Protecting the Earth against Collisions with Asteroids and Comet Nuclei

Andrey M. Finkelstein (Russia)
Walter F. Huebner (USA)
Viktor A. Shor (Russia)
Editors

Proceedings of the International Conference
"Asteroid-Comet Hazard-2009"

Saint Petersburg
"Nauka"
2010

УДК 521
ББК 22.655
340

Защита Земли от столкновений с астероидами и кометными ядрами // Труды Международной конференции «Астероидно-кометная опасность-2009» / под ред. А. Финкельштейна, У. Хюбнера, В. Шора. — СПб.: Наука, 2010. — 427 с.

ISBN 978-5-02-025514-2

В сборнике представлены материалы Международной конференции по проблеме астероидно-кометной опасности, проходившей с 21 по 25 сентября 2009 г. в Институте прикладной астрономии Российской академии наук в Санкт-Петербурге. На конференции обсуждался широкий круг проблем, связанных с происхождением и физическими свойствами малых тел Солнечной системы, способных сталкиваться с Землей, обнаружением и слежением за подобными телами, разрушительными последствиями их столкновений с планетами и их спутниками. Особое внимание в представленных на конференции работах уделялось динамике сближения тел с Землей, предвычислению опасных сближений и организации защиты Земли от столкновений с достаточно крупными небесными телами.

Сборник рассчитан на специалистов в области изучения малых тел Солнечной системы и организации защиты Земли от катастрофических столкновений с небесными телами.

“Protecting the Earth against collisions with asteroids and comet nuclei”. Proceedings of the International Conference “Asteroid-Comet Hazard-2009”. A. Finkelstein, W. Huebner, V. Shor (Eds).

The volume contains the proceedings of the International Conference “Asteroid-Comet Hazard-2009” held in St. Petersburg, Russia, September 21–25, 2009. The conference was held in the Institute of Applied Astronomy of the Russian Academy of Sciences. The subjects of considerable discussion at the conference were the origin and physical nature of minor bodies of the Solar System that can collide with the Earth, detection and follow-up of such bodies and the devastating consequences of their collisions with planets and satellites. Special attention was paid to the dynamics of Earth approach of these bodies, predictions of dangerous collisions, and organization for protecting the Earth from collisions with dangerously large bodies (larger than about 25 m in diameter).

Papers presented in the Proceedings are of considerable interest for the Solar System science community and for all who are involved in study of small objects of the Solar System and in protecting the Earth against catastrophic collisions with celestial bodies.

ISBN 978-5-02-025514-2
© Институт прикладной астрономии РАН, 2010
© Издательство «Наука», 2010

Contents

Program and Local committees VIII

Welcome speech by A. M. Finkelstein X

Preface XII

Part 1. SMALL BODIES OF THE SOLAR SYSTEM 1

A. M. Finkelstein, Yu. D. Medvedev, V. A. Shor. Our View of Objects of ACH-2009 2

G. V. Pechernikova, A. V. Vityazev. Origin of the Small Solar System Bodies 9

D. F. Lupishko, Zh. A. Pozhalova. Physical Properties and Internal Structure of Near-Earth Objects 19

E. M. Drobyshevski. Electrolysis of Ices as a Key to Understanding of the Minor Bodies' Nature 29

F. A. Novikov, V. A. Shor, T. G. Vega, O. M. Kochetova, Yu. D. Medvedev, I. N. Netsvetaev, G. A. Netsvetaeva, U. N. Tihonova, N. B. Zheleznov. AMPLE 3 — Multi-purpose Software Package for Asteroids and Comets 32

E. Yu. Aleshkina, V. V. Kouprianov, A. V. Devyatkin, I. A. Verestchagina, V. Slesarenko. Analysis of Observations of Earth Impact Object 2008 *TC*3 37

V. V. Busarev, V. V. Prokofjeva-Mikhajlovskaya, A. N. Rublevsky. Spots on Asteroids as Evidence of Collisions 43

Yu. A. Chernetenko, A. V. Ivantsov. Masses of Asteroids 10 Hygiea and 152 Atala Obtained by the Dynamical Method 46

N. M. Gaftonyuk, Yu. N. Krugly, I. E. Molotov. Results of Photometric Observations of Potentially Hazardous Asteroids 49

P. Kankiewicz, I. Włodarczyk. Possible Origin of Asteroids on Retrograde Orbits 52

K. V. Kholshevnikov. Estimates for the Set-theoretic Distance between Orbits of Celestial Bodies 55

Yu. N. Krugly, N. M. Gaftonyuk, J. Durech, D. Vokrouhlicky, M. Kaasalainen, V. G. Shevchenko, M. A. Ibrahimov, A. L. Marshalkina, V. V. Rumyantsev, I. E. Molotov, Z. Donchev, V. Ivanova, A. V. Ser-

geyev, N. Tungalag. Detection of the YORP Effect from Photometric Observations of Near-Earth Asteroids 58

N. N. Gorkavyi, A. N. Rublevsky, V. V. Prokofjeva-Mihajlovskaya. The Sizes of Impact Craters and Ejecta Spots on Asteroids 62

V. A. Shefer. Method for High-accuracy Determinations of Orbits of Small Bodies from Three Observations 65

V. A. Shefer. Determination of an Intermediate Perturbed Orbit from Range and Range Rate Measurements at Three Time Instances 70

M. D. Zamarashkina. Improving the Orbital Parameters of Phobos and Deimos by Using the Universal Programming Complex ERA..... 75

E. I. Yagudina. Databases for Observations and Orbit Elements for Asteroids and Comets in ERA System 79

Part 2. OBSERVATION AND DETECTION OF NEOS 83

A. L. García. Automatic Detection of NEOs in CCD Frames 84

A. A. Golubov, Yu. N. Krugly. YORP: Influence on Rotation Rate 90

Yu. V. Batrakov, V. V. Prokofjeva-Mikhajlovskaya, L. G. Karachkina. The Small Libration of the Satellite in the System of the Asteroid 39 Laetitia 95

A. F. Zausaev, A. A. Zausaev, V. V. Abramov, S. S. Denisov. Database Development for Solar System Small Bodies' Orbital Evolution Based on Modern Mathematical Models and Methods 102

A. A. Berezhnoy. Analysis of the Systematic Errors of CCD-observations of Asteroids Performed in 2007–2008 107

M. S. Chubey, L. I. Yagudin, V. N. L'vov, S. D. Tsekmejster, V. V. Kouprianov, G. I. Eroshkin, E. A. Smirnov, A. V. Petrov. Solving of the ACH Problem in the Project "Interplanetary Solar Stereoscopic Observatory" ... 110

M. Kocer, M. Honkova, J. Ticha, M. Tichy. KLENOT Project — Contribution to Follow-up Astrometry of PHAs and VIs..... 115

Part 3. COMETS: PHYSICAL NATURE AND MOTION 119

V. V. Emel'yanenko. Short-Period Comets: Origin and Terrestrial Impact Hazard..... 120

Yu. S. Bondarenko, Yu. D. Medvedev. Method of Calculating Cometary Orbits 129

M. D. Zamarashkina, O. F. Ogneva. Nongravitational Effects on Cometary Motion due to Jupiter 134

M. G. Ishmukhametova, E. D. Kondrat'eva, V. S. Usanin. Variation of Nongravitational Parameters for Comet Encke as a Result of its Decay 139

N. I. Perov, D. V. Kolesnikov. On the Problem of Searching for Undiscovered Cometary Families Colliding with Terrestrial Type Planets 146

Yu. S. Bondarenko. Electronic Catalogue of Comets "Halley" 152

O. G. Gladysheva. From the Tunguska Space Body to the Evolution of the Protoplanetary Nebula 157

Part 4. METEOR COMPLEXES. TUNGUSKA 163

N. V. Kulikova, V. I. Tischenko. Origin and Dynamic Evolution of Meteor Complexes in the Problem of Asteroid-Comet Hazard 164

E. N. Tikhomirova. Meteor Streams: the Relation to Hazardous Celestial Bodies 168

M. I. Gritsevich. Modern Dynamic Methods of Determination of Parameters of Meteor Bodies 174

G. A. Nikolsky, Yu. D. Medvedev, E. O. Schultz. The Tunguska Catastrophe is the Consequence of a Series of Explosions of Comet Nucleus Fragments 179

O. G. Gladysheva. Atmospheric Discharge in the Tunguska Disaster 184

T. Yu. Galushina, E. M. Drobyshevski, M. E. Drobyshevski. In Searching for Comet P/Tunguska–1908 189

V. A. Alekseev, N. G. Alekseeva, I. G. Golovnev, S. Yu. Zheltov, A. I. Morgachev, E. Ya. Fal'kov. Likely Impact Sites of Large Fragments of the Tunguska Cosmic Body 196

Part 5. DEVASTATING CONSEQUENCES OF IMPACTS. STUDY OF TRACES OF PAST COLLISIONS 199

V. V. Svetsov. Consequences of Impacts of Cosmic Objects in Circumstances of Changing Climate 200

An. G. Marchuk, K. V. Simonov, S. A. Peretokin. Detection of Possible Impact Structures at the Bottom of the Ocean by Gravimetric and Magnetometric Data Processing 206

V. L. Masaitis. Prospective Zones of Damage Caused by the Popigai Impact Event 211

N. A. Makhutov, Yu. G. Matvienko, M. A. Bubnov. Hydrocode Modeling of a High-velocity Impact of an Asteroid Particle on a Steel Surface 216

L. A. Egorova, V. V. Lokhin. Destruction Models for Bodies Entering a Planetary Atmosphere 222

V. K. Gusiakov, Z. A. Lyapidevskaya. Expert Database on the Earth Impact Structures 228

V. A. Alekseev, V. V. Kopeikin, N. G. Alekseeva, L. Pelekhan. Georadar and Hydrogen Studies of the Tunguska Meteorite Craters 233

E. V. Pitjeva. Influence of Asteroids and Trans-Neptunian Objects on the Motion of Major Planets and Masses of the Asteroid Main Belt and the TNO Ring 237

Part 6. DYNAMICS OF NEOS. COLLISION PREDICTIONS 243

D. K. Yeomans, S. R. Chesley, P. W. Chodas. NASA's Near-Earth Object Program Office 244

L. K. Kristensen. Demands on Observation Campaigns for Accurate Predictions 255

Yu. D. Medvedev, A. S. Zabotin. Determination of Orbits and Dispersion Ellipsoids of Asteroids Potentially Hazardous for the Earth 262

P. Kankiewicz, I . Włodarczyk. The Orbital Evolution of 2007 VA85, an Amor-type Asteroid on a Retrograde Orbit. 268

V. A. Shor, Yu. A. Chernetenko, O. M. Kochetova. How Precise is the Orbit of (99942) Apophis and how Probable is its Collision with the Earth in 2036? 272

L. L. Sokolov, N. P. Pitjev, V. Sh. Shaidulin. About Zones of Resonant Returns of Asteroid Apophis 279

I. Włodarczyk. Methods of Computing Impact Orbits 284

Yu. A. Chernetenko. The Yarkovsky Effect in the Motion of NEAs 289

J. Desmars, J.-E. Arlot, A. Vienne. Estimating the Accuracy of Asteroid Ephemerides Using the Bootstrap Method 294

I. Włodarczyk. Paths of Risk of Selected Dangerous Asteroids 299

I. Włodarczyk. Impact Solutions for Asteroid (101955) 1999RQ_{36} 302

N. B. Zheleznov. The Study of the Probability of an Asteroid Collision with a Planet by Monte Carlo Method 305

Part 7. INVESTIGATION OF NEOS IN SITU. COUNTERACTION TO THE NEO HAZARD 311

A. W. Harris. Estimating the NEO Population and Impact Risk: Past, Present and Future 312

M. F. A'Hearn. Deep Impact and Deflection of NEOs 327

W. F. Huebner, D. C. Boice, P. Bradley, S. Chocron, R. Clement, A. Ghosh, P. T. Giguere, R. Goldstein, J. A. Guzik, L. N. Johnson, J. J. Keady, J. Mukherjee, W. Patrick, C. Plesko, M. Tapley, J. D. Walker, R. P. Weaver, K. Wohletz. The Engagement Space for Countermeasures Against Potentially Hazardous Objects (PHOs) 337

C. Maccone. Description of a NASA Study to Deflect Hazardous Asteroids 347

A. V. Zaitsev, A. Koroteev, B. Liaschuk, S. Popov. The Level of Rapid Response Reaction of the Planetary Defense System 362

V. A. Emelyanov, Yu. K. Merkushev. Design Parameters and Efficiency of a Space System for Warning about Small Celestial Bodies Approaching the Earth along Collision Trajectories 369

N. A. Makhutov, V. A. Puchkov, D. Reznikov, A. Taranov, A. V. Zaitsev. About Measures on Minimization of Damage from Collisions with Asteroids and Nuclei of Comets 376

Z. M. Ilitz. Rotational Mass Driver — an Efficient NEO Deflection Concept 381

J. J. Smulsky, Ya. J. Smulsky. Evolution of Apophis Orbit for 1000 Years and New Space Targets 390

A. V. Zaitsev, A. A. Klapovsky. On the Approach to Form International-Legal Foundations to Ensure Planetary Defense 396

B. I. Semyonov, S. N. Torgovkin, V. V. Treckin, A. V. Zaitsev. About the Interaction of the "Citadel" Planetary Defense System with the Missile-Space Defense Systems 402

The Resolution of the ACH-2009 Conference 407

INTERNATIONAL CONFERENCE
"Asteroid-Comet Hazard-2009"
September 21–25, 2009,
St. Petersburg, Russia

Program committee

Finkelstein A. M. (Chairman)	Institute of Applied Astronomy of RAS, Russia
Shor V. A. (Vice-chairman)	Institute of Applied Astronomy of RAS, Russia
Medvedev Yu. D. (Scientific secretary)	Institute of Applied Astronomy of RAS, Russia
Adushkin V. V.	Institute of Geosphere Dynamics of RAS, Russia
Akim E. L.	Keldysh Institute of Applied Mathematics of RAS, Russia
Emelyanov V. A.	Central Scientific-Research Institute for Mechanical Engineering of Federal Space Agency, Russia
Fortov V. E.	Institute for High Energy Densities of RAS, Russia
Harris A.	Space Science Institute, USA
Lupishko D. F.	Astronomical Institute of V. N. Karazin Kharkiv National University, Ukraine
Marov M. Ya.	Keldysh Institute of Applied Mathematics of RAS, Russia
Marsden B. G.	Minor Planet Center, USA
Milani A.	University of Piza, Italy
Muinonen K.	University of Helsinki, Finland
Pittich E.	Slovak Academy of Sciences, Slovakia
Pol' V. G.	S. A. Lavochkin Scientific-Production Association, Russia
Rickman H.	Uppsala University, Sweden
Rykhlova L. V.	Institute of Astronomy of RAS, Russia
Shustov B. M.	Institute of Astronomy of RAS, Russia
Simonenko V. A.	Russian Federal Nuclear Center — E. I. Zababakhin Research Institute of Technical Physics, Russia
Sukhanov K. G.	S. A. Lavochkin Scientific-Production Association, Russia

Yatskiv Ya. S.	Main Astronomical Observatory of National Academy of Sciences of Ukraine, Ukraine
Yeomans D. K.	NASA Near Earth Object Program Office, USA
Zajtsev A. V.	Non-profitable Partnership “Planetary Defense Center”, Russia

Local organizing committee

Medvedev Yu. D. – Chairman
Chernetenko Yu. A. – Vice-chairman
Shuygina N. V. – Secretary
Bondarenko Yu. S.
Lysenkov E. A.
Sal’nikov A. I.
Valyaev V. I.
Zabotin A. S.

Welcome Speech by A. M. Finkelstein, Director of the Institute of Applied Astronomy

Dear colleagues and friends!

I am happy to welcome you in Saint Petersburg to our conference "Asteroid-Comet Hazard-2009". More than 150 participants from 18 countries and from 135 different institutions will take part in the Conference, and they will present about 140 reports.

So large an attendance at the Conference shows that the problem of asteroid-comet hazard is a really vital and challenging scientific problem.

I would like to note that this Conference brings together specialists from many different fields of science, such as astronomers and physicists, geophysicists and geologists, engineers and designers, lawyers and even mass media. It shows how complex the problem of the asteroid-comet hazard is. One of the goals of this meeting is to strengthen cooperation and to build stable bridges between the specialists of different "colors" for better understanding and for improvement of studies.

It is well known that during four and half billions years the Earth was repeatedly exposed to collisions with asteroids, comet nuclei, and large meteoroids. The impacts of such cosmic bodies shaped the surface of the Earth and later created the conditions for the beginning and the evolution of life on our planet. These space phenomena caused global climatic changes, changes of flora and fauna, loss of thousands of living species and appearance of thousand of new ones including the mammalians and as a consequence man. A lot of interesting physical processes were connected with these phenomena and they attract the attention of many scientists.

One of the most practical questions of the asteroid-comet hazard problem is the question of how serious the risk of a collision of the Earth with an asteroid or a comet nucleus is, and what can be the consequences of this collision. This question concerns not only the specialists, but also the general public.

Our Conference should give answers to these questions and I hope that we will be able to summarize the most important answers for the mass media during a press-conference on Wednesday.

This Conference is held here in Russia, in the Institute of Applied Astronomy, which has worked for many years on the dynamics of small bodies

of the Solar System. In particular, you probably know, that the IAA publishes annually by order of the International Astronomical Union "Ephemerides of Minor Planets", which is distributed to different world astronomical institutions. Recently we started to use the VLBI-Network "Quasar" for observations of asteroids approaching the Earth. I hope that some of you will visit on Thursday the radio astronomical observatory "Svetloe", one of three observatories of the VLBI-Network "Quasar" which is situated in Leningrad Province, relatively near here.

This screen demonstrates all three "Quasar" observatories in on-line mode via optical fiber lines. They are situated in Leningrad Province, in the North Caucasus and near Baikal Lake in Siberia**.**

I hope that in 2011–2012, in accordance with our plans, we will put into service the large radar using the 70-meter radio telescope located in the Far East of Russia, which we are planning to use with the same aims.

I would like to mention that in Russia, the Russian Space Agency, the Russian Academy of Sciences, and some other governmental departments work together on the creation of various technical facilities for the observation of and development of countermeasures against asteroids and comets approaching the Earth. It is obvious that in order to design and to construct such facilities it is necessary to solve many complicated scientific and engineering problems, as well as, to coordinate a number of delicate juridical questions. It is clear that most of these problems can be solved as a whole only in the framework of international cooperation, using international resources.

We hope that our Conference will be the stimulus for the solution of all these questions.

The success of our Conference depends on the contributions of all participants.

Highly interesting and important contributions will be provided by oral and poster presentations and during discussions. As chairman of the Program Committee I would like to thank all the speakers and all the authors for preparation of their excellent presentations.

I would like also to express my thanks to members of the Program Committee who have set up a very interesting program.

Papers will be printed shortly after the Conference in Proceedings. Thanks to all — let us keep up the momentum and prepare our papers for the Proceedings in time.

I wish all participants to enjoy the Conference, useful meetings as well as a pleasant stay in our remarkable city.

Thank you!

Preface

The International Conference "Asteroid-Comet Hazard-2009 (ACH-2009)", organized on the initiative of the Institute of Applied Astronomy of RAS with financial support from the Russian Academy of Sciences and the Russian Fund for Basic Research, was held from 21 to 25 September, 2009, in St. Petersburg, Russia. The Conference is the most recent in a series of conferences about the same subject that are traditionally conducted by IAA RAS. Plenary sessions of the meeting were held daily in the IAA building in Kutuzov Quay, 10, with exception of 24-th September when an excursion to the radio observatory "Svetloe" on the Karelian Isthmus took place.

The Conference was attended by more than 140 participants from about 20 countries. About 70 oral presentations (13 Invited and 55 contributed papers) were presented during the Conference. In addition about 50 presentations were made in poster form. All oral reports were presented in seven sessions each pertaining to a certain subject. Names of the sessions are given bellow:

1. Small Bodies of the Solar System.
2. Observation and Detection of NEOs.
3. Comets: Physical Nature and Motion.
4. Meteor Complexes. Tunguska.
5. Devastating Consequences of Impacts. Study of Traces of Past Collisions.
6. Dynamics of NEOs. Collision Predictions.
7. Investigation of NEOs in situ. Counteraction to the NEO Hazard.

More than half of participants made use of the opportunity to submit their papers for publication in the Proceedings of the Conference. In the present Proceedings of ACH-2009 all papers accepted for publication are grouped in sections named for the sessions of the Conference. Every paper is put into the section to which it is related by subject. Every section begins with Invited presentations (in case they are published), these papers are followed by contributed oral communications. Each section ends with papers that were originally presented as posters. In each section papers are arranged in the order of their presentation at the Conference. To keep the size of Proceedings within reasonable limits, ten pages were allotted to invited papers, five pages for papers corresponding to oral presentations, and three pages for papers associated with posters, but this rule was not strictly enforced. An authors index placed at the end of the book facilitates finding of papers.

The papers presented for publication in the Proceedings were critically considered by Editors. In many cases the manuscripts were returned to authors for corrections, answering questions and correlating data. As we hope, this process has led to improving quality of papers included in the Proceedings. However, the editors also considered some papers for publication that were not fully mature for publication because they presented some novel and promising ideas that need considerable additional work. In all instances the papers reflect the authors' points of view even if they varied from standard accepted views or were at variance with that of the Editors. In case of some doubts upon correctness of results or proposed ideas the Editors preferred to give authors an opportunity to outline their results or ideas instead of rejecting the paper or insisting on complete correctness of the solutions. Only in small number of cases, when according to Editors' opinion the submitted exposition can lead to misunderstandings or wrong estimates of the attained result, the Editors take the liberty of inserting a footnote with an appropriate explanation.

It is not our aim here to give a comprehensive assessment of the Conference and those papers that appear in its Proceedings. Nevertheless, one will note that approximately three fourths of Conference participants came from countries of the former Soviet Union (FSU). By virtue of some selective process their papers comprise an even higher percentage in the Proceedings. Perhaps for the first time the papers of representatives of this geographical region on the subject of asteroid-comet hazard are collected in great diversity and completeness with Proceedings published in English. This provides an opportunity for English speaking readers to gain insight in the directions and levels of research in the field of asteroid-comet hazards that are conducted in the countries of the FSU. We hope that it also encourages international participation in the common defense of Earth against the asteroid-comet hazard.

Aside the geographical factors, the reader will hopefully find in the Proceedings a number of interesting ideas and developments regarding the study of small Solar System bodies, about problems of interaction of meteor matter with the Earth's atmosphere, and the study of the collision of the Tunguska space body and other space bodies with the Earth and other planets. At the ACH-2009 Conference (and to a lesser degree, in the Proceedings) research results devoted to catastrophic consequences of collisions of cosmic bodies with planets and their satellites were presented. Comprehensive expert information is presented on predictions of encountering dangerous celestial bodies with the Earth and other planets and on prospects for enlarging the scope of the Spaceguard survey to cover dangerous bodies of hectometer size. Finally, possible schemes of organization of Earth protection against

collisions with asteroids and comet nuclei are described in papers by several groups of researchers working on different continents.

Thus, in our opinion, the contents of the Proceedings is of broad interest for a wide section of researchers involved in the study of the problem of counteracting the asteroid-comet hazard, involving experts in the fields of physics, dynamics, the origin of small Solar System bodies, and meteor matter.

We are happy to use this opportunity to thank the members of the Scientific Committee and members of the Local Organizing Committee of ACH-2009 for organization and successfully carrying out the Conference and for co-operation during publication of its Proceedings. We are especially indebted to Diana Ryzhkova, staff member of the IAA RAS for preparation of the Proceedings and to the staff of the St. Petersburg branch of the Publishing house of RAS for preparation and publication of the Proceedings. We also thank Yurij A. Bondarenko, the author of several papers incorporated into the Proceedings, for designing the Conference logo presented on the Proceedings cover.

Andrey M. Finkelstein, Walter F. Huebner , Viktor A. Shor

Standard scenario of evolution of gas-dust pre-planetary disk around the early Sun
ACH - 2009

Part 1. Small Bodies of the Solar System

SMALL BODIES OF THE SOLAR SYSTEM

Our View of Objects of ACH-2009

A. M. Finkelstein, Yu. D. Medvedev, V. A. Shor

Institute of Applied Astronomy of RAS, St. Petersburg, Russia

Abstract. The report is prepared in anticipation of the International Conference "Asteroid-Comet Hazard-2009" (21–25 September, 2009, St. Petersburg). Some considerations on the subject of what can be done and what should be done to enlarge contribution of Russian researches to solution of the problem of the asteroid-comet hazard are presented. In connection with transition to the second stage of Spaceguard survey an important task is the development of national program of Russian participation in NEOs monitoring. An important element for the national program is to upgrade the radio telescope RT-70 in Ussurijsk (Far-East of Russia), which could be used starting in 2011 as regular radar, as well as in the scheme of a VLBI — for radio location. An urgent task seems to be organizing in Russia a regional center for NEO monitoring. Such a center would take over the task of coordination of Russian observatory efforts on NEO observations, on one hand, and would be involved in computation of close approaches and possible collisions of small bodies with planets, on the other hand, similar to that done now at JPL and NEODyS.

As is well known, scientific conferences are organized with the aims of exchanging ideas, experiences, achievements, and for determination of prospective directions of research. All these points undoubtedly have direct relationship to the ACH-2009. However, present Conference has its own specific features connected with place and time of its holding. It would be appropriate for us as the initiators of the Conference to express some thoughts on the subject.

It should be mentioned at first that the Conference takes place in Russia and three fourths of its participants are working in this country. This, on one hand, indicates that the problem of asteroid-comet hazard as a whole or at least some of its branches attract attention in wide circles of scientific workers and technical experts in this country. On the other hand, it gives grounds for us to consider the problem with special emphasis on its Russian aspect.

Different areas of the problem are presented in Russian researches to variable degree of completeness. In some areas, say, in the research of traces of past collisions of Earth with space bodies or in modeling the processes of their impacts, the Russian researches are, as we think, at a level of high standards. Here we have what may be demonstrated and what we can share with our foreign colleagues. "The geographical factor" traditionally provides leading positions of Russian scientists in the research of Tunguska phenomenon. This topic is widely presented in the program of the Conference. It is interesting that two presentations simultaneously report on possible discovery of Tunguska meteorite crater. If the discovery will be confirmed, as well as similar preceding reports of other groups of researches, then our view of Tunguska phenomenon could be significantly changed.

In a number of other divisions our achievements are more modest. Positional observations and physical researches of minor planets in Russia are not numerous. It is primarily the result of a poor instrumental base, as will be mentioned later in detail. The country has been falling behind in such problems as monitoring of potentially hazardous celestial bodies and prediction of their collisions with the Earth. It would be extremely interesting for us to use experience gained in this respect in other countries. A vast field for mutual exchange of ideas and developments is the implementation of the counteractions to the actual collisions.

It would not be a great exaggeration to say that the problem of asteroid-comet hazard experiences now a specific moment of its history.

The peculiarity of the present moment firstly lies in the fact that the transition from the first stage of the program "Spaceguard" to the stage "Spaceguard-2" is now underway. The second stage, as it is known, is intended for discovering and cataloguing 90 % of all potentially hazardous bodies from 140 m to 1 km in size during the next 15–20 years. The corresponding work is approximately two orders of magnitude greater than that fulfilled at the first stage. Solving this sophisticated task requires new, much more powerful instruments for discovery of objects and new approaches for follow-up observations. Prediction and analysis of all possible collisions with the Earth and other massive bodies will become a complicated and time-consuming task.

Secondly, especially after discovering a number of objects that have small, but non-negligible probability of colliding with the Earth during the 21st century, it has become clear that human civilization is not ready to repulse the hazardous objects, first of all because of a lack of political agreement between countries about such actions. Who has to take the responsibility for implementation of counteractions? What is the measure of responsibility of a state or a group of states initiating the preventing actions against a hazardous body in case of failure or unforeseen tragic mistake? There are

no universally accepted answers to these questions. The procedures of informing the population about the collision hazard with a specific body and the extent of this hazard still remain to be developed.

Certainly these questions disturbed experts earlier. But these questions become especially topical during execution of "Spaceguard-2" when the probability of discovery of a dangerous body on a collision course with the Earth increases many-fold. Absence of international agreement on the problem of asteroid-comet hazard counteraction becomes absolutely intolerable. The Committee on NEO of the Association of Space Explorers and its International Panel on Asteroid Threat Mitigation were guided by similar considerations when preparing the report "Asteroid Threats: A Call for Global Response", which was submitted to the UN Committee on Peaceful Uses of Outer Space at the end of last year.

It is needless to say that Russia as one of the leading space powers, possessing necessary means and technologies for participating in counteractions against the NEO threat, is interested in the legal status of these actions, to ensure preparation and implementation of counteractions within the framework provided by the United Nations. Without international agreement the preparation for counteractions can contribute to the rise of international tensions and a new armaments race. There is good reason to hope that, given the legal status of the asteroid-comet hazard and the consideration of the problem on an international level within the UN, the necessity to provide some specific obligations for participating in collective actions will result in raising attention to the NEO hazard on the side of governments and legislators, secure financial support of development, and further creation of corresponding space apparatuses and equipment.

Up to now the financial provision of research on asteroid-comet hazard in Russia was carried out only within the framework of common support of scientific and applied research. For a number of areas it was insufficient. The Russian contribution to the Spaceguard program was insignificant. As a result of the disintegration of the former Soviet Union the majority of southern observatories with their sufficiently powerful instruments are abroad. Under economic pressures of the nineties of the last century the majority of these observatories terminated their activities. The few observatories that remain within Russia also were in difficult circumstances. Their cooperation with observatories beyond Russia's boundaries, drastically dwindled. Observations at their own southern stations actually stopped due to financial difficulties. The fate of the Crimean group of minor planet and comet observers, previously being a part of the Institute of Theoretical Astronomy in Leningrad, is typical in this respect. During the 1970–1980-ies the Group was among the world's three most productive observers of minor planet and comet positions. After disintegration of the Soviet Union it merged into the

staff of the Crimean Astrophysical Observatory (Ukraine) and after a lapse of time it stopped activity.

Currently the situation with respect to observations of minor planets and comets in Russia is getting gradually better. Some southern observatories, now the institutes of independent states, develop their activities in cooperation with astronomical institutions of Russia (Simeiz Observatory, Terskol Observatory, Maidanak Observatory). A joint observational program has been established by Turkey and Russia at TÜBITAK National Observatory, Antalya. Some new observatories and observational stations aimed particularly at observations of small bodies are created on the territory of the Russian Federation. Here we can mention in the first turn the North Caucasus Observational station of Pulkovo Observatory, Kourovka Observatory of the Ural University, and the South station of Moscow University in the North Caucasus. The project of the 2-m telescope intended for discovery of NEOs, and that of the twin telescope with a lesser field of view intended for follow-up observations have been developed.

Though a significant percentage of all available astrometric instruments in Russia have small diameters (0.4–1.0 m), they can contribute to world-wide efforts directed to follow-up observations of discovered objects. As a rule, the available telescopes are aided by equipment for automatic operation. For their efficient use for the purposes of astrometry and astrophysics a well-thought-out program is required. This program still needs to be refined and reconciled.

The amateurs of astronomy who have sometimes the instruments of professional quality at their disposal also can make their own contribution to observations of minor bodies.

Of prime importance is the creation of the radar at Ussurijsk (Far East of Russia) on the base of RT-70 (radio telescope with the dish of 70 m in diameter). This telescope earlier was used for deep space communications. The radar will become operational in 2011. Its parameters are similar to those of the Goldstone radar, one of the two radars most often used for minor planet and comet research.

Construction of a powerful radar at Ussurijsk makes it possible to observe small bodies by the recently elaborated method of VLBI-location. In this method the classic ("usual") radar observations providing measurements of relative velocity of an irradiated body and its distance are supplemented by registration of echo-signals by a number of radio telescopes working together as a VLBI (Very Long Baseline Interferometer). As compared with classic radar, the VLBI enables position determination of an object on the celestial sphere with very high precision; on the order of 0.01″ for a single measurement and on the order of 0.001″ for a series of observations. In so doing, the position of a body is determined directly with respect to the

sources of radio emission (quasars) that fix the celestial reference system. In this way VLBI can provide high precision measurements simultaneously of four quantities that can be used for improving orbital parameters. In this way it will be possible to determine orbits of a number of small bodies to very high precision.

The radio telescope RT-70 together with three other radio telescopes is now included in the Russian VLBI network "Quasar" that has the control center and the center of data processing in St. Petersburg, in IAA RAS. Now the VLBI equipment is mounted on the telescope. After completion of upgrading RT-70, the observations of small bodies will be available in the regime of radar, as well as in the regime of VLBI-location using the telescopes of "Quasar" network and possible the other radio telescopes.

To this we can add that the participation of Russia in the program of discovery and follow-up observations of NEOs seems to be of significant importance because of geographical factors — the great extent of its territory from east to west, in particularly in those time zones where few other observatories exist.

Thus, participation of Russia in monitoring potentially hazardous objects is desired and possible. Nevertheless, it must be stated that a great deal needs to be done in this respect. As was said above, the detailed project of participation of Russia in NEO monitoring is required. At present those observatories where some useful work is fulfilled act in conformity with their own traditions and programs, which are not always in agreement with modern tasks and with modern practices. We feel that in so great a country as Russia, there is need for some scientific body (council or committee) to manage and track work at observatories, put forward new tasks and ideas, and provide useful guidance. It is our opinion that observations at different observatories are in need of more strict coordination, the equipment used is partially in need of modernization, and observers are in need of exchange of experiences and other help including financial incentives. It would be desirable to organize observatory work in close contact with a computing center that analyzes observations and provides feed-back to the observatories. This would be of assistance in raising the precision and accuracy of observations and at the same time it would give observers the feeling of usefulness of their work.

As was noted above, in the second stage of the Spaceguard program, after putting PanSTARRS (the Panoramic Survey Telescope & Rapid Response System), the LSST (Large Synoptic Survey Telescope), and the DCT (Discovery Channel Telescope) in service, the number of potentially hazardous objects that need monitoring and the predictions of possible collisions with Earth and other planets will grow rapidly. As we think, under these conditions it would be advisable to organize in Russia a regional center for

monitoring such bodies. It is quite natural that such center will operate in close contact with other centers abroad, exchanging relevant information with them. For such a great country as Russia, having a very large territory and a long coast line and, consequently, being exposed to a relatively high probability to suffer an impact of a space body on its territory or in a nearby ocean, the availability of special services for keeping track of possible collisions with space bodies is a prime necessity. The interest in such services is displayed by the Ministry of the Russian Federation for Affairs of Civil Defence, Emergencies, and Disaster Relief. We note that Russia has experienced three impacts from cosmic bodies in less than one hundred years (Tunguska on June 30, 1908; Sikhote-Alin on February 12, 1947; and Vitim River basin near Bodaybo on September 25, 2002), more frequently than any other country in modern times.

Creation of a regional center for hazardous space body monitoring will be useful not only for Russian national purposes, but also for counteraction of asteroid-comet hazards world-wide. The Russian center could take over some part of the work necessary for all objects or the whole work for some objects. It is not unreasonable to perform the work in various centers in parallel, as at least in our case all computations will be made on the ground with completely original and independent software and theory of motion of major planets and the Moon (EPM) that has been developed and is maintained in IAA RAS. A comparison of independently obtained results will be useful, necessary, and informative, especially in critical cases. Such a comparison of expected results is of paramount importance when planning orbit deflection of dangerous body, eliminating the threat of dangerous approaches in the future.

Certain provisional work for countering hazardous asteroids and comets has been done in IAA RAS, and we hope that the Conference will give additional impetus for its subsequent development.

One of the important events of the last years was the discovery of threatening asteroid Apophis whose very close approach with the Earth in 2029 is unprecedented for the bodies of hectometers in size. Moreover, there is small probability that this asteroid will collide with the Earth in 2036.

Apophis' motion demonstrates a number of peculiarities that are characteristic properties of bodies having orbits similar to that of the Earth and having very close approaches with the planet. Among these are the possibility of resonant returns of the small body and the Earth to the same mutual positions several years after a close approach, the existence of a number of keyholes passing through which leads to collision with the Earth some revolutions later, the loss of precision of motion predictions after close approach down to full unpredictability of motion after several close encounters, the long time intervals between periods suitable for groundbased observations,

significant influence of nongravitational forces on the motion, etc. Without doubt the implementation of the program Spaceguard-2 will result in discovery of many bodies possessing similar or still more exotic properties. Apophis' properties should be thoroughly studied and taken into consideration when similar bodies are discovered.

A main enigma of Apophis' motion is its minimum distance from the Earth center on 13 April, 2029: will it pass through the keyhole to cause a collision in 2036 or not? The precision of present-day knowledge of Apophis' orbit and nongravitational forces influencing its motion is insufficient to answer this question today.

The limiting values of Apophis' minimum distance from the Earth center in 2029 that distinguish trajectories leading to collision in 2036 from those that will pass by the Earth differ by 600 meters (the keyhole width). It follows from this that, at least in some situations, one needs to know the Apophis orbit to a much higher precision (of two or more orders of magnitude) than presently known. These demands are behind a number of projects to deliver a transmitter to Apophis' surface or on the orbit of its satellite. Processing the radio signals transmitted over several months will provide the opportunity to determine the Apophis orbit with great precision and to solve in this way if it is in need of correction to prevent collision of Apophis with the Earth in 2036.

A project of reconnaissance and tracking mission to Apophis suggested by researches of S. A. Lavochkin Scientific-Production Association and INASAN will be presented at the Conference. The main purpose of the mission is to deliver the radio transmitter on the orbit of Apophis' satellite and possible solution of other tasks of Apophis' investigation. Discussion of the project at the Conference will aid more thorough considerations for the project with the aim of possibly including it in future plans of the Russian Space Agency.

In conclusion, one can state that one of the important aims of the present Conference, according to opinion of its initiators, is to intensify the Russian participation in solving problem of the asteroid-comet hazard. We hope that discussion of presented reports, informal personal contacts of Russian participants with each other and with foreign colleagues will contribute extensively to solving this task.

SMALL BODIES OF THE SOLAR SYSTEM

Origin of the Small Solar System Bodies

G. V. Pechernikova, A. V. Vityazev

Institute of Geosphere Dynamics of RAS, Moscow, Russia

Abstract. During the last decades of the twentieth century joint efforts of scientist from different countries made it possible to develop a standard scenario of the origin of the Sun, planets and other bodies of the Solar System that satisfied basic observational data accumulated by astrophysics and comparative planetology. Following are brief description of this scenario and the problem of the origin of the small Solar System bodies. Small Solar System Body (SSSB) is a term defined in 2006 [1] by the International Astronomical Union to describe objects in the Solar System (SS) that are neither planets nor dwarf planets. In the framework of the standard scenario of the origin of the Solar System SSSBs are considered as some kind of the remnants of building material of the Solar planetary system.

Introduction

For the first time the systematic elaboration of the theory of planet formation from solid particles of the pre-planetary circumsolar cloud was begun by O. Yu. Schmidt in 1944. O. Yu. Schmidt proposed to divide the problem of SS origin into three parts. At that time elaboration of each part could be done to some extent independently:

1. The explanation of the Sun's origin and the way of pre-planetary cloud formation.
2. The development of the theory of planet formation in the course of evolution of pre-planetary cloud — central problem of planetary cosmogony.
3. Construction of the theory of the Earth evolution during the following 4.5 milliard years by the use of the results obtained in the solution of the second problem as initial data.

This allowed O. Y. Schmidt and his followers to begin to address the central problem in the department he founded in the Institute of Physics of the Earth [2].

The theory of formation of the Earth and other planets must explain first of all the following groups of facts:

A — planetary orbits are almost circular and lie in the same plane. Circulation of planets (and rotation of most of them as well) occurs in the direction of rotation of the Sun;

B — distribution of planetary distances from the Sun is evidently not random (the rule of Titius–Bode);

C — partition of planets into two sharply distinguished groups: (1) inner — small, denser, with slower rotation, with small number of satellites (or without them), and (2) outer — large in dimension, with lower density, high rate of rotation and numerous satellites.

Later on:

D — the distribution of angular momentum: while more than 99 % of the total mass of the SS is concentrated in the Sun, less than 2 % of the total angular momentum is accounted by the Sun, the rest (98 %) belongs to the planets;

E — variations in chemical composition and isotopic data.

Standard scenario of the origin of the Solar System

The sequence of stages reflecting the basic features of formation of planetary system of the Sun is shown in Fig. 1. At the left from top to bottom — settling of dust to the central plane and forming of dust subdisk, flattening of dust subdisk, gravitational instability in it and breakdown into dust-gas clusters, shrinking of dust concentrations and forming of swarm of dense bodies with the sizes of asteroids. At the right — integration of planetesimals into planets: birth of large bodies, shock heating, strong metamorphism, melting and vaporization of material, recondensation, dissipation of gas from the Solar

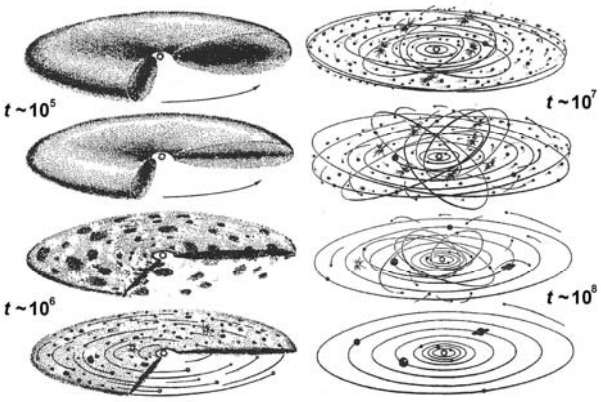

Fig. 1. Evolution of gas-dust pre-planetary disk around the early Sun.

System and accretion on Jupiter and Saturn, formation of Oort cloud and Kuiper belt, completion of the process of formation of planets and satellite systems [3, 4].

"Russian" model, which V. S. Safronov represented, has been termed by the most weighed and promising from 6 models presented at the International Symposium on the Origin of the Solar System, Nice, 1972.

The eighties — revision of the upper boundary for sizes of the largest bodies that formed the planets (from 100 to 1000 km) [5], and, as a consequence, change of the paradigm for the early Earth — hot (of the order of melting temperature) interior of the growing Earth, differentiation in the course of planetary growth [6, 7].

During the last decades of the twentieth century joint efforts of scientist from different countries made it possible to develop a standard scenario of the origin of SS that satisfied basic observational data accumulated by astrophysics and comparative planetology. The general description of this scenario, as well as solutions of related problems, can be found in [4, 6–8].

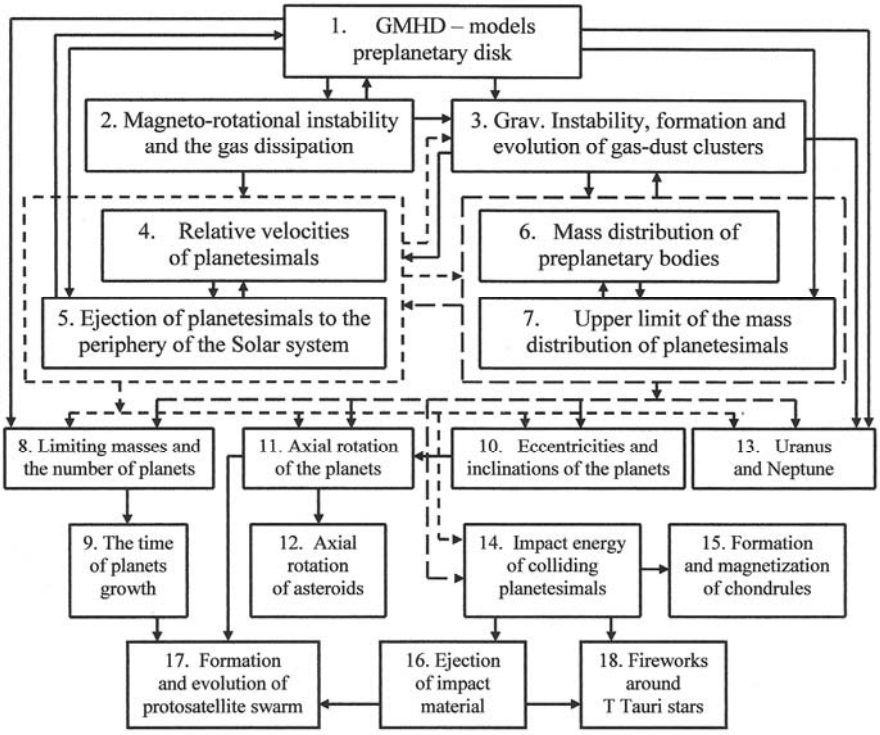

Fig. 2. Block-diagram of gravitational-magnetic-hydrodynamic models of protoplanetary disks around young solar-type stars.

The key problems of a standard scenario of the origin of SS are shown in the block-diagram (Fig. 2).

Every unit in this scheme is, as a matter of fact, a separate line of theoretical and/or experimental investigations for the explanation of observational data. Shown on the scheme are also connections between separate lines of investigations and dependence of solutions of some problems and tasks from others. Units 3–11 were the problems of classical cosmogony. By the end of the eighties, their principal solution has been obtained (the groups of facts A, B and C have been explained) in the framework of the model "Sun + disk". We point out that discussions concerning units 3–7, 13–17 going on with computer calculations are carried out using more and more complicated models. Units 1 and 2 represent the latest modification of the scenario. Unit 18 is our suggestion to astrophysicists [9, 10] — to search for the flashes caused by macro-impacts in forming planetary systems around today's young stars.

Cosmochemistry and geochemistry

New technologies for detection of nano-abundances of the remnants of short-lived radioactive elements (^{26}Al, ^{60}Fe, ^{182}Hf, etc.) enable us to clock separate stages of planetary formation and early evolution with an accuracy of a million years.

Data on Australian zircons and a group of Xe isotopes testify that the atmosphere and hydrosphere existed beginning from 4.4 milliard years ago [11].

The present estimates of the total age of the SS (4.6 Ga) and duration of the final stages of the Earth's formation (~100 Ma) are confirmed by isotope data. However, the Earth's growth rate at the early stages, a crucial period for its future evolution, has so far remained unclear. A consistent consideration of the role of large bodies in the evolution of the preplanetary swarm allowed researchers for the first time to obtain durations of formation of massive (but probably differentiated) bodies (Fig. 3). These durations conform to modern isotope data generated by the Hf-W system [12].

Small Solar System Bodies

SSSB is a term defined in 2006 [1] by the International Astronomical Union to describe objects in the SS that are neither planets nor dwarf planets. SSSBs currently include the classical asteroids, with the exception of Ceres, the Centaurs and Neptune trojans, the trans-Neptunian objects (TNOs), with the exception of dwarf planets, and all comet nuclei. The orbits of the vast majority of SSSBs are located in three distinct areas, namely the Main asteroid belt (between the orbits of the planets Mars and Jupiter), the Edgeworth–Kuiper belt (in the region beyond Neptune), and the Oort cloud. Other

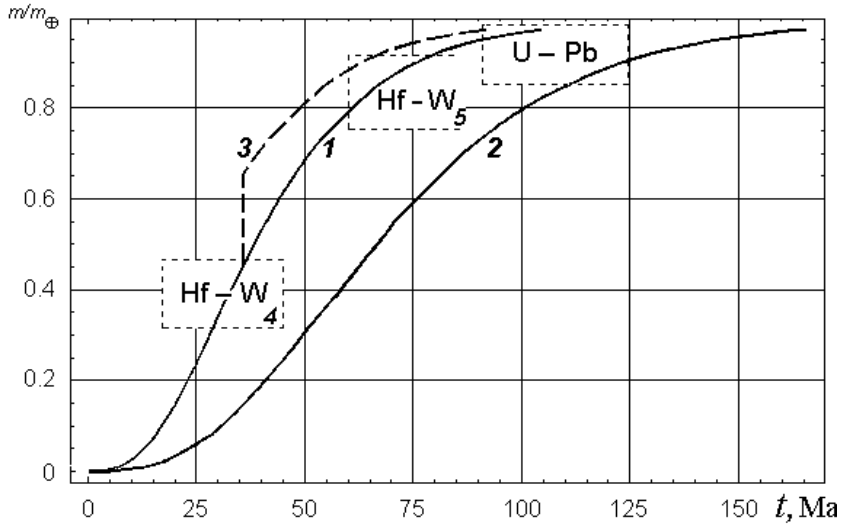

Fig. 3. Increase in the relative mass of the Earth:
1 — present model [12]; *2* — model with expanding feeding zones [4]; *3* — model 1 with megaimpact; *4* — formation of the Earth's core [13–15]; *5* — lunar differentiation [16, 17].

areas of the SS include the near-Earth asteroids, Centaurs, comet nuclei, and scattered disc objects. In the framework of the standard scenario of the origin of the SS ([4], see Fig. 1) all small bodies of the SS are considered as some kind of the remnants of building material of the Solar planetary system. However, the formation of each of the three major reservoirs had its own characteristics.

Main asteroid belt located in the area between 2 and 4 AU from the Sun. Its population is considered as a relict of the stage of planet formation on the boundary of the areas of terrestrial planets and giant planets ("a might-have-been planet"). When the relative velocities of planetesimals were small, the bodies united in collisions. However, gravitational perturbations from the giant planets have led to a rise in the relative velocities of planetesimals, and instead of sticking together, the planetesimals shattered and disrupted. As a result, most of the main belt's mass has been lost since the formation of the SS [4, 18]. The observable gradient of composition of so-called "S", "C", etc. asteroids indicates either incomplete mixing of substance in this zone or features of late condensation on the surfaces of planetesimals.

Edgeworth–Kuiper belt is a region of the SS beyond the orbit of Neptune (30–55 AU from the Sun). It is similar to the asteroid belt, although it is much larger — 20 times as wide and 20–200 times as massive. The Kuiper

belt objects are composed largely of frozen volatiles (termed "ices") such as methane, ammonia, and water. The Kuiper belt is believed to consist of planetesimals — fragments from the original protoplanetary disk around the Sun that failed to fully coalesce into planets and instead formed into smaller bodies. The Kuiper belt objects are clustered near the plane of the SS, whereas Oort cloud comets tend to arrive from any point in the sky.

In 1943, Kenneth Edgeworth suggested that beyond the orbit of Neptune there should be a zone of small bodies, the source of comets. However, for a long time no objects were found in this region, except Pluto (discovered in 1930) and its satellite Charon (discovered in 1978). It was only in 1992 that the first direct evidence for the existence of Kuiper belt objects was found. Since the first discovery in 1992, the number of known Kuiper belt objects has increased to over a thousand. In 1996, V. S. Safronov showed that in the trans-Neptunian zone *in situ* formation of large planetesimals is possible [19]. The precise origins of the Kuiper belt and its complex structure are still unclear.

Oort cloud is a spherical cloud of comet nuclei. Planetesimals from "dirty ice" were formed in the giant planet zone. With growth of massive bodies in the giant planet zone the relative velocities of planetesimals have increased so that eccentricities and inclinations of their orbits have reached critical values $e \sim i \sim 1/3$. This led to the ejection of part of the planetesimals to the periphery of the SS and the formation of the Oort cloud [4]. Some estimates place the outer edge at between 50 000 and 100 000 AU. Although no confirmed direct observations of the Oort cloud have been made, astronomers believe that it is the source of all long-period and Halley-type comets entering the inner Solar System.

Some years ago a group of authors [20, 21] suggested some variant of the standard model of SS formation, the so called "Nice model". In this model the 4 outer giant planets of the early SS were in a compact configuration after the dissipation of the gaseous disk. A few hundred million years later, a global instability drove the planets to their present orbits, producing the Late Heavy Bombardment. The "Nice model" proposes the migration of the giant planets into their present position. In this model originally the Kuiper belt was much denser and closer to the Sun, with an outer edge at 30 AU. Its inner edge would have been just beyond the orbits of Uranus and Neptune. As Neptune migrated outward, it approached the objects in the proto-Kuiper belt, capturing some of them into resonances and sending others into chaotic orbits [22]. Even though the Nice model is able to produce the hot population of the Kuiper belt, it can not explain the low-inclination cold population. Those objects scattered by Jupiter into highly elliptical orbits formed the Oort cloud [22]. Some features of the scattered disk remain an enigma.

Formation of planetary systems within a cluster of stars

Astrophysics: by now, more than 300 exo-planets are found around young stars, about 10000 gas-dust disks, probably proto-planetary disks, are discovered around young stars.

Understanding that stars do not form singly but arise in groups in huge nebulas of the type of the famous Orion nebula has been achieved more than half a century ago. However, the consequences of such collective births of planetary systems, in fact, remain unexplored.

Detection of newly formed planets around hundreds of young stars allows a broader look at the problem of the origin of planetary systems. The launch of the Space Telescope Herschel (May 2009) gives hope for the detection of planetary systems during their formation. It is possible that in the coming decade it will be possible to observe the bright flash ("fireworks") during macroimpacts of planetesimals [9, 10, 23].

Main questions:

- How long did our SS abide inside the nebula and, probably, afterwards in a star cluster of the type of Pleiades or Hyades (without gas-dust environment)?
- What cosmochemical and dynamic consequences of close star environment took place for the young SS?

In connection with the first question we note that typical life-times of nebulas, where stars are born with (and without) planetary systems, are of the order of tens of millions of years. Blue giants disperse the gas-dust component by their stellar winds and star clusters remain at the place of the nebula. Star clusters breakdown much slower; we know NGC 752, M 67, Hyades, Praesepe (M 44), which exist from millions of years to many hundreds of millions of years. What is the astrophysical situation at the observed protoplanetary disks in young nebulae?

Cosmic rays are massive particles, protons, helium nuclei, etc, photons (gamma, X-rays, ultraviolet and infrared). Total energy is 1 eV/cm^3; for comparison, the density of light radiation of stars is 0.3 eV/cm^3. At the time of SS formation in the cluster, the radiation density was higher by two or three orders of magnitude.

A typical protoplanetary disk near a young star of solar type, which experiences the strongest influence of stellar wind, X-ray and UV radiation from a near blue giant, is shown in Fig. 4.

The last modification of the standard scenario of SS origin [24] views formation of the SS in a close surrounding of young active stars and episodically flashings supernovae (SN). Fresh portions of short-lived radionuclides (^{26}Al, ^{60}Fe, …, ^{182}Hf, …) may have been added to the substance of a circumsolar disk by powerful streams of stellar winds from young giants and near supernova explosions. Impinging on the surface of particles, they may have

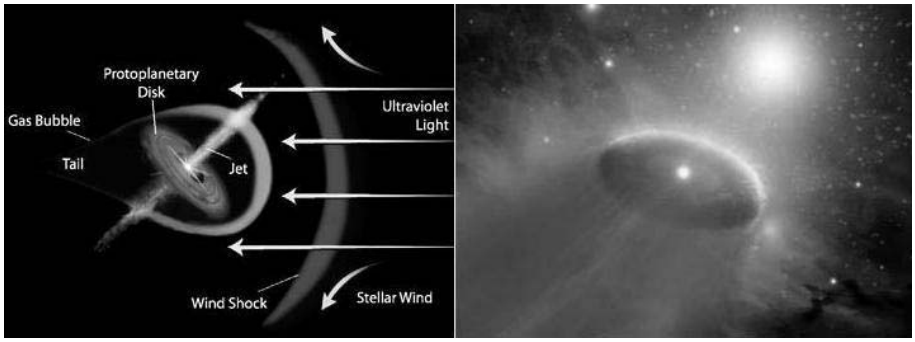

Fig. 4. Protoplanetary disk (schematic) and Protoplanetary disk (art).

reset measured "initial" abundances and thereby "rejuvenated" cosmo- and geo-chronometers. Proximity of other planetary system formations could lead to delivery of separate ice and rock asteroids to the young SS.

Fresh material from a surrounding star population can, as before, enter the young SS with large bodies and protoplanets already formed during the first tens of millions of years after the Sun's formation. If fresh radioactive nuclides of short-lived elements, by who's daughters we clock the early stages of SS evolution, are injected, this could be of great importance for renormalization of the cosmo- and geo-chronometers of the early stages of evolution of the SS and the Earth.

The presence of significant amounts of short-lived radionuclides could result in heating of the interior of icy planetesimals and large rocky asteroids sufficient to melt and differentiate matter in intervals between their destructive collisions.

Consequences of a long residence time of the SS in the parent star cluster:

- contamination of the surfaces of young SS bodies by interstellar material,
- intense exposure of their surfaces to hard UV and X-ray radiation,
- bombardment by the bodies from the Oort cloud could be caused by closely passing of stars.

Conclusion

Many questions about the origin of SSSB remain unsolved. However, the main idea that in the framework of Standard Scenario of the origin of the Solar System SSSBs are considered as remnants of building blocks of the planetary system remains unchanged. Running dynamical models of the early SS with different initial conditions will produce the various populations of objects within the modern SS. Each population will be more or less numerous, and will have particular orbital properties, composition, etc. At the

present time, computer models of the SS origin that are beginning with the initial mass of preplanetary disk of about 3–5 % of Solar mass best match many aspects of the SS.

References

1. IAU News Release — IAU0603: IAU 2006 General Assembly: Result of the IAU Resolution votes.
2. *Schmidt O. Yu*. Meteoritnaya teoriya proishozhdeniya Zemli i planet (Meteorite theory of origin of the Earth and planets) // Doklady Academii nauk SSSR. M., 1944. Vol. 45, N 6. P. 245–249 (in Russian).
3. *Levin B. Yu.* Proishozhdenie Zemli i planet (Origin of the Earth and Planets). M., 1964 (in Russian).
4. *Vityazev A. V., Pechernikova G. V., Safronov V. S.* Planety zemnoj gruppy: Proishozhdenie i rannyaya evolutsiya (Terrestrial Planets: Origin and Early Evolution). M., 1990 (in Russian).
5. *Pechernikova G. V.*, *Vityazev A. V.* Masses of the largest bodies and dispersion of velocities during planet accumulation // Astronomy Letters. 1979. Vol. 5, N 1. P. 54–60.
6. *Safronov V. S., Vityazev A. V.* Origin of the Solar System / Ed. R. Syunyaev // Soviet Scientific Reviews, Section E. Astrophysics and Space Physics Reviews. Vol. 4. Harwood Academic Publishers, 1985. P. 1–98.
7. *Vityazev A. V., Pechernikova G. V.* Late stages of accumulation and early evolution of the planets / Eds T. M. Donahue, K. K. Trivers, D. M. Abramson // Proc. US-USSR Workshop on Planetary Sciences, Washington, D. C.: National Academy Press, 1991. P. 143–162.
8. Origin of the Earth and the Moon / Eds R. Canup, K. Righter. Tucson: Univ. Arizona Press, 2000.
9. *Vityazev A. V., Pechernikova G. V.* Fireworks around naked T Tauri stars // XXV Lunar and Planet. Sci. Conf. 1994. P. 1443–1444.
10. *Vityazev A. V., Pechernikova G. V.* Fireworks in Forming Planetary Systems // Astronomy Letters. 1995. Vol. 21, N 2. P. 271–278.
11. *Pechernikova G. V.*, *Vityazev A. V.* Impacty i evolutsiya rannej Zemli / Eds V. V. Adushkin, I. V. Nemchinov // Catastrophicheskie vozdejstviya kosmicheskih tel. IDG RAN. M.: IKC “Akademkniga”, 2005. P. 251–265. English translation: Pechernikova G. V., Vityazev A. V. Impacts and Evolution of Early Earth / Eds V. V. Adushkin, I. V. Nemchinov // Catastrophic Events Caused by Cosmic Objects. The Netherlands, Dordrecht: Springer, 2008. P. 333–350.
12. *Pechernikova G. V.* Time of the Earth’s growth // Dokl. Earth Sci. 2005. Vol. 401A, N 3. P. 409–412. Translated from Doklady Akademii Nauk. M., 2005. Vol. 401, N 3. P. 391–394.

13. *Kleine T., Moenker C., Mezger K. et al.* Rapid accretion and early core formation on asteroids and the terrestrial planets from Hf-W chronometry // Nature. 2002. Vol. 418. P. 952–955.
14. *Yin Q. Z., Jacobsen S. B., Yamashita K. et al.* A short time scale for terrestrial planet formation from Hf-W chronometry of meteorites // Nature. 2002. Vol. 418. P. 949–952.
15. *Shoenberg R., Kamber B. S., Collerson K. D. et al.* New W isotope evidence for rapid terrestrial accretion and very early core formation // Geochim. Cosmochim. Acta. 2002. Vol. 66, N 17. P. 3151–3160.
16. *Kleine T. et al.* Dating the first ~100 Ma of the Solar System: From the formation of CAIs to the origin of the Moon // Goldschmidt Conference Abstracts 2008a, A480.
17. *Kleine T. et al.* Hafnium-Tungsten chronometry of lunar differentiation // Goldschmidt Conference Abstracts 2008b, A480.
18. *Safronov V.S.* On the origin of asteroids / Ed. T. Gehrels. Asteroids, Tucson: Univ. Arizona Press, 1979. P. 975–991.
19. *Safronov V. S.* Accumulyatsiya malyh tel na vneshnej granice planetnoj sistemy (accumulation of small bodies at the outer edge of the planetary system) // Astronomicheskii Vestnik (Solar System Research). 1996. Vol. 30, N 4. P. 291–298 (in Russian).
20. *Gomes R., Levison H. F., Tsiganis K. et al.* Origin of the cataclysmic Late Heavy Bombardment period of the terrestrial planets // Nature. 2005. Vol. 435. P. 466–469.
21. *Tsiganis K., Gomes R., Morbidelli A. et al.* Origin of the orbital architecture of giant planets of the Solar System // Nature. 2005. Vol. 435. P. 459–461.
22. *Levison H. F., Morbidelli A., Laerhoven C. V. et al.* Origin of the Structure of the Kuiper Belt during a Dynamical Instability in the Orbits of Uranus and Neptune // Icarus. 2007. Vol. 196. P. 258–265.
23. *Vityazev A. V., Pechernikova G. V., Safronov V. S.* Formation of Mercury and removal of its silicate shell / Eds F. Vilas., C. R. Chapman, M. S. Matthews. Mercury, Tucson: Univ. Arizona Press, 1988. P. 667–669.
24. *Adushkin V. V.*, *Vityazev A. V., Pechernikova G. V.* V razvitie teorii proishozhdeniya i rannej evolutsii Zemli (In the development of the theory of the origin and early evolution of the Earth) / Ed. E. M. Galimov // Problemy zarozhdeniya i evolutsii biosphery (Problems of the origin and evolution of the biosphere). M., 2008. P. 275–296 (in Russian).

SMALL BODIES OF THE SOLAR SYSTEM

Physical Properties and Internal Structure of Near-Earth Objects

D. F. Lupishko[1], Zh. A. Pozhalova [2]

[1]V. N. Karazin Kharkiv National University, Kharkiv, Ukraine
[2] Research Institute Nikolaev Astronomical Observatory, Nikolaev, Ukraine

Abstract. The review contains the most recent data on near-Earth objects such as their sizes and densities, rotation and shapes, taxonomy and mineralogy, optical properties and structure of their surfaces, binary systems among the NEOs and internal structure of asteroids and comets constituted the NEO population. The European space mission ISHTAR for investigation of NEOs 4660 Nereus and 5797 Bivoj, which is planned to be launched in Sept. 2011, is briefly described.

Introduction

Near-Earth objects (NEOs) are defined as asteroids and comets having orbits with perihelion distances of 1.3 AU or less. About 30 % of the entire NEO population may reside in orbits having a Jovian Tisserand parameter < 3, and among them roughly half are observed to have comet-like physical properties such as albedos and spectra. Thus, about 10–15 % of the NEO population may comprise extinct or dormant comets [1–3]. The rest are the near-Earth asteroids (NEAs). They are traditionally divided into three groups (the relative abundances are estimated by Bottke et al. [4]):

Amor	$a \geq 1.0$ AU	$1.017 < q \leq 1.3$ AU	$(32 \pm 1$ %)
Apollo	$a \geq 1.0$ AU	$q < 1.017$ AU	$(62 \pm 1$ %)
Aten	$a < 1.0$ AU	$Q > 0.983$ AU	$(6 \pm 1$ %)

Besides these, there is an additional group of rather dangerous asteroids whose orbits reside entirely inside of the Earth's orbit (Q < 0.983 AU). According to [5] objects of this inner-Earth asteroid group and Aten group together can constitute about 20 % of the km-sized Earth-crossing population.

About 6600 NEOs were discovered by the beginning of November 2009. They are the objects of special interest not only from the point of view of basic science, but also of applied science (the problem of asteroid and comet hazard, the NEAs as the potential sources of raw materials in near Earth space, etc.).

Sizes, densities and axis rotation

In general NEOs are much smaller in size in comparison with main-belt asteroids. The size distribution of NEO population can be approximated as

$$N\,(>D\ \text{km}) = k\,D^{-b}$$

with an exponent $b = 1.95$ and $k = 1090$ [6].

This expression indicates that there are 1090 NEOs with $D \geq 1$ km. Including uncertainties, Stuart and Binzel [7] give this result as 1090 ± 180 objects that are 1 km or lager within the NEO population, which agrees well with previous estimates. Below, the sizes of some individual objects are presented that display the whole range of sizes of cataloged NEOs overlapping four orders of magnitude.

Largest NEOs		Smallest discovered NEOs	
1036 Ganymed	D = 38.5 km		
433 Eros	16.5	2000 *WL*107	D = 38 m
3552 Don Quixote	12÷15	2003 *QB*30	17
1866 Sisyphus	8.9	2003 *SQ*222	10
		2008 *TC*3*	4

* Discovered on 6 Oct. 2008, collided with the Earth on 7 Oct. 2008 and disintegrated in the atmosphere over northern Sudan.

Below, the most reliable estimates of bulk densities (g/cm^3) for S, Q, and C-type NEOs are summarized. Discovery of binary NEOs gives a good opportunity to determine their bulk densities, however those estimates are usually not accurate enough due to an uncertainty of binary system parameters.

433 Eros"	2.67 ± 0.03	S
6489 Golevka*	2.7 (+ 0.4, –0.6)	Q
25143 Itokawa"	1.95 ± 0.14	S, Q
1999 *KW*4*	1.97 ± 0.24	S
2100 Ra-Shalom*	1.1 – 3.3	C
1996 *FG*3	1.4±0.3	C
2000 *DP*107	1.6 (+1.2, –0.9)	?
2000 *UG*11	1.5 (+0.6, –1.3)	?

" Space mission data; * Radar data.

Comparing bulk densities of these NEOs with densities of their meteorite analogues (ordinary or carbon chondrites) we have to suppose about 30–50 % porosity of NEO. The 4-m F-type NEO 2008 *TC*3 that disintegrated in the atmosphere (but some pieces were found) displayed also about 50 % porosity. It means that at least some of NEOs are not monolithic bodies but "rubble-pile" structures, which have no coherent tensile strength and are held together weakly by their own mutual gravity. One example of such bodies is the Apollo-object 25143 Itokawa [8].

The distribution of the spin rates of NEOs (Fig. 1) is quite different in comparison with that of small main-belt asteroids (MBAs) and it shows the prominent excesses of slow and fast rotators [9]. Among the reasons for that may be the difference in asteroid diameter distributions within these two populations, influence of the radiation pressure torques (YORP-effect), the influence of the rotational parameters of binaries and may be some selection effects. The whole interval of NEO spin periods ranges over four orders of magnitudes from 500–600 h (96590 1998 *XB* and 1997 *AE*12) to 1.3 min (2000 *DO*8). It is clear that such small (a few 10 m in size) and super-fast spinning bodies are beyond the rotational breakup limit for aggregates like "rubble piles" and therefore they are monolithic fragments.

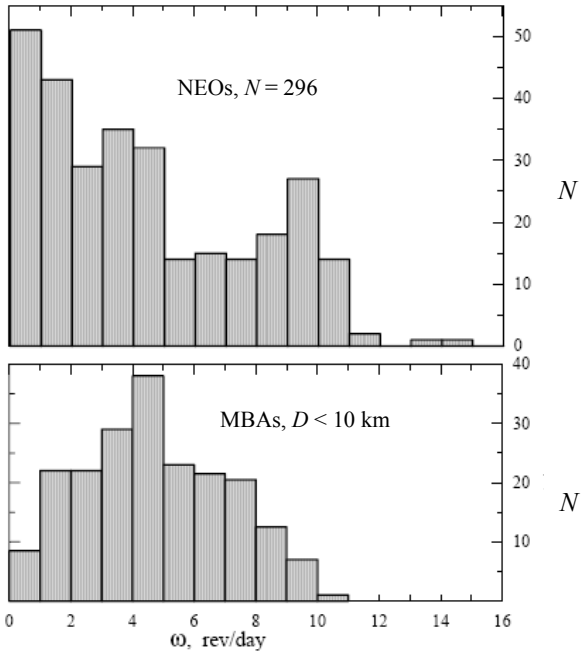

Fig. 1. Distribution of the spin rates of NEOs and small ($D \leq 10$ km) main-belt asteroids.

Taxonomy and mineralogy

As a first step toward estimating the nature of any NEO is determination of its taxonomic class, that is, the object's total mineralogy. Practically all taxonomic classes identified among main-belt asteroids have also been found in the NEO population, including the C, P and D classes that are typical of the outer main belt. Binzel et al. [10] from their spectroscopic survey of 252 NEAs and Mars-crossers noted that 25 of 26 Bus' taxonomic classes [11] of main belt asteroids were represented in the NEO-population. The most common taxonomic classes among them are however S and Q (silicate) types. Recent spectroscopic investigation of 150 NEAs [12] have summarized that 62 % of them belong to S-complex, 20 % to X-complex, 12 % to C-complex, and 6 % to other classes of Bus' taxonomy. Stuart and Binzel [7] modeled the bias-corrected distribution of taxonomic classes and concluded that C and other low-albedo classes constitute 27 % and S + Q classes 36 % of all NEOs.

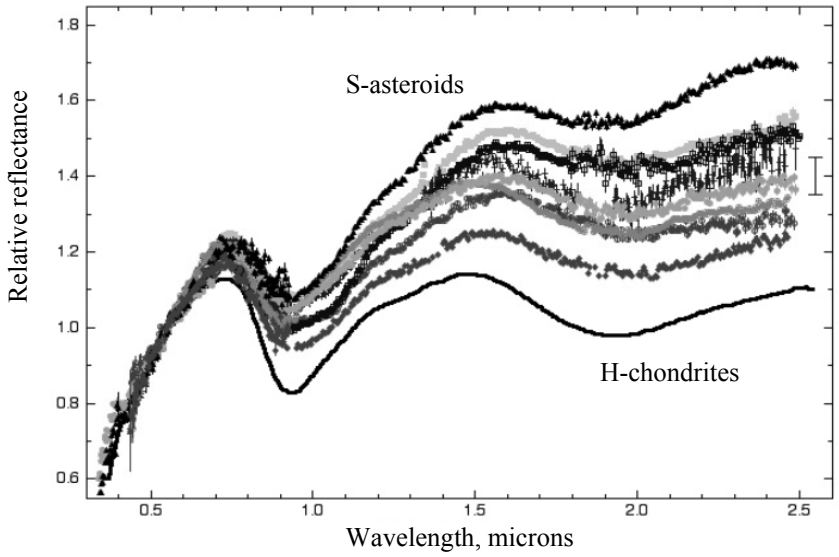

Fig. 2. Continuous range of NEO spectra from S-types to ordinary H-chondrite meteorites (that is, to Q-types) [13].

Observing smaller and smaller *S*-objects Binzel et al. [13] showed a continuous range of NEO spectra from those of *S*-types to ordinary chondrites (Fig. 2). That is, there is a continuous transition from spectra of S-types to those of Q-types. At the same time Q-objects are smaller in size and brighter than S-objects, that is, their surfaces are "younger, fresher". Therefore, this continuum is interpreted as a result of space weathering

process, that is, the process of alteration of the young surface of Q-asteroid to look more and more redder like S-type surfaces [10]. Lazzarin et al. [12] found that only 17 % of NEOs and 6 % of MBAs are compatible with ordinary chondrite spectra but other objects are much redder. They also found the statistically valid linear increase of spectral slope with increase of asteroid exposure (that is, amount of Sun's radiation that a body receives along its orbit), which supported the idea of space weathering. Fevig and Fink [14] reported the results of spectrophotometry of 55 NEOs which revealed the statistically significant evidence for orbit-dependent trends in their data: while observed S-types reside primarily in Amor-Apollo-Aten orbits which do not cross the asteroid main belt, the majority of objects with spectra consistent with ordinary chondrites (Q-types, that is, fresh and relatively unweathered NEOs) are in highly eccentric Apollo orbits that enter the asteroid main belt. It is very likely that these objects have recently been injected into such orbits after a collision in the main belt.

Optical properties and surface structure

The analysis of available data clearly demonstrates that the surfaces of NEOs display in general the same optical properties as the surfaces of MBAs [9, 15, 16]. The whole range of NEO albedos (0.05÷0.50) is basically the same as that of MBAs and it corresponds to the same in general mineralogy within these two populations. But the strict similarity of the other photometric and polarimetric parameters (such as phase coefficient, polarization slope and others, that are related to surface structure) gives evidence of the similar surface structures on a submicron scale.

The polarimetric, radiometric data and direct imaging of Eros and Itokawa give evidence that most NEOs are covered with regolith (fine granulated rocks and dust). Despite their low gravities, even the smallest NEOs appear capable of retaining some regolith coating. As it was estimated a minimum 2.3 ± 0.4 m thick layer of regolith exists in the lowlands of Itokawa, which, if spread evenly across the entire asteroid, corresponds to a 42 ± 1 cm layer. The recent studies of NEO thermal IR emission showed that the average thermal inertia of km-size NEOs is 200 ± 40 $\mathrm{Jm^{-2}s^{-0.5}}K^{-1}$, that is about four times that of the Moon [17]. Furthermore, those authors identify a trend of increasing thermal inertia with decreasing asteroid diameter.

Radar observations showed that even the relatively small NEOs 4179 Toutatis and 1999 *JM*8 ($D \sim 3$ km both) are cratered about to the same extent as MBAs 951 Gaspra and 243 Ida. The radar data also showed evidence that NEO surfaces are rougher than surfaces of large MBAs on the length scale of decimeters and meters. Recently the radar observations have also revealed a link between NEO composition and surface roughness. As is

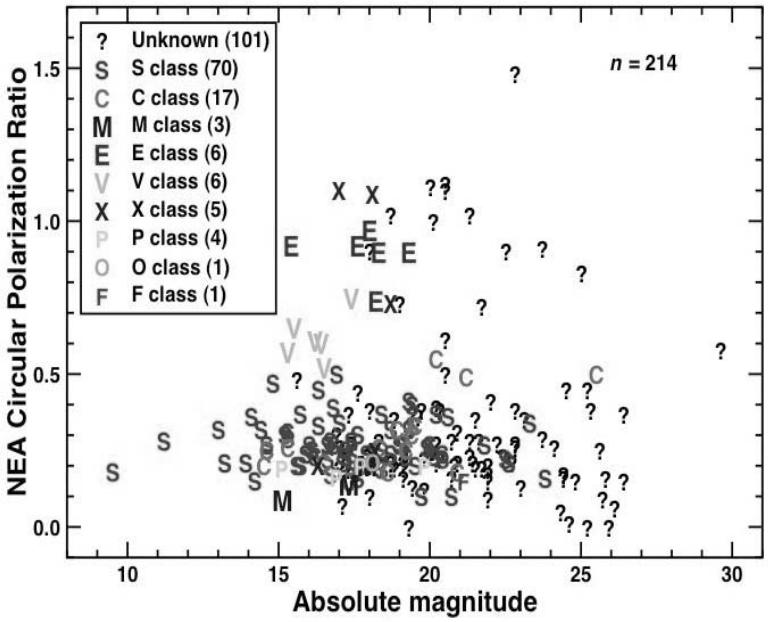

Fig. 3. A radar link between composition and surface roughness (*http://echo.jpl.nasa.gov/*).

clear from Fig. 3 the objects of different composition types have different radar circular polarization ratios, which characterize a measure of centimeter-to-decimeters surface roughness. The roughest are the high-albedo objects of E and V-types, the meteorite analogs of which are enstatite chondrites and HED-meteorites (basalts), and they are most probably rougher because of higher material strength.

Binary and triple systems among the NEOs

By the beginning of November 2009, 37 binary near-Earth asteroids (one with two satellites) have been discovered. They show the similarity of their parameters, for example, spin periods of primaries are within the interval of 2.3–3.6 h and orbital periods of secondaries are in the range of 0.5–1.8 days (which may be due to observational selection effects). A fraction of binary systems among the NEAs is estimated to be 15–17 % [18], though among the Aten-asteroids the fraction can be significantly higher [19].

The NEA 2001 *SN*263 has been revealed as the first near-Earth triple asteroid ever found. It was discovered by Mitchal Nolan and his colleagues using the Arecibo radar. The central body is spherical of $D \approx 2$ km across,

while the larger of the two moons is about half that size. The smallest object is about the size of the Arecibo telescope. Pravec and Harris [20] suggest that binaries formed from parent bodies spinning at the critical rate by some sort of fission or mass shedding, and the YORP-effect is a candidate to be the dominant cause of spin-up to instability. This suggestion is in a good agreement with results obtained by Walsh and Richardson [21] that tidal disruption due to close planetary encounters should account for about 1–2 % of binary NEAs and that there are other formation mechanisms that contribute significantly to this population.

Discovery and study the binary or triple systems allows one to determine the density of the NEOs and type of their material.

On the internal structure of NEOs

The internal structure of NEOs is key information to planning a mitigation strategy. Unfortunately, there are only indirect data on the internal structure of NEOs such as bulk densities and porosities, their spin rates, the events of comet nuclei disintegration, existence of large craters, crater chains and grooves on asteroids and satellites, and the recent data from the Japanese space mission Hayabusa to asteroid 25143 Itokawa. Campo Bagatin [22] analyzed these indirect evidences in order to extract information on the internal structure of NEOs. Taking into account the results of his analysis one can summarize the following.

- The estimated bulk densities of S and especially C-type NEOs (see [9]) are well below the density of their meteorite analogues, which suggests 30–50 % NEO macroporosity. Such porosity can result if a body is completely shattered and reassembled, creating a gravitational aggregate (GA). It means that some NEOs are not monolithic bodies but “rubble-pile” or GA structures, which have no coherent tensile strength and are only weakly held together by their own mutual gravity.
- Comet nuclei also show surprisingly low bulk densities: 0.1–0.5 g/cm^3 (Churyumov–Gerasimenko), 0.18–0.36 g/cm^3 (Borrelly), 0.36–0.76 g/cm^3 (Tempel 1), 0.26 ± 0.15 g/cm^3 (Halley). For these comets bulk porosities (that is, macroporosity) on the order of 70 to 80 % would apply [22]. For example, in July 1992 Shoemaker–Levy 9 passed very close to Jupiter inside the tidal breakup (Roche) limit for unconsolidated water ice and its nucleus was disrupted into many fragments. The estimated tidal stress on the inferred parent body is found to be very small ($\sim 10^4$ bar). It means that before breakup the nucleus was very likely an incoherent aggregate of fragments. Several other tidal disruptions and even spontaneous nucleus splitting of comets are known (e. g., C/1999 S4 LINEAR, Schwassmann–Wachmann 3).
- In spin periods of 1–10 km sized asteroids, Harris and Pravec [23] have found a “spin rate barrier” — the lack of periods less than 2.2 h (spin

faster than ~11 cycles/day). It suggests that even such small asteroids are GA or "rubble-piles", that is, with no substantial tensile strength. At the same time some much smaller objects ($D \leq 100$ m) show a super fast spin with periods ~2 minutes; this is much faster than the "spin barrier", indicating that they are monolithic bodies with sufficient tensile strength.

- The existence of relatively large craters ($d_{\text{crater}} \sim R_{\text{object}}$), grooves, doublet craters, and crater chains on asteroids and satellites also suggests processes of body disruption with subsequent reassembly of fragments creating a GA. In particular, the absence of any correlation between the inferred parent body mass and the number of craters in the chain supports the idea that the fragments reaccumulated via gravitational instability just prior to impact [22].
- NEO 25143 Itokawa is considered as the most striking example of GA, when considering its density, which corresponds to about 40 % of void space (macro-porosity), an availability of large blocks (boulders) on the asteroid, and other evidence of a catastrophic disruption scenario for the formation of Itokawa.

Thus, the NEO population presents at least three very different types of body internal structures. They are: a) monolithic objects (the fragments of larger parent main-belt asteroids) including the metal ones with a tensile strength of about 10^9 dyn/cm^2; b) the structures of "rubble-piles" type or GA; c) about 10 % [1–3] of extinct or dormant comet nuclei with a tensile strength of about 10^2–10^3 dyn/cm^2.

Summary

The European Space Agency works on a NEO space mission preparation named ISHTAR (Internal Structure High-resolution Tomography by Asteroid Rendezvous). Its program foresees the investigation of Apollo-object 4660 Nereus (C-type, $D \sim 1.2$ km) and Amor-object 5797 Bivoj (S-type, $D \sim 0.5$ km) with determination and study of:

- mass and bulk density of target NEOs;
- internal structure, mass distribution, detailed shape;
- spin rate including axis orientation and precession (if any);
- detailed surface geology, characterization of regolith, etc.

Mission ISHTAR will be launched in Sept. 2011 with a Ukrainian Dnepr rocket to reach 4660 Nereus in 2014. After a stay at Nereus of nearly 15 months, during which extensive science measurements can be performed, ISHTAR will then transfer to asteroid 5797 Bivoj in order to repeat the same type of science measurement during a period of at least 3 months. The total mission duration is approximately 7 years.

References

1. *Lupishko D. F., Lupishko T. A.* On the origin of Earth-approaching asteroids // Solar System Res. 2001. Vol. 35, N 3. P. 227–233.
2. *Binzel R. P., Lupishko D. F.* Properties of the near-Earth object population: the ACM 2005 view // Asteroids, Comets, and Meteors / Eds D. Lazzaro et al. Proc. of IAU Symp. 229 "ACM 2005" Aug. 7–12, 2005. Buzios, Rio de Janeiro, Brazil. Cambridge Univ. Press, 2006. P. 207–214.
3. *Michel P., Bottke W. F.* Origin of near-Earth objects and implications on their physical properties and mitigation strategies // Book of Abstracts of Intern. Conf. "Asteroid-Comet Hazard-2009", St. Petersburg, Sept. 21–25, 2009. P. 14–15.
4. *Bottke W. F. Jr., Morbidelli A., Jedicke R. et al.* Debiased orbital and absolute magnitude distribution of the near-Earth objects // Icarus. 2002. Vol. 156. P. 399–433.
5. *Michel P., Zappala V., Cellino A., Tanga P.* Estimated abundance of Atens and asteroids evolving on orbits between Earth and Sun // Icarus. 2000. Vol. 143. P. 421–424.
6. *Stuart J. S.* Observational constraints on the number, albedos, sizes, and impact hazards of the near-Earth asteroids. Ph. D. Thesis. Massach. Inst. of Technology, Cambridge, Massachusetts, 2003.
7. *Stuart J. S., Binzel R. P.* Bias-corrected population, size distribution, and impact hazard for the near-Earth objects // Icarus. 2004. Vol. 170. P. 295–311.
8. *Fujiwara A., Kawaguchi J., Yeomans D. K. et al.* The rubble-pile asteroid Itokawa as observed by Hayabusa // Science. 2006. Vol. 312. P. 1330–1334.
9. *Lupishko D. F., Di Martino M., Binzel R. P.* Near-Earth objects as principal impactors of the Earth: Physical properties and sources of origin // Near Earth Objects, our Celestial Neighbors: Opportunity and Risk. Proc. IAU Symp. N 236. 2006 / Eds A. Milani et al. 2007. P. 251–260.
10. *Binzel R. P., Rivkin A. S., Scott J. S. et al.* Observed spectral properties of near-Earth objects: results for population distribution, source regions, and space weathering processes // Icarus. 2004. Vol. 170. P. 259–294.
11. *Bus S. J.* Compositional structure of the asteroid belt: Results of a spectroscopic survey. Ph. D. thesis, Massach. Inst. of Technol., Cambridge, 1999.
12. *Lazzarin M., Magrin S., Marchi S.* SINEO: Spectroscopic investigation of near Earth objects // Mem. S. A. It. Suppl. 2008. Vol. 12. P. 20–27.
13. *Binzel R. P., Harris A. W., Bus S. J. et al.* Spectral properties of near-Earth objects: Palomar and IRTF results for 48 objects including space-

craft targets 9969 Braille and (10302) 1989 *ML* // Icarus. 2001. Vol. 151. P. 139–149.
14. *Fevig R. A., Fink U.* Spectral observations of 19 weathered and 23 fresh NEAs and their correlations with orbital parameters // Icarus. 2007. Vol. 188. P. 175–188.
15. *Lupishko D. F., Di Martino M.* Physical properties of near-Earth asteroids // Planet. Space Sci. 1998. Vol. 46, N 1. P. 47–74.
16. *Binzel R. P., Lupishko D. F., Di Martino M. et al.* Physical properties of near-Earth objects // Asteroids III / Eds W. Bottke, A. Cellino, P. Paolicchi, R. Binzel. Tucson: Univ. Arizona Press. 2002. P. 255–271.
17. *Delbo M., Dell'Oro A., Harris A. W. et al.* Thermal inertia of near-Earth asteroids and implications for the magnitude of the Yarkovsky effect // Icarus. 2007. Vol. 190. P. 236–249.
18. *Merline W. J., Weidenschilling S. J., Durda D. D. et al.* Asteroid do have satellites // Asteroids III / Eds W. F. Bottke et al. Tucson: Univ. of Arizona Press. 2002. P. 289–312.
19. *Polishook D., Brosch N.* Photometry of Aten asteroids – More than a handful of binaries // Icarus. 2008. Vol. 194. P. 111–124.
20. *Pravec P., Harris A. W.* Binary asteroid population: 1. Angular momentum content // Icarus. 2007. Vol. 190. P. 250–259.
21. *Walsh K. J., Richardson D. C.* A steady-state model of NEA binaries formed by tidal disruption of gravitational aggregates // Icarus. 2008. Vol. 193. P. 553–566.
22. *Campo Bagatin A.* On the internal structure of asteroids and comets // Mem. S.A. It. Suppl., 2008. Vol. 12. P. 150–163.
23. *Harris A. W., Pravec P.* Rotational properties of asteroids, comets and TNOs // Asteroids, Comets, and Meteors / Eds D. Lazzaro et al. Proc. of IAU Symp. 229, Aug. 7–12, 2005. Buzios, Rio de Janeiro, Brazil. Cambridge Univ. Press. 2006. P. 207–214.

SMALL BODIES OF THE SOLAR SYSTEM

Electrolysis of Ices as a Key to Understanding of the Minor Bodies' Nature

E. M. Drobyshevski

Ioffe Physical Technical Institute of RAS, St. Petersburg, Russia

Abstract. The electrolysis of dirty ices constituting massive envelopes of Ganymede-like bodies is shown to be crucial for understanding of (explosive) origin and manifestations of different types of minor bodies and related objects in the inner Solar System. Moreover, the magneto-electrochemical processes in the Galilean satellites' ensemble were, possibly, responsible for incipiency of life in its known forms. To prevent dramatic consequences for the Earth of probable explosion of yet intact Callisto's electrolyzed ice envelope, one has to attach the highest priority to exploration of this satellite.

Introduction. Whence minor bodies?

Traditional Nebular Cosmogonies (NCs) of the Solar System consider minor bodies as the planet building waste. These purely speculative cosmogonies were put forward when the stars' structure, their formation and evolution, to say nothing of stellar multiple systems, were not understood properly. As a result, NCs are inevitably facing difficulties in (*a posteriori*) explanation of known facts, no their predictions were confirmed [1].

The Close Binary Cosmogony (CBC) of the Solar System considers the Sun-Jupiter system as a limiting case of a close binary system. It results from modern ideas on multiple star system formation and its gas-dynamic evolution, easily explaining all the known facts and predicting as many new ones [2, 3]. According to the CBC, minor bodies are the result of destruction of planet-like bodies due to their collisions and/or explosions of their ices. The long-period (L-P) comets are mainly produced by very rare collisions of scores of Pluto-like icy planets in a *joint planetary-cometary cloud* at 50–300 AU from the Sun, whose existence stems from the CBC [1, 3]. This is being confirmed by discoveries of numerous plutinos (Sedna, Xena, etc.)

in disordered orbits during the last decade. This quasi-toroidal cloud is essentially neither the distant Oort cloud, nor the narrow (40–50 AU) Edgeworth–Kuiper comet belt or the scattered comet disk [3, 4].

Role of electrochemistry in origin and properties of minor bodies

Minor bodies in the inner Solar System are mainly a product of explosions of electrolyzed ices. Laboratory experiments demonstrate that the electrolysis of ice, a proton-type conductor, is inevitable if (*i*) it carries electric current that (*ii*) flows into it from a conductor with electronic or hole conductivity. The first condition is met always if a planet-like body is engulfed by the plasma of the solar or a planetary magnetospheres, and the second condition is met if the dirty ices contain large enough carbonaceous or rocky inclusions. When current flows through the inclusion/ice interface, H_2O molecules undergo electrolytic decomposition and release molecular H_2 and O_2. At high concentrations of inclusions, it is permissible to speak of bulk electrolysis [5, 6]. If a body is large enough (of the Ganymede type, e. g.), the ices of its massive (up to ~50 wt. %) envelope is in solid-state convection, which spreads $2H_2 + O_2$ all over the ice volume. On accumulation of 15÷20 wt. % of $2H_2 + O_2$, such a solid solution becomes capable of detonation [5–7]. Global explosions (seven to eight in the history of the Solar System) of ices of moonlike bodies can account in the framework of this common approach for the origin and many, heretofore unexplained properties, of short-period (S-P) comets, asteroids, small satellites and planetary rings, the recent formation and composition of Titan's atmosphere, the differences among the Galilean satellites etc., as well as provide a sound basis for predictions of the properties of these objects [5, 6, 8–10].

While some results amassed in the *Deep Impact* and *Stardust* cometary missions have come in conflict with the traditional condensation-sublimation concepts concerning the cometary origin, they provide supportive evidence for the new paradigm of the planetary origin of S-P comet nuclei and of the presence in them of $2H_2 + O_2$ in the form of clathrates [4, 10].

Some inferences

Magnetic field-assisted electrochemical processes in the icy envelopes of Galilean satellites, and the appearance on them after the ice explosions of oceans of warm and nearly fresh water with the originally high content of abiogenic organics (that removes the concentration and salt problems complicating the origin of life on the Earth), offer additional prospects for the synthesis and evolution of real (optically active — laevorotatory) biomolecules [11].

It appears that only Callisto's ices have thus far escaped explosion. If they explode, the Earth will experience the heavy bombardment by comet nuclei, which will create "impact winters" about once every 60 years on the

average. Therefore, the highest priority should be assigned to *in situ* exploration of Callisto aimed on determining the degree of saturation of its ices with the electrolysis products [6, 8, 12].

References

1. *Drobyshevski E. M.* Facts of space epoch versus two-century-old paradigm // Evolution and Source Regions of Asteroids and Comets, Proc. IAU Coll. 173 / Eds J. Svoreň, E. M. Pittich, H. Rickman. Astron. Inst. Slovak Acad. Sci., 1999. P. 375–380.
2. *Drobyshevski E. M.* Was Jupiter the protosun's core? // Nature. 1974. Vol. 250. P. 35–36.
3. *Drobyshevski E. M.* The origin of the Solar System: Implications for transneptunian planets and the nature of the long-period comets // Moon Planets. 1978. Vol. 18. P. 145–194.
4. *Drobyshevski E. M.* Stardust findings favor not only the planetary origin of comets but the underlying close-binary cosmogony of the Solar System as well // Icarus. 2008. Vol. 197. P. 203–210; arXiv:astro-ph/0702601v2.
5. *Drobyshevski E. M.* Electrolysis in space and fate of Phaethon // Moon Planets. 1980. Vol. 23. P. 339–344.
6. *Drobyshevski E. M., Chesnakov V. A., Sinitsyn V. V.* The electrolytical processes in dirty ices: Implications for origin and chemistry of minor bodies and related objects // Adv. Space Res. 1995. Vol. 16. P. (2)73–(2)84.
7. *Drobyshevski E. M.* The structure of Phaethon and detonation of its icy envelope // Earth Moon Planets. 1986. Vol. 34. P. 213–222.
8. *Drobyshevski E. M.* Jovian satellite Callisto: Possibility and consequences of its explosion // Earth Moon Planets. 1989. Vol. 44. P. 7–23.
9. *Drobyshevski E. M.* The young long-period comet family of Saturn // Mon. Not. Roy. Astron. Soc. 2000. Vol. 315. P. 517–520.
10. *Drobyshevski E. M., Kumzerova E. Yu., Schmidt A. A.* Deep Impact mission to Tempel 1 favours New Explosive Cosmogony of comets // Astron. Astrophys. Trans. 2007. Vol. 26. P. 251–266; arXiv:astro-ph/0605389.
11. *Drobyshevski E. M.* Galilean satellites as sites for incipient life, and the Earth as its shelter // Astrobiology in Russia / Eds M. B. Simakov, A. K. Pavlov. St. Petersburg, 2002. P. 47–62; arXiv:q-bio/0312031.
12. *Drobyshevski E. M.* Threat of every day Tunguska-type events as result of Callisto's ice envelope explosion // Intnl. Conf. "100 years since Tunguska Phenomenon: Past, Present and Future" (Abstracts). Moscow, 2008. P. 175, 176.

SMALL BODIES OF THE SOLAR SYSTEM

AMPLE 3 — Multi-purpose Software Package for Asteroids and Comets

F. A. Novikov, V. A. Shor, T. G. Vega, O. M. Kochetova, Yu. D. Medvedev, I. N. Netsvetaev, G. A. Netsvetaeva, U. N. Tihonova, N. B. Zheleznov

Institute of Applied Astronomy of RAS, St. Petersburg, Russia

Abstract. An integrated multi-purpose software package AMPLE 3 for dealing with asteroids and comets is described.

To deal with minor bodies of the Solar System one urgently needs an appropriate software tool to plan and treat observations, to estimate parameters of selected groups of objects, to visualize orbital motion, and more. There are many tools of that kind that scientists and amateurs have at their disposition, nevertheless we would like to present a new one, AMPLE 3, that has many merits.

The AMPLE 3 software package has a profound background and is based on rich experience accumulated in the implementation of its preceding versions. The first version of the AMPLE (Adaptable Minor PLanet Ephemerides) package had been put forward in 1995 [1]. The package received acknowledgement and respect within the astronomical community due to its various abilities and features. These specific features are simple, ready to use, and easy to understand. Potentialities of the package are based in part on high precision elements of minor planets, annually published by the Institute of Applied Astronomy [2]. They are prepared with retention of full accuracy on the basis of orbital elements of new minor planets and elements of improved orbits distributed monthly by the Minor Planet Center.

The last fifteen years have seen tremendous progress in both the printed version of the minor planet ephemerides yearbook and the accompanied software package AMPLE. Numerous improvements were made in all parts of the package. For instance, a user may update the package database monthly with data published on the IAA website (this feature is known as

MUSE package) [3]. Some clones of the package were developed and put in use for specific tasks, i. e., AMPLE for Comets. AMPLE obtained a first class imbedded numerical integrator and can deal with unnumbered non-catalogued bodies by specifying their coordinates and velocities or elements [4]. However, it was felt that all these achievements were too sparse and insufficiently uniform.

The idea of the new version is to put all innovations together and produce a stand-alone, consistent, multi-purpose, cross-platform, robust, and easy to use software package.

AMPLE 3 is an integrated software package to deal with a number of problems concerning minor bodies of the Solar System. Among these problems are the following.

- Select minor bodies from catalogues based on orbital elements (or on their functions) and/or photometric parameters and represent the resulting data in different graphical forms. We call attention to a new feature called 'Slicing' — a new form of presentation for 3-D distributions. Using slicing one can view 2-D distributions slice by slice along the third dimension.
- Compute ephemerides for specified bodies at given moments in various coordinate systems and with different methods.
- Compare observed positions with computed ones (computation of *O–C*).
- Identify numbered minor bodies, whose computed positions are sufficiently close to the observed position of an unknown object.
- Determine all numbered minor bodies that can be seen at a certain moment within a specified sky region.
- Draw the picture of apparent motion of minor bodies in the sky with respect to fixed stars.
- Visualize the orbital motion of minor bodies in different ways. We mention specially that we offer a diversity of tools for visualization and analysis of various approaches.

The use of the AMPLE 3 package for case models is presented in Fig. 1.

What are the most important new features of the AMPLE 3 in comparison with previous versions and clones? Briefly, there are five.

1. The package is intended for dealing with all numbered minor planets, numbered periodic comets and non-catalogued objects as well.
2. The package is implemented in modern programming environment, and it runs on both Windows and Linux platforms.

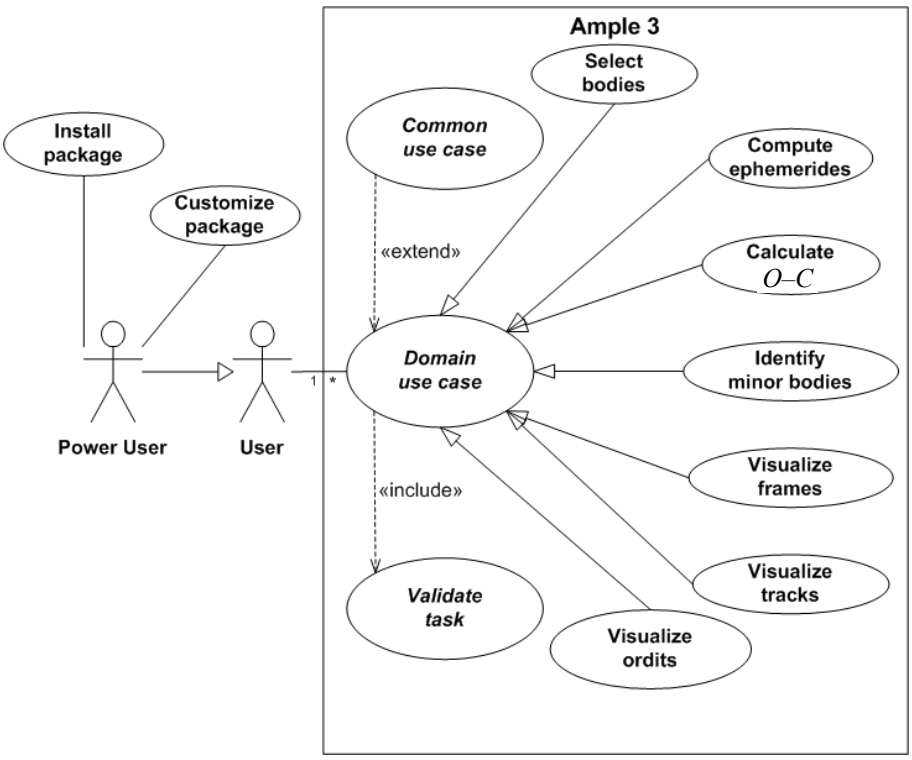

Fig. 1. Use Cases of the AMPLE 3 Package.

3. The package has new smart graphics with effects and animations, including visualization of approaches and impacts (Fig. 2).
4. The package has a modern, natural looking graphical user interface, in which the user always sees what he is about to do in the form of a tree-like structured task description (Fig. 3).
5. The package can be customized and fine-tuned in depth by a power user. Every entity that could be considered a parameter is really the parameter in the AMPLE 3 and could be reset if needed. It can be done by editing XML files with configuration information. For example, we can alter definitions of families and groups (Fig. 4).

The package is open for further improvements: we will compute ephemerides for parabolic and hyperbolic element systems, generate command files for telescope control, and more.

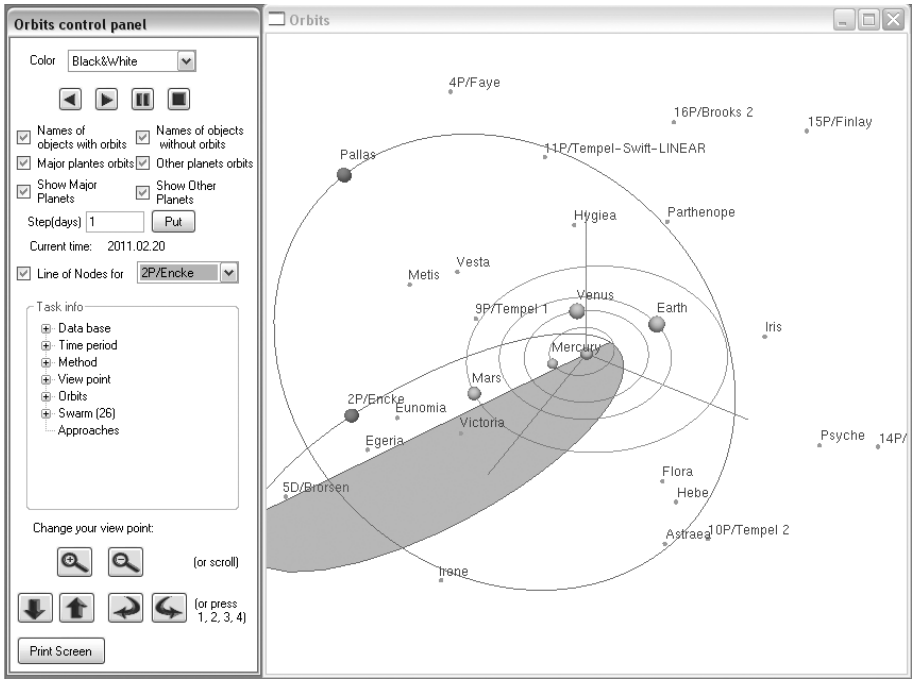

Fig. 2. Sample graphics of the AMPLE 3 Package.

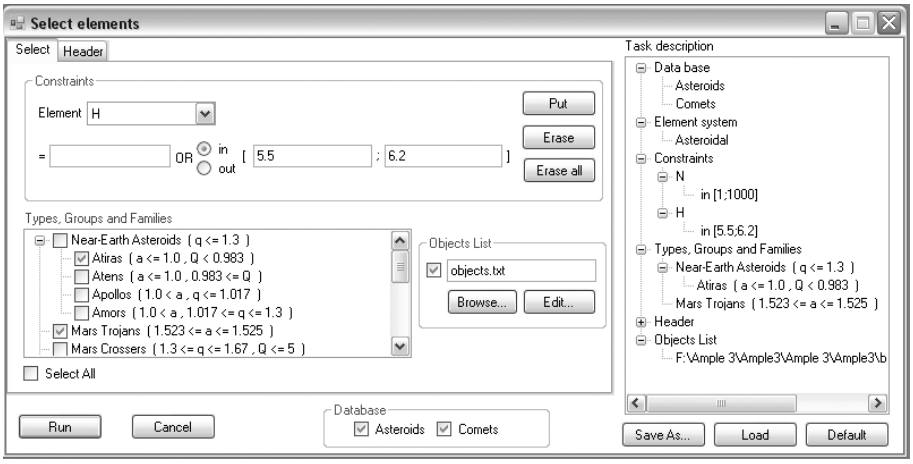

Fig. 3. Sample dialog of the AMPLE 3 Package.

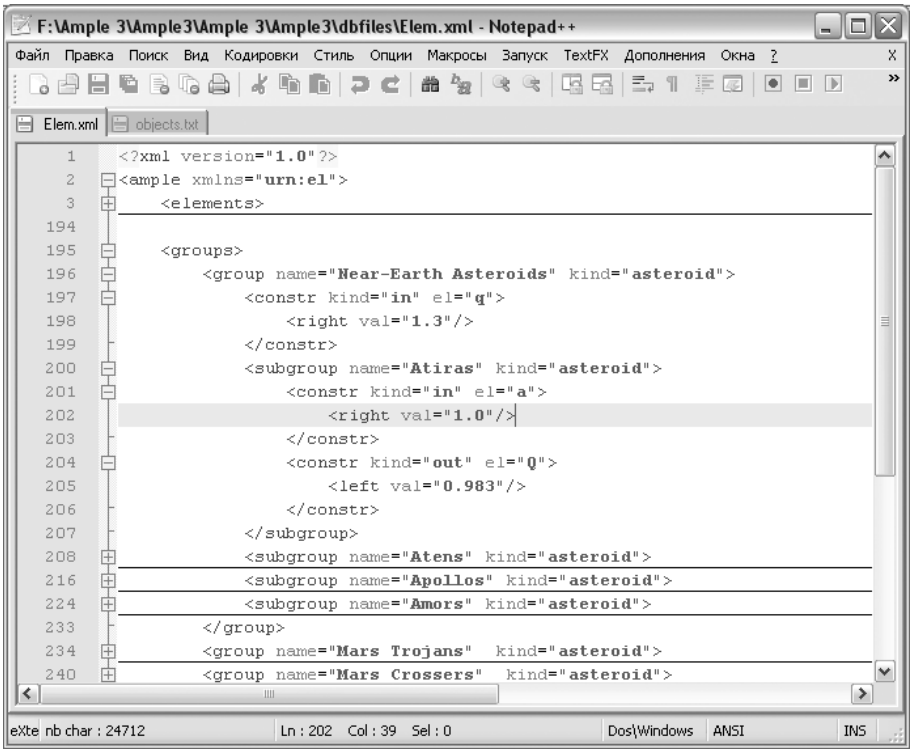

Fig. 4. Part of the parameters definition file.

References

1. *Shor V. A.* New integrated software package for minor planets // Abstracts of the papers presented at the Symposium IAU N 172. Paris, 3–8 July, 1995. P. 67–68.
2. Ephemerides of minor planets for 2009 / Ed. V. A. Shor. St. Petersburg, IAA RAS. 2008. 972 p.
3. *Shor V. A., Bytsin A. Yu., Chernetenko Yu. A., Kochetova O. M. et al.* New possibilities for ephemeris support of minor planets // St. Petersburg. IAA Transactions. N 8. “Celestial Mechanics”, 2002. P. 159–160.
4. *Shor V. A., Chernetenko Yu. A., Kochetova O. M., Netsvetaeva G. A. et al.* AMPLE — integrated multi-purpose software package for minor planets. Version 1.4 // Communications of the IAA RAS St. Petersburg, 2008. N 180. P. 1–58.

SMALL BODIES OF THE SOLAR SYSTEM

Analysis of Observations of Earth Impact Object 2008 *TC*3

E. Yu. Aleshkina, V. V. Kouprianov, A. V. Devyatkin, I. A. Verestchagina, V. Slesarenko

Central (Pulkovo) Astronomical Observatory of RAS, St. Petersburg, Russia

Abstract. On-line astrometric and photometric observations of asteroid 2008 *TC*3, discovered 19 hours before its impact on Earth [1], were carried out with the mirror astrograph ZA-320*M* at Pulkovo observatory at night of 7th October, 2009. We obtained 270 frames during 4 hours, which constitutes about 1/3 of the world's observations of the object. Results of analysis of the of 837 observations taken at 26 observatories worldwide are presented. Estimates of the asteroid's absolute magnitude and its size have been obtained. Frequency analysis of observations for determining the probable periodic brightness variations has been carried out.

Introduction

At 6:39 UTC on October 6, 2008, Richard Kowalski, using 1.5-meter Catalina Sky Survey telescope at Mount Lemmon Observatory in Arizona, discovered a small asteroid approaching the Earth [1]. Preliminary orbit estimates revealed that the asteroid would impact Earth 19 h after the moment of discovery, presumably in North of Sudan [2]. By the time the asteroid entered the Earth's atmosphere, more than 26 observatories worldwide performed more than 800 positional measurements of the asteroid, which received designation 2008 *TC*3. One-third of all measurements were obtained with the ZA-320*M* telescope of Pulkovo observatory [3]. The object entered the atmosphere above Northern Sudan at 02:45:40 UTC with relative velocity of 12.4 km/s and five seconds later exploded in the atmosphere at an altitude of 37 km [2, 4]. Explosion fragments, from small (~1 g) to large (~1 kg), fell on the Earth surface following the body's path [2]. A search in the vicinity of its path uncovered 47 meteorites weighing 3.95 kg in total. Based on chemical and spectral analysis of the asteroid debris the important

characteristics of the asteroid were found: its albedo 0.046 ± 0.005 and mean density 2.3 ± 0.2 g/cm^3. Furthermore, spectral analysis allowed one to determine that the asteroid belonged to taxonomic class F [2]. It should be pointed out that this asteroid is also unusual for class F, since the typical density for objects of this class is ~ 1.29–1.38 g/cm^3 [5]. It is possible that the density of 2008 *TC*3 is higher because of frictional compaction while traveling through Earth's atmosphere.

Observations of asteroid 2008 *TC*3

837 observations of this fast moving asteroid were performed at 26 observatories around the world. Most of these observations fall in the interval from 7:00 UTC till 9:00 UTC. Fig. 1 shows the diagram of the number of observations for different observatories. 270 observations are credited to the Pulkovo observatory, which is almost one-third of the total.

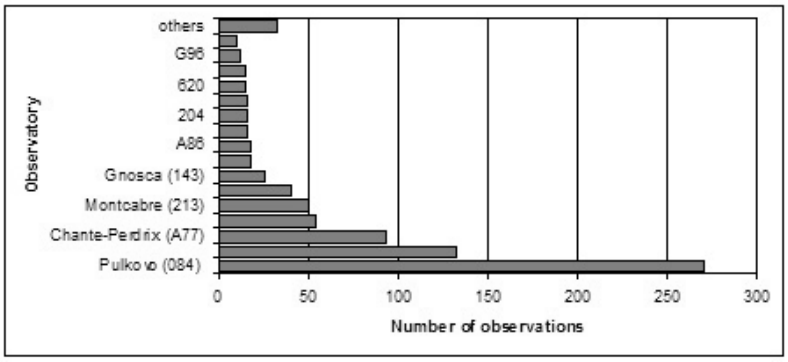

Fig. 1. Distribution of observations of asteroid 2008 *TC*3.

For our analysis we used three different groups of observations: a) all observations obtained with *R* filter; b) all observations obtained with *V* filter; c) observations of Pulkovo observatory. All these groups are shown in Fig. 2.

Three series of observations being studied were acquired in different photometric bands: *V*, *R*, and integral band for Pulkovo series. Based on these observations we have obtained estimates of the asteroid's absolute magnitude M_{abs} in the above bands, given in Tab. 1. Here we used the relation $M_{abs} = m_{obs} - 5\log(rR) + 2.5\log[(1 - G)\Phi_1 + G\Phi_2]$, where m_{obs} is the observed magnitude, r is the topocentric distance to the object, R is Sun to object distance. Φ_1, Φ_2 are functions of the phase angle [5]. Observational accuracy and phase angle range do not allow reliable determination of the parameter G. Therefore, an a priori value $G = 0.15$ was used as in [2]. The dependence of absolute magnitude on phase angle for asteroid 2008 *TC*3 is shown in Fig. 3.

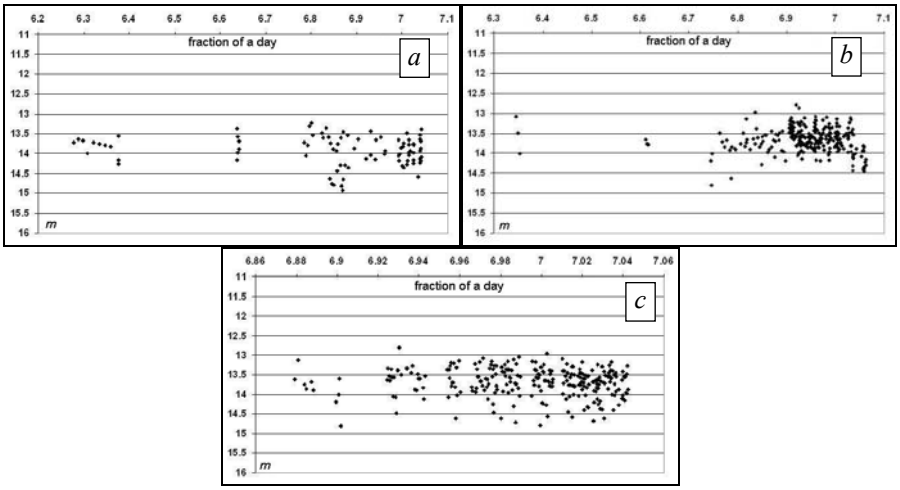

Fig. 2. Observations of asteroid 2008 *TC*3:
a – Pulkovo observatory; *b* – all observations in *V* band; *c* – all observations in *R* band.

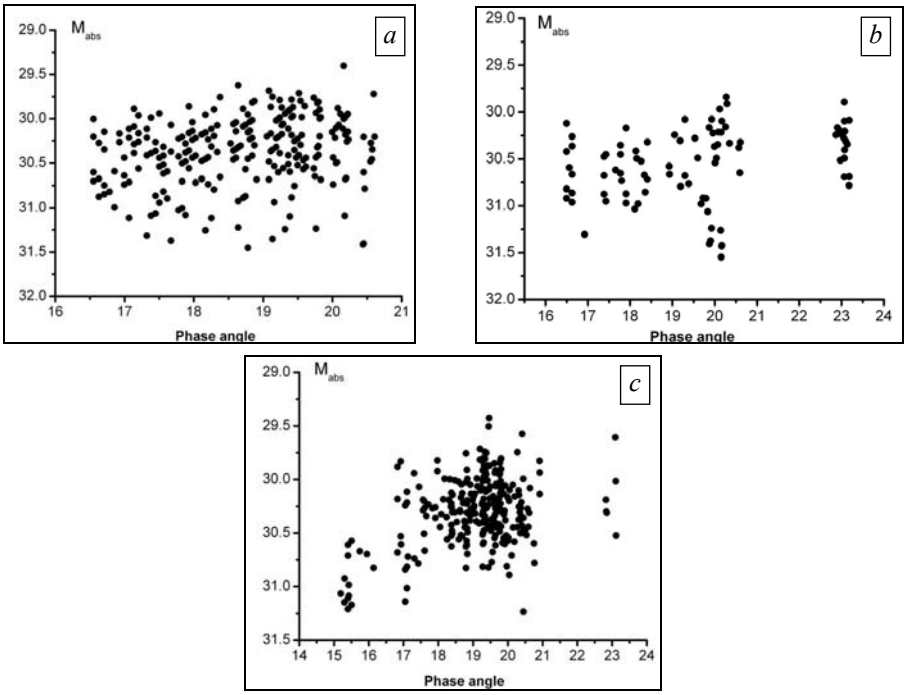

Fig. 3**.** Dependence of absolute magnitude on phase angle for asteroid 2008 *TC*3:
a — Pulkovo observatory; *b* — all observations in *V* band; *c* — all observations in *R* band.

Table 1. Absolute magnitude *M* estimates for asteroid 2008 *TC*3 in Johnson *V*, *R,* and integral bands and color index

V filter	*R* filter	Integral band	Color index *(V–R)*
30.56 ± 0.38	30.31 ± 0.31	30.35 ± 0.37	0.3 ± 0.2

Frequency analysis of asteroid 2008 *TC*3 lightcurves

To uncover the possible periodic components in variations of the asteroid's brightness that could be caused, e. g. by its spin, we have performed frequency analysis of all three series of observations. Three different techniques were employed: the CLEAN method [6], Lomb–Scargle method [7], and a technique involving wavelets [8]. All these methods have different mathematical approaches. CLEAN involves Fourier transform. Lomb–Scargle method is based on least-squares adjustment. The last technique exploits the special form of three-dimensional wavelet function. Hence one may consider these three methods as complementing each other.

Tab. 2 contains the results of our frequency analysis by all methods described above, for different series of observations.

Table 2. Frequency analysis results for series of observations of asteroid 2008 *TC*3. Periods are given in days

Series	CLEAN	Lomb–Scargle	Wavelets
All observatories *R* band	$P_1 = 0.287 \pm 0.005$ $P_2 = 0.09 \pm 0.01$	$P_1 = 0.287 \pm 0.03$ $P_2 = 0.09 \pm 0.004$	$P_1 = 0.287 \pm 0.001$
All observatories *V* band	$P_1 = 0.287 \pm 0.02$ $P_2 = 0.10 \pm 0.009$	$P_1 = 0.11 \pm 0.018$	$P_1 = 0.287 \pm 0.035$
Pulkovo observatory Integral band	$P_1 = 0.0071 \pm 0.00003$ $P_2 = 0.0125 \pm 0.00005$	$P_1 = 0.0071 \pm 0.00003$ $P_2 = 0.0125 \pm 0.00005$	$P_1 = 0.287 \pm 0.001$

The Pulkovo series is likely to contain the periods of 0.287 days (6.89 h) with 0.2^m amplitude and 0.0125 days (18 min) with 0.17^m amplitude. *R* and *V* band series contain periods of 0.287 days (6.89 h) and 0.1 days (2.4 h) with 0.15^m amplitude. The latter period is a clear fraction of 24 h and can be explained by reasons unrelated to the observed object. The 0.287-day period is present in all series of observations and is detected by all techniques used, which suggests that it is most reliable and belongs to the object itself. The 18-minute period might be real as well, but it is not clearly revealed from *R* and *V* observations due to their high off-duty factor.

According to [2], the object had two periods of 49 и 97 s. It was impossible to detect such periods from *R* and *V* band series of observations studied here, because consecutive frames were acquired with intervals of several

minutes. The Pulkovo series had consecutive frames with intervals of 10–20 s so it allowed us to reveal such periods. Because of the fast motion of the asteroid against the background, we had to divide our series for differential photometry into 8 groups of frames with the same reference stars in each frame. The mean value of accuracy is equal to 0.05^m. Frequency analysis was performed for each group and revealed the mean period of (48.5568 ± 0.6048) s. This period is in good agreement with that obtained in [2]. Therefore we consider that this period is inherent to asteroid 2008 *TC*3.

Estimates of the possible size of asteroid 2008 *TC*3

The possible size of asteroid was estimated using the formula $\log(D) = 3.122 - 0.5 \log(p) - 0.2M$, where M is absolute magnitude, p is the albedo, and D is the diameter of the object in km.

From data given in [2], the absolute magnitude of the asteroid is 30.9 in V band with $G = 0.15$. Asteroid debris found allowed one to determine its albedo, which appeared to be 0.046 ± 0.005. This result, accompanied by spectral data from the meteorites found, allows one to attribute 2008 *TC*3 to taxonomic class F [2, 4, 5]. However, the mean density for asteroids of F class is 1.29–1.38 g/cm^3 [5], whereas the mean density of 2008 *TC*3, as determined from its fragments, is 2.3 g/cm^3. This suggests that this asteroid is uncharacteristic of its class. According to observations the estimates of absolute magnitude is $\boldsymbol{M_V} = 30.56^m$ (see Tab. 1).

The possible size and mass of the asteroid are given in Tab. 3 as functions of albedo.

Table 3. Estimates of size and mass of 2008 *TC*3 for two value of M

Albedo	$M = 30.9^m$		$M = 30.56^m$	
	Diameter, m	Mass, kg	Diameter, m	Mass, kg
0.042	4.27	93.724	4.99	149.917
0.043	4.22	90.474	4.93	144.718
0.044	4.17	87.407	4.88	139.812
0.045	4.12	84.510	4.82	135.178
0.046	**4.08**	**81.769**	**4.77**	**130.794**
0.047	4.04	79.173	4.72	126.642
0.048	3.99	76.712	4.67	122.705
0.049	3.95	74.376	4.62	118.968
0.05	3.91	72.156	4.58	115.417

Conclusion

On-line astrometric and photometric observations of asteroid 2008 *TC*3, discovered 19 h before its impact on Earth, were carried out with the mirror astrograph ZA-320*M* at Pulkovo observatory in the night from 6th to the 7th

of October, 2009 [3]. We obtained 270 frames during 4 h. This is about one-third of the world observations.

Results of analysis of the whole block of observations (837) from 26 world observatories were presented. The estimated absolute magnitude of 2008 *TC*3 is $M_V = 30.56^m$**,** its size with a priori value of albedo 0.046 was 4.77 m. From frequency analysis of observations we conclude that asteroid 2008 *TC*3 had spin periods of 6.89 h and 49 s.

References

1. *Kowalski R. A. et al.* // MPEC 2008-T50 / Ed. G. V. Williams. P. 1 Minor Planet Center, Smithsonian Astrophysical Observatory, 2008.
2. *Jenniskens P., Shaddad M. H., Numan D. Elsir S. et al.* The impact and recovery of asteroid 2008 *TC*3 // Nature. 2009. Vol. 458. P. 485–488.
3. *Devyatkin A. V., Aleshkina E. Yu., Kouprianov V. V.* // Minor Planet Circular. 65326. 1. 2009
4. *Kwok R.* The rock that fell to Earth // Nature. 2009. Vol. 458. P. 401–403.
5. *Vinogradova T. A. et al.* // Transactions of IAA RAS. 2003. Vol. 9. 218 p. (in Russian).
6. *Vityazev V. V.* Analysis of irregular time series. St. Petersburg University press, 2001. 67 p. (in Russian).
7. *Scargle J. D.* Studies in astronomical time series analysis. II. Statistical aspects of spectral analysis of unevenly spaced data // Ap. J. 1982. 263. P. 835–853.
8. *Vityazev V. V.* Wavelets analysis. St. Petersburg University press, 2001. 58 p. (in Russian).
9. *Harris A. W.* A Practical Guide to Lightcurve Photometry and Analysis. Springer, 2006. 297 p.

SMALL BODIES OF THE SOLAR SYSTEM

Spots on Asteroids as Evidence of Collisions

V. V. Busarev[1], V. V. Prokofjeva-Mikhajlovskaya[2], A. N. Rublevsky[2]

[1]Sternberg State Astronomical Institute of M. V. Lomonosov Moscow State University, Moscow, Russia;
[2] Scientific Research Institute Crimean Astrophysical Observatory, Nauchnyj, Ukraine

Abstract. The spectral-frequency method (SFM) was developed in SAI and SRI CrAO [1]. It was used for investigations of sizes of hydro-silicate spots on the surfaces of asteroids 21 Lutetia and 4 Vesta. The results are in agreement with data from other observations. Spots are the result of small body collisions.

Introduction

Because of the large number of asteroids and meteoroids discovered in the Solar System, their physico-chemical parameters will remain unknown for a long time. However, these properties are needed to study the origin and evolution not only of these bodies but also those of the whole Solar System, and to solve the problem of asteroid and comet impact hazards. As is well known, particle sizes of regolith of solid airless bodies are very different. For example, the smallest fraction having an elevated mobility could form regions with specific laws of reflection of light. They could appear as surface details or spots on these bodies. Another reason of spots on solid bodies may be difference in the chemical-mineral content of their matter which may be connected with impact events. Since celestial bodies have a proper rotation, the heterogeneous structure of their surface could manifest itself in variations of photometric or spectral characteristics. To study them we have developed a SFM [1]. One purpose of the method is to estimate sizes of spectral and/or photometric details or spots on the surface of solid airless bodies.

Observations

Investigations of (21) Lutetia and (4) Vesta (asteroids of M and V types, respectively), targets of "Rosetta" and "Dawn" space missions, were performed with SFM. From August 31 to November 20, 2000, V. V. Bochkov obtained 186 spectra (0.37–0.84 μm) of 21 Lutetia with a 0.5-m meniscus

telescope MTM-500 in the Crimean Astrophysical Observatory (Fig. 1). A slitless spectrograph with two exchangeable transparent gratings, which provided a resolution of 40 or 30 Å, was used for the spectrophotometric observations. The spectra were calibrated by star standards and then converted to conditions beyond the terrestrial atmosphere. On the other hand, spectral observations (0.40–0.90 μm with a spectral resolution of 7–8 Å) of (21) Lutetia were performed by V. V. Busarev on 31 August, 2000 and 4–8 November, 2004 with a spectrograph and ST-6 SBIG CCD mounted on the 1.25-m telescope of SAI in Nauchnyj (Fig. 2).

An absorption band of phyllosilicates at 0.44 μm was discovered in reflectance spectra of (21) Lutetia. A frequency analysis of the equivalent width values of the band led us to estimate sizes of phyllosilicate spots on the asteroid surface (mainly 30–40 km) [2]. Then, the same absorption band at 0.44 μm

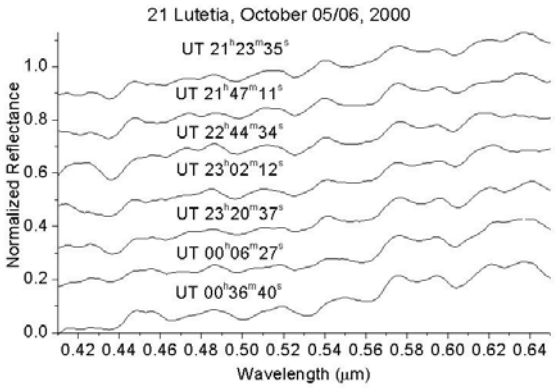

Fig. 1. Reflectance spectra of Lutetia obtained with a television facility mounted on the 0.5-m telescope MTM-500.

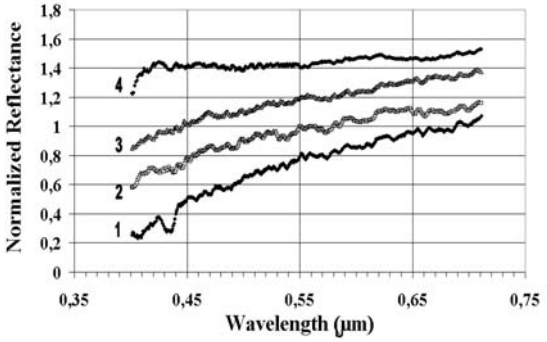

Fig. 2. Reflectance spectra of asteroid (21) Lutetia obtained with a CCD-spectrograph of 1.25-m telescope of SAI on 7/8.11.2004 with 10 min intervals.

was detected in reflectance spectra of Vesta obtained in CrAO (February 2002) [3]. It was found with SFM 16 independent periods in the row of equivalent width values of the band. Corresponding sizes of phyllosilicate spots on the asteroid surface mainly turned out not to be large.

Since formation temperatures of igneous asteroids Vesta and Lutetia could reach 1000–1500 °C, presence of phyllosilicates is not typical for them. Such low-temperature compounds could be delivered to the asteroids only during collisions with hydrated bodies at relatively low velocities. Small sizes of phyllosilicate spots on (21) Lutetia and (4) Vesta point also to small sizes of corresponding colliding bodies. Small sizes of the spots probably indicate a recent time of their formation. Another explanation of the spots may be a gravitational accumulation of hydrated dust particles on the surface of the asteroids. In the process of collisions and due to other space factors the dust particles could settle on the bodies in lowlands. The results support a hypothesis of V. V. Busarev [4] on delivery of phyllosilicates from the periphery of the Solar System. The compounds could originate in interiors of proto-planetary silicate-icy bodies at a stage of their initial thermal evolution. Then, the bodies might have been ejected by proto-Jupiter to the adjacent asteroid zone. As the result of crushing of the fragile objects during collisions with asteroid parent bodies, their fragments might remain there until the present time.

Conclusions

We have developed and used a SFM. It is based on registration of a row of spectra of a point object and on a frequency analysis of their parameters. It allows us to conclude that spots on asteroids are probably results of falls of small primitive bodies.

References

1. *Busarev V. V., Prokof'eva-Mikhailovskaya V. V., Bochkov V. V.* Spectral and spectral-frequency methods for studying atmosphere less bodies in the Solar System // Uspekhi Fisicheskikh Nauk. 2007. Vol. 177. P. 667–675 (in Russian).
2. *Prokof'eva V. V., Bochkov V. V., Busarev V. V.* The Surface Structure of the M-Type Asteroid 21 Lutetia: Spectral and Frequency Analysis // Solar System Research. 2005. Vol. 39. P. 410–420.
3. *Prokofjeva-Mikhailovskaja V. V., Rublevskij A. N., Bochkov V. V.* Water combination on the surface of the asteroid 4 Vesta / Izvestiya Astrophysicheskoy Observatorii. 2008. Vol. 104. P. 162–170 (in Russian).
4. *Busarev V. V.* Hydrated Silicates on M-, S-, and E-Type Asteroids as Possible Traces of Collisions with Bodies from the Jupiter Growth Zone // Solar System Research. 2002. Vol. 36. P. 35–42.

SMALL BODIES OF THE SOLAR SYSTEM

Masses of asteroids 10 Hygiea and 152 Atala obtained by the dynamical method

Yu. A. Chernetenko[1], A. V. Ivantsov[2]

[1]Institute of Applied Astronomy of RAS, St. Petersburg, Russia
[2] Research Institute Nikolaev Astronomical Observatory, Nikolaev, Ukraine

Abstract. Masses of asteroids 10 Hygiea and 152 Atala have been obtained by the dynamical method. Some other asteroids were used as test particles. We evaluated the contributions from different perturbing asteroids and the additional acceleration caused by the Yarkovsky effect in determining the masses. The influence of different criteria for elimination of erroneous observations on the value of determined mass was studied. The final mass values were obtained by common solutions based on optical observations of eight perturbed asteroids for 10 Hygiea [$m_{10} = 4.03 \pm 0.10$ (10^{-11} M_{Sun})] and of three perturbed asteroids for 152 Atala [$m_{152} = 1.34 \pm 0.27$ (10^{-11} M_{Sun})].

Introduction

This paper deals with problems of asteroid mass determination by the dynamical method when some other asteroids are used as perturbed bodies. The main parts of this approach are: a) appropriate model of motion; b) choice of perturbed asteroids; c) elimination of erroneous observations.

Choice of perturbed asteroids was made in accordance with the approach proposed in the paper [1]. The approach is based on the value of the mass error of perturbing asteroid obtained from observations of each perturbed asteroid. This criterion implicitly incorporates such often used criteria as value of minimal distance between bodies, number of close approaches, number of observations of perturbed asteroids and so on. However, some small values of mass error correspond to nonrealistic (very large or negative) mass estimations.

Therefore we try to investigate what factors have influence on the obtained mass values. It is proposed to evaluate contributions of: a) different sets of perturbing asteroids; b) different criteria of elimination of erroneous

observations; c) additional acceleration due to the Yarkovsky effect. Also it is not quite clear what kind of the perturbed asteroids are more preferable: if perturbed asteroid is rather large, the mutual perturbations should be taken into account; if perturbed asteroid is small, then there is a possibility of influence by the Yarkovsky effect on the mass estimate. These questions were considered in the evaluation of masses of asteroids 10 Hygiea and 152 Atala.

Results

Perturbed asteroids (PAs) were selected from the numbered asteroids in accordance with values of the mass errors of perturbing asteroid obtained from observations of each PA. Optical observations were taken from MPC catalogue. We have used observations starting from 1900.

Calculations were fulfilled using two independent software programs ("IAA" and "Nikolaev" [2]), however, models of motion and the sample of observations were the same. The gravitational perturbations from all the major planets and Pluto were taken into account. The coordinates of the main perturbing bodies were calculated using DE405 ephemeris. Relativistic perturbations from the Sun were included into the model. The possibility of accounting perturbations from: a) Ceres, Pallas, and Vesta; b) 300 asteroids in accordance with DE405; c) 307 asteroids (300 asteroids and large asteroids 152, 153, 190, 279, 334, 675, 1180) were considered. The phase correction and the gravitational deflection of light were taken into account. Numerical integration of the equations of motion and variation equations was performed by the 15th-order Everhart method. Erroneous observations were rejected by the 3 σ criterion ("IAA") or by application of a robust regression ("Nikolaev"). The final mass values have been defined by common solutions using observations of a number of selected PAs for each perturbing asteroid. The least squares method was used to fit conditional equations. Two variants of weights were used: a) equal weights; b) the weight 0.7 was given for all observations made before 1950.

Distributions of masses of perturbing asteroids and their mass errors versus diameters of perturbed asteroids show the advantage of large asteroids because they produce the lesser range of the mass values and the lesser mass errors as compared with small asteroids. It may be the result of the smaller mean residuals of these bodies, the larger intervals of observations, or the greater number of approaches. Hence the large perturbed asteroids (d > 150 km) can give a useful contribution to mass determination. However, it is necessary to take into account that mutual perturbations of perturbed and perturbing asteroids can be considerable. It should be noted that this conclusion was obtained for perturbing asteroids having diameters 429 and 287 km.

A number of common solutions were obtained for the mass of Hygiea. All of them are in good agreement with each other. We give here the mass

value 4.03 ± 0.10 (10^{-11} M_{Sun}), which was found using eight numbered PAs: 20, 3946, 6143, 11215, 15187, 24433, 48499, and 113976. The mass of 152 Atala 1.34 ± 0.27 (10^{-11} M_{Sun}) was found using observations of PAs 250, 264, and 651.

The estimates of a possible influence by additional acceleration from the Yarkovsky effect on the mass value were obtained for some PAs (see Table). We determined orbital parameters, mass correction and the transverse component of the acceleration, A_2, on the assumption that its value depends on the heliocentric distance as $1/r^2$. It should be noted that the so determined parameter A_2 can include not only the Yarkovsky effect but also some other accelerations not taken into account explicitly.

Estimates of mass of Hygiea (the third column) and estimates of its mass together with additional acceleration A_2 (the fourth column)

Perturbed asteroid	Diameter, km	M, 10^{-11} M_{Sun}	m, 10^{-11} M_{Sun}	A_2, 10^{-14}AU day^{-2}
3946	13.6	4.05 ± 0.16	3.41 ± 0.29	–33.5 ± 13.3
15187	6.5	3.52 ± 0.54	3.47 ± 1.13	–1.2 ± 3.4

Conclusions

- The mass values of asteroids 10 Hygiea and 152 Atala were obtained: m_{10} = 4.03 ± 0.10 (10^{-11} M_{Sun}), mean density = 2.0 g·cm^{-3};
  m_{152} = 1.34 ± 0.27 (10^{-11} M_{Sun}), mean density = 2.8 g·cm^{-3}.

The mass obtained for Hygiea is close to its value, 3.7 (10^{-11} M_{Sun}), assumed when constructing DE405.

- Final mass values practically do not depend on the criterion of rejecting erroneous observations.
- It was shown that mass estimates depend on completeness of accounting for perturbations. Therefore accounting for perturbations from asteroids should be as complete as possible.
- The additional acceleration acting on some perturbed asteroids was evaluated. It seems to be useful to include in the common solution the unknown parameter A_2 for each relatively small perturbed asteroid, in addition to the orbital parameters and mass correction.

References

1. *Chernetenko Yu. A., Kochetova O. M.* Determining the masses of some minor planets by the dynamical method // Near-Earth Astronomy-2003. Proc. of the conf. 2003. P. 233–239 (in Russian).
2. *Ivantsov A. V.* Determining the masses of large asteroids by the dynamical method // Kinematika i Fizika Nebesnykh Tel. 2007. Vol. 23, N 3. P. 108–115 (in Russian).

SMALL BODIES OF THE SOLAR SYSTEM

Results of Photometric Observations of Potentially Hazardous Asteroids

N. M. Gaftonyuk[1], Yu. N. Krugly[2], I. E. Molotov[3]

[1]Scientific Research Institute Crimean Astrophysical Observatory, Nauchnyj, Ukraine
[2]V. N. Karazin Kharkiv National University, Kharkiv, Ukraine
[3]Keldysh Institute of Applied Mathematics of RAS, Moscow, Russia

Abstract. We report results of CCD observations of 23 potentially hazardous asteroids that were made with the 1-m telescope in Simeiz Department of CrAO.

Introduction

NEAs whose orbits approach the Earth orbit at a distance $\Delta \leq 0.05$ AU and have absolute magnitude $H \leq 22.0^{\,\mathrm{m}}$ are considered as potentially hazardous asteroids (PHAs). According to the list of the Minor Planet Center, 6108 NEAs were discovered as of April 2, 2009. Approximately 20 % of them are PHAs. Studying these asteroids is of great interest since they can collide with the Earth and cause enormous devastation.

One method of studying physical properties of asteroids is based on photometric observations and their analyses. Photometric observations of NEAs allow one to determine parameters of rotation, shape, size, surface optical properties, etc. In the report we present results of NEA studies according to the joint project of the Crimean Astrophysical Observatory and the Institute of Astronomy of Karazin Kharkiv National University. Among NEAs observed within the frame of the project approximately 30 % are PHAs.

Observations and results

Observations of 23 PHAs were made with the 1-m Zeiss telescope of CrAO in Simeiz using CCD cameras SBIG ST-6, Apogee Alta U-42, FLI PL09000, and FLI IMG1001E. Method and reduction of observations are described in [1]. Results of observations are presented in Table. According to

Results of observations of PHAs

Asteroid	Type of orbit	Opposition	*H*, mag	Diameter, km	Spin Period, h	Amplitude, mag
1620 Geographos[(YORP)]	Ap	2008	15.6	2.26	5.2233	1.2–2.0
1862 Apollo [B] [(YORP)]	Ap	2005,7	16.1	1.55	3.065	0.26
1981 Midas	Ap	2006	15.18	2.2	5.220	0.65–0.8
3200 Phaethon	Ap	2004,6,7	14.51	5.1	3.604	0.11–0.3
4179 Toutatis	Ap	2004	15.3	2.8	129.84	1.2
16960 1998 QS52	Ap	2008	14.3	5.5	2.899	0.2–0.27
35107 1991 VH [B]	Am	2008	16.9	1.7	2.62	0.08
52768 1998 OR2	Ap	2009	15.9	2.3	5.7	0.17
54509 2000 PH5[(YORP)]	Am	2003,4	22.7	0.15	0.2029	0.86
65803 Didymos [B]	Ap	2003	18.4	0.8	2.2593	0.07–0.09
68216 2001 CV26 [B]	At	2007	16.4	1.7	2.429	0.08
87684 2000 SY2	At	2008	16.4	2.1	Short?	0.13
138137 2000 EE14	Ap	2007	17.1	1.2	—	> 0.2
138971 2001 CB21	Am	2006	18.4	0.7	3.76	0.11
143651 2003 QO104	Ap	2009	16.0	2.5	>80	> 1.
164400 2005 GN59	Ap	2008	17.3	1.5	38.3	> 1.3
2004 XP14	Ap	2006	19.4	0.45	>24	~ 0.05
2005 NB7 [B]	Ap	2008	18.9	0.5	3.48	0.1
2006 RZ	Ap	2006	20.3	0.3	4.96?	> 0.1
2006 VV2 [B]	Ap	2007	16.8	1.8	2.429	0.48
2007 DT103	Ap	2007	19.2	0.6	2.65	0.5–0.1
2007 TU24	Ap	2008	20.6	0.3	~26.	> 0.5
2007 TS19	Ap	2007	20.7	0.3	6.60	> 0.32

[(YORP)] Asteroid with the YORP effect discovered; [B] binary asteroid.

the Table, diameters of observed asteroids lay in the range from 0.3 to 5.5 km. The exception is asteroid 54509 2000 PH5, which has a diameter of 150 m.

Ten asteroids from our sample have spin periods in the range of 2.2–4.0 h and amplitudes of light curves typically less than 0.2 mag. Five asteroids have long spin periods ($P > 24$ h). For example 16960 1998 QS52 ($P = 2.899$ h) and 164400 2005 GN59 ($P = 38.3$ h) are asteroids with short- and long spin periods. Observations of these asteroids were carried out in the autumn of 2008 and their spin periods were determined for the first time.

Among the observed PHAs are six binaries or probable binary asteroids: 65803 Didymos, 1862 Apollo, 68216 2001 CV26, 2006 VV2, 35107 1991 VH, 2005 NB7. Four of them were previously discovered as binary systems by radar observations and were confirmed by our observations.

Several asteroids were observed to have a YORP effect. Observations of asteroids 1862 Apollo and 1620 Geographos allowed one to find changes of their spin rates that can be explained by the YORP effect. For the asteroid 1862 Apollo the YORP effect was revealed from observations during the interval from 1980 to 2005 [2]. For asteroid 1620 Geographos the spin period has decreased by 0.1 s during the interval of observations from 1969 to 2008 [3]. The YORP effect was also directly measured for the super-fast spinning asteroid 54509 2000 PH5 (P = 12.173 min) [4]. We observed this asteroid in 2003 and 2004.

An interesting object among PHAs is 3200 Phaethon. Its orbit is genetically connected with the Geminides meteor stream, so it can be assumed that Phaethon is an extinct comet nucleus. Our observations of Phaethon, which were carried out in 2004, 2006, and 2007 have confirmed that its spin period is equal to 3.604 h, in conformity with that found earlier [1].

Conclusion

When studying potentially hazardous asteroids it is expedient to carry out observations by various techniques to obtain as much information on physical characteristics of these objects as possible in order to solve the asteroid hazard problem. Study of binaries and asteroids with long spin periods requires long observation times and needs the cooperation of other observatories located at different longitudes. One can hope that observatories included in the International Scientific Optical Network (ISON) will join us in PHA studies.

References

1. *Krugly Yu. N., Belskaya I. N, Shevchenko V. G, Cherny V. G. et al.* The Near-Earth Objects Follow-up Program. IV. CCD Photometry in 1996–1999 // Icarus. 2002. Vol. 158. P. 294–304.
2. *Kaasalainen M., Ďurech J., Warner B. D., Krugly Yu. N. et al.* Acceleration of the rotation of asteroid 1862 Apollo by radiation torques // Nature. 2007. Vol. 446. P. 420–422.
3. *Ďurech J., Vokrouhlický D., Kaasalainen M., Higgins D. et al.* Detection of the YORP effect in asteroids (1620) Geographos // Astron. Astrophys. 2008. Vol. 489. L25–L28.
4. *Taylor P. A., Margot J.-L., Vokrouhlický D., Scheeres D. J. et al.* Spin rate of asteroid (54509) 2000 PH5 increasing due to the YORP effect // Sci. 2007. Vol. 316. P. 274–277.

SMALL BODIES OF THE SOLAR SYSTEM

Possible Origin of Asteroids on Retrograde Orbits

P. Kankiewicz[1], I . Włodarczyk[2]

[1]Institute of Physics of Astrophysics Division of Kochanowski University, Kielce, Poland
[2]Chorzów Astronomical Observatory, Chorzów, Poland

Abstract. Asteroids on retrograde orbits ($i > 90°$) are known since 1999. Some of them are Centaurs, small Transneptunian bodies, or potential comet nuclei. Their possible origin is still not explained in detail. They can be transported into the inner part of Solar System by perturbations, especially secular resonances with outer planets. Such scenarios are shown in the presented work.

Initial data and methods

We list 18 objects on retrograde orbits (see Table). Taking into account their astrometrical observations, we computed their orbits with the use of the OrbFit software [*http://adams.dm.unipi.it/~orbmaint/orbfit/*]. Here are our results:

We computed clones of each asteroid with the multiple solution method [1] and with the settings: 3 sigma, 1001 clones, JPL DE405/406 (as the source of planetary perturbing forces). Next, the orbital elements were propagated backwards in time to the epoch "now minus 10^6 years" with the use of the Mercury software [2]. During the integration we averaged orbital elements of all clones of the given asteroid.

Results

In Figure are presented results of our computations. Shown are the orbital evolution of semi-major axis and eccentricity for selected asteroids on retrograde orbits (10^6 years backward). The Figure is based on similar diagrams, presented by Horner et al. [3]. We present here the classification scheme for objects under the control of giant planets. First letter denotes the planet controlling the perihelion and the second letter the aphelion. It is important to mention that the current number of objects with $i > 90°$ increased in the last few months to ~25, so we expect to update our results in the near future.

Keplerian elements of 18 known asteroids on retrograde orbits and corresponding rms values (epoch JD2454400.5 = 2007/10/27)

Ast. name	*a,* AU	*e*	*i,* deg	Long. Node, deg	Arg. peric., deg	Mean anom., deg
20461 Dioretsa	23.93799	0.90002	160.43311	297.58331	102.9424	24.41532
rms	8.7E-4	4E-6	2E-5	7E-5	1.2E-4	0.00133
65407 (2002 RP120)	54.31628	0.95461	119.11975	39.19562	357.83143	4.54868
rms	0.00441	4E-6	3E-5	1E-5	7E-5	5.5E-4
1999 LE31	8.13248	0.46524	151.85909	292.07679	32.50918	137.8434
rms	2.4E-4	1E-5	4E-5	1.7E-4	0.00162	0.00654
2000 DG8	10.77006	0.79365	129.26807	279.11021	222.14185	69.22792
rms	6.8E-4	1E-5	7E-5	4E-5	2.7E-4	0.0065
2000 HE46	23.65609	0.89965	158.52169	313.4354	82.5552	23.75313
rms	0.02559	1.1E-4	1.7E-4	6.6E-4	9.4E-4	0.03853
2002 CE10	9.76865	0.79057	145.45305	147.39903	126.01911	51.3141
rms	6E-5	1E-6	2E-5	2E-5	4E-5	5E-6
2004 NN8	99.84446	0.97658	165.51226	165.32294	262.835	1.0824
rms	0.0839	2E-5	5E-5	1.9E-4	3.5E-4	0.00136
2005 NP82	5.87742	0.4788	130.59804	123.6837	254.47095	34.46231
rms	0.01249	6.3E-4	0.01641	0.00434	0.14804	0.06972
2005 SB223	29.63412	0.90653	91.40343	219.7129	252.57607	4.34151
rms	0.02649	8E-5	2.1E-4	3.7E-4	0.00311	0.00576
2005 TJ50	9.14575	0.58656	110.30737	218.08345	211.79868	19.78503
rms	0.16772	0.00719	0.10114	0.00729	0.14249	0.50977
2005 VD	6.67438	0.25385	172.8279	171.3717	176.20638	33.5047
rms	0.00161	1.5E-4	2.6E-4	4.9E-4	0.03255	0.00916
2006 BZ8	9.65909	0.8036	165.27009	183.46277	82.14575	15.81708
rms	9E-5	2E-6	2E-5	5E-5	7E-5	2.3E-4
2006 EX52	43.43511	0.94068	150.25362	247.92036	163.4085	1.21934
rms	0.00897	1E-5	5E-5	3E-5	1.7E-4	3.8E-4
2006 GZ2	54.73004	0.94028	168.59243	355.53157	193.39382	1.02914
rms	35.6239	0.03864	0.0605	0.13015	1.30239	0.34877
2006 RG1	25.50298	0.92089	133.32121	305.6988	344.03656	2.57238
rms	0.75126	0.0023	0.00435	0.01507	0.06496	0.11267
2006 RJ2	9.80472	0.76433	164.65505	190.81699	160.65958	15.01771
rms	0.12047	0.00282	0.00623	0.00386	0.06547	0.28316
2007 VA85	4.15347	0.7348	132.48411	115.34374	25.33612	10.57766
rms	0.02525	0.00138	0.01114	0.01406	0.12327	0.10806
2007 VW266	5.45518	0.39009	108.29225	276.50904	226.01761	336.75775
rms	0.03008	0.00332	0.05022	0.00255	0.0883	0.11302

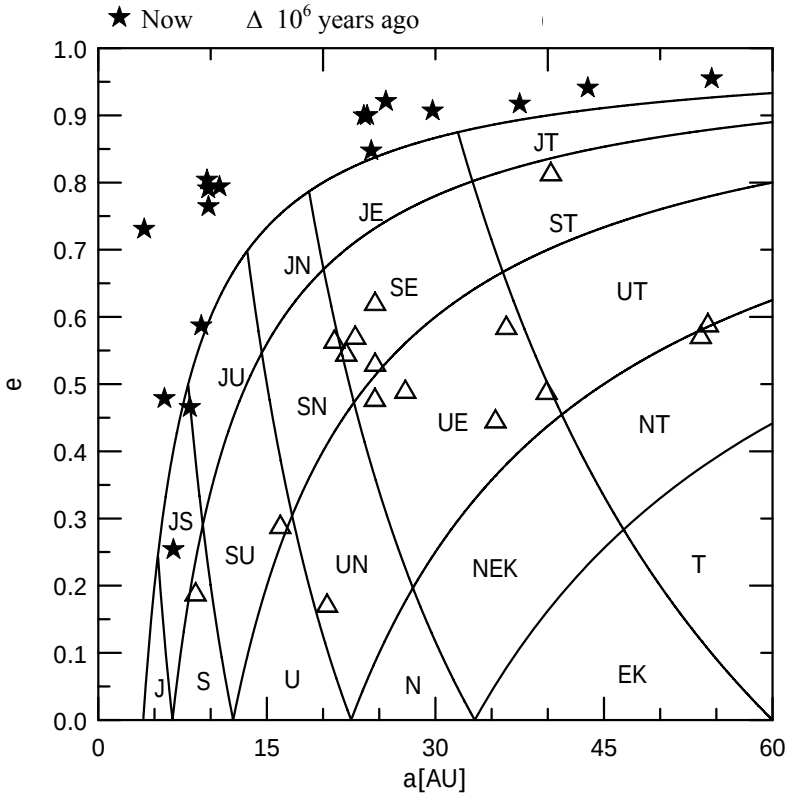

The evolution of asteroids on retrograde orbits in the plane of semi-major axis and eccentricity. First letter denotes the planet controlling the perihelion and the second letter the aphelion.

Conclusions

It is apparent that about 10^6 years ago the perihelia of selected objects were controlled mainly by outer planets. Now they are closer to the inner planets of the Solar System.

References

1. *Milani A., Sansaturio M. E., Tommei G., Arratia O. et al*. Multiple solutions for asteroid orbits: Computational procedure and applications // Astron. Astrophys. 2005. Vol. 431. P. 729–746.
2. *Chambers J. E.* A hybrid symplectic integrator that permits close encounters between massive bodies // Mon. Not. 1999. Vol. 304. P. 793–799.
3. *Horner J., Evans N. W., Bailey M. E., Asher D. J.* The populations of comet-like bodies in the Solar System // Mon. Not. 2003. Vol. 343. P. 1057–1066.

The Asteroid-Comet Hazard Conference Proceedings, 2009

SMALL BODIES OF THE SOLAR SYSTEM

Estimates for the Set-theoretic Distance between Orbits of Celestial Bodies

K. V. Kholshevnikov[1, 2]

[1]Sobolev Astronomical Institute of St. Petersburg State University, St. Petersburg, Russia
[2]Institute of Applied Astronomy of RAS, St. Petersburg, Russia

Abstract. Prediction of close encounters of celestial bodies with the Earth or other planets requires enormous calculations. It is reasonable to use preliminary simple criteria for the proximity to intersection based on estimates of set-theoretic distance $\rho(\mathbf{E}, \mathbf{E_0})$ between orbits $\mathbf{E}$, $\mathbf{E_0}$ of celestial bodies P, P_0. As a first step it is sufficient to consider orbits as unperturbed. We describe here two simple criteria and one more complicated one. The first one uses the most unfavorable orientation of orbits with given semi-major axes and eccentricities. The second one uses the topological notion of linkage. Both give us lower and upper bounds of the distance. The third one requires calculation of the distance itself and it amounts to solving a trigonometric equation of the 8-th degree.

Introduction

Prediction of close encounters of celestial bodies with the Earth or other planets requires enormous calculations. It is reasonable to use preliminary simple criteria for the proximity to intersection based on estimates of set-theoretic distance $\rho(\mathbf{E}, \mathbf{E_0})$ between orbits $\mathbf{E}$, $\mathbf{E_0}$ of celestial bodies P, P_0. By definition

$$\rho\left(\mathbf{E}, \mathbf{E_0}\right) = \min \tilde{\rho}\left(P, P_0\right), \tag{1}$$

$\tilde{\rho}(P, P_0)$ being the distance between points P, P_0; the minimum is taken over all possible positions of the points P, P_0 lying in the orbits $\mathbf{E}$, $\mathbf{E_0}$. As a first step it is sufficient to consider orbits as unperturbed. Note, that if the orbits are situated far from the mean motion resonance there exist moments when the distance between the bodies P, P_0 differs from $\rho(\mathbf{E}, \mathbf{E_0})$ by a negligible quantity. In case of a strong resonance $\tilde{\rho}(P, P_0)$ may always be much greater

than $\rho(\mathbf{E}, \mathbf{E_0})$. This is the case for the pairs Neptune–Pluto, Titan–Hyperion, and several others.

Remark. One often uses the term Minimal Orbit Intersection Distance for ρ. This term is regrettable. *Intersection* is possible only in the case ρ = 0. The notion of a minimum is already included in the definition of a distance between sets.

Let us describe three criteria of estimates for ρ in order of increasing accuracy. Let *q, Q, p, a, e,* θ being the distance from the Sun at perihelion, the distance from the Sun at aphelion, semi-latus rectum, semi-major axis, eccentricity, and true anomaly, respectively.

Criterion using distances at perihelion and aphelion

Let index 0 relate to the Earth.

$$\text{If } q > Q_0, \text{ then } \rho(\mathbf{E}, \mathbf{E_0}) \geq q - Q_0. \tag{2}$$

For asteroids of Atira type

$$q_0 > Q, \ \rho(\mathbf{E}, \mathbf{E_0}) \geq q_0 - Q. \tag{3}$$

In spite of simplicity of inequalities (2) and (3) they are exact: equality is attained if lines of apsides are anticoincident .

Criterion using linking coefficient

Two disjoint elliptic orbits **E** and $\mathbf{E_0}$ can be embedded in three-dimensional space in two ways: with a linkage (case A_1) and without a linkage (case A_2). Continuous transit from one type of embedding to another is possible through the intersection (case A_3) only. Let us derive a simple criterion for distinguishing types A_k. We restrict ourselves to a case of two non-coplanar ellipses (rare cases of coplanarity, as well as unboundedness of **E** orbit are examined in [1, 2]). Let **L** be a ray directed from the Sun to one of common nodes of orbits **E**, $\mathbf{E_0}$. Denote by $M(r,\theta)$ the unique point in **E**, lying in **L**. Analogously we obtain a point $M_0(r_0,\theta_0) \in \mathbf{E_0}$ lying on the same ray. Construct also points $N(r,\theta-\pi) \in \mathbf{E}$, $N_0(r_0,\theta_0-\pi) \in \mathbf{E_0}$, lying in the line of nodes on the other side from the Sun.

Definition. Quantity

$$l(\mathbf{E}, \mathbf{E_0}) = (r - r_0)(R - R_0) \tag{4}$$

is called the linking coefficient. It is negative, positive, or equal to zero in the cases A_1, A_2, A_3, respectively. Evidently,

$$\rho^2(\mathbf{E}, \mathbf{E_0}) \leq |l(\mathbf{E}, \mathbf{E_0})|, \tag{5}$$

$$\rho(\mathbf{E}, \mathbf{E_0}) \leq \min\{|r - r_0|, |R - R_0|\}. \tag{6}$$

Quantities r, r_0, R, R_0, l can be expressed via orbital elements by simple formulas given in [1, 2].

For what purpose is the linking coefficient useful, if the estimate (6) is more effective than (5)? Under the effects of perturbations the orbits of celestial bodies change. They may intersect at an epoch only when l vanishes. For example, osculating orbits of the Earth and 2201 Oliato intersected in 1962. Osculating orbits of the Earth and 1981 Midas intersected several times in 1889.

Calculation of ρ

If the two first criteria show a proximity of orbits to intersection, it is necessary to find the distance $\rho(\mathbf{E_0}, \mathbf{E})$. The algorithm for calculating ρ is adduced in [1, 3]. The algorithm output contained in [3], is an extension to a case of arbitrary orbits contained in [4]. Analogous construction using another parametrization contained in [5]. Computer program calculating ρ is contained in [6].

References

1. *Kholshevnikov K. V., Titov V. B.* Zadacha dvukh tel (Two Body Problem). St. Petersburg: St. Petersburg University Press. 2007. 180 p. (in Russian).
2. *Kholshevnikov K. V., Vassiliev N. N.* On the linking coefficient of two Keplerian elliptic orbits // Celest. Mech. Dyn. Astron. 1999. Vol. 75, N 1. P. 69–74.
3. *Kholshevnikov K. V., Vassiliev N. N.* On the distance function between two Keplerian elliptic orbits // Celest. Mech. Dyn. Astron. 1999. Vol. 75, N 2. P. 75–83.
4. *Baluyev R. V., Kholshevnikov K. V.* Distance between two arbitrary unperturbed orbits // Celest. Mech. Dyn. Astron. 2005. Vol. 91, N 3–4. P. 287–300.
5. *Gronchi G. F.* An algebraic method to compute the critical points of the distance function between two Keplerian orbits // Celest. Mech. Dyn. Astron. 2005. Vol. 93, N 1–4. P. 295–329.
6. *Shor V. A., Chernetenko Yu. A., Kochetova O. M., Netsvetaeva G. A. et al.* AMPLE — integrated multi-purpose software package for minor planets. Version 1.5. St. Petersburg: Publ. Institute of Applied Astronomy. 2009.

SMALL BODIES OF THE SOLAR SYSTEM

Detection of the YORP Effect from Photometric Observations of Near-Earth Asteroids

Yu. N. Krugly[1], N. M. Gaftonyuk[2], J. Durech[3], D. Vokrouhlicky[3], M. Kaasalainen[4], V. G. Shevchenko[1], M. A. Ibrahimov[5], A. L. Marshalkina[5], V. V. Rumyantsev[2], I. E. Molotov[6], Z. Donchev[7], V. Ivanova[7], A. V. Sergeyev[1], N. Tungalag[8]

[1]V. N. Karazin Kharkiv National University, Kharkiv, Ukraine
[2]Scientific Research Institute Crimean Astrophysical Observatory, Nauchnyj, Ukraine
[3] Astronomical Institute of Charles University, Prague, Czech Republic
[4]Department of Mathematics and Statistic of Rolf Nevanlinna Institute of University of Helsinki, Helsinki, Finland
[5]Ulugh Beg Astronomical Institute of Uzbek Academy of Sciences, Tashkent, Uzbekistan
[6]Keldysh Institute of Applied Mathematics of RAS, Moscow, Russia
[7]Institute of Astronomy of Bulgarian Academy of Sciences, Sofia, Bulgaria
[8]Research Center for Astronomy and Geophysics of Mongolian Academy of Science, Ulanbator, Mongolia

Abstract. In this report we present summary of photometric observations of near-Earth asteroids (NEAs) obtained to search for YORP effect. New additional observations of 1862 Apollo in 2007 have confirmed YORP detection. Observations of 1620 Geographos in 2008 and 3103 Eger in 2009 are used to detect the acceleration of the asteroids rotation rates in agreement with the computed theoretical values due to YORP effect. Now there are four asteroids with the YORP effect detected. Rotation periods for co-orbital NEAs 138175 2000 EE104 and 138852 2000 WN10 are determined for the first time.

Introduction

An asteroid absorbing sunlight and reemitting it mainly in thermal range is subjected to a recoil force. For an asymmetrical asteroid this force can result in a torque that modifies its spin period and obliquity, which named as effect of Yarkovsky-O'Keeffe-Radzievskii-Paddack, or YORP [1]. The main

factors determining evolution of asteroid's spin vector under YORP are the asteroid size, shape, surface properties, and average distance from the Sun.

Here we report the results of the project on the YORP effect detection from lightcurve observations of NEAs. Our observations in 2005 have been used to detect the YORP effect for 1862 Apollo [2], which is one of two asteroids with the YORP effect detected for the first time. In 2007–2009 we have carried out new photometric observations of several NEAs, which are supposed to be candidates for detection of YORP acceleration in the near future. Also lightcurves of so-called Earth co-orbitals (NEAs with orbital periods close to the Earth's one) are obtained.

This work is performed in frame of the joint project of the Institute of Astronomy of Karazin Kharkiv National University and the Crimean Astrophysical Observatory for NEAs study. The observations in Rozhen Observatory are a part of the joint project of IA KhNU and the Institute of Astronomy of the Bulgarian Academy of Sciences for small bodies of Solar System research. The work was supported by International Scientific Optical Network (ISON) [3], which includes more than 20 observatories in nine countries. All these observatories participate in coordinated CCD-observations of NEAs in frame of this work.

Observations and results

The observations were mainly carried out with the 0.7 m telescope at the Chuguevskaya Station (70 km to the South-East from Kharkiv, Ukraine) and with the 1 m Zeiss telescope at the Simeiz Observatory (Crimea). The observations of more faint objects were done with the 2.6 m ZTSh telescope of the Crimean Astrophysical Observatory (Nauchny, Crimea), the 2 m Zeiss telescope at the Rozhen Observatory of the Bulgarian Academy of Sciences (Rhodope Mountains, Bulgaria), the 1.5 and 0.6 m telescopes at the Maidanak Observatory (Uzbekistan). All telescopes are equipped with CCD-cameras. The observations were obtained using BVRI filters of the standard Johnson-Cousins photometric system (mainly R-filter was used as more sensitive band for CCD). Reduction of the observations and the brightness measurements with the aperture photometry routine were done in standard way [4]. Differential photometry between the asteroid and the comparison stars in the CCD-frame provides uncertainty on the order of 0.01–0.03 mag (rms). Special attention was paid to the asteroid absolute calibration which was fulfilled in photometric nights.

Obtained results for the individual asteroids are shown in the Table. It includes type of orbit, year of last observations, absolute magnitude, effective diameter, determined spin period, lightcurve amplitude, and quality of the period determination. In 2007 we observed Apollo and confirmed previously detected YORP acceleration of its spin rate [5]. New observations of

Orbital parameters and obtained physical parameters of observed asteroids

Asteroid	Orbit type	Opposition	H[1], mag	D[2], km	Spin period, h	Observed amplitude, mag	Quality[3]
1862 Apollo [B,Y]	Apollo	2007	15.68 [R]	1.5	3.0646 ± ± 0.001	0.26	3
1620 Geographos [Y]	Apollo	2008	15.25	3.5	5.2225 ± ± 0.001	1.14–1.58	3
1865 Cerberus	Apollo	2008	16.34 [R]	1.3	6.8033 ± ± 0.001	1.78	3
3103 Eger [Y]	Apollo	2009	(15.61)	2.1	5.706	0.7	3
54509 2000 PH5 [Y]	Apollo	2004	21.99 [R]	0.11	0.20288 ± ± 0.00005	1.0	3
85770 1998 UP1 [C]	Aten	2007	(20.37)	0.26	–	0.1	–
138175 2000 EE104[C]	Apollo	2007	(20.30)	0.27	13.56 ± ± 0.03	> 0.8	1
138852 2000 WN10[C]	Apollo	2008	20.2	0.29	4.44 ± 0.1	0.4	2

[B]binary; [Y]with YORP detected; [C]co-orbital; [R]absolute magnitude in *R*-band; [1]*H* values in brackets are taken from MPC; [2]diameters estimated from *H*; [3]quality of the period determination.

Geographos, Cerberus, and Eger in 2008–2009 have allowed detecting the YORP effect for Geographos and Eger [6, 7]. As result of observations of co-orbital NEAs the spin periods are determined for 138175 2000 EE104 and 138852 2000 WN10 for the first time.

Discussion and Conclusions

Detection of the YORP effect for an asteroid is based on analysis of its lightcurves obtained on time intervals that are sufficient to develop the asteroid's shape model and to determine its spin period precisely. NEAs undergo the strongest influence of YORP effect among all the small Solar System bodies due to their stronger heating by the Sun. Value of change of the spin rate of km-sized NEAs caused by YORP is comparable with the measuring precision of this value attainable after several decades of observations. For asteroids with size of about hundred meters the effect can be measured after several years of observations. Co-orbital NEAs, whose orbital periods are close to the Earth's year, are the most convenient for this kind of detection.

References

1. *Rubincam D. P.* Radiative spin-up and spin-down of small asteroids // Icarus. 2000. Vol. 148. P. 2–11.

2. *Kaasalainen M., Ďurech J., Warner B.D. et al.* Acceleration of the rotation of asteroid 1862 Apollo by radiation torques // Nature. 2007. Vol. 446, N 7134. P. 420–422.
3. *Molotov I., Agapov V., Titenko V. et al.* International scientific optical network for space debris research // Advan. Space Res. 2008. Vol. 41, Issue 7. P. 1022–1028.
4. *Krugly Yu. N., Belskaya I. N., Shevchenko V. G. et al.* CCD photometry of near-Earth asteroids in 1996–1999 // Icarus. 2002. Vol. 158. P. 294–304.
5. *Durech J., Vokrouhlický D., Kaasalainen M. et al.* New photometric observations of asteroids (1862) Apollo and (25143) Itokawa — an analysis of YORP effect // Astron. Astrophys. 2008. Vol. 488. P. 345–350.
6. *Durech J., Vokrouhlický D., Kaasalainen M. et al.* Detection of the YORP effect in asteroid (1620) Geographos // Astron. Astrophys. 2008. Vol. 489. L25–L28.
7. *Durech J., Vokrouhlicky D., Polishook D., Krugly Y. N. et al.* Detection of the YORP Effect in Asteroid (3103) Eger // 41th DPS Meet. AAS. 2009. Id. 56.04.

SMALL BODIES OF THE SOLAR SYSTEM

The Sizes of Impact Craters and Ejecta Spots on Asteroids

N. N. Gorkavyi, A. N. Rublevsky, V. V. Prokofjeva-Mihajlovskaya

Scientific Research Institute Crimean Astrophysical Observatory,
Nauchnyj, Ukraine

Abstract. The formation of ejecta during the cratering process is characteristic for meteoritic impacts. On a simple impact model, analytic expression for a size of impact crater and ejecta spot are derived.

Introduction

Scientific interest in the process connected with the collision of two Solar System bodies started in the middle of the last century. Investigations led to the important conclusion that meteorite bombardment causes reduction of mass of small bodies of the Solar System and can be the cause for the origin of the Moon and asteroid satellites [1].

Estimates of the sizes of spots around craters

The energy balance during crater formation is based on the assumption that the kinetic energy of a meteorite is spent on breakup of the meteorite of mass m and asteroid material of mass M_i (M_i << total mass of asteroid) and for moving the ejected mass M_e to a height h against gravity g

$$mV^2 / 2 = m\,E_{\rm m} + M_i E_a + M_e\, g\, h, \qquad (1)$$

where V is the velocity of a meteorite relative to the asteroid and E_m and E_a are the breakup energies per unit mass of the meteorite and the asteroid materials, respectively. We assume that the meteorite has the form of a sphere of diameter L, and a crater has the form of a hemisphere of diameter D, and $M_i = M_e = M$, $h = D/2$. Part of the ejecta will be dispersed in space, but we expect this part to be small compared with the ejecta remaining around the crater. Considering that

$$M = (\rho_a \pi D^3) / 12;\; m = (\rho_m \pi L^3) / 6, \qquad (2)$$

where ρ_m and ρ_a — are the densities of the meteorite and the asteroid, respectively, we obtain from the equation (1):

$$L^3 \rho_m(V^2 - 2 E_m) = D^3 \rho_a (E_a + gD/2) \quad (3)$$

Let's consider equation (3) in a limiting case of dominance of strength or breakup energy $E_a >> gD/2$ and high-velocity impacts $V^2 >> 2E_m \sim 10^2$ m/s. Then we obtain

$$D = (\rho_m/\rho_a)^{1/3} L V^{2/3} E_a^{-1/3} . \quad (4)$$

Parameter E hides in itself a number of complex effects of impact interaction: breakup with formation of a free surface, heating, fusion, and evaporation. For example for destruction of monolithic ice $E = 10^7 - 10^8$ erg/g. Thus E is not a real constant, and it grows with energy of impact as it has been experimentally shown for low-velocity impacts of two bodies with a regolith layer. We will estimate E, using semi-empirical expression for D, obtained from the analysis of results of nuclear explosions [2]:

$$D = 0.00124 \rho_m^{1/3} L V^{2/3} . \quad (5)$$

Substituting (5) in (4), we obtain $E_a\rho_a = 5.2 \cdot 10^8$ erg/cm^3. Allen (1977) published the expression similar to (5) from which it is possible to obtain estimates for $E_a \rho_a = 1.5 \cdot 10^8$ erg/cm^3. For studying crater formation on asteroids with typical density $\rho_a = 2 \div 4$ g/cm^3 we can use value $E_a = 10^8$ erg/g. We will estimate the size of a crater D_{cr}, at which effects of gravitation and strength are comparable (see (3)): $D_{cr} = 2 E_a/g \sim 2$ km for the Earth, ~ 12 km for the Moon and ~ 120 km for an asteroid with a diameter of 350 km. For calculation of the size of the craters close to D_{cr}, it is necessary to use the full equation (3), which can be solved numerically. We will write down the equation useful to estimates. For $E_a = 10^8$ erg/g the diameter of a crater divided by diameter of a meteorite gives

$$D/L = 4.6 (\rho_m/\rho_a)^{1/3} V_1^{2/3} , \quad (6)$$

where V_1 in km/s.

For $\rho_m = \rho_a$ and velocity of impact equal to 1 km/s, we obtain $D/L = 4.6$. The relative density of impactor is not so important: if it is 4 times less than asteroid density, then we have $D/L = 2.9$. A change of velocity to 0.5 km/s will result in some reduction of the size of a crater.

Let's consider the problem of the size of spot of ejecta thrown out of a meteoritic crater, assuming that the size of a crater is known from (4). The density of ejecta that settled on the asteroid surface smoothly varies with distance from the crater. The border of the spot can be defined by acceptance of the minimum thickness of layer H of ejecta. It is clear that very thin ejecta layer will be simply absorbed by uneven regolith and will not give observa-

ble changes in properties of the surface. We consider that the total mass of the ejecta is equal to mass of the material that has been thrown out from crater. Since the size of the crater is known, it gives a way of calculating the distribution of ejecta surface density around the crater. From the Collins et al. paper and for such preconditions (dependence of thickness of regolith (H) with distance (R) measured from the center, and crater diameter including the wall surrounding it $D_0 = 1.25D$) one obtains [2]

$$H = 0.0037\, D_0^4/R^3. \quad (7)$$

Conclusion

In Solar System small bodies with primitive structure migrate from its periphery toward the Sun [3, 4]. Collisions of bodies occur continuously. In such collisions scattered ejecta settle around the craters as a bright spots with different chemical characteristics.

References

1. *Gorkavyi N. N.* The Origin of the Moon and Binary Asteroids // Izvestiya Astrophysicheskoy Observatorii. 2007. Vol. 103, N 2. P. 143–155 (in Russian).
2. *Collins G. S., Melosh H., Marcus R. A.* Earth Impact Effects Program: A Web-based computer program for calculating the regional environmental consequences of a meteoroid impact on Earth // Meteoritics & Planetary Science. 2005. 40, N 6. P. 817–840.
3. *Eneev T. M.* About the possible structure of external areas of the Solar System. // Astronomical J. Lett. 1980. Vol. 6, N 5. P. 295–300 (in Russian).
4. *Ipatov S. I.* Migration of Celestial Bodies in the Solar Systems // M.: Editorial URSS, 2000. 320 p. (in Russian).

The Asteroid-Comet Hazard Conference Proceedings, 2009

SMALL BODIES OF THE SOLAR SYSTEM

Method for High-accuracy Determinations of Orbits of Small Bodies from Three Observations

V. A. Shefer

Research Institute of Applied Mathematics and Mechanics
of Tomsk State University, Tomsk, Russia

Abstract. A new method is suggested for finding the preliminary orbit of a small celestial body from three pairs of angular measurements of its position at three moments. The method uses the intermediate orbit that we previously constructed from three position vectors and the corresponding times. This intermediate orbit allows for most of the perturbations in the motion of the body under study. The methodical error of orbit computation by the proposed method is generally three orders smaller than the corresponding error of the traditional approach based on the construction of the unperturbed Keplerian orbit.

Introduction

Now, with the availability of modern high-precision optoelectronic and radiotechnical positional observations, which are several orders of magnitude more accurate than classical astrometric measurements, the accuracy of the preliminary orbit obtained via the traditional methods based on the solution of the two-body problem [1, 2] may turn out to be much lower than that of the reference observations. In view of the discovery of a great number of objects observed on short orbital arcs in the zones of close approaches with major planets (mainly within the neighborhood of the Earth) the problem of constructing the preliminary orbit with an accuracy matching the ever-increasing accuracy of the observations employed is especially important today.

In our previous study [3] we suggested a method for finding the intermediate perturbed orbit of a small celestial body from three position vectors and the corresponding time instants. The method allows one to construct the orbit that in the vicinity of the reference time interval is three orders of magnitude more precise than the traditional Keplerian orbit.

In the present paper a method is proposed for determining the orbit from three positions of a small body on the celestial sphere at three time instants taking into account the principal perturbations. The perturbing effects are allowed for via the intermediate orbit derived in [3].

Method description

Let us consider the motion of a small body (asteroid, comet, large meteoroid, or spacecraft) in the heliocentric rectangular equatorial coordinate system. The differential equations of motion can be written in the form

$$\ddot{\mathbf{x}} = -\frac{k^2 M}{r^3}\mathbf{x} + \mathbf{F} \equiv \mathbf{G}, \tag{1}$$

where $\mathbf{x}$ is the position vector of the small body, $r = |\mathbf{x}|$, k is the Gaussian gravitational constant, M is the mass of the Sun, and $\mathbf{F}$ is the perturbing acceleration vector.

Suppose that for each of three time instants t_1^0, t_2^0, t_3^0 ($t_1^0 < t_2^0 < t_3^0$) we have a pair of observed angular coordinates: the right ascension α_i^0 and declination δ_i^0 of the small body ($i = 1, 2, 3$). We assume that angular coordinates are the topocentric coordinates referring to the observation point. Heliocentric and topocentric coordinates of the small body are related to each other via the vector equations

$$\mathbf{x}_i = \rho_i \mathbf{L}_i - \mathbf{S}_i;\ i = 1, 2, 3, \tag{2}$$

where $\mathbf{x}_i$ is the heliocentric position vector of the small body determined at the time t_i^0; $\mathbf{S}_i$ is the topocentric position vector of the Sun determined at the observing time t_i^0; ρ_i is the topocentric distance, and $\mathbf{L}_i$ is the unit vector of the form

$$\mathbf{L}_i^T = (\cos\delta_i^0 \cos\alpha_i^0,\ \cos\delta_i^0 \sin\alpha_i^0,\ \sin\delta_i^0).$$

We now use the formulas of the classic approach [1, 2] to obtain ρ_i in the first approximation. After this stage, we put into observing time the correction to account for the time it takes the ray of light (signal) to cover the distance from the small body to the observer and turn to the time instant t_i:

$$t_i = t_i^0 - \rho_i / c;\ i = 1, 2, 3, \tag{3}$$

where c is the speed of light. Then, according to (2), we determine the position vectors $\mathbf{x}_1$, $\mathbf{x}_2$, $\mathbf{x}_3$ at time instants t_1, t_2, t_3 ($t_1 < t_2 < t_3$), respectively. The values of the vectors $\mathbf{x}_1$, $\mathbf{x}_2$, $\mathbf{x}_3$ at this stage are approximate and require further refinement.

Let us introduce the notation

$$t_{12} = t_2 - t_1;\ t_{23} = t_3 - t_2;\ t_{13} = t_3 - t_1;$$
$$T_1 = 2/(t_{12}t_{13});\ T_2 = -2/(t_{12}t_{23});\ T_3 = 2/(t_{13}t_{23}).$$

In accordance with [3], let us compute the position vectors $\mathbf{q}_1^*$, $\mathbf{q}_2^*$, $\mathbf{q}_3^*$ on the intermediate orbit relative to the fictitious attracting centre, the position vectors $\mathbf{Z}_1$, $\mathbf{Z}_2$, $\mathbf{Z}_3$ of the fictitious centre, and the gravitational constants μ_1, μ_2, μ_3:

$$\mathbf{q}_i^* = -\lambda_i \mathbf{G}_i,\ \mathbf{Z}_i = \mathbf{x}_i - \mathbf{q}_i^*,\ \mu_i = \lambda_i R_i^* \hat{\mathbf{G}}_i^2;\ i = 1, 2, 3, \tag{4}$$

where

$$\hat{\mathbf{G}}_i = \mathbf{G}_i - \ddot{\mathbf{Z}},\ R_i^{*2} = \lambda_i^2 \hat{\mathbf{G}}_i^2;\ i = 1, 2, 3,$$
$$\ddot{\mathbf{Z}} = \frac{\mathbf{G}_2 - A_1\mathbf{G}_1 - A_3\mathbf{G}_3}{1 - A_1 - A_3};\ A_j = \frac{(\mathbf{Q}_j \cdot \mathbf{G}_2)}{\Delta};\ j = 1, 3,$$
$$\mathbf{Q}_1 = (\mathbf{G}_3 \cdot \mathbf{G}_{23})\mathbf{G}_{12} - (\mathbf{G}_3 \cdot \mathbf{G}_{12})\mathbf{G}_{23};\ \mathbf{Q}_3 = (\mathbf{G}_1 \cdot \mathbf{G}_{12})\mathbf{G}_{23} - (\mathbf{G}_1 \cdot \mathbf{G}_{23})\mathbf{G}_{12};$$
$$\Delta = (\mathbf{G}_1 \cdot \mathbf{G}_{12})(\mathbf{G}_3 \cdot \mathbf{G}_{23}) - (\mathbf{G}_1 \cdot \mathbf{G}_{23})(\mathbf{G}_3 \cdot \mathbf{G}_{12});$$
$$\mathbf{G}_{12} = \mathbf{G}_2 - \mathbf{G}_1 \neq 0;\ \mathbf{G}_{23} = \mathbf{G}_3 - \mathbf{G}_2 \neq 0.$$

We determine the parameters λ_1, λ_2, and λ_3 in the following way [3].

The parameter λ_2 can be found as the solution of an algebraic equation

$$A\lambda_2^4 + B\lambda_2^3 + C\lambda_2^2 + D\lambda_2 + E = 0, \tag{5}$$

where

$$A = P_1^2 |\hat{\mathbf{G}}_1|^3 |\hat{\mathbf{G}}_2|^3 t_{12} + P_3^2 |\hat{\mathbf{G}}_2|^3 |\hat{\mathbf{G}}_3|^3 t_{23} - P_1^2 P_3^2 |\hat{\mathbf{G}}_1|^3 |\hat{\mathbf{G}}_3|^3 t_{13};$$
$$B = 2(P_1 S_1 |\hat{\mathbf{G}}_1|^3 |\hat{\mathbf{G}}_2|^3 t_{12} + P_3 S_3 |\hat{\mathbf{G}}_2|^3 |\hat{\mathbf{G}}_3|^3 t_{23} - P_1 P_3 Q |\hat{\mathbf{G}}_1|^3 |\hat{\mathbf{G}}_3|^3 t_{13});$$
$$C = S_1^2 |\hat{\mathbf{G}}_1|^3 |\hat{\mathbf{G}}_2|^3 t_{12} + S_3^2 |\hat{\mathbf{G}}_2|^3 |\hat{\mathbf{G}}_3|^3 t_{23} -$$
$$-(Q^2 + 2P_1 S_1 P_3 S_3 |\hat{\mathbf{G}}_1|^3 |\hat{\mathbf{G}}_3|^3 t_{13};$$
$$D = -2S_1 S_3 Q |\hat{\mathbf{G}}_1|^3 |\hat{\mathbf{G}}_3|^3 t_{13};$$
$$E = -S_1^2 S_3^2 |\hat{\mathbf{G}}_1|^3 |\hat{\mathbf{G}}_3|^3 t_{13};\ Q = P_1 S_3 + P_3 S_1;$$
$$P_j = -\frac{T_2}{T_j} A_j;\ S_j = -\frac{(\mathbf{Q}_j \cdot \mathbf{R})}{T_j \Delta};\ j = 1, 3;\ \mathbf{R} = T_1\mathbf{x}_1 + T_2\mathbf{x}_2 + T_3\mathbf{x}_3.$$

The root that we need is selected among the real nonzero roots of equation (5) as follows. We find the root λ_2 that is not smaller than all the re-

maining roots in absolute value. If the signs of λ_1 and λ_3, which are then determined from formulas

$$\lambda_1 = \lambda_2 P_1 + S_1;\ \lambda_3 = \lambda_2 P_3 + S_3,$$

coincide with the sign of the root found by the above rule, then the latter is taken as the required parameter λ_2. Otherwise, this root and a multiple of it (if it exists) are discarded and the search for the needed root among the remaining real roots using the described procedure is continued.

According to [3], we obtain three positions on the intermediate orbit in the space of variables **u**. These positions are determined by the vectors

$$\mathbf{u}_1 = \frac{\mu_1}{\mu_2}\mathbf{q}_1^*;\ \mathbf{u}_2 = \mathbf{q}_2^*;\ \mathbf{u}_3 = \frac{\mu_3}{\mu_2}\mathbf{q}_3^* \tag{6}$$

and the corresponding fictitious time instants

$$\theta_1 = -\frac{\mu_1}{\mu_2}t_{12};\ \theta_2 = 0;\ \theta_3 = \frac{\mu_3}{\mu_2}t_{23}. \tag{7}$$

Since the Keplerian orbit, which we have in the parametric space [3], is planar, in view of (2), (4), (6), and (7), we can write

$$d_1\mu_1\rho_1\mathbf{L}_1 - \mu_2\rho_2\mathbf{L}_2 + d_3\mu_3\rho_3\mathbf{L}_3 = d_1\mu_1\mathbf{Y}_1 - \mu_2\mathbf{Y}_2 + d_3\mu_3\mathbf{Y}_3, \tag{8}$$

where

$$d_1 = \frac{\eta_{13}(\theta_3 - \theta_2)}{\eta_{23}(\theta_3 - \theta_1)};\ d_3 = \frac{\eta_{13}(\theta_2 - \theta_1)}{\eta_{12}(\theta_3 - \theta_1)};\ \mathbf{Y}_i = \mathbf{S}_i + \mathbf{Z}_i;\ i = 1, 2, 3,$$

η_{pq} is the ratio of the areas of the conic sector and the triangle constructed for the vector pair $\{\mathbf{u}_p, \mathbf{u}_q\}$ $(p = 1, 2;\ q = 2, 3;\ p \neq q)$. The equations (8) are obtained by analogy with the fundamental equations of the Gauss method [1, 2]. The Gaussian equations result from (8) as a special case, if we put $\mu_1 = \mu_2 = \mu_3 = k^2;\ \mathbf{Z}_1 = \mathbf{Z}_2 = \mathbf{Z}_3 = \mathbf{0}$.

Solving the system of equations (8), we find more accurate values for the topocentric distances ρ_1, ρ_2, and ρ_3. Now, relations (2) and (3) can be used again to refine $\mathbf{x}_i$ and t_i. The calculation process is repeated, until the topocentric distances are determined with the preassigned accuracy.

Based on the three finally refined position vectors $\mathbf{x}_1$, $\mathbf{x}_2$, $\mathbf{x}_3$ and the corresponding refined time instants t_1, t_2, t_3, we find the velocity vector $\dot{\mathbf{x}}_2^*$ on the intermediate orbit using the algorithm developed in [3]. The values of vectors $\mathbf{x}_2^* = \mathbf{x}_2$, $\dot{\mathbf{x}}_2^*$ are the parameters of motion for the required orbit at

time $t_2^* = t_2$. This orbit will fully satisfy the three given pairs of angular measurements.

Remark. The above-described iteration procedure requires the fulfillment at each step the following constraining conditions [3]:

$$\boldsymbol{\delta} \equiv T_1\mathbf{Z}_1 + T_2\mathbf{Z}_2 + T_3\mathbf{Z}_3 = \mathbf{0};\ \gamma \equiv \mu_1\mu_2 t_{12} + \mu_2\mu_3 t_{23} + \mu_1\mu_3 t_{13} = 0.$$

The nonfulfilment of these conditions, due to errors in the computation, can lead to misconvergence of the iterative process. To eliminate this defect we propose the use of the corrections

$$\Delta\mathbf{Z}_i = -\frac{T_i\boldsymbol{\delta}}{T_1^2 + T_2^2 + T_2^2};\ \Delta\mu_i = -\frac{\alpha_i\gamma}{\alpha_1^2 + \alpha_2^2 + \alpha_3^2};\ i = 1, 2, 3,$$

where

$$\alpha_1 = \mu_2 t_{12} - \mu_3 t_{13};\ \alpha_2 = \mu_1 t_{12} + \mu_3 t_{23};\ \alpha_3 = \mu_2 t_{23} - \mu_1 t_{13}.$$

The corrections $\Delta\mathbf{Z}_i$ and $\Delta\mu_i$ are added to the computed values of $\mathbf{Z}_i$ and μ_i included in (8) correspondingly at each step of the iteration procedure.

Conclusions

In this paper we proposed a new method for the determination of the preliminary orbit using three positions of a small body on the celestial sphere and the corresponding time instants. We developed this method in line with the underlying scheme of the classic Lagrange–Gauss method as far as our approach allowed. The principal and fundamental deviation from the classic scheme is that instead of the unperturbed Keplerian orbit we construct an orbit that allows for most of the perturbations in the motion of the celestial body. We achieve it by using our earlier derived intermediate perturbed orbit based on three position vectors and the corresponding time intervals. Our orbit is generally three orders more accurate than the orbit constructed by traditional methods.

Acknowledgements

The work was supported by the Ministry of Education and Science of Russia ("Development of the Scientific Potential of the Higher School (2009–2010)" Program; project number: 2.1.1/2629).

References

1. *Escobal P. R.* Methods of Orbit Determination. New York–London–Sydney: John Wiley and Sons, 1965.
2. *Subbotin M. F.* Vvedenie v teoreticheskuyu astronomiyu (Introduction to Theoretical Astronomy). M.: Nauka, 1968 (in Russian).
3. *Shefer V. A.* Determination of an Intermediate Perturbed Orbit from Three Position Vectors // Astron. Lett. 2007. Vol. 33. P. 270–282.

The Asteroid-Comet Hazard Conference Proceedings, 2009

Determination of an Intermediate Perturbed Orbit from Range and Range Rate Measurements at Three Time Instances

V. A. Shefer

Research Institute of Applied Mathematics and Mechanics
of Tomsk State University, Tomsk, Russia

Abstract. A new method for computing the preliminary orbit of a small celestial body from three pairs of range and range rate observations is proposed. The method is based on using the intermediate orbit with a fourth-order tangency to the trajectory of perturbed motion previously constructed by the author. The degree of approximation of the real motion by the constructed intermediate orbit near the middle observation time is three orders higher than by the Keplerian orbit determined by traditional methods.

Introduction

Modern radiotechnical and laser gauges allow us to measure the distance between the observation point and the celestial body (range) and radial velocity (range rate) with precision that is several orders higher than by optical observations. The use of such high-precision measurements requires a non-traditional approach for the solution of the preliminary orbit problem. Below we state a new method for construction of an intermediate perturbed orbit from the above three sets of observational data.

Method description

Consider the motion of a small celestial body in the heliocentric rectangular equatorial coordinate system that is described by equations

$$\ddot{\mathbf{x}} = -\frac{k^2 M}{r^3}\mathbf{x} + \mathbf{F} \equiv \mathbf{G}, \qquad (1)$$

where $\mathbf{x}$ is the vector of the position of the body, $r = |\mathbf{x}|$, k is the Gaussian gravitational constant, M is the mass of the Sun, **F** is the perturbing acceleration vector.

Let us assume that, for each of the three time instants t_1, t_2, t_3 ($t_1 < t_2 < t_3$), we have a pair of measured values for the ranges ρ_i and range rates $\dot{\rho}_i$ of the small body ($i = 1, 2, 3$). We assume that the measured quantities are the topocentric parameters referring to the point of observation.

For the heliocentric position vector $\mathbf{x}_i$ of the small body, topocentric position vector $\mathbf{S}_i$ of the Sun, and the vector $\rho_i \mathbf{L}_i$ at the time t_i we have the relation:

$$\mathbf{x}_i = \rho_i \mathbf{L}_i - \mathbf{S}_i, \quad i = 1, 2, 3, \tag{2}$$

where $\mathbf{L}_i$ is the unit vector directed from the observer to the small body. Differentiating (2) with respect to time *t*, we obtain

$$\dot{\mathbf{x}}_i = \dot{\rho}_i \mathbf{L}_i + \rho_i \dot{\mathbf{L}}_i - \dot{\mathbf{S}}_i, \quad i = 1, 2, 3. \tag{3}$$

The unknowns in (2) and (3) are the quantities $\mathbf{x}_i$, $\dot{\mathbf{x}}_i$, $\mathbf{L}_i$, $\dot{\mathbf{L}}_i$. Eliminating from (2) and (3) the vectors $\mathbf{L}_i$ и $\dot{\mathbf{L}}_i$ gives

$$(\mathbf{x}_i + \mathbf{S}_i)^2 = \rho_i^2; \quad (\mathbf{x}_i + \mathbf{S}_i) \cdot (\dot{\mathbf{x}}_i + \dot{\mathbf{S}}_i) = \rho_i \dot{\rho}_i, \quad i = 1, 2, 3. \tag{4}$$

We accept the middle time instant $t = t_2$ as an initial time. Suppose that we know at this time, as a first approximation, the position and velocity vectors of the small body, that is

$$\mathbf{x}(t_2) = \mathbf{x}_2; \quad \dot{\mathbf{x}}(t_2) = \dot{\mathbf{x}}_2.$$

Introduce a fictitious attracting centre with the gravitational parameter μ and locate it at the point defined by the vector

$$\mathbf{Z} = \mathbf{Z}_2 + \dot{\mathbf{Z}}_2 (t - t_2) + \frac{1}{2} \ddot{\mathbf{Z}}_2 (t - t_2)^2, \tag{5}$$

where $\mathbf{Z}_2$, $\dot{\mathbf{Z}}_2$, $\ddot{\mathbf{Z}}_2$ are the initial position, velocity, and acceleration vectors of the fictitious centre, respectively. Then the equations of motion of the small body about the fictitious centre will be written in the form

$$\ddot{\mathbf{q}} = \mathbf{G} - \ddot{\mathbf{Z}} \equiv \hat{\mathbf{G}}; \quad \mathbf{q} = \mathbf{x} - \mathbf{Z}; \quad \ddot{\mathbf{Z}} = \ddot{\mathbf{Z}}_2. \tag{6}$$

In the same coordinate system, in which the real motion (6) is considered, we specify an intermediate motion by the equations

$$\ddot{\mathbf{q}}^* = -\frac{\mu}{R^{*3}} \mathbf{q}^*; \quad R^* = |\mathbf{q}^*| \tag{7}$$

and the initial conditions

$$\mathbf{q}^*(t_2) = \mathbf{q}_2^*; \quad \dot{\mathbf{q}}^*(t_2) = \dot{\mathbf{q}}_2^*.$$

Let us assume that the gravitational parameter μ is a function continuously varying with time according to the formula [1]

$$\mu = \frac{\mu_2^2}{\mu_2 - \dot{\mu}_2(t - t_2)}, \quad \mu_2 \neq 0. \tag{8}$$

Let us require performing the following conditions:

$$\mathbf{q}_2^* = \mathbf{q}_2 = \mathbf{x}_2 - \mathbf{Z}_2; \quad \dot{\mathbf{q}}_2^* = \dot{\mathbf{q}}_2 = \dot{\mathbf{x}}_2 - \dot{\mathbf{Z}}_2; \quad \ddot{\mathbf{q}}_2^* = \ddot{\mathbf{q}}_2 = \mathbf{G}_2 - \ddot{\mathbf{Z}}_2 \equiv \hat{\mathbf{G}}_2; \tag{9}$$

$$\mathbf{q}_2^{*(3)} = \mathbf{q}_2^{(3)} = \dot{\mathbf{G}}_2; \quad \mathbf{q}_2^{*(4)} = \mathbf{q}_2^{(4)} = \ddot{\mathbf{G}}_2; \quad \ddot{\mathbf{Z}}_2 \perp \dot{\mathbf{G}}_2; \quad \ddot{\mathbf{Z}}_2 \perp \ddot{\mathbf{G}}_2. \tag{10}$$

The superscript in parentheses denotes the order of the derivative with respect to time *t*.

From (9) and (10) due to (7) we will have [1]

$$\mu_2 = \lambda R_2^* \hat{\mathbf{G}}_2^2; \quad \dot{\mu}_2 = (3b - \beta)\mu_2; \tag{11}$$

$$\mathbf{q}_2^* = -\lambda \hat{\mathbf{G}}_2; \quad \dot{\mathbf{q}}_2^* = \lambda\left(\frac{1}{2}\beta \hat{\mathbf{G}}_2 - \dot{\mathbf{G}}_2\right); \tag{12}$$

$$\hat{\mathbf{G}}_2 = \frac{1}{c - b\beta}(\ddot{\mathbf{G}}_2 - \beta \dot{\mathbf{G}}_2); \quad \frac{1}{\lambda} = \frac{3}{2}a - \frac{15}{2}b^2 + \frac{1}{2}c + 4b\beta - \frac{3}{4}\beta^2; \tag{13}$$

$$a = \frac{\mathbf{U}_2^2}{\mathbf{V}_2^2}\dot{\mathbf{G}}_2^2; \quad b = \frac{\mathbf{U}_2^2}{\mathbf{V}_2^2}(\mathbf{G}_2 \cdot \dot{\mathbf{G}}_2); \quad c = \frac{\mathbf{U}_2^2}{\mathbf{V}_2^2}(\mathbf{G}_2 \cdot \ddot{\mathbf{G}}_2); \quad \beta = \frac{(\mathbf{V}_2 \cdot \ddot{\mathbf{G}}_2)}{(\mathbf{V}_2 \cdot \dot{\mathbf{G}}_2)}; \tag{14}$$

$$\mathbf{V}_2 = (\mathbf{G}_2 \cdot \dot{\mathbf{G}}_2)\ddot{\mathbf{G}}_2 - (\mathbf{G}_2 \cdot \ddot{\mathbf{G}}_2)\dot{\mathbf{G}}_2; \; \mathbf{U}_2^2 = \dot{\mathbf{G}}_2^2 \ddot{\mathbf{G}}_2^2 - (\dot{\mathbf{G}}_2 \cdot \ddot{\mathbf{G}}_2)^2; \; R_2^{*2} = \lambda^2 \hat{\mathbf{G}}_2^2.$$

We assume that $\mathbf{G}_2 \neq \mathbf{0}$; $\dot{\mathbf{G}}_2 \neq \mathbf{0}$; $\ddot{\mathbf{G}}_2 \neq \mathbf{0}$; $\mathbf{V}_2 \neq \mathbf{0}$; $\lambda \neq 0$.

Using the quantities a, b, c, and β calculated by the formulas (14), we determine the parameter λ and the vector $\hat{\mathbf{G}}_2$ from (13). Then we find, according to (11) and (12), the scalars μ_2, $\dot{\mu}_2$ and the vectors $\mathbf{q}_2^*$, $\dot{\mathbf{q}}_2^*$ that uniquely determine the intermediate orbit. From (9) we obtain the vectors $\mathbf{Z}_2$, $\dot{\mathbf{Z}}_2$, and $\ddot{\mathbf{Z}}_2$ that specify the position of the fictitious centre (5).

Introduce the transformations of coordinates and time of the form

$$\mathbf{u} = \frac{\mu}{\mu_2}\mathbf{q}^*; \quad d\theta = \left(\frac{\mu}{\mu_2}\right)^2 dt. \tag{15}$$

Then the solution of the equations of intermediate motion (7) are reduced to solution of the following system of equations:

$$\mathbf{u}'' = -\frac{\mu_2}{|\mathbf{u}|^3}\mathbf{u}\,; \quad t' = \left[1 - \frac{\dot{\mu}_2}{\mu_2}(t - t_2)\right]^2. \tag{16}$$

Here, the prime denotes the differentiation with respect to the new independent variable θ (fictitious time).

For the specified instant t of physical time we calculate the fictitious time θ by the formula

$$\theta = \frac{\mu}{\mu_2}(t - t_2). \tag{17}$$

Next, at the calculated instant θ the position vector $\mathbf{u}$ and the velocity vector $\mathbf{u}'$ of the small body in the intermediate orbit in $\mathbf{u}$ — space are determined by the formulas of the classical two-body problem in accordance with the first equation from (16):

$$\mathbf{u} = f\mathbf{u}_2 + g\mathbf{u}_2'\,; \quad \mathbf{u}' = f'\mathbf{u}_2 + g'\mathbf{u}_2'. \tag{18}$$

The functions f, g, f', and g' are defined by the well-known expressions [2]. The initial conditions referred to the instant $\theta = 0$ are given by

$$\mathbf{u}_2 = \mathbf{q}_2^*\,; \quad \mathbf{u}_2' = \frac{\dot{\mu}_2}{\mu_2}\mathbf{q}_2^* + \dot{\mathbf{q}}_2^*. \tag{19}$$

Finally, the transformations

$$\mathbf{q}^* = \frac{\mu_2}{\mu}\mathbf{u}\,; \quad \dot{\mathbf{q}}^* = \frac{\mu}{\mu_2}\mathbf{u}' - \frac{\dot{\mu}_2}{\mu_2}\mathbf{u} \tag{20}$$

enable us to find respectively the position and velocity vectors of the small body in the intermediate orbit relative to the fictitious centre in the physical space at the moment of time t. The position and velocity vectors of the small body in the intermediate orbit in the initial coordinate system are determined from the formulas:

$$\mathbf{x}(t) = \mathbf{Z}_2 + \dot{\mathbf{Z}}_2(t - t_2) + 0.5\ddot{\mathbf{Z}}_2(t - t_2)^2 + \mathbf{q}^*(t)\,; \tag{21}$$

$$\dot{\mathbf{x}}(t) = \dot{\mathbf{Z}}_2 + \ddot{\mathbf{Z}}_2(t - t_2) + \dot{\mathbf{q}}^*(t). \tag{22}$$

At $t = t_1$, t_3, according to (21) and (22), we may obtain

$$\mathbf{x}_j = \mathbf{Z}_2 + \dot{\mathbf{Z}}_2(t_j - t_2) + 0.5\ddot{\mathbf{Z}}_2(t_j - t_2)^2 + \mathbf{q}_j^*\,;$$

$$\dot{\mathbf{x}}_j = \dot{\mathbf{Z}}_2 + \ddot{\mathbf{Z}}_2(t_j - t_2) + \dot{\mathbf{q}}_j^*, \tag{23}$$

where, in view of (20),

$$\mathbf{q}_j^* = \frac{\mu_2}{\mu_j}\mathbf{u}_j\,; \quad \dot{\mathbf{q}}_j^* = \frac{\mu_j}{\mu_2}\mathbf{u}_j' - \frac{\dot{\mu}_2}{\mu_2}\mathbf{u}_j, \quad j = 1, 3. \tag{24}$$

The position and velocity vectors of the small body in the parametric space of variables $\mathbf{u}$ and the fictitious time instants corresponding to these vectors at $t = t_1$, t_3 are determined, according to (18) and (17), by the formulas

$$\mathbf{u}_j = f_j \mathbf{u}_2 + g_j \mathbf{u}_2'; \quad \mathbf{u}_j' = f_j' \mathbf{u}_2 + g_j' \mathbf{u}_2'; \quad \theta_j = \frac{\mu_j}{\mu_2}(t_j - t_2), \quad j = 1, 3. \quad (25)$$

We represent the vectors $\mathbf{u}_2$ and $\mathbf{u}_2'$ included in (8), in accordance with (19) and (9), in the form

$$\mathbf{u}_2 = \mathbf{x}_2 - \mathbf{Z}_2; \quad \mathbf{u}_2' = \frac{\dot{\mu}_2}{\mu_2}(\mathbf{x}_2 - \mathbf{Z}_2) + \dot{\mathbf{x}}_2 - \dot{\mathbf{Z}}_2. \quad (26)$$

We substitute expression (23) into (4), on account of (24)–(26). Then we obtain a system of six equations with respect to the six unknown components of the vectors $\mathbf{x}_2$ and $\dot{\mathbf{x}}_2$. Solving this system using an appropriate iterative procedure (for example by the Newton–Raphson method) with accepted initial approximation we can define more accurate values of the vectors $\mathbf{x}_2$ and $\dot{\mathbf{x}}_2$. The process of construction of the intermediate orbit by means of the suggested algorithm is repeated until the prescribed accuracy of calculation is achieved.

Methods of obtaining the initial estimates of the vectors $\mathbf{x}_2$ and $\dot{\mathbf{x}}_2$ one can find in the book [3].

Conclusions

In the present study, we proposed a new method for construction of the preliminary orbit of a small celestial body from three pairs of range and range rate measurements and the corresponding time instances. According to [1], the degree of approximation to the real motion by the constructed orbit in the neighborhood of the reference epoch t_2 is three orders higher than by the Keplerian orbit determined by traditional methods.

Acknowledgements

The work was supported by the Russian Foundation for Basic Research (project number: 08-02-00359-a).

References

1. *Shefer V. A.* Superosculating intermediate orbits: fouth- and fifth-order tangencies to trajectories of perturbed motion // Astron. Lett. 2006. Vol. 32. P. 845–858.
2. *Escobal P. R.* Methods of Orbit Determination. New York–London–Sydney: John Wiley and Sons, 1965.
3. *Baker R. M. L. Makemson M. W.* An Introduction to Astrodynamics. New York: Academic Press, 1967.

SMALL BODIES OF THE SOLAR SYSTEM

Improving the Orbital Parameters of Phobos and Deimos by Using the Universal Programming Complex ERA

M. D. Zamarashkina

Institute of Applied Astronomy of RAS, St. Petersburg, Russia

Abstract. The present paper is the first stage of our study of Martian satellite dynamics. The ERA system was used for developing the numerical dynamical theory of Phobos and Deimos. The database of the observations of different types was constructed in the form of ERA tables. At present the main features of the model are realized in the framework of the ERA system. Our results are in good agreement with those obtained by other authors. A further development of the theory (for example, inclusion of the secular acceleration) and expansion of the database of the satellites observations is assumed.

For calculating ephemerides of celestial bodies it is possible to use the available programs developed in the different astronomical organizations (JPL, SAI/IMCCE, IAA RAS etc.). The basic deficiency of such systems under a variety of their functions is the limitation in the area of solving problems. In IAA RAS the universal programming system ERA (Ephemeris Research in Astronomy) [1] was created. The ERA system allows one to solve the problems from a wide range of applications in ephemeris and dynamical astronomy. For convenience to users a compact and easy-to-learn interface was constructed. ERA is realized as a programming system based on using a specialized, high level language SLON. In the present paper the dynamical model of the motion of Martian satellites (Phobos and Deimos) is considered. A database of the satellites' observations was constructed. The database was presented in the universal table form adopted in the package. Such tables are specific feature of the SLON language. The dynamical models are embedded into the ERA package for a large number of celestial bodies.

In particular, for Phobos and Deimos, the analytical theory ESAPHO [2] is embedded.

In this work the original numerical dynamical theory of Phobos and Deimos was constructed by using the ERA system. The scheme of this process is presented below.

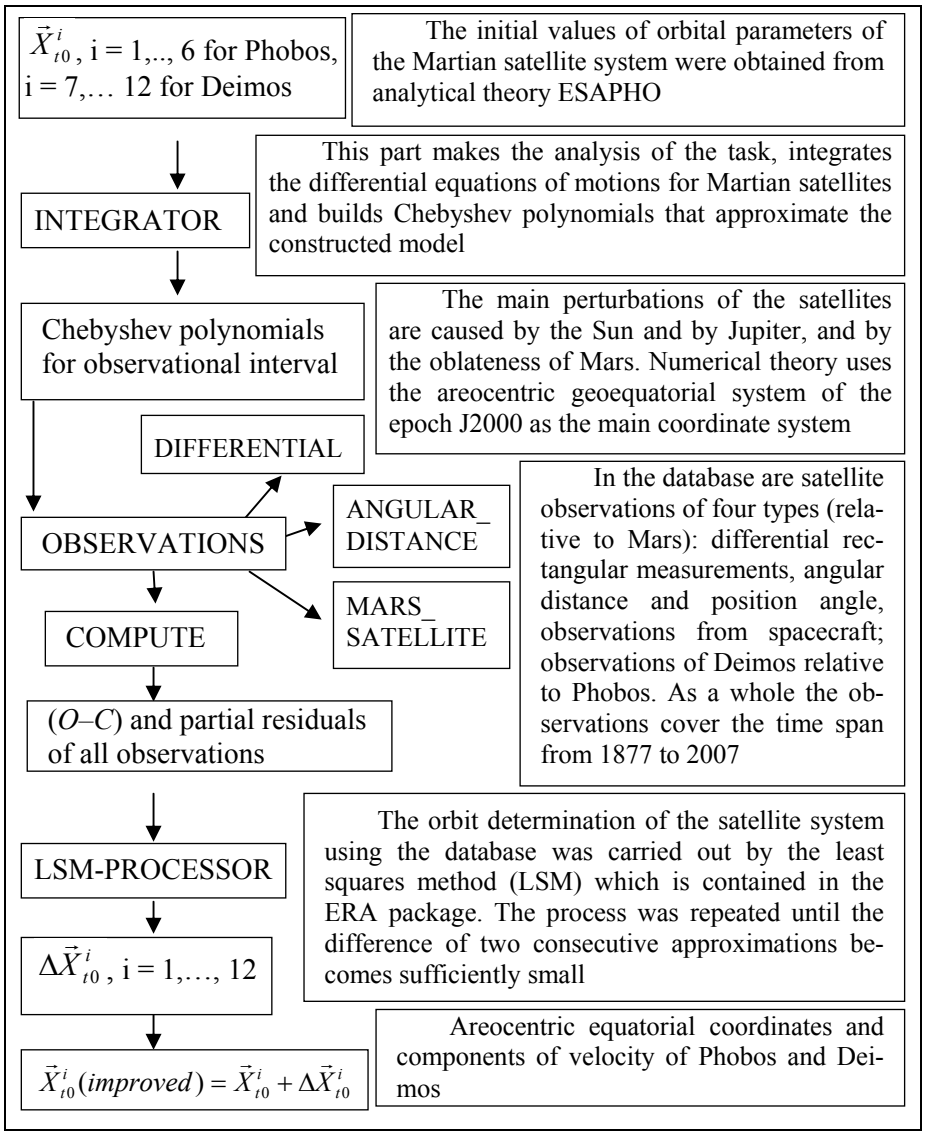

Block-scheme of processing Phobos and Deimos observations in the ERA system.

The list of the observations utilized in this study includes 8079 observations of all four types and covers the time span 1928–1988. The standard derivation of residuals is equal 0″.77.

The sets of the orbital parameters of Phobos and Deimos obtained by different authors are given in the Table. As can be seen from this Table, the orbits of Martian satellites constructed by using the ERA system are in the good agreement with analogous results of other authors.

Coordinates and components of velocities of Martian satellites

x, km	y, km	z, km	$\dot{x}$, km/s	$\dot{y}$, km/s	$\dot{z}$, km/s	Author
(T_{epoch} = 2447558.50 TDB = 1989–Feb–01)						
Phobos						
–3682.655	**6640.434**	**5268.697**	**–1.72295**	**–1.26184**	**0.37093**	**ERA***
–3622.256	6583.690	5372.588	–1.732944	–1.25540	0.35633	2
–3628.648	6620.922	5328.077	–	–	–	3
–3722.325	6543.083	5356.358	–1.71994	–1.27489	0.34793	4
–3626.170	6611.965	5336.648	–1.73115	–1.25205	0.36436	6
–3627.542	6613.507	5338.031	–1.730978	–1.25509	0.36407	6
–3722.445	6540.972	5356.169	–1.720039	–1.27525	0.34823	7
Deimos						
19510.999	**12086.242**	**–4883.707**	**–0.460258**	**1.03836**	**0.73118**	**ERA***
19677.440	11768.270	–4973.596	–0.43775	1.04388	0.73755	2
19588.890	11953.094	–4913.510	–	–	–	3
19554.827	12011.724	–4883.399	–0.45379	1.03796	0.73601	4
19585.017	11948.220	–4917.534	–0.450144	1.04041	0.73479	5
19592.464	11946.352	–4908.496	–0.450115	1.04037	0.73487	6
19559.043	12009.991	–4874.412	–0.453925	1.03796	0.73583	7

*Results obtained by the author of present paper.

References

1. *Krasinsky G. A., Vasiliev M. V.* ERA: knowledge base for ephemeris and dynamical astronomy // Proc. of IAU Coll. 1996. 165. P. 239–244.
2. *Chapront-Touze M.* Orbits of the Martian satellites from Esapho and Esadei theories // Astron. and Astrophys. 1990. Vol. 240. P. 159–172.
3. *Sinclair A. T.* The orbits of the satellites of Mars determined from Earth-based and spacecraft observations // Astron. and Astrophys. 1989. Vol. 220. P. 321–328.
4. *Kudryavtsev S. M. et al.* New Analytical Theory of Motion of Phobos and Deimos for Navigation Support of Mission to Mars // Proc. of the 12th Int. Symp. on Space Flight Dynamics. 1997. P. 377–382.

5. *Jacobson R. A.* Ephemerides of the Martian Satellites— MAR080 // JPL IOM 343R–08–006. 2008.
6. *Emelyanov N. V. et al.* The dynamics of Martian satellites from observations // Astron. and Astrophys. 1993. Vol. 267. P. 634–642.
7. *Lainey V. et al.* First numerical ephemerides of the Martian moons // Astronomy and Astrophys. 2007. Vol. 465. P. 1075–108.

SMALL BODIES OF THE SOLAR SYSTEM

Databases for Observations and Orbit Elements for Asteroids and Comets in ERA System

E. I. Yagudina

Institute of Applied Astronomy of RAS, St. Petersburg, Russia

Abstract. The programming system ERA (Ephemeris Research in Astronomy) has been developed in IAA RAS to support scientific research in ephemeris and dynamical astronomy as well as for aims of astronomical education. The main feature of the system is its versatility: user not limited by a predefined set of ephemeris tasks but easily develops his/ her applications practically in any branch of positional astronomy. In the frame of the ERA system, a user has easy access to an embedded universal package to process high precision observations of Solar System bodies, including those that are hazardous for humanity, such as NEAs and comets. In the present paper the databases for both observations and elements of asteroids and comets in the ERA system are described, as well as examples of the orbit determination and the processing of observations for these objects. The peculiarities of computations are described and examles of usage of the ERA system for orbit determination are presented.

A brief description of the main concept of the ERA system

The ERA system [1] has its special language (problem-oriented language SLON). SLON is the language of a relational type, i. e., a database management system with data in the form of tables ("relations") is embedded into the language. SLON compiler automatically calls subroutines of the universal applied program package to compute observables and to confront them with observations for analyzing the residuals and estimating parameters of the mathematical model. In the ERA system, data (observations of objects, elements of initial orbits, coordinates of observational stations from different sources, such as MPC and others) have been transformed into special forms (tables), which are the databases within the ERA system. Different kinds of tables such as tables of observations of asteroids (optical and radar), that of elements of asteroids and periodic comets, have already been

described briefly [2]. In the present paper a table of comet observations is shown and a description how to use ERA tables for orbit improvement is given. As an example of a ERA table the table for comet observations is shown in Table.

Table of comet observations

Comet number	Date of observation, calendar date	Right ascension, hms	Declination, dms	Station Number
1	18350821.000556832	00 50 55.800	23 32 53.30	75
1	.....	.....	.....	.....
2	18810826.014834560	04 02 14.370	33 31 38.50	522
2	.....	.....	.....	.....
164	20050117.002408064	11 04 28.430	27 08 59.40	48
164	.....	.....	.....	.....
164	20050220.003857120	10 38 16.680	32 37 35.80	170

In the last column of the table the numbers of observational stations according to ERA catalog are given. The catalog includes all stations that were once used for processing of observations.

For the ERA system the elements of comets taken from MPC have been transformed into corresponding coordinates (to be used directly for orbit determination) and so the data in the relevant ERA table are the following: name of a comet as in MPC, all previous apparitions of the comet, the moment of perihelion passage in each apparition, time-scale, the coordinates and velocities at epoch, the non-gravitational parameters given in Marsden–Sekanina form, epoch of osculation of the comet elements, proper name of comet.

To calculate the orbit of any comet, it is necessary either to write a simple program in SLON language (in Manual of the ERA system there is built-in HELP that includes a large number of source code examples), or to use a bat-file for orbit determination of any comet in the database of the ERA system. The first program of bat-file from table of elements reads the line with initial values of coordinates and velocities of the comet identified by number or by name. Then the program writes the data into the corresponding table ("initial.sln"). This table is used in the program of integration for calculation of *O–C* for all observations of the comets included into the ERA tables ("orbit.sln"). The corrections to coordinates and velocities of the comet and to non-gravitational parameters are determined by the least-squares method ("orbit.lsm"). During the work of the LSM procedure the graphs of the residuals in right ascentions and declinations can be obtained. After introducing

the corrections into the initial coordinates and velocities the integrations are repeated and comparisons with observations are made again. Iteration process continues till corrections to the evaluated parameters become small (smaller than one tenth of the mean square error) ("cor.sln"). The order of usage and titles of programs involved in bat-file are shown in brackets. The final result — the improved values of coordinates and velocities at definite epoch and corrections to non-gravitational parameters are recorded into the initial table of elements (coordinates) of the comet.

Conclusion

In conclusion one can emphasize the following. Language of the ERA system SLON is a high level language whose lexicon is very close to the standard astronomical terminology. The available LSM package can process large systems of equations with several hundreds of unknowns. Therefore the package is suitable for the orbit determination of the different Solar System objects, including comets and asteroids, with high accuracy.

In the current state the ERA system is used in standard DOS-version. A 32-bit version of the system for two operational systems, Windows and LINUX, is now being developed.

The Manual with embedded HELP is available at FTP address:

FTP://quasar.ipa.nw.ru/incoming/era .

On the page one can find the file "era_manual.ps" with Manual of ERA and file "dirinfo" where users can read instructions how to install ERA system.

References

1. *Krasinsky G. A., Vasiliev M. V.* ERA: knowledge base for ephemeris and dynamical astronomy / Eds Wytrzyszczak et al. // Proc. of IAU Colloquium 165, Poznan, Poland, July 1–5, 1997. P. 239–442.
2. *Yagudina E. I.* Database of comet observations and determination of comet orbits using ERA system // Materials of the conf. "Aseroid-Comet hazard-2005" (ACH-2005). 3–7 October 2005. St. Petersburg. P. 359–361 (In Russian).

PART 2. OBSERVATION AND DETECTION OF NEOS

OBSERVATION AND DETECTION OF NEOS

Automatic Detection of NEOs in CCD Frames

A. L. García [1,2]

[1]Astronomy and Astrophysics Department of Valencia University, Valencia, Spain
[2]Astronomical Observatory, Valencia, Spain

Abstract. Detection of transient phenomena is of great interest in many astronomical projects. CCD frames obtained with modern telescopes with robotic operation allow carrying out standard observation programs for detection of peculiar objects on stellar backgrounds, as is the case of Near Earth Objects (NEOs).

Valencia Observatory new telescope TROBAR (altazimutal 60 cm Ritchey-Cretien telescope) placed at University of Valencia astronomical station will be operated from Valencia headquarters and an automatic detection programs will be carried out with several CCD devices [1].

In this paper, we present original algorithms for automatically detecting dim NEO images in telescope frames, considering both sidereal and differential tracking [2]. In both cases, detection can be done from peculiar characteristics of a NEO image or from the comparison of two frames of the same stellar zone.

Algorithms and codes are based on the previous experience of the author in minor planet astrometry with CCD images at Valencia Observatory since 2001 and in differential tracking applied to photographic plates at La Silla in 1992. Peculiar algorithms have been developed for several kinds of images [3, 4].

Visual Basic platform is used. "Masks" or "filters" are not applied and algorithms are original, robust and fast.

This work can be applied to automatic detection of transient phenomena with different equipments and under different conditions, introducing small modifications to the algorithms and adapting them.

Introduction

Instrumentation and techniques

Valencia Observatory has new telescopes (TROBAR, altazimutal 60 cm Ritchey-Cretien and 40 cm Schmidt-Cassegrain) placed at Valencia astronomical station 110 km from the city at a high plateau. Both telescopes will be applied to automatic detection of NEOs with several CCD devices [1].

In this paper we present our results on development of detection algorithms and their application to NEO observations. Both sidereal and differential tracking techniques are considered [2].

Observations

Three NEOs were observed (2004 XJ3, 2005 NJ63 (Fig. 1) and 2006 WN1) on June 26–27, 2009 with 40 cm Schmidt–Cassegrain (f 10) telescope and CCD Apogee USB Net of 2049 × 2049 (2x binning). 30, 70 and 15 exposures of 120 seconds have been obtained, with sidereal and differential tracking. Observations were prepared using MPC Ephemeris Service.

Automatic detection

Identification by sweeping

First step consists in the detection of field objects by sweeping along pixels columns and files. After a "bright" pixel is detected, object contour is obtained and "bottom" value is assigned to pixels inside the contour (Fig. 2). Object center and "radius" are stored and the sweeping process continues until the entire CCD field is analyzed.

Fig. 1. 2005 NJ63 zoom detail.

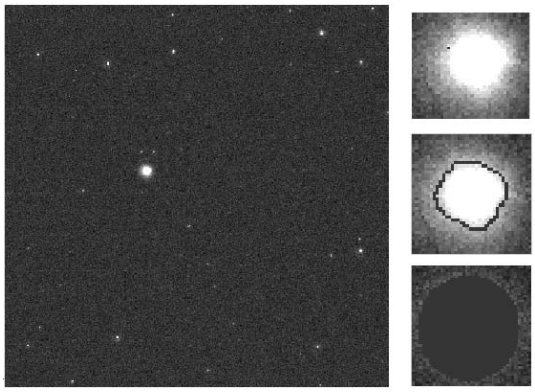

Fig. 2. Details of sweeping.

NEO detection vs. tracking system

In the case of **sidereal tracking** two methods can be applied:

1) in the first method we try to distinguish an NEO's elongated image from round star images. After the objects are detected, a parameter related to the image's shape is used to distinguish the NEO images from field star images;

2) when the NEOs and stars images are similar, two similar frames of the same field obtained in a sufficient time interval must be compared.

When **differential tracking** is used, similar methods can be used:

1) in some cases, elongated star images will be distinguished from NEO images as in the previous first method;

2) in general, comparison of two similar frames will be the selected method.

Single frame analysis

Model construction in differential tracking.

An object's aspect depends on several factors: exposure time, NEOs proper motion, tracking quality, and object magnitude. To define an "object model" can be very useful before object detection by sweeping.

To construct an object model several objects are selected, corresponding to stars with different magnitudes. Several image parameters are obtained and fitted versus big diameter (Fig. 3). Slope and image elongation are considered constant parameters of the model.

When sweeping is applied, "normal" images can be eliminated applying the corresponding model. "Peculiar" images (NEOs and spurious images) are analyzed one by one and assigned to their categories.

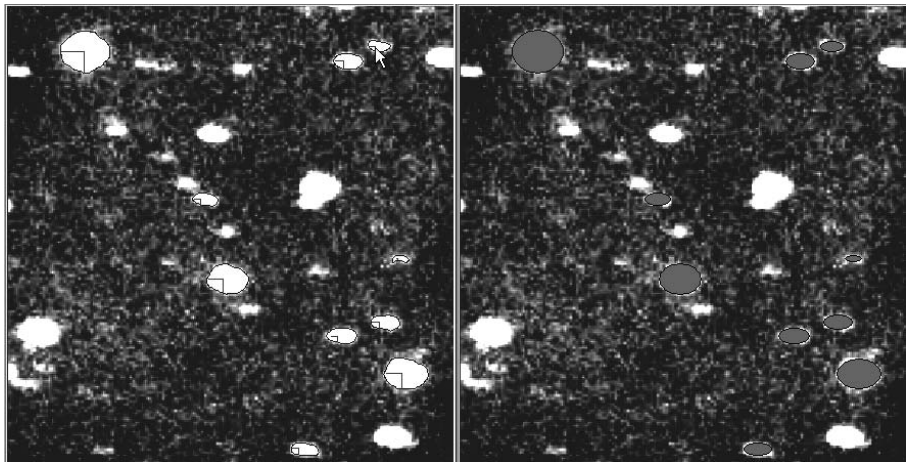

Fig. 3. Model construction and image elimination.

A more physical model is composed of an alongated gaussian image plus two semicircular gaussian images in both sides.

Model application in complex images

In crowded fields or when NEO image is close to a star image the solution is more difficult. Before eliminating an image, we must deduce the real size and shape of the object from model data.

Our algorithm detects and eliminates every object, trying not to disturb the remaining images in the group. The process is repeated until all objects are considered in the field [3].

Singular objects like NEOs are detected through its peculiar shape.

Two frames comparison

This method is applied to sidereal and differential tracking when no differences between stars and NEO images are presented [4]. Main steps are:

Images detection

Sweeping process is applied to both frames (working and reference). Only bright objects are detected and their coordinate centers are stored.

Triangles identification

Two equivalent triangles are detected in both frames in order to eliminate rotation and scale change between them.

If automatic detection fails, vertices are selected by hand. Although the first method is not as robust as the second one, it must be preferred in the case of full automatic detection.

Working field reconstruction

Working field is reconstructed from reference frame, applying linear transformation parameters obtained by fitting both triangles.

NEO's identification

For the identification of single objects (moving NEO with respect to fixed stars), two methods can be applied.

Fields blinking

Optical blinking devices were used in the past for photographic plates.

Both frame images are displayed alternatively on the computer screen and moving objects are detected easily.

Fields subtraction

When we need an automatic analysis of both plates (detection of new NEOs, RGB, novae or supernovae) prior to an accurate study of each frame, a good solution is to "substract" working and reference frames, giving as a result a "difference" image of working and reference frames. Algorithm detects small "real" differences, but spurious objects appear also in final image (Fig. 4).

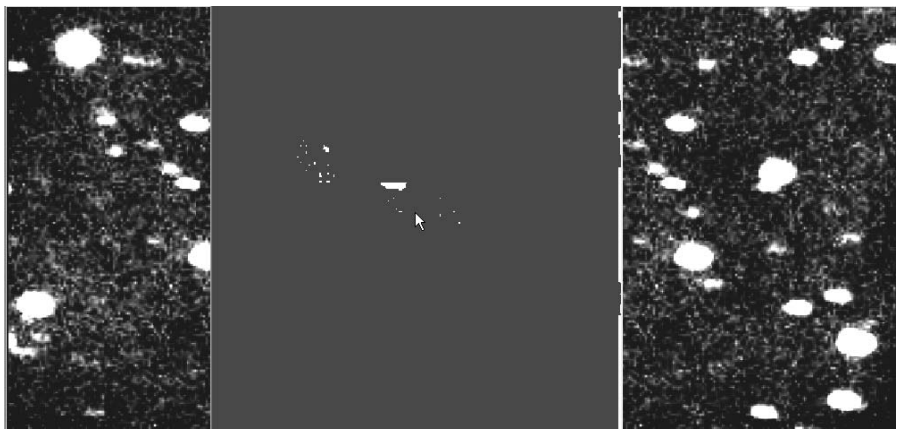

Fig. 4. Working, difference and reference frames.

Frame measuring process

Automatic measuring of NEOs can be done in the same way as in the case of other asteroid frames. Main steps are the following:

Frame image and catalogue map comparison

CCD frame and zone map from stellar catalogue are presented on screen.

Searching process in selected windows

Operator can select one or several windows for sweeping. In this way, frame zones with defects can be avoided. After object's detection by sweeping, single objects can be detected one by one.

Objects identification in CCD frame and in stellar map

Three frame objects and corresponding map stars are selected by hand. Fitting of both sets of coordinates allows observer to identify frame objects with map stars.

Object coordinates and magnitude

When the previous process is ended, the object image is marked by a click and corresponding coordinates and magnitude are found (Fig. 5).

Checking of results

Object coordinates can be checked in real time. Stored values are compared with integrated coordinates for the epoch of observation. Residuals in right ascension and declination less than a few seconds of arc are accepted.

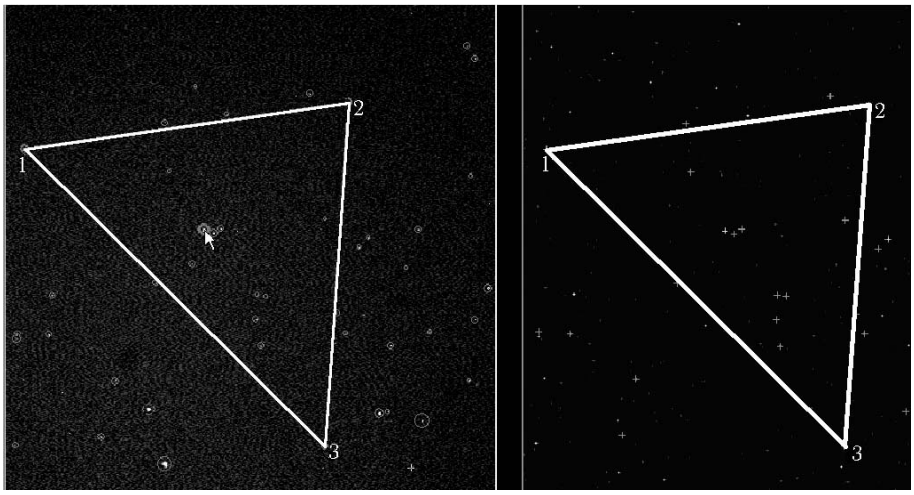

Fig. 5. Object identification in CCD frame (left) and in stellar map (right).

References

1. *Lopez A*. *et al.* Photographic and CCD Observations of Minor Planets from Valencia Observatory // Proc. of "Workshop Ceres 2001". Paris, 2001. IMCCE, 2004. P. 81–86.
2. *Lopez A*. Automatic detection of transient phenomena in Solar System observations // Proc. of "Mutual Events of the Uranus' satellites in 2007–2008 and further observations in network". Paris, 2006. IMCCE, 2008. P. 63–70.
3. *Lopez A*. *et al*. Observaciones CCD de asteroides y planetas // Proc. of "Jornadas Científicas 250 años de Astronomia en España 1753–2003". San Fernando, Cádiz. 2003. Published by Centro de Ayudas a la Enseñanza de la Armada. 2004.
4. *Lopez A*. Minor Planet Astrometry with CCD Frames // Proc. of "Astrometry in the Age of the Next Generation of Large Telescopes". Flagstaff, AZ. USA. 2004. ASP Conference Series. 2005. Vol. 338. P. 111–117.

OBSERVATION AND DETECTION OF NEOS

YORP: Influence on Rotation Rate

A. A. Golubov[1], Yu. N. Krugly[2]

[1]Astronomisches Rechen-Institut of University of Heidelberg, Heidelberg, Germany
[2]V. N. Karazin Kharkiv National University, Kharkiv, Ukraine

Abstract. We have developed a semi-analytical model for calculating angular acceleration of asteroids due to Yarkovsky–O'Keefe–Radzievskii–Paddack (YORP) effect. The calculation of the YORP effect has been generalized for the case of elliptic orbits. It has been shown that the acceleration does not depend on thermal inertia of the asteroid's surface. The model was applied to the asteroid 1620 Geographos and led to acceleration $2 \cdot 10^{-18}$ s^{-2}. This value is close to the acceleration obtained from photometric observations of Geographos by Durech et al. [1].

Introduction

Thermal radiation by a surface of an irregular shaped object results in a torque that may secularly affect both the rotation frequency and the obliquity of the spin axis [2]. This effect called YORP is interesting for several reasons. It has implications on the statistical distribution of rotation periods of small asteroids. It is thought to be responsible for formation of close binaries as product of rotational fission. Another very important implication of the YORP effect is related to the Yarkovsky orbital effect, which leads to an opposite orbital effect when the asteroid's prograde spin is changed to the spin rotation.

In this paper we concentrate on angular component of the YORP torque, omitting studying of obliquity changes. Such a consideration has two reasons. The first reason is observational. Angular acceleration of asteroids by the YORP has already been detected in photometric observations, while attained precision is by far insufficient to observe a change of obliquity. The second reason is theoretical. In contrast to obliquity component, angular component does not depend on thermal properties of the asteroid's surface that allows using different methods for its consideration.

Analytical model

We have developed a theoretical model of the YORP torque that is based on the following assumptions.

1. Lambert law is used to express an isotropic thermal emission from the asteroid surface, which is a simplification of properties of a real object. This law is also applied for scattered light.
2. We consider a convex shape of the asteroid.
3. Thermal energy is conserved under a surface element. So, there is no heat exchange between different surface elements.
4. The asteroid is in principal-axis rotation state.

Recoil force acting on a surface element *dS* is given by expression

$$df = -2LdS/3c, \tag{1}$$

where *L* is power emited by unit surface, *c* is speed of light, and factor 2/3 is due to accepted Lambert's indicatrice.

To obtain an influence of YORP effect on long-term spin dynamics of the asteroid we must average the torque (1) for a surface element over time and integrate the average torque over the surface. The first step can be done analytically, yielding to the following expression for the average YORP torque acting on the asteroid relative to its spin axis

$$\langle M_z \rangle = \frac{2\Phi_0 R_0^2}{3ca^2\sqrt{1-e^2}} \int_S f\left(\psi(\vec{r}),\varepsilon\right) \left[\vec{r}\times\vec{e}_z\right] d\vec{S}. \tag{2}$$

Here Φ_0 is light flux of solar radiation at the sun-asteroid distance $R_0 = 1$ AU, a is the semi-major axis of the asteroid's orbit, e is the orbit's eccentricity, ε is obliquity of the asteroid's equator to its orbital plane, $\psi = \pi/2 - \angle(\vec{r},\vec{e}_z)$ is latitude, $\vec{r}$ is a radius vector going from center of gravity of the asteroid to the surface element $d\vec{S}$, $\vec{e}_z$ is unit vector of the asteroid rotational axis. Integration is done over the entire asteroid's surface. Function f is given by

$$f(\psi,\varepsilon) = \frac{1}{\pi^2}\int_0^{\pi} d\phi \sqrt{1-\left(\cos\phi\cos\psi\sin\varepsilon - \sin\psi\cos\varepsilon\right)^2}. \tag{3}$$

The function f can be called the latitude factor because of its dependence on latitude ψ. The function is universal for any shape of the asteroid and can be calculated numerically.

By the way we must mention two important points. Firstly, the average torque does not depend on surface thermal properties. Secondly, we consider a general case of elliptic orbits, and the eccentricity naturally appears in formula (2).

Application to asteroid 1620 Geographos

Our YORP model can be applied to asteroids that have numerical models of the shapes. There are three sources that give such models. Firstly, shapes can be obtained by photometric techniques. Usually an ellipsoidal shape model was used to describe an asteroid's shape. But recently the model of arbitrary shape obtained by lightcurve inversion becomes the most commonly used. The method was developed by Kaasalainen and collaborators [3–6]. Secondly, in case of an asteroid's close approach to the Earth (near-Earth asteroid) radar observations are carried out. This allows constraining asteroids' shapes (radar models). Thirdly, we know shapes of several asteroids from a few spacecraft missions.

We used our analytical model for the YORP torque calculation. We created a computer program and applied it to the photometric model of the asteroid 1620 Geographos, whose spin rate increase has already been measured in analysis of the photometric observations [1]. In this paper observational data for the asteroid could be interpreted only in model, which included gradual increase of rotational period. Shape model for Geographos was also obtained in [1] by method of lightcurve inversion [3, 4]. Three projections of this shape model are presented in Fig. 1.

We used this model for our calculations. The YORP acceleration for Geographos-shaped body as a function of obliquity is presented in Fig. 2. Solid curve shows results of our program for different obliquities. Black square is observational result [1]. Vertical error bars correspond to observational errors, horizontal error bars — to uncertainty in obliquity of Geographos. Black triangle marks the result of numerical simulation in [1].

Our YORP torque calculations for Geographos demonstrate a good agreement with observations that allows using it to predict the YORP acceleration of asteroids with known shapes and for numerical experiments with synthetic shapes. It is also in agreement with YORP calculations in [1].

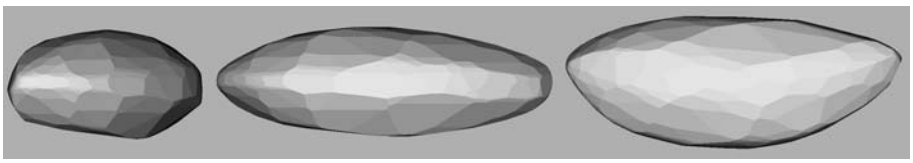

Fig. 1. Shape model of the asteroid 1620 Geographos.

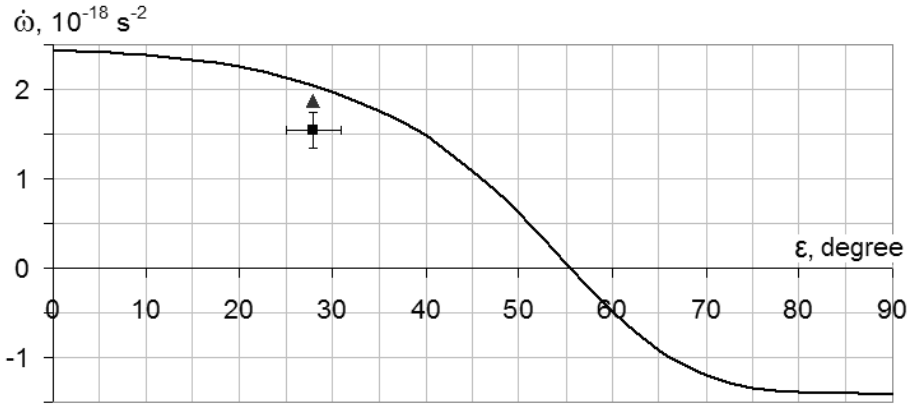

Fig. 2. YORP acceleration of Geographos as function of its obliquity.

Discussion and concluding remarks

Consideration of absorption and re-emission of solar light by an asteroid surface allows one to evaluate the recoil force, which defines changing of the asteroid's orbit (Yarkovsky effect) [7] and rotational properties, i. e. rotational velocity and obliquity (YORP effect) [2]. We give an analytical expression for the calculation of influence of the YORP on asteroid's rotation rate. The calculation of YORP effect is generalized for the case of elliptic orbits. Influence of YORP effect on rotation rate of asteroid is shown to not depend on thermal inertia of its surface.

Application of YORP calculations to shape model of the asteroid 1620 Geographos demonstrates a good agreement with the value of YORP acceleration obtained from photometric observations during time interval from 1969 to 2008 [1].

Our program can be used for predictions and numerical experiments. The same method of averaging over time and then integrating the result over the surface can be used to get an analytical formula for obliquity component of YORP. In this case thermal inertia is important and a heat model of the surface is needed. It makes the problem more complex, but if done gives an opportunity to study self-consistently asteroid's rotational state evolution in phase plane $\omega - \varepsilon$. Understanding of such an evolution can be thought of as the main aim of the YORP studying.

YORP is an important factor of NEAs evolution. Firstly, it can accelerate spin rates of asteroids, induce their decay, and therefore form distribution of asteroids over sizes. Secondly, when YORP changes spin rate of an asteroid and its spin axis orientation, it influences drift of main belt asteroids induced by Yarkovsky effect. So it appears to be an important factor that affects a number of NEAs. Thus, YORP effect comprehension is crucially

important to explain the size distribution and the number of NEAs, and it should be taken into account for prognosing evolution of NEA population. The YORP effect can be mentioned as one of factors that can be used for long-term defense of the Earth from dangerous asteroids.

References

1. *Durech J., Vokrouhlicky D., Kaasalainen M., Higgins D. et al.* Detection of the YORP effect in asteroid (1620) Geographos // Astron. Astrophys. 2008. Vol. 489. L25–L28.
2. *Rubincam D. P.* Radiative spin-up and spin-down of small asteroids // Icarus. 2000. Vol. 148. P. 2–11.
3. *Kaasalainen M., Torppa J.* Optimization methods for asteroid lightcurve inversion. I. Shape determination // Icarus. 2001. Vol. 153. P. 24–36.
4. *Kaasalainen M., Torppa J.* Optimization methods for asteroid lightcurve inversion. II. The complete inverse problem // Icarus. 2001. Vol. 153. P. 37–51.
5. *Kaasalainen M., Torppa J., Piironen J.* Models of twenty asteroids from photometric data // Icarus. 2002. Vol. 159. P. 369–395.
6. *Durech J., Kaasalainen M.* Photometric signatures of highly nonconvex and binary asteroids //Astron. Astrophys. 2003. Vol. 404. P. 709–714.
7. *Chesley S. R., Ostro S. J., Vokrouhlický D., Čapek D. et al.* Direct Detection of the Yarkovsky Effect via Radar Ranging to Asteroid 6489 Golevka // Sci. 2003. Vol. 302. P. 1739–1742.

OBSERVATION AND DETECTION OF NEOS

The Small Libration of the Satellite in the System of the Asteroid 39 Laetitia

Yu. V. Batrakov[1], V. V. Prokofjeva-Mikhajlovskaya[2], L. G. Karachkina[2]

[1]Institute of Applied Astronomy of RAS, St. Petersburg, Russia
[2]Scientific Research Institute Crimean Astrophysical Observatory, Nauchny, Ukraine.

Abstract. Observations of asteroids at the Crimean astrophysical observatory (CrAO) were conducted since the 1980s. The Maksutov 50-cm telescope and TV installation were used, allowing to automate the process of observation. Brightness of asteroid was investigated in VBR bands simultaneously. The resulting light curves are processed on a computer by the method of frequency analysis, which reveals the hidden periodicity of changes of asteroid brightness. According to the observations of the asteroid brightness of 39 Laetitia at CrAO it was confirmed that this asteroid is a binary. The satellite orbital period of the binary system of 39 Laetitia and the period of axial rotation of components have been identified with the observed frequencies. In this paper we assume that the satellite has not yet fully stabilize its orientation with respect to its orbital radius vector and there is residual libration in the orbital plane with a small amplitude. The first six harmonics of the expansion of the gravitational potential of the satellite were taken into account. Emerging from their influence the theoretical values of the libration period due to these harmonics were compared with those obtained from observations by frequency analysis of light curves.

It was proven that there is a sufficiently close match with one of the periods obtained by frequency analysis of light curves. This circumstance can be seen as confirmation of the hypothesis of the existence of small libration of the satellite in the binary system of 39 Laetitia. The dynamics of this binary system deserves a more complete study.

Introduction

Binary asteroids attract increasing attention by astronomers since their percentage in the total number of asteroids is not too small. All structural peculiarities of the ring of asteroids and even the group of the near Earth asteroids have binary asteroids. Binary asteroids deserve much more attention than single ones from the point of view of asteroid hazard. Protection of the Earth from a binary asteroid is a more complicated task than from a single asteroid. So, study of dynamic characteristics of double and multiple asteroid systems is a highly topical scientific task.

Observation of asteroids have been conducted at the CrAO since the 1980s. The Maksutov 50 cm telescope with a TV installation was used for observations. Observations are conducted simultaneously in three bands (VBR), the sensitivity of the installation is up to 20^m, accuracy is up to $0.1–0.2^m$. Frequency analysis of light curves gives reliable values for the frequencies corresponding to the orbital motion of the asteroid and axial rotation of satellite components. But apart from these fundamental frequencies analysis provides a whole range of other frequencies. Their identification with certain features of the dynamics of the asteroid can be very difficult, as it is necessary to have a fairly complete theory of component motions and the characteristics of the surface structure of the asteroid.

We assume in this paper that the satellite in the asteroid 39 Laetitia system fluctuates around its axis of inertia, whose direction is normal to the plane of the satellite's orbit, deviating from the radius vector of the direction from main component to the satellite at small angles. This means that the libration takes place only in the orbital plane and in the rotating coordinate system tied to the orbital radius vector of the satellite. The gravitational potential of the satellite is approximated by the six first harmonics of its development. Sequential consideration of these harmonics makes it possible to judge the accuracy of approximation. The orbit of the satellite is circular. We take into account in the analytical representation of the attractive potential of the satellite only terms containing the angle of libration in the second degree. The main component is considered as the material point, because its shape is closer to the ball than the figure of the satellite. The values of libration period were obtained for three options of accounting the harmonics of the satellite: only the second harmonic, only the second and the fourth harmonics, and all harmonics up to the sixth. The period, corresponding to the third option should be close to that obtained from observations. Indeed, it was proven to be possible to identify the theoretical and observed periods of libration.

Coordinate systems

We considered as a reference coordinate system the so-called orbital system, the axes of which are tied to the orbital radius vector and rotate with it around the center of mass of the system. Coordinates in this system will be denoted by *x, y, z.* Axis *x* of the orbital system is tangential to the orbit of the satellite in the direction of its motion. Axis *y* is normal to the plane of the satellite orbit, and axis *z* is directed along the radius vector of the satellite in its orbital motion. The second system, which will be used by us, is the system of axes, coinciding with the principal axes of inertia of the satellite. Coordinates in this system are denoted as *x′, y′, z′.* It is also mobile system, whose axis *y′* coincides with axis y in accordance with condition of plane libration.

The double asteroid 39 Laetitia system

Determining the parameters of the double asteroid 39 Laetitia engaged many authors, but the data presented in their works differ quite widely. We chose here to use the work of Cellino (1985), which seemed to be more complete and convincing. According to this work, the main component of the asteroid has roughly an ellipsoidal shape with semi-axes a_1 = 72.5 km, b_1 = 65 km, c_1 = 60 km. The satellite also has an ellipsoidal shape with semi-axes a_2 = 60 km, $b_2 = c_2$ = 35 km. The distance between the centers of inertia of the components is equal to 168 km, and the density of the components is equal to 4.5 g/cm^3.

Development of the gravitational potential of the satellite

Expansion will be built around the axes x', y', z'. Coordinates of the main component will be $x' = R\sin\theta$; $y' = 0$; $z' = R\cos\theta$, where R = 168 km is the distance between the components, θ is the angle between the axis x′ with respect to the axis x (the current angle of libration). Since these coordinates will appear only in even degrees, we can make the change $z'^2 = R^2\cos^2\theta = R^2 - x'^2$. Then the potential expansion at the point of the main component can be simplified by retaining only the terms containing x'^2. In addition, we discard terms of the potential expansion, which do not affect the change in the orientation of the satellite. Since the main component of the figure is closer to the ball, then we will assume the main component is the material point.

Position of an element of the satellite mass is defined by the vector $\bar{\rho}(\xi,\eta,\varsigma)$, where ξ, η, ς are the components of $\bar{\rho}$ in axes x', y', z'. The position of the component m_1 is determined by the vector $\overline{R'}(x',\ y',\ z')$

and the position m_1 relative to the element of mass dm_2 is determined by the vector $\vec{r}'(x'-\xi,\ y'-\eta,\ z'-\xi)$ (see Figure).

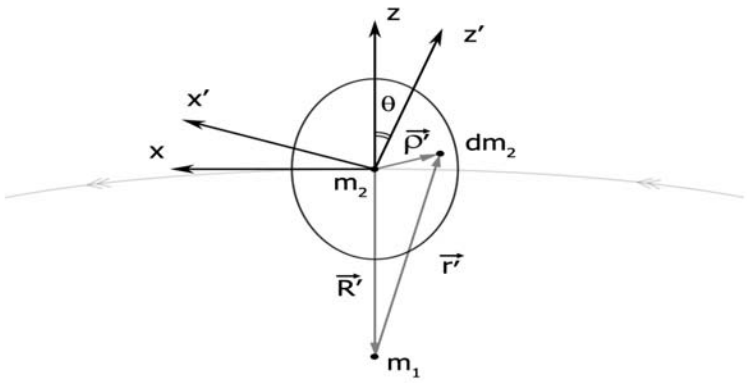

Moving coordinates *x, z* and x', z'.

If we now expand the potential of point masses m_1 and dm_2 in a row along with harmonics, integrate their joint potential $dV = \dfrac{k^2 m_1 dm_2}{r'}$ over the volume of the satellite ellipsoid, and introduce the agreed simplifications, then for joint potential of bodies m_1, m_2 we obtain the expression

$$V = \frac{k^2 m_1 m_2}{R'}\left\{1 + \frac{3}{10}\frac{(a_2^2 - c_2^2)\ x'^2}{R'^4}\ \left[1 + \frac{\chi_4}{R'^2} + \frac{\chi_6}{R'^4}\right]\right\}, \tag{1}$$

where the coefficient before the square brackets describes the influence of the second harmonic potential of the satellite, and χ_4, χ_6 describe the influence of the fourth and sixth harmonics.

We have

$$\begin{aligned} \chi_4 &= \frac{5}{14}\left(4c_2^2 - 3a_2^2 - b_2^2\right), \\ \chi_6 &= \frac{5}{24}\left(5a_2^4 + b_2^4 + 8c_2^4 - 12a_2^2c_2^2 - 4b_2^2c_2^2 + 2a_2^2b_2^2\right). \end{aligned} \tag{2}$$

One should bear in mind that a_2, b_2, c_2 are consistent with the coordinate axes x', y', z'. In another orientation of the satellite one should change the names of the semi-axes so that they conform to this order of following coordinates. It is important to note that the satellite bodies oriented along with axes *x′, y′, z′* are stable in the sense of Lyapunov, which corres-

pond to conditions $B > A > C$, where *A, B, C* are the main moments of inertia that successively correspond to axes *x′, y′, z′* [1]. In our case we have $A = B$ so, we do not have a strong Lyapunov stability. Though later it will be shown that the libration in this case does exists. If one calculates the moments of inertia for the case of constant density, then the same condition will go into the inequality for the semi-major axes of the ellipsoid $c > a > b$. Therefore, we choose the orientation of the satellite ellipsoid in such a way that the largest axis of the ellipsoid corresponds to the axis *z′*, the smallest axis of the ellipsoid corresponds to the axis *y*', and the intermediate one is directed along the axis *x′*.

Equations for the libration motion of the satellite

The relationship of coordinate systems are given by the matrix equation

$$(x', y', z')^T = \begin{pmatrix} \alpha & \alpha' & \alpha'' \\ \beta & \beta' & \beta'' \\ \gamma & \gamma' & \gamma'' \end{pmatrix} (x, y, z)^T , \tag{3}$$

where $\alpha = \cos\Theta$; $\alpha' = 0$; $\alpha'' = -\sin\Theta$; $\beta = 0$; $\beta'=1$; $\beta'' = 0$; $\gamma = \sin\Theta$; $\gamma' = 0$; $\gamma'' = \cos\Theta$. In the case of plane libration components of the relative angular velocity of the satellite will be

$$\overline{p} = \overline{r} = 0;\ \overline{q} = \dot{\Theta}. \tag{4}$$

Components of the absolute angular velocity will be

$$p = r = 0;\ q = \overline{q} + \omega_0. \tag{5}$$

Let us apply the Lagrange function $L = T + U$, where $T = \frac{1}{2} B(\overline{q} + \omega_0)^2$ is kinetic energy and $U = -V$. Let us introduce an impulses

$$p_1 = p_2 = 0;\ \tilde{p}_3 = \frac{\partial L}{\partial \dot{\Theta}} = Bq .$$

We introduce also a new Hamiltonian

$$H' = \tilde{p}_3 \dot{\Theta} - L = \frac{1}{2} B\overline{q}^2 - U$$

and a new generalized impulse $p_3 = \tilde{p}_3 - B\omega_0$. Then we obtain

$$\overline{q} = \frac{p_3}{B};\ \mathrm{H}' = \frac{1}{2}\frac{p_3^2}{B} - U.$$

Canonical equations of the libration will take the view

$$\dot{\Theta} = \frac{\partial H'}{\partial p_3};\ \dot{p}_3 = -\frac{\partial H'}{\partial \Theta},$$

then

$$\dot{\Theta} = \frac{p_3}{B};\ \dot{p}_3 = \frac{\partial U}{\partial \Theta}. \tag{6}$$

If one puts the force function $U = -V$ into the second equation of (6) and differentiates the first equation with respect to time, it becomes possible to put $\dot{p}_3$ into the first equation and one obtains

$$\ddot{\Theta} + 3\omega_0^2 \frac{c_2^2 - a_2^2}{c_2^2 + a_2^2}\left(1 + \frac{x_4}{R'^2} + \frac{x_6}{R'^4}\right)\Theta = 0, \tag{7}$$

where $\omega_0 = \sqrt{k^2 m_1 / R'^3}$ is the unperturbed angular velocity of the point mass m_2 in its orbital motion around the body m_1, and where only the terms containing Θ in the first powers are taken into account.

Equation (7) describes the usual harmonic oscillations, whose period is independent of amplitude.

Let us introduce the designations:

- $P_0 = 2\pi / \omega_0$ for the unperturbed orbital period of the satellite $(\omega_0^2 = k^2 m_1 / R'^3)$;
- $P_2 = 2\pi / \omega_2$ is the period of libration due to the second harmonic of the satellite potential $\left(\omega_2^2 = 3\omega_0^2 \frac{c_2^2 - a_2^2}{c_2^2 + a_2^2}\right)$;
- $P_4 = 2\pi / \omega_4$ is the period of libration due to the common action of the second and the forth harmonics of the satellite potential $\left(\omega_4^2 = \omega_2^2\left(1 + x_4 / R'^2\right)\right)$;
- $P_6 = 2\pi / \omega_6$ is the period of libration due to the common action of the second, the forth, and the sixth harmonics of the satellite potential $\left(\omega_6^2 = \omega_2^2\left(1 + x_4 / R'^2 + x_6 / R'^4\right)\right)$.

For the parameters of the binary system of the asteroid 39 Laetitia the calculations give

$$P_0 = 0^d.26562;\ P_4 = 0^d.20652$$
$$P_2 = 0^d.21858;\ P_6 = 0^d.20544.$$

In this case the largest semi-axis of the ellipsoid was directed along the axis z, the other semi-axes were directed along the axes x', y'. Other equilibrium orientations of the satellite ellipsoid failed to provide an oscillatory character of the movement.

From the periods, obtained by frequency analysis at CrAO, the period $0^d.202$ comes closest to the theoretical value $P_6 = 0^d.20544$. From the closeness of the obtained value of the period of libration (both theoretical and observed) results we conclude that a small-amplitude libration of the satellite in the system 39 Laetitia can exist and deserves more detailed investigation.

Conclusions

Investigation of the libration of the satellite of asteroid 39 Laetitia showed that the theoretical period of libration, obtained with allowance for six harmonics of the gravitational potential of the satellite, is sufficiently close to the period $0^d.202$, obtained by the frequency analysis of light curves. This allows us to assume that the appearance of the period $0^d.202$ in changes of the asteroid brightness could be explained by small-amplitude libration of the satellite. Therefore, the motion of the components of the double asteroid 39 Laetitia deserves more detailed study.

References

1. *Beletsky V. V.* Satellite motion around center of masses in gravity field. Moscow University Publishers, 1975. 308 p. (in Russian).
2. *Cellino A., Pannunzio R., Zappala V., Farinella P. et al.* Do we observe light curves of binary asteroids? // Astron. and Astroph. 1985. Vol. 144, N 2. P. 355–362.
3. *Prokofjeva V. V., Demchik M. I., Karachkina L. G., Pavlenko E. P.* Photometry and colorimetry of the asteroids with digital television complex // Solar System Res. 1992. Vol. 26, N 5. P. 3–13.

OBSERVATION AND DETECTION OF NEOS

Database Development for Solar System Small Bodies' Orbital Evolution Based on Modern Mathematical Models and Methods

A. F. Zausaev, A. A. Zausaev, V. V. Abramov, S. S. Denisov

Samara State Technical University, Samara, Russia

Abstract. The modified Everhart method up to order 33 and algorithms for the Adams methods up to order 16 inclusive were developed. A software package for calculating the Solar System small bodies' orbital evolution and automating the processes of database development were created. Research of the orbital evolution of 6163 asteroids belonging to Apollo, Amor, Aten groups and 197 short-period comets was performed for the time period from 1800 to 2206. 815 objects have been identified among asteroids approaching closely to inner planets, in particular 612 objects passing through the Earth's sphere of action. On the basis of performed research the website SmallBodies.Ru was created. The information offered in the website can be used by specialists when studying the orbital evolution of asteroids and short-period comets, investigating problems of the orbits stability and revealing objects presenting potential hazard to the Earth.

Introduction

Cataloguing of the Solar System small bodies is an important stage for the "Asteroid-Comet Hazard" problem solution. Catalogues of asteroids and comets contain valuable information on distribution of small bodies in the Solar System and the evolution of their orbital elements.

When investigating orbital evolution of the Solar System's small bodies (asteroids and comets) it is necessary to apply modern mathematical models for the motion of celestial bodies and high-precision numerical methods for solving differential equations.

The research work of the orbital evolution of the Solar System small bodies approaching the Earth is the product of a collective work. It was per-

formed with the financial support of the Federal Agency of Education of the Russian Federation (project codes RNP 2.1.1.1689 and RNP 2.1.1.745). It resulted in three published papers [1, 2, 3].

1. Mathematical modeling

For solving the differential equations of motion we developed the modified Everhart method up to order 33 inclusive as well as algorithms and the software program implementing Adams–Bashforth and Adams–Moulton methods up to and including order 16.

Research of the orbital evolution of 6163 asteroids belonging to Apollo, Amor, and Aten groups and 197 short-period comets were performed for the time period from 1800 to 2206. 815 objects have been identified among asteroids approaching closely to inner planets, including 612 objects passing through the Earth's sphere of action.

The cited results were obtained by the numerical integration of 72 combined equations by means of the modified Everhart method of order 27 with variable integration step-size [4]. The criterion of step change was the minimum distance between investigated body and objects of the Solar System (with the exception of the asteroid belt bodies).

The differential equations of motion in barycentric coordinate system considering Newton and Schwarzschild forces conditioned by mutual interaction of the Sun and planets [5] were used as a mathematical model describing the motion of a small body. We also took into account the influence of the shapes of the Earth and the Moon and perturbations from 50 most massive bodies of the asteroid belt.

2. Software package

To create the database it was necessary to calculate the evolution of thousands of objects. In order to achieve the objective it was necessary to develop not only the program for calculating the evolution of an object's motion, but also the application allowing to automate the process of developing the database. The software package consists of the following applications [6].

Calculation Server. This program performs calculations in automatic mode. A user just needs to choose required objects and specify the calculation period. The application is adapted for multi-core systems.

Database Manager. With this program a user can add the information to the database, retrieve the list of objects approaching a planets etc.

Object Viewer. It allows viewing the orbital evolution of the asteroid, chosen from the database, for specific time periods. The application represents the table and graphs of orbital elements evolution, list of the closest approaches and 3D animation of the object's motion.

We developed the database for the time period between 1800 and 2206 containing barycentric coordinates and velocities of nine planets (Mercury – Pluto), the Sun and the Moon, the orbital elements of asteroids belonging to Apollo, Amor, and Aten groups and short-period comets at standard dates with the interval of 100 days, the small bodies' closest approaches to planets, the Moon and the Sun, initial data and the objects general information. The initial data of orbital elements of asteroids were retrieved from the database DASTCOM (Database of ASTeroids and COMets) of the Jet Propulsion Laboratory (JPL).

The calculated coordinates and velocities were conformed to DE405 — high-precision numerical theory of motion of major planets, the Sun and the Moon. Distances and dates of approaches of asteroids and the Earth are in good agreement with observations. This testifies to the accuracy of the calculations.

With the course of time new objects are discovered and the orbits of existing objects are updated, so the database is replenished and the orbits of approaching asteroids are recalculated and entered in the database every 100 days. The database was developed in DBMS MySQL 5.

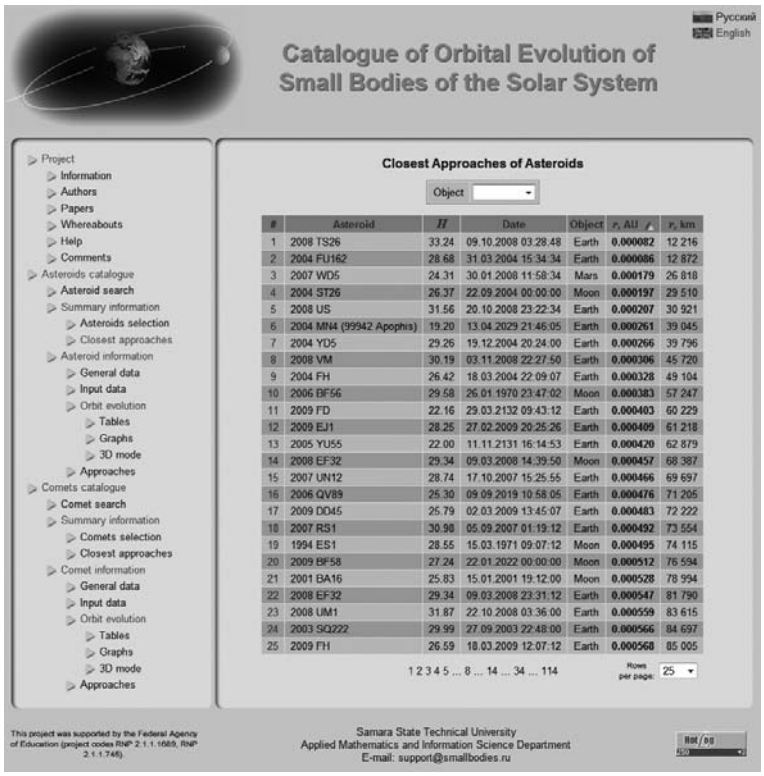

Website SmallBodies.Ru.

3. Website

On the basis of the performed research the website *SmallBodies.Ru* (see Figure) was created [7]. It allows access to ephemerides of asteroids and short-period comets entered into the developed database. For viewing the website information in the form of scalable graphs and three-dimensional scene of the objects motion we developed two Java applets.

The site allows:

- implementing the search for a specific object by name;
- viewing the list of the objects' closest approaches with major planets;
- filtering asteroids and comets by orbital elements and other criteria;
- view the list of their approaches to the Sun, major planets;
- view initial data for calculation;
- view the list of object approaches to the Sun, major planets, and the Moon;
- view the data of object orbital evolution in forms of tables, graphs, and in three-dimensional mode.

The scene for motion of objects is animated and a user can set the speed of displayable time, change it, or stop the animation. User also can choose any specified time moment at which the orbit of asteroid or comet will be displayed. One can zoom and move the camera point relative to the central object which can be the Sun, the planet, the asteroid, or the comet.

The applet has a number of features stated below that foreign analogs do not have, e. g., the applet located at the Jet Propulsion Laboratory website. The orbits are constructed in heliocentric or planetocentric coordinate systems or a coordinate system associated with the comet or asteroid. The lengths of the orbits are chosen on the basis of the orbital periods, but the user can change them for the Solar System's small bodies. Thus, is possible to view more obviously the orbit change owing to a close approach.

It should be noted that the algorithm uses all the information contained in the database, and the mathematical model considers disturbances from the Sun, nine planets, and the Moon. So the applet correctly shows the orbital evolution of objects with close approaches to planets, wherein it significantly surpasses foreign analogues using simplified mathematical models.

Conclusion

The information offered at the website can be used by specialists when studying the orbital evolution of asteroids and short-period comets, investigating problems of the orbits stability and revealing objects presenting potential hazard to the Earth.

The results of this work can be useful in research activities. As long as the information is represented in accessible form, the developed site can be used in teaching physics and astronomy in educational organizations.

References

1. *Zausaev A. F., Abramov V. V., Denisov S. S.* Katalog orbitalnoj evolutsii asteroidov, sblizhauschikhsya s Zemlej s 1800 po 2204 gg. (Catalogue of orbital evolution of asteroids approaching to the Earth from 1800 to 2204). M.: Mashinostroenie–1, 2007. 610 p.
2. *Zausaev A. F., Zausaev A. A.* Katalog orbitalnoj evolutsii korotkoperiodicheskih komet s 1800 po 2204 gg. (Catalogue of short-period comets' orbital evolution from 1800 to 2204). M.: Mashinostroenie–1, 2007. 410 p.
3. *Zausaev A. F., Zausaev A. A.* Matematicheskoe modelirovanie orbitalnoj evolutsii malykh tel Solnechnoj sistemy (Mathematical modeling of the Solar System small bodies' orbital evolution). M.: Mashinostroenie, 2008. 250 p.
4. *Zausaev A. F., Zausaev A. A., Olhin A. G.* Primenenie metoda Everharta dlya resheniya uravnenij dvizheniya bolshih planet (Application of the Everhart method in the solving of major planets' motion equations // Trudy GAISH (SAI Transactions). 2006. Vol. 76. P. 75–82.
5. *Newhall X. X., Standish E. M., Williams Jr. and JG.* DE 102: A numerically integrated ephemeris of the Moon and planets spanning forty-four centuries // Astron. Astrophys. 1983. N 125. P. 150–167.
6. *Denisov S. S.* Sozdanie bankov dannykh asteroidov, sblizhauschikhsya s Zemlej (Databanks development for the asteroids approaching to the Earth) // Tezisy dokladov Mezhdunar. konf. "100 let Tungusskomu fenomenu: proshloe, nastoyaschee, buduschee" (Abstracts of the Intern. Conf. "100 Years since Tunguska Phenomenon: Past, Present and Future"). M., 2008. P. 114–115.
7. *Abramov V. V.* Elektronnyj katalog orbitalnoj evolutsii malyh tel Solnechnoj sistemy: razrabotka informatsionnoj bazy i Internet-resursa (Electronic catalogue of the Solar System small bodies' orbital evolution: database and website development) // Vestnik SamGTU. Seriya: Fiz.-Mat. nauki (Herald of the SSTU. Series of "Phys. and Math. Sci.). Samara: SSTU, 2008. N 2. P. 275–278.

OBSERVATION AND DETECTION OF NEOS

Analysis of the Systematic Errors of CCD-observations of Asteroids Performed in 2007–2008

A. A. Berezhnoy

Central (Pulkovo) Astronomical Observatory of RAS, St. Petersburg, Russia

Abstract. Analysis of systematic errors based on CCD-observations taken with Normal Astrograph (D/F = 0.33 m/3.5 m, FOV = 18 × 16 arcmin, scale = 1 arcsec/pix) of Pulkovo observatory during 2007–2008 has been made. About 5000 CCD-images of 150 asteroids were processed and reduced to UCAC2 system. A statistical approach that used mean (*O–C*) values obtained for positions of reference stars within the field of view separated on square bins and magnitude ranges was applied. The positions of reference stars and asteroids were corrected according to parameters of magnitude equation and common distortion.

Introduction

A preliminary investigation [1] of (*O–C*) differences has shown a relevance of the magnitude equation which can reach values about 100 mas for bright object and 100–200 mas for fainter ones. Great volume of observational material obtained and processed in the last year makes it possible to obtain more relevant fragmentation of data (by 2D focal plane positions and magnitudes) for application of bicubic interpolation. Investigation of systematic errors of coordinates of stars and asteroids based on observations made with Normal Astrograph of Pulkovo Observatory allows one to improve accuracy of present and future observations.

Vector fields

The field of view was separated into bins and mean (*O–C*) values of positions of reference stars were calculated for each. A similar approach was used in construction of CPC2 [2] and USNO-B [3] catalogs. Also all reference stars were separated by their values of U2R magnitudes in order to investigate the magnitude equation. Vector fields constructed according to

such procedure represent systematic positional errors for each range of 2D coordinates and magnitudes and allow to correct positions of reference stars or asteroids by interpolation procedure on a regular grid.

Material features of observations

First observation	10 January 2007
Last observation	17 November 2008
Reference catalog	UCAC2
Reduction model	6 constants
Number of reference stars	~240000
Number of asteroid positions (series)	~400
PSF	Lorenzian
Theory of motion	DE405 / LE405 (from *www.imcce.fr*)

Figure shows vector fields for two magnitude ranges. The mean residuals for the faintest magnitude range can reach 200 mas and even more.

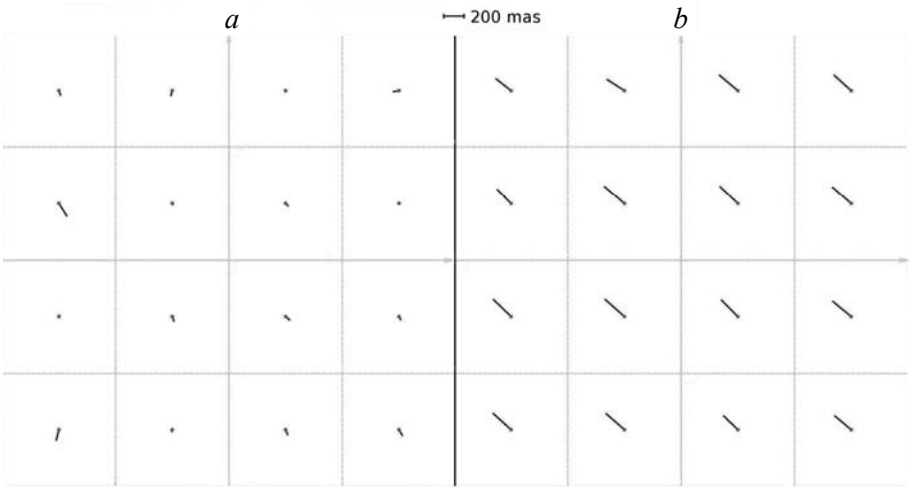

Vector fields:
a — $10 < m \leq 11$, b — $13 < m \leq 14$.

Magnitude equation

It was established that the magnitude equation was the main source of systematic errors of observations with the Normal Astrograph. There are two main reasons of systematic errors of this kind in our case: optical aberration and irregularity of tracking. As a result profiles of stellar images became elongated, and brighter stars gain greater elongation. The reduction proce-

dure is performed with brighter reference stars, therefore fainter objects gain additional bias relatively to their true positions in the frame system.

The bicubic interpolation method was used to calculate corrections to individual positions of each reference star used. Further calculations showed that the magnitude equation was significantly decreased. Obtained corrections were applied to asteroid positions.

Conclusion

The statistical approach based on the mean values of (*O–C*) residuals of reference stars was successfully employed to stars and asteroid positions and allowed improvement in the accuracy of coordinates of asteroids. A similar approach tested for the results of CCD-observations can also be applied for reduction of digitized photographic plates taken with the Normal Astrograph in the past.

References

1. *Khrutskaya E. V., Khovritchev M. Yu., Kalinin S. I., Berezhnoj A. A.* Astrometria malykh tel solnechnoj sistemy na Pulkovskom Normal'nom astrografe. (Astrometry of small bodies of the Solar System with the Pulkovo Normal astrograph) // Proc. of International astronomical meeting "Dynamics of Solar System Bodies". Tomsk, 2008. P. 43. (in Russian).
2. *Zacharias N., de Vegt C., Murray C. A.* CPC2 Plate Reductions with HIPPARCOS Stars: First Results. 1997 // Proc. of the ESA Symposium "Hipparcos – Venice 97". P. 85–90.
3. *Monet D. et al*. The USNO-B Catalog // Astron. J. 2003. Vol. 125, Issue 2. P. 984–993.

OBSERVATION AND DETECTION OF NEOS

Solving of the ACH Problem in the Project "Interplanetary Solar Stereoscopic Observatory"

M. S. Chubey[1], L. I. Yagudin[1], V. N. L'vov[1], S. D. Tsekmejster[1], V. V. Kouprianov[1], G. I. Eroshkin[1], E. A. Smirnov[2], A. V. Petrov[2]

[1]Central (Pulkovo) Astronomical Observatory of RAS, St. Petersburg, Russia
[2]St. Petersburg State University, St. Petersburg, Russia

Abstract. The extended modeling of the on-board observational process within the Interplanetary Stereoscopic Observatory concept [3] during a 6 year mission and the expected single NEO-observation errors are presented. It is shown that the accuracy of the distance to an asteroid can be achieved in the interval from 2.5 km to 15.0 km depending on the revolution period and maximal distance of the NEO. Every synchronous on-board long-focus astrograph observation gives a 3D-vector of the NEO's position with an angular accuracy at a level of ±0.001″. The effectiveness of the Observatory in supporting ACH-investigations is evident.

Introduction

Modern ground-based global monitoring of near-Earth objects (NEOs) is performed using automatic telescopes with CCD-registration of images and radio telescopes [1]. Some space missions for NEO observations are also planned and executed.

We note that radio locating of NEOs is effective for limited distances from the Earth, depending on the object's size and on its sky position. Radio locating can be employed for the study of NEOs only episodically. Thus, the main part of the activity in discovering and monitoring these objects can be fulfilled only by optical telescopes — both ground-based and space-based. Modern ground-based telescopes give a subsecond accuracy that is not sufficient for monitoring all NEOs. Newly discovered objects are often lost and must be redetected later. Thus, the use of space-based technology is an urgent task.

NEO observations from on-board of the Interplanetary Solar Stereoscopic Observatory

The main task of the Interplanetary Solar Stereoscopic Observatory (ISSO) [2] are quasi-synchronous observations of objects with two identical groups of instruments placed in Lagrange points L_4 and L_5 of the "Sun – Earth – Moon barycenter" system. The estimated active time for the project is up to eleven years. This time is planned for 3D monitoring of celestial bodies. The goal of this article is to estimate the ISSO efficiency in such monitoring.

There are two main tasks in this area:

1. Orbit improvement of known objects for more accurate prediction of approach parameters.

2. Detection of new NEOs — asteroids and comets.

The second task assumes continuous monitoring in all directions of space and demands great instrumental resources. It can be successively solved only if it is the basic purpose of the considered mission. On the other hand, solving the first task (observations for high-accuracy NEA orbit determination) could be fulfilled at the expense of less than 7 % of the ISSO resources. Moreover, the error of an object position may be reduced to the diffraction limit $\pm 0''.001$, that is not achievable under atmospheric conditions.

The final result of orbit improvement is defined by the observational accuracy and the distribution of observations along the orbit. The accuracy of observations is determined exclusively by the technical parameters of the telescopes and recording equipment, and does not depend on the space environment. We assumed the value for mean error of a single observation to be equal to $\pm 0''.001$ for a long-focus astrograph.

The possibility of successful distribution of observations along the orbit is determined by the mutual positions of NEO, two ISSO spacecraft and the Sun during the entire time of the mission. The observations are restricted by the need to avoid the "blind" zone — the cone with 50° apex angle where the CCD-matrix may be damaged. The important factor is the shape of the triangle produced by the two spacecraft and the observed object. All this can be estimated only by numerical modeling of observations.

The computational model approach

Fig. 1 helps to understand that the accuracy of object's derived position is defined mainly by two parameters: the distances from the two spacecraft (the error is proportional to them) and the angle at the object (the error attaines a minimum at $\varphi = 90°$ and tends to infinity when φ approaches 0° or to 180°).

Thus the upper estimate for the NEO positional error is expressed by the formula $\sigma = \max(R_1, R_2)\,\mathrm{tg}(\sigma_1)/\sin\phi$, where σ_1 is the direction error of a single observation in radians and R_1 and R_2 are the corresponding distances from the NEO to the two spacecraft.

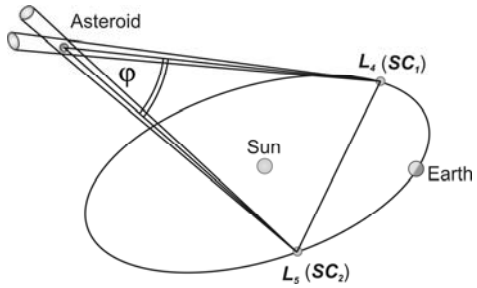

Fig. 1. Observations of an NEO from on-board of ISSO.

Modeling of observations

The list of NEOs is adapted from the MPC database (*ftp://cfa-ftp.harvard.edu/pub/MPCORB/MPCORB.DAT*). There are about 400 numbered asteroids and more than 2000 unnumbered asteroids, mainly of the Apollo and Aten types. The JPL Planetary and Lunar Ephemerides DE405/LE405 were used in the calculations.

The mission time was assumed to be from January 1, 2010 to December 31, 2015. In general, the start time of mission is indifferent, but its duration for 5–6 yr is appropriate. A one day step was used in the calculations.

For each NEA we estimated the possibility of its synchronous observations from both spacecraft and if observations are possible we calculated the error of determining the corresponding space coordinates.

The results are presented in the form of numerous graphs. Here we demonstrate only three graphs illustrating the typical results for asteroids with various orbits (Figs. 2, 3).

All graphs have been constructed in accordance with the same form. The upper part of a figure includes the object's name and the minimum and maximum distances from the Earth during the observational interval. Along the *x*-axes the mean anomaly is plotted. So the left and right borders correspond to pericenter of an orbit and the middle — to apocenter. Along the *y*-axis the calculated value of σ — a single observation of NEO position error expressed in km is plotted.

The short-period NEAs give several curves during the six-year mission, but for long-period NEAs this value is no more than two. The gaps in the curves are produced either by the "blind" zones or by the cases when all three objects are in line with each other.

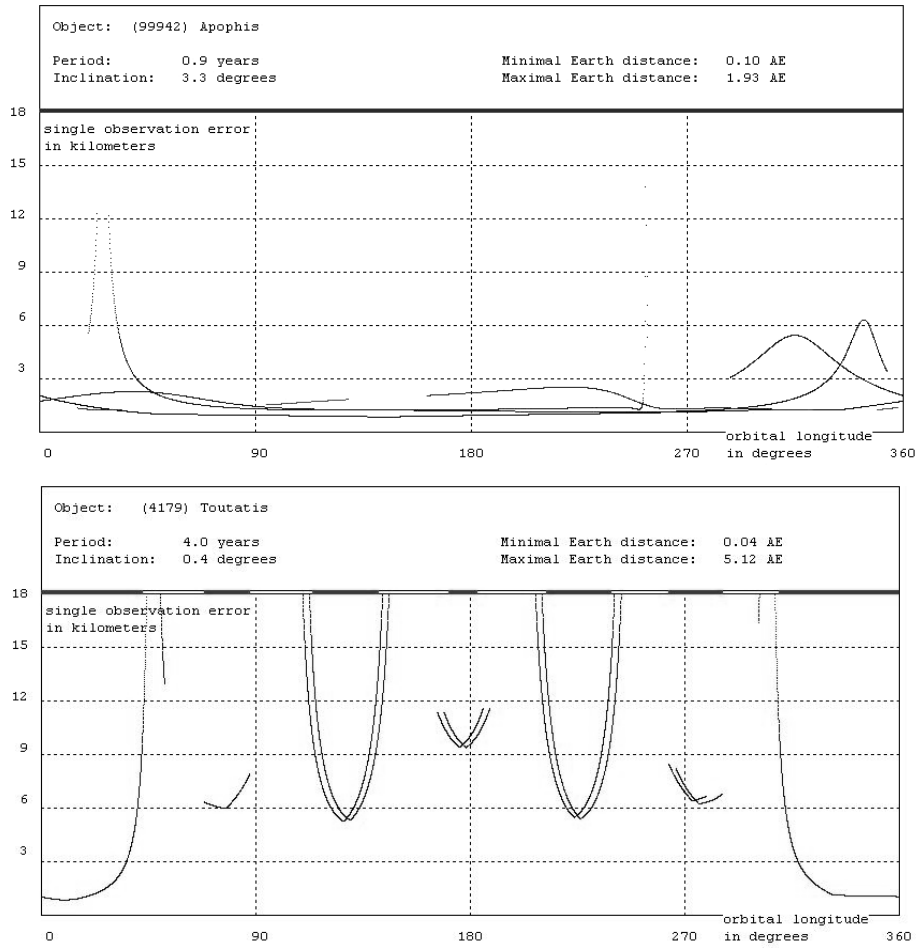

Fig. 2. The error of a single observation for asteroids Apophis with the short revolution period (top) and Toutatis with the long revolution period and large maximal distance (bottom).

Conclusion

According to our analysis about 10 % of the source list objects can be observed on four optimal parts of their orbits with a single-observation accuracy of 2.5–3.0 km; 34 % — as accurate as 3.0–5.0 km; 40 % — as accurate as 5.0–10.0 km; 14 % — as accurate as 10.0–15.0 km. Only 2 % can not be observed close to their aphelia. Nevertheless, the orbits of even such NEAs can be significantly improved. The results permit calculation of the most precise orbits for practically all NEAs.

In case of special circumstances, non-synchronous, single-mode observations with one telescope are possible, like ground-based observations, but

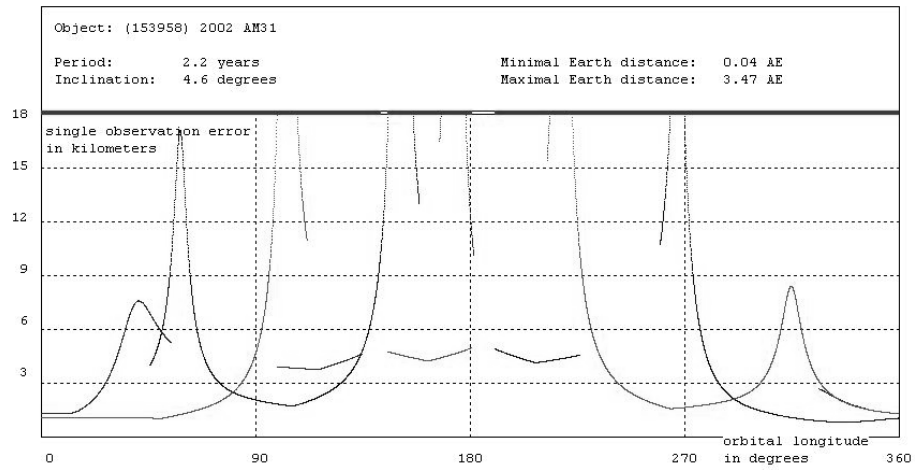

Fig. 3. The error of a single observation for asteroid (153958) 2002 AM31.

with two differences. First, the accuracy is higher by an order of magnitude. Second, the ISSO configuration [2] permits exclusion of the "blind" zones, unobservable from the Earth.

Long-period NEAs are in the least favorable situation. An augmentation of the mission duration may be useful to solve that problem.

Thus, the advantages of the ISSO project are obvious. The systematic and long-term prognosis of every NEO's motion with the accuracy of a few tens kilometers is unachievable now by any other method.

References

1. Asteroid&Comet Hazard / Ed. A. G. Sokol'sky. St. Petersburg: ITA RAS, MIPAO, 1996 (in Russian).
2. *Grigor'ev V. M., Papushev P. G., Chuprakov S. A., Chubey M. S. et al.* Interplanetary Solar Stereoscopic Observatory // J. Opt. Technol. 2006. 73. P. 251–255.

OBSERVATION AND DETECTION OF NEOS

KLENOT Project — Contribution to Follow-up Astrometry of PHAs and VIs

M. Kocer, M. Honkova, J. Ticha, M. Tichy

Klet Observatory, South Bohemia, Czech Republic

Abstract. Near Earth Object research is important not only to solar System science, but for protecting human society from asteroid and comet hazard as well. An integral part of NEO discovery is astrometric follow-up fundamental for precise orbit computation and for the reasonable judging of future close encounters with the Earth including possible impact solutions. The KLENOT project is aimed especially to do so. It ranks among the worlds most prolific professional NEO follow-up programs. Here we present KLENOT project and its contribution to follow-up astrometry of PHAs and VIs, our observing strategy as well as our plans for the future.

Introducting the KLENOT project

The 1.06-m KLENOT telescope [1], put into regular operation in 2002, is the largest telescope in Europe used exclusively for observations of asteroids and comets and full observing time is dedicated to the KLENOT team. KLENOT project gives the highest priority to potentially hazardous asteroids (PHAs) and virtual impactors (VIs) [2]. Confirmatory observations [3], follow-up astrometry, recoveries, and search for new asteroids and comets are also performed as part of the project. KLENOT telescope (MPC Code 246) is the main observing device of the program while the brighter objects are left to the smaller 0.57-m reflector (MPC Code 046). The acquired data are processed by a software package developed at Klet Observatory.

KLENOT project first phase results

Near-Earth asteroids (NEAs) observations

Results of the first phase obtained during 2002–2008 [4] consist of 58071 positions of 6422 Solar System objects sent to the Minor Planet Center, including 16659 positions of 1650 NEAs, 295 of which were PHAs, 299

of NEAs were VIs at the time of observation. We also discovered 3 new NEAs on our images, including the smallest NEA discovered in Europe [5]. The observations were centered on newly discovered NEO candidates of typical apparent brightness $m_V = 19.5^m$ and apparent motion of 2″/min.

VIs observations

A special consideration is given to virtual impactors coming from Sentry [6] and CLOMON [7] automatic monitoring systems. Data obtained by the KLENOT team enabled one to remove predicted impact solutions in many cases (see Figure). The KLENOT team also took part in the process of determining the impact of asteroid 2008 *TC*3, which hit the Earth on 2008 Oct 7.

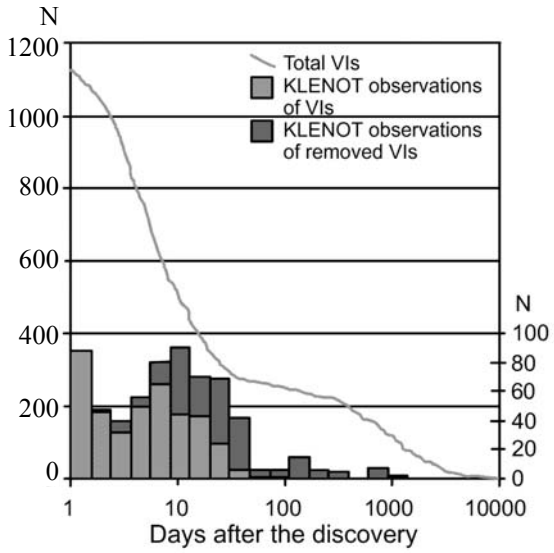

VI observations are performed mainly close to their discovery, contributing to the determination of their orbits.

KLENOT next generation

A fundamental improvement of the KLENOT telescope was started in 2008. The telescope will be able to cover a larger area of the sky, also the number, accuracy, and limiting magnitude of the observations will increase.

Conclusion

KLENOT project significantly participates in the follow-up of PHAs and VIs. Since KLENOT telescope is the largest telescope in Europe used exclusively for astrometric observations of asteroids and comets, observations focus on faint and fast moving objects. KLENOT observations are used

to confirm a discovery and determine orbit or impact solutions of such objects. Improvement of KLENOT telescope will lead to enhanced output from the program.

References

1. *Ticha J., Tichy M., Kocer M.* NEO-related scientific and outreach activities at KLENOT // Near Earth Objects, our Celestial Neighbors: Opportunity and Risk. Proc. of IAU Symp. 236. 2007. P. 371–376.
2. *Larson S.* Current NEO surveys // Near Earth Objects, our Celestial Neighbors: Opportunity and Risk. Proc. of IAU Symp. 236. 2007. P. 323–328.
3. *Marsden B. G., Williams G. V.* The NEO confirmation page // Planetary and Space Sci. 1998. Vol. 46. P. 299–302. (*http://www.cfa. harvard.edu/iau/NEO/ToConfirmRA.html*).
4. *Tichy M., Ticha J., Kocer M., Honkova M.* KLENOT project 2002–2008 — European Contribution to NEO Astrometric Follow-up // Proc. of 1st IAA Planetary Defense Conf.: Protecting Earth from Asteroids. 2009 (in press).
5. National Aeronautics and Space Administration NASA Near-Earth Object Survey and Deflection Analysis of Alternatives Report to Congress. 2007.
6. *Chamberlin A. B., Chesley S. R., Chodas P. W., Giorgini J. D. et al.* Sentry: An Automated Close Approach Monitoring System for Near-Earth Objects // Bull. of the American Astronomical Soc. 2001. Vol. 33. P. 1116. (*http://neo.jpl.nasa.gov/risk/*).
7. *Chesley S. R., Milani A*. NEODyS: an online information system for near-Earth objects // American Astronomical Soc. DPS meet. 31, 28.06. 1999. (*http://newton.dm.unipi.it/neodys/*).

Part 3. Comets: Physical Nature and Motion

The Asteroid-Comet Hazard Conference Proceedings, 2009

COMETS: PHYSICAL NATURE AND MOTION

Short-Period Comets: Origin and Terrestrial Impact Hazard

V. V. Emel'yanenko

Institute of Astronomy of RAS, Moscow, Russia

Abstract. A model of the Solar System cometary cloud is developed to explain the observed orbital distributions and numbers of both Jupiter-family and Halley-type short-period comets. The model is consistent with the basic observed distributions of near-parabolic comets, short-period comets, Centaurs and high-eccentricity trans-Neptunian objects.This model requires that initial objects in the early Solar System are concentrated to the outer planetary region, and the physical lifetime of comets in the inner planetary region at the present epoch is an increasing function of initial perihelion distances. The mean physical lifetime of active comets does not exceed 200 revolutions in the region $q < 1.5$ AU.The uncertain physical behaviour of comets leads to large uncertainties in estimates of a cometary contribution to the terrestrial impact hazard.

Introduction

The main difficulty in explaining the origin of short-period comets is the inconsistency between distributions of so-called Jupiter-family (JF) (Tisserand parameters $T > 2$, mainly periods $P < 20$ yr) and Halley-type (HT) ($T < 2$, mainly $P > 20$ yr) comets. First, the number of observed HT comets is too small in comparison with the number of observed JF comets, while dynamical theories predict that the number of HT comets captured from the outer Solar System should be much larger. Secondly, neither trans-Neptunian objects, nor the near-parabolic flux can produce the distribution of orbital elements (in particular, inclinations) for observed short-period comets. Therefore, sources of JF and HT comets are often separated: JF comets originate largely in the trans-Neptunian region, and HT comets are captured from the near-parabolic flux. But even in this case we need to assume very different properties for comets of these classes. While HT comets should disintegrate very quickly to explain the small observed number of

these objects and asteroids in HT orbits, JF comets should survive for a much longer time. This approach also cannot explain the observed distribution of orbital elements for short-period comets.

New constraints on the pathways by which comets reach short-period orbits from the outer Solar System come from observations of the Centaur population. The existence of Centaurs with large inclinations and semi-major axes indicates that the Oort cloud makes a large contribution to cometary objects in the inner planetary region [1]. In the paper [2] we developed the model of the Oort cloud formed under the action of planetary, stellar, and galactic perturbations for 4.5 Gyr and showed that this model is consistent with basic features of various classes of cometary objects in the Solar System.

In the present paper, the results [3] of a major extension of the calculations of [2] are discussed, considering a much larger number of objects in order to obtain data with greater statistical significance. It is shown that our model of the cometary cloud together with a unified model for lifetimes of comets in the inner Solar System can explain the basic features of the observed SP comet population [3].

Model and methods

For this work, we use the model of the Oort cloud developed in the paper [2]. In that paper we took particles with initial semi-major axes distributed uniformly in the range $50 < a < 300$ AU, initial inclinations distributed according to a "sine law" scaled to the interval $0 < i < 40$ degrees, and perihelion distances distributed uniformly in the range: $5 < q < 36$ AU. Results for different initial models can be obtained by applying appropriate weights. This initial distribution of orbits was integrated, taking account of planetary perturbations. All objects that reached the Oort cloud region ($a > 1000$ AU) were then evolved for the age of the Solar System under the action of planetary, stellar, and galactic perturbations.

In the present work, we took 8925 objects that survived after 4.5 Gyr, cloned them 200 times and integrated these particles for a further 300 Myr under the action of planetary, stellar, and galactic perturbations. The dynamical evolution of the test particles was calculated using the symplectic integrator [4] until the orbit reaches $q < 2.5$ AU and the symplectic integrator [5] beyond that. In order to weaken fluctuations connected with the initial conditions for these objects we analyzed results on the interval 50–300 Myr. More details about the numerical procedure were given in the paper [2].

In order to compare our model with the observed features of short-period comets we have taken data from the JPL and MPC lists about discovered comets that have $P < 200$ years and perihelion distances $q < 1.5$ AU near the present epoch. We excluded the SOHO comets have rather uncer-

tain physical and dynamical characteristics. This affects only the distribution near very small perihelion distances that we do not study here. We also excluded multiple-apparition comets that have not been observed for many revolutions and are now treated as dead comets. For split comets we assumed only one orbit of the main nucleus. In the end we obtained the list of 103 objects that we regard as present-day active short-period comets with $q < 1.5$ AU. 75 of them have $T > 2$ (JF comets) and 28 have $T < 2$ (HT comets). The actual number of active short-period comets is rather uncertain, especially for HT comets. But there are many arguments about the high-degree of completeness of the observed sample with $q < 1.5$ AU [6, 7]. Levison et al. [7] estimated that the number of active HT comets with $q < 1.3$ AU is 57. This number can be extrapolated to about hundred objects for $q < 1.5$ AU. For JF comets, Fernandez et al. [6] found that about hundred active comets exist in the region $q < 1.5$ AU. Although after discoveries of comets in past decade this estimate should be modified, these changes are not drastic. Thus, we conclude that there are roughly hundred active JF comets and hundred active HT comets in the region $q < 1.5$ AU near the present epoch.

Figs. 1 and 2 show the distribution of orbital elements for the present-day observed set of 103 short-period comets with $q < 1.5$ AU. The distribution of inclinations shows that not only JF comets are concentrated to the ecliptic plane, but also prograde HT comets outnumber retrograde HT comets [7, 8]. Fig. 2 shows an interesting correlation between Tisserand parameters and perihelion distances of short-period comets.

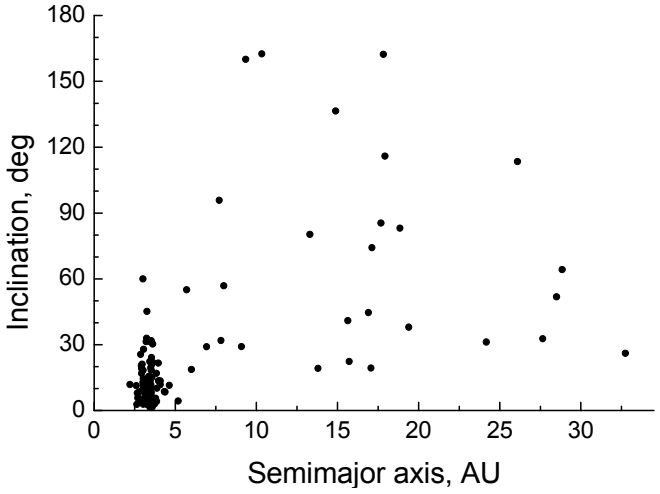

Fig. 1. The distribution of a and i for observed short-period comets with $q < 1.5$ AU.

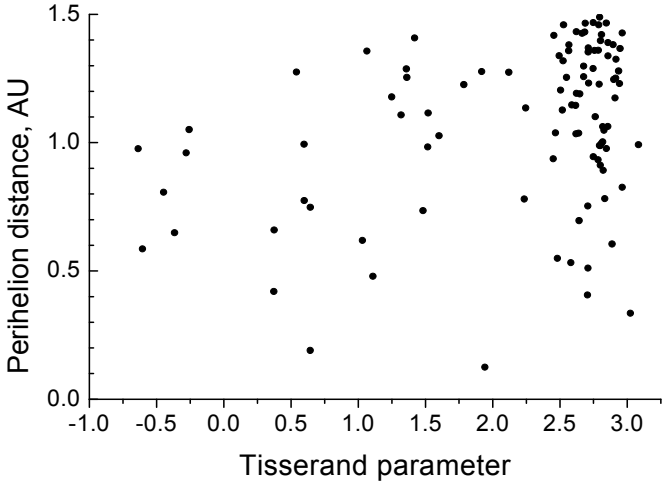

Fig. 2. The distribution of T and q for observed short-period comets with $q < 1.5$ AU.

The flux of dynamically new comets is a basic parameter of many models in cometary astronomy, including this paper. The estimates of the value ν for comets passing perihelia with $a > 10000$ AU per year per AU have some uncertainties, but ν is usually estimated between 2 and 4 for present-day comets in near-Earth space [9, 10]. We use $\nu = 2.5$ for quantitative estimates in this paper.

In order to estimate the contribution of trans-Neptunian objects to short-period comets we use results of the works [1, 11] where the near-Neptune high-eccentricity (NNHE) region defined by orbits with $28 < q < 35.5$ AU, $60 < a < 1000$ AU was found as a source of JF comets. Unfortunately, current knowledge of the distribution of trans-Neptunian objects is limited. In this respect, Centaurs as a transition population en route from the outer Solar System to near-Earth space provide valuable information. Following the definition in paper [2] we call all small bodies moving in heliocentric orbits with $5 < q < 28$ AU and $a < 1000$ AU Centaurs (except for a few resonant trans-Neptunian objects and Trojans). It was shown in [1] that Centaurs with $a > 60$ AU come mainly from the Oort cloud. Many of them reach orbits with $a < 60$ AU. Our results show that approximately 5/8 Centaurs with $a < 60$ AU come from the Oort cloud and the others are produced by a primordial trans-Neptunian population. A list of observed Centaurs that have a probable source in the Oort cloud is given in Tab. 1. Here only Centaurs with an observational arc larger than 100 days from the Minor Planet Center list and comets of Classes 1 and 2 [12] are included.

Table 1. Centaurs that have a probable source in the Oort cloud. The majority of such objects have $a > 60$ AU. Centaurs with $a < 60$ AU are listed if $i > 40$ degrees

Name	a, AU	q, AU	i, deg
(29981) 1999TD10	98.2	12.3	6.0
(87269) 2000OO67	658	20.8	20.1
(127546) 2002XU93	66.5	21.0	78.0
2003FH129	70.8	27.6	18.7
(65489) 2003FX128	100	17.8	22.3
2005VD	6.7	5.0	172.9
2007JK43	46.4	23.6	44.9
2007UM126	12.9	8.5	41.7
2008KV42	41.8	21.2	103.4
2008QD4	8.4	5.4	42.0
2008YB3	11.7	6.5	105.1
2009MS9	412	11.0	68.0
C/1984U1	646	5.5	179.2
C/1998M6	972	6.0	91.5
C/1999K2	145	5.3	82.2
C/2001Q1	176	5.8	66.9
C/2002K2	561	5.2	130.9
C/2002P1	497	6.5	34.6
C/2002VQ94	189	6.8	70.5
C/2003J1	514	5.1	98.3
C/2005R4	914	5.2	164.0
C/2007D3	765	5.2	45.9
C/2007K1	425	9.2	108.4

Predicted lifetimes and initial orbital distributions

An important factor that allows us to find out features of the dynamical and physical evolution of comets is the orbital distribution of JF comets. In particular, the distribution of inclinations is very sensitive to the physical lifetime of comets [13]. Our investigations show that the modeled inclination distribution of JF comets is close to the observed inclination distribution only if we assume that the physical lifetime of JF comets does not exceed 200 revolutions in the region $q < 1.5$ AU.

But if we apply such physical lifetime restrictions to all short-period comets, we have the well-known problem of numbers: the ratio of the numbers of HT and JF comets is too large and the absolute number of JF comets is too small in comparison with the present-day values based on observations. For example, in the case of the q^{-2} distribution for the initial perihelion distances in the early Solar System the HT/JF ratio is 4.6 and the number of JF comets is equal to 32 compared to values of 1 and 100, respectively.

First, this does not favor models with the initial number of objects as a decreasing function of initial perihelion distances. Secondly, this indicates the need to introduce one more factor, namely a dependence of the physical lifetime on initial positions of comets in the early Solar System.

In order to find consistency with both numbers and orbital distributions of observed short-period comets we consider a simple model for the dependence of the physical lifetime on initial q. Let us assume that the physical lifetime of comets is constant for all objects from the outer range 25–36 AU, and it changes as q^{β} for initial $q < 25$ AU. We study the power law q^{α} for the initial distribution of perihelion distances with $\alpha > 0$ because $\alpha < 0$ gives too small a number of JF comets and a wrong value of the HT/JF ratio.

Our calculations show that the models with $\beta \geq 1$ give results that are close to observations. It is impossible to derive exactly the restrictions on the cometary lifetimes and the values of α, β simultaneously because of uncertainties in the number and the orbital distribution of short-period comets. Nevertheless we have found that the best parameters are close to the following values: the restriction of about 150 revolutions in the region $q < 1.5$ AU for objects from the initial range 25–36 AU, the restriction of about 400 revolutions in the region $q < 2.5$ AU for objects from the initial range 25–36 AU, the value of about 1–2 for α and the value of about 1–2 for β. Thus, in our calculations the mean physical lifetime of objects from the initial range (10, 25) AU is 1.43 times as small as that of objects from the range 25–36 AU at $\beta = 1$ (for both $q < 2.5$ AU and $q < 1.5$ AU), and the corresponding factor is 1.92 at $\beta = 2$.

Tab. 2 gives results of calculations for one of the best solutions with the following parameters: the restriction of 420 revolutions in the region $q < 2.5$ AU for objects from the initial range 25–36 AU, the restriction of 150 revolutions in the region $q < 1.5$ AU for objects from the initial range 25–36 AU, $\alpha = 1$, $\beta = 2$. The consistency of our model with observed features of short-period comets, Centaurs, and trans-Neptunian objects allows us to estimate the distribution of different cometary populations. In Tab. 2, the data about the numbers of cometary objects coming from various original positions in q are presented. Here we show the number from each range of initial q for present-day objects from the Oort cloud and the number of objects originating from the trans-Neptunian (TN) population that have never been in the Oort cloud listed in the final column.

The basic features of the modeled orbital distributions for short-period comets are also consistent with those of the observed distributions in Fig. 1 and 2.

Table 2. The number of cometary objects in different dynamical classes

Initial region	5–10	10–25	25–36	TN
N_{OC}	0.1×10^{10}	1.8×10^{11}	4.3×10^{11}	
N_N	0	0.3×10^{9}	7.9×10^{9}	8.3×10^{9}
$N_C\ a<60$	0	0.1×10^{7}	6.6×10^{7}	4.2×10^{7}
N_{JF}	0	1	41	51
N_{HT}	0	7	101	0

N_{OC} — the number of objects in the Oort cloud, N_N — the number of objects in the NNHE region, $N_C\ a < 60$ — the number of Centaurs with $a < 60$ AU, $N_{\rm JF}$ — the number of JF comets, $N_{\rm HT}$ — the number of HT comets.

Remnants in short-period orbits

Restrictions on the physical lifetime imposed above assume that comets disintegrate during perihelion passages in the inner planetary region. If comets just fade and become dormant, then the large population of "cometary asteroids" exists. However, Levison et al. [14] showed that this assumption is not consistent with the observed number of asteroids in cometary orbits. Thus the majority of comets must disrupt into boulders or dust after losing the capacity to undergo outgassing. Details of final stages of the cometary evolution are not clear yet, and this problem is very important for estimating the terrestrial impact hazard.

If there is no limit on the physical lifetime of comets, our calculations give the steady-state numbers of 8300 HT objects with $q < 1$ AU. If comets evolve into objects of mass m_b, then let us assume that the total mass of these objects is a fraction f of active comets with the mean mass $m_c = 4\times10^{16}\ g$ [14]. The mean interval for collisions of these cometary remnants with the Earth is given by $\Delta t \approx P/(Np_E)$, where $p_E = 2.2\times10^{-9}$ is the probability of collisions with the Earth for near-parabolic comets with q < 1 AU per revolution [15], $P \approx 70$ years is the mean period of Halley-type comets, $N = 8300\, f m_c / m_b$ is the number of bodies with $q < 1$ AU in HT orbits. Then for Tunguska-sized bodies with $m_b \approx 10^{11}\ g$, $\Delta t \approx 9.6/f$. For example, if $f = 0.01$, then such bodies collide with the Earth approximately every thousand years, on average.

For remnants in Jupiter-family orbits the collisional frequency is much larger. To show this we use the estimate of [13] that $p_E / P = 4\times10^{-10}$ for JF comets with $q < 2$ AU. If there is no limit on the physical lifetime of comets, our calculations give the steady-state numbers of 9800 JF objects with $q < 2$ AU. Then for bodies with $m_b \approx 10^{11}\ g$, $\Delta t \approx 0.6/f$. For exam-

ple, if $f = 0.01$, then Tunguska-like events occur about once every sixty years.

Conclusions

1. The developed model of the Solar System cometary cloud is consistent with the basic characteristics of near-parabolic comets, short-period comets, Centaurs, and high-eccentricity trans-Neptunian objects.2. No model with the initial number of objects as a decreasing function of q is able to explain the observed distribution of short-period comets.

3. A simple model with initial objects concentrated in the outer planetary region and a physical lifetime of comets in the inner planetary region as an increasing function of initial perihelion distances is consistent with the orbital distribution and the number of both JF and HT comets.

4. The mean physical lifetime of active comets does not exceed 200 revolutions in the region $q < 1.5$ AU.5. The uncertain physical behavior of comets leads to large uncertainties in estimates of a cometary contribution to the terrestrial impact hazard.

Acknowledgments

This work was supported by RFBR Grant 09-02-00511 and RFBR-Ural Grant 07-02-96002.

References

1. *Emel'yanenko V. V., Asher D. J., Bailey M. E.* Centaurs from the Oort cloud and the origin of Jupiter-family comets // Mon. Not. 2005. Vol. 361. P. 1345–1351.
2. *Emel'yanenko V. V., Asher D. J., Bailey M. E.* The fundamental role of the Oort cloud in determining the flux of comets through the planetary system // Mon. Not. 2007. Vol. 381. P. 779–789.
3. *Emel'yanenko V. V., Asher D. J., Bailey M. E.* A unified model for short-period comets: implications for the early Solar system // Mon. Not. 2009 (in press).
4. *Emel'yanenko V. V.* An explicit symplectic integrator for cometary orbits // Celest. Mech. Dyn. Astr. 2002. Vol. 84. P. 331–341.
5. *Emel'yanenko V. V.* A method of symplectic integrations with adaptive time-steps for individual Hamiltonians in the planetary *N*-body problem // Celest. Mech. Dyn. Astr. 2007. Vol. 98. P. 191–202.
6. *Fernandez J. A., Tancredi G., Rickman H., Licandro J.* The population, magnitudes, and sizes of Jupiter family comets // Astron. Astrophys. 1999. Vol. 352. P. 327–340.
7. *Levison H. F., Dones L., Duncan M. J.* The origin of Halley-type comets: probing the inner Oort cloud // Astron. J. 2001. Vol. 121. P. 2253–2267.

8. *Fernandez J. A., Gallardo T.* The transfer of comets from parabolic orbits to short-period orbits: numerical studies // Astron. Astrophys. 1994. Vol. 281. P. 911–922.
9. *Bailey M. E., Stagg C. R.* Cratering constraints on the inner Oort cloud — Steady-state models // Mon. Not. 1988. V. 235. P. 1–32.
10. *Francis P. J.* The demographics of long-period comets // Astrophys. J. 2005. Vol. 635. P. 1348–1361.
11. *Emel'yanenko V. V., Asher D. J., Bailey M. E.* High-eccentricity trans-Neptunian objects as a source of Jupiter-family comets // Mon. Not. 2004. Vol. 350. P. 161–166.
12. *Marsden B. G., Williams G. V.* Catalogue of Cometary Orbits 2008. Cambridge, MA: Smithsonian Astrophys. Obs. 2008.
13. *Levison H. F., Duncan M. J.* From the Kuiper belt to Jupiter-family comets: the spatial distribution of ecliptic comets // Icarus. 1997. Vol. 127. P. 13–32.
14. *Levison H. F., Morbidelli A., Dones L., Jedicke R., Wiegert P. A. et al.* The mass disruption of Oort cloud comets // Sci. 2002. Vol. 296. P. 2212–2215.
15. *Weissman P. R.* Long-period comets and the Oort cloud / Ed. J. L. Remo // Proc. Int. Conf. "Near-Earth Objects". Annals of the New York Academy of Sci. 1997. Vol. 822. P. 67.

COMETS: PHYSICAL NATURE AND MOTION

Method of Calculating Cometary Orbits

Yu. S. Bondarenko, Yu. D. Medvedev

Institute of Applied Astronomy of RAS, St. Petersburg, Russia

Abstract. A method of constructing a numerical theory of comet motion covering large intervals of time is presented. It involves the determination of individual values of the constants A_1, A_2, A_3 (radial, transverse, and normal components of non-gravitational acceleration) and the displacement of the photo center in each apparition. In difficult cases, such as close approaches to the major planets, sudden increase of brightness, or considerable asymmetric outgassing about perihelion, when Marsden's model of non-gravitational acceleration does not allow one to present observations with sufficient accuracy, the instantaneous variation of velocity in the cometary motion is assumed. Based on this methodology, a unified numerical theory of the motion of comet Kopff during the time interval 1906–2002 was developed. It links 16 cometary apparitions with an RMS residual $\sigma = 1.40''$.

Description of methodology

A method of improving the orbit of a comet with large and quickly changing nongravitational accelerations is presented. In addition to orbital parameters the values of constants A_1, A_2, A_3 (radial, transverse, and normal nongravitational parameters of Marsden's model [1]) and displacement of the photo center in each cometary apparition are determined by this method. We choose the following strategy. The values of the root mean squares (RMS) residuals free from errors of dynamic models are calculated. The value of photo center displacement, d_e, is also calculated; in cases when its error is acceptable, the value was included into the list of improved parameters. It is assumed that the photo center displacement takes place along the radius-vector of the comet nucleus and does not depend on heliocentric distance. The following values are calculated: orbital parameters (position and

velocity vector components at initial moment), value of photocenter displacement (in case when its value is acceptable), and the RMS values, $\sigma_{T_i}^a$, see equation for each apparition, T_i. These values are calculated by using the observations from two adjacent apparitions. RMS values, $\sigma_{T_i}^a$, determined in such a way are referred further as a priori observational errors.

$$\sigma_a\left(T_i\right)=\sqrt{\frac{\sum_{j=1}^{n_i}\left(\left(\alpha_j^o-\alpha_j^c\right)^2\cos^2\delta_j^c+\left(\delta_j^o-\delta_j^c\right)^2\right)}{n_i-1}}\,.$$

All available observations of a comet are combined according to the following scheme. At first the observations of three apparitions are combined. The orbital parameters, the nongravitational acceleration values and the values of the photo centre displacement as well as the RMS values for each apparition are calculated. These RMS values are referred to as posterior errors. Then subsequent apparitions are linked one by one. We suppose that nongravitational accelerations are changed in cases when at least one value of a posterior error is much larger than an a priori error for the same apparition. The new parameters A_1, A_2, A_3 are added to the improved parameters in this case. In difficult cases such as close approaches to the planets, sudden increases of brightness, considerable asymmetric outgassing relative to perihelion, when Marsden's model of nongravitational acceleration does not allow one to represent the observations with sufficient accuracy, an instant variation of velocity of the cometary motion is assumed. Three components of instantaneous variation of cometary velocity are added to the improved parameters.

This procedure of orbit improvement has been realized in a computer program. It gives the possibility to derive the minor planet or comet orbits with high efficiency. To increase accuracy we used the modified Encke method of the numerical integration of motion equations. Modification of Encke method consists in changing the unperturbed osculation orbit at every step of integration. Unperturbed motion is calculated with quadruplicated accuracy using FORTRAN variables of the form REAL*16.

Numerical theory of motion of comet Kopff

To prove the efficiency of this procedure the improvement of the orbit of comet 22/P Kopff was done. The comet is moving along an elliptical orbit with period equal to 6.5 years. It was discovered in 1906. After discovery the comet performed 16 revolutions around the Sun. The comet was observed in 15 apparitions. The apparition in 1912 was missed because of bad observational conditions. Nevertheless, the comet was rediscovered in 1919 and

later was observed every time when it approached the Sun. Comet Kopff belongs to the Jupiter comet family. Its aphelion is not far from Jupiter's orbit. On March 30, 1954 it approached Jupiter up to a distance of 0.174 AU. During its observational history the comet's brightness periodically increased and considerable displacements of nucleus outgassing maximum relative to perihelion took place. All these circumstances complicated creation of a comprehensive numerical theory of motion. There are 7 sets of orbital parameters for this comet in Marsden's cometary catalogue [2]. Strictly speaking, it means that the trajectory is represented by several separate orbits not joined together. Our goal is to calculate the comprehensive numerical theory of motion of comet Kopff suitable for all available observations (1370 positional observations of this comet in the interval 1906–2002). At the preliminary stage we calculated orbital parameters by linking observations of adjacent apparitions by two over all investigated intervals. Then we calculated a priori RMS for each apparition. The RMS for observations in 1906 is obtained from improvement based on observations in just one apparition because of the absence of the adjacent one (the one that was missed). As for apparitions from 1906 to 1996 which had two RMS error values, the a priori error was considered to be the average of these values. An improvement of the orbit is carried out step by step. At each step the combined interval was increased, then a posterior errors of observations were calculated and the optimal number of improved parameters was defined. We assumed that two impulse velocity changes took place in the comet's motion. The first change of velocity took place at the moment when the comet approached close to Jupiter. The next moment of velocity change was selected by variation and dated February 1, 1973, when it was close to its aphelion. This velocity change can be explained by a brightness outburst of the comet marked by observers and also by considerable displacement of the outgassing maximum relative to its perihelion.

For linking all 16 apparitions 32 parameters were required: three position components, three velocity components, eighteen nongravitational acceleration parameters and two photocenter displacement values, and two sets of instant velocity changes. The numerical theory of motion presenting observations during the time interval 1906–2002 (16 apparitions) with mean square error $\sigma = 1.40''$ has been calculated. Figure shows changes of nongravitational accelerations A_1, A_2, A_3 from apparition to apparition. In these figures time is plotted on the abscissa. Time is shown in years. Along the ordinates the values of A_1, A_2, A_3 are shown in 10^{-9} AU/day^2, and vertical dotted lines mark moments of impulse changes of velocity. The analysis of the figures points at considerable changes of nongravitational accelerations. In the interval from 1906 to 1951 the nongravitational

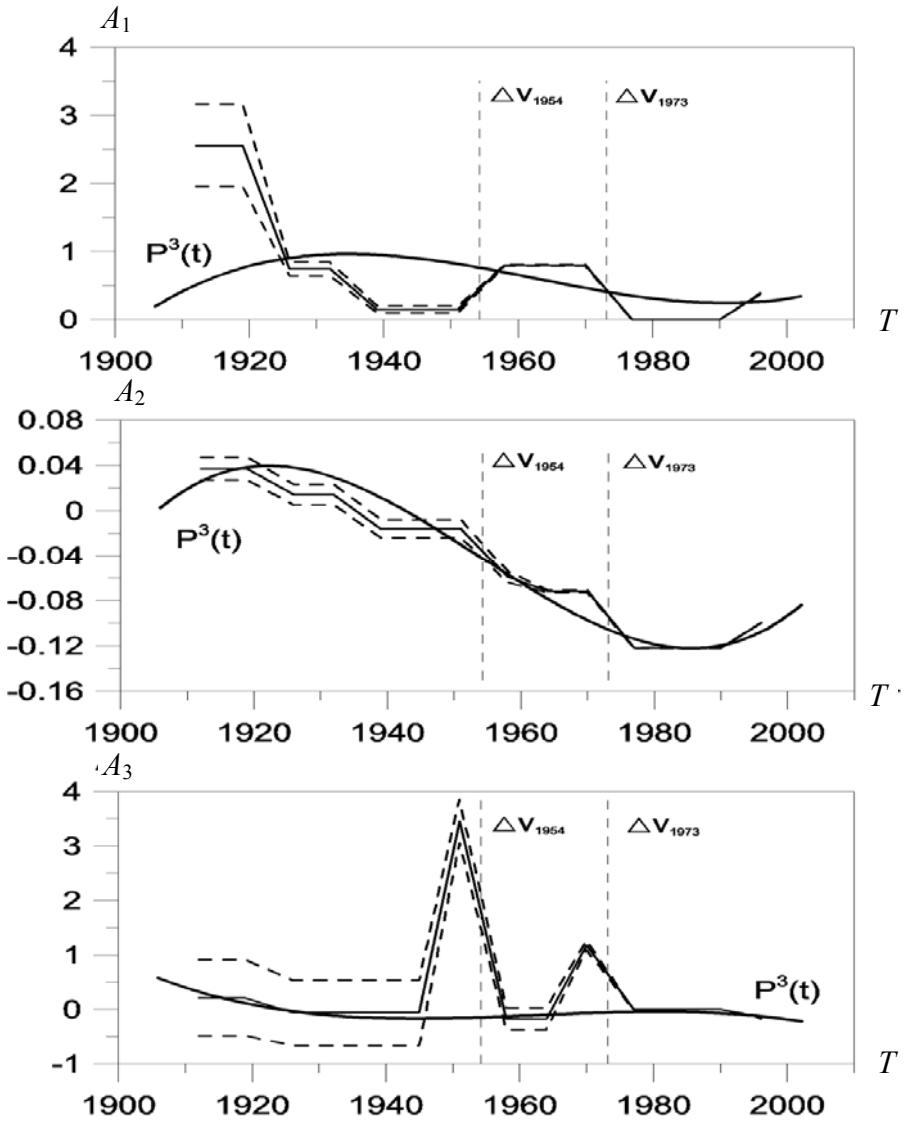

Change of components of nongravitational acceleration A_1, A_2, A_3.

acceleration components diminished, which is typical for most comets. Even before the comet approached Jupiter, the value of A_2 changed sign from positive to negative and component A_3 had a considerable jump. However, the following approach to Jupiter further complicates the evolution of its acceleration components. Value A_1 rises. This fact can be explained by im-

perfection of Marsden's model, which can be compensated for by a considerable increase of the value of A_3 and by assuming an impulse velocity change at the time of the closest pass by Jupiter. While investigating cometary dynamics, we discovered another moment when its orbital motion was influenced by nongravitational accelerations. It was its appearance in 1970 for which we also had to adopt the hypothesis about an impulse velocity change.

Conclusions

A method to improve cometary orbits with large non-gravitational accelerations has been developed. It enables one to link a large number of comet apparitions by a common orbit. A combined numerical theory for comet Kopff has been created for the period from 1906 to 2002. It links 16 cometary apparations with an RMS error $\sigma = 1.40''$. Linkage of 16 apparitions was attained at the cost of additional 26 parameters.

References

1. *Marsden B. G., Sekanina Z., Yeomans D. K.* Comets and nongravitational forces // Astron. J. 1973. Vol. 78. N 2. P. 211–229.
2. *Marsden B. G., Williams G. V.* Catalogue of Cometary Orbits. 16th ed. SAO. Cambridge. 2005.

COMETS: PHYSICAL NATURE AND MOTION

Nongravitational Effects on Cometary Motion due to Jupiter

M. D. Zamarashkina[1], O. F. Ogneva[2]

[1]Institute of Applied Astronomy of RAS, St. Petersburg, Russia
[2]Yaroslavl State Technical University, Yaroslavl, Russia

Abstract. The problem of linking cometary apparitions before and after the approach of a comet to Jupiter was investigated. A hypothesis of possible existence of additional acceleration, perturbing the motion of comets in the vicinity of Jupiter, was considered. This nongravitational perturbation is described by a function of the jovicentric distance, written in a standard "force law" form. The values of its coefficients are determined along with the osculating orbital elements by the least squares method in the process of fitting the comet positional observations. Numerical dynamical theories of comets Harrington-Abell, Kopff, and Shoemaker-Levy 9 were constructed. An additional acceleration in the cometary motion in the vicinity of Jupiter was included into the equations of motion along with the well-known gravitational and nongravitational perturbations. It was shown that inclusion of nongravitational acceleration enables one to reduce standard derivations of residuals for all considered objects.

Numerical dynamical theories of three comets were constructed. The dynamical model includes the main gravitational perturbations caused by the Sun, by the major planets (DE403 [1]), by the Galilean satellites (ERA system [2]), by the oblateness of Jupiter (J_2, J_4), and nongravitational effects of two types. The first acceleration caused by cometary sublimation was calculated according to B. Marsden's model [3]. The second is an additional acceleration in the vicinity of Jupiter. The authors consider this additional parameter as a formal one used to better fit observational data. Nongravitational perturbations from Jupiter are introduced into the equations of motion by simple expressions for the radial, transverse, and normal components in orbital jovicentric motion.

We assumed that these nongravitational perturbations are described by a function of the jovicentric distance, written in a standard "force law" form. The values of the coefficients A_i^j are determined along with the osculating orbital elements by the least squares method in the process of fitting the comet positional observations

$$a_i = \begin{cases} A_i^j \dfrac{1}{R_j^2}, & \text{if} \quad R_j \le 0.5 \text{ AU}, \\ 0, & \text{if} \quad R_j > 0.5 \text{ AU}. \end{cases} \tag{1}$$

In (1) a_i ($i = r, \tau, n$) are radial (axis is directed from the center of Jupiter), transverse (along normal to radius-vector in orbital plane), and normal to orbital plane components of nongravitational acceleration from Jupiter, R_j is the jovicentric distance, A_i^j ($i = r, \tau, n$) are coefficients whose values are determined along with the osculating orbital elements.

Three comets having close approaches to Jupiter and observed before and after approaches — 52/P Harrington–Abell, 22/P Kopff, and SL9 — have been chosen as objects for this study. The information about approaches of these comets is presented in Tab. 1.

Table 1. The moment ($T_{\min}$) and distance ($r_{\min}$) of the close approach of comet to Jupiter

Object	$T_{\min}$	$r_{\min}$, AU
52/P Harrington-Abell	12 Apr 1974	0.037
22/P Kopff	30 Mar 1954	0.111
Shoemaker-Levy 9 (SL9)	Comet was located in satellite orbit of Jupiter	

Comet P/52 Harrington-Abell

This comet was discovered in 1955. It had a few close approaches to Jupiter. The closest one was in 1974. Due to it the orbit of the comet was significantly changed. Reliable orbits could be calculated before and after 1974. S. Nakano [4] linked 4 apparitions containing close approaches to Jupiter. In this work we tried to link all available apparitions of this comet.

At the first stage (Tab. 2) two systems (I, II) of orbital parameters were obtained. Secondly, the linkage of seven comet apparitions in 1955–1999 was done. An attempt of the orbit determination on the whole interval including the approach to Jupiter with unified system of elements was not successful — large errors in (O–C) were obtained (system III). At the third stage the dynamical model of cometary motion was expanded. An additional jovicentric acceleration was included into the equations of motion. The va-

lues of its components were defined together with the cometary parameters (system IV) in the process of fitting the comet positional observations.

The data presented in Tab. 2 show that inclusion of an additional perturbation allows one to reduce the standard residuals (σ) and link seven apparitions of Comet Harrington–Abell.

Table 2. The characteristics of the systems of orbital parameters of Comet Harrington-Abell

System	Observational period	Approaching Jupiter	Inclusion of additional acceleration	σ
I	1955–1969	Before	No	0.84″
II	1975–1999	After	No	0.91″
III	1955–1999	Contains	No	1.11″
IV	1955–1999	Contains	Yes	0.91″

Comet Kopff

The comet was observed from 1906. It had four close approaches to Jupiter. The closest one was in 1954. Under the assumption that the nongravitational acceleration changed in the course of the approach of the comet to Jupiter the accuracy of orbit determination was increased. 12 apparitions of the comet (1906–2003) were linked. Including an additional acceleration allows one to reduce differences between the observed and calculated positions of comet Kopff in 1906, 1919 and 1932 apparitions.

Comet of Shoemaker-Levy 9 (SL9)

Comet SL9 broke up into many fragments (which have been designated by letters from A to W) during its approach to Jupiter at 1.3 Jupiter radii in 1992. Precovery images of the comet (dating back to March 1993) were not found. It is possible to calculate only probable orbit before 1992. As a result, a generally accepted pre-impact orbit of SL9 parent body is not known.

The orbits of 13 fragments of SL9 were calculated in two ways. In the first variation the jovicentric acceleration was not included into the equations of motion, in the second one it was included. The orbit of fragment H was chosen as base-orbit. The retrospective orbital evolution of fragment H was investigated. In the first variation (see Figure, var. 1) fragment H orbited Jupiter at least a century before the disruption in 1992 and probably longer. In the second one (see Figure, var. 2) the fragment was located on a Jupiter satellite orbit only for one rotation.

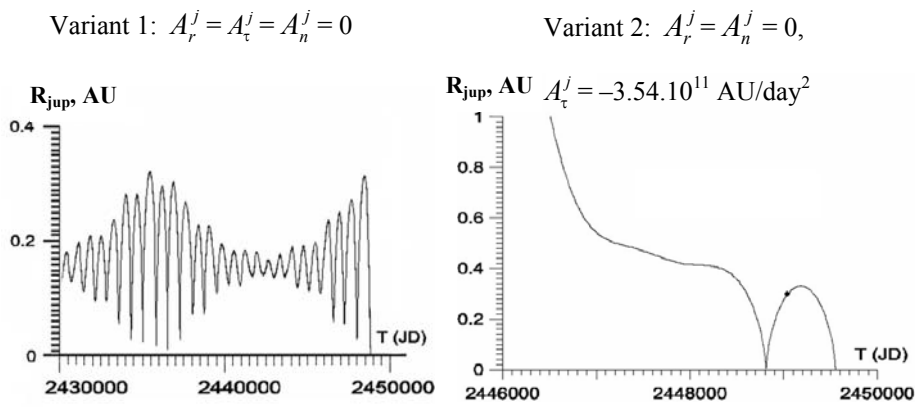

Jovicentric trajectory of fragment H of Comet SL9.

The result of improvement and additional nongravitational parameters for three comets as obtained from observations are presented in the Tab. 3.

Table 3. The results of improvement of orbital parameters

Object	ΔT	n	σ^j	σ	N	$A_r^j \cdot 10^8$, AU/day^2	$A_\tau^j \cdot 10^8$, AU/day^2
52/P	1955–1999	494	0.91″	1.11″	7	0.0456 ± 0.0045	0.0720 ± 0.0041
22/P	1906–2003	1224	1.86″	1.90″	12	0.0950 ± 0.0010	–0.0146 ± 0.0015
SL9	1993–1994	203	0.57″	0.62″	1	Detected with large errors	0.0234 ± 0.0097

In the Tab. 3 ΔT is the observational interval, n is the number of observations, σ^j are standard deviations of the residuals taking into account additional acceleration, σ are the standard deviations without additional acceleration, N is the number of apparitions of the comet, A_r^j, A_τ^j are radial and transverse components of the nongravitational acceleration from Jupiter. Calculations have shown that for all three comets the normal component has been derived with large errors.

Conclusion

1. The hypothesis of the possible existence of an additional nongravitational acceleration in the cometary motion, when a comet is approaching Jupiter, was considered. The method of determination of these acceleration parameters was developed.

2. The values of components of additional nongravitational perturbations were calculated for three comets.

3. The numerical pre-impact theory of the orbital evolution for the SL9 parent body was constructed [6].

4. Allowing for additional acceleration in the comet motion, 7 apparitions of the comet Harrington–Abell were linked with $\sigma = 0.91''$ [5] and 12 apparitions of the comet Kopff were linked with $\sigma = 1.86''$. The standard deviations of residuals for different fragments of SL9 were reduced up to $0.01''$–$0.04''$ [6].

References

1. *Standish E. M. et al.* JPL planetary and lunar ephemerides DE403/LE403 // JPL IOM 314.10–127. 1995.
2. *Krasinsky G. A., Vasilyev M. V.* ERA: knowledge base for ephemeris and dynamical astronomy // Proc. of IAU Coll. 165. 1997. P. 239–244.
3. *Marsden B. G. et al.* Comets and nongravitational forces // Astron. J. 1973. Vol. 78. P. 211–225.
4. *Marsden B. G., Williams G. V.* Catalogue of cometary orbits // Minor Planet Center. Smithsonian Astrophys. Obs., Cambridge, MA. 2005.
5. *Grigoryan O. F., Medvedev Yu. D., Tomanov V. P.* The hypothesis of additional acceleration in the motion of the comet Harrington-Abell from Jupiter // Solar System Res. 2004. Vol. 38, N 5. P. 394–402.
6. *Zamarashkina M. D.* Possible models of capture of a comet to Jupiter satellite orbit // Proc. of the Int. Conf. “Near-Earth Astronomy-2003”. Terskol, Russia. Sept. 8–13. 2003. P. 108–115 (in Russian).

COMETS: PHYSICAL NATURE AND MOTION

Variation of Nongravitational Parameters for Comet Encke as a Result of its Decay

M. G. Ishmukhametova[1, 2], E. D. Kondrat'eva[1], V. S. Usanin[1, 2]

[1]Kazan State University, Kazan, Russia
[2]Engelhard Astronomical Observatory, Zelenodolsky region, Russia

Abstract. An assumption is made that variations of nongravitational parameters of comet Encke in Marsden's model are caused by its secular decay. To account for decrease of nongravitational parameters three variants of physical processes are proposed: 1) deposition of a substantial nonvolatile mass not impeding the sublimation; 2) generation of a little-massive mantle shrinking the effective area linearly; 3) generation of a little-massive mantle shrinking the area exponentially. The corresponding equations are derived. The adequacy of the first two models over more than 150 years is shown.

Many models [1] explain the behavior of Marsden's parameters [2] of comet Encke [3] by the rotation pole precession of the spotty nucleus as proposed by Whipple and Sekanina [4]. Since the comet decay is not considered, they are not self-consistent. Other shortcomings are reviewed by Chernetenko [5].

In the present work we examine three models for secular decay of comet Encke assuming a constant shape of the nucleus. (Keeping nearly constant shape of a cometary nucleus was confirmed by Medvedev [6].) Since not all the mass is ejected in the same direction, Meshcersky's equation for the reactive force acting on the comet nucleus of mass m is given by

$$\vec{F}_r = \lambda \vec{u} \frac{dm}{dt}, \tag{1}$$

where λ is the anisotropy factor and $\vec{u}$ is the velocity of the matter escaping from the nucleus in the orbital coordinate system; in Marsden's model [2]

both being considered as constants. The number of particles in mass m is given by

$$N = mN_A / M\,, \tag{2}$$

where N_A is the Avogadro number and M is the mean molecular mass. In Marsden's model the number of ejected particles from a unit pure area during unit time is given by

$$-\frac{1}{\beta S}\frac{dN}{dt} \equiv Z = Z_0 g(r(t))\,, \tag{3}$$

where S is the geometrical area, $0 \le \beta \le 1$ is the ratio of the effective area to geometrical area, $r(t)$ is the heliocentric distance (in AU), and

$$g(r) = 0.111262 \cdot 10^{-8} (r / 2.808)^{-2.15} (1 + (r / 2.808)^{5.093})^{-4.6142}\,. \tag{4}$$

In preliminary calculations one can use $\langle g(r(t)) \rangle = g(a,\ e)$ depending on the size and shape of the orbit. One obtains the acceleration in orbital coordinates (i = 1; 2; 3 are radial, transverse, and normal directions):

$$w_i = -\frac{\lambda u_i M Z_0 \beta S}{N_A m} g(r)\,. \tag{5}$$

By definition, one finds Marsden's parameters (units are AU/(104 days)2):

$$A_i = -\frac{\lambda u_i M Z_0 \beta S}{N_A m}\,. \tag{6}$$

1. Assume a substantial nonvolatile mass is deposited. To continue this deposition, it should not impede the sublimation ($\beta = 1$). Before Style II Marsden's model was introduced, a similar case was considered by Sekanina [7] but it was not developed. If the nucleus shape is constant, then

$$\frac{S}{m_{\text{ice}}} = \frac{\varphi}{\rho_{\text{ice}} R}\,, \tag{7}$$

where φ depends on the shape ($\varphi = 3$ for a sphere), ρ_{ice} and m_{ice} are the density and the mass of the ice, R is its mean radius defined as

$$R = \sqrt[3]{\frac{3m_{\text{ice}}}{4\pi\rho_{\text{ice}}}}\,. \tag{8}$$

Analogically R_{end} is defined using the nonvolatile mass $m_{\text{end}} = m - m_{\text{ice}}$:

$$R_{\text{end}} = \sqrt[3]{\frac{3m_{\text{end}}}{4\pi\rho_{\text{end}}}}. \tag{9}$$

Hence Marsden's parameters and their variations due to the ablation are

$$A_i = -\frac{\lambda u_i M Z_0 \varphi}{N_A \rho_{\text{ice}}} \frac{R^2}{R^3 + (\rho_{\text{end}} R_{\text{end}}{}^3 / \rho_{\text{ice}})}, \tag{10}$$

$$\frac{dA_i}{dR} = -\frac{\lambda u_i M Z_0 \varphi}{N_A \rho_{\text{ice}}} \frac{2R(R^3 + (\rho_{\text{end}} R_{\text{end}}{}^3 / \rho_{\text{ice}})) - 3R^4}{(R^3 + (\rho_{\text{end}} R_{\text{end}}{}^3 / \rho_{\text{ice}}))^2}. \tag{11}$$

And also their combination is

$$\frac{dA_i}{A_i dR} = \frac{2}{R} - \frac{3R^2}{R^3 + (\rho_{\text{end}} R_{\text{end}}{}^3 / \rho_{\text{ice}})}. \tag{12}$$

Combining (2), (3), (7), and (8) if $\beta = 1$, one obtains

$$\frac{dR}{dt} = -\frac{\varphi M Z_0}{3 N_A \rho_{\text{ice}}} g(r). \tag{13}$$

Designating $\sqrt[3]{\frac{\rho_{\text{ice}}}{\rho_{\text{end}} R_{\text{end}}{}^3}} R = \chi \geq 0$ and $\frac{\phi M Z_0}{3 N_A \rho_{\text{ice}}{}^{2/3} \rho_{\text{end}}{}^{1/3} R_{\text{end}}} = \alpha \geq 0$ in (12) and (13), one writes the final set

$$\begin{cases} \dfrac{dA_i}{d\chi} = A_i \left(\dfrac{2}{\chi} - \dfrac{3\chi^2}{1+\chi^3}\right), \\ \dfrac{d\chi}{dt} = -\alpha g(r(t)), \\ \alpha = \text{const}. \end{cases} \tag{14}$$

Table 1. Parameters of solution in Fig. 1 for beginning and ending dates of model

Year	A_2	α, day^{-1}	χ
1786	–0.0461	$3.24 \cdot 10^{-5}$	0.945
2032	0		0

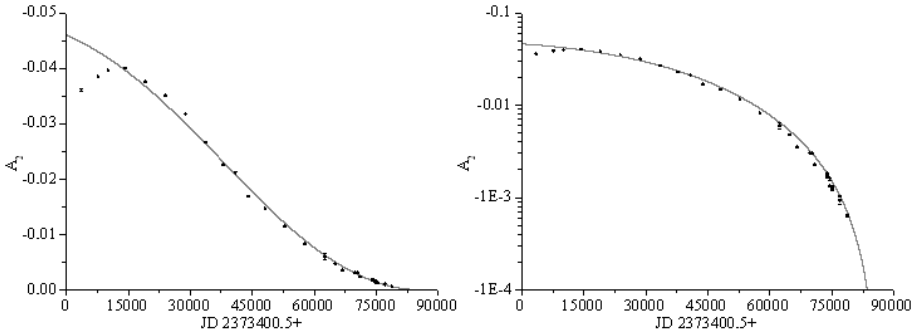

Fig. 1. Formal solution of set (14) on linear and logarithmic scales.

The formal (because input data are A_2 with mean errors from [2, 3, 8] and other sources, not astrometry) solution of (14) for A_2 (which is much more accurate than both A_1 and A_3) is in Fig. 1, its parameters are in Tab. 1. Here and below elements a, e, are assumed as equal to their mean values. The accuracy of A_2 increased with time when its value decreased, thus the graph on the logarithmic scale is a better representation for the weighted accuracy. One can see that the model reproduces A_2 adequately over more than 170 years and predicts the total decay about 2022.

2. Suppose a little-massive mantle is generated shrinking the effective area linearly with the thickness. This is equivalent to Shul'man's assumption that the mantle formation is completed when the volume containing the covering area equal to the nucleus area has sublimated [9]. In analogy to (7) one has

$$\frac{S}{m} = \frac{\varphi}{\rho R}, \tag{15}$$

where ρ is the nucleus density (assumed uniform), R is the mean radius:

$$R = \sqrt[3]{\frac{3m}{4\pi\rho}}. \tag{16}$$

Hence Marsden's parameters and their variations due to the ablation are

$$A_i = -\frac{\lambda u_i M Z_0 \varphi \beta}{N_A \rho R}, \tag{17}$$

$$\frac{dA_i}{dR} = -\frac{\lambda u_i M Z_0 \varphi}{N_A \rho} \frac{d(\beta / R)}{dR}. \tag{18}$$

And also their combination is

$$\frac{dA_i}{A_i dR} = \frac{R}{\beta}\frac{d(\beta / R)}{dR} = \frac{1}{\beta}\frac{d\beta}{dR} - \frac{1}{R}. \tag{19}$$

By the model assumption, one gets

$$\beta = 1 - h / h_0, \tag{20}$$

where h_0 is the mantle thickness terminating the sublimation,

$$h = \frac{f(m_{\text{begin}} - m)/\rho}{S} \tag{21}$$

is its current thickness, m_{begin} is the initial mass, and f is the nonvolatiles bulk part. Substituting (15) and (16) one has

$$h = \frac{f}{\varphi}\frac{R_{\text{begin}}{}^3 - R^3}{R^2}. \tag{22}$$

Derivating (20) with respect to *R*, considering (22), and substituting R_{begin} from them, one obtains

$$\frac{d\beta}{dR} = \frac{3f}{\varphi h_0} + \frac{2(1-\beta)}{R}. \tag{23}$$

Hence one sets (19) to:

$$\frac{dA_i}{dR} = A_i\left(\frac{1}{\beta}\frac{3f}{\varphi h_0} + \frac{2}{\beta R} - \frac{3}{R}\right). \tag{24}$$

Combining (2), (3), (15), and (16), one obtains

$$\frac{dR}{dt} = -\frac{\varphi M Z_0}{3N_A\rho}\beta g(r). \tag{25}$$

Designating $\frac{3f}{\varphi h_0}R = \chi$ and $\frac{MZ_0 f}{N_A \rho h_0} = \alpha$ in (24), (23), and (25), one writes

$$\begin{cases} \dfrac{dA_i}{d\chi} = A_i\left(\dfrac{1}{\beta} + \dfrac{2}{\beta\chi} - \dfrac{3}{\chi}\right), \\ \dfrac{d\beta}{d\chi} = 1 + \dfrac{2(1-\beta)}{\chi}, \\ \dfrac{d\chi}{dt} = -\alpha\beta g(r(t)), \\ \alpha = \text{const}. \end{cases} \tag{26}$$

The formal solution of (26) for A_2 is in Fig. 2, its parameters are in Tab. 2. It reproduces A_2 adequately over more than 150 years and suggests that on discovery the comet surface was nearly pure ice ($\beta > 1$ makes no sense).

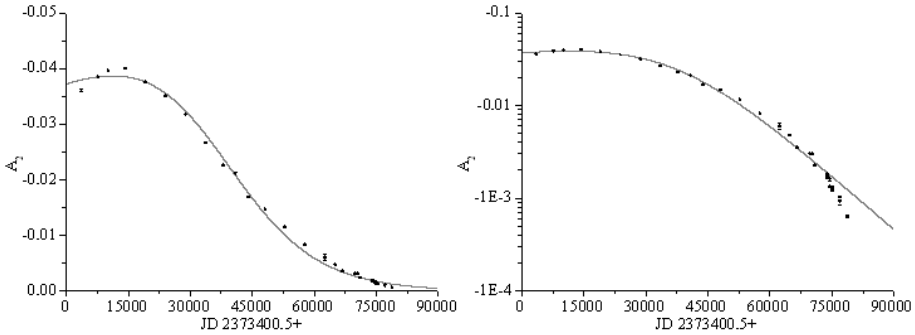

Fig. 2. Formal solution of set (26) on linear and logarithmic scales.

Table 2. Parameters of solution in Fig. 2 for beginning and ending dates of model

Year	A_2	α , day^{-1}	β	χ
1786	–0.0372	$3.32 \cdot 10^{-5}$	0.99	0.637
2032	–0.000455		0.00547	0.288

3. A case of the generation of a little-massive mantle shrinking the effective area exponentially was also considered. It was shown that this model represents the variation of A_2 only qualitatively and is of no interest.

Solutions obtained in the present work leave significant offsets. Causes of offsets may be not only in model assumptions, but also out of them. These are the solution procedure formality, the cometary stochasticity, and accidental errors in A_2 multiplied by the correlation with little-significant A_1.

References

1. *Yeomans D. K., Chodas P. W., Sitarski G., Szutowicz S., Królikowska M.* Cometary Orbit Determination and Nongravitational Forces / Eds M. C. Festou, H. U. Keller, H. A. Weaver. Comets II. Tucson: Univ. Arizona Press, 2004. P. 137–151.
2. *Marsden B. G., Sekanina Z., Yeomans D. K.* Comets and nongravitational forces. V. // Astron. J. 1973. Vol. 78. P. 211–225.
3. *Marsden B. G., Sekanina Z.* Comets and nongravitational forces. VI. Periodic comet Encke 1786–1971 // Astron. J. 1974. V. 79. P. 413–419.
4. *Whipple F. L., Sekanina Z.* Comet Encke: precession of the spin axis, nongravitational motion, and sublimation // Astron. J. 1979. Vol. 84. P. 1894–1909.

5. *Medvedev Yu. D., Sveshnikov M. L., Sokolsky A. G., Timoshkova E. I. et al.* / Ed. A. G. Sokolsky. Asteroid-Comet Hazard. St. Petersburg: ITA RAS, 1996 (in Russian).
6. *Medvedev Yu. D.* Effekty sublimatsii v orbital'nom i vrashchatel'nom dvizhenii kometnogo yadra. Avtoref. diss… dokt. fiz.-mat. nauk. (Effects of sublimation in orbital and rotational motion of cometary nucleus. Abstr. ScD thesis.) St. Petersburg: IAA RAS, 1995 (in Russian).
7. *Sekanina Z.* Dynamical and Evolutionary Aspects of Gradual Deactivation and Disintegration of Short-Period Comets // Astron. J. 1969. Vol. 74. P. 1223–1234.
8. *Kozlov E. A., Medvedev Yu. D., Zamarashkina M. D., Pittichová J. et al.* Catalogue of short-period comets. Bratislava: Astronomical Institute, Slovak Academy of Sci. 2005.
9. *Shul'man L. M.* Dinamika kometnykh atmosfer. Neitral'ny gaz. (Dynamics of cometary atmospheres. Neutral gas.) Kiev: Naukova dumka, 1972 (in Russian).

COMETS: PHYSICAL NATURE AND MOTION

On the Problem of Searching for Undiscovered Cometary Families Colliding with Terrestrial Type Planets

N. I. Perov, D. V. Kolesnikov

Yaroslavl State Pedagogical University, Yaroslavl, Russia

Abstract. The process of the transition of a comet nucleus from an initial heliocentric parabolic orbit into a heliocentric elliptical (parabolic with different parameters or hyperbolic) trajectory is investigated in terms of a pairwise three dimensional two-body problem: the Sun – comet nucleus and terrestrial planet — comet nucleus. Analytical formulas are reported for the orbital parameters of a nucleus after its passing through the sphere of influence of a terrestrial planet. It should be noted that the new minimal values of the orbital periods of the nuclei P_{min} are within the limits 10–10^4 years (P_{min} for "families" of comets of Mercury, Venus, Earth, and Mars is equal to 10130, 34, 19, 632 tropical years, respectively). The angles between directions "the Earth – the Sun" and "the Earth – the planet (Mercury, Venus)", corresponding to the epochs of collisions of the comet nuclei with the Earth (or epochs of appearance of new meteor streams associated with existing or disintegrated comet nuclei) are determined. The bottleneck of revealing of such meteoroid complexes is concerned with the small value of the corresponding impact parameter. The value is on the order of magnitude of 10 % of the radius of the terrestrial type planet (whereas for the giant planets it is equal to 10 radii).

Introduction

It is assumed [1, 2] that there are 10^{12}–10^{13} comets in the Oort cloud, moving along elliptical orbits. Perturbations from stars and gigantic molecular clouds, passing near the Sun, force some comets of Oort's cloud to move into the inner Solar System and these comets turn into short- or long-period comets, or parabolic or hyperbolic comets. The major planets may play an important role in this process [3]. There are only about 4000 comets in modern comet catalogues [1–3]. Development of theoretical methods of localiza-

tion in space-time of undiscovered comets, radiants of meteor streams, and forecasting appearances near the Earth of uncatalogued minor bodies is of a special interest [1]. (It is believed up to now that discoveries of comets are random and unpredictable [4], [5]). Based on interaction of minor bodies with major planets of the Solar System a model of forecasting the appearances of yet undiscovered minor bodies including those hazardous for Earth's civilization is presented below.

A non-traditional model of migration of comets

Let us consider a model of interaction of a comet in parabolic heliocentric orbit, and a planet of mass M_{pl}. The comet at the perihelion of the heliocentric orbit approaches the planet, which moves in a circular orbit of radius r_{pl} with velocity V_{pl}. An initial angle between the orbital planes of the comet and the planet is equal to i_0 (Fig. 1). The process of interaction of the comet and the planet will be considered as a momentary turn of the velocity vector V_c of the comet, having a close approach with the planet (Fig. 2).

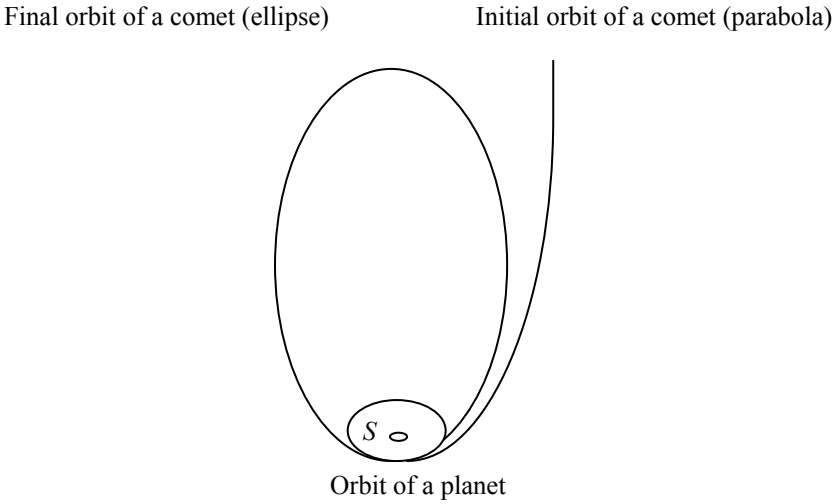

Fig. 1. A comet on a parabolic orbit approaches a terrestrial type planet. The new perihelion is placed near the orbit of the planet. The new aphelion is placed far beyond the Sun (*S*): 13 AU (in a case of a comet approaching the Earth) and 930 AU (in a case of a comet approaching Mercury).

The angle of turn of the comet velocity vector (within the sphere of action of the planet) is maximum, if the comet approaches the planet at the minimal distance without colliding. For this distance we take the radius of the planet R_{pl}. (roche limit is not taken into account). A target parameter of the comet ρ should be in excess of ρ_{crit} (for ρ_{crit} $r_{min} = R_{pl}$), otherwise the comet will collide with the planet and will subsequently not be considered. The

comet with velocity of V enters into the sphere of influence of the planet, whose mass is M_{pl}. Setting for the heliocentric motion $r \approx r_{pl}$ (at the moment of time of "collision" of comet and planet) we determine analytically an angle of turn θ of a velocity vector of the comet in the sphere of action of the planet, a semi-major axis a, an eccentricity e, inclination i, true anomaly v of the comet for the new heliocentric orbit (after scattering the comet by gravitational field of the planet and egress of this object from the sphere of the planet's action) and an angle α between the heliocentric radius-vector of comet r and the vector of the heliocentric velocity V. The new perihelion distance of the comet is denoted by r_{pl}. The parameters of the final orbit (without indexes) of the comet are connected with some parameters of the original (parabolic in accordance with the model) orbit (index "0") and with that of the planet by the following formulae (1–5), corrected as compared with [3]. Some results are presented in Tab. 1.

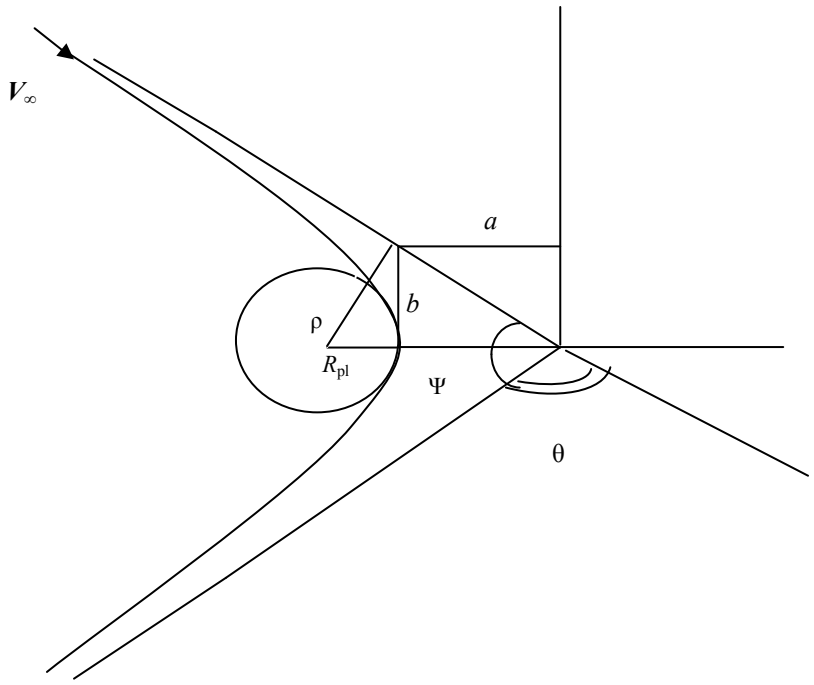

Fig. 2. Comet **a**pproaching a planet. V_∞ is the velocity of the comet at the boundary of the sphere of action of the planet. R_{pl} is the radius of the planet. ρ is the impact parameter of the comet, a and b are real and imaginary semi-major axes of the hyperbola, θ is the angle by which the velocity of the comet turns in the sphere of action of the planet), 2Ψ is the angle between asymptotes of the hyperbola.

$$\nu' = \frac{1}{\left[\frac{M_{\text{Sun}}}{M_{\text{pl}}} \cdot \frac{R_{\text{pl}}}{r_{\text{pl}}}(3 - 2\sqrt{2}\cos i_0) + 1\right]^2}, \quad (1)$$

$$a = \frac{r_{\text{pl}}}{4\nu'(\sqrt{2}\cos i_0 - 1)}, \quad (2)$$

$$e^2 = 1 - 8\nu'(\sqrt{2}\cos i_0 - 1)\{[1 - \sqrt{2}\nu'(\sqrt{2} - \cos i_0)]^2 + 2\nu'^2 \sin^2 i_0\}, \quad (3)$$

$$\tan i = \pm \frac{\sin i_0 (1 - 2\nu')}{\cos i_0 - \sqrt{2}\nu'(\sqrt{2}\cos i_0 - 1)}, \quad (4)$$

$$\cos v = \frac{2 \cdot \left\{\left[1 - \sqrt{2}\nu'(\sqrt{2} - \cos i_0)\right]^2 + 2\nu'^2 \sin^2 i_0\right\} - 1}{e}. \quad (5)$$

The relation between impact parameters ρ, measured in terms of the radius of the planet, for $i_0 = 0^\circ$ and $i_0 = 180^\circ$ (invariant for all planets of the solar and extrasolar systems) is given by

$$\frac{\rho^2(0^\circ) - 1}{\rho^2(180^\circ) - 1} = 17 + 12\sqrt{2}. \quad (6)$$

Table 1. Capture of comets by terrestrial type planets at the perihelia of the initial parabolic comet orbits with subsequent ejection

Planet	ν'	α, deg.	a, AU	e	v, deg.	i, deg.
Mercury	$0.498 \cdot 10^{-3}$	90.766	468.822	0.999174	1.499	0
	$0.451 \cdot 10^{-6}$	90.415	–88845.681	1.000004	0.263	180
Venus	0.041	96.785	10.654	0.933092	14.059	0
	$0.550 \cdot 10^{-4}$	91.451	–1362.070	1.000530	2.900	180
Earth	0.0842	99.731	7.169	0.864789	20.954	0
	$0.141 \cdot 10^{-3}$	92.333	–732.540	1.001363	4.648	180
Mars	0.0124	93.742	73.921	0.979476	7.562	0
	$0.135 \cdot 10^{-4}$	90.720	–11638.875	1.000131	1.440	180

Hypothetical ephemerides of undiscovered hazardous comets

In Tab. 2 Ephemerides of undiscovered periodic comets and radiants of unknown meteor streams for the epochs of their collisions with the Earth are presented for the case i = 0º.

Table 2. Ephemerides of undiscovered periodic comets and radiants of unknown meteor streams for the epochs of theirs collisions with the Earth (after approaching the cometoids, migrated from the periphery of the Solar System, with major planets). γ is the angle at the Earth between directions to the Sun and to the planet (elongation of the planet from the Sun); χ – is the angle at the Earth between directions to the Sun and to the comet (radiant of the meteor stream); λ and β are ecliptical coordinates (for the ecliptical circle orbits of the planet and ecliptical elliptical orbits of the comets (and the streams). The angles γ and χ are constant and they determine the epoches of searching for unknown comets and radiants of meteor streams. $i = 0^{\circ}$. *

Epochs yyyy mm dd	Right ascension α h m	Declination δ ° '	Planet with which comet approaches	γ ° '	χ ° '
2009 09 07	13 23 08 35	–08 46 18 35	Mercury	21 58	38 29
2010 01 18	17 13 22 32	–23 15 –09 21			
2010 02 08	18 47 23 49	–22 46 –01 22			
2009 12 13	13 21 21 28	–09 01 –15 08	Venus	07 09	58 13
2010 02 10	17 31 01 11	–23 02 07 36			
Daily	$\lambda = \lambda_{Sun} + \chi$ $\beta = 0$		Earth	–	80 16

Conclusion

The considered model of the transition of comets from parabolic into elliptical orbits makes it possible to do the following: a) choose more definitely the initial conditions for the process of comet migration; b) dynamically explain the adopted classification of comets into planetary families; c) explain the deficit of observed comets with perihelion distance $r_P < 2.5$ AU; d) interpret the formation of the association between a number of short-period comets, on the one hand, and Jupiter ("six-year" comets), Saturn ("13-year" comets), on the other hand. Discrepancies are found to

* Editorial note: One should emphasize that the probability of observing comets or meteor radiants in accordance with these ephemerides is very low, since they are based on suppositions that are usually not fulfilled for the few new comets.

exist for the well-known families of Uranus ("33-year" comets) and Neptune ("75-yar" comets), because it follows from our study that comets with periods of 43 and 81 years must be ascribed to these families, whereas comets with period of 34 and 19 years must be ascribed to the families of Venus and Earth, respectively; e) compute ephemerides of undiscovered hazardous comets and radiants of unknown meteor streams.

The work is carried out in the frame of the Federal special purpose program "Scientific and scientific — pedagogical personnel of innovation in Russia" for 2009–2013 (state contract N P539).

References

1. *Ipatov S. I.* Migratsiya nebesnykh tel v Solnechnoi sisteme (Migration of Celestial Bodies in the Solar System). M.: Editorial URSS, 2000. (in Russian).
2. *Levison H. F., Morbidelli A., Dones L. et al*. The mass disruptions of Oort cloud comets // Sci. 2002. Vol. 296. N 5576. P. 37–50.
3. *Perov N. I.* Model of the Origin of Planetary Comet Families // Solar System Res. 2005. Vol. 39, N 3. P. 281–287.
4. *Belton M. J. S., Thomas P., Veverka J. et al.* The internal structure of Jupiter family cometary nuclei from Deep Impact observations: The "talps" or "layered pile" model // Icarus. 2007. Vol. 187, N 1. P. 332–344.
5. *Moehlmann D.* The enigma of cometary nuclei // Solar System Res. 2009. Vol. 43, N 3. P. 215–219.

The Asteroid-Comet Hazard Conference Proceedings, 2009

COMETS: PHYSICAL NATURE AND MOTION

Electronic Catalogue of Comets "Halley"

Yu. S. Bondarenko

Institute of Applied Astronomy of RAS, St. Petersburg, Russia

Abstract. In this paper we give a description of the Electronic Catalogue of Comets "Halley", which makes it possible to calculate the evolution of the orbits of comets, to visualize orbital motion, to determine the circumstances of a comet's close approach to planets within a given time interval, as well as a number of other opportunities. The database of cometary orbits contains elements of short-period comets, calculated with the original method developed at the IAA RAS for constructing numerical theories of comet motion, covering large intervals of time. It involves the determination of individual values of the constants A_1, A_2, A_3 (radial, transverse, and normal components of non-gravitational acceleration according to Marsden's model [1]) and the displacement of the photocenter for each apparition.

Introduction

The Electronic Catalogue of Comets "Halley" is an application for management and working with the database of comets (DC), containing information on comet elements and other parameters. The DC contains not only the orbital elements derived from existing catalogues of comets [2], but also elements of short-period comets, calculated using the original method developed at the IAA RAS. Besides Keplerian orbital elements, a record of the DC may include additional parameters used in the improvement and information about the physical characteristics of the comet, its observed apparitions, and other data. The tasks performed by an electronic catalogue, in addition to database management, include the calculation of the orbital evolution of comets and their visualization, identification of close approaches to the planets in a given time interval, as well as a number of other actions. The catalogue is intended for use with a personal computer with Microsoft Windows 98, Microsoft Windows XP, or Microsoft Windows Vista operating system.

General view of the catalogue

Designed for Microsoft Windows, the electronic catalogue is built into the GUI, which simplifies user interaction with the program. The catalogue is implemented as a dialog Windows application designed for the most convenient and efficient work. The main window contains the panel with the application menu and is divided into "work area" and "output area". The catalogue is divided into section tabs. Switching between sections is done by selecting the appropriate tab. The current version of the catalogue includes two sections:

• Start Page — this section takes the form of the cover, in its role as the title page. It has a certain number of possibilities: a) the "work area" section of the Start Page displays basic information about the catalogue; b) the "output area" section of the Start Page is used as a text editor.

• Elements — is the section for management and working with the catalogue. The "Work area" of the Elements section is intended to set the conditions for selection from the database. A table with the generated results is created in the "output area".

Features

Work with the Elements section (see Figure) can be formally divided into two types — database management and work with the database.

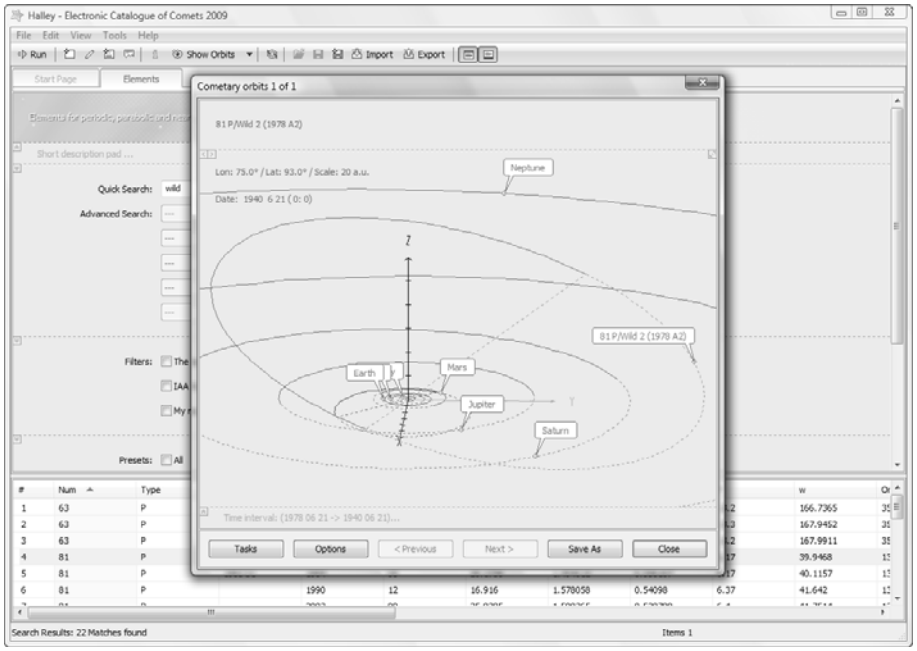

Elements section.

Database Management

The database of cometary orbits is the basis of the catalogue, so the DC management has a special place when working with the catalogue. DC provides information about all available apparitions of comets. Each record of database contains:

• The old and the new provisional designation, number and name of the comet.

• Type of cometary orbits.

• Epoch, date of perihelion passage, and the dates of the first and the last observations.

• Elements of the Keplerian orbit (perihelion distance, eccentricity, orbital period, inclination of the orbit, the argument of perihelion and longitude of the ascending node with respect to the ecliptic of 2000.0).

• The number of observations used for obtaining the orbit.

• The version of ephemerides of major planets used.

• Perturbations taken into account when determining the orbit.

• Components of nongravitational acceleration, asymmetric outgassing about perihelion, and displacement values of the photocenter.

• The values of the root mean square errors of observations.

• References to the source of catalogue data.

• History of the apparitions of a comet.

• Time of changing the record (added automatically).

The catalogue allows the user to perform the following operations with the DC records: a) adding new records "user records"; b) editing existing records; c) creating copies of existing records with the possibility of their editing; d) removing the existing records. (It should be noted that the "user records" can not be restored); e) importing records to DC from a file; f) exporting data from the DC to a file; g) updating or restoring DC from the IAA RAS internet server (this operation is possible only in case of an existing Internet connection).

Working with a database of comets

Work with the catalogue begins with selecting the necessary records from the database. This selection is done in the "work area" of the Elements section. The "Work area" for convenience is divided into several panels that can be hidden or expanded: a) A short description panel with useful tips on working with the DC; b) a quick and advanced search panel; c) a query filters panel, performs filtering records on the last apparition, "user records", and IAA RAS referenced records; and d) elements presets, standard elements, and calculated elements panels.

After specifying the necessary conditions index, a user query will be sent to the database. The "output area" creates a table with the found results.

The number of results is displayed in the lower left corner on the status bar, as well as in the first column of the table. If the user is not satisfied with the result, then he can make a re-assignment of conditions and further researches. If the result is satisfactory, further work is carried out in the "output area". Selected records by default are in ascending order of the first element. Also, the user has the ability to customize a convenient form of the output table.

It is important to note that any transaction relating to the work with the DC, is carried out only with the selected records. Current version of the electronic catalogue has the following features to work with DC: a) saving the information from the DC to a file; b) output the additional information of the selected records such as date of reopening, the number of observations in this apparition, brightness outbursts, etc. (only if such information is contained in the relevant records); c) visualization of a three-dimensional projection of the comet's orbits of selected records within a specified period of time; d) calculating the position and velocity, Keplerian orbital elements, data on close-approaches and perihelion passages of comets of selected records at the given moment.

It is important to note that in each type of the selected task it is possible to set proper preferences.

Implementation

Intel Visual Fortran and Intel Visual ++ compilers were used to create an Electronic Catalogue of Comets "Halley". The envelope of the catalogue is written in FORTRAN using the Win32 API functions. SQL database management is performed using the SQLite library. The method of calculation of cometary orbits has been implemented in FORTRAN. It allows for the possibility to perform high-precision improvements of comet orbits using available optical and radar observations. The method allows for a large number of apparitions to be linked by a common orbit. High accuracy of numerical integration is achieved through the use of the modified Encke's method. The modification consists of performing the change of the osculation epoch at each step of integration. The parameters of the unperturbed motion are calculated with quadruple precision by using variables of type REAL*16 (32 decimal).

Support and distribution

The Electronic Catalogue of Comets "Halley" contains updatable databases of cometary elements. It is assumed that monthly updates of DC will be stored on the Internet server of IAA RAS and that they will be automatically added to the database of application. Preparation of new elements of comets, observed during the current month, will be produced in IAA RAS

using specially designed software. Also new features as well as “bug” fixes will be made.

It is planned that the website of IAA RAS will contain a page of basic information about the catalogue and the latest news. Probably, a release version of the application will be ready for use during the next year.

References

1. *Marsden B. G., Sekanina Z., Yeomans D. K.* Comets and nongravitational forces // Astron. J. 1973. Vol. 78, N 2. P. 211–229.
2. *Marsden B. G., Williams G. V.* Catalogue of Cometary Orbits. 16th ed. Cambridge: SAO, 2005.

The Asteroid-Comet Hazard Conference Proceedings, 2009

COMETS: PHYSICAL NATURE AND MOTION

From the Tunguska Space Body to the Evolution of the Protoplanetary Nebula

O. G. Gladysheva

Ioffe Physical Technical Institute of RAS, St. Petersburg, Russia

Abstract. A model for the structure of comet nuclei is proposed based on the results of the investigations of carbonaceous substances from the epicenter of the Tunguska cosmic body (TCB) explosion. According to this model the comet nucleus structure is a conglomerate of micron sized ice granules covered with organic materials that have dust particles as their nuclei. Such structure could be formed at a stage of continuous temperature decrease in the protoplanetary nebula. After the water vapour has condensed onto the dust particles, organic molecules and gases such as NH_3, CO_2, H_2S, etc. are precipitated on the surfaces of ice-covered grains. Under the influence of different types of radiation (for example, cosmic rays) and thermal processing the polymerization of the initial components takes place and as a result carbon-chain and more complex molecules are formed*.

The structure of the Tunguska cosmic body

The peat bogs around the place of the Tunguska disaster (TD) are unique natural "archives" of matter that has fallen from the atmosphere. Since the growing mosses are located considerably higher than the subsoil water levels and receive the water-mineral nutrition from the atmosphere only, they are ideal depositories for substances that fell on their surfaces.

---

* Editorial note: This paper suggests several new ideas about the solar nebula and the formation and composition of comet nuclei based on investigations of the Tunguska event. However, many of these ideas are hypotheses that still need experimental verification or theoretical modeling based on well-established principles of physics and chemistry.

Radiocarbon analysis showed that peat sediments that corresponded to the TD time contain "ancient" carbon (depleted ^{14}C) in somewhat excessive amounts [1]. In Earth's atmosphere, ^{14}C is continually generated by galactic cosmic rays and is then assimilated as carbon oxides by plants. An essential decrease of ^{14}C suggests insertion of considerably mass of other carbon. The presence of matter from space in the "catastrophe's" levels of peat deposits was confirmed by the investigations conducted by Kolesnikov et al. [2, 3, 4].

Isotopic analyses of peat sediments showed that peat levels located a short distance from the epicenter of the disaster are characterized by an anomalous variation of both ^{13}C and D abundances (enrichment in the isotopic composition of carbon, and depletion in deuterium) [2, 3] while the maximum of the nitrogen isotope variation falls on the permafrost boundary [5]. It has been suggested that nitrogen oxides were washed out from the atmosphere by rain, and trickled down to permafrost level because of the porosity of peat. The fact that carbonaceous matter was able to reach the earth's surface and deposit on it points to the fact that this matter was neither liquid, nor gaseous; therefore, we conclude that this substance was either solid or sufficiently viscous.

Heavy carbon (^{13}C) has been found in cellulose molecules of dead plants [2], i. e., carbonaceous substances decomposed under the influence of bacteria, solar/earth radiation, and air components into CO_2, and were then assimilated by growing moss. This and the presence of C and H isotope variations in the same layers of peat sediments suggest that carbonaceous substances contain hydrocarbons, i. e. organic components. Thus, we can conclude that the TCB has transported interplanetary organic material (that is either solid or sufficiently viscous at Earth's surface temperatures) to Earth.

It was found that falls of carbonaceous organic compounds occurred extremely irregularly, as clearly shown by separate areas [1, 3]. Samples poor in carbonaceous compounds were located close by rich ones. Based on the sizes of the samples under investigation we can conclude that the organic fragments were considerably more massive ($>10^{-3}$ kg) than silicate particles ($< 5 \cdot 10^{-6}$ kg), which were identified as the TCB remnants [6]. On the assumption of homogeneity of "ice-dust" mixture we suggest that organic matter bound particles together, without which a formation so heavy fragments is impossible[**].

Moreover, an interesting peculiarity of the allocation of the TCB remnants on Earth's surface is the fact that the amount of organic compounds in peat samples exceeds the amount of dust (silicate) particles many times over

---

[**] Editorial note: This is a hypothesis that needs experimental verification or theoretical modeling based on well-established principles of physics and chemistry.

[1, 4]. Therefore, the organic substance was able to be released from the dust and this was possible only if silicates and organic components were segregated one from the other by water ice.

Based on the preceding, the following model of the matter of the TCB is suggested (Fig. 1, *c*): — covered with organic, bound together iced grains (1÷10 μm in size), having dust particles as their nuclei. These grains are similar to typical particles of comet Halley, which consist of a silicate core often covered by refractory (and icy) organic material [7].

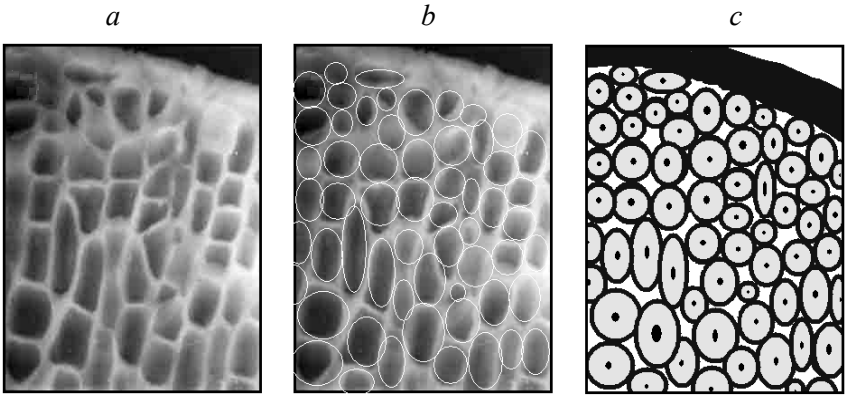

Fig. 1. Reconstruction of the TCB structure from the internal structure of the carbonaceous globule:
a — the chip of carbonaceous globule. Scanning electron microscope T-29 (Japan), magnification 2000. Photo courtesy of B. F. Bidyukov; *b* — cellular structure with marked granules of ~5 μm in size; *c* — model of the TCB structure that consists of particles covered with organics, bound together by icy grains with silicate dust cores.

The evolution of the protoplanetary cloud

The suggested structure could form only on the periphery of the protoplanetary nebula (PN). During the decreasing temperature of the initial nebula, the water vapour started condensing onto the dust particles. During the subsequent continued temperature decrease, the surfaces of the ice-covered particles served as places for the precipitation of organic molecules, which existed in the initial nebula as gases such as CH_4, NH_3, CO_2, H_2S, etc. Subsequently, chemical reactions, enhanced by UV light and gamma rays changed this mixture of volatile organic compounds. Furthermore, some thermal processes, i. e. the increased reaction rate during the heating of the grain surfaces, for example, by shock waves, furthered the chemical reactions. As a consequence the organic molecules were transformed into a high-molecular weight carbon backbone chain mixed up with high molecular weight organic compounds.

The carbonaceous particles (~1 mm in size) were found near the epicenter of the TCB explosion in the "catastrophe" layers of peat deposits (Fig. 2). The nature of these particles is not determined but terrestrial analogues are absent. The elemental composition of the carbonaceous globules (C — 45.0 %; O — 38.5 %; H — 4.3 %; N — 1.3 %) [8] is similar to composition of bituminous compound in meteorites (Mokoia: C — 46.4 %; O — 39.4 %; H — 5.0 %; N — 2.1 %). The dust inclusion was found on the surface and inside of globules. Some of them have magnetic properties, others look like black and white crystals, still others are similar to different color glasses [8]. The model structure (Fig. 1, *c*) could transform in the cellular structure (Fig. 1, *a*) under gradual heating. Since the structure (Fig. 1, *c*) has a cosmic origin, vacuum space between granules will "collapse" during slow defrosting, and partitions between cells will be represented as connected coverings of neighboring granules. If we deal with quick heating the increased volume of the granules' shells led to an extrusion or outlier of melted iced grains. As a result we will have a destruction of cellular structure (Fig. 2, *f*), formation of pores on the granule surface (Fig. 2, *c*), and formation of organic fragments without silicate dust.

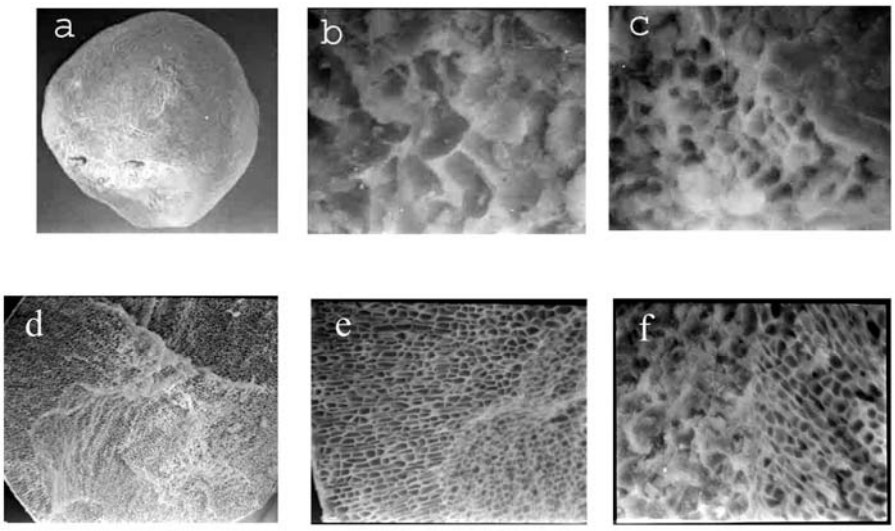

Fig. 2. The carbonaceous globules. Scanning electron microscope T-29 (Japan), magnification 2000. Photo courtesy of B. F. Bidyukov:
a — the globule ~1 mm in size (magnification 75); *b* — the surface of this globule (× 2000); *c* — near-surface layer of this globule (x 2000); *d* — the chip of globule (magnification 150); *e* — the same chip (× 500); *f* — near-surface layer of this chip (× 1000).

The covering of ice grains by organics, which become viscous at some temperatures, enables separate grains to cling together in order to form complicated multi-component objects (Fig. 1, *c*). A short-term heating of the surface layer, for example under the influence of shock waves, could form shells[***].

This TCB structure could be formed only in the beginning of the evolution of protoplanetary nebula (PN). From comparison the elemental composition of the Solar System with the TCB (Fig. 3) we can assume that the TCB was formed on periphery of the PN, beyond the ecliptic plane. The differentiation of the elements in the PN took place, probably, via variation in speeds of precipitation. It is known that heavy and large particles move more quickly through protoplanetary gas cloud to the ecliptic plane than light and small particles.

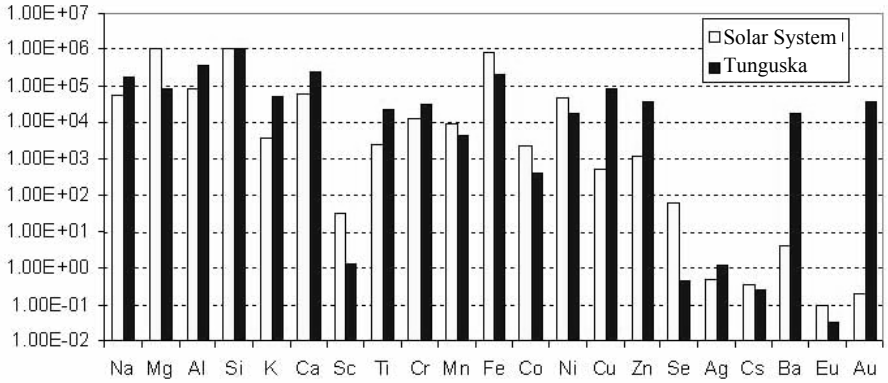

Fig. 3. Comparison the space abundance of chemical elements [9] with the approximate elemental composition of the TCB remnants [6].

References

1. *L'vov Yu. A.* Carbon in the Tunguska meteorite composition / Ed. N. V. Vasil'ev. Meteorite investigations in Siberia (75 years of the Tunguska phenomena), Novosibirsk: Nauka. 1984 (in Russian).
2. *Kolesnikov E. M.* Isotope anomalies H and C from the peat of the place of the Tunguska meteorite fall // DAN SSSR. 1982. Vol. 266 (4), P. 993–995 (in Russian).

[***] Editorial note: This is a hypothesis that needs experimental verification or theoretical modeling based on well-established principles of physics and chemistry.

3. *Kolesnikov E. M., Boettger T., Kolesnikova N. V.* Finding of probable Tunguska cosmic body material: isotopic anomalies of carbon and hydrogen in peat // Planet. Space Sci. 1999. Vol. 47. P. 905–916.
4. *Rasmussen K. L., Olsen H. J. F., Gwozdz R., Kolesnikov E. M.* Evidence for a very high carbon/iridium ratio in the Tunguska impactor // Meteoritics and Planet. Science, 1999. Vol. 34. P. 891–895.
5. *Kolesnikov E. M., Kolesnikova N. V., Boettger T.* Isotopic anomaly in peat nitrogen is a probable trace of acid rains caused by 1908 Tunguska bolide // Planet. Space Sci. 1998. Vol. 46(2/3). P. 163–167.
6. *Gladysheva O. G.* On the Problem of the Tunguska meteorite material // Solar System Res. 2007. Vol. 41(4). P. 314–321.
7. *Kissel J., Krueger F. R.* The organic component in dust from comet Halley as measured by the PUMA mass spectrometer on board Vega 1 // Nature. 1987. Vol. 326 (6115). P. 755–760.
8. *Mul'diyariv E. Ja., Sal'nikova G. A.* About a nature of dark globules from the Tunguska catastrophe area / Ed. G. F. Plekhanov. Reading Yu. A. L'vov memory. Tomsk: Univer. Pr. 1995 (in Russian).
9. *Lodders K.* Solar System abundances and condensation temperatures of the elements // Astrophys. J. 2003. Vol. 591. P. 1220–1247.

Part 4. Meteor Complexes. Tunguska

Origin and Dynamic Evolution of Meteor Complexes in the Problem of Asteroid-Comet Hazard

N. V. Kulikova, V. I. Tischenko

State Technical University for Nuclear Power Engineering, Obninsk, Russia

Abstract. The life cycle of a comet and its meteoroid complex from discovery to its last return with no time gap is reconstructed using computer technology. Simulation results of comeraty nucleus disintegration, meteoroid complex and its position in the near solar space with consideration for Keplerian and disturbed motion are analyzed and compared with observational data. The results obtained turned out to be rather unexpected.

Introduction

One of the reasons why civilization has an interest in the problem of outer space population is safety of life on the Earth. Comets are only a part of objects approaching the Earth, however, they possess specific destructive effects because of their dynamic characteristics. The dynamic evolution of comets is determined not only by gravitational and nongravitational effects, but also by disintegration processes of their nuclei on approach to the Sun as well as at great heliocentric distances. Background data on the recent cometary activity show that many comets have split into independent fragments. Such disintegration processes are generally followed by solid substance ejections with the subsequent formation of meteoroid complexes. The total meteor mass in interplanetary space is not so much of interest as the place and the process of formation, its spreading, initial structure, subsequent development, the velocity of motion, fragment masses, and so on. Of primary concern are the established fine and superfine structures of young meteor formations and the regions of fragment concentration. The entry of celestial bodies into the near Earth space is already classified as one of geospace problems including all catastrophic consequences of their passage through the atmosphere and the impact of these objects or their disintegration fragments on the Earth's surface.

Method

The current research trend is the development of computer technologies on the module principle. This enables us to enlarge the range of applied mathematical models of disintegration and algorithms of the evolutionary development of meteoroid complexes, and to assess the quantitative and qualitative characteristics of the criteria developed for identifying some meteors as specific stream elements. The technology allows simulation of meteor complex formation and its evolution in the light of gravitational effects to be realized using a probability model [1, 2]. The technology involves an individual unit for calculating the generality criteria D_{SH} (Southworth–Hokkins), D_D (Drummond), D_H (Jopek), geocriterion, dynamic criterion in order to determine the affiliation of some meteors to a certain meteor stream associated with a given comet [3, 4].

Objects and results

The technology is applied to study meteoroid complexes of some comets (Tab. 1) during their observational periods. Fig. 1 presents some results obtained by this technology for these objects.

Table 1. Studied objects

Comet	Number of appearances	Years of appearances
Halley (1910 I)	26	1404 B. C. – 1986 A. D.
Giacobini–Zinner	11	1910–1985
Tempel–Tuttle II	10	1533–1899
Grigg–Skjellerup	18	1907–1999
Pons–Winnecke	19	1819–1983

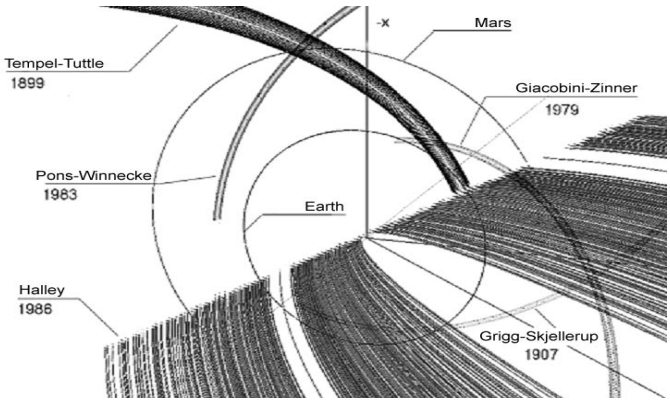

Fig. 1. Expected meteoroid complexes between the Earth and Mars formed by comets Halley, Giacobini–Zinner, Pons–Winnecke, Tempel–Tuttle II and Grigg–Skjellerup in the process of disintegration from 1900 to 2000.

Recent studies allow the determination of the migration regions of a specific small body not observable during some predicted appearance and time-space reconstruction of the whole object trajectory to be performed (see an example in Tab. 2 for Holmes' comet; not observed but predicted appearances are shaded).

Table 2. Evolution of orbit of Holmes' comet (from modeling)

N	Date of perihelion passage	*A*, AU	*E*	*Q*, AU	*P*, yr	ω, deg	Ω, deg	*I*, deg
1	15.06.1892	3.625	0.4095	2.1406	6.9018	14.28	333.22	20.805
2	09.04.1899	3.615	0.4113	2.1281	6.8732	14.06	333.14	20.814
3	16.03.1906	3.609	0.4123	2.121	6.8561	14.26	333.08	20.826
4	21.07.1913	3.778	0.3798	2.3431	7.3433	22.08	330.72	19.520
5	30.11.1920	3.788	0.3786	2.3538	7.3725	22.189	330.66	19.498
6	09.04.1928	3.783	0.3802	2.3447	7.3579	22.084	330.66	19.508
7	01.08.1935	3.764	0.3843	2.3175	7.3025	21.892	330.49	19.528
8	24.11.1942	3.762	0.3843	2.3163	7.2967	22.141	330.40	19.524
9	19.03.1950	3.782	0.3798	2.3451	7.3550	21.997	330.24	19.472
10	28.07.1957	3.790	0.3778	2.3581	7.3783	21.959	330.21	19.442
11	09.12.1964	3.779	0.3796	2.3445	7.3462	22.075	330.18	19.463
12	21.02.1972	3.670	0.418	2.1359	7.0307	23.88	327.79	19.050
13	10.03.1979	3.675	0.417	2.1424	7.0451	24.048	327.72	19.036
14	24.03.1986	3.681	0.416	2.1497	7.0623	23.80	327.68	19.027
15	15.04.1993	3.686	0.414	2.1599	7.0767	23.69	327.67	18.997
16	14.05.2000	3.677	0.416	2.1473	7.0508	23.81	327.64	19.01
17	04.05.2007	3.615	0.435	2.0424	6.8732	24.65	326.57	18.95

Fig. 2 presents the projection of Holmes' comet meteoroid complex evolution on the ecliptic plane. Fig. 2, *a* shows the space distribution and time evolution of a meteoroid complex; observed orbital elements in years of the comet appearances (9 cases) have been used as input data in modeling. So far, as in modeling, there are certain deviations of orbital elements of ejected fragments within $\pm \delta f$ (where *f* presents orbital elements *a, e, i,* Ω, ω). The complex has two branches relative to the parent body's orbit for each comet revolution. Fig. 2, *b* presents a similar pattern obtained for all 17 comet revolutions from the original data (Tab. 2). Clearly seen are three regions of the complex concentration limited by time intervals of comet observations: 1892–1906 (region I), 1964 (region II), 1972–2007 (region III). The spatial movement of a complex takes place from region I to region III. Orbits of non-observed comet revolutions with their complexes, reconstructed by modeling, are grouped in region II.

a *b*

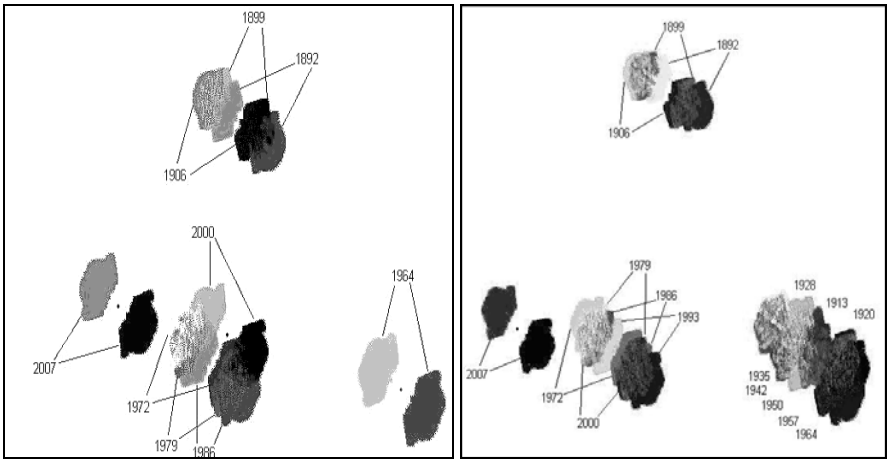

Fig. 2. Ecliptic intersection regions for orbits of fragments ejected from Holmes' comet nucleus in years of appearances:
a — reference data; *b* — simulation.

Conclusion

The considered time intervals allow one to assume that the comet is found in a specific region of space during all eight orbits, thereafter it moves into another one. If it is true, the comet was discovered during the eruption, after which it had abruptly changed its orbit in two revolutions.

References

1. *Kilikova N. V., Tischenko V. I.* Computer technologies for processing and presenting simulation results and astronomical observational data. 2003 // Astronomical and Astrophysical Transaction. 2003. Vol. 22, N 4–5. P. 535–541.
2. *Tischenko V. I.* Computer technology for studying meteoroid complexes in the near space // Candidate's thesis in physics and mathematics. Obninsk, 2005, 91 p.
3. *Valsecchi G. B., Jopek T. J., Froeschle Cl.* Meteoroid stream identification: a new approach – I. Theory // Mon. Not. R. Astron. Soc. 1999. N 304. P. 743–750.
4. *Jopek T. J., Froeschle Cl., Valsecchi G. B.* Asteroid Meteoroid Streams. Asteroids III. 2000. P. 645–652.

Meteor Streams: the Relation to Hazardous Celestial Bodies

E. N. Tikhomirova

Astronomical Observatory of Yaroslavl State Pedagogical University, Yaroslavl, Russia

Abstract. Analytically tractable, the evolution of meteor particles' elliptic orbits in a gravitational field of the Sun is considered in view of light pressure, the Poynting–Robertson effect, and the corpuscular analogue of Poynting–Robertson effect. The compact formula connecting parameters of initial and final elliptic orbits (semi major axis and eccentricity; perihelion and aphelion distances) of meteor particles are deduced. In the context of the model for the evolution of meteor particles' orbits, the method of estimating the meteor stream's life time is derived.

In the context of the perturbed two-body problem, the criterion for the probable meteor particles parent bodies are identified. Some known meteor streams and their parent comets are linked by the suggested criteria. According to the model, the parent comets for meteor streams β Cancrids, λ Cygnids and κ Cygnids are 3*D*/Biela, 73*P*/Schwassmann-Wachmann, and 177 *P*/Barnard, respectively.

Introduction

The asteroid and comet hazard is one of the most important problems of astronomy today. It is well known that asteroids and comets are the sources of meteor streams. It should be noted that parent bodies of many meteor streams have not been identified. The research of meteor streams evolution and meteor streams identification would help in solving some problems connected with dangerous objects [1].

Several methods of searching for the relation between parent body (comet, asteroid) and its possible meteor stream have been worked out during the last several tens of years. The known methods use physical, geometrical, and observational bases, either separately or simultaneously. The models making predictions for linking "parent body–meteor stream"

pairs have some inconsistencies. This problem needs be investigated thoroughly.

The nongravitational effects in the motion of meteor particles is considered first. Analytically tractable, the evolution of meteor particles' elliptic orbits in a gravitational field of the Sun is considered in view of light pressure, the Poynting–Robertson effect, and solar wind interaction. The compact formulae connecting parameters of initial and final elliptic orbits of meteor particles are deduced.

The fundamental equation

The differential equation of motion presented in vector form, for an absolutely black spherical body, isotropically reradiating solar energy and moving with velocity *v*, making an angle *u* with a direction of a heliocentric radius vector ***r*** is [2]:

$$\ddot{\vec{r}} = -GM'\vec{r}/r^3 - \frac{2\pi R^2 q r_{S-E}^2}{Mc^2} v\cos u\frac{\vec{r}}{r^3} - \frac{\pi R^2 q r_{S-E}^2}{Mc^2 r^2} v\sin u\vec{e}_t, \quad (1)$$

where G is the gravitational constant, r the distance between the Sun and a particle, R the radius of a particle, c the speed of light, q the solar constant, $r_{S\text{-}E}$ the average distance from the Sun to the Earth, e_r and e_t are unit vectors of radial and transverse accelerations, and M' is a reduced mass of the Sun (M_S) and (spherical) particle (M) system given by

$$M' = M_S - \pi R^2 q r_{S-E}^2/(GMc). \quad (2)$$

Equation (1) is applicable in case $R > \lambda$, is the radiation wavelength. The Poynting-Robertson effect is characteristic for particles with radii from 1 μm up to 1 cm.

To apply perturbation theory to the motion, we assume that the first term ("photogravitational" acceleration — f_0) on the right side of Eq. (1) exceeds the second and the third terms (f_r and f_t, i. e., the perturbating accelerations) by a large factor.

Solution of the fundamental equation

Using Lagrange equations we'll find perturbations of semi-major axes and eccentricity after one revolution of a meteor particle

$$\Delta a' = -4\pi^2 a^2 R^2 q r_{S-E}^2 (3/2e^2 + 1)/(Mc^2 (GM'p^3)^{1/2}), \quad (3)$$

$$\Delta e' = -5\pi^2 R^2 q r_{S-E}^2 e/(Mc^2 L), \quad (4)$$

where $p = a(1-e^2)$, $L = (GM'p)^{1/2}$.

Below, we assume that the minimum interval of time is greater than Keplerian period of the particle.

In [3] the influence of the solar wind on the motion of meteoroids is taken into account in semianalytical form. We use an average value of the solar wind velocity (in the radial direction) $\overline{U}$ = 400 km/s (for distance 0.3 AU < r < 10 AU). The concentration of protons n_p in the solar wind varies as n_p= 8.1 $(r_{S-E}/r)^2$ (400/w)·cm^{-3}. We also use $U = w - v$, n_α/n_p = 0.05. The action of electrons and heavy ions on meteoroids is not taken into account. The parameter of the model is ψ, which takes on values: 1.6 (water ice), 1.4 (magnetite), 1.1 (obsidian).

The averaged equations of motion for $\Delta a''$ and $\Delta e''$ of the meteoroid's orbit under the influence of the solar wind (the analogue of Poynting–Robertson effect) are reduced to the formula analogous to (3), (4), see Eqs. (5) and (6). In [3] the equations for $\Delta a''$ and $\Delta e''$ assuming some numerical values (in CGS) are:

$$\Delta a'' = -3.65\cdot 10^3 \Psi \overline{U} (GM')^{\frac{1}{2}} \left(A/M\right)(2+2e^2)/2\pi a^{\frac{3}{2}}(a(1-e^2)^{\frac{3}{2}}) \qquad (5)$$

$$\Delta e'' = -3.65\cdot 10^3 \Psi \overline{U} (GM')^{1/2} \left(A/M\right)(2e)/2\pi a^{3/2}(a^2(1-e^2)^{1/2}), \qquad (6)$$

where A is the cross section area of a meteoroid particle. For spherical particles, we take $A = \pi R^2$.

The basic theoretical results of the meteor bodies' motion are cast numerically. Unlike [3] we solve Eqs. (3), (4) and (5), (6) not numerically, but analytically simulating the simultaneous action of photons, protons, and α-particles.

Assuming that $\Delta a \approx \Delta a' + \Delta a''$, $\Delta e \approx \Delta e' + \Delta e''$, $\Delta a/\Delta e \approx da/de$ and the time interval cannot exceed the orbital period of the meteoroid. Replacing Δa and Δe with da and de we get the differential equation

$$\frac{da}{de} = \frac{a}{1-e^2}\cdot\frac{(6+2k)e^2+4+2k}{e(5+2k)}. \qquad (7)$$

For a case of small perturbations integration of Eq. (7), gives

$$e^{\frac{4+2k}{5+2k}}/a(1-e^2) = \text{const}. \qquad (8)$$

In view of the initial conditions

$$a/a_0 - (1-e_0^2)e^{\frac{4+2k}{5+2k}}/(1-e^2)e_0^{\frac{4+2k}{5+2k}} = 0\ . \qquad (9)$$

It should be noted for k = 0 Eq. (9) coincides with the formula of [4].

In Eqs. (7)–(9):

$$k = k_w / k_p , \tag{10}$$

$$k_w = 3.65 \cdot 10^3 \Psi \overline{U} , \tag{11}$$

$$k_p = \frac{\pi q r_{S-E}^2 a_0^{3/2}}{\sqrt{GM'} c^2 T_0} , \tag{12}$$

where k_w and k_p are the values proportional to the accelerations of meteoroids caused by the action of protons (of the solar wind) and photons, respectively; and a_0 and e_0 are the initial values of the semi-major axis and the eccentricity of the meteoroid's orbit.

According to the possible maximal and minimal values of k_w and k_p (see Eqs. (10)–(12)):

$$0 < k < 1.5 . \tag{13}$$

Determining k, using the Eq. (9), gives

$$k = \left(5 \ln \frac{a(1-e^2)}{a_0(1-e_0^2)} - 4 \ln \frac{e}{e_0} \right) \Big/ \left(\ln \frac{e}{e_0} - \ln \frac{a(1-e^2)}{a_0(1-e_0^2)} \right) . \tag{14}$$

Application: the method of meteor streams and identification of parent comets

According to the assumed method of linking meteor streams to their parent comets taking into account the light pressure, Poynting–Robertson effect, and its corpuscular analogue we apply Eq. (9). We also assume that the inclinations of comet and meteor stream orbits differ from each other by less than 10º and close approaches of comets and meteoroids to major planets are absent (at least, in the considered interval of time).

To estimate the reliability of the relationship between meteor streams and comets criterion k can be used, in particular the ratio (14). In Table the average values (semi-major axis a, eccentricity e, inclination i) of some meteor streams and comets are considered [1]. We will check the applicability of Eq. (9) and criterion (13). As shown in Table 1, we attempt to link the meteor streams β Cancrids, λ Cygnids, κ Cygnids to comets 3D/Biela; 73P/Schwassmann-Wachmann, 1920 III; 177 P/Barnard, and 1905 III, respectively.

The elements of comets 1920 III and 1905 III orbits indicated by "*" are taken from the catalogue of long period comets (Epoch 1950.0) in Laplacian coordinate system (the coordinates of Laplacian system were converted to ecliptic coordinates).

The comets – candidates for parent bodies of meteor streams. The criterion k is in the interval $0 < k < 1.5$ (interaction of comets and meteor particles with planets is not considered)

Meteor stream		Comet (Epoch 2000 01 01)	*k*
β Cancrids		3D/Biela	0.130
a, AU	2.105	3.533	
e	0.638	0.768	
i, deg.	2.8	8.1	
λ Cygnids		73P/Schwassmann–Wachmann	0.622
a, AU	2.522	3.060	
e	0.641	0.694	
i, deg.	11.2	11.4	
λ Cygnids		1920 III (Epoch 1950.0)*	1.368
a, AU	2.532	193.949	
e	0.620	0.994	
i, deg.	11.2	20.4	
κ Cygnids		177P/Barnard	1.179
a, AU	3.533	24.065	
e	0.719	0.954	
i, deg.	32.7	31.2	
κ Cygnids		1905 III (Epoch 1950.0)*	1.085
a, AU	3.533	37.107	
e	0.719	0.970	
i, deg.	32.7	39.2	

Conclusion

Identification, predictions of appearance, or increasing the activity of meteor streams are possible with a help of the above dynamical method. It is important for clarifying interrelations between comets and meteoroids related to the early history of the Solar System. According to the model the parent comets for some meteor streams are found.

References

1. *Gajdoš Š., Porubčan V.* Bolide meteor streams. Dynamics of populations of planetary systems / Eds Z. Knežević, A. Milani. Cambridge University Press, 2005. P. 393–398.
2. *Radzievskii V. V.* Photogravitational celestial mechanics / Eds Yu. A. Nickolaev. Nizhniy Novgorod, 2003.

3. *Ryabova G. O*. On the dynamical consequences of the Poynting–Robertson drag caused by solar wind. Dynamics of populations of planetary systems / Eds Z. Knežević, A. Milani. Cambridge University Press, 2005. P. 411–414.
4. *Wyatt S. P., Whipple F. L.* The Poynting–Robertson effect on meteor orbits // Astrophys. J. 1950. 111. P. 134–141.

METEOR COMPLEXES. TUNGUSKA

Modern Dynamic Methods of Determination of Parameters of Meteor Bodies

M. I. Gritsevich[1,2]

[1] European Space Research and Technology Centre of European Space Agency, Noordwijk, The Netherlands
[2] Institute of Mechanics of M. V. Lomonosov Moscow State University, Moscow, Russia

Abstract. In this study we will consider a dynamical approach to evaluating meteoroid parameters from observational data. The study takes an approach in modelling the fireballs' mass and other properties from the rate of body deceleration in the atmosphere as opposed to conventionally used luminosity. An analytical model of the atmospheric entry is calculated for registered fireballs using published observational data and evaluating parameters describing drag and ablation of meteors and bolides along the luminous segment of the trajectory. One of the special features of this model is the possibility of considering a change in body shape during its motion in the atmosphere.

Nomenclature

H^* — effective destruction enthalpy;
h — height;
M — meteoroid mass;
V — velocity;
S — middle section area;
γ — slope with the trajectory;
α — ballistic coefficient;
β — mass loss parameter;
μ — shape change parameter;
σ — ablation coefficient;
ρ_0 — gas density at sea level;
ρ — meteoroid density;
c_d — drag coefficient;
c_h — heat-transfer coefficient,

h_0 — scale height, $y=h/h_0$;
M_e — preatmospheric mass, $m = M/M_e$;
V_e — velocity at the entry into the atmosphere; $v = V/V_e$;
S_e — middle section area at the entry into the atmosphere;
A_e — shape factor at entry into the atmosphere.

Special mathematical function used exponential integral:

$$\overline{Ei}(x) = \int_{-\infty}^{x} \frac{e^z dz}{z}.$$

Introduction

The interpretation of the observations of meteors and fireballs is usually based on the photometric or dynamical methods. Photometric methods are based on the fireball luminosity. They usually assume that a given fraction of the kinetic-energy of the body is converted into visible radiation. The greatest uncertainty then is the not well-known value of the luminous efficiency coefficient [1, 2]. The validity of the photometric approach in general usually is supported by the fact that the spectral lines of elements of most meteorites dominate in the meteor spectra. This suggests that the dominating contribution to the meteor luminosity comes from the emission of the material vaporized from the body surface. However, other important sources of emission have been ignored.

The dynamical methods determine the body mass from the analysis of the observed drag in the atmosphere. The main drawback of these methods is the necessity of the a priori assumption on the density and the shape factor of the body. These parameters cannot be directly obtained from the observations. The dynamical methods are often used if the falling of meteorites is expected. The mass of a fireball in the lower part of the trajectory is used to estimate the masses of the possible meteorites. The mass is usually directly calculated from the projection of the motion equation onto the tangent to the trajectory (see [3] for a review).

The method of calculations

The solution of equations of meteor physics (see e. g. [10])

$$m = \exp\left[-\beta\left(1-v^2\right)/(1-\mu)\right], \quad y = \ln 2\alpha + \beta - \ln(\overline{Ei}(\beta) - \overline{Ei}(\beta v^2)) \quad (1)$$

shows the dependence of the luminous trajectory segment shape on the two non-dimensional parameters:

$$\alpha = \frac{1}{2} c_d \frac{\rho_0 h_0 S_e}{M_e \sin\gamma}, \quad \beta = (1-\mu)\frac{c_h V_e^2}{2 c_d H^*}. \quad (2)$$

The ballistic coefficient α characterizes the drag intensity as it is equal to the ratio of the mass of the atmospheric column with the cross section S_e along the trajectory to the body mass. The mass loss parameter β is proportional to the ratio of the fraction of the kinetic energy of the body's unit mass that is supplied to the body in the form of heat to the effective destruction enthalpy. It characterizes the relative roles of the disintegration, deceleration, and evaporation of meteor body [9]. β ~ 1 corresponds to the entry of quite heat-resistant objects with relatively low velocities. If the strength of the body is low, it is disintegrated into numerous fragments, whereas mass loss owing to the blowing off of a liquid film, as well as the evaporation of the body material from the front side, is relatively small. As a result, this case corresponds to the fall of numerous fragments on the surface of a planet, which is accompanied by the formation of meteorite and crater fields [7].

For the well registered fireballs the values of the parameters α and β providing for the best fit of observed physical process can be found by the method proposed by Gritsevich [4]. The sum of the squared deviations of the $\exp(-y_i)$ values corresponding to the given (observed) altitudes h_i of motion at certain points (i = 1, 2, …, n) from the corresponding values $\exp(-y_i)$ calculated using (1) for each given velocity value V_i is used as the fitting criterion [4].

Then the desired parameters are unambiguously determined by the following formulas:

$$\alpha = \sum_{i=1}^{n} \exp(-\beta - y_i) \cdot \Delta_i \,/\, (2\sum_{i=1}^{n} \exp(-2y_i)),$$

$$\sum_{i=1}^{n} \left[\left(\Delta_i \left(\sum_{i=1}^{n} \exp(-2y_i) \right) - \left(\sum_{i=1}^{n} \Delta_i \, \exp(-y_i) \right) \exp(-y_i) \right) \cdot \left(\Delta_i - (\Delta_i)'_\beta \right) \right] = 0.$$

$$\frac{\sum_{i=1}^{n} e^{-2y_i} \sum_{i=1}^{n} \left(\left((\Delta_i)'_\beta - \Delta_i \right)^2 + \left(\Delta_i - 2\alpha \exp(\beta - y_i) \right) \right) \left((\Delta_i)''_\beta - 2(\Delta_i)'_\beta + \Delta_i \right)}{\left(\sum_{i=1}^{n} \exp(-y_i)(\Delta_i - (\Delta_i)'_\beta) \right)^2} > 1.$$

Here

$$v_i = V_i/V_e,\ y_i = h_i/h_0,\ \Delta_i = \overline{Ei}(\beta) - \overline{Ei}(\beta v_i^2),\ (\Delta_i)'_\beta = \frac{d\Delta_i}{d\beta},\ (\Delta_i)''_\beta = \frac{d^2\Delta_i}{d\beta^2}.$$

The value of β here describes the mass-loss efficiency along the entire studied segment of the meteoroid trajectory due to both evaporation and melting of the outer layer followed by blowing-off of the liquid film by the

flow and detachment of secondary-size fragments from the parent body [5]. Let us note, that the value of the ballistic coefficient α and mass loss parameter β allow us to estimate the ablation coefficient of a meteor body and its preatmospheric mass under the formulas:

$$\sigma = \frac{2\beta}{(1-\mu)V_e^2}, \quad M_e = \left(\frac{1}{2} c_d \frac{\rho_0 h_0}{\alpha \sin\gamma} \frac{A_e}{\rho^{2/3}} \right)^3.$$

Results and conclusions

The obvious distribution of the parameters α and β can be obtained as a result of the thorough analysis of the available natural materials. We restrict this analysis to consideration of bolides reliably observed in the Earth's atmosphere in the framework of Canadian Observation and Recovery Project running from 1971 until 1985. The detail data of observations that were used as input parameters are published in [8]. The values of the parameters (lnα and lnβ) corresponding to the observational data are presented in the Figure. The numerical values for these parameters and mass estimates are published elsewhere [6]. As seen, all the points are located in the region $\alpha > 1$. This completely corresponds to the absence of catastrophic events within the indicated time intervals in the geographic zones covered by the fireball Network under consideration. It is remarkable that the leftmost point in Figure corresponds to the bolide Innisfree. It means that the ballistic coefficient for Innisfree was the smallest among all fireballs registered by the Canadian Network (it corresponds to a rather big value of initial mass divided by

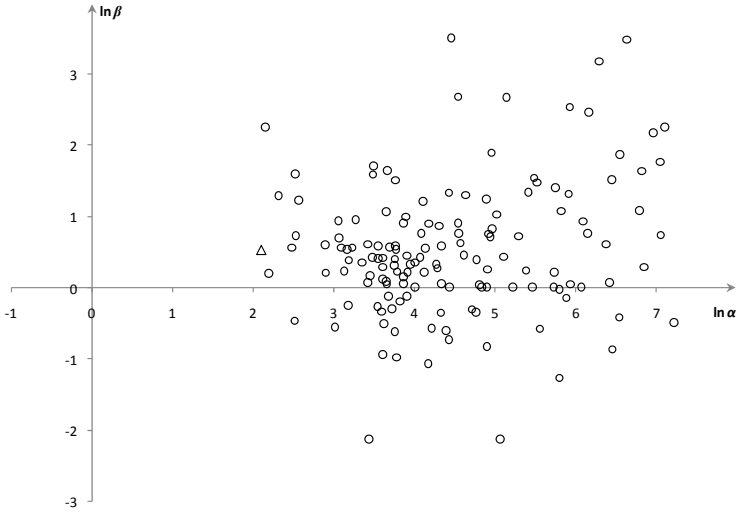

The obtained distribution of parameters α and β for the Canadian Network fireballs. Δ — meteorite Innisfree.

a sine of a slope). On the other hand among all these fireballs Innisfree was a unique fall for which fragments of a meteorite have been found on the Earth's surface [3].

The approximation of the actual data using theoretical models in general makes it possible to achieve additional estimates, which do not directly follow from the observations. As an example, the correct mathematical modeling of meteor events in the atmosphere is necessary for further estimates of the key parameters, including the extra-atmospheric mass, the ablation coefficient, and the effective destruction enthalpy of entering bodies. In turn, this information is needed by some applications, namely, those aimed at studying the problems of asteroid and comet nucleus security, to develop measures of planetary defense, and to determine the bodies that can reach Earth's surface. Surely, the detailed review of the existing models for evaluating parameters of meteor bodies serves a separate future publication.

References

1. *Campbell-Brown M. D., Koschny D.* Model of the Ablation of Faint Meteors // Astron. & Astroph. 2004. Vol. 418. P. 751–758.
2. *Gritsevich M. I.* Validity of the Photometric Formula for Estimating the Mass of a Fireball Projectile // Doklady Physics. 2008. Vol. 53 (2). P. 97–102.
3. *Gritsevich M. I.* The Příbram, Lost City, Innisfree, and Neuschwanstein falls: An analysis of the atmospheric trajectories // Solar System Res. 2008. Vol. 42 (5). P. 372–390.
4. *Gritsevich M. I.* Identification of Fireball Dynamic Parameters // Moscow Univ. Mechanics Bull. 2008. Vol. 63 (1). P. 1–5.
5. *Gritsevich M. I.* Estimating the Mass of a Fireball Projectile // Doklady Physics. 2008. Vol. 53 (11). P. 588–593.
6. *Gritsevich M. I.* Determination of Parameters of Meteor Bodies based on Flight Observational Data // Advances in Space Res. 2009. Vol. 44 (3). P. 323–334.
7. *Gritsevich M. I., Stulov V. P., Turchak L. I.* Classification of Consequences for Collisions of Natural Cosmic Bodies with the Earth // Doklady Physics. 2009. Vol. 54 (11). P. 499–503.
8. *Halliday I., Griffin A. A., Blackwell A. T.* Detailed Data for 259 Fireballs from Canadian Camera Network and Inferences Concerning the Influx of Large Meteoroids // Meteoritic & Planetary Sci. 1996. Vol. 31. P. 185–217.
9. *Stulov V. P.* Large Fireballs: Evaporation and Fragmentation // Solar System Res. 2006. V. 40 (3). P. 198–207.
10. *Stulov V. P., Mirskii V. N., Vislyi A. I.* Aerodinamika bolidov (Aerodynamics of Bolides). M.: Nauka, 1995 (in Russian).

METEOR COMPLEXES. TUNGUSKA

The Tunguska Catastrophe is the Consequence of a Series of Explosions of Comet Nucleus Fragments

G. A. Nikolsky[1], Yu. D. Medvedev[2], E. O. Schultz[1]

[1]Department of Physics of St. Petersburg state University, St. Petersburg, Russia
[2]Institute of Applied Astronomy of RAS, St. Petersburg, Russia

Abstract. In this work the author's concept of the Tunguska event (TE) is briefly submitted. For the first time in history of Tunguska research the generalized concept of all essential phenomena starting with the most probable origin of tandem comet nucleus fragments intruding into the Earth's atmosphere up to the detonation of these products and the disintegration and meteorological, climatic, atmospheric, and geomagnetic consequences of this event is presented.

Introduction

As a base for the construction of a picture of Tunguska event, we accept the following reasonable hypotheses: 1) bodies intruded into the Earth atmosphere formed as a result of past disintegration of a comet nucleus (possibly — Encke–Baklund); 2) the mass of the intruded fragments was significant ≥ 32 Mt, 3) the body was captured into a satellite orbit; 4) in the final stages the body was destroyed and its fragments had rather low speed (~ 2 km/s); 5) the basic source of the devastating energy was a volume explosion of a detonating gas-air mixture of hydrocarbon (CH) components of cometary substances with oxygen of the air.

Different constituents of this multidimensional model concept are elaborated and accurate to a variable extent. The amount of entering mass of a single intruding fragment of the comet bodies was found by numerical solution of an inverse problem, namely, launching into space an ice sphere of 200 meters in diameter. It is launched as a simulated body with characteristics similar to those of the Tunguska Comet Body that intruded into the Earth atmosphere along the Tunguska bolide's trajectory that ended with an explosion in a place with coordinates (60°53′ N, 101°53′ E). The gravitational acceleration from the Earth, the Moon, and the Sun were included in the model

of reverse motion as well as acceleration due to braking in the atmosphere of the Earth. Values of the velocity magnitude, azimuth, and inclination angle, mass of the body, and height of the TCB explosion were varied in numerical experiments.

The reverse run of the body's motion puts severe restrictions on all the initial values of the considered TCB parameters.

Results

When setting the heat of evaporation to be equal to 400÷800 cal/g and choosing the break point stress of the ice body to be equal to 0.2÷0.02 MPa, only an object with mass of 6.4 Mt (1 Mt = 10^6 ton), rising along the southern trajectory inclined at a small angle to Earth's surface, managed to "shoot out" into space after completing three revolutions. Fig. 1 represents the calculated trajectory of the ice sphere while getting up the speed and entering a hyperbolic orbit.

Calculations [1] have demonstrated that the volumetric explosion of 10^{17} J per sec needs 2.7 to 3.3 Mt hydrocarbons depending on water content of a comet nucleus fragment. However, since a single fragment would consume no more than 0.5–0.6 Mt because of the immense ablation rate with a water content as high as 70 %, there must be at least 5 (or 6) fragments in tandem. The volumetric explosion, having the energy efficiency between nuclear and chemical explosions, is most reliable. This supposition is supported by the picture of damage and destruction and is in good agreement with a supposed cometary origin of fragments and their total mass.

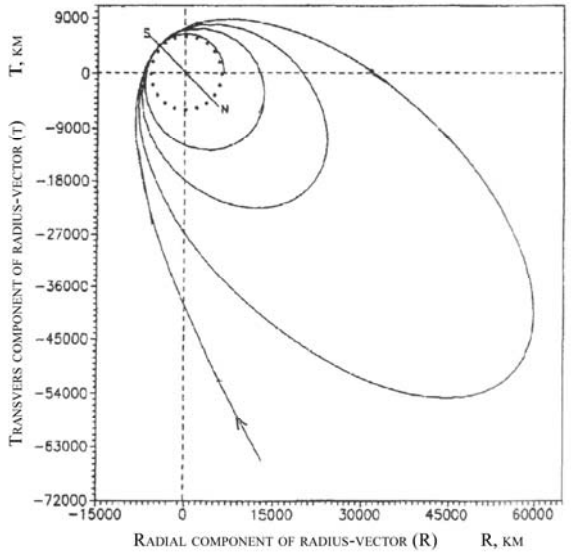

Fig. 1. Model of evolution of Tunguska body's orbit in the gravitational field of the Earth before explosion on June 30, 1908 at 00^{h} 14.5^{m} UT.

The total mass of the comet substance interacting with the atmosphere during the Tunguska catastrophe was estimated by us from the data of the Smithsonian Astrophysical Observatory (SAO) on atmosphere spectral transparency [2]. At the moment of catastrophe the observatory on Mount Wilson was the only one in the world where spectral measurements of atmospheric transparency were taken. These and some other data make it possible to state that, firstly, the post explosion air mass had reached Mount Wilson and, secondly, some of the registered deviations in the SAO data were caused by the catastrophe. Corrections to repeatable errors have been estimated for the SAO data; a novel method has been developed to separate a spectral optical thickness into components in absorption bands; to estimate the TCB mass (V. G. Fesenkov, R. Ganapahty) and the ozone losses (R. Turko) [2, 3], the errors and their origins have been determined. It was found that somewhere between the end of April and beginning of May a tandem of three large bodies behaving like carbon-bearing chondrites intruded into the Earth's atmosphere and exploded at the height of the ozone layer maximum. They formed an optically dense dust cloud in the stratosphere at altitude of 22–27 km, which went over the observatory three times with a period of 60 days. It is from this cloud that V. G. Fesenkov estimated the mass of dust as 1 Mt. We estimated the value as about 0.1 Mt. When going over the observatory at the second time, the cloud optically superposed the post explosion air mass; the mass was moving at an altitude of about 16–19 km, hardly had any dust, and was rich in water and nitrogen oxides. Fig. 2 represents the variations of spectral transparency, total water content and total ozone content which concordantly support the dynamic and optical processes registered in the Northern hemispheric stratosphere while driving the post explosion air mass from Eurasia to North America. The water content remained excessive (0.8 cm in the average) from July 15th till August 12th, which supports not only the time (fourteen 24-hour periods) taken by the post explosion air mass to reach Mount Wilson, but also the fact that the air stream in the mid-latitude Ferrell cell drew the products of ablation and of volumetric explosions from the catastrophe region during twenty-eight 24-hour periods. Note that in June of the last decade before the TE, experts observed a solar halo in a quite cloudless sky indicating that the Earth entered the zone of daytime β-Taurids meteor shower, the stream reaching maximum on June 30th, 1908. The southern trajectory of the TCB intrusion, which the authors have accepted, is sustained by log-book notes of the British Antarctic expedition that was stationed in vicinity of the magnetic pole in summer 1908. The notes will lead one to another conclusion: the TCB intrusion had a low impact parameter; the body significantly slowed down, intensively broke up and formed plasma; the plasma extended up into the ionosphere and may have had a global impact on the geomagnetic field.

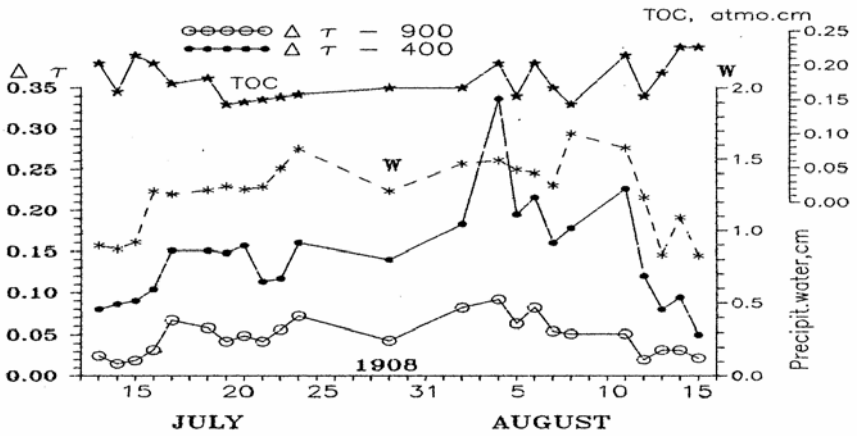

Fig. 2. Observations at the Mount Wilson station, California, July–August 1908. TOC — total ozone content; $\Delta\tau$ — optical thickness of the atmosphere at 400 and 900 nm; *W* — total content of the water vapor. The variations of the optical characteristics of atmosphere during July 15–August 12 testify to movement above Mount Wilson of diverse air masses (in lower stratospheric layers 16–19 km and 22–27 km). The *W*-curve shows an excess of water vapor (above 0.7–0.8 cm from Tunguska explosions), and surplus of aerosol — not of Tunguska origin ($\Delta\tau \sim 0.16$).

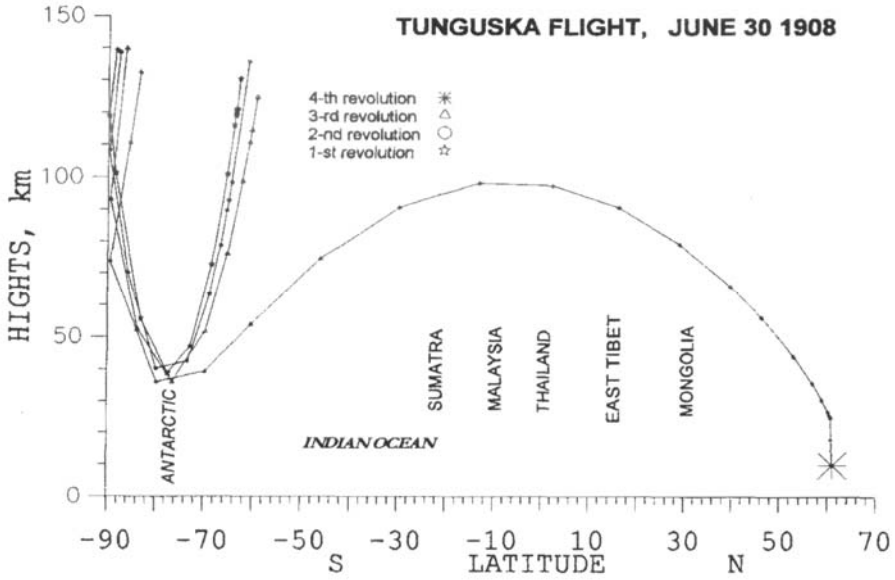

Fig. 3. Projection of Tunguska body motion on plane of meridian 102° E.

Fig. 3 demonstrates four perigees of the passes of probable TCB as well as the final sections of flight trajectories along the meridian plane of 102° E. As the seismogram made in the Irkutsk observatory has shown important details of a local earthquake caused by the fall of some parts of TCB fragments, it became possible to elucidate why the seismic events were anomalously prolonged. Apparently, the effects of interaction of air shock waves (formed by five powerful volumetric explosions) with the terrestrial surface manifested themselves as seismic surface waves.

Thus, the long duration of the Irkutsk seismogram suggests that alongside with shock-caused seismic waves the oscillations of the terrestrial surface caused by shock air waves were serially archived by the observatory seismograph. A possible interpretation of the long-duration seismogram of the Irkutsk observatory is that it has recorded fluctuations of the terrestrial surface caused by volumetric explosions of five multi-ton icy nuclei that survived despite huge ablation during their long flight through the atmosphere. The event eyewitnesses, residing in the area of the catastrophe, confirmed that the impact of a leading fragment of the nucleus with the ground was not preceded by a volumetric explosion. In such case it is possible to speak of about six large fragments, since the Slutsk and English micro barograms testify to only five explosions.

Conclusion

The report has discussed not all but just a number of points of the conception. Stress was put on novel approaches to lay the foundation of this concept.

References

1. *Tsinbal M. N., Schnittke V. E.* The specified model of gas-air explosion of the Tunguska bolide and its consequence // 100 years to the Tunguska Comet Body. St. Petersburg branch of Russian Geographical Soc. 2008. P. 62–73 (in Russian).
2. *Kondratyev K. Ya.* Climate shocks: Natural and Anthropogenic. N. Y. John Wiley & Sons, Inc., 1988. P. 220–253.
3. *Kondratyev K. Ya., Nikolsky G. A., Shultz E. O.* Tunguska space body — nucleus of a comet // Aktual'nye voprosy meteoritiki v Sibiri. Novosibirsk, 1988. P. 114–143 (in Russian).

METEOR COMPLEXES. TUNGUSKA

Atmospheric Discharge in the Tunguska Disaster

O. G. Gladysheva

Ioffe Physical Technical Institute of RAS, St. Petersburg, Russia

Abstract. Based on the fact that an explosion of the Tinguska cosmic body, which caused trees to fall over a wide area, and radiant energy release during the Tunguska disaster were separated in space and in time, it is proposed that these events are interrelated but of different origin. We propose that the emission during the Tunguska disaster was caused by an atmospheric discharge at altitudes of 10–90 km above the Earth's surface. We propose these separate but interrelated events as an explanation for the Tunguska cosmic body destruction mechanism over the epicenter.

Introduction

A theory that can explain the observed and reported features of the release of radiant energy during the Tunguska disaster (TD) is absent. Attempts to explain the emission of radiant energy by the processes that accompany flight and destruction of a cosmic body remain unexplained and they disagree with observationally established evidence found from investigations at the epicenter.

Observations and facts

First of all, eyewitnesses of the TD observed an astonishing phenomenon. They saw a flash like a fiery column. Kulesh, the observer of the meteorological station at Kirensk (~500 km from the epicenter) wrote: "On the 30th of June an extraordinary phenomenon was noticed… At a quarter past seven a fiery column appeared in the north-west. It looked like a spear. The column having disappeared, we heard five strong abrupt blows, like from a gun. They followed one another quickly and distinctly; then we saw a thick cloud in that place… The fiery column was seen by lots of people, but even more people heard blows…" [1].

A flare was observed at a distance of ~ 500 km. The atmosphere had to glow to an altitude of ~ 80÷90 km in order to make the light observable at such a distance on a sunny day. We note that about 35 % of the more than 30 eyewitnesses of the TD saw a flame that blazed up over the place where the object had disappeared from the scene and about 47 % saw smoke that rose from the place below the explosion [1, 2]..

After a very brief flash that may have signaled the destruction o the body entering the upper atmosphere, an atmospheric discharge took place according to eyewitnesses. The lifetime of a gigantic luminous column was shorter than the time of human response to a strong external stimulus according the eyewitness Seminov [3]. The estimated approximate duration of luminosity was about 1 to 3 seconds [4].

In addition, it is difficult to explain some unusual properties of the emission source that operated during TD. For example, the emission was so powerful that live needles from trees and dry grass started to burn within distances of 40 and 50 km from the epicenter, while an absolutely sound, about 50 years old larch without burn traces was found in the southern bog almost in the explosion's epicenter. The selective impact of the emission might be explained by a time delay between the destruction of the body and the "switching" to an emission source. In this case dust (including water vapor spray) that was blown up by the explosive shock wave in the epicenter, might have protected some plants from the emission source.

Moreover, several tens of explosions have occurred over the epicenter. These explosions were interpreted by inhabitants as sound of falling stones, at a distance of 65 kilometers, and an artillery cannonade at a distance of 200÷300 kilometers. Many hypotheses have been proposed to explain the Tunguska disaster. A likely explanation is that the original cosmic body exploded and broke into pieces over the epicenter as it entered the atmosphere and these pieces caused the additional explosions.

Spatial and temporal discrepancies

It has been established that the location of the Tunguska cosmic body (TCB) explosion epicenter, determined by and based on the fall of trees, does not coincide with the center of the liberated emission energy. It is important to note that the emission source is confined to the paleovolcano central conduit. The distance between the explosion epicenter and the center of the light energy release is ~ 2 km [4].

The emission energy release and the explosion that caused the fall of trees did not coincide in space or in time. The results of studying the tree destruction in the explosion epicenter unambiguously indicated that a burn took place after the explosive shock wave [5, 6]. This makes it possible to assume that the fall of trees and the burn of vegetation, including that of

felled trees, were caused by two different phenomena rather than one phenomenon.

Infrasonic waves generated during TD were registered at numerous stations. According to Whipple [7], four almost equal oscillations with periods of ~ 2 min were followed by strong fast oscillations. Whipple assumed that low oscillations at the beginning of a wave and fast oscillation are of different nature. We also assume that the explosions caused the initial stage of oscillations, whereas the following oscillations were generated by a discharge [4]. The very beginning of a wave (low oscillations) propagated at a velocity of 323 m/s, but a short compressed shock front (fast oscillations) moved at a velocity of 308 m/s. It is known that the average velocity of sound is 320 m/s at an altitudes of 0–10 km and 302 m/s at an altitude of 10–30 km. According to estimates, the TCB was destroyed below 10 km altitude; therefore, it is not surprising that the velocity of sound propagation at this altitude corresponds to the velocity of propagation of the wave onset. Since the velocities of propagation of fast oscillations is much closer to the velocity of sound at an altitudes of 10–30 km, we assume that the radiation emission source was located much above the zone of the body's explosive destruction.

Destruction of the Tunguska cosmic body

Tsynbal and Schnitke [8] were first to suggest that the explosion of the TCB was a volume-detonation of a mixture of cometary gases emitted during the destruction of the TCB. Volume-detonations require formation of an aerosol mixture of volatile gaseous, liquid, or solid materials, releasing huge amounts of energy when burning. This mixture gets ignited accidentally or by means of detonators.

Judging by the model suggested above [9], the TCB was a porous construction made of various-sized particles (1 mm to 10 m in diameter) (Fig. 1). Having interacted with the atmosphere, the particles gradually broke up to the initial structural elements. The point is that atmospheric pressure is on the outside of the spheres, but vacuum is inside of these particles that were formed in space. If the shell of the body is broken, a shock wave transforms the particles to an aerosol mixture of their fragments. Further destruction of these fragments, for example under influence of subsequent explosions, leads to disintegration of these particles down to granules of ~5 μm in size.

Let's consider that the TCB had a diameter of ~100 meters and was filled by carbonaceous pellets of ~1 mm diameter [9]. Then its inner organic combustible surface was ~ 10^{10} m^2. The combustible surface increases considerably when the body disintegrates into granules.

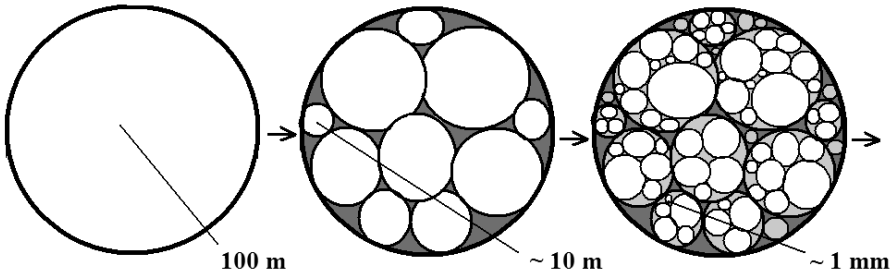

Fig. 1. Structure of the TCB.

Thus, having interacted with the atmosphere, the TCB transformed to an aerosol mixture of small granules covered with organic fragments. In this suggested model, the organic surface layer is the largest available for combustion. Lightning discharges could be a detonator, which are needed for explosion of the aerosol mixture.

Atmospheric discharge

Atmospheric discharges that appear at ionospheric altitudes are the only known natural phenomenon, the nature of which is close to that of the TD emission source. The main reddish luminosity of such discharges, which was observed at altitudes of 50–90 km, has lateral dimensions of 5–30 km, and a bluish emission descends beyond the main "body" and reaches an altitude of 20 km. However, an atmospheric discharge that took place during TD was much stronger. According to eyewitnesses of the TD, a fiery column looked like a spear (see above). This is the usual form for ionospheric discharges.

If we have a cloud, where charges were separated for any of several reasons, and one type of the charges flows to the ground, a discharge can originate between the upper part of a cloud and the ionosphere.

The initial explosion could be detonated by a lightning discharge between the body and the ground. As a result the TCB disintegrated forming a cloud of fragments. If we consider that the TCB fragments carry positive charge downward, the heated air will carry a flow with predominant negative charge upward. Lightning discharges that might inevitably originate between centers of positively and negatively charged regions, will result in subsequent volume-detonations. This will lead to heating of fragments, burning of the body's shell, intensification of crushing, enhancement of convective flows, and, consequently, further separation of charges in a dust cloud [4].

As crushed fragments approach the Earth under the action of gravity, the field strength between the Earth and the total charge carried by fragments will increase until it reaches the breakdown value. Then, positive charge will flow onto the ground via numerous lighting discharges (Fig. 2). When a pos-

itive charge flows to the ground, such conditions can originate that the electric field strength in the entire atmospheric interval (10–100 km) will exceed the threshold value. Since electrons in strong fields are produced in the form of an avalanche, the emission intensity should increase with increasing lifetime of such fields.

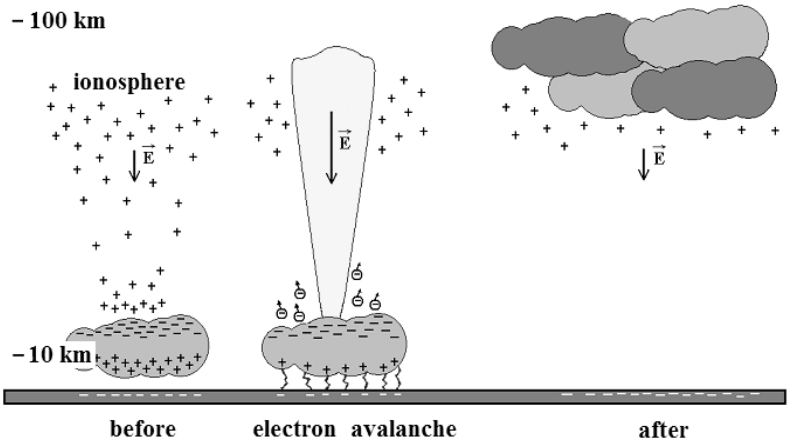

Fig. 2. The picture of the TD.

References

1. *Voznesensky A. V.* Meteorite fall of June 30, 1908, in Khatanga river upper reaches // Mirovedenie, 1925. 14(1). P. 25–38 (in Russian).
2. *Konenkin V. G.* Reports of eyewitnesses to the Tunguska meteorite of 1908 // Probl. Tungus. Meteor. 1967. 2. P. 31–35 (in Russian).
3. *Krinov E. L.* Messenger of the Universe. Moscow: GIGL, 1963.
4. *Gladysheva O. G.* Atmospheric discharge as a source of emission during the Tunguska disaster // Geomag. and Aeronomy. 2009. 49 (3). P. 397–404.
5. *Florensky K. P., Vronsky B. I., Emel'yanov Yu. M. et al.* Preliminary results of the Tunguska meteoritic expedition of 1958 // Meteoritika. 1960. 19. P. 103–134 (in Russian).
6. *Krinov E. L.* Tunguska meteorite. M.: Akad. Nauk SSSR, 1949.
7. *Whipple F. J. W.* The great Siberian meteor and the waves, seismic and aerial, which it produced // Quart. J. R. Meteorol. Soc. 1930. Vol. 56 (236). P. 287–301.
8. *Tsynbal M. N., Shnitke V. E.* Gas-air model of the Tunguska comet's explosion // Space matter and the Earth. Novosibirsk: Nauka. 1986. P. 98–117 (in Russian)
9. *Gladysheva O. G.* From the Tunguska space body to the evolution of the protoplanet clouds // (see this book).

METEOR COMPLEXES. TUNGUSKA

In Searching for Comet P/Tunguska–1908

T. Yu. Galushina[1], E. M. Drobyshevski[2], M. E. Drobyshevski[2]

[1] Scientific and Research Institute of Applied Mathematics and Mechanics of Tomsk State University, Tomsk, Russia
[2] Ioffe Physical Technical Institute of RAS, St. Petersburg, Russia

Abstract. The reason for the horizontal turn of the Tunguska–1908 bolide trajectory remains difficult to understand. It finds explanation, however, in the New Explosive Cosmogony of minor bodies as having been caused by an explosion of a part (M up to 10^{12} g) of the comet nucleus whose ices contained products of their electrolysis, $2H_2 + O_2$. In detonation, this part was repelled from the more massive unexploded nucleus remnant, changed the direction of its own motion by ~10° and imparted its kinetic energy, in expanding and slowing down, to the air in producing an effect of a high-altitude explosion. On passing through the Earth's atmosphere, the unexploded remnant again entered a heliocentric orbit (the Vernadskiy's hypothesis, 1932). A search for this comet, P/Tunguska–1908, among the 6077 known NEAs shows the 2005 NB56 object to be the most appropriate candidate for a number of its parameters (its size is ≈ 170 m, P = 2.106 y, e = 0.473 and i = 6.8°). Back integration of its orbit without allowing for non-gravitational effects suggests that it had passed the Earth on June 27, 1908 at a distance of 0.0659 AU. It is quite possible that a proper inclusion of even fairly weak non-gravitational forces might make its orbit consistent with parameters of the Tunguska bolide.

1. Introduction

The Tunguska–1908 phenomenon (TP) was triggered by a high-altitude (~5÷10 km) atmospheric explosion of a body that was moving with V ~ 20÷30 km/s along a slightly sloping ($\delta \approx 0 \div 20^{o}$) trajectory with a kinetic energy $W \approx 10 \div 50$ Mt TNT (1 Mt TNT = $4.2 \cdot 10^{22}$ erg) [1,2]. This energy could transform to that of an explosion itself, i. e., the energy of the air overheated to $T > 104$ K, as it was slowing down the rapidly dispersing meteoroid.

Two major mechanisms of its breakup are most frequently considered (see refs. in [3]), namely, (*i*) the so-called "explosion in flight", when the dynamic head of the air $\rho_a V^2/2$ exceeds the strength of the material (rock or ice) of the body, and (*ii*) chemical explosion of the cometary ices saturated with the solid solution of $2H_2 + O_2$, the products of ice electrolysis (for details, see [3] and below) (this chemical explosion energy is far less than W).

The crucial aspect in unraveling the origin of the TP is the final turn of its trajectory. It is deduced both from the fact that (*i*) continuation of the original fireball trajectory with an azimuth $\varphi \approx 120 \div 137^o$, as testified by numerous eyewitnesses, passed to the north of the final tree-fall, Kulik's epicenter [1, 2, 4], and that (*ii*) the azimuth of the symmetry axis $\varphi \approx 116 \div 99^o$ of this tree-fall, as also of the zone of radiation burn of the trees, deviates by $\Delta\varphi \approx 10^o$ to the west of the original trajectory direction.

The concepts underlying the New Explosive Cosmogony (NEC) of minor bodies, which explains formation of SP cometary nuclei (and of a number of other bodies, of the type of MB asteroids, the Trojans, small satellites etc.) as due to extremely rare (7÷8 in 4.5 aeons) global explosions of thick (~ 800 km) electrolyzed icy envelopes of distant moonlike bodies, of the type of Titan, permitted [3] to show that all aspects of the TP, including the final turn of the trajectory, can be accounted for by detonation of the electrolysis products, $2H_2 + O_2$ (present in the concentration of 15÷20 wt. %), dissolved in a part, or, better, in a layer up to $\sim 10^{12}$ g in mass (and $\sim 20 \times 200 \times 200$ m^3 in size) of a much more massive icy cometary nucleus. This yields ~200 m for the lower estimate of the size of the original nucleus. Judging from the visible size of the bolide (0.5÷2.0 km by [4]), the diameter of the meteoroid could be as large as ~500 m (which increases its mass to $\approx 10^{13} \div 10^{14}$ g).

The exploded layer was repelled with a velocity V_r = 1.54÷1.63 km/s from the much more massive nucleus, which would account for the observed turn of the visible trajectory. The gaseous products of the layer's detonation expanding with $V_t \approx 2$ km/s were slowed down efficiently by the air, with the initial kinetic energy (up to $W \sim 50$ Mt TNT) and the momentum of the layer imparted to the air heated in the process to $T > 10^4$ K, and this is what created the phenomenon of a moving high-altitude TP explosion.

An essential point of the above scenario is the conclusion that the larger part of the cometary nucleus would be left intact in its tangential passage through the Earth's atmosphere and that it could escape into space to enter again a heliocentric orbit. A similar, while hardly realizable possibility was mentioned as far back as 1932 by Vernadskiy [6].

The fall of the main body with a mass of $\approx 10^{13} \div 10^{14}$ g on the Earth with $W \sim 250 \div 3000$ Mt TNT would have produced a crater ~3.5÷8.0 km in di-

ameter with the resultant climatic catastrophe of the type of the Younger Dryas cooling, which occurred ~ 13÷11.5 ky ago (see refs. in [3]). Fortunately, this fall did not occur, which suggests the only conclusion that the main body of the Tunguska bolide (we call it P/Tunguska–1908 comet, or P/T subsequently) left the Earth on passing through the atmosphere at a distance of only ~10 km from its surface.

2. From trajectory of Tunguska bolide to that of P/Tunguska-1908

It would seem that the simplest approach to search for the P/T would be, starting from the trajectory of the Tunguska fireball near the Earth's surface within the Earth's atmosphere and assuming only a small part of it to have exploded, to reconstruct its previous trajectory (see, e. g., [7–11]) and project it, on a mathematically sound basis, up to the present time.

However, one can see that the original meteoroid experienced so close an encounter with the Earth and the complex gravitational maneuver accompanied by a partial explosion and experienced atmospheric drag that it had to change its initial orbit substantially. Thus, the starting parameters needed for calculation of the original P/T orbit have uncertainties so large to be beyond acceptable limits. This makes their use in a search for this body in the present epoch hardly reasonable.

Our approach based on the NEC permits one *to invert the problem*, and in place of looking for the trajectory of the original body, as this was done heretofore, we shall rather try to find this body now!

3. Trajectory signatures of the P/Tunguska-1908 comet

The P/T-1908 comet is an orbitally young object that has not yet had time enough to enter an orbit commensurate with that of the Earth. Assuming its orbital period $P \approx 3.5$ yr ($a \approx 2.3$ AU) to be comparable to that of P/Encke [7–9], then, in the absence of commensurability with the Earth, and disregarding perturbations caused by other planets, non-gravitational effects and the like, the probability for the residue of the Tunguska meteoroid to make a new passage through the Hill's gravitational sphere of the Earth ($\Delta = 0.01$ AU) is about $3 \cdot 10^{-6}$ per year. Nevertheless, P/T approaches the Earth to a distance ≤1 AU once every ~25 yr, when it may be discovered as an asteroid-like body, even if presently it is "dormant" and does not reveal signs of cometary activity.

It appears fairly obvious that:

1. A NEO-candidate for the P/T nucleus should cross the Earth's orbit sometime around June 30.

2. The distance to which the object approaches the Earth should not be large ($\Delta \leq 0.05$ AU); i. e., the search for P/T should be started among the Potentially Hazardous Asteroids.

3. Subsequent approaches (close to June 30) should occur with intervals from the TP date, which are approximately multiples of the P/T orbital period.

4. Back integration of the orbit of the P/T should demonstrate its close passage by the Earth (if not colliding with it) on June 30, 1908.

5. The orbit of the P/T, notwithstanding drastic perturbations that had occurred in passage through the Earth's atmosphere and explosion of a part of its nucleus, could nevertheless retain some orbital parameters of the original body (say, of a fragment of the P/Encke nucleus or of the member of the β-Taurid meteor stream).

6. The size of the P/T body is confined within ø ≈ 200÷500 m [5].

7. The non-gravitational forces which, generally speaking, may be considered being proportional to the surface area of the nucleus should impart to the small P/T nucleus an order-of-magnitude higher acceleration than to the nucleus of a conventional comet, because the size of such a comet nucleus, as specified in the next paragraph, is measured in km.

For instance, the orbital period of P/Encke changes after every revolution around the Sun, on the average, by 2.7 h, which is equivalent to an averaged acceleration of $\sim 2 \cdot 10^{-6}$ cm/s^2. The radius of its nucleus is ~ 2.5÷4 km. It is conceivable therefore that for the same surface activity (and volume density) the P/T nucleus (with a radius of 100÷250 m) would feel an order-of-magnitude higher non-gravitational acceleration.

4. A search for P/T among the Potentially Hazardous Asteroids (PHAs)

In accordance with item 2, Sec. 3, we started a search for candidates for the P/T with PHAs, i. e., among the bodies that are expected to approach the Earth to within $\Delta \leq 0.05$ AU in the time period from the present to the year 2178 (see *http://www.cfa.harvard.edu/iau/lists/PHACloseApp.html*). Altogether, 27 objects satisfying the requirements of item 1 have been found, which make the closest approach around June 30 (± 10 days). Back integration performed with the use of NEODyS (*http://newton.dm.unipi.it/neodys*) codes revealed that none of these objects approached the Earth close enough on June, 1908. The closest objects were found to be 65909 1998 FH12 with $\Delta = 0.179$ AU and the famous asteroid 25143 Itokawa (1998SF36) with $\Delta = 0.269$ AU. The integration with the MPC (*http://www.cfa.harvard.edu*) and the Tomsk (see Sec. 5 and Tab. 1 below) codes has yielded practically the same results (e. g., $\Delta = 0.1449$ AU for 65909 1998 FH12 on 21 June, 1908, and $\Delta = 0.2422$ AU for 25143 Itokawa on 19 July, 1908, by the Tomsk calculations).

5. A search for the P/T among other near-Earth asteroids (NEAs)

The search was continued among all NEAs. This was accomplished by integrating the motion of the 6077 NEAs back to January 1, 1908. The asteroid trajectories were integrated using the codes developed at the Institute of

Applied Mathematics and Mechanics, Tomsk State University [12, 13]. The starting data were taken from the catalogue of Bowell compiled up to January 12, 2009 (*ftp:/ftp.lowell.edu/pub/elgb/astorb.dat*). The integration was performed by the 19-order method of Everhart. Effects of all planets, Pluto and the Moon were included. The coordinates of the perturbing bodies were calculated on the basis of the DE404 ephemerises.

Our study revealed that two objects, 2005 MB (Aton) and 2005 NB56 (Apollo), selected within this model approached fairly close the Earth at the end of June 1908. We subjected the motion of these asteroids and of the two PHA objects mentioned in the preceding Sec. 4 to a more comprehensive study. The force model was complemented by the Earth oblatness and three asteroids (Ceres, Pallas, Vesta) (see Tab. 1).

Table 1. Asteroids that approached the Earth close to June 30, 1908

Name	25143 Itokawa	65909 1998 FH12	2005 MB	2005 NB56
Δ, AU	0.2728 (30.06.1908)	0.1746 (30.06.1908)	0.0971 (26.06.1908)	0.06945 (27.06.1908)
P, days	556.4798	416.4360	357.2113	769.2369
a, AU	1.3240	1.0914	0.9853	1.6430
E	0.2800	0.5397	0.7928	0.4728
i, deg	1.6219	3.5585	41.4163	6.7633
q, AU	0.9533	0.5024	0.2042	0.8661
Q, AU	1.6948	1.6804	1.7663	2.4199
H	19.2	19.2	17.07	22.94
d, m	520 × 270 × 230	970	2600	170

Note. Δ — the approach distance; *P* — period of revolution around the Sun; *a*, *e*, *i* — major semi-axis, orbital eccentricity, and inclination; *q*, *Q* — perihelion and aphelion of the object; *H* — stellar magnitude; *d* — size of the object (for albedo 0.04; except Itokawa).

6. Main conclusions. Is 2005 NB56 the P/Tunguska-1908?

As seen from Tab. 1, the most appropriate candidate for P/T among the known NEOs is the 2005 NB56 asteroid.

This statement is corroborated not only by (1) the closeness of the date (June 27, 1908) to the time of the TP and (2) the smallest distance to the Earth among the four objects found at the time, but (3) by its orbital parameters being closest to those of P/Encke and of the β-Taurid stream and, finally and most significantly, (4) by the size of the object (≈ 170 m) practically coinciding with the lower estimate derived from the angle of turn of the Tunguska fireball trajectory [3, 5], while the dimensions of the other three objects exceed the value derived from the TP observations.

There is a problem in that back integration of the orbit of the 2005 NB56 object does not terminate at the exact location of the TP event. The matter is that these calculations disregard the forces of other than gravitational origin, which should inevitably manifest themselves in our case, where we deal with a remnant of a cometary nucleus (for more details see [14]).

One cannot exclude the possibility that careful observations of the 2005 NB56 object when it will approach the Earth closer (see Tab. 2), will show it to reveal certain cometary manifestations (regrettably, in June 2009, its $\Delta \approx 1.5$ AU).

Table 2. Close approaches of 2005 NB56 in future

Date	Δ, AU
2045.07.11	0.04249
2064.06.22	0.09505
2123.07.06	0.03090
2163.06.25	0.09344

References

1. *Bronshten V. A.* Tungusskiy Meteorit: Istorija Issledovanija (Tunguska Meteorite: History of Studies). M.: Publ. A. D. Seljanov, 2000.
2. *Vasilyev N. V.* Tungusskiy Meteorit: Kosmicheskiy Phenomen Leta 1908 G (Tunguska Meteorite: Space Phenomenon of 1908 Summer). M.: Publ. NP ID "Russkaja Panorama", 2004 (in Russian).
3. *Drobyshevski E. M.* Tunguska–1908 and similar events in light of the New Explosive Cosmogony of minor bodies // arXiv:0903.3309, 2009.
4. *Epiktetova L. E.* Trajectory of Tunguska Cosmic Body on the basis of witness testimonies // Intern. Conf. "100 years since Tunguska Phenomenon: Past, Present and Future" (Abstracts). Moscow. 2008. P. 77–79.
5. *Astapovich I. S.* Air waves caused by the fall of the meteorite on 30th June, 1908, in Central Siberia // Q. J. Roy. Meteorol. Soc. 1934. Vol. 60, N 257. P. 498–504.
6. *Vernadskiy V. I.* On study of space dust // Mirovedenie. 1932. Vol. 21(5). P. 32–41 (in Russian).
7. *Zotkin I. T.* Anomalous twilight related with the Tunguska meteorite // Meteoritika. 1969. Vol. 29. P. 170–176 (in Russian).
8. *Kresák L.* The Tunguska object: a fragment of comet Encke? // Bull. Astron. Inst. Czechosl. 1978. Vol. 29. P. 129–134.
9. *Asher D. J., Steel D. I.* On the possible relation between the Tunguska bolide and comet Encke // Planet. Space Sci. 1998. Vol. 46(2/3). P. 205–211.

10. *Jopek T. J., Froeschlé C., Gonczi R., Dybczyński P. A.* Searching for the parent of the Tunguska cosmic body // Earth Moon Planets. 2008. Vol. 102(1–4). P. 53–58.
11. *Zabotin A. S., Medvedev Yu. D.* On possible heliocentric orbit of the Tungus meteorite before entrance to the Earth's atmosphere / Eds L. V. Rykhlova, V. K. Tarady // Near-Earth Astronomy 2007, Nalchik; 2008. P. 149–154.
12. *Galushina T., Bykova L.* Applied program system for study of motion and orbital evolution of asteroids / Eds V. V. Orlov, A. V. Rubinov. Resonances, Stabilization, and Stable Chaos in Hierarchical Triple Systems. St. Petersburg University, 2008. P. 5–11.
13. *Bykova L. E., Galushina T. Yu., Baturin A. P.* The algorithms and programs for investigations of near-Earth asteroids // Astron. Astrophys. Trans., 2009 (in press).
14. *Drobyshevski E. M., Galushina T. Yu., Drobyshevski M. E.* A search for a present-day candidate for the Comet P/Tunguska-1908 // arXiv:0903.3313, 2009.

Likely Impact Sites of Large Fragments of the Tunguska Cosmic Body

V. A. Alekseev[1], N. G. Alekseeva[1], I. G. Golovnev[2], S. Yu. Zheltov[2], A. I. Morgachev[2], E. Ya. Fal'kov[2]

[1]Troitsk Institute for Innovation and Fusion Research, Troitsk, Russia
[2]State Research Institute of Aviation Systems, Moscow, Russia

Based on the large-scale stereo aerial survey of the Tunguska catastrophe region and application of three-dimensional models, we determined the possible impact sites of Tunguska cosmic body (TCB) fragments. Some of these sites were earlier determined by L. A. Kulik.

Kulik schematized the tree fall around the Cranberry Hole and at the Southern Bog in order to elucidate the possible location of meteorite fragments. We cut a channel in the Suslov Hole, and drained water from it [1]. A stub was found at the crater bottom. Ice of unknown (possibly cometary) origin was also discovered. Comparing the stub photographs from the Suslov hole with the photographs of a stub from the Sikhote Alin holes, we can assume that trees were possibly broken in a similar manner when large meteorite fragments fell [2].

Then we drilled three boreholes at the bottom, the first one on the northern slope since Kulik considered that the meteorite flew from south to north and could get deep into the hole on the northern slope. This borehole penetrated a 25-m-thick permafrost layer and 6-m aquifer below the permafrost. The second borehole was drilled at the hole center to a depth of 20 m. The third borehole was drilled on the southern slope.

Kulik schematized tree fall on the Southern Bog and around the Cranberry Hole and selected the centers where TCB fragments might be located. However, he did not find any Tunguska meteorite fragments in the Suslov Hole. We consider that it is necessary to verify the Kulik proposal and to perform at first georadar investigations in the Suslov and Cranberry holes and then drill in the craters to find possible meteorite fragments.

Pit layer enrichment of different elements and isotopes relating to 1908 that was found by E. M. Kolesnikov et al., might have purely terrestrial causes. Firstly, deep structures of a paleovolcano may release gases during an explosive earthquake [3]. Gaseous and aerosol elements are redistributed during any earthquake [4]. These elements differ from a refractory matter of

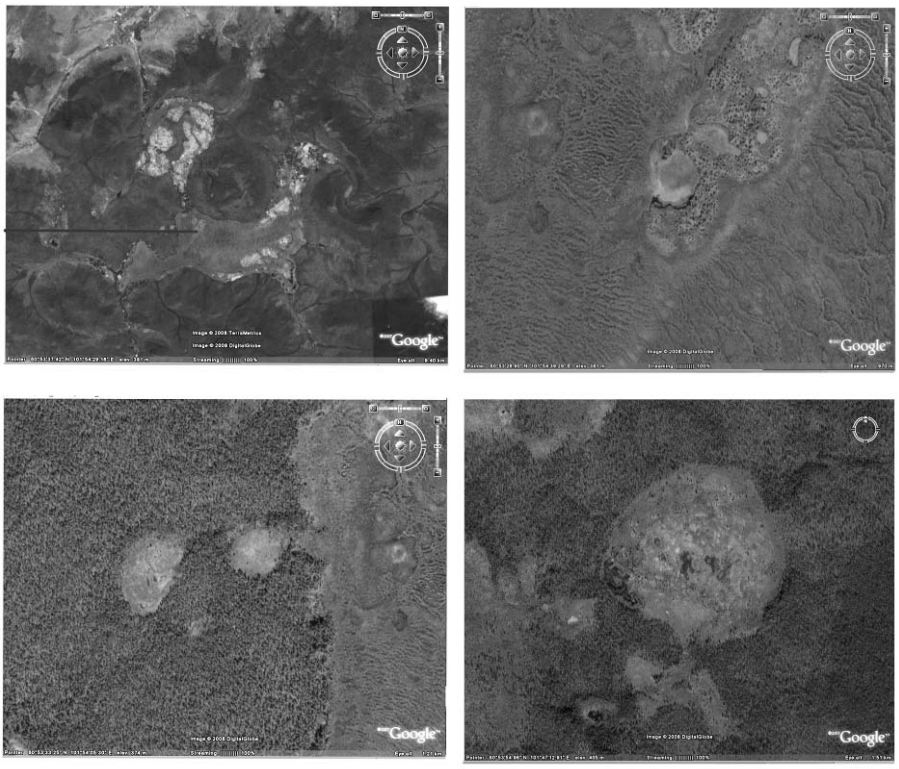

Possible sites where TCB fell.

traps. Secondly, aerosols erupted from the Ksudach volcano in Kamchatka in 1907 could change the composition of precipitation in the Tunguska region. Thirdly, recent data indicate that comets are mostly enriched in deuterium, whereas Kolesnikov et al. thought that comets have a decreased content of this element. Different positive and negative isotopic anomalies are observed when tectonic structures (fault and mud volcanoes) release gases. At last, enrichment in iridium and platinum-group elements can be related to volcanic activity. Extremely high concentrations of iridium were registered during the eruption of the Kilauea volcano [5]. Rhenium and platinum-group elements deposits are formed in Kuril volcanoes.

Thus, element and isotope anomalies are possibly not pertinent to the Tunguska meteorite. One should search for large pieces of meteorite in order to elucidate the real situation.

Large TCB fragments can be sought in Cranberry and Suslov holes studied by Kulik (see Figure), near northern tributaries of the Ugakit Creek, and in the Bagel bog region. Lake Cheko, studied by V. A. Koshelev as long ago as 1961, can also contain TCB pieces.

This work, executed by modern 3D methods both remote sensing and ground ones, has studied the zone of probable dissemination of the Tunguska space body fragments a little to the east from its main trajectory. Further task is to explore all the zone of possible dissemination of the fragments as L. A. Kulik planned some time ago. The next task is to calculate parameters of the dissemination.

References

1. *Kulik L. A.* Dannyje po Tungusskomu meteoritu k 1939 godu // Doklady Akad. Nauk SSSR. 1939. Vol. 22. P. 520–524 (in Russian).
2. *Alekseev V. A.* Modern state of search of material of Tunguska cosmic object // Intern. conf. "100 years since Tunguska phenomenon: past, present and future". M., 2008. Russia. June 26–28, 2008. P. 14 (in Russian).
3. *Kolesnikov E. M., Boettger T., Kolesnikova N. V.* Finding of probable Tunguska Cosmic Body material: isotopic anomalies of carbon and hydrogen in peat // Planetary and Space Sci. 1999. Vol. 47. P. 905–916.
4. *Alekseev V. A., Alekseeva N. G.* Particularities of the astroblem of the Tunguska body // All-Russian conference "Asteroid-Comet Hazard-2005 (ACH-2005)". St. Petersburg, 2008. Russia. Oct. 3–7, 2005. P. 19–23 (in Russian).
5. *Zoller W. H., Paveington J. R., Phelan Kotra G. M.* Iridium Enrichment in Airborne Particles from Kilauea Volcano: January 1983 // Sci. 1983. Vol. 222. P. 1118–1121.

Part 5. Devastating Consequences of Impacts. Study of Traces of Past Collisions

The Asteroid-Comet Hazard Conference Proceedings, 2009

DEVASTATING CONSEQUENCES OF IMPACTS. STUDY OF TRACES OF PAST COLLISIONS

Consequences of Impacts of Cosmic Objects in Circumstances of Changing Climate

V. V. Svetsov

Institute of Geosphere Dynamics of RAS, Moscow, Russia

Abstract. The consequences of the impacts of asteroids about 1 km in size on the Earth are considered from the viewpoint of their negative effects under conditions when the climate changes. These effects are ejection of greenhouse gases, fires, changes in surface albedo, and global dispersion of asteroid material. Estimates show that the impacts of this size do not pose a direct threat of climate change, however, they can lead to substantial damage. Dispersion of iron contained in asteroids over the ocean surface can have a strong influence on the ecosystem (development of phytoplankton, sequestration of carbon dioxide, blooms of toxic algae); but it is not yet possible to predict consequences of ocean fertilization with any assurance.

Introduction

Due to Spaceguard survey the risk from large impacts of asteroids about 10 km in diameter, which can cause global disaster and wipe out civilization in the next 50–100 years, has been greatly reduced [1]. Asteroids about 1 km in size are likely to remain the most dangerous to humanity in the nearest future. Typically such asteroids cause regional devastations (on areas $\sim 10^6$ km^2) [2], although water injections to the atmosphere and subsequent ozone losses can be significant. However, it is generally believed that ejection of dust and water by the impact of a 1-km asteroid cannot cause a global catastrophe or substantially change the climate.

Climate changes occurring for one or another reason can be dangerous for mankind. The modern threat of climate warming is associated with the increase in atmospheric concentration of greenhouse gases and the related rise of the sea level. Alteration of the environment can lead to substantial material losses and expenditures for overcoming the climate changes. Nega-

tive climate changes create a stressful situation in which some (yet poorly studied) consequences of asteroid or comet impacts can turn out extremely dangerous to humanity. The impacts can significantly aggravate the critical situation by acceleration of negative processes or destructive influence upon those defensive methods that will be applied for counteraction to climate changes. Some consequences of the impacts of 1-km-diameter asteroids are considered here using estimates and numerical simulations.

Increase of carbon dioxide in the atmosphere

A large quantity of carbon dioxide can originate from the impact on a rock target rich in carbonates. Assume the target consists of calcite and the projectile is a sphere with a density 3 g/cm^3 and mass $1.6 \cdot 10^{15}$ g. At the impact velocity 20 km/s the vaporized target mass will be about $8 \cdot 10^{15}$ g, and a melted mass ~$4 \cdot 10^{16}$ g [3]. If all the vapor forms CO_2, and another part of CO_2 emanates from the two-phase fraction of $CaCO_3$, the total mass of carbon dioxide ejected into the atmosphere immediately after the impact will be about $3 \cdot 10^{16}$ g (1 % of the present-day mass of atmospheric CO_2). This estimate agrees with the maximum amount of CO_2 estimated in [4] to have been ejected into the atmosphere after the impact of a 10-km-diameter body (Chicxulub) with a mass of $1.6 \cdot 10^{18}$ g.

At the same time the impact of a 1-km-diameter asteroid (at 20 km/s) on a surface covered by forests fells all trees within a radius of 200 km and part of the trees within 300 km [5] (taking into account that minor damage of trees occurs at a wind speed of ~30 m/s and all trees fall at wind speeds above 60 m/s). Such area of deforestation is about 6 times larger than the existent annual reduction of forest areas on Earth, which is estimated to be $7.3 \cdot 10^4$ km^2/yr. At an impact velocity of 40 km/s the area of felled trees will be almost 2.5 times larger than at 20 km/s. Present-day deforestation results in ~18 % of the total global CO_2 emissions into the atmosphere. Note that mature forests act as a sink of carbon dioxide. The emission of CO_2 can be higher after the impact in the region of densest forests. The maximum density of biocarbon above the soil is about $1.9 \cdot 10^9$ g per hectare in eucalyptus forests of Australia. Thus, if all the carbon from the impact-killed wood is converted into carbon dioxide (combustion and decay), about $3 \cdot 10^{17}$ g of CO_2 will be emitted into the atmosphere. The impact can also release carbon from soil; on average there is more carbon in soil down to a depth of 3 m than in biomass above the surface.

Thermal radiation from the fireball produced by the impact of a 1-km asteroid can ignite dry wood (dead leaves, dry twigs and branches) at a distance of ~300 km from the impact site [5]. At appropriate weather conditions, fires can cover far larger areas. Fires that constantly happen over the

Earth (mainly in Africa), emit into the atmosphere on average $3.4 \cdot 10^{15}$ g of CO_2 per year. The fires generated by the impact can emit more CO_2 than usual fires produce during several decades.

Iron dispersion, planktons, and carbon dioxide

After impacts at velocities above 20 km/s, the bulk of asteroid material is vaporized and ejected to high altitudes. Numerical simulations show that in 30 s after the impact of a 1-km asteroid on a rock target asteroidal material reaches altitudes from 50 to 250 km and continues to move upward. Atmospheric winds disperse asteroid material over the Earth. The same effect takes place after the impacts on shallow water basins. The mass of ordinary H-chondrite includes 1/3 of iron. The impact-vaporized iron condenses only partly into microparticles; a significant portion of iron is dispersed as atoms [6]. The mean surface density of iron precipitated on the Earth after the impact will be 1 g/m^2, and this iron will fall on the surface over years.

Fertilization of the ocean by iron can have significant influence on the ecosystem. Indeed, a hypothesis has been advanced that iron is a necessary component of phytoplankton growth and a deficit of iron restrains algae blooms [7]. Experiments made in small areas of the ocean confirm this suggestion [8]. After the Mount Pinatubo Volcano eruption of 1991, about 80 g/km^2 of iron fell on the ocean surface and an increase in atmospheric concentration of CO_2 and a decrease in O_2 have been registered [9]. Moreover, it was suggested to use the effect of iron fertilization on the growth of phytoplankton for sequestration of carbon dioxide from the atmosphere.

In a recent experiment, LOHAFEX, 6 tons of iron have been dispersed over an area of 300 km^2 in the Southern Ocean [10]. The observations have shown that phytoplankton, intensively consuming carbon dioxide, doubled its mass during two weeks. However, thereafter crustaceous zooplankton ate the algae and cancelled the effect of reduction in CO_2. This attempt shows that the effect of iron fertilization on the ecosystem is unpredictable. The unexpected result is the main argument against suggestions for future large-scale experiments with ocean fertilization.

Among several possible causes of mass extinctions in Phanerozoic, it has been hypothesized that blue-green (cyanobacteria) and probably other types of algae produced toxins that caused or contributed to major mass extinctions [11]. Four of five major mass extinctions are associated with peaks in the relative abundances of stromatolites (fossil remnants of blue-green algae). Climatic warming and increased nutrient supply might have promoted the algae expansion. There is no stromatolite increase in the case of the mass extinction at the K-T boundary. Evidence shows the onset of cooling at the very end of Cretaceous [12]. Increased concentrations of O_2 and reduction in CO_2 at the K-T boundary could create a stressful situation for

plants, so that weakened biota could have been predisposed to the negative consequences of the impact that happened 65 million years ago [13]. Ocean fertilization by dispersed asteroid material could result in development of algae blooms (e. g., diatoms) which consumed CO_2 and reduced its atmospheric concentration to a catastrophic level. Recently observed toxin-producing algal blooms may be related to the present global warming. It is highly plausible that iron fertilization of the ocean by an asteroid impact can be crucial for another massive biotic crisis.

The impacts onto polar regions

The impact of a 1-km-diameter stony asteroid or comet nucleus on land produces an earthquake with a magnitude of about 7.9. Earthquakes of such magnitude are not uncommon in Antarctica and they do not produce significant geologic effects on this continent. The impact on a thick ice sheet will not eject substantial amounts of mineral dust into the atmosphere.

The impact could influence the ice sheets of the Antarctic, Arctic, and Greenland by decreasing surface albedo due to the ejecta blanket. After the impact of a 1-km-diameter body at 20 km/s on a rock outcrop, the area of ejecta blanket is about 10^6 km^2, that is about 10–20 times smaller than the total area of the Antarctic ice sheet. In this area the albedo will be several times smaller than the albedo of ice. Antarctica is a dry region and annual amount of atmospheric precipitations in central regions is lower than 5 g/cm^2. However, on average, the annual increase in ice sheet is about 15 g/cm^2 (precipitations minus sublimation and melting). The thickness of impact ejecta blanket diminishes from ~10 cm at a distance of 100 km from the impact site to ~1 mm at 500 km. These ejecta will be covered by snow soon afterwards. Therefore, although the Antarctic and Arctic albedo influences significantly the radiation balance, the impact of a 1-km-diameter asteroid cannot diminish significantly the ice sheet masses either by shock or by albedo reduction.

Conclusions

The impact of a 1-km-diameter asteroid can lead to emission of carbon dioxide with a mass that is at the worst (a carbonaceous target, development of wildfires) no more than 10 percent of present-day CO_2 atmospheric abundance. High atmospheric concentrations of water can arise after an impact on a water basin, but preimpact levels of water vapor will be approached in less time than a decade. Formation of hydrogen from water in the upper atmosphere is dangerous for the ozone layer, and the hydrogen will persist in the atmosphere for about a decade. Such ejections bring no great threat to humanity via climate change; however expenditures for overcoming the impact contribution to CO_2 and water (in addition to human and economic losses)

can be substantial as compared to the modern carbon dioxide capture costs. The impacts in Antarctica do not pose considerable threat.

The most dangerous global effect may result from dispersion of asteroidal iron, development of algal blooms, production of toxins, consumption of CO_2, and formation of deep-water anoxic regions. Despite the influence of iron fertilization on the ocean and the whole ecosystem is still unpredictable, it is not improbable that in the circumstances of changing climate the ocean fertilization by an asteroid impact could result in biotic mass extinctions.

References

1. *Harris A.* What Spaceguard did // Nature. 2008. Vol. 453. P. 1178–1179.
2. *Nemchinov I., Shuvalov V., Svetsov V.* Main factors of hazards due to comets and asteroids / Eds V. Adushkin, I. Nemchinov. Catastrophic events caused by cosmic objects. Dordrecht: Springer, 2008. P. 1–89.
3. *Melosh H. J.* Impact cratering: A geologic process. New York: Oxford University Press, 1989.
4. *Gerasimov M. V.* Production of toxins during an impact and their possible role in a biotic mass extinction // Int. conf. on catastrophic events and mass extinctions: Impacts and beyond, Vienna, 2001. Abst. 3051.
5. *Collins G. M., Melosh H. J., Markus R. A.* Earth impact effects program: A web-based computer program for calculating the regional environmental consequences of a meteoroid impact on Earth // Meteoritics & Planetary Sci. 2005. Vol. 40. P. 817–840.
6. *Raizer Yu. P.* Condensation of a cloud of vaporized matter expanding in vacuum // Soviet Phys. JETP. 1959. Vol. 37. P. 1741–1750.
7. *Martin J. H., Coale K. H., Johnson K. S. et al.* Testing the iron hypothesis in ecosystems of the equatorial Pacific Ocean // Nature. 1994. Vol. 371. P. 123–129.
8. *Boyd P. W., Jickells T., Law C. S. et al.* Mesoscale iron enrichment experiments 1993–2005: Synthesis and future directions // Science. 2007. Vol. 315. P. 612–617.
9. *Watson A. J.* Volcanic iron, CO_2, ocean productivity and climate // Nature. 1997. Vol. 385. P. 587–588.
10. *Smetacek V., Naqvi S. W. A.* The next generation of iron fertilization experiments in the Southern Ocean // Phil. Trans. Royal Soc. A 2008. doi:10.1098/rsta.2008.0144. P. 1–21.
11. *Castle J. W., Rodgers J. H. Jr.* Hypothesis for the role of toxin-producing algae in Phanerozoic mass extinctions based on evidence from the geologic record and modern environments // Environmental Geosciences. 2009. Vol. 16. P. 1–23.

12. *Barrera E*. Global environmental changes preceding the Cretaceous-Tertiary boundary: Early-late Maastrichtian transition // Geology. 1994. Vol. 22. P. 877–880.
13. *Gale J., Rachmilevitch S., Reuveni J., Volokita M.* The high oxygen atmosphere toward the end-Cretaceous; a possible contributing factor to the K/T boundary extinctions and to the emergence of C_4 species // J. of Experimental Botany. 2001. Vol. 52. P. 801–809.

DEVASTATING CONSEQUENCES OF IMPACTS. STUDY OF TRACES OF PAST COLLISIONS

Detection of Possible Impact Structures at the Bottom of the Ocean by Gravimetric and Magnetometric Data Processing

An. G. Marchuk[1], K. V. Simonov[2], S. A. Peretokin[3]

[1]The Institute of Computational Mathematics and Mathematical Geophysics of RAS, Novosibirsk, Russia
[2]The Institute of Computational Modeling of RAS, Krasnoyarsk, Russia
[3]Siberian Federal University, Krasnoyarsk, Russia

Abstract. A new attempt to detect hidden impact craters on the Earth surface and on ocean bottoms was made using high-tech computational methods. For detection and allocation of such structures, a fast two-dimensional wavelet transformation of the gridded gravimetric data was used. The method was tested on reliably known impact structures. The results obtained are promising. Known hidden circle structures are effectively detected and clearly distinguished in the selected areas.

Introduction

It is a rather difficult problem to discover traces of large celestial body impacts at the ocean bottom. The reason is more intensive erosion processes and covering of structure morphology by bottom sediments. Because of this, only few reliable impact structures are discovered compared to hundreds identified on dry land. In addition to morphological characteristics the impact craters have also some geophysical indications. For example, most of the impact structures are characterized by a negative gravity field anomaly [1]. Gravity anomaly value for some reliable impact structures are given in the Tab. 1.

Table 1. Gravity anomaly value at some impact structure locations

Structure's name	Diameter, km	Gravity Anomaly, mGal
Haughton	20.500	–11
Gosses Bluff	22.000	– 3
Clearwater East Lake	22.000	–13
Rochechouart	23.000	–10
El'gygytgyn	23.000	–12
Ries (Nordlinger Ries, Rieskessel)	24.000	–20
Clearwater West Lake	32.000	–16
Manson	32.000	?
Carswell	37.000	–10
Kara	60.000	–20–25

Anomaly of the Earth's magnetic field is typical for "young" or very large structures (such as "Chicxulub"). Therefore, magnetic and gravity field analysis can help to discover hidden and ocean bottom impact craters. Visualization of the gravity field at the impact crater "Chicxulub" is presented in Fig. 1 (deep color means low gravity).

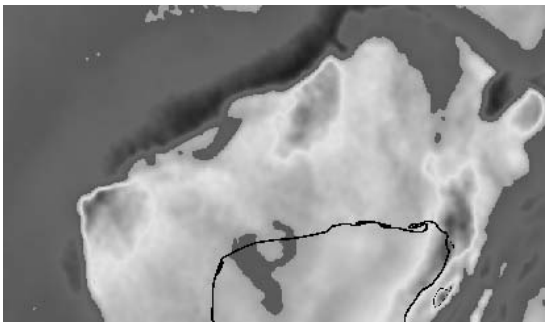

Fig. 1. Gravity field around "Chicxulub" impact crater. The Yukatan peninsula coastline is drawn as a black line.

Application of the wavelet transformation for impact craters detection

Digital Earth elevation and gravity data are presented as an *NxL* array of the Earth surface elevation or gravity field values at rectangular grid-point locations. It is necessary to distinguish an impact crater from other kinds of relief and gravity heterogeneities. The following algorithm of the bi-variable wavelet-transformation of the function *f(x,y)* is proposed:

$$f'(x_0, y_0) = \int_{-\infty}^{\infty} \int_{-\infty}^{\infty} \phi(x, y) f(x, y) dxdy \, . \qquad (1)$$

First it is necessary to set up the "mother" wavelet. For practical application it is important to know indications that should have a wavelet function: localization in space (time) and frequency; zero mean and L2 norm

$$\int_{-\infty}^{\infty}\int_{-\infty}^{\infty}\phi(x,y)dxdy = 0;\ \int_{-\infty}^{\infty}\int_{-\infty}^{\infty}\left|\phi(x,y)\right|^2 dxdy < \infty\ . \qquad (2)$$

In our case the basis is a square matrix with constant elements. Its dimensions will be changed according to the diameter of the structures to be detected. The proposed algorithm uses the following denotations:

$$x, y \in (-M, M);$$
$$\phi(t) = -(1-t)\cdot e^{-t};$$
$$\Phi_{x+M,y+M} = \phi\left(\frac{10((x-M)^2 + (y-M)^2)}{M}\right);$$

where M is the scale of the wavelet transform and $\Phi_{x+M,y+M}$ are elements of the basis (mother) wavelet matrix.

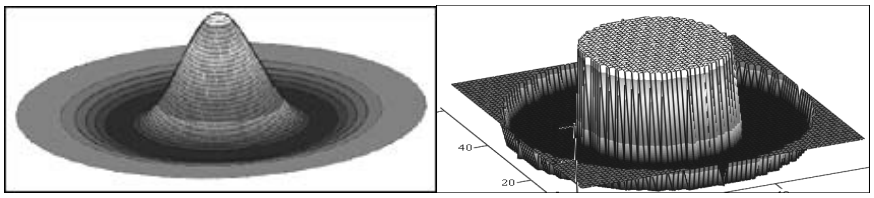

Fig. 2. Some basis wavelet profiles, that were used for data processing. Gauss wavelet function (left) and Haar function (right).

The possible wavelet functions that were used for crater detection is shown in Fig. 2. In our case the basis wavelet is the square matrix with constant elements, but matrix dimensions are varying depending on the diameter of the structure to be discovered. The most simple formula for the wavelet filter, that uses $M \times M$ matrix, can be expressed as an integral sum:

$$W_{x,y} = \frac{1}{M^2}\cdot\left(\sum_{k=-M/2}^{M/2}\cdot\sum_{l=-M/2}^{M/2}\Phi_{k,l}\cdot F_{x+k,y+l}\right). \qquad (3)$$

The main goal of such a transform is to magnify all the circle structures of chosen diameter $D = MDx$ (Dx is the step of a grid) and to eliminate circles having other sizes. In order to discover a possible impact crater we need to repeat the data filtering, changing the effective diameter of the basis wavelet.

Testing of the algorithm

The method was tested on some reliably known impact structures on dry land and the impact crater "Burckle" located in the Indian Ocean (30.865 S, 61.365 E). The diameter of this structure is 29 km. The Haar wavelet function (Fig. 2) with effective size of 60 km was used for data filtering. The size of whole computational area was 400×300 km with a 1 km grid step (Fig. 3).

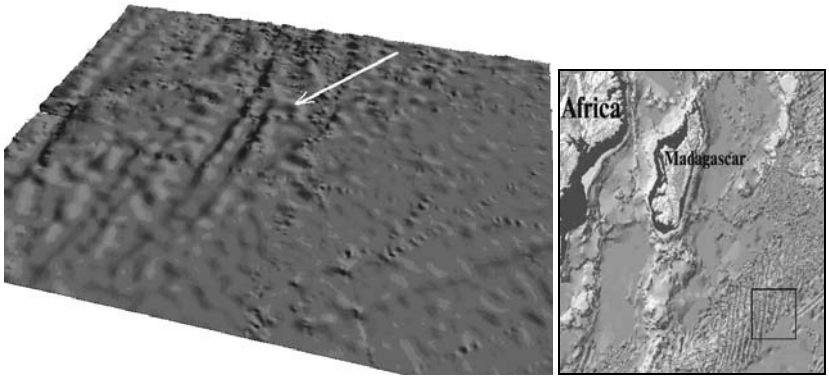

Fig. 3. Gravity field visualization around the "Burckle" impact crater.

The results of gravity field processing are presented in Fig. 4, where after three stages (*a, b* and *c*) of filtering (wavelet transformation) the "Burckle" crater was discovered. The location of this impact crater is indicated by the white arrow in the Fig. 3.

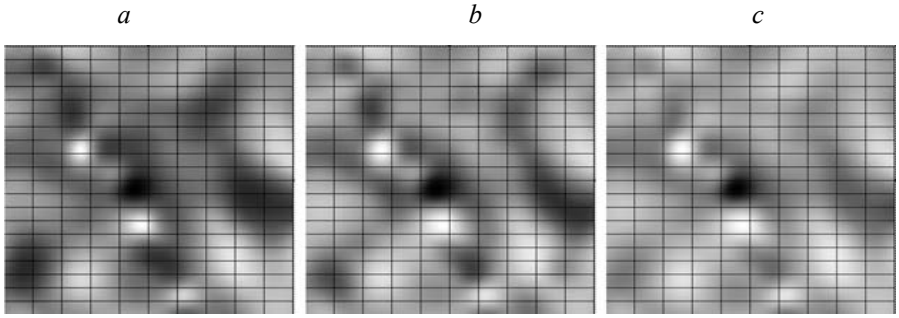

Fig. 4. Three stages of the "Burckle" gravimetric data wavelet filtering.

Another example of the proposed wavelet analysis application is shown in the Fig. 5. On the left part the bottom relief of a small area of the Indian Ocean is visualized. This data was obtained by multi-beam measurements. On the right part of Fig. 5 the result of wavelet filtering is presented. A possible impact structure of 20 km diameter is detected at the location 40º 55′ S, 78º 40′ E.

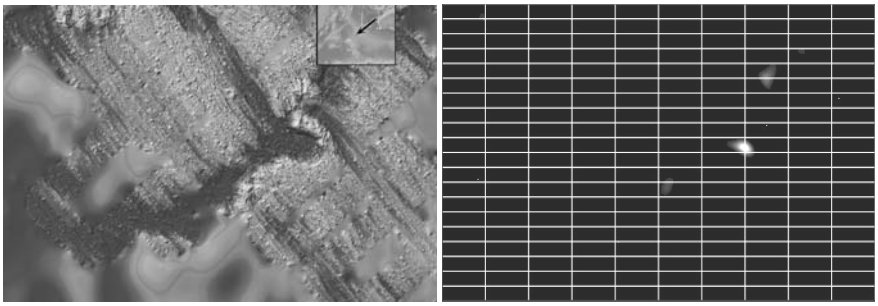

Fig. 5. Detection of a circle structure by processing bottom relief data.

Conclusion

The possibility of discovering hidden impact circle structures by wavelet processing the digital geophysical data was shown in this study. The method for effective wavelet filtration of the digital elevation, gravimetric and magnetometric data was proposed and tested.

References

1. *Petrenko V. E., Lyapidevskaya Z. A.* Data bank for impact structures of the Earth // Bull. of the Novosibirsk Computing Center. Ser. Math. Modeling in Geophysics. Issue 7. Novosibirsk, 1998. P. 161–185 (In Russian).

The Asteroid-Comet Hazard Conference Proceedings, 2009

DEVASTATING CONSEQUENCES OF IMPACTS. STUDY OF TRACES OF PAST COLLISIONS

Prospective Zones of Damage Caused by the Popigai Impact Event

V. L. Masaitis

Russian Geological Research Institute, St. Petersburg, Russia

Abstract. The Popigai impact event occurred about 36 Ma ago, and had not produced a global catastrophe and extinction. Several concentric zones of damage in which intensity decreases with the distance from the impact site may be reconstructed and evaluated in rankings ranging from 10 (evaporation, target perturbation) to 1 (mostly dust settling).

The Popigai crater in central Arctic Siberia with diameter 100 km was formed 35.7 ± 0.2 Ma ago by the collision of an asteroid, which had ordinary chondrite composition and was about 7 km across [1, 2]. Paleogeographical reconstruction shows that the territory where the impact event occurred at the end of Eocene was characterized by a relatively flat relief and was covered by forest vegetation of a transition type from subtropical to moderate thermophilic [3]. The original crater, which is only insignificantly modified by erosion, has a multi-ring inner structure, and is filled in with lithic impact breccias and impactites, resulting from destruction and melting of a two-layered target made of crystalline basement (Archean gneiss) and a platform cover 1.5 km thick (Upper Proterosoic, Cambrian, Permian and Cretaceous siliciclastic and carbonate sedimentary rocks). The impactites (tagamites and suevites) contain impact diamonds formed by shock transformation of graphite crystals and aggregates contained in gneisses. The total volume of from erosion preserved diamond-bearing impactites is about 1750 km^3; their layer has a maximal thickness 600 m [1]. The energy of the impact may be evaluated as equivalent to $E = 2.10^7$ Mt of TNT, peak pressure at the compression stage of $P = 6.24 \cdot 10^{11}$ Pa, and seismic magnitude at the point of impact of 8.3–9.5 on the Richter scale [1, 4, 5]. The zone of complete destruction of

target rocks during cratering had the radius of about 50 km, it may be divided into three subzones: evaporation ($R \sim 9.5$ km), melting ($R \sim 11.3$ km), and intensive deformation ($R = 50$ km), respectively. The ballistic ejecta, seismic wave, thermal radiation caused by fireball heating, blast wave in the atmosphere, and high-velocity wind were responsible for the principal damage outside the area of complete destruction. Several zones of decreasing damage with distance from the impact point may be distinguished. The approximate radii of various types of damage that influenced the environment to different degrees may be reconstructed by means of evaluated impact energy [4, 5, 6], and local environmental conditions. The near crater zone of local destruction and severe damage ($R \sim 1.500$ km) embraced the central and northern parts of Eastern Siberia, parts north-east of Western Siberia, north-west of the Verkhojansk range, and a part of the Arctic ocean (see Figure). This zone consists of three concentric subzones characterized by different degrees of damage. At a distance of about 100 km from the impact point intensive ground displacement, very strong air blast, incineration due to fireball radiation, base surge, and ejecta fallout occurred. Remnants of the ejecta blanket are preserved out to a distance of 70–80 km from the crater center [1], but ballistic ejecta originally had extended out to 500 km where its thickness was only some centimeters or a little more. The evaluation of maximal distance of ballistic transport of impact melt bombs and droplets is in agreement with the distribution of impact diamonds scattered in the river beds around the crater and caused by destruction of these diamond-bearing particles [1, 7]. The outer limits of influence of thermal radiation caused wildfires and strong burns as far as 1500 km from the impact point.

The radius of a zone of moderate or light short-term damage of biotic systems may extend still further out; it embraced northern Eurasia and a significant part of the adjoining Arctic ocean down to the modern northern coasts of Greenland and Canadian archipelago. The deforested land of this zone produced by violent storms probably propagated to a distance of about 2000 km, and areas of slight damage to the vegetation caused by storms and strong gales may have reached to distances up to 2500 km. Some disturbances caused by seismic-generated tsunamis and gales may have occurred on the shores of internal, shallow seas and Arctic ocean coasts up to 3000 km. The influences of global long-term factors of damage are studied insufficiently. It is known that considerable biotic change at the end of Eocene did not occur. The reconstruction shows that global cold snaps (about 4–5 ^{o}C) and biotic changes took place at the Eocene/Oligocene boundary, and is considered as the result of common climatic change, but this cold snap might have been enhanced due to blanketing of the atmosphere with dust clouds. In the part of Siberia under review a change of species of forest vegetation occurred, these species became less thermophilic, and the flowering

plants and fern families underwent more significant extinction [3]. However, the probable contribution of the Popigai event to these processes is not clear. In general, the intensive and moderate damage areas caused by this event covered about 5.5 % of the Earth's surface. Taking into consideration the absence of evidences of a world-wide effect, the Popigai event could not have produced a global catastrophe, but gave rise to rather significant regional effects and destruction.

Nevertheless, the influence of the Popigai event may be traced to a distance of more than 15.000 km based on the distribution of dust carried by atmospheric or gas currents and apparently affected all of the Earth.

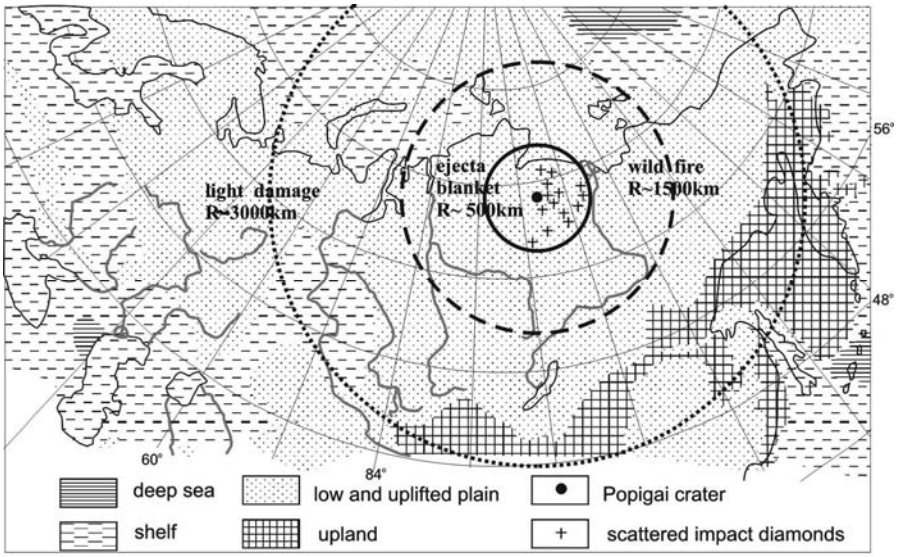

Map showing the paleogeographical settings at the time of the Popigai event (E/O) and the reconstructed zones of damage of various intensity.

The fine spheroids of impact melt (microkrystites) and particles of transformed minerals (shocked quartz, etc.) are found in the Late Eocene deposits in Italy, in Spain, in deep drill holes DSDP (Deep Sea Drilling Project) and ODP (Ocean Drilling Project) in subequatorial area of world oceans and in the southern part of Atlantic ocean [8, 9, 10, 11]. The bulk composition of impactites from Popigai and tiny spheroids (microkrystites) recovered from the core of drill holes are similar [1, 10]. Moreover, isotope measurements of particles and spheroids and their dating compared well with data on impactites and thus are consistent with materials that have been thrown out from the Popigai crater [12].

In general, concentric zones of damage have had irregular contours depending on the local geological setting, on the topography, and atmospheric

conditions at the moment of impact. Thus, their radii may be estimated only approximately. The quantitative scale of intensity of impact damage caused by the Popigai event may be estimated (Impact Damage Index or IDI scale, see Table). The scale can have gradation in points, evaluated as indicators of damage, e. g. from 10 down to 1 or zero if no effect is estimated (see Table). The intensity of destruction depends both on impact energy and distance from the impact site. The IDI scale may be used for reconstruction of any area of destruction caused by impact events that occurred in the past or may happen in the future.

Intensity of impact damage caused by the Popigai event

Index	Description	Principal factors	Damage effects	Approx R, km
10	Impact site, complete destruction	Shock compression of target rocks and accompanying processes	Vaporization, expanding fireball	9.5
9			Melting, jetting	11.3
8			Shock metamorphism, plastic deformation, brecciation, rock displacements, fluidized ejecta, base surge	50
7	Local destruction and severe damage	Seismic wave, shock wave, thermal radiation, ejecta fall	Damaging earthquake, rock displacement, base surge, ballistic ejecta fallout, incineration, very strong air blast	100
6			Strong earthquake, ballistic sedimentation, incineration, strong air blast	500
5			Moderate earthquake, wildfires, burn, air blast, hurricane, dust settling	1500
4	Moderate or light damage	Seismic wave, shock wave, dust cloud	Weak earthquake, violent storm, dust settling	2000
3			Weak earthquake, storm or strong gale, dust settling	2500
2			Very weak earthquake, gale, high wind, oceanic wave, dust settling	3000
1	Light or no damage	Long-term factors (acid rain, darkening, greenhouse effect?)	Light breeze, dust settling, climate change	Up to 15.000

References

1. *Masaitis V. L., Mashchak M. S., Raikhlin A. I., Selivanovskaya T. V. et al.* Almazonosnye impaktity Popigaiskoi astroblemy (Diamond-bearing impactites of the Popigai astrobleme) Saint Petersburg: VSEGEI Publ., 1998. 178 p. (in Russian).
2. *Bottomly R., Grieve R., York D., Masaitis V.* The age of the Popigai impact event and its relation to events at the Eocene/Oligocene boundary // Nature. 1997. Vol. 388. P. 365–368.
3. Geologicheskie i bioticheskie sobytiya pozdnego eozena — rannego oligozena (Geological and biological events of the Late Eocene — Early Oligocene) M.: GEOS, 1996. Part I. 313 p., Part II. 249 p. (in Russian).
4. Katastrophicheskie vozdeistvia kosmicheskikh tel. The catastrophic influence of cosmic bodies / Eds V. V. Adushkin, I. V. Nemchinov. M.: Akademkniga, 2005. 310 p. (in Russian).
5. *Melosh H. J.* Impact cratering. A geological process. Oxford University Press. 1989. 245 p.
6. *Collins G. S., Melosh H. J., Marcus R. A.* Earth impact effects program: a web-based computer program for calculating the regional environmental consequences of a meteorite impact on Earth // Meteoritics and Planetary Sci. 2005. 40. N 6. P. 817–840.
7. *Grakhanov S. A., Shatalov V. I., Shtyrov V. A., Kychkin V. R. et al.* Rossypi almazov Rossii. Diamond placers of Russia. Novosibirsk: GEO Publ. House, 2007. 454 p. (in Russian).
8. *Montanari A., Koeberl C.* Impact stratigraphy. Springer-Verl., 2000. 364 p.
9. *Molina E., Cruz L. E., Gonzalvo C., Ortiz S., Robin E.* Evidencias de impacto meteoritico en el Eoceno Superior de Fuente Caldera (Granada, Cordilleras Beticas) // Geo-Temas. 2004. 6(4). P. 365–368.
10. *Glass B. P., Koeberl C.* Ocean Drilling Project Hole 689B spherules and upper Eocene microtektite and clinopyroxene-bearing spherule strewn field // Meteoritics and Planetary Sci., 1999. 34. P. 197–208.
11. *Vonhof H. B., Smit J.* Late Eocene mikrokrystites and microtektites at Maud Rise (Ocean Drilling Project Hole 689B; Southern Ocean) suggest a global extension of the approximately 35.5 Ma Pacific impact ejecta strewn field // Meteoritics and Planetary Sci. 1999. 34. P. 747–755.
12. *Kettrup B., Deutsch A., Masaitis V.* Homogeneous impact melts produced by a heterogenous target? Sr-Nd isotopic evidence from the Popigai crater, Russia // Geochimica and Cosmochimica Acta. 2003. Vol. 67, N 4. P. 733–750.

DEVASTATING CONSEQUENCES OF IMPACTS. STUDY OF TRACES OF PAST COLLISIONS

Hydrocode Modeling of a High-velocity Impact of an Asteroid Particle on a Steel Surface

N. A. Makhutov, Yu. G. Matvienko, M. A. Bubnov

A. A. Blagonravov Mechanical Engineering Research Institute of RAS, Moscow, Russia

Abstract. Present work deals with physical-mathematical modeling of hyper-velocity impacts up to 80 km/s. This problem is very important for asteroid protection systems and other critical nuclear and military objects.

The main method of solution of this problem is numerical modeling. As a result of modeling, new models and criteria of extreme states of solids will be developed to describe hyper-velocity impacts.

A problem is solved with an arbitrary Lagrangian-Eulerian algorithm (ALE). The LS-DYNA 3D hydrocode was used. The material behavior has been defined by a linear-polynomial model with phase transformations.

The impact process was finished after 10 μs. The results of modeling describe a physical picture of deformation and fracture under hyper-velocity impacts as well as parameters of the produced crater.

Introduction

Increasing risks of natural and technical catastrophes lead to tremendous losses. These catastrophes can be characterized by phenomena of hyper-velocity impact. Thus, the problem merits attention of specialists from all scientific and technical spheres [1].

Solution of this interdisciplinary engineering problem can be based on an analysis and substantiation of models to describe extreme states of solids. Moreover, physical-mathematical modeling of deformation, damage, and fracture processes under hyper-velocity impact loading should be employed. The models have to take into account phase transformations and to be applied in the case of various scales including nano-, micro- and macro-levels.

Actuality of formulation and solution of hyper-velocity impact problem is generated by a need of creation of adequate models and criteria of deformation, damage and fracture processes under high-velocity impacts for the exploitation of asteroid protection systems as well as critical plants such as nuclear energy stations and military objects [1–3].

Impact and deformation processes with characteristic velocities of interaction 10–80 km/s are accompanied by substantial strain intensity and strain rate as well as by increasing the material plasticity up to phase transformations (melting and vaporization).

Since experimental research in this problem is difficult or impossible, the main method of solution of this problem is numerical modeling. As a result of modeling, new models and criteria of extreme states of solids will be developed to describe hyper-velocity impact.

Various models with phase transformations (melting, vaporization, ionization, etc) define material behavior [3–4]. This problem was solved with arbitrary Lagrangian-Eulerian algorithm (ALE) [5]. The LS-DYNA 3D [6] hydrocode was used.

Results for different models

Fig. 1 presents the model for the investigated process. Near the elastic-plastic semi-space 1, we place the kinetic body 2, formed as a cube in the initial approximation. Around this kinetic body the calculation area 3 is simulated as vacuum.

The main problems to be solved in this work, are:

- choice of a method for solution and models of material behavior to produce an adequate physical picture of the impact process;
- estimate consequences of the impact via analysis of the numerical modeling results ;
- development of fracture criteria for hyper-velocity impact problems;
- development of a defense against bodies with hyper-velocity impacts such as asteroids.

In the first approximation both the penetrating body and the target are described by the Johnson–Cook EOS model [6] without taking into account phase transformations. In the deformation process, the hyper-velocity kinetic body penetrates into the target and spreads as a liquid.

In the initial stage of penetration it is possible to use the hydrodynamic approximations.

Hereafter we will consider only the initial stage of the process of penetration, since this stage defines the consistency of the physical picture.

The dependence of temperature as a function of time is shown in Fig. 2. The moment, where our calculation scheme is no longer applicable (negative absolute temperatures appear), can be seen in the figure.

Thus, the process of hyper-velocity impacts cannot be described in the frames of the classical model of the Johnson–Cook equation of state.

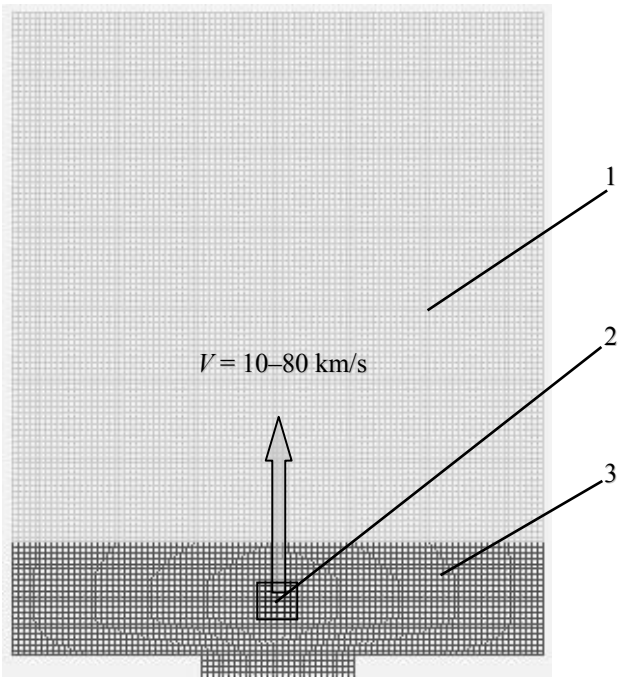

Fig. 1. Calculation scheme.

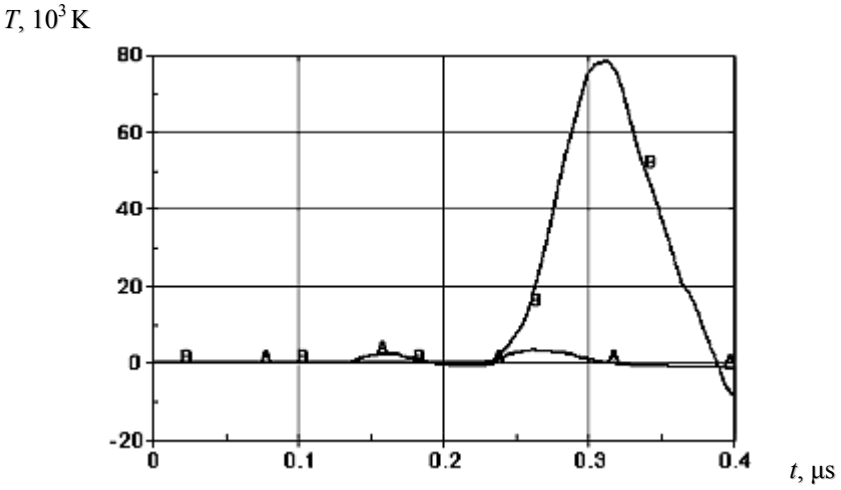

Fig. 2. Temperature time dependence gives inadequate results after 0.35 μs.

Comparison of penetrator and crater shapes in the calculations, both taking into account the processes of thermal conductivity and without them, does not show any essential difference of the shapes of the craters in the model, at least not in the initial stages.

Behavior of penetrator and target materials is described by linear-polynomial model of the equation of state. The equation of that model is following [6]

$$P = C_0 + C_1\mu + C_2\mu^2 + (C_4 + C_5\mu + C_6\mu^2)\,E,$$

where P is hydrodynamic pressure, $\mu = \frac{\rho}{\rho_0} - 1$, where ρ, ρ_0 is a current and initial density, E — internal energy, C_0–C_6 are selectable constants. This equation of state may be used to describe behavior of materials such as liquid and gas after melting and vaporization.

Characteristic current form (time moment 10 μs) of crater for iron penetrator and target at impact velocity 80 km/s as well as contours of fluid density is shown in Fig. 3. The dark shades correspond to regions with highest density (up to 10,000 kg/m^3).

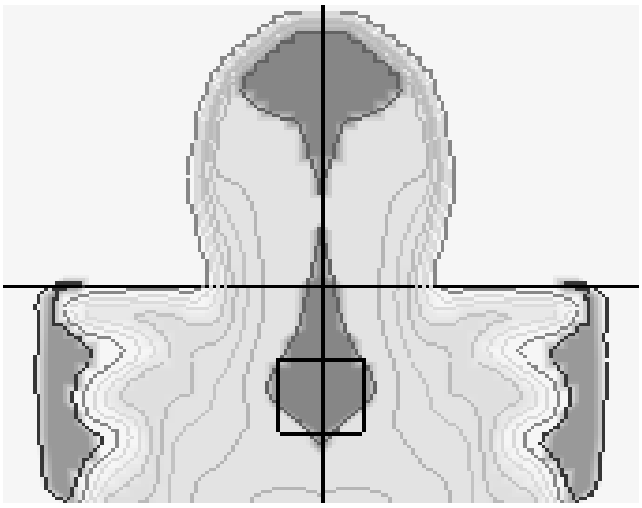

Fig. 3. Crater form after 10 μs.

Also, in the frames of our work, the analysis of the balance of the mechanical (kinetic and internal) energy was done in three different approaches for the description of the materials, namely, Johnson–Cook model, coupled analysis with consideration for the processes of thermal conductivity, and linear-polynomial model that in the simplest case describes the processes of melting and vaporization. In first approximation the criteria for phase trans-

formations is at a constant temperatures of melting (1800 K) and vaporization (> 3000 K). For all these three cases, the essential part of losses of non-mechanical types of energy can reach 60 percent of total kinetic energy of impacting body [7]. These losses are assumed to be connected with ionization, radiation, etc.

The comparison of the results of modeling the hyper-velocity impact process with usage of the Johnson–Cook model and the described linear-polynomial model with phase transformations have been discussed.

The phase transformations were included in the present model by means of changing parameters of equation (1). Thus, calculations of the material deformation under temperature less 1800 K were carried out with initial parameters of the equation (1), which describe the behavior of material as a metal. Deformation under the higher temperature is calculated with another initial parameters of the equation (1), which describe the behavior of material as a liquid and gas. Formulation of the complex equation of state for solid-gas-liquid mixture is very important and should be considered and discussed in future research. An analysis of the obtained results was based on two criteria, namely, maximum temperature in the first shock wave front, and maximum hydrodynamic pressure. However, both models provide a maximum temperature of order 100,000 K, high enough to reach plasma conditions. For the definition of the true order of temperatures further investigations are required.

Conclusions

The following main results have been obtained. Modeling of hyper-velocity impact is carried out by means of different numerical methods. Moreover, the comparison of the results with physical picture of the process is done. Effects of thermal conductivity, melting, and vaporization have been observed.*

At the same time, ionization and radiation effects should be considered in future research.

References

1. Bezopasnost' Rossii. Pravovye, social'no-ekonomicheskie i nauchno-technicheskie aspekty. (Russia's Safety. Lawful, social-economical and scientifical-technical aspects) / Pod obsch. red. akad. K. V. Frolova

---

* Editorial note: The results of the conclusions and the calculations are very interesting, but because of generally unknown physical properties of asteroids it would be interesting to know more about the assumed values for C_0, C_1, C_2, C_4, C_5, C_6, and E in the author's equation.

(Ed. Acad. K. V. Frolov). Vol. 1–31. M.: MGF "Znanie", 1997–2008 (in Russian).
2. *Makhutov N. A.* Prochnost' I bezopasnost': fundamental'nye I prikladnye issledovaniya (Durability and safety: fundamental and applied researches). Novosibirsk: Science, 2008. 528 P. (in Russian).
3. *Matvienko Yu. G.* Modeli I kriterii mekhaniki razrusheniya (Models and criteria of fracture mechanics). M.: Physmatlit, 2006. 328 p. (in Russian).
4. *Stanyukovitch K. P.* Neustanovivshiesya dvizheniya sploshnoj sredy. (Impermanent motions in continuous medium). M.: Science, 1971. 856 p. (in Russian).
5. *Bubnov M. A.* Issledovanie processa metaniya odnosloynogo nabora kompaktnykh gotovykh porazhayuschikh elementov s ploskogo torca prizmaticheskogo zaryada vzryvchatogo veschestva (Research of compact ready fragments throwing from the plane butt-end of prism-formed high explosive charge) // Izv. RAN. 2006. Vol. 1. P. 48–56. (in Russian)
6. LS-DYNA Keyword User's Manual. Vol. 970. LSTC, Livermore, USA, 2003.
7. *Bubnov M. A, Matvienko Yu. G.* Modelirovanie razrusheniya vysokoriskovyh technicheskih sistem posredstvom reshatelya LS-DYNA-3D (Modeling of fracture of high-risk technical systems by means of the LS-DYNA-3D hydrocode) // Proc. of XVI Winter Sci. School for mechanics of solid mediums. Russia, Perm, 2009. P. 74. (in Russian).

DEVASTATING CONSEQUENCES OF IMPACTS. STUDY OF TRACES OF PAST COLLISIONS

Destruction Models for Bodies Entering a Planetary Atmosphere

L. A. Egorova, V. V. Lokhin

Institute of Mechanics of M. V. Lomonosov Moscow State University, Moscow, Russia

Abstract. A body moving in a planet atmosphere is under the influence of aerodynamic loads, the forces of inertia, and heat flux. As a result, the body undergoes ablation and even could be completely destroyed. First of all, the stressed state within the body at any time is determined through an accurate solution of the Lamé equations. Based on the solution, one can investigate the nature of the destruction of the body and evaluate the altitude of destruction for well-known meteoroids if their composition and space velocities are known. During the flight of small fragments thermoelastic forces become significant. Unlike large fragments smaller fragments heat up in a short time resulting in accelerating the process of destruction, which also contributes to the ablation, i. e., reduces the fragment's size. The state of stress in the hot object of decreasing radius is under consideration in this paper. Finally, "thermal explosion" due to the rapid evaporation of small fragments in a typical size range of the fragments was considered. Assessment of the length of run and time of evaporation of small particles allows one to speak about the explosive outbreak and disappearance of the asteroid in the final stages of its demise.

Introduction

Before a body reaches critical loads implying its failure, one should estimate the elastic stress within the body. This involves calculation and distribution of compressive, tension, and tangential (shear) stresses. This problem was first discussed by Yu. Fadeenko [3] for an elastic ball. But there were no solutions of the problem while the places of maximum compressive, tension, and tangential stresses were shown. The necessity to solve the elastic stress problem for meteoroids entering atmosphere was noted by S. Grigorian [4].

In the work of V. Korobeinikov et al. [5] the stress state of a ball was first calculated without shear stresses.

Elastic stress state

The body entering a planetary atmosphere with supersonic speed is under the load of aerodynamic forces. Therefore elastic stresses act on the body. When stresses reach critical values the body may fail and disintegrate. we will examine the elastic stress state of a ball entering the atmosphere. The equations for the of elastic stress problems with boundary conditions from aerodynamics are [1, 7]:

$$\begin{cases} \dfrac{1}{1-2\nu}\,\text{grad div}\,\mathbf{u} + \Delta\mathbf{u} = \dfrac{\rho_b}{G}\dfrac{d\mathbf{V}}{dt}, \\ \sigma_r = \sigma(\theta), \quad r = R, \\ \tau_{r\theta} = \tau(\theta), \quad r = R; \end{cases} \tag{1}$$

$$\sigma_r = \sigma(\theta) = \begin{cases} -\alpha\rho V^2 \cos^2\theta, & 0 \le \theta \le \dfrac{\pi}{2}, \\ 0, & \dfrac{\pi}{2} \le \theta \le \pi; \end{cases} \tag{2}$$

$$\tau_{r\theta} = \tau(\theta) = \begin{cases} \beta\rho V^2 \cos\theta \sin\theta, & 0 \le \theta \le \dfrac{\pi}{2}, \\ 0, & \dfrac{\pi}{2} \le \theta \le \pi. \end{cases} \tag{3}$$

Here **u** is the displacement vector, σ_r is the normal pressure at the surface of a sphere, $\tau_{r\theta}$ is the shear stress on the surface, ν is Poisson's ratio, G is the shear modulus, R is the radius of the body, r, θ are spherical coordinates, ρ_b is the density of the body, ρ is the density of air, V is the speed of the body, and α, β are the aerodynamic resistance coefficients.

The solution was found as a superposition of particular integrals and complimentary functions. Particular integrals:

$$\begin{cases} u_r = -r^2 \cos\theta \dfrac{1-2\nu}{1+\nu}\dfrac{3}{32}\dfrac{(\alpha+\beta)\rho V^2}{GR}, \\ u_\theta = -r^2 \sin\theta \dfrac{1-2\nu}{1+\nu}\dfrac{3}{32}\dfrac{(\alpha+\beta)\rho V^2}{GR}. \end{cases} \tag{4}$$

Complimentary functions were found in terms of Legendre polynomials:

$$u_r^0 = \sum_{n=1}^{\infty} \left[A_n (n+1)(n-2+2\nu) r^{n+1} + B_n n r^{n-1} \right] P_n(\cos\theta),$$

$$u_\theta^0 = \sum_{n=1}^{\infty} \left[A_n (n+5-4\nu) r^{n+1} + B_n n r^{n-1} \right] \frac{dP_n(\cos\theta)}{d\theta}, \quad r = Rx. \qquad (5)$$

The solutions in terms of displacements permit us to find the strain tensor and elastic stress tensor. For further estimates we choose the stress intensity expressed by the second invariant of the stress tensor:

$$\tau_i = \sqrt{I_2} = \sqrt{\frac{1}{6}\left[(\sigma_r - \sigma_\theta)^2 + (\sigma_r - \sigma_\varphi)^2 + (\sigma_\theta - \sigma_\varphi)^2 + \tau_{r\theta}^2 \right]}. \qquad (6)$$

The value of stress intensity is shown in Fig. 1. As a criterion of breaking strength we chose the following: the potential energy density of a change in shape must be less than the critical strength of the material [1, 2]:

$$\sqrt{3}\tau_i = \sqrt{3}\sqrt{I_2} < \sigma_*. \qquad (7)$$

Knowing velocity and density of the body one can estimate the altitude at which the body disrupts. We consider velocity as constant at the given part of trajectory. So the value of second invariant changes only because the atmosphere density changes. Using the barometric formula for the density, the equations above give the relation for the destruction altitude. We consider the start of breakup as a point when the critical value of stress is attained in the ball. The final breakup is the point when critical values of stress are reached in most parts of the volume. Let us consider examples to show the relation. If we have a material with critical stress of 700 atm entering with 30 km/s it will survive. If the critical stress is only 50 atm it will break up at an altitude of about 8 km.

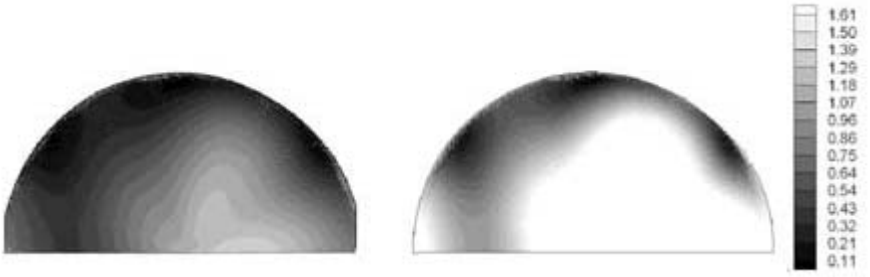

Fig. 1. Stress intensity of the ball.

Thermoelastic stress state

Knowing the linear nature of the problem we can solve the thermoelastic stress separately from the elastic stress and then add the component solutions. To find the thermoelastic stress we solve the thermal conductivity problem. To solve for the temperature we substitute into the known relations for thermoelastic stress:

$$\sigma_{rr} = \frac{2}{3}\frac{E\kappa}{1-\nu}\left[\overline{T}(R,t) - \overline{T}(r,t)\right],$$

$$\sigma_{\varphi\varphi} = \frac{2}{3}\frac{E\kappa}{1-\nu}\left[\overline{2T}(R,t) + \overline{T}(r,t) - 3T(r,t)\right] = \sigma_{\theta\theta}, \qquad (8)$$

$$T(r,t) = \frac{2RT_0}{\pi r}\sum_{n=1}^{\infty}\frac{(-1)^{n+1}}{n}\sin\frac{\pi nr}{R}e^{-\kappa\pi^2x^2t/R^2},\ \overline{T}(r,t) = \frac{3}{r^3}\int_0^r x^2T(x,t)dx,$$

$$\overline{T}(r,t) = \frac{6RT_0}{(\pi r)^2}\sum_{n=1}^{\infty}\frac{(-1)^{n+1}}{n}\left(\cos\frac{\pi nr}{R} - \frac{R}{n\pi r}\sin\frac{\pi nr}{R}\right)e^{-\kappa\pi^2x^2t/R^2} \qquad (9)$$

.

It should be mentioned that thermoelastic stress influences the body breakup only for small bodies. The time of flight is enough for heat to spread into the body. For large bodies thermoelastic stress will cause only ablation. Adding the thermoelastic stress solutions to the elastic stress we have the following pictures for small bodies (Fig. 2).

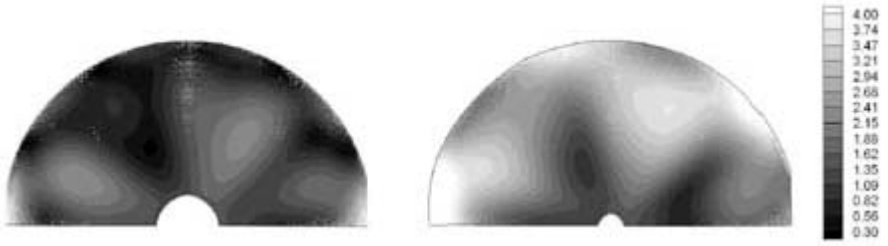

Fig. 2. Stress intensity of a ball taking into account thermoelasticity effect.

To estimate the influence of vanishing effect on the stress inside the body we state the Stephan problem for the ball vanishing with rate alpha and melting temperature at the surface. The solution of the heat transfer problem was substituted into relations (9). Then the elastic stresses were added to see the complete solution.

"Heat explosion"

We assume that a body moving in the atmosphere with high velocity breaks up several times by elastic fragmentation. The resulting small particles break up again by thermoelastic stresses and the smallest ones melt and vaporize. This raises the question: What is the maximum size of a particle that will not break up because of elastic stress at the given velocity and altitude? We can find the radius from the condition at which the impact air pressure reaches its maximum:

$$\frac{d}{dt}\left(\rho V^2\right) = 0, \quad r = \frac{3}{4}\frac{H\rho_0}{\rho_b}\exp(-\frac{h}{H}), \tag{10}$$

where H is the atmospheric scale height.

The smaller particles are destroyed by thermoelastic stress and vaporization, the larger ones are destroyed by elastic fragmentation.

The final problem we set ourselves was that of explaining the thermal explosion hypothesis. As we conclude, at a final stage the body is broken to pieces [6]. As we do not know exactly the particle size distribution we suppose, that particles have the distribution as that in a body immediately after breakup by explosion. The distribution is well known from the literature: $\frac{dN_m}{dm} = Cm^{\frac{k}{3}-2}$, $k = 1.2$. From this relation we could find the number of particles having mass m. The equation of mass loss permits us to find the time of vanishing. So we could find the luminosity of the cloud of dust at the final stage of meteoroid destruction:

$$I = -\tau\frac{V^2}{2}\frac{dM}{dt} \tag{11}$$

Conclusions

Using Legendre polynomials the exact solution was found for the stress state of an elastic sphere when entering a planetary atmosphere with cosmic speeds. Thermoelastic stress and vaporization were also under consideration.The solution shows the destruction character and the heat explosion of a meteoroid.

The work was carried out with financial support from Program of support to Leading Scientific Schools (397.2008.1).

References

1. *Lurie A. I.* Prostranstvennye zadachi teorii uprugosti (Three-dimensional problems of elasticity), M.: 1955 (in Russian).

2. *Belyaev N. M.* Trudy po teorii uprugosti i plastichnosti *(*Works on theory of elasticity and plasticity). M. 1955 (in Russian).
3. *Fadeenko Yu. I.* Destruction of meteoroids in the atmosphere // Combustion, Explosion, and Shock Waves. 1967. Vol. 3, N 2. P. 172–174.
4. *Grigoryan S. S.* Motion and destruction of meteors in planetary atmospheres // Cosmic Res. 1979. Vol. 17. P. 724–740.
5. *Korobeinikov V. P., Gusev S. B., Semenov I. V.* Simulation of Celestial-Body Disruption in the Earth's Atmosphere // Solar System Res. Vol. 31, N 4. 1997. P. 330.
6. *Tirskiy G. A., Khanukaeva D. Yu.* Ballistics of a Fragmenting Meteor Body with Allowance Made for Ablation in the Non-isothermal Atmosphere. II // Cosmic Res. 2008. Vol. 46, N 2. P. 120–132.
7. *Lunev V. V.* Giperzvukovaja aerodinamika (Hypersonic Aerodynamics). M.: Mashinostroenie, 1975 (in Russian).

DEVASTATING CONSEQUENCES OF IMPACTS. STUDY OF TRACES OF PAST COLLISIONS

Expert Database on the Earth Impact Structures

V. K. Gusiakov, Z. A. Lyapidevskaya

Institute of Computational Mathematics and Mathematical Geophysics of RAS, Novosibirsk, Russia

Abstract. An Expert Database on the Earth Impact Structures (EDEIS) has been compiled and is being maintained in the Tsunami Laboratory of the Institute of Computational Mathematics and Mathematical Geophysics of SD RAS in Novosibirsk. This database is somewhat more liberal than the well-known Earth Impact Database maintained by the Planetary and Space Science Centre, University of New Brunswick, Canada. In addition to including the fully validated impact structures, the EDEIS also lists proposed structures whose impact genesis still needs validation. For any structure, the degree of confidence of impact origin is reflected by its validity index V, which varies from 4 (confirmed) to 0 (rejected) with intermediate values of 3 (probable), 2 (perspective) and 1 (proposed for further study). Classification of structures over the validity index is based on some sort of expert judgment and reflects the availability of impact criteria found at four different levels — morphological, geological, petrological, and mineralogical. Currently, the database contains 1020 structures, among them 214 with $V = 4$, 211 with $V = 3$, 455 with $V = 2$, and 47 with $V = 1$. 93 structures have validity index $V = 0$, because the once proposed impact origin was later disproved by additional studies.

Cataloging of impact structures discovered on the Earth surface is an important instrument for evaluation of frequency of impacts and for studying the comet and asteroid hazard. Presently there exist more than 10 global catalogs and databases on Earth impact structures. The widely-known Earth Impact Database (EID), maintained by the Planetary and Space Science Centre, University of New Brunswick, Canada [1] is considered to be a reference database in this field. The EID, currently having 176 craters, contains only those structures whose impact genesis has been confirmed over the whole

complex of evidences. Meanwhile, in the scientific literature and on the Internet, the data on many more structures, having some features of an impact origin, are being circulated and discussed. Systematization and cataloging of all these data was the main objective of an Expert Database on the Earth Impact Structures (EDEIS), that has been created and is being maintained by the Tsunami Laboratory of the Institute of Computational Mathematics and Mathematical Geophysics of SD RAS. The EDEIS was built on the basis of the initial catalog of impact structures developed in [2].

As is known [3, 4, 5], the full set of evidences for proving the impact genesis of a suspicious structure includes the study of four groups of criteria found on different spatial levels:

1. morphological criteria discovered on macro-spatial level (10^2–10^5 m) — circular form, presence of edge wall and central uplift (for complex structures), typical diameter/depth ratio, inconsistency with local geological settings and local hydrographic network (for lakes), associated craters;

2. geological criteria discovered on spatial level of 10^{-1}–10^2 m — ejecta layer, breccias, pseudotachylite**,** shatter cones, radial faults, presence of melt sheets and dykes;

3. petrological criteria discovered on spatial level of 10^{-4}–10^{-2} m — high pressure metamorphism of rocks and minerals, disordered structure of grains, presence of plagioclase feldspar, etc.;

4. mineralogical criteria discovered on micro-spatial level (10^{-6}–10^{-5} m) — planar deformation structure (PDFs), shocked quartz, micro spherules of different types (silicate, magnetite, carbon), translucent amorphous C, splash in Fe, Ni, Cr content, Iridium anomaly.

Normally, the process of proving the impact origin of a structure should include the investigation made on all four levels — starting from the initial identification on maps or satellite images (level 1), through the field study on level 2 followed by laboratory analysis on levels 3 and 4. However, for too many structures this process is still limited to the first, second or third levels, thus leaving some degree of uncertainty on the impact origin of a structure. In the EDEIS, this uncertainty is reflected by the validity index V varying from 4 (confirmed on all four levels), through 3 (probable) and 2 (perspective) to 1 (proposed for further study). Thus, classification of the structures over the validity index is based on some sort of expert judgment and reflects the availability of impact criteria found at four different levels listed above. This classification constantly changes thus reflecting availability of data in the literature and on the Internet.

Currently, the database contains the parametric catalog of 1020 structures, among them 214 structures with the validity index $V = 4$, 211 structures with $V = 3$, 455 structures with $V = 2$, 47 structures with $V = 1$, and 93

structures with $V = 0$. The last group of records includes the structures whose impact origin has once been proposed, but further investigation demonstrated clear evidence against the impact genesis. We keep these rejected structures in the database, because information about them is still circulating in the literature and on the Internet. In addition to the main parametric table, the database contains over 2440 photos and maps, 765 textual descriptions and 980 bibliographical references. For each structure, the main table contains the basic parametric data on geographical location, diameter, depth of depression, estimated age, etc., as well as additional data on availability of further impact criteria, degree of erosion, geophysical anomalies, finding extraterrestrial materials, etc. Each structure is provided with bibliographical references to the original publications, catalogs and web-sites that list this particular structure.

Geographical location of 648 impact structures, having the age estimates and validity from 4 to 1 is shown in Fig. 1. Spatial distribution of structures on the Earth surface is quite uneven reflecting geological conditions on the surface and the level of geological mapping of the territory.

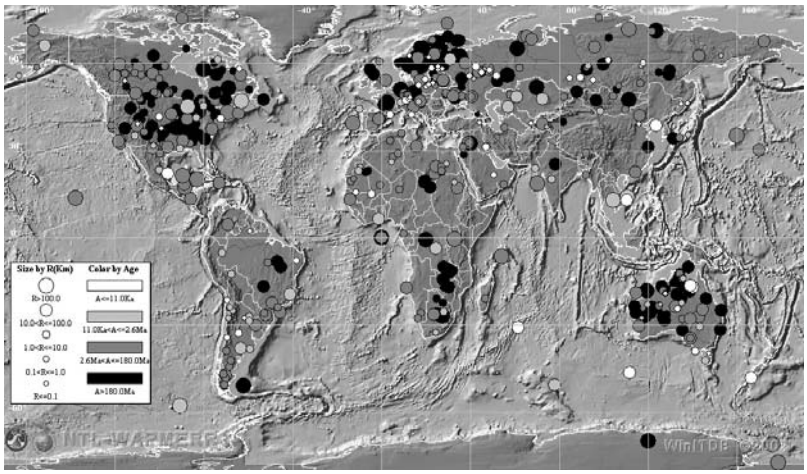

Fig. 1. Geographical distribution of 648 impact structures on the Earth surface, having age estimates. Size of circles is proportional to the crater diameter. Density of the grey color corresponds to four groups of age (see inserted legend).

The database was constructed in the DBMS MS Access and is provided with a specially developed user interface — PDM (Parametric Data Manager) graphic shell allowing a quick and efficient handling of data (retrieval, listing, editing, sorting, processing, and analysis). The PDM shell gives the user possibility to work with different type of information — table, textual, graphical. Some examples of the screen outputs provided by the graphic shell are shown in Figs. 2 and 3.

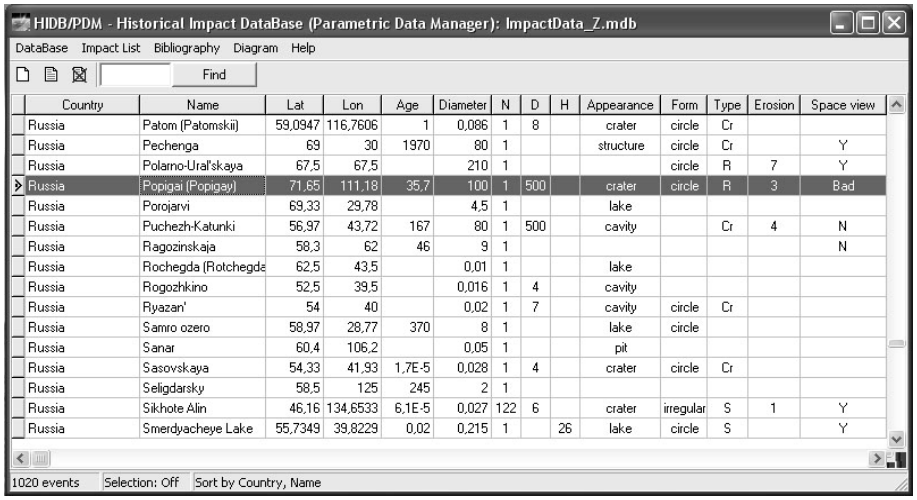

Country	Name	Lat	Lon	Age	Diameter	N	D	H	Appearance	Form	Type	Erosion	Space view
Russia	Patom (Patomskii)	59,0947	116,7606	1	0,086	1	8		crater	circle	Cr		
Russia	Pechenga	69	30	1970	80	1			structure	circle	Cr		Y
Russia	Polarno-Ural'skaya	67,5	67,5		210	1				circle	R	7	Y
Russia	Popigai (Popigay)	71,65	111,18	35,7	100	1	500		crater	circle	R	3	Bad
Russia	Porojarvi	69,33	29,78		4,5	1			lake				
Russia	Puchezh-Katunki	56,97	43,72	167	80	1	500		cavity		Cr	4	N
Russia	Ragozinskaja	58,3	62	46	9	1							N
Russia	Rochegda (Rotchegda	62,5	43,5		0,01	1			lake				
Russia	Rogozhkino	52,5	39,5		0,016	1	4		cavity				
Russia	Ryazan'	54	40		0,02	1	7		cavity	circle	Cr		
Russia	Samro ozero	58,97	28,77	370	8	1			lake	circle			
Russia	Sanar	60.4	106,2		0,05	1			pit				
Russia	Sasovskaya	54,33	41,93	1,7E-5	0,028	1	4		crater	circle	Cr		
Russia	Seligdarsky	58,5	125	245	2	1							
Russia	Sikhote Alin	46,16	134,6533	6,1E-5	0,027	122	6		crater	irregular	S	1	Y
Russia	Smerdyacheye Lake	55,7349	39,8229	0,02	0,215	1		26	lake	circle	S		Y

Fig. 2. Parametric catalog of the impact structures listed in the main screen window of the PDM graphic shell.

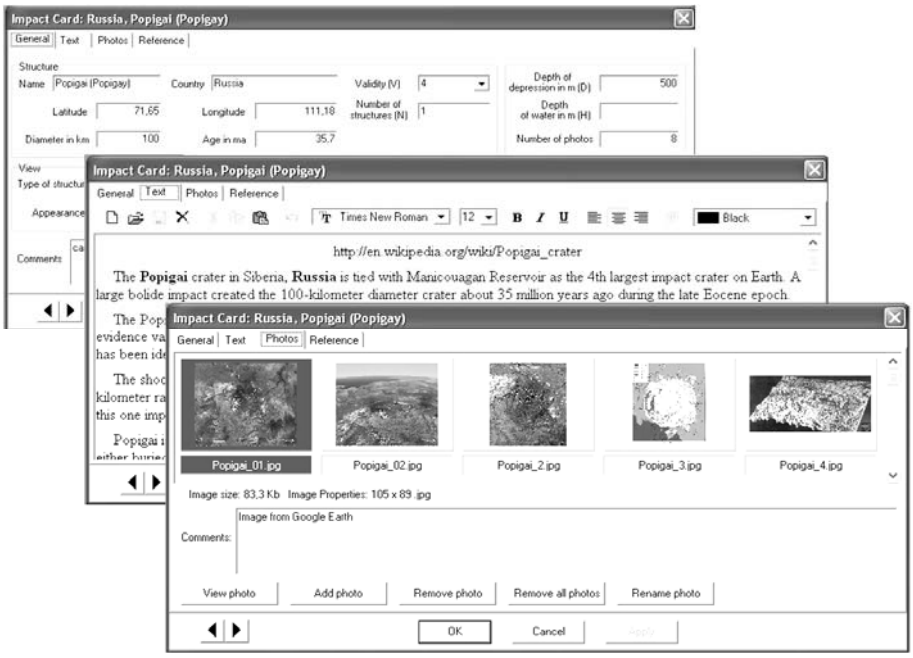

Fig. 3. Additional dialog windows provide detailed parametric data, textual description and collected graphic images for the selected structure (in this example — Popigai crater in the northern Siberia).

The main screen window lists the parametric catalog of impact structures containing the basic set of quantitative information related to a particular structure. By default, they are sorted by geographical location and structure's name. The user can easily re-sort the list (in ascending or descending order) by clicking on header of any column in the table. Double-click on any line in the table opens the additional dialog windows with more detailed data and information available for this structure (Fig. 3).

The full version of the database contains about 300 Mb of data and information and is distributed on a CD-ROM. The Internet version, providing the access to the main parametric catalog, can be found at the Tsunami Laboratory web-site: *http://tsun.sscc.ru/nh/impact.php*.

The work was supported by the RFBR grants 08-07-00105 and 09-05-00294.

References

1. *Spray J., Hines J.* Earth Impact Database // Planetary and Space Sci. Centre. University of New Brunswick. Canada, 2009. *http://www.unb.ca/passc/ImpactDatabase/index.html*.
2. *Petrenko V. E., Lyapidevskaya Z. A.* Bank dannykh dlya impactnykh struktur Zemli (Data bank on the impact structures of the Earth) // Trudy IVMiMG. Matematicheskoe modelirovanie v geofizike. Issue 7. Novosibirsk, 1998. P. 161–185. (in Russian).
3. *Grive R. A. F.* Terrestrial impact structures // Ann. Rev. Earth Planet Sci. 1987. Vol. 15. P. 245–270.
4. *Masaitis V. L. et al.* Geologia astroblem (Geology of astroblems). Leningrad: Nedra, 1980. 231 p. (in Russian).
5. *Khryanina L. P.* Meteoritnye cratery na Zemle (Meteorite craters on the Earth). Leningrad: Nedra, 1987. 112 p. (in Russian).

DEVASTATING CONSEQUENCES OF IMPACTS. STUDY OF TRACES OF PAST COLLISIONS

Georadar and Hydrogen Studies of the Tunguska Meteorite Craters

V. A. Alekseev[1] , V. V. Kopeikin[2], N. G. Alekseeva[1], L. Pelekhan [3]

[1]Troitsk Institute for Innovation and Fusion Research, Troitsk, Moscow region, Russia
[2] Institute of the Earth Magnetism and Propagation of Radio Waves of RAS, Troitsk, Moscow region, Russia
[3] Complex Self-made Surgut Expedition, Surgut, Russia

Abstract. Tunguska meteorite craters were studied during July 7–22, 2009. The distribution of the craters over the 2.5 × 0.3 km area between the North and South bogs are very similar to the crater arrangement of Sikhote Alin meteorite shower, which suggests that the Tunguska meteorite, during its explosion, was divided into fragments. Our studies support the idea by L. A. Kulik [1, 2] on abundant formation of the craters of impact nature.

Introduction

The crater structure was studied using a "Loza" georadar penetrating the ground to a depth of 40 m. The craters selected as caused by impacts preserved their shapes because of permafrost: they are cones dissecting the bog to the depth of approximately 40 m. The crater structure consists of (1) the upper layers of the present-day permafrost, (2) lower, destructed layers, and (3) possible fragments of the disrupted cosmic body, which should be studied by drilling.

We found and studied 13 craters. They were visually selected by their anomalous morphology of the low peat bogs and peat billows from other craters of the forest. To study the craters, boards were laid through their centers and the georadar measurements were performed with a step size of 10 cm in the form of a "north-south" and "west-east" cross.

It should be noted that we used the "Loza" georadar whose sensitivity and depth of propagation are many times higher than those of all modern world analogs, and the inventor took part in the measurements.

We studied in detail the Suslov crater and its daughter side craters. Our measurements confirm their impact origin, as was assumed by L. A. Kulik. However, he could not detect fragments of the Tunguska cosmic body, since the fragments are non-uniformly distributed in the crater bottom and cannot be detected by drilling if their location is unknown.

The search for the impact structures and the georadar investigation should be continued in other regions of the Tunguska reserve in order to obtain a complete picture of the dispersal of the fragments after the explosion and the distribution of the craters of the Tunguska meteorite shower.

Results of craters geo-profiling radar (GPR) survey

In July 2009 a GPR survey was performed in the region of Podkamennaya Tunguska to survey the number of craters in the epicenter of the Tunguska meteorite falls. The epicenter of the Tunguska phenomenon was first identified in an investigation by L. A. Kulik using the directions of the fallen trees.

The profiling and sounding was carried out using the "Loza" GPR, which has the following parameters:

1. Frequency band 1–500 MHz,
2. Time sampling 1 ns,
3. Sensitivity of receiver 100 mkV,
4. Pulse power of transmitter 1 MW,
5. Central frequency of antennas 100 MHz.

Positioning was determined with a GARMIN Venture GPS.

Survey on July 11, 2009.

Objective 1. Suslov crater. Coordinates: N 60°54′13.5″, E 101°54′23.8″.

The depth and the dielectric constant were calculated via sounding.

In Figs. 1 and 2 the wave forms of reflected signals are presented with the time scale as vertical coordinate. The left hand scale shown in the figures is approximate. The exact boundary depths for sounding points is indicated on leaders.

It is still necessary to study once more the composition of inclusions in the craters that have just been studied by the georadar using drilling. We appeal to the world fellowship to support the work on drilling of the detected impact structures.

Objective 2. During the expedition, hydrogen flows were measured on the routes to the Farington and Stoikovich mountains and around the Suslov crater. In some areas, the hydrogen flows related to degassing of breakage structures of the paleovolcano are anomalously high. This fact also confirms a possible endogenous origin of the geochemical anomalies (elevated concentration of microelements in the 1908 moss layers). Anomalous hydrogen flows suppress plant growth as identified in satellite photographs.

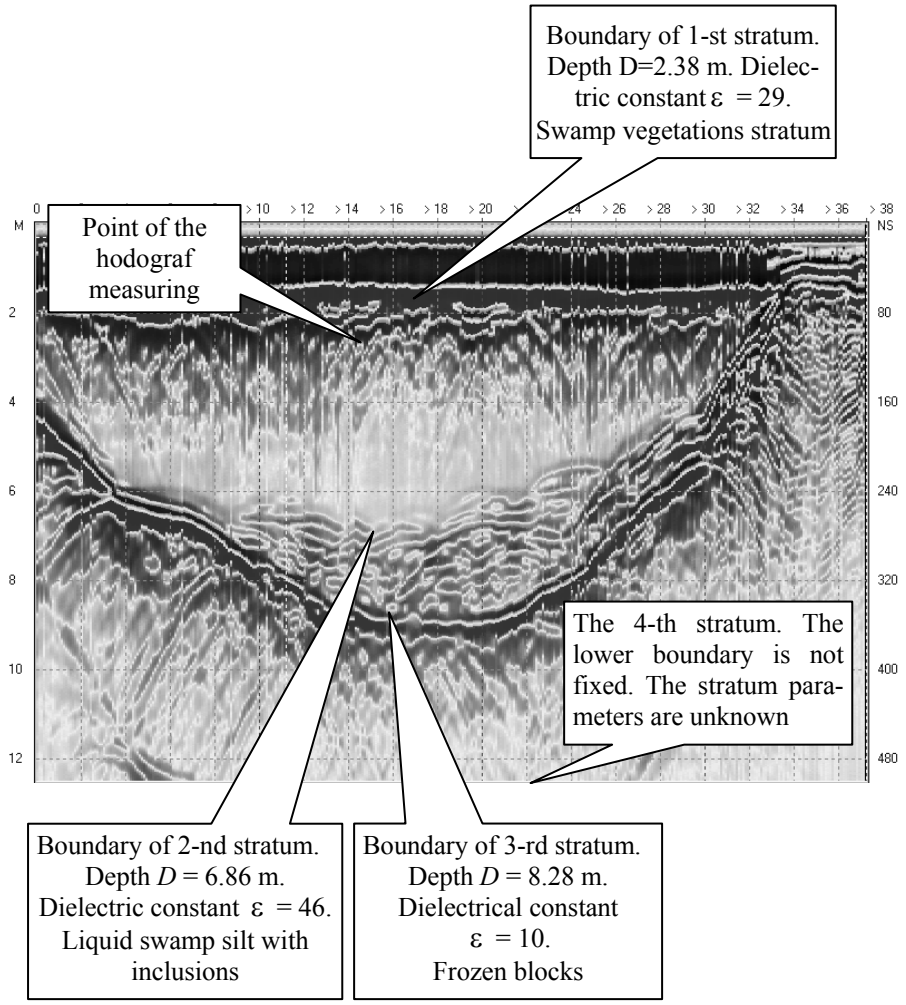

Fig. 1. North-south crater section.

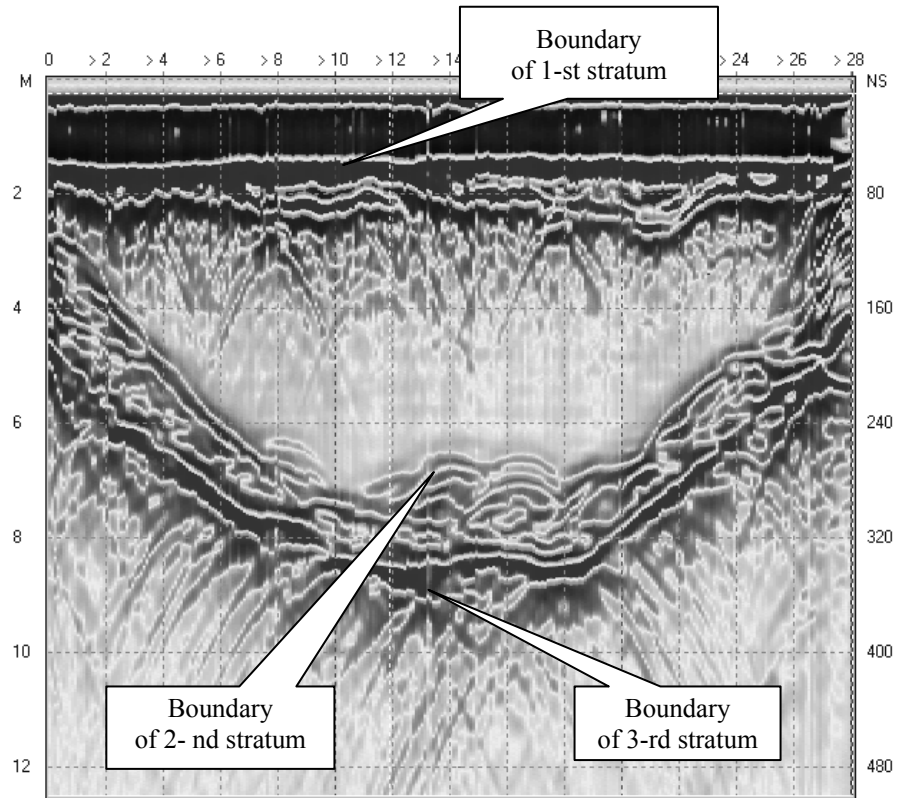

Fig. 2. West-east crater section.

References

1. *Kulik L. A.* Dannyje po Tungusskomu meteoritu k 1939 godu (Information on Tunguska meteorite as of 1939) // Doklady Akad. Nauk SSSR. 1939. Vol. 22. P. 520–524 (in Russian).
2. *Kulik L. A.* Meteoritnaja ekspeditsija na Podkamennuju Tungusku v 1939 g. (Meteorite expedition to Podkamennaya Tunguska in 1939) // Doklady Akad. Nauk SSSR. 1940. Vol. 28. P. 597–601 (in Russian).

The Asteroid-Comet Hazard Conference Proceedings, 2009

DEVASTATING CONSEQUENCES OF IMPACTS. STUDY OF TRACES OF PAST COLLISIONS

Influence of Asteroids and Trans-Neptunian Objects on the Motion of Major Planets and Masses of the Asteroid Main Belt and the TNO Ring

E. V. Pitjeva

Institute of Applied Astronomy of RAS, St. Petersburg, Russia

Abstract. Perturbations from asteroids and Trans-Neptunian Objects (TNOs) produce a significant effect on the orbits of planets and should be taken into account when high-accuracy planetary ephemerides are constructed. On the other hand, from an analysis of motion of the major planets some physical parameters of the asteroids and TNOs may be obtained. The experiment showed that fitting ephemerides from only several of the largest asteroids is insufficient; at present the perturbations from more than 300 asteroids have been taken into account. Methods of estimating asteroid masses are discussed in this paper. Influence of TNOs on the motion of major planets is also considered. Masses of several asteroids that perturb Mars most strongly, the mass and the radius of the asteroid ring, the mass of the TNO ring, as well as the total masses of the main belt asteroids and all TNOs have been estimated while fitting the high-precision numerical ephemerides EPM2008 of IAA RAS to accurate ranging data (1961–2008) of planets and spacecraft orbiting near planets or landing on them.

Introduction: precision of observations and dynamical models

At present, the accuracy of ranging observations of spacecraft orbiting near planets reaches a precision of 1 m, which is the twelfth significant figure in distances. The construction of high-precision ephemerides of major planets, which corresponds to 1 m accuracy of ranging data, requires the creation of an adequate mathematical and dynamical model of the motion of planets on the basis of general relativity and must take into account all perturbing factors. Perturbations from asteroids and Trans-Neptunian Objects affect significantly the orbits of planets and should be taken into account

when high-accurate planetary ephemerides are constructed. On the other hand, from analysis of these perturbations it is possible to derive values of some physical parameters of the asteroids and TNOs through processing of precise spacecraft measurements. The EPM2008 ephemerides (Ephemerides of Planets and the Moon) of IAA RAS originated in the 1970s at about the same time as DE ephemerides were developed to support space flights. Since that time they have been extensively developed and used for data analysis.

EPM2008 ephemerides

For the construction of the EPM2008 ephemerides a numerical integration of the equations of motion of the major planets, the Sun, the Moon and the lunar physical libration, asteroids and TNOs, taking into consideration perturbations from solar oblateness has been performed in the Parameterized Post-Newtonian metric for the harmonic coordinates $\alpha = 0$ and general relativity values $\beta = \gamma = 1$.

A serious problem in the construction of planetary ephemerides arises due to the necessity to take into account the perturbations caused by minor planets. The experiment showed that the fitting of ephemerides accounting for the perturbations from only several of the largest asteroids (DE200 and EPM87) to the Viking lander data was poor. The perturbations from 300 and more asteroids have been taken into account in the ephemerides starting with DE403, and EPM98. However, masses of many of these asteroids are quite poorly known, which deteriorates the accuracy of the planetary ephemerides.

Masses of most large asteroids that affect Mars and Earth more strongly can be estimated from observations of Martian landers and other spacecraft orbiting Mars. Five of the 300 largest asteroids proved to be binaries and their masses are now known. The masses of (243) Ida, (433) Eros, (253) Mathilda, and (951) Gaspra have been derived from perturbations on the Galileo and NEAR spacecraft during flybys. Unfortunately, the classical method of determining masses of asteroids for which close encounters occur can give an accurate determination of asteroid masses only for separate cases when very close encounters are provided with useful data before and after encounters.

The masses of the rest of the 301 large asteroids have been estimated by the astrophysical method from analysis of data concerning their diameters and spectral classification. The mean densities of the three asteroid taxonomical classes (C, S, M) that were used in this case were estimated from ranging observations. However, the total mass of asteroids not included in the list of 301 asteroids is large enough to affect the orbits of the major planets. The total contribution of all remaining small asteroids is modeled as the acceleration caused by a solid ring with the constant mass distribution in the ecliptic plane [1].

By now hundreds of large TNOs have been found including Eris which surpasses Pluto in mass. The updated model of EPM2008 includes the 21

largest TNOs (Eris, Haumea, Makemake, Sedna, Quaoar, Orcus, Varuna, Ixion, and others) into the process of the simultaneous numerical integration. In order to investigate the influence of trans-Neptunian objects on the motion of planets, positions of planets obtained with two versions of EPM ephemerides, with and without the 21 TNOs, have been compared. The maximum differences in right ascension ($d\alpha$), declination ($d\delta$), and heliocentric distance (dR) obtained on the time interval 1913–2020 are shown in Tab. 1. These differences are on the order of the magnitude less than the formal uncertainties of planet positions. After adjusting ephemerides to the present set of observational data, the difference in residuals for these versions of ephemerides (with and without TNO) was not found. However, the total shift of the barycenter of the Solar System due to the 21 largest trans-Neptunian objects is 6140 m within the lifetime of GAIA (2011–2020).

Table 1. The maximum differences in $d\alpha$, $d\delta$, and dR, 1913–2020, for ephemerides with and without the 21 largest TNOs

Planet	$d\alpha$, mas	$d\delta$, mas	dR, m
Mercury	0.006	0.003	2.4
Venus	0.006	0.010	6.1
Mars	0.068	0.025	15.5
Jupiter	0.260	0.110	199
Saturn	0.298	0.103	311
Uranus	1.688	0.744	5932
Neptune	2.321	0.279	50332
Pluto	2.578	1.064	60821

Some tests have been made for estimating the effect of other TNOs on the motion of planets. Their perturbations have been modeled by considering the perturbation from a circular ring having a radius of 43 AU and different masses. The minimum mass (EPM_{1-TNO}) of this ring is taken to be equal to the mass of 100,000 bodies 100 km in diameter with density equal to 2 g/cm^3. It amounts to 110 masses of Ceres. The maximum mass (EPM_{5-TNO}) of the ring is expected to be 100 times the minimum mass. Masses of EPM_{2-TNO}, EPM_{3-TNO}, EPM_{4-TNO} amount 25, 50, and 75 % of the maximum mass respectively. The effect of the ring is only noticeable for more accurate observations — the spacecraft data. The rms residuals and the weight unit errors for these data after fitting the standard and test EPM ephemerides are given in Tab. 2.

It is seen that all the masses of the TNO ring except the minimum mass ($EPM_{1-TNO} = 5.26 \cdot 10^{-8}$ $M_\odot$) are too large and make the data residuals worse. These results allow for the possibility to estimate the upper limit of the total mass of all TNOs and to include the mass value of the TNO ring into the set of the adjusted parameters.

Table 2. The rms residuals expressed in meters and the weight unit errors σ_0 for EPM ephemerides with different masses of the TNO ring

Observations	Martian Landers	Martian spacecraft	Venus Express	Spacecraft at Jupiter	Spacecraft at Saturn	σ_0
Interval	1976–1997	1998–2008	2006–2007	1973–2001	1979–2006	1913–2008
Num. n. p.	1348	13903	547	7	734	97101
EPM2008	11.82	2.04	2.59	13.09	3.04	0.876
EPM_{1-TNO}	12.00	1.87	2.59	13.08	3.02	0.876
EPM_{2-TNO}	13.16	1.90	2.63	13.20	64.35	1.000
EPM_{3-TNO}	13.35	2.00	2.68	13.29	129.7	1.305
EPM_{4-TNO}	13.83	2.05	2.74	17.74	195.0	1.696
EPM_{5-TNO}	14.26	2.06	2.80	27.43	200.3	2.126

Thus, the dynamical model of EPM2008 ephemerides takes into account the following:

- mutual perturbations from major planets, the Sun, the Moon and the 5 most massive asteroids;
- perturbations from 296 other asteroids chosen due to their strong perturbations on Mars and the Earth;
- perturbation from the massive asteroid ring with constant mass distribution in the ecliptic plane;
- perturbations from the 21 largest TNOs;
- perturbation from a massive ring of TNOs with the radius of 43 AU;
- perturbations due to the solar oblateness $J_2 = 2 \cdot 10^{-7}$.

The modern EPM2008 ephemerides have resulted from a least squares adjustment to observational data totaling about 550,000 position observations of different types including different American and Russian radiometric observations of planets and spacecraft (VEX, MGS, Odyssey, MRO, Cassini, etc.) during 1961–2008, CCD astrometric observations of outer planets and their satellites, meridian transits and photographic observations of the XX century, as well as the VLBI spacecraft data. Data used for the production of ephemerides were taken from databases of the JPL website (*http://ssd.jpl.nasa.gov/iau-comm4/*) created by Standish, and continued by Folkner, and extended to include Russian radar observations of planets *(//www.ipa.nw.ru/ PAGE/DEPFUND/LEA/ENG/englea.htm*).

The significance of the high precision radiometric observations of planets beginning in 1961 (and afterwards also spacecraft) and continuing with the increasing accuracy is stressed. These observations have made it possible to determine and improve a broad set of astronomical constants. The detailed description of the EPM2008 ephemerides is given in the papers [2, 3].

Values of the adjusted parameters

More than 260 parameters have been determined while improving the planetary part of EPM2008. In addition to the orbital elements of all the planets and the main satellites of the outer planets, different physical constants have been estimated including masses of ten asteroids that perturb Mars most strongly, mean densities for three taxonomic classes of asteroids (C, S, M), the mass and the radius of the asteroid ring, and the mass of the TNO ring. In Tab. 3 the adjusted values of several of these parameters are presented. The parameters are shown with their real uncertainties estimated by comparing the values obtained in different test LS solutions, as well as by comparing parameter values produced by independent groups.

Table 3. Masses of Ceres, Pallas, Juno, Vesta, Iris, Bamberga in 10^{-10} M⊙

	Ceres	Pallas	Juno	Vesta	Iris	Bamberga
	4.71	1.06	0.129	1.32	0.040	0.046
σ_{formal}	±0.007	±0.003	±0.003	±0.001	±0.001	±0.001
σ_{real}	±0.03	±0.03	±0.008	±0.03	±0.008	±0.008

Two parameters that characterize the ring modeling the effect from small asteroids (its mass M_{ring} and radius R_{ring}) have been determined:

$$M_{ring} = (0.87 \pm 0.35) \cdot 10^{-10} M_\odot, \quad R_{ring} = (3.13 \pm 0.05) \text{ AU}.$$

Thus, the estimated total mass of the main belt asteroids represented by 301 asteroids and the asteroid ring is:

$$M_{belt} = (13 \pm 2) \cdot 10^{-10} M_\odot \text{ (about 3 Ceres mass)}.$$

The mass value of the ring of TNOs has been obtained:

$$M_{TNOring} = (498 \pm 14) \cdot 10^{-10} M_\odot, (5\sigma).$$

Thus, the total mass of all TNOs including Pluto, the 21 largest TNOs and the TNO ring of other TNO objects with 43 AU radius is

$$M_{TNO} = 775 \cdot 10^{-10} M_\odot, \text{ (about 164 } M_{Ceres} \text{ or } 2M_{Moon}).$$

References

1. *Krasinsky G. A., Pitjeva E. V., Vasilyev M. V., Yagudina E. I.* Hidden mass in the asteroid belt // Icarus. 2002. Vol. 158, N 1. P. 98–105.
2. *Pitjeva E. V.* Ephemerides EPM2008: the updated model, constants, data / Eds M. Soffel, N. Capitane // Proc. JOURNEES-2008, Astrometry, Geodynamics and Astronomical Reference Systems. Dresden, 2009. P. 157–160.
3. *Pitjeva E. V.* EPM ephemerides and relativity / Eds S. Klioner, P. K. Seidelmann, M. Soffel // Proc. IAU Symp. No. 261, Relativity in fundamental astronomy. Cambridge University Press, 2009. P. 170–178.

Part 6. Dynamics of NEOs. Collision Predictions

The Asteroid-Comet Hazard Conference Proceedings, 2009

NASA's Near-Earth Object Program Office

D. K. Yeomans, S. R. Chesley, P. W. Chodas

Jet Propulsion Laboratory of California Institute of Technology, USA

Abstract. This paper briefly presents the history, interactions and current activities of NASA's Near-Earth Object Program Office. The Program Office utilizes near-Earth object (NEO) astrometric data from the international community, received from the Minor Planet Center, to refine orbits and provide predictions for coming Earth close approaches. For those objects for which an Earth impact cannot be ruled out, an automatic Sentry system computes Earth impact probabilities. These predictions are often compared and verified with a similar process that is underway in Pisa Italy (NEODyS). The sophisticated techniques used within the Sentry system are described. Recent studies of some of the issues surrounding the deflection of an Earth threatening NEO are also described. In particular, the viability of the gravity tractor concept is discussed in connection with avoiding an asteroid's passage through a dynamical keyhole at the time of a close Earth approach — an event that ensures a subsequent Earth impact event at a later time.

History of NASA's near-Earth observations program

In 1998, the NASA Headquarters Science Director for Solar System Exploration announced the so-called Spaceguard goal to the U.S. House Subcommittee on Space & Aeronautics. This goal, which arose as a result of two previous NASA reports [1,2], was to find and track 90 % of NEOs whose diameters are greater than 1 km by the end of 2008. A subsequent NASA report in 2003, documented a cost benefit study and recommended that the search be extended to include potentially hazardous objects down to those larger than 140 meters [3]. This target size was selected because it represents the level of survey needed to reduce the hazard from sub-global catastrophes by a factor of ten. With the Spaceguard having already reduced the global hazard by more than a factor of ten, completion of the new survey would reduce the total risk from objects of all sizes to less than 1 %. Potentially Hazardous Objects (PHOs), a subclass of the NEO population, can ap-

proach the Earth's orbit to within 0.05 AU. NASA initiated a Near-Earth Object Observations program in 1998, the same year the Near-Earth Object Program Office began operations at JPL. At NASA Headquarters, Lindley Johnson is the Program Executive for the NEO Observations program and Don Yeomans manages the NEO Program Office at JPL.

At the request of the U.S. Congress, NASA completed, in 2006, an Analysis of Alternatives that could be employed to carry out a survey program to discover and track 90 % of the NEOs larger than 140 meters. Also requested was an analysis of possible alternatives that NASA could employ to divert an object on a likely collision course with Earth. This report recommended that NEO survey programs should consider potentially hazardous objects (PHOs) larger than 140 meters rather than all NEOs. The Agency could reach the stated goal by partnering with other agencies on potential future optical ground-based observatories and building a dedicated NEO survey asset. Space-based IR systems, combined with shared ground-based assets could reduce the overall time to reach the goal by at least three years. Radar could be used to rapidly refine tracking and determine object sizes for NEOs of high interest. Nuclear stand-off explosions were assessed to be 10–100 time more effective than non-nuclear alternatives. Kinetic energy impacts are the most mature technique and could be used effectively for single, small solid bodies[4].

As of mid-2009, the U.S. Congress and NASA are awaiting the results of a National Research Council study that is to provide advice on the most efficient techniques for reaching the goal of finding 90 % of the PHOs larger than 140 meters and the most effective techniques for dealing with PHOs that are found to be upon an Earth threatening trajectory. Until additional actions are taken, the NASA goal will remain to find and track 90 % of the NEOs larger than one kilometer.

The success of the current NASA goal of finding and tracking 90 % of all NEOs larger than one km is demonstrated in Fig. 1 where the cumulative number of discoveries of all NEAs (black) and NEAs larger than one km in diameter grey) are plotted by year (Fig. 1). By mid-2009, the number of discoveries of near-Earth objects larger than one km was 778 and the estimated total population of near-Earth asteroids larger than one kilometer is 940 ± 50 [5].

NASA-supported near-Earth object observational surveys and the Minor Planet Center

In addition to the Minor Planet Center, there are currently three NEO observational surveys being supported by NASA, the Catalina Sky Survey, LINEAR, and Spacewatch.

Catalina Sky Survey: The Catalina Sky Survey (CSS) is currently the most efficient NEO survey program for finding new near-Earth objects. CSS utilizes three refurbished telescopes all using identical thinned, multi-channel cryogenically cooled 4K × 4K CCD cameras: 1) the original Catalina Sky Survey (CSS, MPC Code 703) using a 0.7-meter f/1.8 Schmidt telescope with a 2.9 × 2.9 degree field at the Steward Observatory Catalina Station (2510 m elevation, 20 km northeast of Tucson, Arizona); 2) the Siding Spring Survey (SSS, MPC Code E12) using the Uppsala 0.5-m f/3.5 Schmidt telescope with a 2.0 × 2.0 degree field operated jointly with the Australian National University Research School for Astronomy and Astrophysics at Siding Spring Observatory, Australia (1150 m elevation); 3) The Mt. Lemmon Survey (MLS, MPC Code G96) using the 1.5-meter f/2.0 prime focus telescope with a 1.0 × 1.0 degree field at the Steward Observatory Mt. Lemmon station (2790-m elevation, 18 km north of Tucson). The 1.5-meter Mt. Lemmon and 1.0-meter Siding Spring telescopes are also used for astrometric follow-up and physical observations of interesting NEOs.

CSS personnel: Edward Beshore, Principal Investigator; Steve Larson, and Rob McNaught (SSS), Co-investigators; Andrea Boattini, Gordon Garradd, Alex Gibbs, Al Grauer, Rik Hill, and Richard Kowalski, Observers.

For additional information on CSS, see:
http://www.lpl.arizona.edu/css/ and http://msowww.anu.edu.au/~rmn/

Lincoln Near-Earth Asteroid Research (LINEAR): In cooperation with the Air Force, MIT's Lincoln Laboratory has been operating a near-Earth object discovery facility using one-meter aperture GEODSS telescopes. GEODSS stands for Ground-based Electro-Optical Deep Space Surveillance and these wide field Air Force telescopes were designed to optically observe Earth orbital spacecraft. The GEODSS instruments used by the LINEAR program are located at the Lincoln Laboratory's experimental test site in Socorro, New Mexico. Tests in early 1996 indicated that the search system, now known as LINEAR, had considerable promise. In the period between March and July 1997, a 1024 × 1024 CCD pixel detector was used in field tests and, while this CCD detector filled only about one fifth of the telescope's field of view, four NEOs were discovered. In October 1997, a large format CCD (1960 × 2560 pixels) that covered the telescope's 2 square degree field of view was employed successfully to discover a total of 9 new NEOs. Five more NEOs were added in the November 1997 through January 1998 interval when both the small and large format CCD detectors were employed. Beginning in October 1999, a second one-meter telescope was added to the search effort.

Currently, LINEAR telescopes observe each patch of sky 5 times in one evening with most of the efforts going into searching along the ecliptic plane where most NEOs would be expected. The sensitivity of their CCDs, and

particularly their relatively rapid read out rates, allows LINEAR to cover large areas of sky each night.

LINEAR personnel: Grant Stokes, Principal Investigator; Scott Stuart and Eric Pearce, Co-Investigators.

For additional informaiton on LINEAR, see:

http://www.ll.mit.edu/LINEAR/

Spacewatch: Beginning in 1984, the 0.9-meter, Newtonian f/5 Steward Observatory Spacewatch telescope began being used full time to survey for comets and asteroids under the leadership of Tom Gehrels. First installed on the University of Arizona campus in 1923, this telescope had been moved to Kitt Peak, Arizona in 1963. In 1982, this instrument was donated to the Spacewatch team and in 1984 it became the first telescope to detect and discover asteroids and comets with electronic detectors (CCDs, as opposed to photographic plates or film).

The initial 320 × 512 RCA CCD detector used from 1984 to 1988 was replaced with a large format 2048 × 2048 CCD detector used during the interval 1989–1992. This system had a field width of 38 arc minutes and limiting magnitude of 20.5. The sensitivity of the CCD (quantum efficiency) was doubled to 70 % in 1992 when a thinned 2048 × 2048 CCD was installed and extended the limiting magnitude down to 21.0. The 0.9-meter telescope is used about 23 nights per month to search for near-Earth objects. By locking the right ascension axis in place and allowing the star fields to drift through its field of view ("drift-scan") while the CCD detector was constantly read out, this telescope scanned at a rate that covered about 200 square degrees of sky each month down to magnitude 21. Each region of sky was scanned three times, about thirty minutes apart, to examine which objects moved relative to the background stars.

This system was the first to discover NEOs with CCDs, the first to discover a comet with a CCD, and the first to discover an NEO with automated image processing software. In 2000, large minor planet (20000) Varuna in the outer solar system was discovered with this system. Spacewatch has discovered many of the smaller near-Earth objects that pass close to the Earth, including a 10-meter sized asteroid (1994 XM1) that had a then record close Earth passage (105,000 km on 1994 Dec 9). Discoveries of Potentially Hazardous Asteroids (PHAs) with the 0.9-m drift scan system total 45, NEOs total 274, and follow-up observations of NEOs many thousands.

In 2001, the Spacewatch group began observing with a newly built 1.8-meter aperture telescope designed for follow-up of asteroids that get fainter after discovery. In late 2002, a large-mosaic CCD camera (four 4608 × 2048 CCDs) was added to the 0.9-meter, and the optical system was replaced to allow a wider field-of-view (2.9 square degrees). The 0.9-meter design now operates in the "stare" mode rather than in the previous "drift-

scan" mode, whereas the 1.8-meter telescope operates in the "drift-scan" mode.

From 2005 through 2008 the Spacewatch group gradually shifted their emphasis to follow-up observations that are critical for securing accurate orbits. In addition to these activities, the Spacewatch team has been involved with studies of the Centaur and Trans-Neptunian minor planet populations and the sizes of short period comet nuclei.

Spacewatch personnel: Robert S. McMillan, Principal Investigator; Robert Jedicke and Jeff Larsen, Collaborators; Joe Montani and Jim Scotti, Senior Research Specialists.

For additional information on Spacewatch, see:
http://pirlwww.lpl.arizona.edu/spacewatch/

The Minor Planet Center (MPC) acts as a central clearinghouse for astrometric and photometric data on comets, asteroids and other bodies of the Solar System. Together with the co-located Central Bureau of Astronomical Telegrams (CBAT), the MPC also provides orbital and ephemeris information for these bodies, assigns discovery credit as well as official designations and names. For near-Earth objects, the MPC collects, organizes and verifies data, provides preliminary orbits and ephemerides, posts a list of tentative NEO objects that need confirmation via additional observations and, if appropriate, provides Earth impact predictions.

The MPC operates at the Smithsonian Astrophysical Observatory in Cambridge Massachusetts under the auspices of Division III of the International Astronomical Union (IAU). Currently, the operations of the MPC are largely funded through the Near-Earth Object Observations program within NASA with additional funding coming from the IAU, individuals and foundations.

MPC personnel: Tim Spahr is the MPC Director; Brian Marsden, Director Emeritus; Gareth Williams, Associate Director and Sonia Keys, Software Specialist.

For additional MPC information, see:
http://www.cfa.harvard.edu/iau/mpc.html

The activities of the Near-Earth Object Program Office at JPL

The current activities of NASA's Near-Earth Object Program Office include the maintenance of up-to-date orbits, physical characteristics and close approach circumstances for all NEOs. This information is contained within a sophisticated relational database [6]. Investigations have also been carried out to investigate the often-neglected perturbations that can significantly affect the long-term motion of near-Earth objects including the thermal re-radiation accelerations (Yarkovsky effect) that depend upon the NEA's mass and surface characteristics [7]. Recent studies have also been carried out to

investigate the prevalence and nature of narrow dynamical "keyholes" in space that can occur during an Earth close approach. A NEO passage through a keyhole would ensure an Earth impact at a subsequent resonant return [8]. JPL's interactive Horizons system continues to provide ephemeris information for nearly 500,000 objects including the known planets, natural satellites, comets, asteroids and 59 spacecraft [9]. Horizons is currently providing an average of about 10,000 ephemeris products per day to the international scientific community.

The Sentry automatic orbit/close approach update process

Every day, observations and orbit solutions for Near-Earth Asteroids (NEAs) are received from the Minor Planet Center in Cambridge, Massachusetts. Once classified as an NEA, the asteroid is thereafter given automatic orbit updates within JPL's Sentry system. A new orbit solution for an NEA is automatically computed whenever new optical or radar observations for that object become available.

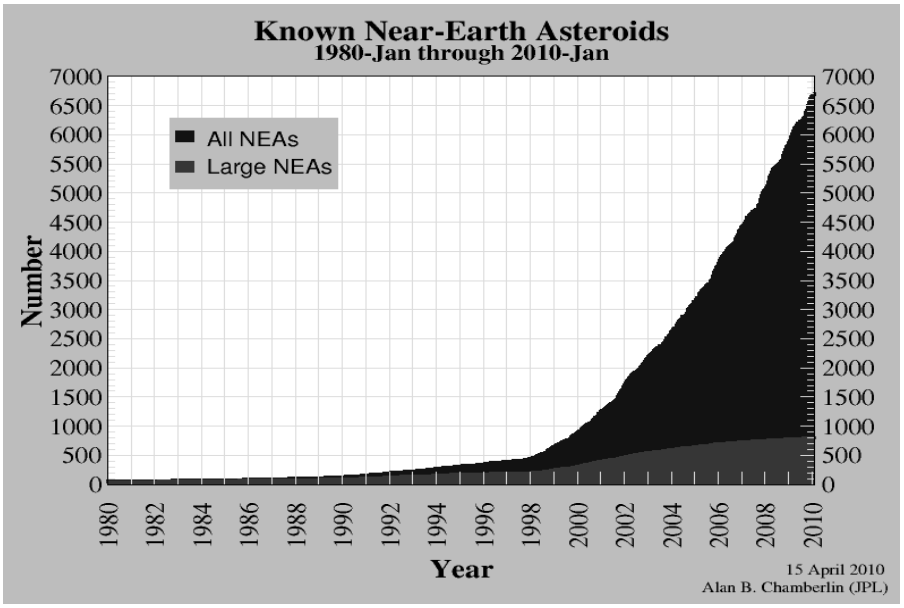

Fig. 1. The cumulative discoveries of all near-Earth asteroids (black curve) and the subset of these objects that are 1 km and larger (grey curve).

Once the nominal orbit and its associated uncertainty region have been determined, the object's motion is numerically propagated forward in time for up to 100 years in order to determine its close approaches to the Earth. These nominal orbit close approach predictions are tabulated in our Earth Close Approach Tables along with other uncertainty-related information

such as the minimum possible close approach distance, and the impact probability [10]. The uncertainty-related parameters are computed by projecting the uncertainty region from the epoch to the respective close approach times via so-called linearized techniques [11]. Since these techniques lose accuracy when the uncertainties become large, we include only reasonably certain predictions in our Close Approach Tables. As a result, close approaches may be tabulated decades into the future for objects with well-known orbits, but only a few months or years into the future for objects with poorly known orbits. On the other hand, Sentry assesses the long-term possibilities of an Earth impact for all objects whose orbits can bring them close to the Earth, even those with poorly known orbits. To perform this risk analysis it uses more sophisticated non-linear methods.

The Sentry impact risk analysis system

Non-linear analysis is required whenever the uncertainties in a close approach prediction are large. The position uncertainty of an asteroid is usually relatively small over the time span of the observations, but it usually grows, or stretches, as the object's position is predicted farther and farther into the future. This uncertainty growth is especially fast along the track of the orbit. The evolution of uncertainties can be understood using the notion of so-called virtual asteroids (VAs). Suppose the uncertainty region around the nominal orbital solution is filled with a swarm of thousands or tens of thousands of virtual asteroids, each having slightly different orbital elements, but all fitting the observations acceptably well. Only one of these virtual asteroids is real, but we don't know which one, although the central, nominal orbit is most likely to be the real one. The further a VA is from the nominal position within the swarm, the less likely it is to represent the real asteroid. If the three-dimensional positions of the VAs are plotted around the time of the observations, the swarm will take the shape of an elongated ellipsoid.

When the VAs are all numerically integrated forward in time, their slightly different positions in space allow each to undergo slightly different gravitational nudges (perturbations) from the planets and other perturbers. Over time, this swarm of virtual asteroids will spread out along the path of the nominal orbit, demonstrating how the uncertainty ellipsoid surrounding the asteroid's nominal position evolves into a very elongated tube centered on the asteroid's nominal orbit. Long-term orbital extrapolations can cause the asteroid's position uncertainty tube to grow to great lengths, even extending one or more times around the asteroid's entire orbit, and close planetary encounters can cause the uncertainty region to even double back on itself by folding. This type of numerical analysis, whereby many orbits are propagated forward in time to represent a single asteroid's position uncertainty region, is the basis of the non-linear techniques used by Sentry [12, 13].

In practice, the non-linear analysis is made computationally more efficient if only virtual asteroids along the central axis of the asteroid's elongated uncertainty region are integrated forward in time. The assumption is then made that virtual asteroids along this "Line of Variations" (LOV) are representative of the nearby off-axis portions of the uncertainty region (Fig. 2). The first step in the risk analysis is to numerically integrate the VAs on the LOV forward in time, and detect close approaches to the Earth. When a stream of consecutive VAs experience essentially the same close encounter, an automatic search is conducted to find the virtual asteroid that passes closest to the Earth. The motion of this particular virtual asteroid and its own local uncertainty region is then analyzed using linear techniques to determine if an impact is possible and, if so, to estimate the probability of impact. For pathological cases where an asteroid's uncertainty region folds back on itself (due to a previous close planetary encounter) or where several complex streams of virtual asteroids are evident, a second form of non-linear analysis may be undertaken.

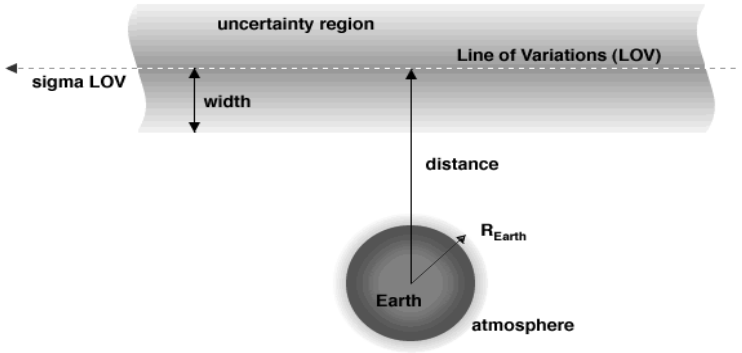

Fig. 2. An illustration of some of the concepts used in the Sentry system.

This technique, called Monte Carlo, samples the complete uncertainty region at epoch, not just the central axis, and uses a great many more virtual asteroids. Once again, all the VAs are integrated forward to the time of a close Earth approach, and monitored for possible impact. If, for example, a total of 100,000 virtual asteroids were integrated forward and two of these VAs manage to collide with the Earth in the year 2040 then the impact probability for the real asteroid in 2040 would be approximately 2/100,000, or 1/50,000.

If we assume a particular asteroid's position uncertainty region is a long three-dimensional tube stretched along its orbit, then a projection onto the target plane will reduce the uncertainty region to a two-dimensional strip

centered on the Line of Variations and passing a certain Distance from the Earth's center. If this Distance is less than 1 Earth radius then one of the virtual asteroids is known as a virtual impactor since it can strike the Earth. Sigma LOV is a measure of the deviation of the virtual impactor from the position of the central, or nominal, virtual asteroid. Sigma LOV is a measure of how well the impacting orbit fits the available observations. It is equal to zero for the best-fitting (nominal) orbit while orbits with values between –3 and +3 ("3-sigma") comprise about 99 % of the virtual asteroid swarm. The farther Sigma LOV is from zero, the less likely the collision with Earth. Since the intersection of the uncertainty region with the impact plane will form a narrow strip on the impact plane, three times the Width of this region in Earth radii will include more than 99 % of the entire localized uncertainty region.

The mitigation of a threatening near-Earth asteroid

Although Hollywood has created some colorful methods for stopping an object that is on a collision path with Earth, no government agency, national or international, has been tasked or accepted the responsibility to stop such an asteroid, should one be discovered. But there have been a number of academic and some technical studies, not to mention numerous movies, on how a devastating asteroid impact might be avoided. Since asteroids outnumber comets 100 to 1 in the inner solar system, the asteroids, rather than comets, represent the majority of the nearer-term threat to our planet.

Because of the wide range of possible sizes, trajectories and warning times for Earth-threatening asteroids, there will be a corresponding wide range in the levels of challenge in providing an appropriate response. Unless there are a few decades of warning time, hazardous asteroids larger than a few hundred meters in diameter will require enormous energies to deflect or fragment. In the rare case of a large threatening asteroid, nuclear explosions that could push or fragment the object might provide a sufficient response.

For the far more numerous asteroids that are smaller than a few hundred meters in diameter, if we have adequate early warning of several years to a decade, a weighted robotic spacecraft could be targeted to collide with the object, thereby modifying its velocity to nudge the trajectory just enough that the Earth impact would be avoided. The spacecraft navigation technology for impacting a small body was successfully demonstrated when the Deep Impact spacecraft purposely rammed comet Tempel 1 on July 4, 2005, to scientifically examine its composition.

Nuclear explosions and spacecraft impacts are two of the more relatively mature options for deflecting Earth-threatening objects and they have been studied in some detail [4]. Another option has been suggested for the

small subset of asteroids that might also pass close to the Earth a few years prior to the predicted Earth impact. For these unique cases, the pre-impact close encounter affects the asteroid's motion so strongly that a relatively tiny change in its velocity prior to the close approach will be multiplied several fold during the flyby, thus allowing the asteroid to miss the Earth on the next pass. In these relatively infrequent cases, even the very modest gravitational attraction between the asteroid and a nearby "micro-thrusting" spacecraft (nicknamed a "gravity tractor") could provide enough of a change in the asteroid's velocity that an Earth collision could be avoided [8].

Successful mitigation requires that a threatening asteroid must be discovered and physically characterized soon enough to allow the appropriate response; the current NASA Near-Earth Object Observations program is operated with this in mind. But, since the number of near-Earth asteroids increases as their sizes decrease, we are most likely to be hit by the relatively small objects that are most difficult to find ahead of time. As a result, consideration must also be given to the notification and evacuation of those regions on Earth that would be affected by the imminent collision of a small, recently-discovered impactor. However, if the object could be found far enough ahead of time and our space technology used to deflect it from the Earth threatening trajectory, it would be a tremendous demonstration of our space-faring capabilities!

References

1. The Spaceguard Survey Report of the NASA International Near-Earth-Object Detection Workshop / Ed. D. Morrison. Pasadena, Jet Propulsion Laboratory, January 25, 1992. *http://impact.arc.nasa.gov/downloads/spacesurvey.pdf*
2. Report of the Near-Earth Objects Survey Working Group, June 1995 (Gene Shoemaker, Chair). *http://impact.arc.nasa.gov/downloads/neosurvey.pdf*
3. Study to Determine the Feasibility of Extending the Search for Near-Earth Objects to Smaller Limiting Diameters: Report of the Near-Earth Object Science Definition Team, Aug. 22, 2003 (Grant Stokes, Chair). *http://neo.jpl.nasa.gov/neo/report.html*
4. Near-Earth Object Survey and Deflection Study Final Report, Dec. 28, 2006. *http://neo.jpl.nasa.gov/neo/report2007.html*
5. *Harris A. W.* The population of NEAs and PHAs and the current status of surveys, 33 pp, private communication, 2007.
6. Link to SSD database: http://ssd.jpl.nasa.gov/sbdb_query.cgi
7. *Giorgini J. D, Benner L. A. M., Ostro S. J., Nolan M. C., Busch M. W.* Predicting the Earth encounters of (99942) Apophis // Icarus. 2008. Vol. 193. P. 1–19. *http://neo.jpl.nasa.gov/apophis/*

8. *Yeomans D. K., Bhaskaran S., Broschart S., Chesley S. R. et al.* Deflecting a Near-Earth Object. 2009 // 1st IAA Planetary Defense Conference: Protecting Earth from Asteroids.
http://neo.jpl.nasa.gov/neo/pdc_paper.html
9. Link to Horizons web site: *http://ssd.jpl.nasa.gov/?horizons*
10. Link to Close Approach Tables: *http://neo.jpl.nasa.gov/ca/*
11. *Chodas P. W., Yeomans D. K.* Predicting Close Approaches and Estimating Impact Probabilities for Near-Earth Objects // Paper AAS. AAS/AIAA Astrodynamics Specialists Conference, Girdwood, Alaska, 1999. P. 99–462.
12. *Milani A., Chesley S. R., Chodas P. W., Valsecchi G. B.* Asteroid Close Approaches: Analysis and Potential Impact Detection // Chapter in Asteroids III / Eds W. Bottke, A. Cellino, P. Paolicchi, and R. P. Binzel. 2002.
13. The Sentry web site: *http://neo.jpl.nasa.gov/risk/*

The Asteroid-Comet Hazard Conference Proceedings, 2009

Demands on Observation Campaigns for Accurate Predictions

L. K. Kristensen

Institute of Physic and Astronomy, Aarhus University, Denmark

Abstract. Accurate predictions of close encounters require optimum times of observations, positions with dependences, and rigorous least squares adjustment accounting for correlations.

Introduction

The day will come when special observation campaigns are needed to monitor the "potentially hazardous objects" (PHO) which may hit the Earth. The main goal of such campaigns is to predict, as accurate as possible, the error ellipse on the impact plane. This requires: 1) a selection of observatories with good astrometry and small systematic errors, 2) optimize the times for observations, 3) observations are published with dependences, and 4) the least squares adjustment should account rigorously for correlations between observations.

Analysis of observations and selection of observatories

The purpose of a critical analysis of observations is to estimate observational mean errors and check for systematic errors. Mean errors and averages of the *O–C* residuals for all observatories are published by the Minor Planet Center [7]. Similar lists are given by Bykov et al [2]. As a specific example: In the period 1999–2008 LINEAR (observatory code 704) had a remarkably constant mean error $\sigma = \pm 0.65''$ in both α and δ. However, δ contained systematic errors between $+0.3''$ and $+0.4''$. The mean of $\cos\delta \cdot \Delta\alpha$ showed a yearly variation from $-0.05''$ in August–September to between $+0.30''$ and $+0.40''$ in March–April, probably due to a temperature dependent instrumental error. For discoveries and surveys such observations are very valuable but the systematic errors are too large for accurate predictions. Accurate astrometry can, for instance, be provided by Bordeaux–Floirac (code 999) with $\sigma = \pm 0.15''$ and bias $<0.05''$.

Optimal distribution of the observations

How the distribution of the observations can be optimized will be shown by a simple example.

Suppose we have a ruler with three division marks for an unknown unit x. Measuring the distances with equal weights gives the observational equations:

$$1x = o_1,\ 2x = o_2 \text{ and } 3x = o_3. \tag{1}$$

Adjustment by least squares gives normal equations, the solution of which is

$$x = (o_1 + 2o_2 + 3o_3)/14. \tag{2}$$

If the observational mean error of unit of weight is σ_0 then the mean error of x is

$$\sigma_x = \sigma_0/\sqrt{14} = \pm 0.267\sigma_0. \tag{3}$$

As shown by (2), o_3 seems to be more important than the others so we will try to observe with different observational errors σ_i or weights $p_i = (\sigma_0/\sigma_i)^2$ (i = 1, 2, 3) while retaining the sum:

$$p_1 + p_2 + p_3 = 3. \tag{4}$$

This condition is added with a Lagrange multiplier λ to the variance of (2)

$$\sigma_0^2(1/p_1 + 4/p_2 + 9/p_3)/14^2 + \lambda p_1 + \lambda p_2 + \lambda p_3. \tag{5}$$

Differentiation by p_i determines the minimum

$$\frac{\sigma_0^2}{p_1^2}\cdot\frac{1}{14^2} = \frac{\sigma_0^2}{p_2^2}\cdot\frac{4}{14^2} = \frac{\sigma_0^2}{p_3^2}\cdot\frac{9}{14^2} = \lambda\,. \tag{6}$$

The Lagrange multiplier is determined by the condition (4) and we obtain the better weights

$$p_1 = ½,\ p_2 = 2/2 \text{ and } p_3 = 3/2. \tag{7}$$

The mean error of x, as determined by (2), is now reduced to $\pm 0.247\sigma_0$. Least squares with the new weights, gives normal equations with the solution

$$x = (o_1 + 4o_2 + 9o_3)/36 \tag{8}$$

and mean error

$$\sigma_x = \sigma_0/\sqrt{18} = \pm 0.236\sigma_0\,. \tag{9}$$

Again we improve x, this time given by (8), by minimizing the expression similar to (5) and obtain

$$\frac{\sigma_0^2}{p_1^2}\cdot\frac{1}{36^2}=\frac{\sigma_0^2}{p_2^2}\cdot\frac{4^2}{36^2}=\frac{\sigma_0^2}{p_3^2}\cdot\frac{9^2}{36^2}=\lambda \tag{10}$$

or

$$p_1 = 3/14,\ p_2 = 12/14,\ p_3 = 27/14. \tag{11}$$

With these weights the least squares adjustment gives

$$\sigma_x = \sigma_0 / \sqrt{21} = \pm 0.218\sigma_0 \tag{12}$$

Table gives the different weights and illustrates how the accuracy improves after a few iterations, evidently because p_3 increases at the expense of p_1 and p_2. After iteration n the relative weights become $1{:}2^n{:}3^n$ so in the limit the optimum is $p_3 = 3$ and $p_1 = p_2 = 0$. This gives

$$\sigma_x = \sigma_0 / \sqrt{27} = \pm 0.192\sigma_0 \tag{13}$$

To achieve this accuracy with the equal distribution of weights, requires about twice (≈27/14) the former number of observations. Planning of observations for a specific purpose may thus be very efficient. The main problem is to avoid observations — here especially of o_1 — which contributes little to the determination of the wanted quantity.

Dependence of the accuracy on the weights and iterations

o_1	1	1/2	3/14	0	3
o_2	1	2/2	12/14	0	0
o_3	1	3/2	27/14	3	0
σ_x/σ_0	0.267	0.236	0.218	0.192	0.577

The above example is trivial, but to determine the nights which are not useful for the determination of a collision is not! However, the method to optimize observations is the same. In the example above we can easily see that the choice $p_1 = 3$ with $p_2 = p_3 = 0$ is unfavourable but the complex case of asteroid observations requires some computations.

Near the epoch of a close encounter we define coordinates (ξ, η, ζ) of the asteroid relative to the centre of the Earth and with the ζ-axis parallel to the relative velocity ($d\xi/dt = d\eta/dt = 0$). The (ξ, η)-plane is the so called "impact plane" and the main purpose of an observation campaign is to obtain ξ and η as accurately as possible. That is, to make the predicted mean errors σ a minimum:

$$\sigma_\xi^2 + \sigma_\eta^2 = \text{Minimum.} \qquad (14)$$

Given the distribution of observations and their adopted weights in a least squares adjustment we can compute the effect of an infinitesimal change of each observation in (α,δ) on the predicted position by the linear expression:

$$d\xi = A \cos\delta \, d\alpha + B \, d\delta \quad \text{and} \quad d\eta = C \cos\delta \, d\alpha + D \, d\delta. \qquad (15)$$

These expressions are differential forms similar to (2) and (8) and can be obtained from the observational equations and solution of the least square adjustment programmes. A part of $\cos\delta \, d\alpha$ and $d\delta$ is random observational errors with variance σ_0^2/p and the sum over all observations contributes to the variance (14) with:

$$\sigma_0^2 \sum (A^2 + B^2 + C^2 + D^2)/p = \sigma_\xi^2 + \sigma_\eta^2. \qquad (16)$$

We assume that the cost of a single observation is c_p and that the total cost is

$$\sum c_p = C. \qquad (17)$$

It is realistic to assume different costs for individual observations because more observations are needed at low altitudes to obtain the same accuracy. We now minimize (16) under the condition (17) having the Lagrange multiplier λ. This is similar to (6) and (10). Differentiation gives:

$$-\sigma_0^2 \, (A^2 + B^2 + C^2 + D^2)/p^2 + \lambda c = 0 \qquad (18)$$

or

$$p = \sigma_0 \sqrt{(A^2 + B^2 + C^2 + D^2)/\lambda c} \qquad (19)$$

If we had used the relative coordinates (ξ, η, ζ) and their time-derivatives at the epoch of closest approach as elements, then the coefficients *A*, *B*, *C* and *D* in (15) indicate how sensitive the observations (α, δ) are to a small variation in ξ and η. Clearly, observation should be avoided when these coefficients are small.

As in the example above the iterations start with the assumption of an equal distribution of weights $p = 1$. After a few iterations the useless nights can be spotted and these observations saved. Numerical examples are given in [5], [6] and [9].

Dependences

When the achievement of the highest systematic accuracy, without regard to efforts, is the goal it is necessary to state the observations with their dependence on the reference stars. Let the tangential or plate-coordinates of

the object and the N reference stars be respectively (x, y) and (x_i, y_i). The dependences d_i are defined by:

$$x = \sum d_i x_i,\ y = \sum d_i y_i \text{ and } 1 = \sum d_i, \text{ and if } N>3 \ \sum d_i^2 = \text{Minimum.} \quad (20)$$

The former good habit to state accurate observations with dependencies is unfortunately now abandoned. Due to the much larger number of stars in the modern catalogues the distances to the reference stars will now be much smaller. This facilitates the conversion of tangential coordinates to the spherical coordinates (α, δ). Use of nearby reference stars diminishes the effects of differential refraction, the position of the tangential point, radial and other distortions, and coma. Dependences have many advantages:

1. The positions can always be re-reduced with improved star positions in a well defined system.
2. Corrections can be computed for systematic effects due to color and magnitude. The color index and magnitude of the object will in general differ from the average of the stars. Examples of systematic errors are given in [1] and [4]. Their influence can be estimated from the A, B, C and D coefficients in (15). It is especially dangerous if these coefficients contain a constant part that is summed up when multiplied by the systematic errors. The characteristic time of their variation is the synodic period so they vary little within a couple of weeks.
3. With a linear ephemeris correction the mean error of measuring σ can be separated from the catalogue star error ε by:

$$\langle (O-C)^2 \rangle = \sigma^2 + (\sigma^2 + \varepsilon^2) \langle d_i^2 \rangle, \quad (21)$$

where $\langle\ \rangle$ denotes statistical averages. A correct analysis of errors is essential for the computation of probabilities.

4. The correlation between the observations using the same reference stars can rigorously be accounted for in the least squares adjustment.

Least squares adjustment with correlations

The general problem of least squares adjustment with correlated observations is treated in [6]. The main effect of the correlations is a reduction of the effective number of observations, which again increases error estimates.

The correct treatment of the error estimates is of great importance for the correct computation of probabilities. Orbits determined from essentially the same observations may give nearly the same elements while the error estimates still differ by a factor two, as illustrated by Shor et al [8]. Suppose we have the same observations O which are adjusted with two different sets of weights p and p'. The solutions are respectively x and x' and the computed observations C and C'. It can be shown that the difference $x'–x$ is obtained by substituting for O in the normal equations a fictitious observation

$$(p'/p - 1)(O–C'). \tag{22}$$

If p' and p are proportional or $O–C' \approx 0$, then the two sets of elements are nearly equal. Classically the error estimates are based on subjective evaluation of the relative weights followed by a determination of the unit of weight by the square sum $\sum(O–C)^2$ of the residuals.

A practical method to handle the problem of correlated observations is to include the star positions as unknown elements. Each observation then gives an equation of condition between the corrections to the six elliptical elements (a, e, …) and the positions of the reference stars. In declination the observational equation is:

$$\delta_{\text{obs}} - \delta_{\text{comp}} = \frac{\partial\delta}{\partial a}\Delta a + \frac{\partial\delta}{\partial e}\Delta e + \cdots + \sum_i d_i \cdot \Delta\delta_i \,. \tag{23}$$

Here δ_{obs} is the observation and δ_{comp} is the computed by the adopted set of six elements and the catalogue positions of reference stars. Similar observational equations come from right ascension. The observational mean error of (23) is $\pm\sigma\sqrt{(1 + < d_i^2 >)}$, with σ the measuring error from (20). In addition we have the "observations" in the catalogue

$$\Delta\delta_i = 0 \pm \varepsilon_i \tag{24}$$

where ε_i is the mean error of the individual stars. The matrix of the normal equations is thus very great, but is of the "banded-bordered" type, which, with partial eliminations of stars no longer used, is easy to handle.

Acknowledment. The author is greatly indebted to Anette Skovgaard and Grete Flarup for preparing the electronic manuscript.

References

1. *Berezhnoy A. A.* Analysis and taking into account the systematic errors of CCD observations performed in 2006–2008 // Book of Abstracts. Intern. conf. "Asteroid-Comet Hazard-2009". St. Petersburg, 2009. P. 196–197.
2. *Bykov O. P., L'vov V. N., Izmailov I. S., Kastel G. R.* Accuracy of the near-Earth asteroid observations // Book of Abstracts. Intern. conf. "Asteroid-Comet Hazard-2009". St. Petersburg, 2009. P. 200.
3. *Kristensen L. K.* Demands on observation campaigns for accurate predictions // Book of Abstracts. Intern. conf. "Asteroid-Comet Hazard-2009". St. Petersburg, 2009. P. 149–153.
4. *Kristensen L. K.* Equator and Equinox of FK4 by 2240 observations of (51) Nemausa // Mitt. d. Astron. Ges. N 48, 1980. P. 50–55.

5. *Kristensen L. K.* Optimum observing strategies // Astron. Nachr. 322. 2001. P. 47–56.
6. *Kristensen L. K.* Optimizing collision predictions and information to the public // Book of Abstracts. All-Russian conf. "Asteroid-Comet Hazard-2005". St. Petersburg, 2005. P. 194–199.
7. Minor Planet Center 2009 // *www.cfa.harvard.edu/iau/special/residuals2.txt.*
8. *Shor V. A., Chernetenko Yu. A., Kochetova O. M.* How precise is the orbit of (99942) Apophis // Book of Abstracts. Intern. conf. "Asteroid-Comet Hazard-2009". St. Petersburg, 2009. P. 154–159.
9. *Kristensen L. K.* Initial orbit determination for distant objects // Astron. J. 2004. 127. P. 24–35.

The Asteroid-Comet Hazard Conference Proceedings, 2009

Determination of Orbits and Dispersion Ellipsoids of Asteroids Potentially Hazardous for the Earth

Yu. D. Medvedev, A. S. Zabotin

Institute of Applied Astronomy of RAS, St. Petersburg, Russia

Abstract. The influence of the observation error distribution on the orbits of 22 asteroids potentially hazardous for the Earth has been studied. First, we computed the mean errors of orbit parameters on the assumption of the linear connection of them with observation errors and then we compared obtained estimates with those resulting from the assumption of the nonlinearity of this connection. Secondly, we correlate orbital parameters and their errors obtained by the method of the least modulus with those obtained by the least-squares method. The general conclusion is that the dispersion ellipsoids calculated on the assumption of nonlinearity are more plausible, and the orbits and estimates of their errors calculated by the least modulus method are more robust compared to those obtained by the least-squares method.

Introduction

To estimate the hazard for the Earth posed by a newly discovered asteroid one must solve two problems: 1) to determine the most accurate orbit (nominal orbit) and 2) to obtain reliable estimates of the size of the dispersion ellipsoid for initial values of orbital parameters. During the first approach (opposition) the number of observations and the observed arc are generally not large enough for these asteroids. Therefore, in some cases the use of the conventional method of least squares does not yield a very accurate nominal orbit and because a linear approximation was used, the size of the dispersion ellipsoid is not very accurate. In the present article we try to apply procedures that allow one to solve these problems more precisely.

Comparison of dispersion ellipsoids computed by two different methods

In the first part of this work the dispersion of orbital parameters considered as accidental functions of accidental observational errors are determined by the Monte Carlo method that takes into account the nonlinear de-

pendence of orbital parameters on observations. The following procedure has been used for each asteroid. Using observations in the first opposition the nominal orbit (the components of position and velocity vectors at initial moment) has been calculated by the least-squares method. With the obtained nominal orbit the rms value σ_0 (mean residuals of observations) has been calculated. Then 10,000 variants of the normal distributed errors of each observation have been computed using the Intel Math Kernel Library. In so doing the mean value equal to zero and the dispersion equal to $\sigma_0{}^2$ were assumed in these calculations. The model errors have been added to the calculated positions at the moments of real observations in the first opposition. In such a way 10,000 sets of artificial asteroid observations in this opposition have been obtained. Using these observations 10,000 variants of orbits have been calculated for each asteroid. The parameters of these 10,000 orbits form a field. We interpret it as a field of concentration derived by taking into account the nonlinear propagation of parameter errors. The statistical estimates of components of the covariance matrix *K* for orbital parameters of each asteroid have been computed on the basis of these variants of orbit by the following formula

$$k_{i,j} = \frac{1}{N-1}\sum_{m=1}^{N}(y_{i,m} - y_i)(y_{j,m} - y_j),\ \ i,j = \overline{1,6}\,, \tag{1}$$

where y_i is *i*-th component of the state vector of the nominal orbit, $y_{i,m}$ is *i*-th component of the state vector for the *m*-th variant of 10,000 varied orbits, and *N* being the number of variants (10,000).

The covariance matrix *K* was also calculated, as accepted in the least-square method, by the following formula

$$K = \sigma_0^2\left(A^T A\right)^{-1}, \tag{2}$$

where A is the matrix of conditional equations formed on the basis of real observations in the first opposition.

Then the dispersion ellipsoids were calculated by the formula

$$(Y - Y_0)^T \cdot K^{-1} \cdot (Y - Y_0) = k^2\sigma^2, \tag{3}$$

where *Y* is the state vector, Y_0 is the state vector of the nominal orbit, *K* is the correlation matrix [calculated by (1) or by (2)], *k* is a factor that determines the probability of initial values being contained in the dispersion ellipsoid. Usually we accept $k = 3$.

Next we consider the question whether the initial values of parameters of the nominal orbit calculated on the basis of observations at all available

oppositions are situated inside or outside the dispersion ellipsoids. Those ellipsoids that contain values of the nominal orbit for the majority of asteroids under study should be considered as more reliable. With this question in view, we consider results of corresponding calculations fulfilled for 22 potentially hazardous asteroids (Tab. 1). The table contains: asteroid numbers; the ratios of the mean positional errors calculated by our (nonlinear) method to those calculated by the least squares method (linear one) A_x, A_y, A_z in corresponding coordinates *x, y, z;* and the ratios of the velocity components A'_x, A'_y, A'_z. The table contains also the indices N_{lin} and N_{nonlin} that indicate whether the initial values of the nominal orbit parameters (determined on the base of all available oppositions) are located inside the corresponding ellipsoid. The index N_{lin} is for the linear case and the index N_{nonlin} is for the nonlinear case. A three-point system is adopted: 0 means that the initial values of parameters of the nominal orbit lie outside the ellipsoid, 1 means that they belong to the boundary, and 2 means that they lie inside the ellipsoid.

Table 1. Ratios between the mean positional errors in coordinates *x, y, z* for nonlinear and linear cases and that of for velocity

Number	A_x	A_y	A_z	A'_x	A'_y	A'_z	N_{lin}	N_{nonlin}
8566	0.85	0.82	0.96	0.87	0.79	0.89	2	2
23187	1.16	1.16	1.17	1.13	1.22	1.17	1	2
31669	1.68	1.68	1.65	1.65	1.60	1.69	2	2
35107	1.28	1.24	1.36	1.37	1.25	1.31	0	0
35396	1.15	1.16	1.19	1.12	1.28	1.29	0	0
37655	1.23	1.23	1.23	1.23	1.23	1.23	1	2
53319	1.26	1.26	1.26	1.26	1.26	1.27	2	2
66391	0.83	0.83	0.84	0.82	0.85	0.82	2	2
85713	1.17	1.17	1.17	1.17	1.16	1.16	1	2
85989	0.94	1.09	1.11	1.26	1.26	1.19	0	0
86039	1.40	1.40	1.41	1.41	1.44	1.44	0	2
86819	1.20	1.21	1.28	1.21	1.21	1.22	0	0
89958	1.43	1.44	1.43	1.46	1.42	1.46	0	2
103067	1.28	1.28	1.26	1.28	1.28	1.28	1	2
111253	1.54	1.48	1.52	1.51	1.19	1.29	1	2
136618	1.40	1.40	1.39	1.40	1.52	1.49	2	2
137126	1.26	1.26	1.26	1.26	1.26	1.26	2	2
137427	1.05	0.83	1.13	1.09	1.04	1.10	2	2
138524	1.13	1.15	1.16	1.14	1.15	1.21	0	1
139359	1.62	1.61	1.61	1.62	1.61	1.61	2	2
141851	1.08	1.08	1.08	1.09	1.08	1.08	0	2
154276	1.46	1.46	1.46	1.46	1.46	1.46	1	2

As can be seen from the table the dispersion ellipsoids calculated by the nonlinear method are more plausible and more reliable since values of N_{nonlin} are equal to or exceed N_{lin}.

Comparison of the least modules method and the least-squares method

In the second part of this work we compare asteroid orbits calculated by two methods: by the least modules (LM) method [1] and by the least-squares (LS) method [2–4]. The orbits have been computed using the observations in the first opposition. They are compared with the orbit calculated by the least-square methods on the basis of all available observations. The data of comparison are presented in Tab. 2. The first column contains the asteroid number, the second column the distance between the initial positions obtained by LS using observations in the first opposition and the initial position obtained by LS using all observations, R_{LS}, the third column contains the distance between the initial position obtained by LM using observations in the first opposition and the initial position obtained by LS using all observations, R_{LM}. The fourth and fifth columns contain corresponding values for phase space of velocities, V_{LS}, V_{LM}. The sixth and seventh columns contain the sign of the differences between R_{LS}, R_{LM} and V_{LS}, V_{LM}. The dispersions for orbits obtained by LM are determined by the Monte Carlo method.

Table 2. Difference between positions and velocities obtained by LS and LM methods. Distances are expressed in km, velocities in cm/s

Number	R_{LS}	R_{LM}	V_{LS}	V_{LM}	$R_{\text{LS}}-R_{\text{LM}}$	$V_{\text{LS}}-V_{\text{LM}}$
8566	160.8	59.7	3.4	0.8	+	+
23187	1105.4	2068.2	16	30.8	–	–
31669	5479.3	332.4	63.9	24.9	+	+
35107	951.3	683.8	16.1	11.8	+	+
35396	4273	4016.8	97.1	87.4	+	+
37655	51981.5	3776.1	3575.7	258.4	+	+
53319	328.9	776.6	5.5	12.5	–	–
66391	2496.7	1445	120.9	71.1	+	+
85713	4183.4	5876.3	115.2	162.6	–	–
85989	910.2	711.4	11	9.5	+	+
86039	113518.5	149146.2	1298.6	1633	–	–
86819	1636	1735.7	31.4	33.5	–	–
89958	10718.1	5815.9	293.4	156.9	+	+
103067	2957.6	5371.5	75	137.1	–	–
111253	4106.5	4014.8	32.5	31.8	+	+
136618	2121.8	154.1	4.3	15.3	+	–
137126	3550.2	1384	74.9	29.1	+	+
137427	660.2	742.4	5.5	6.2	–	–
138524	1367.9	1149.1	15.9	13.6	+	+
139359	2312.7	15131.1	80.7	526.6	–	–
141851	5734.4	7730.2	941.9	1281.8	–	–
154276	524.9	231.4	10.2	4.6	+	+

Comparison of dispersion ellipsoids obtained by the least modules method and by the least squares method

To compare dispersion ellipsoids obtained from the above two methods we have used the same procedure that was applied for comparison of linear and nonlinear methods of the covariance matrix computation.

Using observations in the first opposition the components of position and velocity vectors at the initial moment (the nominal orbit) have been calculated by LM method. In the present case the nominal orbits provide the minimum of the sum of modulus of residuals. Using the nominal orbit the rms value σ_0 has been calculated. Then 10,000 variants of Laplace distributed errors of observations have been obtained using the Intel Math Kernel Library. The dispersion equal to $\sigma_0{}^2$ is assumed in these variants. The model errors were added to the calculated observations and the 10,000 sets of asteroid observations in the first opposition were obtained. Then, with these

Table 3. Ratios between diagonal elements of covariance matrices obtained by the LM and LS methods and three-point indices of relative position of dispersion ellipsoid for the nominal orbit with respect to the dispersion ellipsoids computed by the LM and LS methods

Number	B_x	B_y	B_z	B'_x	B'_y	B'_z	LS	LM
8566	3.11	2.15	4.31	4.05	3.82	6.88	2	2
23187	3.33	3.64	3.51	3.04	3.59	3.58	1	2
31669	3.13	3.16	2.77	3.05	2.91	3.15	2	2
35107	3.67	3.72	4.37	4.88	3.81	4.65	0	1
35396	3.03	2.87	3.37	3.48	3.22	2.99	0	0
37655	5.79	5.79	5.99	5.79	5.8	5.74	1	2
53319	3.22	3.26	3.85	3.25	3.24	4	2	2
66391	2.44	2.45	3.28	2.4	2.5	2.28	2	2
85713	3.08	3.07	3.03	3.09	3.06	2.98	1	2
85989	4.9	4.55	4.34	3.94	4.76	5.59	0	2
86039	2.42	2.38	2.43	2.37	2.05	2.34	0	2
86819	4.52	4.61	7.65	4.56	4.59	4.85	0	2
89958	5.98	6.08	6.16	6.3	6.04	6.17	0	2
103067	6.49	6.67	6.47	6.53	6.75	6.37	1	2
111253	2.12	2.06	2.13	2.07	1.8	1.93	1	2
136618	3.18	2.34	3.65	2.57	1.74	1.85	2	2
137126	4.28	4.29	4.26	4.29	4.3	4.2	2	2
137427	3.48	4.47	3.95	3.69	3.99	3.73	2	2
138524	5.66	5.7	6.52	5.6	5.64	5.82	0	2
139359	5.68	5.66	5.68	5.67	5.66	5.68	2	2
141851	3.72	3.72	3.68	3.81	3.76	3.71	0	2
154276	3.28	3.26	3.29	3.28	3.26	3.26	1	2

observations 10,000 variants of orbits for each asteroid have been calculated. The parameters of these orbits form a field of concentration. With these parameters the statistical estimates of the covariance matrix for parameters of each asteroid orbit have been calculated by formula (1). The data to judge the size of the field of concentration are given in Tab. 3. It contains: the number of the asteroid; the ratios between diagonal elements of covariance matrixes obtained by the LM method and LS method (the ratios of the mean positional errors calculated by LM method to those calculated by LS one), B_x, B_y and B_z; and the ratios between the mean velocity errors calculated by the same methods, B'_x, B'_y, B'_z. It also contains indices LS and LM that point out the nominal orbit falling within dispersion ellipsoid calculated by the appropriate method. The same three-point index system has been applied as in Tab. 1.

Conclusion

The calculations show that for 13 asteroids the dispersion ellipsoids computed by the method of the least modules are more reliable than the ones computed by the method of the least squares. The dispersion ellipsoid calculated by the method taking into account the nonlinear relations is also more reliable. Orbits computed by the method of least modules are more accurate than orbits computed by the method of least squares for 13 asteroids. Therefore the orbital parameters for newly discovered asteroids should be computed not only by conventional method of the least squares, but also by the method of least modules.

References

1. *Linnik Yu. V.* The method of least squares and the basic theory of processing observations. M.: State Publisher of Physical-Mathematical Literature, 1962 (in Russian).
2. *Mudrov V. I., Kushko V. L.* Some experiments using the method of least-squares in problems of processing orbital data // Space Res., 1968. Vol. 6, N 4. P. 502–514 (in Russian).
3. *Mudrov V. I., Kushko V. L.* Methods of processing measurements. Quasi plausible estimates. M.: Publisher of Radio and Communications, 1983 (in Russian).
4. *Makarova E. N.* The processing of observations of selected minor planets by least modules method // Trudy IPA RAN (IAA RAS Transactions). 2000. Vol. 5. P. 190–196 (in Russian).

DYNAMICS OF NEOS. COLLISION PREDICTIONS

The Orbital Evolution of 2007 VA85, an Amor-type Asteroid on a Retrograde Orbit

P. Kankiewicz[1], I . Włodarczyk[2]

[1]Institute of Physics of Astrophysics Division of J. Kochanowski University, Kielce, Poland
[2] Chorzów Astronomical Observatory, Chorzów, Poland

Abstract. Among the known population of asteroids on retrograde orbits ($i > 90°$) we found an object classified as an Amor-type asteroid. During the analysis of the first results of astrometry, we found some possible Earth-impact solutions for this asteroid. After taking into account the latest observations, we excluded any significant impact solution. However, this asteroid is the first known example of potentially hazardous object on a retrograde orbit. We also investigated the orbital evolution of 2007 VA85 (1 Myr in the past), obtaining possible scenarios of its dynamical origin.

Introduction

The asteroid 2007 VA85 is the first small body on a retrograde orbit inside Jupiter's orbit (P = 8.7 yr, i = 131.8°). It was discovered in November, 2007 and was considered during some time as dangerous for the Earth (till first 55 observations). Currently, this body is categorized as the Amor-type asteroid. Any potential cometary activity of this object has not been confirmed yet. We present our latest results concerning the analysis of orbital evolution of 2007 VA85 in the past (1 Myr). Our data are based on averaged result of tracking (by numerical integration) a large number of so-called 'clones'. It allowed us to take into account the propagation of orbit determination errors and to improve the long-term orbital solution. Finally, we obtained possible evolutional paths of this asteroid. Additionally, we present some results of the impact risk estimates in the near future, based on similar methods.

Data and methods

Due to presence of errors in the determined orbital elements, we decided to compute sets of elements fitted to observations with fixed rms residuals. For this purpose we chose the method proposed by Milani [1] (included in the OrbFit computation tool [*http://adams.dm.unipi.it/~orbmaint/orbfit/*]). Typically, we used a set of 1000 massless test particles ("clones") distributed uniformly according to Gaussian probability density. Then we propagated these sets of orbital elements backward in time (1 Myr), calculating their mean values. In our dynamical model, we took into account gravitational perturbations from eight planets, from Mercury to Neptune, and the Moon. In the numerical integration we used initial positions of planets and Moon taken from the JPL DE406 Ephemeris. The motion of massive bodies was numerically integrated backward.

Results

Averaging of orbital elements allows us to improve the long-term estimates of changes in the orbital elements in the past.

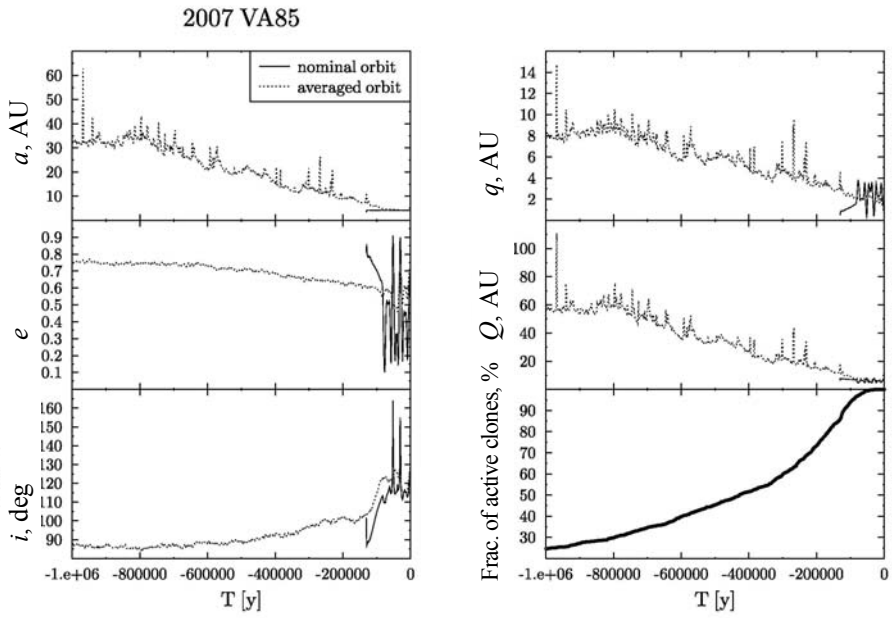

Fig. 1. The orbital evolution of the asteroid 2007 VA85 during 1 Myr obtained from a numerical backward integration.
Results representing nominal solution (solid line) ends at 150000 yr in the past due to "escape" to hyperbolic orbit ($e > 1$, $r > 1000$ AU) and became inactive. The mean solution (dotted line) is based on averaged elements of active clones.

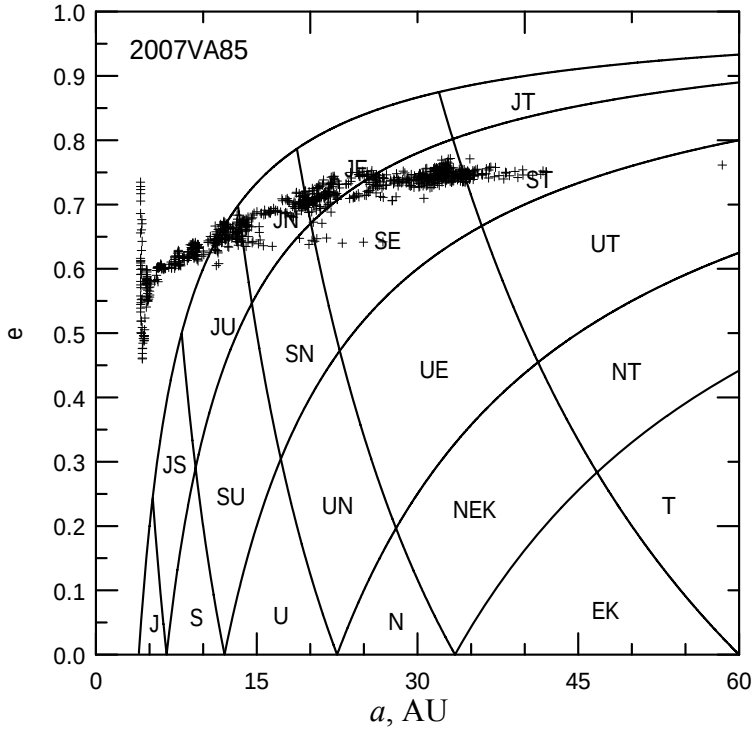

Fig. 2. The evolutionary path of averaged clones of asteroid 2007VA85 during the time-span 10^6 yr (in the past).
The evolution goes from right to left. The diagram and abbreviations are based on the classification of Horner et al. [2] where the first letter denotes the planet controlling the perihelion and the second letter the aphelion.

To increase the significance of solutions located closer to the nominal orbit, we used the Gaussian distribution probability density for weighting. The large fraction of "clones" escaped (were ejected) during backward integration (Fig. 1). Averaged results for 2007 VA85 indicate greater values of semi-major axis in the past. Mean value of inclination also indicates that the motion of the asteroid became retrograde in a relatively short time-span (10^5–10^6 yr). This conclusion is based on the averaged solution for limited number of clones — about 25 % at the end of integration. There is a relatively large probability that 2007 VA85 was captured into planetary region from hyperbolic orbit or from the Solar System periphery (Fig. 2).

Based on the current observational material (84 obs.) there will be no significant threat from this asteroid in the near future. However, during the analysis of the first 55 optical observations, we found some Earth-impact solutions (see Table). The collision probabilities were calculated using 1200 clones of the asteroid. We also applied the extended dynamical model, in-

cluding additional perturbations from Ceres, Pallas, Vesta, and Hygiea. Currently, observational results contain 84 obs. (231 days arc, with rms = 0.5176″). After the update of observational data, we do not expect any close approaches to planets in the next 100 y, except the approach to Jupiter (2009/01/23.22710, at 0.67440015 AU, which is now in the past).

2007 VA85 impact predictions based on first 55 optical observations (of which 1 was rejected as outlier) from 2007/11/04.090 to 2007/11/09.059. Arc length: 5 days, rms = 0.530″

Date	MJD	Sigma	Dist +/– (in Earth radii)	Probability
2082/01/16.453	81510.453	–2.311	7.55 +/–	4.24E-10
2083/01/16.773	81875.773	–2.227	1.89 +/–	6.43E-10
2089/01/16.205	84067.205	–2.185	12.13 +/–	2.70E-10

Conclusions

We obtained the most probable evolutionary scenario expected for 2007 VA85 in the past. It is the capture into the inner Solar System from a prograde orbit with high eccentricity and inclination (timescale: 1 Myr). Taking into account the latest (updated) results, no potential collisions with any planets in the near future (100 yr) were found. We expect to confirm and improve our solution after obtaining new observations of this asteroid. We also hope that applied "cloning" methods can improve such solutions and connect them to real observational errors.

References

1. *Milani A., Chesley S. R., Chodas P. W., Valsecchi G. B.* Asteroids III, 2002 / Eds W. F. Bottke Jr., A. Cellino, P. Paolicchi, R. P. Binzel. Tucson: Univ. of Arizona Press. 55.
2. *Horner J., Evans N. W., Bailey M. E., Asher D. J.* The populations of comet-like bodies in the Solar system, Mon. Not. 2003. 343. P. 1057–1066.

DYNAMICS OF NEOS. COLLISION PREDICTIONS

How Precise is the Orbit of (99942) Apophis and how Probable is its Collision with the Earth in 2036?

V. A. Shor, Yu. A. Chernetenko, O. M. Kochetova

Institute of Applied Astronomy of RAS, St. Petersburg, Russia

Abstract. At present the orbit of asteroid (99942) Apophis and the forces acting on it are not known with sufficient accuracy to predict with certainty its motion after the close approach to the Earth in April of 2029. As a result of this approach the current heliocentric orbit of the asteroid will be changed by Earth's gravity. The amount of change depends substantially on the minimum geocentric distance of the asteroid during its close approach. We compare published solutions for Apophis' orbit and discuss the consequences that follow from the uncertainty of Apophis' orbit, including the probability of its collision with the Earth in April 2036. New determinations of Apophis' orbit that appeared after the end of the Conference ACH-2009 support our conclusion that the widely quoted value of Apophis' collision probability with the Earth in 2036 of 1/45000 is an overestimate.

Present day knowledge of Apophis' orbit

Apophis' orbit having a semi-major axis of 0.922 AU and aphelia distance 1.098 AU is situated mainly inside the Earth's orbit. The orbit has small inclination to the ecliptic plane. The asteroid can be observed during comparatively short periods of time when its elongation from the Sun is greater than $\sim 55^\circ$. In one of these periods it was discovered on 19 June, 2004, at Kitt Peak Observatory. In the period since 15 March, 2004, (five positions were fixed before official discovery) till 16 August, 2006, slightly more than one thousand optical observations and seven radar observations were obtained.

There are at least four determinations of Apophis' orbit from optical and radar observations that we will designate as solutions from Jet Propulsion Laboratory (JPL), *http://ssd.jpl.nasa.gov/sbdb.cgi?sstr=99942*, from NEODyS *http://newton.dm.unipi.it/neodys/epoch/99942.eq1*, from IAA RAS [1], and

from Giorgini et al. [2]. Shortly after finishing the Conference ACH-2009, the web sites of JPL and NEODyS posted two more solutions found from a substantially larger number and corrected measurements of Apophis positions provided by Dave Tholen. In the present paper we do not consider these new solutions.

All four solutions were found by the weighted least squares method. In so doing, the different groups of researchers have determined different sets of orbital parameters, ascribing different weights to observations, and using various criteria for rejecting observations. They also used somewhat different models of motion. Finally, solutions were found from the use of a different number of optical observations and with different formal precision. Solutions of JPL and of NEODyS are close to each other and so are the estimates of the mean errors of elements in them. While our solution [1] is sufficiently close to the other two solutions, the precision of orbital elements in it is noticeably better than those in the solutions of JPL and NEODyS. This difference gave us justifiable concern until solution [2] was published. In this solution estimates of element errors are found to be substantially closer to ours. Since formal criteria do not permit conclusions about which solution is more precise, it is interesting to follow the results emerging from the distinctions between them.

Recall that the nominal solution is not the only one compatible with the used set of observations. In the six-dimensional space of orbital elements (coordinates and velocities) the nominal solution is located at the center of an ellipsoid, whose axes lengths depend on the mean errors of elements of the nominal solution. If one restricts consideration within limits $\pm 3\sigma_{E_i}$, then inside of this ellipsoid with semi-axes equal to $3\sigma_{E_i}$ are the great majority of permissible initial conditions of motion.

Each point of space, restricted by the ellipsoid, can be considered as a virtual asteroid [3]. Virtual asteroids move with time along trajectories more or less closely to the trajectory of the nominal solution. Some fraction of virtual asteroids can collide with the Earth and some fraction can pass by. Thus, the problem of collision prediction has probabilistic character.

The points of intersections of virtual asteroids with some plane form a scattering field. Special interest has the scattering field on the target plane. By this term is meant a plane passing through the Earth's center normal to the relative velocity of the potentially colliding body. Connected with this plane is the coordinate system ξ, η, ζ having its origin O at the center of the Earth. Its η axis is directed along the relative velocity of the body, the ξ-axis is directed along the vector product of the heliocentric velocity of the Earth and the relative velocity of the small body. The ζ axis completes the

right-handed coordinate system. In this coordinate system the target plane coincides with the coordinate plane $\xi O \zeta$.

When a cloud of virtual asteroids crosses the target plane a dispersion ellipse is formed on it with semi-major axis parallel to the ζ-axis and the semi-minor axis parallel to the ξ-axis. The position of the dispersion ellipse on the target plane with respect to the projection of the Earth on the plane determines the possibility of collisions of all or some virtual asteroids with the Earth in the given approach.

Within the frame of linear approximations there exists a simple dependence of the semi-axes of the ellipsoid of initial values to the semi-axes of the dispersion ellipse on the target plane. Omitting details, we indicate that for our solution [1] the position of the ellipse center on the target plane at moment T = 2462240.407115 (the moment of closest approach of Apophis to the Earth on 13 April, 2029) is given by coordinates ξ = 7124.5 ± 15 km and ζ = 37550.7 ± 351.6 km. It follows that the minimum distance of Apophis from the Earth's center in 2029 will be 38220.5 km (see Figure). Our computations for the solutions of JPL, NEODyS, and [2] indicate that the minimum distances for them will be 38240.5 km, 38228.1 km, and 38027.2 km, respectively. We don't wish to exaggerate the significance of the fact that for the first three solutions the minimal distances are very similar to each other while the forth solution is somewhat different. Giving different weights to observations makes it possible to change the position of the center of the ellipse along the ζ-axis significantly more than was found, as evidenced by the relatively large value of σ_ζ (± 351.6 km).

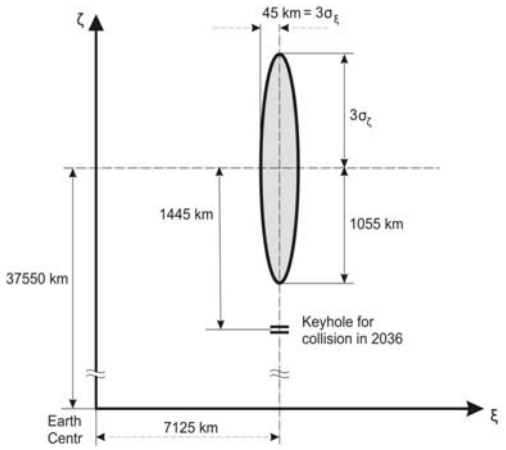

Dispersion ellipse on target plane at the moment of closest approach in 2029.

Key hole for collision in 2036

Various bodies belonging to the cloud of virtual asteroids cross the target plane, generally speaking, at different moments. Those virtual asteroids that move ahead of Apophis overtake the target plane at an earlier time and the ζ coordinate of their crossing point turns out to be smaller. Alternatively, if a virtual asteroid moves behind the nominal solution for Apophis, it overtakes the target plane later and the ζ coordinate of its crossing point is larger. If in the nominal solution one varies the mean motion within the limits from $n + 3\sigma_n$ to $n - 3\sigma_n$ and follows up the motion of the virtual asteroids generated in such a way, then their crossing points on the target plane will run along the major axis of the dispersion ellipse starting from its end closest to the Earth to its most distant end. Corresponding virtual asteroids pass by the Earth at different distances and their orbits undergo different perturbations. The orbital period of the asteroid passing through the nearest end of the semi-major axes will be changed from 0.88570 to 1.1677 yr, whereas that of the asteroid passing through the more distant end will be changed from 0.88570 to 1.1537 yr. Within the interval 1.1677–1.1537 there are many periods commensurate with a year, for example 1.16666… $\approx 7/6$. During seven Earth years an asteroid with such a period will accomplish six revolutions along its orbit and again approach the Earth practically at the same point of its orbit. In reality one must also take into account the perturbations from other bodies. This can lead to enlargement or reduction of the minimum distance. One can obtain a more realistic situation for April of 2036 by following up the large number of virtual asteroids with varied mean motions (Tab. 1). As seen from the Table, if the variation of the mean motion in the nominal solution [1] lies within the limits $(11252 - 11256.8) \cdot 10^{-11}$ °/day, then virtual asteroids will collide with the Earth on 13 April of 2036. Such collisions will take place also for other solutions, but under different variations.

Table 1. Minimum distances in 2036 depending on variation of the mean motion

Variation $\times 10^{11}$, °/day	Δt, 2036 04 13.0 + Δt	Δ_{min}, km
11252	0.36942	6415
11254	0.37007	2221
11256	0.37986	4336
11256.8	0.38597	6680

It is not difficult to determine where those virtual asteroids that in April 2036 will collide with the Earth cross the target plane in April 2029. With this aim it is sufficient to express the limiting values of variation, leading to

collisions, in the unit of σ_n. For our solution they are 4.1081–4.1098. Taking into consideration that σ_n on the target plane in 2029 is equal 351.6 km, we find that crossing points are situated on the extension of the major axis directed toward the Earth, at distances from 1444.4 km to 1445.0 km. This length of the axis extension is the so called keyhole or resonance return zone for 2036 (see Figure). The results of similar calculations for this and other solutions are presented in Tab. 2.

Table 2. Probability of collision in 2036 according to different solutions

Quantity	Solution of IAA [1]	Solution of JPL	Solution [2]
n, °/day $\sigma_n \cdot 10^{11}$	1.11281511370 ± 0.2739	1.11281511240 ± 0.4407	1.11280772364 ± 0.1733
$\Delta_{\min}$, km in 2029	38220	38240	38027
Var $n \cdot 10^{11}$	11252–11256.8	11431.4–11436.2	9595.6–9600.3
$\Delta_{\min}$, km in 2036	2110	2115	2114
Δ_{keyhole}, km	36825.7	36823.4	36822.9
keyhole	4.1081 – 4.1098	2.5953 – 2.5960	5.536 – 5.540
P	$1.5 \cdot 10^{-7}$	$1 \cdot 10^{-5}$	$3.5 \cdot 10^{-10}$

The limiting values of variation leading to collision in 2036 are given on line 3. On line 4 are indicated the minimum distances from the Earth's center in 2036. Line 5 shows the distance of the center of the keyhole from the Earth's center. On the last line we give the probability of passage of the asteroid through the keyhole. The main inference is that the estimated probability for collision in 2036 varies according to different solutions by several orders of magnitude. One more important inference is the weak dependence of the keyhole position on the motion models and the initial values of parameters used.

It is worth while to mention that on 7 Oct., 2009 information appeared on the NASA web site (*http://neo.jpl.nasa.gov/news/news164.html*) that NASA had refined asteroid Apophis' path toward the Earth. It stated that Steve Chesley and Paul Chodas refined the asteroid orbit using corrected measurements of Apophis positions. As a result of this improvement, the probability of an Earth encounter on April 13, 2036 for Apophis has decreased from 1/45000 to about four-in-a million. The new value is much closer to the probability of collision indicated in the last Table for the solution of IAA, though the IAA probability is still less than NASA's.

Influence of disregarded accelerations

The preceding results were obtained without regard to Yarkovsky effect, stemming from asymmetrical reradiation of solar insolation by the body moving in a heliocentric orbit and spinning around an axis [4]. Due to the heat inertia of matter the maximum surface temperature is attained not at the subsolar point but to the east or west of it, depending on the sense of the spin. Just as maximum heating of one of two hemispheres is attained not on the day of summer solstice but at a later time. The heat photons, emitted from the heated body produce a small but consistent reactive force. Because of the difference in temperature from different parts of the body a component of the reactive force is directed in opposition to the orbital motion, if the sense of spin is direct, or in orbital direction, if the sense of spin is reverse (diurnal effect). Analogously, because of heat inertia in the course of orbital motion a component directed against the orbital motion appears (seasonal effect). Compounded action of the two accelerations could produce acceleration or retardation of orbital motion (change of the semi-major axis of the orbit). The amount of the effect depends on the orbit, the mass of the body, position of spin axis, speed of spin, and the thermal properties of the body's surface layers. Since most of these parameters are unknown, it is impossible to take this effect accurately into consideration. Nevertheless, it is possible to estimate maximum and minimum possible action of the effect at Apophis, using limiting values of the parameters, as it was done in [2]. Towards 2029, according to [2] the effect can produce displacement of Apophis along its orbit from –720 to +780 km. We proceed from the assumption that the effect is characterized by three components $A_1 r^{-2}$, $A_2 r^{-2}$, and $A_3 r^{-2}$ — radial, transversal, and normal to the orbit plane, r being the heliocentric distance. Available observations provide no way to determine these parameters. In numerical experiments we assume that A_1 and A_3 are equal to zero, whereas for A_2 we accept values $(0, \pm 2, \pm 6) \cdot 10^{-14}$ AU/day^2. In each experiment the parameters of motion and estimates of their errors were determined using a refined model of motion. These changes produced a minute effect on parameters of dispersion ellipse. By the way of subsequent numerical integration the following displacements of asteroids along the orbit and their distances from the Earth's center on 13 April, 2029 were found (Tab. 3). For example, if $A_2 = -6.0 \cdot 10^{-14}$, then $\Delta_{\min} = 37451.4$ km and ζ coordinate of ellipse center is equal to +36767.5 km, that is it decreased to 783 km. At the same time the position of the keyhole for collision in 2036 practically did not change. As a result it turns out to be deeply inside the dispersion ellipse. The estimate for the collision probability increased approximately one thousand times, being as much as $1.1 \cdot 10^{-4}$. Note that Apophis displacement along the orbit in this case is equal to +816 km, which is close to the upper limit found

in [2]. In case of direct spin of the asteroid its additional displacement along the orbit will occur in the opposite direction and the dispersion ellipse as a whole will be displaced even farther from the keyhole, while the collision probability will have values less than $1.5 \cdot 10^{-7}$.

Table 3. Displacement of Apophis under the influence of nongravitational forces

$A_2 \times 10^{14}$, AU/day^2	Sense of spin	$\Delta_{\min}$, km	Change of $\Delta_{\min}$, km	Displacement along orbit, km
0.0		38220.5	0	0
+2.0	Direct	38477.2	+256.7	–272.2
–2.0	Reverse	37964.0	–256.5	+272.0
+6.0	Direct	38991.0	+770.5	–816.9
–6.0	Reverse	37451.4	–769.1	+815.8

References

1. *Vinogradova T. A., Kochetova O. M., Chernetenko Yu. A., Shor V. A. et al*. The orbit of asteroid (99942) Apophis as determined from optical and radar observations // Astronom. Vestn. 2008. Vol. 42, N 4. P. 291–300 (in Russian) (see also Solar System Res. 2008. Vol. 42, N 4).
2. *Giorgini J. D., Benner L. A. M., Ostro S. J., Nolan M. C., Busch M. W.* Predicting the Earth encounters of (99942) Apophis // Icarus. 2008. Vol. 193, Issue 1. P. 1–19.
3. *Milani A., Chesley S. R., Valsecchi G. B.* Asteroid close encounters with the Earth: Risk assessment // Planetary Space Sci. 2000. Vol. 48. P. 945–954.
4. *Bottke W. F., Vokrouhlicky D., Rubicam D. P., Broz M.* The effect of Yarkovsky thermal forces on the dynamical evolution of asteroids and meteoroids. In Asteroids III / Eds W. F. Bottke, A. Cellino, P. Paolicchi, R. P. Binzel. Univ. Arizona Press., 2002. P. 395–408.

The Asteroid-Comet Hazard Conference Proceedings, 2009

About Zones of Resonant Returns of Asteroid Apophis

L. L. Sokolov, N. P. Pitjev, V. Sh. Shaidulin

Sobolev Astronomical Institute of St. Petersburg State University,
St. Petersburg, Russia

Abstract. Asteroid Apophis is one of extremely dangerous NEOs. Different scenarios of the dynamical evolution of Apophis' orbit within the framework of today's knowledge are discussed. Using analytical and numerical tools, we investigate the loss of precision after the Earth approach in 2029 and the possible approach in 2036. After 2036 Apophis' motion may not be determinable. Possible trajectories of collisions with the Earth have been found analytically and numerically in this chaotic region. To construct these trajectories we used quasi-random intermediate motions, made up from resonant collision orbits. The hazard trajectories are derived numerically using Everhart's integrator and Solar System model DE405. The size of the region of initial conditions leading to the collisions in 2040, 2041, 2042, 2044, 2047, 2051 is presented. The possibility of similar behavior of other NEO trajectories is discussed.

Introduction

Asteroid Apophis was discovered on June 19, 2004 at the Kitt Peak National Observatory in Arizona, USA. On April 13, 2029 Apophis will approach Earth at 37–38 thousand kilometers. The accuracy of this distance is about one thousand kilometers.

The initial data accuracy is 1–3 km for coordinates and 1–2 mm/s for velocities [1]. Now, Apophis is out of the region where it could be observed by optical or radar methods. New observations will be possible in 2012–2013 [2]. The last observations of the asteroid were performed in August 2006. The elements of Apophis orbit and its accuracy is discussed in the papers [3, 4].

Possible approaches to Earth after 2029 are associated with resonances. The most probable 6/7 resonance leads to a collision in April of 2036, but the collision probability is estimated as 10^{-5} and even less [3, 4].

Each Earth approach and scattering of possible trajectories leads to a loss of accuracy. The difference of minimum distance to the Earth in 2029 equal to 30 km corresponds to a difference of minimum distance to the Earth in 2036 equal to 10^6 km [5].

Apophis demonstrates important properties of NEO motions that may be typical for other hazardous objects. Before an NEO collision with a planet, several encounters with the planet usually take place [6]. Encounters are more probable than collisions. The probability of an unknown asteroid approach rises with geocentric distance r as r^2.

Our goal is to investigate hazardous trajectories of Apophis, especially after 2036.

Hazardous trajectories after 2036

Let us assume that during the time interval 2029–2036 the asteroid will move in the resonance orbit with the 6/7 commensurability, and in 2036 after close approach to the Earth Apophis will pass to another resonance collision orbit. A list of such elliptic orbits, having collisions before 2052, is presented in [5].

To investigate the motion of asteroid Apophis, we applied the Everhart integrator [7] to take into account the perturbations for eight major planets, Pluto, and the Moon. The computations were performed in the ICRF barycentric equatorial system, for the epoch J2000.0. The integrator parameters NOR = 15, LL = 10, NI = 2 were used in the computations. For coordinates of the major planets and the Moon we use ephemerides DE405 [8]. The initial data were published on 18.05.2006 at NASA sites *http://newton.dm.unipi.it/cgi-bin/neodys/neoibo?objects:Apophis;main* and *http://neo.jpl.nasa.gov/cgi-bin/db?name=99942*. Double-precision computations (16 decimal places) were performed.

The accuracy of the direct numerical integration is obviously insufficient to examine the third approach to Earth. The region of initial conditions in 2006 that leads to collisions and hazardous approaches after 2036 has the sizes of about one centimeter or less. But if we shift this region along the trajectories from 2006 to 2035, a millimeter size will be transformed into kilometer size. In this new, larger region of initial conditions one can search for hazardous trajectories and minimum geocentric distances without major difficulties.

To separate hazardous trajectories, we vary the initial conditions in 2006 and 2035. It is sufficient to change only one variable (mean motion, or semi-major axis, or some coordinate). Some details are given in [5].

In Tab. 1 the minimum geocentric distances, $r_{\min}$ (10^3 km), after 2036 are presented for some possible hazardous trajectories. The necessary change Δa_0 of that semi-major axis value in 2006, which leads to collision in 2036, are given in each line.

Table 1. Minimum geocentric distances (in units of 10^3 km) after 2036

Years	r_{min}, 10^3 km	Δa_0, m
2037	7.4	15
2038	7.3	–4
2039	7.4	–10
2039	51.0	4
2040	2.8	–18
2040	39.0	5
2041	5.5	–7
2042	2.9	–84
2044	6.2	128
2045	12.0	71
2046	22.0	52
2047	3.0	–5
2049	28.0	34
2049	21.0	–182
2051	8.6	8171
2051	2.0	29
2052	17.0	15884

The regions of initial conditions at JD 2464448.5 (2035), corresponding to the collisions, have the sizes presented in Tab. 2.

Table 2. Ranges of initial data variations for each discovered collision (JD 2464448.5, (2035)

Year	Δx	Δy	Δz	ΔV_x	ΔV_y	ΔV_z
	km			mm/s		
2040	0.42	0.26	0.63	0.042	0.132	0.308
2041	0.033	0.019	0.049	0.0035	0.011	0.0028
2042	5.5	3.2	8.4	0.54	1.8	4.1
2044	3.1	1.8	4.8	0.31	1.0	2.3
2047	0.024	0.013	0.035	0.0023	0.0072	0.0202
2051	0.32	0.19	0.49	0.031	0.103	0.209

Table 3. The ranges (Δr) of minimum geocentric distances (r) in 2036 for each discovered collision

Year	Δr, km	r, 10^3 km
2040	5.1	101
2041	0.38	31
2042	69	500
2044	39	772
2047	0.28	21
2051	3.9	164

The regions of initial conditions on 01.05.2029, corresponding to the collisions, have the sizes about ten times smaller, than the sizes in 2035.

The regions of initial conditions leading to a collision in 2036 have the following sizes in coordinate space: in 2006 — 3 m, on 01.03.2029 — 500 m, on 01.05.2029 — 200 km, in 2035 — 1800 km.

In Figure (left) the region of initial conditions in 2006, corresponding to the possible collision in 2036, is presented [5]. This is a strip (line) in the plane: variation of barycentric distance vs. variation of barycentric velocity. The size of Figure (left) corresponds to the accuracy of initial conditions [1]. The small square in the Figure (left) is magnified in Figure (right). The inclined straight lines going from top left to bottom right are the initial data for the collisions in 2042, 2040, 2041, 2047, 2036 (dark strip), 2051, 2044. Lines for collisions in 2041 and 2047 are very close to each other. The lines in the Figure correspond to constant values of semi-major axis of Apophis' orbit.

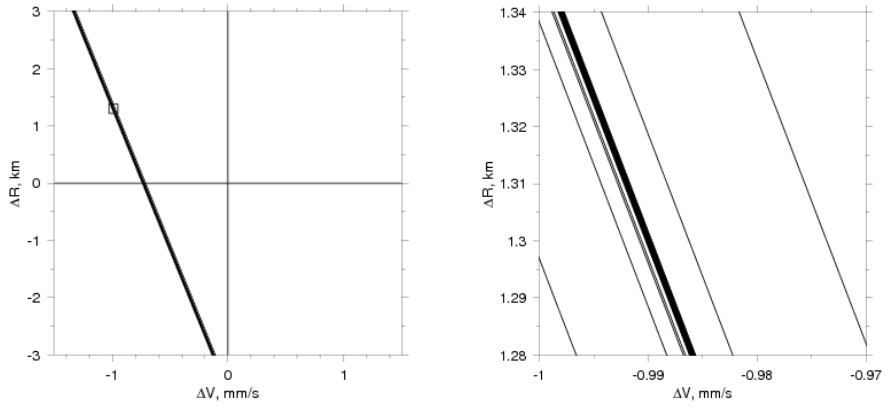

Ranges of initial data in 2006 for discovered collisions. Right figure is magnified small square in left figure.

In the work [9] the possible approaches and collisions of the asteroid Apophis with the Earth after 2036 are presented (see their Fig. 4). The collisions in 2040, 2042, and 2051 in [9] correspond to the collisions given in this work (Tab. 1). We confirm also the possible collisions in 2041, 2045, and 2059 presented in [9]. In particular, the minimum geocentric distances are the same. But two different collisions are possible in 2041: one collision is presented in [9], another one is given in this work.

Conclusions

According to the state-of-the-art knowledge of the orbit of asteroid Apophis, its hazardous approaches and collisions with Earth are possible (though very unlikely) not only in 2036, but also in subsequent years. This

should be kept in mind when measures to prevent the collision in 2036 are planned. We present the possible collisions in 2040, 2041, 2042, 2044, 2047, 2051 and corresponding regions of initial conditions, as well as many close approaches.

Acknowledgments

This study was financially supported by the analytic departmental special-purpose program of the Russian Ministry of Science and Education: Development of Higher School Research Potential (project no. 2.1.1/504) and by Leading Scientific School (project no. NSh-1323.2008.2).

References

1. *Yagudina E. I., Shor V. A.* The Orbit of the NEA (99942) Apophis = 2004 MN4 from Analysis of Optical and Ranging Observations // Materialy Vseros. konf. "Asteroidno-kometnaya opasnost'–2005" (AKO–2005) (Proc. All-Russian Conf. "Asteroid-Cometary Hazard"). St. Petersburg, 2005. P. 355–358.
2. Chesley Steven R. Potential impact detection for Near-Earth asteroids: the case of 99942 Apophis (2004 MN4) // Asteroids, Comets, Meteors. Proc. IAU Symp. N 229. 2005. Cambridge University Press, 2006. P. 215–228.
3. *Vinogradova T. A., Kochetova O. M., Chernetenko Yu. A., Shor V. A. et al.* Orbit of Asteroid (99942) Apophis Determined from Optical and Radar Observations // Solar System Res. 2008. Vol. 42, N 4. P. 291–300.
4. *Kochetova O. M., Chernetenko Yu. A., Shor V. A.* Asteroid (99942) Apophis // Solar System Res. 2009. Vol. 43, N 4. P. 291–300.
5. *Sokolov L. L., Bashakov A. A., Pitjev N. P.* Peculiarities of the Motion of Asteroid 99942 Apophis// Solar System Res. 2008. Vol. 42, N 1. P. 18–27.
6. *El'kin A. V., Sokolov L. L.* On Continuous Passages of NEAs in the Earth's Vicinity // Asteroidnaya opasnost'-95 (Asteroid Danger'-95), ITA RAS, Abstracts. Vol. 2. St. Petersburg, 1995. P. 41.
7. *Everhart E.* Implicit single-sequence methods for integrating orbits // Celest. Mech. 1974. Vol. 10. P. 35–55.
8. *Standish E. M.* JPL Planetary and Lunar ephemerides, DE405/LE405 // Interoffice Memorandum. 1998. 312.F-98-048. 18 p.
9. *Yeomans D. K., Bhaskaran S., Broschart S. B., Chesley S. R. et al.* Deflecting a Hazardous Near-Earth Object // The 1st IAA Planetary Defense Conference: Protecting Earth from Asteroids. Granada, Spain, 27–30 April 2009 (*http://neo.jpl.nasa.gov/neo/pdc_paper.html*).

DYNAMICS OF NEOS. COLLISION PREDICTIONS

Methods of Computing Impact Orbits

I. Włodarczyk

Chorzów Astronomical Observatory, Chorzów, Poland

Abstract. The methods of computing impact orbits with the use of the free OrbFit v.4.0 software [*http://adams.dm.unipi.it/~orbmaint /orbfit/*] are described. Some results are published on the www site of the Chorzów Astronomical Observatory [*http://www.planetarium.edu.pl/irek/ 2009BD.TXT*].

Introduction

If for a given asteroid we find an orbit that exactly crosses the Earth then the probability of this impact is nonzero [Sitarski, 2009, private information]. The idea of impact orbits was introduced by Grzegorz Sitarski [1]. His method is based on computing impact orbits for the epoch close to that of the observed arc and for the epoch usually 7 days before an impact of the asteroid with the Earth. Computed in such a way impact orbits are presented on the www site of Space Research Center of the Polish Academy of Sciences [*http://phas.cbk.waw.pl/neo_impact.htm*].

The author computes impact orbits with the use of the free OrbFit v.4.0 software. Some results are published on the www site of the Chorzów Astronomical Observatory.

Usually the impact solutions are presented in the form similar to the one seen on the Impact Risk Page of NASA (*http://neo.jpl.nasa.gov/risk/*) or on NEODyS: (*http://newton.dm.unipi.it/neodys/index.php?pc=4.0*). For potentially hazardous objects (PHOs) they give the name of the asteroid, dates of possible impacts, probability of impact, impact energy, and risk estimated on the Torino and Palermo scales.

Method of computing

The multiple solution method [2] from the OrbFit software is used for settings: usually 3 sigma or 6 sigma, 1201 clones on each side of the nominal solution along LOV, i. e. the coordinate along the Line of Variations

(LOV) [3] and for the epoch close to the observational arc. Next the possible close approaches of clones to the Earth on intervals 100 year in advance are computed together with prognostic dates and corresponding sigmas of LOV. Then with the OrbFit software we can propagate these clones for the epoch several days before impact. With the computed sigma LOV we can find which clones can impact the Earth.

We can find impact orbits with two main methods. First, we can interpolate orbital elements from clones with sigma_LOVs close to the sigma_LOV of a potential impact for a given year. We use the Lagrange method of 12th to 18th degree and get orbital elements of clones that can impact the Earth. This method was illustrated with an example of asteroid (99942) Apophis [4]. We can also use the second method by first selecting a clone close to sigma LOV and next apply the multiple solution method with the use of the OrbFit software by setting sigma_LOV to small values between 0.02 and 0.000002 around this selected orbit of a clone. Sigma_LOV is the coordinate along the LOV. This value is a measure of how well the impacting orbit fits the available observations. Zero indicates the best-fitting, central (nominal) orbit. The further from zero, the less likely is the event: roughly 99 % of all the uncertainty region lies between –3 and +3. CLOMON 2 of NEODyS usually examines for collisions sigma_LOV within the limits ± 3, Sentry of the JPL NASA — up to ± 5. Sometimes we use sigma_LOV equal to ± 6.

Thus, we compute new clones around the prognostic impact clone. By propagating them we can see on the display which clones impact the Earth around the previously computed date of impact. We illustrate this method with an example of asteroid 2009 FJ which was on the top of the NASA Impact Risk Page in April 2009.

The LOV of asteroid 2009 FJ was computed for 20001 clones within ± 4 sigma variation and for the epoch MJD55000 = JD2455000.5 = 2009 June 18.0 TDB. Observations were taken from the time span 2009 03 17.24376 to 2009 04 05.29170. From 126 observations 7 were discarded. Rms of the nominal orbit = 5.795E-01". In Fig. 1 three clones with the serial numbers 7280, 7281, and 7282 are presented, where clone 7281 is close to the impact orbit in 2058.

Below are listed orbital elements of clone 7281 with their errors:

Keplerian elements: *a*, *e*, *i*, longitude of node, argument of perihelion, mean anomaly [deg]:

2.20061902273646E+00 0.567404607275080 0.8915884972697 353.6453176783613 150.6149307323342 35.5739037655478.

Epoch: MJD 55000.000000000 TDT.

RMS: 1.81341E-03 3.64310E-04 4.26750E-04 4.72626E-04 1.37826E-04 4.48470E-02.

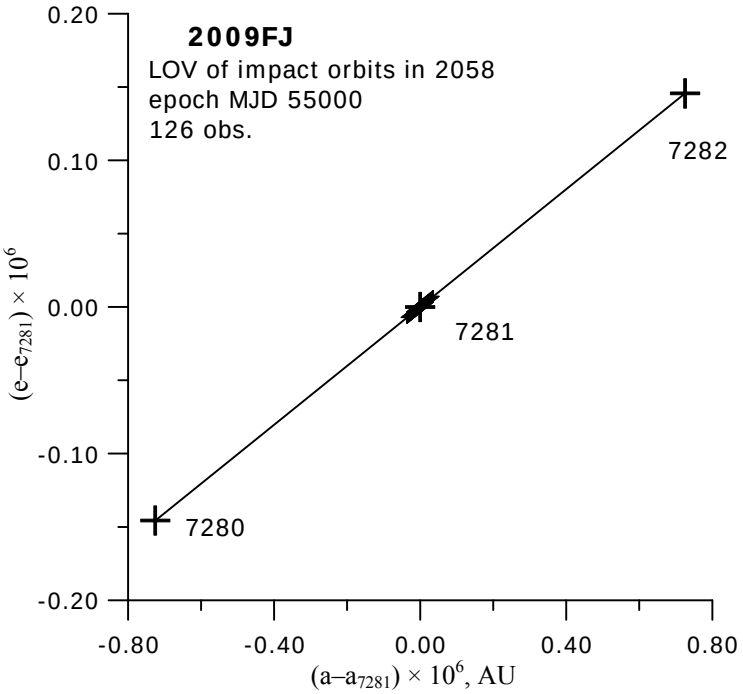

Fig. 1. Search for impact orbits in 2058 for asteroid 2009 FJ (elements for epoch 2009 June 18.0 TDB obtained on the base of the first 126 observations) around the nearest clone on the LOV.
Thin lines connect three neighboring clones of prognostic impact orbit on LOV from computed 20001 clones within ± 4 sigma variation. Thick lines connect LOV for sigma = 0.00002 around prognostic impact orbit.

Around this clone we have computed 201 clones from the multiple solution for sigma = 0.00002 to find orbits that cross the Earth. They are shown in Fig. 2 around clone 7281. Among these clones there were 171 impact clones, from serial number 30 to 201, that impact the Earth. One of them, with the serial number 201, is given below:

orbit: 201.

Close approach to Mars on 2025/10/04.31159 60952.31159 MJD at 0.06943577 AU.

Close approach to Earth on 2045/01/16.06580 67996.06580 MJD at 0.02651729 AU.

Close approach to Earth on 2058/03/13.80695 72800.80695 MJD at 0.00002282 AU — impact! Elements at time 55000.0 (MJD) — epoch close to observational arc.

Keplerian elements: *a*, *e*, *i*, longitude of node, argument of perihelion, mean anomaly [deg]:

2.200619059005824 .567404614561456 .8915885057982892 150.6149307310013 353.6453176690237 35.57390286856596.

Elements at time 72793.0 (MJD) — 7 days before impact:

2.197643237987197 .5667252285901425 .8740977128302188 152.2366017333275 352.5678194058514 4.166654886948607.

Elements at time 72820.0 (MJD) — 20 days after impact:

2.232674537476911 .5582294733651824 7.314581606613035 11.8312582714231 172.620489478256 2.883278852107046.

Between these two last epochs: 72793.0 (MJD) and 72820.0 (MJD) we can see which clones impact the Earth on the display, i. e., their distance is smaller than the Earth's radius.

The path of risk was computed with the use of all of these 171 clones (impact orbits). It is presented in Fig. 2.

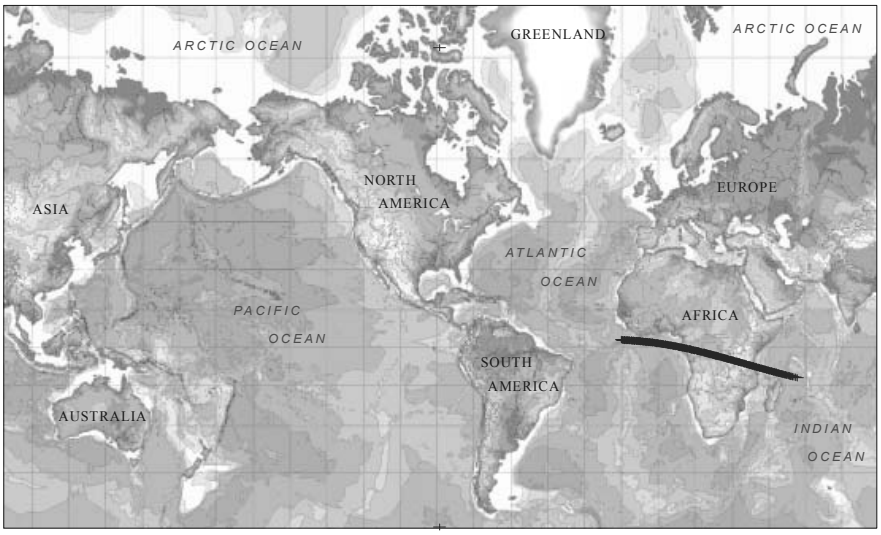

Fig. 2. Path of risk for asteroid 2009 FJ on 2058/03/13.789.

Conclusion

From our computations it is clear that with the use of the free OrbFit software it is possible to compute impact orbits of dangerous asteroids by two different methods. The best method of computing impact orbits is the method of multiple solutions. Using this method one forms clones twice: at first, to find close approaches of clones with the Earth by tracing their motion numerically and then, in the vicinity of prognostic impact orbits, to find orbits leading to real collisions, if any.

References

1. *Sitarski G.* How to find impact orbit for the Earth-asteroid collision // Acta Astronomica. 1999. Vol. 49. P. 422–431.
2. *Milani A., Sansaturio M. E., Tommei G., Arratia O., Chesley S. R.* Multiple solutions for asteroid orbits: Computational procedure and applications // Astron. Astrophys. 2005. Vol. 431. P. 729–746.
3. *Milani A., Chesley S. R., Sansaturio M. E., Tommei G., Valsecchi G.* Nonlinear impact monitoring: Line of variation searches for impactors // Icarus. 2005. Vol. 173. P. 362–384.
4. *Wlodarczyk I.* The impact orbits of the dangerous asteroid (99942) Apophis // Contrib. Astron. Obs. Skalnate Pleso. 2008. Vol. 38. P. 21–32.

The Asteroid-Comet Hazard Conference Proceedings, 2009

The Yarkovsky Effect in the Motion of NEAs

Yu. A. Chernetenko

Institute of Applied Astronomy of RAS, St. Petersburg, Russia

Abstract. In this paper we evaluate the Yarkovsky effect on the motion of NEAs under the assumption that this acceleration depends on heliocentric distance as $1/r^2$ and is characterized by the transverse component A_2 in the orbital coordinate system. For 94 NEAs values of A_2 have been found with errors less than $1.5 \cdot 10^{-14}$ AU/day^2. To evaluate the Yarkovsky effect the model of motion should be as complete as possible. In some instances the Yarkovsky effect can be estimated by using only optical observations. Accounting for the Yarkovsky effect permits to include more optical observations in the orbit fitting process. In determining asteroid masses by the dynamical method it seems to be useful to combine it with A_2 estimates when a small, perturbed asteroid is used as a test particle.

Introduction

This paper deals with evaluation of the Yarkovsky effect [1] from optical and radar observations of asteroids. The Yarkovsky effect (YE) depends on a number of physical and orbital parameters and its accurate accounting is a rather complicated task. In the paper [2] it was proposed to evaluate this additional acceleration on the assumption that it depends on heliocentric distance as $1/r^2$ and can be presented by three (in the general case) components in orbital coordinate system. This approach demands a very accurate model of motion and a precise reduction of observations. The proposed approach shows satisfactory agreement of residuals from radar observations for asteroid 6489 Golevka obtained in the paper with corresponding results in [3]. Therefore, the proposed approach can be recommended for other asteroids.

For 94 NEAs the values of A_2 have been found with errors less than $1.5 \cdot 10^{-14}$ AU/day^2. From these only 36 asteroids have radar observations. Accounting for Yarkovsky effect permits to include more optical observations to improve the process, especially remote observations for asteroids 68950, 85953, 152563, 162004.

Results

The transverse parameter of acceleration, A_2, was evaluated along with orbital parameters for 862 numbered NEAs having $H > 10^m$ ($d < 40$ km) and 593 unnumbered NEAs having more than three oppositions and $H > 10^m$. Optical observations were taken from catalogue of MPC and radar observations were taken from catalogue of JPL (NASA) as of June 2009. Gravitational perturbations from all the major planets and Pluto and from 300 perturbing asteroids were taken into account in the equations of motion of an asteroid. Relativistic perturbations from the Sun and Jupiter, perturbations due to oblateness of the Sun and the Earth and due to light pressure were also included into the model. Perturbations from the Earth and the Moon are considered separately. The coordinates of the perturbing bodies were calculated using DE405 ephemeris. The gravitational deflection of light was taken into account. Numerical integration of the equations of motion and the equations for partial derivatives was performed by the 15th-order Everhart method.

Different components of the model of motion (relativistic perturbations from Jupiter, oblateness of the Sun, uncertainty of the Mercury mass, and gravitational perturbations from asteroids) were tested to evaluate their contribution to the derived values of A_2. These values proved to be very sensitive to the amount of perturbing asteroids included into the equations of motion. So, for asteroid 1036 $A_2 = -2.07 \cdot 10^{-14}$AU/day^2 when perturbations from Ceres, Pallas, and Vesta are taken into account, and $A_2 = -2.44 \cdot 10^{-14}$ AU/day^2 when perturbations from 300 asteroids are included in the equations of motion. For asteroid 4015 corresponding data are –0.41 and –2.86. For asteroid 11054 these data are –1.27 and –0.07. For asteroid 14402 they are –0.13 and –0.95.

The YE is of the order of $(1 \div 10) \cdot 10^{-14}$ AU/day^2 [1], therefore for further consideration the values of A_2 were selected with errors less than $1.5 \cdot 10^{-14}$ AU/day^2. It was proved that 94 asteroids satisfy this criterion and only 36 from them have radar observations. Tab. 1 gives the list of these asteroids and their values of A_2 in increasing order of their errors. Numbers of asteroids having radar observations are printed in the bold type. It is of interest to note that asteroid 4015 Wilson–Harrington is the comet 107 P/ Wilson–Harrington. However, the value of A_2 for this asteroid is of the same order as for other asteroids. If acceleration of the asteroid is caused by sublimation of matter, then the corresponding value of A_2 should be much greater, about 10^{-10}–10^{-11} AU/day^2, as it is for comets. So, this small body should be considered more as an asteroid than a comet.

Figure shows values of A_2 versus diameters of asteroids. One can see that asteroids with the smaller diameters have the largest absolute values of A_2.

Table 1. Values of transverse component, A_2 , in increasing order of errors in A_2 for 94 NEAs

Number	A_2 (10^{-14} AU/day^2)	Number	A_2 (10^{-14} AU/day^2)	Number	A_2 (10^{-14} AU/day^2)
433	0.02 ± 0.03	5011	–2.81 ± 0.50	65679	–2.83 ± 0.93
1862	–0.51 ± 0.04	14402	–0.95 ± 0.51	**2001BE10**	–3.77 ± 0.93
1685	0.06 ± 0.05	**10115**	–0.54 ± 0.54	**5604**	2.65 ± 0.99
1620	–0.14 ± 0.07	1916	3.04 ± 0.56	**4183**	–0.90 ± 1.05
4179	–0.56 ± 0.07	88710	–7.62 ± 0.56	162173	–3.48 ± 1.06
2100	–1.54 ± 0.13	1943	0.18 ± 0.58	21374	0.95 ± 1.11
85953	–1.49 ± 0.16	2340	–2.46 ± 0.58	**4197**	8.46 ± 1.13
152563	–2.54 ± 0.17	3361	1.74 ± 0.59	172034	3.74 ± 1.15
162004	2.16 ± 0.18	**2062**	–0.25 ± 0.60	1917	–3.30 ± 1.15
1566	–0.23 ± 0.18	**1866**	–1.65 ± 0.60	**2201**	1.38 ± 1.18
3200	–0.30 ± 0.18	719	–0.30 ± 0.61	17182	1.13 ± 1.24
1580	–0.62 ± 0.19	**3103**	1.48 ± 0.62	**85774**	4.27 ± 1.26
6489	–1.21 ± 0.19	**6037**	–2.21 ± 0.63	137924	–0.60 ± 1.28
3908	3.60 ± 0.23	11054	–0.07 ± 0.66	**4450**	–3.02 ± 1.28
1627	0.19 ± 0.24	2212	2.52 ± 0.69	85989	3.88 ± 1.30
7350	–2.35 ± 0.29	162080	–1.85 ± 0.71	**7341**	4.96 ± 1.30
1980	0.23 ± 0.31	1863	4.56 ± 0.73	67399	–4.94 ± 1.30
1865	–1.03 ± 0.31	**35107**	2.98 ± 0.76	6047	1.14 ± 1.31
105140	0.13 ± 0.33	137925	3.87 ± 0.77	1994AW1	2.02 ± 1.33
22753	–1.24 ± 0.34	1864	–4.41 ± 0.78	37655	–2.82 ± 1.33
161989	1.13 ± 0.35	4015	–2.86 ± 0.80	4947	5.41 ± 1.34
1036	–2.44 ± 0.35	207945	–1.24 ± 0.80	5693	3.11 ± 1.35
68950	–2.80 ± 0.42	5797	–2.08 ± 0.80	2102	–1.49 ± 1.36
40267	0.31 ± 0.43	99935	0.33 ± 0.82	152561	0.73 ± 1.38
99907	1.34 ± 0.43	137170	–4.04 ± 0.82	**6239**	–3.90 ± 1.39
87684	0.00 ± 0.45	**5660**	–3.33 ± 0.82	**7753**	–7.09 ± 1.41
87309	4.27 ± 0.45	2001MQ3	–3.35 ± 0.84	5143	2.08 ± 1.45
1981	–0.88 ± 0.45	10302	9.54 ± 0.89	**68348**	–4.77 ± 1.45
3753	–2.06 ± 0.45	53789	3.94 ± 0.90	152756	–11.08 ± 1.46
887	–0.32 ± 0.46	85770	–5.86 ± 0.91	152895	7.61 ± 1.49
2063	–2.47 ± 0.46	11284	1.45 ± 0.92		
1221	0.95 ± 0.50	**11500**	6.16 ± 0.93		

The abundance of some negative values of A_2 can be explained by the existence of two components of the YE — seasonal (have negative values of A_2) and daily (have negative or positive values of A_2) effects.

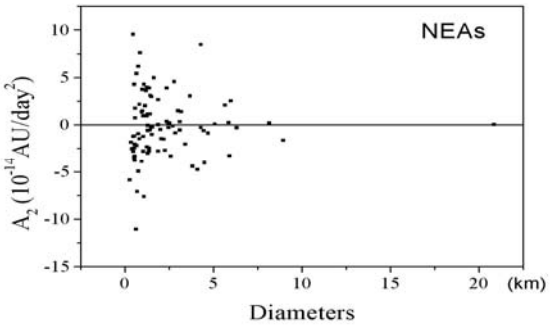

A_2 versus diameters of NEAs.
$\sigma_{A_2} < 1.5\times 10^{-14}$ AU/day^2, diameters < 25 km.

Table 2. Residuals of some optical observations of the asteroids 68950, 85953, 152563, 162004 after fitting without accounting for YE (the second column) and with accounting for YE (the third column) (residuals rejected in the course of fitting are given in brackets)

Date	Δα cos δ, ″	Δδ, ″	Δα cos δ, ″	Δδ, ″
	Without accounting for YE		With accounting for YE	
Asteroid 68950			**$A_2 = -2.9 \pm 0.4$**	
1955.07.23.239942	(1.53)	0.23	–0.31	–0.53″
1955.07.23.274662	(2.06)	(1.46)	0.23	0.69
Asteroid 85953			**$A_2 = -1.6 \pm 0.2$**	
1971.03.26.3063786	0.83	0.28	(–2.54)	0.79″
1971.03.26.3105486	(3.26)	–1.31	–0.12	–0.79
1971.03.26.3147186	(4.21)	–0.19	0.83	0.33
1971.03.26.3452686	0.12	0.49	(–3.26)	1.01
1971.03.26.3494386	(2.64)	–0.42	–0.73	0.10
1971.03.26.3535986	(3.60)	–0.67	0.22	–0.16
Asteroid 152563 *			**$A_2 = -2.5 \pm 0.2$**	
1953.01.10.137162	(6.47)	(2.93)	–0.44	0.48
1953.01.10.144102	(6.90)	(2.97)	0.00	0.52
1953.01.12.137162	(6.64)	(4.99)	0.16	(2.72)
1953.01.12.144102	(6.38)	(5.26)	–0.10	(3.00)
Asteroid 162004			**$A_2 = 2.2 \pm 0.2$**	
1954.11.24.221189	(–2.83)	(–2.11)	0.95	–0.22
1954.11.24.252439	(–3.39)	(–2.46)	0.38	–0.57
1954.11.24.255919	(–3.93)	(–2.17)	–0.15	–0.28
1954.11.24.264249	(–3.98)	(–2.33)	–0.21	–0.44

***** For asteroid 152563 a similar result was obtained in [4] by another method.

As a rule, accounting for the YE results in decreasing the unit weight error.

Moreover, for some asteroids, 68950, 85953, 152563, 162004, (Tab. 2) accounting for the YE permits one to include more optical observations to improve the process, especially remote observations. For asteroid 152563 a similar conclusion was obtained by a different method in [4]. In this table the residuals rejected in the course of fitting are given in brackets.

Conclusions

To evaluate the YE, the model of motion should be as complete as possible.

The YE can be estimated by using only optical observations.

For a number of asteroids taking into account the YE permits inclusion of additional optical observations in the fitting process, especially remote observations.

In determining asteroid masses by the dynamical method it seems to be useful to combine it with A2 estimates when a small, perturbed asteroid is used as a test particle.

References

1. *Bottke W. F., Vokrouhlicky D., Rubicam D. P. et al.* The effect of Yarkovsky thermal forces on the dynamical evolution of asteroids and meteoroids // In Asteroids III / Eds: Bottke W.F., Cellino A., Paolicchi, Binzel R.P. Univ. Arizona Press. 2003. P. 395–408.
2. *Chernetenko Yu. A.*Yarkovsky effect in the motion of asteroids // Trudy Vserossijskoj astronomicheskoj konferentsii "VAK–2007", Kazan'. 2007. P. 103–104 (in Russian).
3. *Chesley S. R., Ostro S. J., Vokrouhlicky D. et al.* Direct Detection of the Yarkovsky Effect via Radar Ranging to Asteroid 6489 Golevka // Sci. 2003. Vol. 302. P. 1739–1742.
4. *Vokrouhlicky D., Chesley S. R., Matson R. D.* Orbital identification for asteroid 152563 (1992 BF) through the Yarkovsky effect // Astron. J. 2008. Vol. 135. P. 2336–2340.

The Asteroid-Comet Hazard Conference Proceedings, 2009

Estimating the Accuracy of Asteroid Ephemerides Using the Bootstrap Method

J. Desmars[1], J.-E. Arlot[1], A. Vienne[1,2]

[1]Institut de Mécanique Céleste et de Calcul des Ephémérides — Observatoire de Paris, Paris, France
[2] Laboratoire d'Astronomie de Lille, Université de Lille, Lille, France

Abstract. The accuracy of solar system object ephemerides can be estimated by the bootstrap method. This method uses minimal assumptions on the observations. We apply the bootstrap method to two NEOs: Toutatis and Apophis. We provide an estimate of the accuracy of their ephemerides and an estimate of the accuracy of their next close approach to Earth.

Introduction

The accuracy of ephemerides can be determined by statistical methods that consist in creating a set of possible orbits. To create possible orbits, the classical way is to apply small variations on initial conditions and to measure the difference of orbits provided by these initial conditions. Small variations can be estimated using the covariance matrix of the problem or by adding noise to the observations and then determine new initial conditions by fitting to these observations. All these methods assume that the distribution of observational errors is Gaussian.

The bootstrap method uses minimal assumptions and allows the estimation of the region of possible motions. This method has been successfully applied to Saturnian satellites and has provided an estimate of ephemerides accuracy of these satellites [1]. We propose to apply the bootstrap method to two near-Earth asteroids: (4179) Toutatis and (99942) Apophis.

The bootstrap method

The idea of the bootstrap is to mimic the whole sampling process in order to create a new set. For a set with N elements, the bootstrap sample is obtained by sampling N times with replacement among the N elements. Then,

the model is fitted to the bootstrap sample through least-squares method (LSM) and a new orbit is determined. This process can be repeated as many times as desired (see [1] for more details). Contrary to other classical methods, the only underlying assumption of the bootstrap is that observations are independent in the sampling process. In particular, the noise level is allowed to vary between observations, and the errors can be non-Gaussian.

Dynamical model and observations

The dynamical model used for an asteroid is the Numerical Orbit and Ephemerides (NOE) based on the work developed in [2] applied to asteroids. Equations of asteroid motions are numerically integrated. The perturbations of the eight major planets, Pluto, and the Moon are taken into account. The positions of the planets, Pluto, and the Moon come from JPL DE406. Variational equations are integrated simultaneously with the equations of motions.

(4179) Toutatis was discovered in 1989. 2701 observations from 1934 to 2007 are tabulated by the Minor Planet Center. Most of observations have been done between 1989 and 2007. (99942) Apophis was discovered in 2004. 1000 observations from 2004 to 2006 are available.

Accuracy of ephemerides

The bootstrap method was applied for Toutatis and Apophis in order to estimate the accuracy of their ephemerides. 500 and 1048 bootstrap samples have been created for respectively Toutatis and Apophis. Fig. 1 represents the RMS distance between positions of asteroid according to the K bootstrap orbits and the nominal one (or the accuracy of the NEO ephemerides for distance). We note that the accuracy is quite good during the observational period (about 30 km for Toutatis) but decreases outside this period.

Accuracy of close approach

The next three close-approaches of Toutatis (less than 0.1 AU) will be in 2012, 2069 and 2322. For each one, we have computed moment and minimum distance from the Earth for the 500 bootstrap orbits, which provides the accuracy of the close approach (Fig. 2). In 2012, the accuracy of the close approach is about 200 km in distance and 15 seconds in time. In 2069, the accuracy is 7 minutes in time but about 130 km in distance. For 2322 computed data are so different (84 hours in time and $2.5 \cdot 10^6$ km in distance) that the prediction of the next close approach is impossible.

We have applied the same method for Apophis. It appears that the accuracy of the close approach on April 13, 2029, is about 2 seconds in time and 6,000 km in distance. Because of the short distance between the Earth and Apophis (less than 40,000 km), the trajectories of different bootstrap orbits will evolve very differently. Thus, there is a non-zero probability of collision with Earth in 2036 because one of the bootstrap orbits reaches a minimum distance less than one Earth radius.

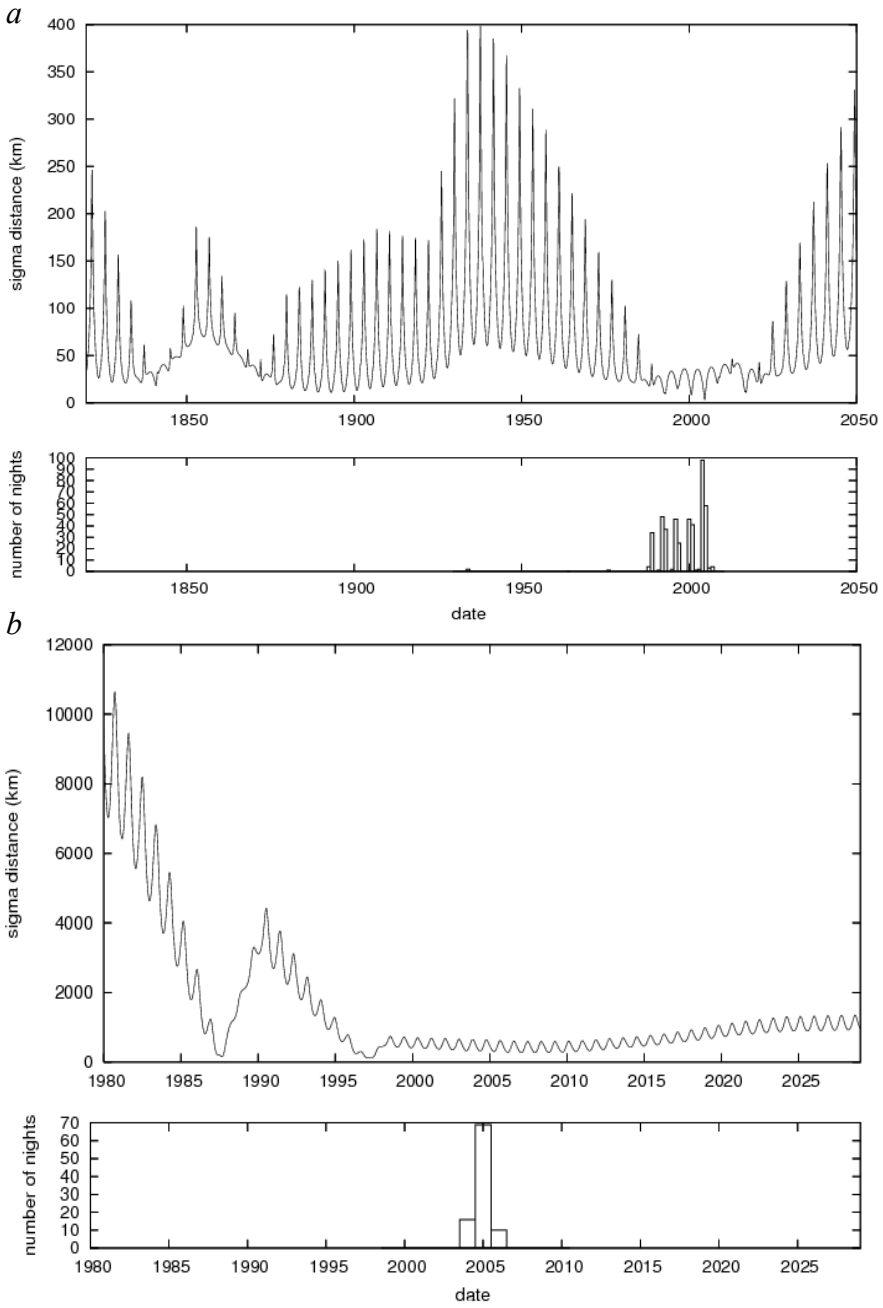

Fig. 1. Extrapolated root mean square for (*a*) Toutatis from 1820 to 2050 and for (*b*) Apophis from 1980 to 2029.
Histograms of observation nights per year are also indicated.

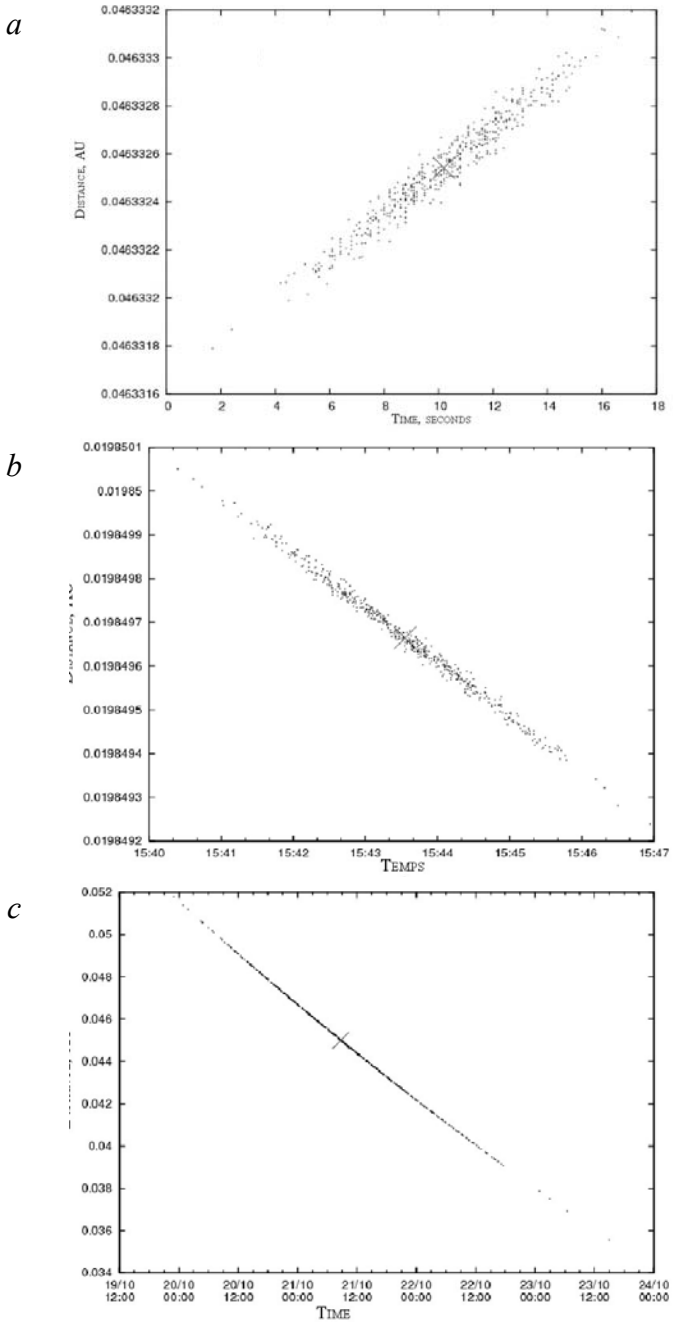

Fig. 2. Minimum distance between Toutatis and Earth for the 500 bootstrap orbits created. Cross represents minimum of reference orbit.
a — on December 12, 2012, at 6^h40^m; *b* — on November 5, 2069; *c* — on October 2322.

Conclusion

The bootstrap method allows estimating the accuracy of NEO ephemerides. Moreover, the bootstrap method uses minimal assumptions and can be easily implemented. The accuracy of close approach can also be quantified by bootstrap method and finally, the risk of collisions can be estimated.

References

1. *Desmars J., Arlot S., Arlot J.-E. et al.* Estimating the accuracy of satellite ephemerides using the bootstrap method // Astron. Astrophys. 2009. Vol. 499. P. 321–330.
2. *Lainey V, Duriez L., Vienne A.* New accurate ephemerides for the Galilean satellites of Jupiter — I. Numerical integration of elaborated equations of motion. 2004 // Astron. Astrophys. 2004. Vol. 420. P. 1171–1183.

The Asteroid-Comet Hazard Conference Proceedings, 2009

Paths of Risk of Selected Dangerous Asteroids

I. Włodarczyk

Chorzów Astronomical Observatory, Chorzów, Poland

Abstract. The paths of risk (corridors of risk) computed by the author for Apophis impact in 2036 and for 2007HJ impact in 2077, taken from Impact Risk Page of the NASA, are presented.

Introduction

Usually impact solutions are presented in the form similar to that of the Impact Risk Page of NASA: (*http://neo.jpl.nasa.gov/risk/*) or that of NEODyS: (*http://newton.dm.unipi.it/neodys/index.php?pc=4.0*). For potentially dangerous objects they give the name of the asteroid, date(s) of possible impact(s), probability of impact, impact energy, and estimate of impact risk by Torino and Palermo scales. Both NASA and NEODyS monitor possibilities of future impacts over the next 100 years.

Method of computing

The author's method of determining the path of risk for an asteroid collision with Earth is as follows:

1. Selecting a dangerous asteroid from NASA's Impact Risk Page.
2. Reading observations of the selected asteroid from the MPC site *http://www.cfa.harvard.edu/iau/services/WebCSAccess.html* or from NEODyS site *http://newton.dm.unipi.it/neodys/*
3. Computing the orbit of the asteroid with the use of the OrbFit software, *http://adams.dm.unipi.it/~orbmaint/orbfit/*
4. Computing clones of the asteroid; following their motion over 100 years in the future and looking for close approaches and impacts with the Earth.
5. Computing impact orbit and clones for the epoch several days before impact.
6. Computing close approaches of impact clones with the use of the Mercury software [1].

7. Drawing the path of risk of impact clones on the map of the Earth with the use of author's software.

As an example, we present in Fig. 1 the path of risk of asteroid (99942) Apophis in 2036 and in Fig. 2. that of asteroid 2008HJ in 2077.

All computations were made with the use of the free software OrbFit ver. 4.0. with settings: multiple solution [2], 3 sigma, 2001 clones, ephemerides JPL NASA DE405, and no additional perturbing massive asteroids.

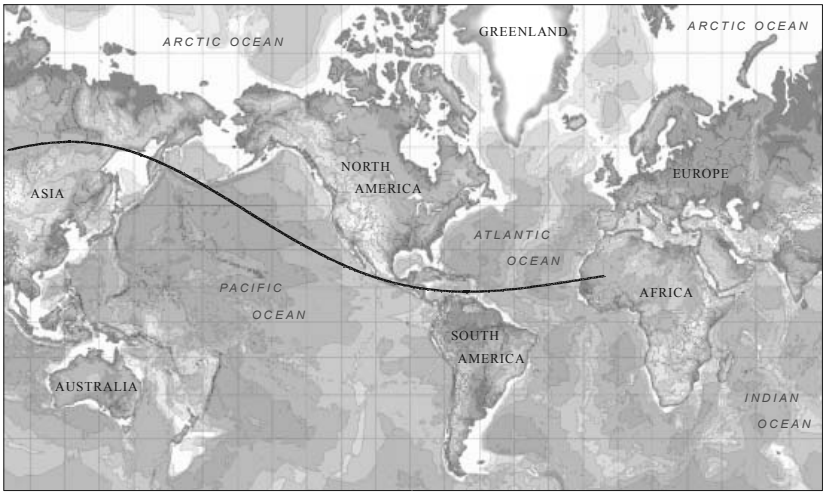

Fig. 1. Path of risk of asteroid (99942) Apophis on 2036/04/13.37.

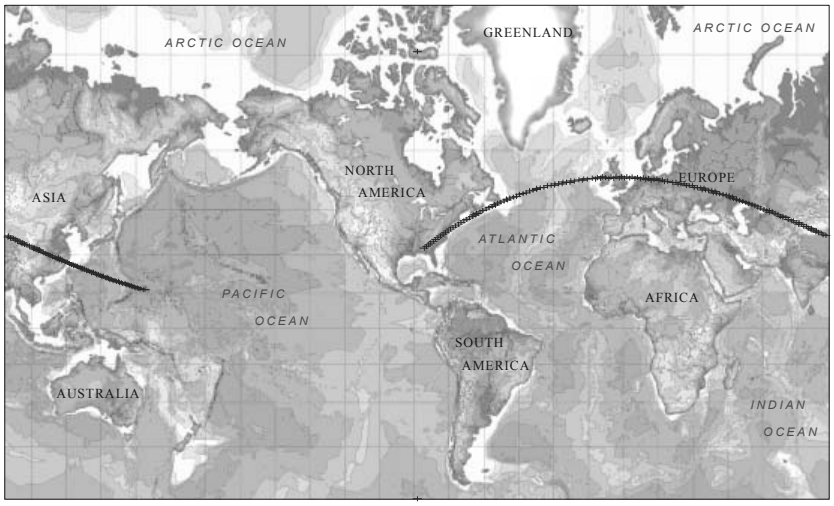

Fig. 2. Path of risk of asteroid 2008HJ on 2077/05/02.71.

Conclusion

From our experience one can conclude that the OrbFit software is well suited for computation of impact orbits of dangerous asteroids and predicting the path of risk on the Earth.

References

1. *Chambers J.* A Hybrid symplectic integrator that permits close encounters between massive bodies // Mon. Not. 1999. Vol. 304. P. 793–799.
2. *Milani A., Sansaturio M. E., Tommei G., Arratia O. et al*. Multiple solutions for asteroid orbits: Computational procedure and applications // Astron. Astrophys. 2005. Vol. 431. P. 729–746.

The Asteroid-Comet Hazard Conference Proceedings, 2009

Impact Solutions for Asteroid (101955) 1999RQ$_{36}$

I. Włodarczyk

Chorzów Astronomical Observatory, Chorzów, Poland

Abstract. Impact solutions for asteroid (101955) 1999 RQ$_{36}$ are presented for different models of the Solar System and with and without the Yarkovsky effect. Also the impact orbit of asteroid for 2185 has been computed.

Introduction

Recently, in a paper by Milani et al. [1], possible impacts of asteroid (101955) 1999RQ$_{36}$ with Earth over a long time period were computed. Usually NEODyS and NASA monitor possibilities of future impacts over the next 100 years. However, this time the work was extended to the second half of the 22nd century. In such long periods of time it is necessary to account for influence of the Yarkovsky effect on the motion of asteroids.

The author of the present paper investigated the influence of different ephemerides of the major planets, that of additional perturbations from the most massive asteroid as well as the Yarkovsky effect on impact solutions for asteroid (101955) 1999RQ$_{36}$. In particular, differences between possible dates of impact solutions obtained with the use of the JPL DE405 and JPL DE406 Ephemerides were found. Also the influences of additional perturbations from Ceres, Pallas, and Vesta were studied. In addition the influence of the Yarkovsky effect on impact solutions was studied using the free software OrbFit v.4.0 (see *http://adams.dm.unipi.it/~orbmaint/orbfit/*). The necessary parameters for computing the Yarkovsky effect were taken from [1].

Method of computing

To compute the influence of the Yarkovsky effect on the motion of the asteroid we used da/dt = –16.80E-4 AU/Myr from [1]. The results are presented in Table.

All computations were made with the OrbFit ver. 4.0. software with settings: multiple solution [2], 3 sigma, and 2001 clones. Observations of asteroid (101955) $1999RQ_{36}$ were taken within the time span from 1999/09/11.40624 to 2006/05/26.19953. Of 303 observations (290 optical and 13 radar) 295 were used. The orbit of the asteroid was computed with the rms = 0.524".

From Table one can see that during such long time span it is necessary to take into account the influence of the Yarkovsky effect as well as perturbations from additional massive asteroids. Moreover, the effect of different dynamical models of the Solar System is noticeable.

Impact solutions of asteroid (101955) $1999RQ_{36}$ with and without Yarkovsky effect.

DE405			
3 asteroids		0 asteroids	
With Y. effect	without Y. Effect	With Y. Effect	without Y. effect
2195/09/25.000	2185/09/24.628	2182/09/24.929	2185/09/24.627
2196/09/24.342	2185/09/24.622	2182/09/24.933	2185/09/24.622
	2185/09/24.598	2187/09/24.858	
	2192/09/24.328	2188/09/24.246	
		2188/09/24.270	
		2191/09/24.983	
		2195/09/25.077	
		2195/09/25.078	
DE406			
2195/09/25.018	2185/09/24.629	2182/09/24.929	2185/09/24.628
2196/09/24.342	2185/09/24.620	2182/09/24.933	2185/09/24.621
2197/09/24.505	2185/09/24.603	2187/09/24.977	2191/09/24.955
	2192/09/24.336	2187/09/24.862	
		2187/09/24.874	
		2188/09/24.248	
		2188/09/24.273	
		2193/09/24.543	
		2195/09/25.077	
		2195/09/25.080	

It is clear that the radar observations play an important role. Without radar observations no impact solution was found for settings: sigma = 1.4, 2001 clones, 0 massive asteroids, and JPL DE405. After the radar observations were included a possible impact in 2185 was found. For prognostic impact in 2185/09/24.628 (JPL DE405, 3 asteroids, without Yarkovsky effect) several impact orbits together with their errors (1-sigma) were found (see Tab. 1). One of them (number 3) is given below:

Starting epoch for all orbits is the same: JD2454800.5 = 2008/11/30.

Keplerian elements — *a, e, i,* longitude of node, argument of perihelion, mean anomaly [deg]:

1.12631446858696E+00 0.203790267574845 6.0347807362354 2.0684643914846 66.2142175087641 193.4207233913870.

RMS: 1.18553E-10 3.43268E-08 4.38898E-06 5.66182E-06 6.48023E-06 3.66332E-06.

Epoch of orbital elements is given for date seven days before impact — JD2519374.5 = 2185/09/17:

1.111314861650991 .1976048925735216 6.283852677924837 359.584277857674 71.15720015725316 302.6858782293254.

The asteroid moving in this orbit impacts the Earth! It is the impact orbit.

Conclusion

From our computations one can see that with the use of the OrbFit software it is possible to construct the precise dynamical model of asteroid motion that is of critical importance for predicting a possible impact with the Earth.

References

1. *Milani A., Chesley S. R., Sansaturio M. E., Bernardi F., Valsecchi G. B., Arratia O.* Long-term impact risk for (101955) 1999 RQ36 // Icarus. 2009. Vol. 203. P. 460–471.
2. *Milani A., Sansaturio M. E., Tommei G., Arratia O. et al*. Multiple solutions for asteroid orbits: Computational procedure and applications // Astron. Astrophys. 2005. Vol. 431. P. 729–746.

The Asteroid-Comet Hazard Conference Proceedings, 2009

The Study of the Probability of an Asteroid Collision with a Planet by Monte Carlo Method

N. B. Zheleznov

Institute of Applied Astronomy of RAS, St. Petersburg, Russia

Abstract. The close approach of asteroid (99942) Apophis to the Earth on April 13, 2029, and 2007 *WD*5 to Mars on January 30, 2008, have been researched taking into account the sets of observations giving maximal estimates of encounter probability. Our estimates of probability obtained by the Monte Carlo method resemble those published on the web site of JPL, NASA.

In the considered examples it is shown that neglecting correlations between orbit parameters in the covariance matrix can lead to poor results for predicted collision probabilities.

Introduction

The collision probability of an asteroid with a planet can be estimated by the Monte Carlo method. The essence of the method is the statistical modeling for possible initial conditions of asteroid motion on the basis of a distribution of the probability density defined by a corresponding covariance matrix, and subsequent tracing of the motion of possible (virtual) asteroids according to the accepted orbital model. As a result the collision probability is defined as the relation of the found number of collisions to the total number of tests.

The basic problem lies in the fact that different components of initial conditions (the elements of an orbit, i. e., the coordinates and velocities) are correlated and cannot be assumed independently from each other. A manifestation of these correlations is the non-diagonal form of the covariance matrix.

Since the covariance matrix is symmetric it can be transformed into diagonal form by an orthogonal transformation of the initial six-dimensional coordinate frame. As a first step the covariance matrix can be transformed

into a three-diagonal form, and then the *QL*-algorithm with implicit shift returns the elements of the diagonal matrix.

In the new (transformed) coordinate system the choice of initial values for each of the six orbital parameters can be set independently from each other by taking into account the normal distribution of the probability density depending on the elements of the diagonal covariance matrix. A program for calculating the normal distribution has been developed on the basis of the central limit theorem using the generator of pseudo-random numbers in Fortran. Each sample of initial values of six parameters of an orbit is transformed into the initial coordinate system by return transformation, and then the asteroid motion is traced by numerical integration for the purpose of determining the possible collision with a planet.

In this study we illustrate using asteroids (99942) Apophis and 2007 *WD*5 as examples that not accounting for correlations can result in appreciable distortions of the estimated collision probability. This occurs when large non-diagonal elements of the covariance matrix are ignored.

Collision probabilities of (99942) Apophis with the Earth on April 13th, 2029, and 2007 *WD*5 with Mars on January 30th, 2008, are calculated based on observations leading to nonzero probabilities of collisions. These results are compared with corresponding results on the website of JPL, NASA.

It is shown by the example of 2008 *TC*3 how, in the case of 100 % collision probability, not accounting for correlations influences the accuracy of determining the place of impact on Earth.

Study of collision probability of (99942) Apophis with the Earth

On the basis of the first 176 observations of (99942) Apophis published in MPEC on December 27th, 2004 [1] it was shown that the probability of its collision with the Earth on April 13th, 2029, is about 2.7 % (1/37).

On the basis of these observations we have computed the state vector and its covariance matrix in the equatorial heliocentric coordinate system using the programs developed in IAA RAS.

Using the covariance matrix, 2000 estimates of an initial state vector (2000 virtual asteroids or clones) were obtained taking into account correlations between the covariance matrix elements as described above. In addition 2000 estimates were obtained of the same vector without considering correlation dependences (another set of 2000 clones). In Figs. 1 and 2 we show for (99942) Apophis the distributions of coordinates of 2000 virtual asteroids obtained at the initial moment of time by these two methods.

Comparison of the figures shows the essential distinction in the distributions of the choice of initial positions made with accounting and without accounting for correlations. A similar distinction is observed for the initial velocities.

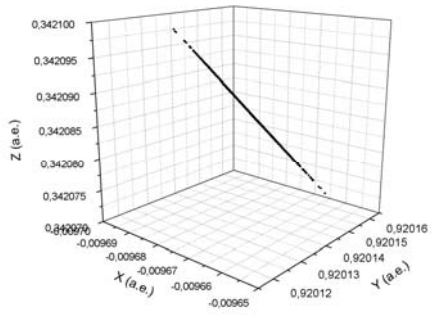

Fig. 1. Initial distribution of coordinates of (99942) Apophis taking into account correlations.

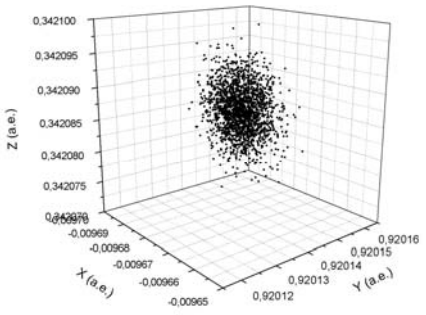

Fig. 2. Initial distribution of coordinates of (99942) Apophis without considering correlations.

The motion of each virtual asteroid in both cases was traced by numerical integration. Integration was carried out taking into account the perturbations from all major planets on the basis of theory DE405, and also from Ceres, Pallas, and Vesta.

In Figs. 3 and 4 the distribution of coordinates of the same virtual asteroids on May 13th, 2031 (JD = 2463000) is shown. For more than 26 years initial ellipsoids "were extended" along all heliocentric orbits of (99942) Apophis, and a portion of orbits, most likely having the closest approach with the Earth on April 13th, 2029, "were removed" from the general group, having formed some loop similar in form of an orbit. The obtained distributions of the virtual asteroids differ strongly. Such distinctions can significantly influence the estimates of collision probabilities.

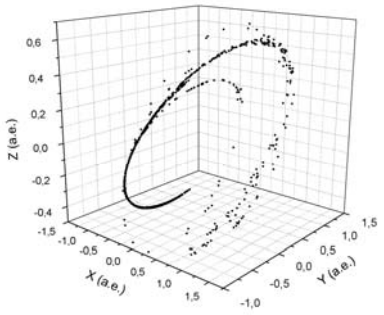

Fig. 3. The distribution of coordinates of (99942) Apophis taking into account correlations.

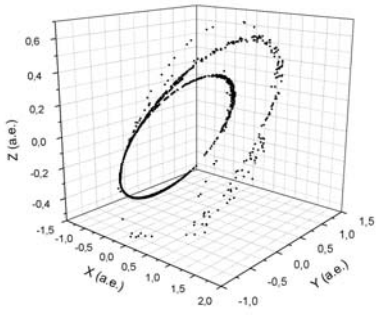

Fig. 4. The distribution of coordinates of (99942) Apophis not taking into account correlations.

For (99942) Apophis not accounting for correlations leads to a larger collision probability (1/29) compared to the case accounting for correlations (1/51).

Study of approaching of 2007 *WD*5 with Mars

The nominal orbit and the covariance matrix of 2007 *WD*5 were defined on the basis of the observations published on NEODyS of the University of Valladolid (Spain). The estimates of collision probability of the asteroid with Mars were calculated for those dates when corresponding estimates on the web site of JPL are available [2].

In total 45 observations covering a time span from November 8th, 2007 to January 8th, 2008 have been used. 4000 initial orbits were chosen. Calculations were carried out taking into account correlations in an initial state vector.

In Tab. 1 in the first column are given the date of calculations; in the second, number of observations as of this date; in the third, the time interval covering observations; in the fourth, the number of orbits out of 4000 that lead to an impact on Mars; in the fifth, the collision probabilities calculated by us; and in the sixth, the collision probabilities published on the JPL web site.

Table 1**.** Collision probability of 2007 *WD*5 with Mars

Date	Number of obs.	Time interval	Number of Impacts	Probability by our estimate	Probability by JPL estimate
21.12.07	25	20.11.07–19.12.07	62	1.5 % 1/65	1.3 % 1/75
28.12.07	28	08.11.07–19.12.07	148	3.7 % 1/27	3.9 % 1/25
02.01.08	32	08.11.07–31.12.07	106	2.7 % 1/38	3.6 % 1/28
08.01.08	44	08.11.07–07.01.08	62	1.5 % 1/65	2.5 % 1/40
09.01.08	45	08.11.07–08.01.08	0	0	0.001 %

In the case without considering correlations the estimate of collision probability of 2007 *WD*5 with Mars was always equal to 0, independently of used observations.

Study of the impact of 2008 *TC*3

It is interesting to study the approach of an asteroid to a planet in the case when the collision probability is equal to 100 %. Such an object is 2008 *TC*3 [3].

In our study the minimum distances (MDs) between virtual asteroids (clones of 2008 *TC*3) and Earth center on the basis of the first 47 observations and for 566 observations was calculated. The calculated minimal distances in all cases were less than the radius of the Earth. In

Tab. 2 results for MDs and root-mean-square error of MDs calculated with accounting correlations in covariance matrix and without accounting for them are given.

Table 2. Minimum distances (MDs) and σ_{MDs} for clones of 2008 *TC*3 calculated with accounting the correlations in the covariance matrix and without accounting for them for the first 47 and 566 observations

Correlations & number of observations	MDs, km	σ_{MDs}, km
Correlations, 47 obs.	5854.7–5860.2	1.69
Without corr., 47 obs.	5799.4–5911.4	14.91
Correlations, 566 obs.	5851.3–5851.7	0.06
Without corr., 566 obs.	5848.8–5854.2	0.82

As seen from Tab. 2, MDs calculated with due regard for correlations between the covariance matrix elements is more precise than in the case without accounting for these correlations for any set of observations.

Conclusion

It is shown that not taking correlations into account can lead to appreciable distortions of the estimates of collision probabilities of asteroids with planets. The estimates of collision probability for asteroids 2007 *WD*5 with Mars and (99942) Apophis with the Earth on the basis of short arc sets of observations leading to probabilities essentially distinct from zero have been obtained. Our estimates are similar to those of on the JPL web site.

References

1. *Williams G.* MPEC 2004-Y66 // MPC. Cambridge, MA 02138, USA. 27 Dec. 2004.
2. *Yeomans D.* Asteroid 2007 WD5 // See *http://neo.jpl.nasa.gov/2007 wd5/*, 2008.
3. *Williams G., Gareth V.* MPEC 2008-T50 // MPC. Cambridge, MA 02138, USA. 08 Oct. 2008.

A'Hearn
Michael
USA

Part 7. Investigation of NEOs in situ. Counteraction to the NEO Hazard

The Asteroid-Comet Hazard Conference Proceedings, 2009

INVESTIGATION OF NEOS IN SITU. COUNTERACTION TO THE NEO HAZARD

Estimating the NEO Population and Impact Risk: Past, Present and Future

A. W. Harris

Space Science Institute, Boulder, Colorado, USA

Abstract. As Near-Earth Object (NEO) surveys continue, we improve our knowledge of the population of NEOs and become better able to estimate both the total population versus size and the fraction that remains undiscovered. As of January 19, 2009, the present surveys had discovered 765 Near-Earth Asteroids (NEAs) larger than 1 km in diameter out of an estimated total population of 940, or about 81 % of that population. Since most of the risk resides in the largest impactors, finding that fraction of the largest bodies, and that none of them has a significant chance of impacting in the next century or so, "retires" more than 90 % of the impact risk, including most of the risk of a globally catastrophic impact event. It appears that ground damage extends to considerably smaller impactor sizes than was previously inferred by modeling them as equivalent to nuclear airbursts. This increases the expected frequency of damaging events, although it only modestly increases the "fatality rate", since the smallest events are not very damaging. In the mid-size range, from ~150 m to ~1 km, the main risk is from tsunami generated by an ocean impact. The detailed analyses of the 2003 NASA SDT report estimated a "persons affected" rate of ~182 per year associated with impact tsunami. They did mention that for earthquake-generated tsunami, the actual death rate is typically only 10 % or less of the population in the inundation zone, but did not take full account of that in their risk analysis. Here we re-evaluate the impact hazard, using our new population and completion estimates, and revised "kill curves" including the airburst damage down to smaller size and lower tsunami fatality rate. We estimate that the *a priori* impact risk (not allowing for any discovered NEAs) is (was) ~40/year for local/regional land impacts, ~6/year from impact tsunami (the dramatic decrease in this number is due to a reduction of a factor of 3 in the estimated population in this size range,

times the factor of 10 reduction due to expected actual deaths in the inundation zone), ~1100/year due to globally catastrophic events, and ~10/year from comet nucleus impacts. With the current level of survey completion, the remaining risk from the undiscovered population is ~20/year from local/regional land impacts, ~4/year from impact tsunami, ~54/year from globally catastrophic events, and still ~10/year from comet nuclei. It is noteworthy that even though the risk from globally catastrophic events has been 95 % retired for the short term, it is still the largest component of the remaining risk. Looking to the future, the "next generation survey", aimed to find 90 % of NEAs larger than 140 m diameter, will further reduce the impact risk, using our models of population, completion, and impact damage, to ~6/year from local/regional land impacts, ~0.3/year from impact tsunami, ~11/year from globally catastrophic events, and ~10/year from comet nuclei. In addition to providing long-term (decades) warning of an impact, optical surveys have the capability to spot an impending impactor days or weeks before an impact, if it is coming from a direction being covered by the survey (currently ~35 % of the sky area), providing short term warning long enough for evacuation of affected area or other "civil defense" measures*.

Introduction

In the 2003 NASA Near-Earth Objects (NEO) Science Definition Team report [1] a simple power law model for the NEO population was assumed, and in the 2006 NASA report [2], the same model was used. Even at the time of the earlier report, a significant deviation from the straight-line (on a log-log plot) population was indicated. A more recent population estimate [3, 4] confirms the deviation, most importantly in the smaller range of size, 50–500 m diameter, important for impact hazard estimation of sub-global consequence events. Additionally, the estimates of damage versus size of impact developed in the 2003 study and used essentially unchanged in the 2006 study, have been questioned in two important aspects. In the smallest size range where damage is due to airburst rather than actual impact, recent studies by Boslough [5] suggest that the earlier estimates used in the NASA reports underestimate damage in the size range up to around 200 m diameter of NEA. In the size range just above that, from about 250 m up to 1–2 km, it was estimated that most damage would be from tsunami generated by an ocean impact. There are recent calculations by Gisler et al. [6] suggesting

---

*This paper by A. Harris is analogous to paper of the same author that will appear in Proceedings of the 2009 IAA Conference, "Planetary Defense", ESA Conference Publication.

that the magnitude of a tsunami caused by an impact into deep ocean may have been over-estimated, and furthermore, the earlier studies, while recognizing that only a minority of the affected population would be expected to die in a tsunami inundation, the non-fatality damage was arguably over-estimated. In this paper we present the revised population estimate. Using that population model to derive an impact frequency vs. size, and a revised "kill curve" over the range of sub-global impacts, we derive a new estimate of the impact hazard. We present estimates of the impact risk vs. size for the intrinsic population, that is what it was before any NEOs were discovered, what the short-term risk is now (over the time, ~50 years, in which we can certify that none of the discovered NEOs will impact), and finally, we estimate the residual impact risk that will remain after the "mandate" of the U. S. Congress is met, of discovering 90 % of all NEOs with D > 140 m.

There is a minor distinction to be made between Near-Earth Asteroids (NEAs) and Near-Earth Objects (NEOs). In either case, "Near-Earth" implies objects whose orbits have perihelia closer to the sun than 1.3 Astronomical Units (AU), thus they cross the orbit of Mars and approach the orbit of the Earth. Among those, NEAs include only asteroids, while NEOs include also comet nuclei, the latter being only a very small fraction of the impact risk [1]. A further subset is the so-called "Potentially Hazardous Asteroids (PHAs), which are asteroids whose orbits come within 0.05 AU of intersection with the Earth's orbit. By analogy, "PHO" would be the same including comet nuclei, even though it is more commonly used as the name of a kind of Vietnamese soup.

Near-Earth asteroid population

The most effective way to estimate the population of NEAs is to go out and look, with a controlled telescope survey. As the survey progresses and more objects are found, our knowledge of the population that remains to be found improves. Fig. 1, taken from my 2007 report to NASA, is the most recent population estimate covering the full range of sizes of NEAs. The actual measured quantities are the absolute magnitude, *H*, and the cumulative number of objects larger (brighter) than the given value of *H*. *H* is an astronomical magnitude scale that is logarithmic with 5 magnitudes representing a factor of 100 in brightness, with smaller numbers corresponding to brighter objects. The normalization of the scale is such that for an assumed albedo of 0.14, $H = 17.75$ corresponds to an object 1 km in diameter. The diameter scale below the plot is adjusted for this equivalence. As the survey progresses to include enough objects to statistically characterize the orbits, it becomes possible to calculate the mean impact frequency of objects from that distribution of orbits. The scale on the right is so derived, and corresponds to

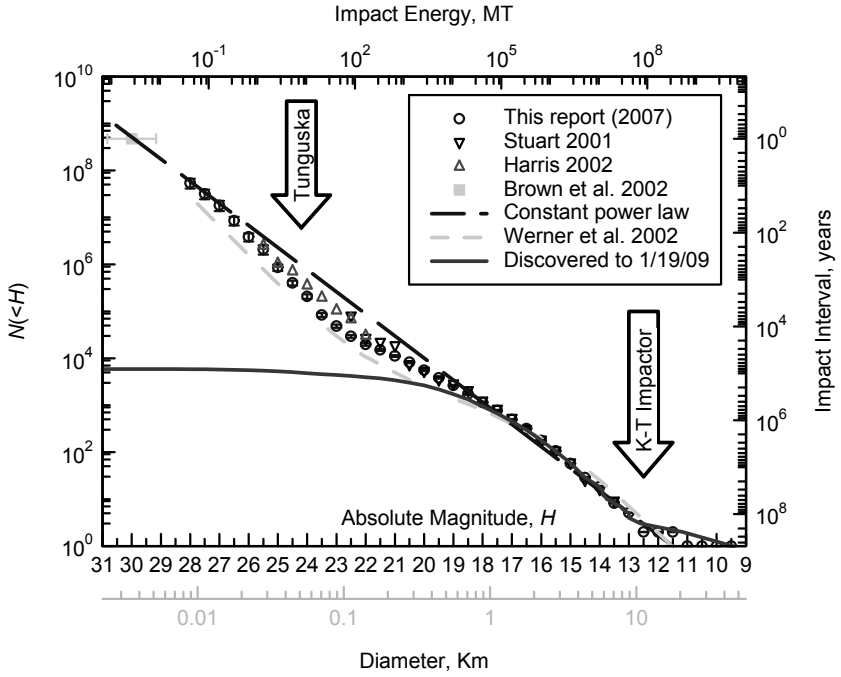

Fig. 1. Cumulative population of NEAs versus size.

a per-object impact frequency of once per 474 million years. Thus, for example, a population of 1,000 NEAs with the observed distribution of orbits would be expected to have an impact with the Earth once in 474,000 years, or in round numbers, a couple times per million years. It is further possible to define the RMS impact velocity of NEAs from such an orbital distribution, which works out to close to 20 km/s. (The dispersion velocity "at infinity" of NEAs in the Earth's vicinity is about 17 km/s, but is increased to a mean impact velocity of ~20 km/s by the acceleration falling into the Earth's gravity.) Using that velocity and assuming a mean density of 2.5 g/cm^3, we can define an equivalent scale of impact energy as a function of diameter of the body, as given across the top of the plot, in MT equivalent of TNT.

Now, within the plot, the bold type curve is the number of discovered NEAs up through January 19, 2009. One way of estimating completeness of a survey, and thereby estimating the full population, is to simply keep track of what fraction of detected objects are already known objects, and what fraction are new discoveries. This varies with size of object, of course, and allows one to estimate completion factors versus size. In my 2007 assessment [3], I have done this, including a correction for the fact that not all asteroids are equally easy to detect. Since one expects the already detected asteroids to be on average among the easier to discover than the ones that have

"hid out" so far, the re-detection ratio is expected to be higher than the completion ratio. By computer modelling surveys that match existing performance, one can estimate these bias corrections and obtain completion estimates down to a level of survey completion of around 10 %, that is, where only of the order of one in ten detections of a survey is a new object not previously observed. In the plot in Fig. 1, that carries down to around $H = 22$ or 23, or about 100 m in diameter. Below that size, one can estimate completion based on relative completion of the computer-simulated survey. That is, one can estimate that if surveying a given area of the sky to a given limiting magnitude yields C_1 completion at magnitude H_1, it will yield C_2 completion to magnitude H_2. Even though it is difficult to accurately determine C_1 and C_2 individually, the ratio C_1/C_2 will be well determined. Thus it is possible to determine relative completion still further down in size and simply "spline fit" the population estimate to match in the range over which absolute numbers can be measured. In this way, we have extended the estimated population down to about $H = 28$ ($D \approx 10$ m). At this small size, only a handful of objects have been discovered by the surveys, so we run out of reliable statistics of discoveries. It is, however, below the smallest size that we expect can make it through the atmosphere to cause ground damage. Several earlier population estimates are also plotted [7, 8, 9, 10], including the one by Brown et al. [10] which is estimated based on the size of the largest bolides observed to have entered the Earth's atmosphere over a period of about a decade.

It is noteworthy in this plot that the population of large NEAs ($D > 1$ km) is very well determined and has not changed significantly since the time of the 2003 NASA study [1]. As we shall see in the following sections of this paper, most of the impact risk comes from impacts of these large objects that have the potential to cause a global climatic catastrophe, so the total impact risk has not changed much. However, as this risk is retired, the risk remaining from smaller impacts becomes relatively more important. Already, just through a more realistic modelling of the population of NEAs in this size range, it appears that the risk from smaller impacts is only about 1/3 what was estimated in the 2003 and 2006 NASA studies. This may call for reconsideration of some of the programmatic recommendations of those earlier reports based on a perceived greater impact risk in the size range to be targeted by the next generation surveys.

A revised "kill curve"

In order to assess the risk from impacts, one must estimate the expected damage as a function of size of impactor. This is a rather difficult task, since the damage that results, at least for a smaller impactor < 1 km in diameter depends greatly on where it hits, on land or sea, or in a populated area or not.

As an example, the Tunguska event of 100 years ago devastated an area of a few millionths of the area of the Earth. Assuming that area constitutes the "death zone", and multiplying it by the population of the Earth, we can estimate that the average "Tunguska" event should lead to about 20,000 fatalities. In fact, it killed no one, and a detailed study reveals that only about ¼ of events would be expected to kill even a single person. Most of the risk is contained in events that chance to affect populated areas. Because human population is so clustered, that amounts to only a tiny fraction of events, even fairly large ones.

In any case, starting from the smallest impacts that can cause ground damage, early estimates of damage were based on the radius of destruction of a nuclear airburst at the altitude where a bolide of that energy would explode. For example, it was estimated that the Tunguska bolide was around 10–20 MT energy and exploded about 8 km above ground. Scaling from these numbers over a range of sizes, Hills and Goda [11], among others, have estimated the range of damage as a function of size for impactors entering at various velocities and composed of various materials. Fig. 2 is a plot from their paper, for "hard stone". In our earlier studies [1,2], we adopted the radius of destruction given by the 20 km/s entry velocity curve, and derived

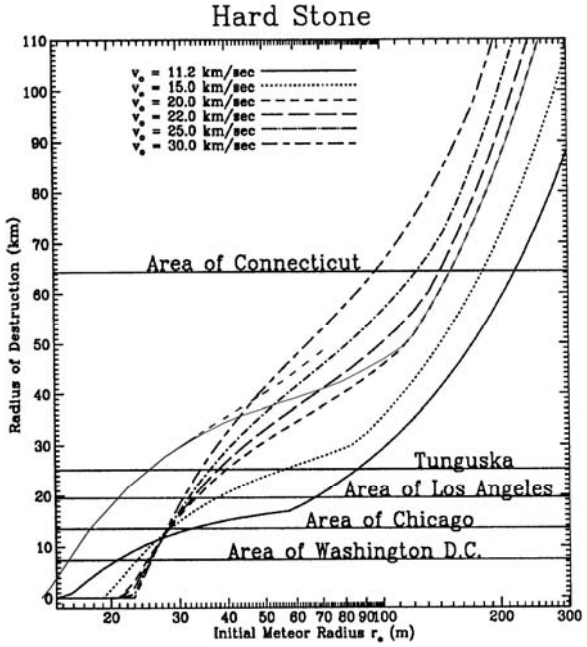

Fig. 2. Area of destruction versus impactor size and velocity, from Hills and Goda [11].

"expected fatalities" by simply multiplying the fraction of the Earth's area contained within the destruction radius by the population of the Earth. This is shown in Fig. 3, to be described presently. Returning for the moment to Fig. 2, the upper part of the 20 km/s impact curve for radius of impactor >100 m (D > 200 m) represents ground impacts. We do not revise these destruction estimates, because as we will see they are not terribly important in the "big picture". In the smaller size range though, the recent work of Boslough [5] suggests that impact airbursts may be more damaging than equivalent energy nuclear blasts, because of the momentum carried by the impact event, which is lacking in a nuclear blast. Essentially, a vortex plume, similar to a "smoke ring" continues downward and produces a hurricane-strength blast of superheated gases on the surface, even though the solid body of the impactor is completely vaporized. Boslough estimates that the area of damage of Tunguska may have been caused by an event as small as 3 MT energy. In Fig. 2, we have revised the Hills and Goda curve by smoothly moving it over by a factor of 1/4 in energy ($0.5^{2/3}$ in radius of impactor). This shift suggests that some ground damage could occur down to an impactor diameter of ~25 m, and implies an energy of the Tunguska impacting body of ~7.5 MT. This is still higher than Boslough's lower limit, but may be a reasonable estimate, certainly more likely than the 30 MT implied by the unaltered Hills and Goda curve. In Fig. 3, *a*, open circle symbols, we plot the estimated fatalities per event, the population of the Earth times fraction of surface destroyed for the Hills and Goda unaltered curve. In Fig. 3, *b*, we apply the shift by a factor of ¼ in energy to obtain a revised

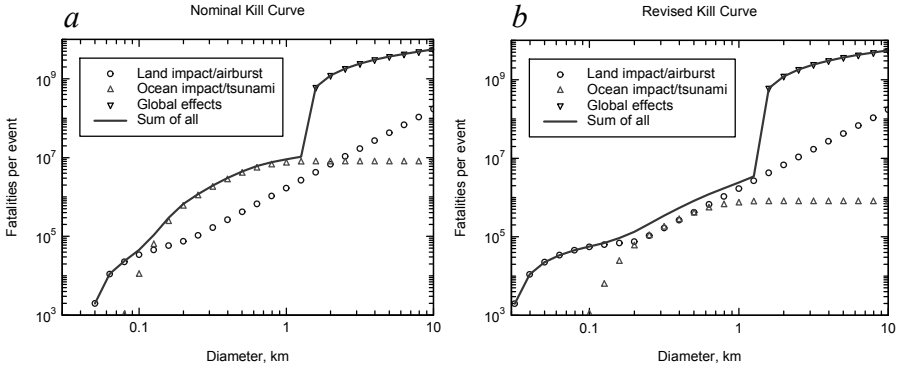

Fig. 3. Different "kill curves":
a — the nominal "kill curve" used in the 2003 and 2006 NASA reports; *b* — the "kill curve" as revised in this work. The open circles are estimated fatalities from land impacts or airbursts over land, moved a factor of ¼ in energy for airbursts on the right. The triangles are the estimated "people affected" (on the left), or "actual fatalities" (on the right, reduced a factor of ten). The "global catastrophe" plot, black inverted triangles, is unchanged in both plots.

"kill curve" for land impacts/airbursts (same plot symbols). Note that to arrive at an estimate of the "mean" fatalities per event, it is not necessary to account for the "clumpiness" of human population, or for that matter even the fact that 2/3 of the area of the Earth is ocean and has essentially zero population. For example, with respect to ocean area, if we allowed for the fact that only 1/3 of impacts hit over land, but increased the estimated population density of the land area by a factor of 3 over uniformly distributed including ocean area, we would get the same answer for the mean fatalities per event.

The second revision we have made in the "kill curve" is in relation to tsunami damage. In the 2003 NASA report, the area of inundation was estimated using a tsunami run-up and run-in model and coastal population model from Chesley and Ward [12]. The numbers of "people affected" are the total population numbers estimated in the inundation zone. It was noted in the NASA report that historically for earthquake generated tsunami, which have perhaps less certain warning and greater and faster inundation, fatalities run on the order of 10 % of the population in the inundation zone, so it is reasonable to assume the actual number of fatalities from an impact tsunami may be only about 1/10 the numbers given. Taking the full number was justified by assuming the full lifetime "value" of an individual is lost, that is, the total amount a person may "earn" in a lifetime. More realistically, an individual may have only a small fraction of one's "lifetime worth" in possession at any given moment. For example, even though an individual in the United States may have a lifetime earnings of $1M, a person at that economic level is likely to have perhaps only $100K of property in possession at the moment of a disaster. Thus, even in terms of property loss, it seems that the tsunami risk was over-estimated by a substantial factor. Without doing a detailed re-modelling of the tsunami hazard, it seems reasonable to down-grade the tsunami risk by about a full order of magnitude, as we show in Fig. 3, *b*, to represent actual fatality estimates as done with the other classes of risk [13]. In particular, the land impact risk involves property loss as well, but we only score "fatalities" in that class. Additionally, recent work by Gisler et al. [6] suggest that impact generated tsunami waves may damp more quickly with distance, at least initially, with the result that the run-up and run-in estimates by Chesley and Ward [12] may be too high. It may be that the tsunami risk is even less than we show, but since the factor of ten reduction brings the tsunami risk down to at most equal to land impacts, and in most sizes even less, we will refrain from assuming an even lower risk. We thus arrive at the revised "kill curve" plotted in Fig. 3, *b*. The "global catastrophe" kill curve is the same in both plots. The full lines in each plot are the sum of the individual components, thus the overall "kill curve" for the impact hazard.

The impact hazard revisited

Having now revised both the impact rate (population curve) and the "kill curve", we can now re-examine the impact hazard using these revisions. Fig. 4, *a* is a histogram of "fatalities per year" versus size of impact event for the population model used in the 2003 NASA report. We show both the histogram for the kill curve used in that report (see Fig. 3, *a*), and for our revised kill curve (see Fig. 3, *b*). Note that the total risk changes very little. The main change is that very small impacts gain in importance and mid-sized events (100 m–1 km) become less important. In Fig. 4, *b* we show the histogram for the new population model, again for the original and new kill curves. The main difference is a considerable reduction for both curves in the mid- to small range, due to the lower population estimate. For both of these plots, we present the *a priori* risk, that is, before any NEAs were discovered. Having now discovered about 90 % of the large NEAs capable of causing global damage, and certifying than none of them pose an impact risk in the near-term (~50 years), we can regard that fraction of the risk as "retired". In Fig. 4, *c*, we present the histogram for the remaining risk from undiscovered NEAs, using the new population model, again showing both the original kill curve and the revised one. Finally, in Fig. 4, *d* we present the same histogram for the risk that we project will remain after the "Congressional mandate" to find 90 % of NEAs larger than 140 m diameter is achieved. We make no presumption on when or how this may be achieved; most surveys from either Earth or space have similar characteristics as far as completion versus size, so the residual risk histogram is not sensitive to method or time.

In Table, we present the above results in tabular form. F and F' are the fatalities/year for the 2003 NASA report kill curve and the revised kill curve, respectively. We list these numbers based on the original "straight line" population used in the 2003 report, and then for the new population model, and for that we list the a priori risk, the residual risk at the current level of completion, and finally the residual risk expected after the next generation survey is achieved, to 90 % completion to 140 m diameter. For each of these columns, we list the fatalities expected from land impacts, from tsunamis generated by impacts into the sea, from large globally-catastrophic impacts, and finally, the total. To each of these totals, one could add an estimated ~10/year due to long-period comet nuclei. The surveys do nothing to reduce this risk, so it is constant across all columns.

As noted previously, the completion vs. size of object is a nearly self-similar function for any survey, that is, a survey that is 50 % complete at absolute magnitude H tends to be about 90 % complete at $H - 3$ and about 10 % complete at $H + 3$, and so forth. Fig. 5 is a plot showing the estimated

a

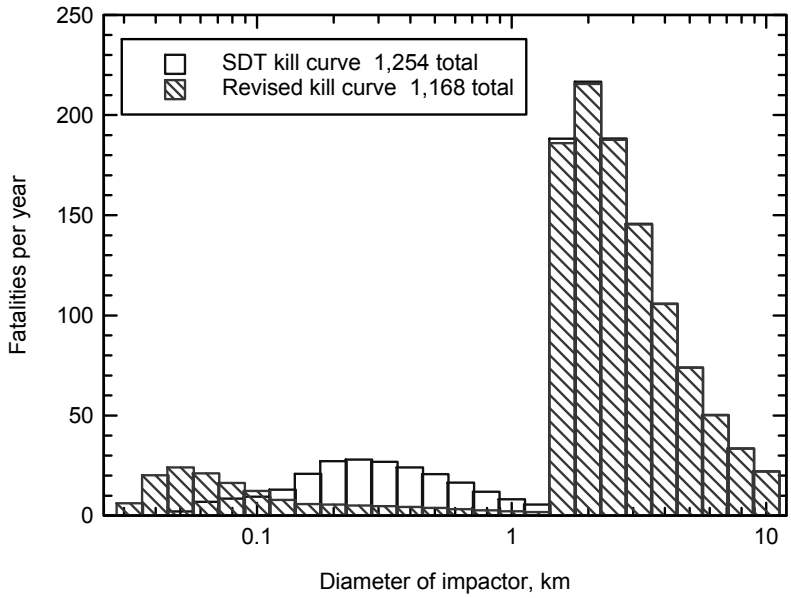
SDT kill curve 1,254 total
Revised kill curve 1,168 total
Fatalities per year
250
200
150
100
50
0
0.1
1
10
Diameter of impactor, km

b

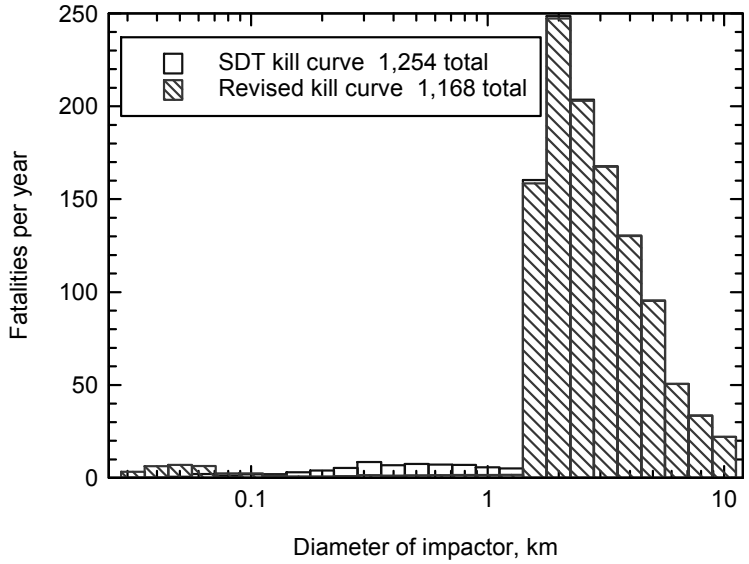
SDT kill curve 1,254 total
Revised kill curve 1,168 total
Fatalities per year
250
200
150
100
50
0
0.1
1
10
Diameter of impactor, km

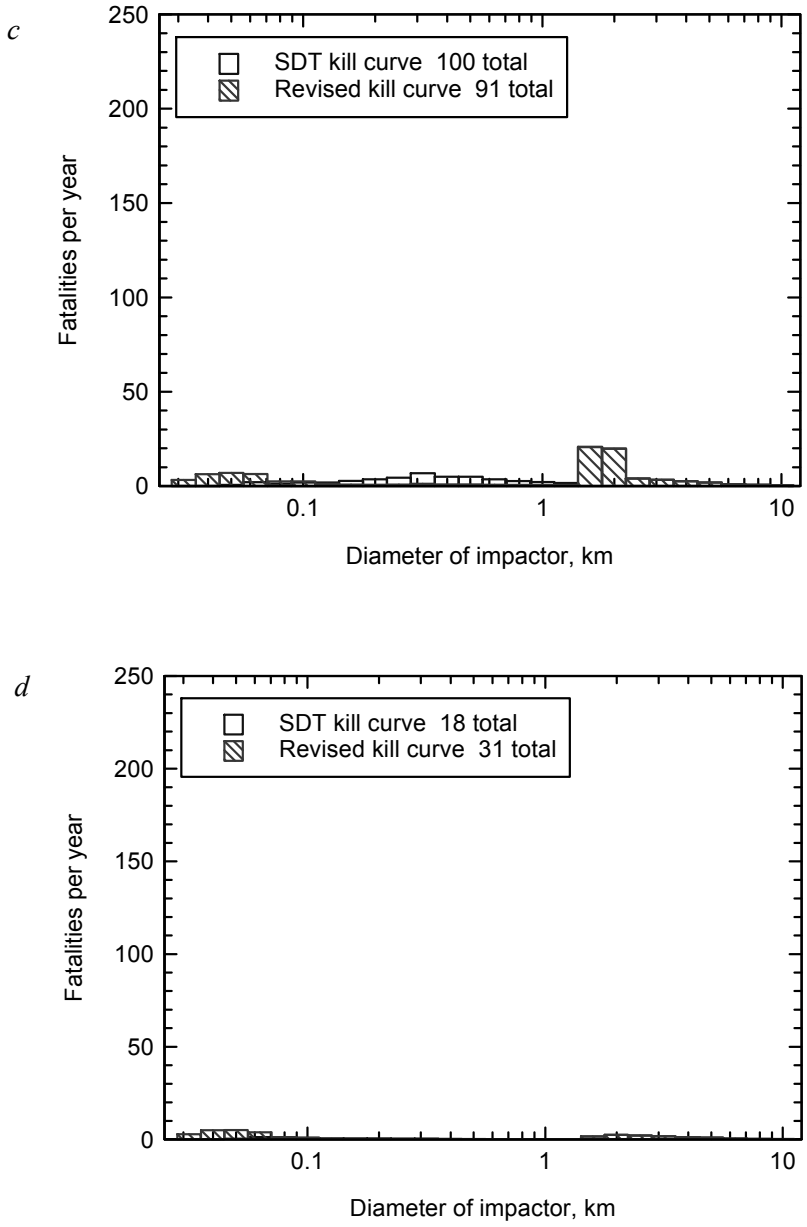

Fig. 4. Impact risk histogram:
a — using the population model 2003; *b* — using the new population model [3]; *c* — histogram of remaining risk, with the current level of completion, using the new population model [3]; *d* — histogram of risk after the next generation "Congressional mandate" goal is achieved, of 90 % completion to 140 m diameter.

Summary of impact hazard, past, present and future.

		SDT Population		New Population		New Pop, current compl		New Pop, Next Gen	
Class	<D>, km	F	F'	F	F'	F	F'	F	F'
Land	0.05–0.15	61	138	23	46	11	34	4	20
Tsunami	0.15–0.70	182	18	59	6	35	4	3	0.3
Global	>1.5	1011	1011	1098	1098	54	54	11	11
Total		1254	1168	1181	1150	100	91	18	31

completion of the present surveys (right curve). We can estimate the expected completion of the next generation survey, i. e. when the "congressional mandate" is achieved, by simply sliding the curve over by about 4 magnitudes of *H* (left curve). It is interesting to note that the present survey is nearly 50 % complete down to the size of Apophis. Thus the claim that "Apophis-like" discoveries will become more frequent, that is objects for which a non-zero chance of impact remains for a long time after discovery, is not true, at least not in the size range of Apophis, since we have already discovered about half of all such objects possible. Going to the smallest sizes that can cause ground damage, however, it may be true that many such objects discovered will continue to have non-zero impact probabilities long after discovery. This is particularly true since the smaller objects are likely to have shorter arcs of observation and be more difficult to follow up in subsequent apparitions. Thus there may be "Apophis-like" persistent non-zero impact probabilities, but only among much smaller sized asteroids. For such

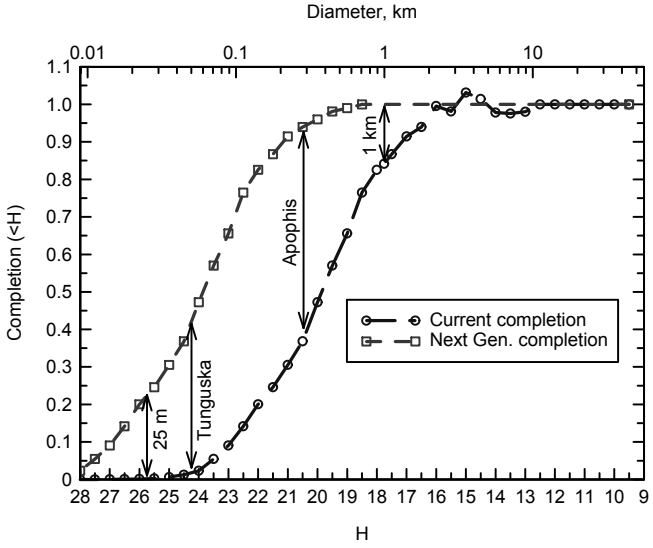

Fig. 5. Completion vs. size of NEA for present level of completion, and expected when the "congressional mandate" is achieved.

a very small asteroid, it may be sufficient to monitor it closely and plan evacuation of limited areas if it is determined that a not too damaging impact is going to occur, rather than contemplating deflection.

Short-term warning from optical surveys

Following the recent discovery of the small asteroid 2008 *TC*3 one day before it entered the Earth's atmosphere over Sudan and deposited meteorites on the ground below [14], the matter of detecting "death plunge" objects only days or weeks before impact has become a popular topic. Since an optical survey can monitor a significant fraction of the entire celestial sphere, there is a substantial probability that an incoming object can be detected with short-term warning, in principle up to the fraction of the sky accessible. From a single station at moderate latitude, the available sky is around 25–35 % of the entire celestial sphere, the rest being hidden below the horizon, too close to the sun or moon, the confusing zone near the galactic plane, and so forth. Given the mean velocity of NEAs relative to the Earth when nearby, and for some average geometry of observation, one can estimate how many days' warning a given depth of survey can provide for asteroids of a given size. Fig. 6 is a plot of such an estimate. The scale on the left is the maximum distance a survey can see a given size asteroid; the scale on the right is the number of days for an asteroid to close from that distance at the RMS velocity of NEAs in the Earth's vicinity, around 17 km/s. The scale across the bottom is the absolute magnitude, and the scale across the top is diameter, with the same normalization as used in Fig. 1, where 1 km diameter corresponds to $H = 17.75$. In this case we are dealing with much smaller objects, with diameter given in meters. For reference, 2008 *TC*3 is plotted, at its absolute magnitude and along the line of the limiting magnitude of current surveys, ~20.5. It was detected about 1 day out, but since it was a particularly low-velocity impactor it was probably visible for a couple days. Present and planned future surveys have a typical repeat frequency of around 5 days, so we can estimate that there was around a 10 % probability of stumbling upon this object in the time before its impact (the product of fraction of sky covered and the fraction of repeat cycle during which it was visible). Thus, the fact that one object of a size expected to hit the Earth about once a year was detected in a decade of surveying is just about what one should expect. Interestingly, even for present surveys, any object large enough to penetrate deeply enough in the atmosphere to cause ground damage should be spotted a week or more before impact, if it is coming from a direction accessible to the survey. This suggests about a 25–35 % chance that such an impactor will be spotted with days to weeks warning time. Future surveys should do even better, providing perhaps a month or more warning [15], and the fraction accessible may also be a bit greater, since over a month or more, orbital cur

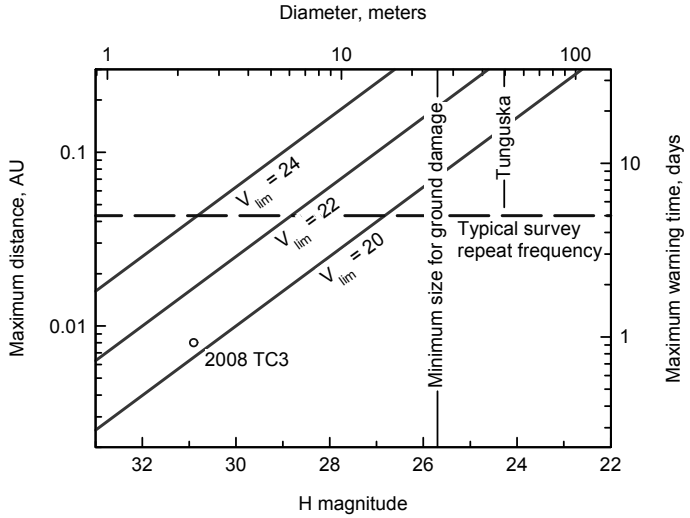

Fig. 6. Short-term warning provided by an optical survey.

vature becomes significant and the object sweeps over a range of the sky rather than just coming in from a constant direction. While such short-term warning from optical surveys cannot be regarded as "complete protection", it is only prudent to be prepared with "civil defense" measures to make all possible use of such warning as may be provided. It should be noted though that future surveys will not have such rapid follow-up as present surveys (in spite of the fact that "Rapid Response" is part of the Pan-STARRS acronym). Thus, while the available lead time for objects large enough to cause ground damage should be sufficient for next generation surveys to identify objects on impact paths before they hit, as presently planned they will have difficulty identifying really small objects like 2008 *TC*3 before they arrive [15].

Conclusions

Within a few years, if not already, we will have found essentially all PHAs large enough to be a risk of global climatic effects. We will be left with some fractional probability that even one such object remains undiscovered. Mid-size impacts, presenting mainly tsunami risk, are less frequent and probably less damaging than previously estimated. In the smallest size range capable of causing ground damage, the next generation survey may find ~25 %, providing long-term warning. Ground-based optical surveys are capable of about 25–35 % chance of detecting a "death plunge" object, down to the smallest size capable of producing ground damage, providing days to weeks' warning, sufficient for some civil defense measures. Thus in a very short time, on the scale of civilizations and even quite short in terms of a human lifetime, the impact hazard should be reduced to a negligible risk.

The one exception to this is the risk from long-period comet nuclei, for which present technology can offer no protection beyond short-term warning. Fortunately this risk is estimated to be quite small.

References

1. *Stokes G.* (Study Lead). Study to Determine the Feasibility of Extending the Search for Near-Earth Objects to Smaller Limiting diameter. Washington: NASA Office of Space Science. 2003. 154 p.
2. *Claybaugh W.* (Study Lead). 2006 Near-Earth Object Survey and Deflection Study. Washington: NASA Office of Program Analysis and Evaluation. 2006. 272 pp.
3. *Harris A. W.* The population of NEAs and PHAs and the current status of surveys // Final report to NASA NEO Program Office, JPL and NASA NEO Observations Program, Washington. 2007. 35 p.
4. *Harris A. W.* What Spaceguard did // Nature. 2008. Vol. 453. P. 1178–1179.
5. *Boslough M.* The Nature of Airbursts and their Contribution to the Impact Threat // The IAA 2009 Planetary Defense Conference.
6. *Gisler G., Weaver R., Gittings M.* Near-field effects of asteroid impacts in deep water // The IAA 2009 Planetary Defense Conference.
7. *Stuart J. S.* A Near-Earth asteroid population estimate from the LINEAR Survey // Sci. 2001. Vol. 294. P. 1691–1693.
8. *Harris A. W.* A new estimate of the population of small NEAs // Bul. Amer. Astron. Soc. 2002. Vol. 34. P. 835.
9. *Werner S. C., Harris A. W., Neukum G., Ivanov B. A.* The near-Earth Asteroid size-frequency distribution: A snapshot of the Lunar impactor size-frequency distribution // Icarus. 2002. Vol. 156. P. 287–290.
10. *Brown P., Spaulding R. E., ReVelle D. O., Tagliaferri E., Worden S. P.* The flux of small near-Earth objects colliding with the Earth // Nature. 2002. Vol. 420. P. 294–296.
11. *Hills J. G., Goda M. P.* The fragmentation of small asteroids in the atmosphere // Astron. J. 1993. Vol. 105. P. 1114–1144.
12. *Chesley S. R., Ward S. N.* A Quantitative Assessment of the Human and Economic Hazard from Impact-generated Tsunami // Natural Hazards. 2006. Vol. 38. P. 355–374.
13. *Chapman C. R.* The hazard of near-Earth asteroid impacts on earth // Earth & Planetary Science Letters. 2004. Vol. 222. P. 1–15.
14. *Jenniskens P. et al.* The impact and recovery of asteroid 2008 TC_3. Nature. 2009. Vol. 458. P. 485–488.
15. *Ivezic Z., Chesley S., Jones L., Juric M. et al.* LSST: Comprehensive NEO detection, characterization, and orbits // The IAA 2009 Planetary Defense Conference.

The Asteroid-Comet Hazard Conference Proceedings, 2009

INVESTIGATION OF NEOS IN SITU. COUNTERACTION TO THE NEO HAZARD

Deep Impact and Deflection of NEOs

M. F. A'Hearn

Department of Astronomy of University of Maryland, College Park MD, USA

Abstract. Deep Impact was proposed and selected purely as a mission for scientific investigation of comets. Nevertheless, it measured parameters that are crucial for understanding how to deflect hazardous NEOs and provides several lessons that need to be taken into account in any planning for mitigation.

Introduction

The Deep Impact mission was selected by NASA through a competitive peer review process as a purely scientific mission to further our understanding of comets and how to use them to understand the formation of the Solar System. The principal goal was to understand the differences in chemical composition of volatiles with depth below the surface of the nucleus and the next most important goal was to determine physical properties of the nucleus. This was to be carried out by delivering an impactor spacecraft at hypervelocity to the nucleus while a flyby spacecraft was used to observe what happened. The two spacecraft were launched on 12 Jan 2005 and they flew joined together, with the flyby spacecraft in control, until one day before impact on comet 9P/Tempel 1. At that point the two spacecraft separated. The flyby spacecraft diverted to miss the nucleus by 500 km and decelerated by a total of 100 m/s in order to provide a 13-minute window for observation between the time of impact and the time at which the flyby spacecraft flew past the nucleus. The impactor navigated to hit the nucleus of the comet in an illuminated area on the side toward the flyby. The first scientific results were published by A'Hearn et al. [1] and numerous papers have followed, a large subset of which are available as a book edited by A'Hearn and Combi [2].

Relevance to NEOs

When the original, scientific proposal was written, we mentioned in passing that some of the scientific results would be of benefit for understanding how to mitigate impactors on Earth. Noting that our target, comet 9P/Tempel 1, is neither an asteroid nor an NEO, it is worth asking how the results can be relevant. According to De Meo and Binzel [3], 30 % of NEOs have a Tisserand invariant, $T_J < 3$, a common dynamical criterion for separating comets from asteroids. Half of these have some physical characteristic suggesting that they are physically comets (very low albedo, etc.) and some of these are known, active comets. They reject half of the objects with cometary physical properties on the basis of a dynamical model, but this seems to me inappropriate in this context so I argue that 15 % of the NEOs are physically either active or dormant comets. There are 151 active comets that are currently NEOs according to the NEO website at JPL [4]. Since NEOs are objects with relatively short dynamical lifetimes that were fed into that state from non-NEO orbits, there is likely very little physical difference between objects that are otherwise of the same type. More specifically, the evolution of comets due to the somewhat smaller perihelion distance of an NEO compared to that of a comet that is not an NEO is unlikely to have drastically altered the physical properties. In fact, one of the conclusions from the Deep Impact mission is that it seems likely that the surface erodes rapidly enough to keep up with the evolutionary sublimation front.

It is worth also pointing out that the closest we have come to a global disaster in recorded history was in 1770 when Lexell's Comet passed within 0.014 AU of Earth only two weeks after it was discovered. Modern integrations [5, 6] show that this comet had been in an orbit with perihelion just inside 3 AU until a close passage near Jupiter in 1767 sent it to the inner solar system. Based on the brightness of the comet, it seems likely that the nucleus was of order 5 km or more in diameter. Thus comets do present a real hazard to Earth and need to be included when studying mitigation.

Deep Impact as Mitigation

It is convenient to divide mitigation measures into 3 different groups: slow push-pull techniques, kinetic impacts, and nuclear explosions. The first is applicable to small NEOs with very long (many decades) warning times and to objects with small, dynamical keyholes. The second is applicable to a much wider range of sizes of NEOs, including small ones with intermediate (1 decade or less) warning times. The third technique is applicable to even larger NEOs but is unlikely to be deployed unless absolutely necessary.

In many ways, Deep Impact was the prototype for deflection of an NEO by kinetic impact. Because Deep Impact was a scientific mission, it was targeted at a large cometary nucleus and because it was a cost-capped mission

the mass of the impactor was relatively small, 1/3 ton, compared to what could have been delivered (up to perhaps 5–10 tons with today's launch vehicles). Thus any change in the orbit of Tempel 1 was much too small to be measured. Nevertheless, the physical parameters learned from the experiment have taught us a lot about how to deflect an NEO with a kinetic impact.

Approach Results

Targeting

The algorithm used for targeting, which was not aimed at maximizing the transfer of momentum, had a circular error, 3-σ, of radius about 200 m based on simulations and the actual delivery was within this. In order to deflect a small NEO (say only a few 100 m in diameter), the accuracy of the targeting will need to be improved significantly. This does not appear to be an insurmountable obstacle but effort will need to be applied. The targeting techniques and their performance have been described by Mastrodemos et al. [7] and by Kubitschek et al. [8].

On approach, the impactor was hit by 4 dust particles that caused the attitude of the spacecraft to vary by amounts large compared to the field of view of the camera. Because of the high speed of approach (10.3 km/s), very small particles are capable of changing the attitude and the three particles that hit prior to the last image transmitted to Earth were estimated to be only between 1 and 10 mg, compared to the 1/3 ton mass of the impactor itself [9]. This was not a problem for delivering the impactor, since the last targeting maneuver took place long before the attitude disturbances, roughly 7.5 minutes before impact, and the dust impacts could not significantly affect the velocity vector of the impactor. However, for an explosive device, the attitude fluctuations are likely to be a problem for triggering the explosive unless they are taken into account. We need to remember that large NEAs are generally thought to be rubble piles, with many of them rotating not far below breakup velocity. Whether there is debris around NEAs that would affect fusing of explosives for deflection is an open question that needs to be investigated.

Heterogeneity

Comet Tempel 1 exhibited substantial heterogeneity in many properties. The topographic features varied dramatically from place to place and we do not yet understand the processes that lead to this diversity [10]. Perhaps even more exciting scientifically, the outgassing of evaporated volatiles occurred in different places for different molecules (notably H_2O and CO_2) [11]. There are large-scale layers present in many places that are thought to be remnants of the original cometesimals that produced the cometary nucleus [12]. Finally, we note that the huge amount of water subliming into the coma

is not coming from ice on the surface, but rather from subsurface ice and percolation through overlying inert material to the surface [13]. Furthermore, the sublimation process also leads to fairly frequent outbursts from a limited number of sites on the nucleus [1, 14]. It is unclear to what extent the variations from place to place on the nucleus imply large variations in the parameters most relevant to mitigation since there was only one impactor, hitting in one place.

In addition to the variation from place to place on comet Tempel 1, there are also substantial variations in gross shape and in topographic features among the 4 comets visited by spacecraft. Some of these may be related to the different evolutionary histories experienced by the four comets, but there is no information that lets us decide reliably whether key parameters for mitigation vary significantly from one cometary nucleus to another. Basilevsky and Keller [15] have argued that the nuclei show similarities that imply that the same processes operate on all comets. This would imply rather little variation in the key properties, or rather in the range of the key properties, among different cometary nuclei.

Impact Results

Energy Balance

There were two separate phases of excavation after the impact. The first phase was a hydrodynamically driven ejection of hot, self-luminous material at high speed. This consisted of very roughly a ton of material moving at ≥5 km/s. The second phase consisted of the traditional, mechanical excavation of a crater by the shock wave that proceeds through the material. This consisted of very roughly 10^4 tons of material, with the earliest ejecta moving at >200 m/s but with the bulk of the material moving much more slowly, much of it moving below escape velocity (1.4 m/s). The material of the first phase carried a kinetic energy comparable to the total energy delivered to the comet by the impactor, 19 GJ. The uncertainty in the mass of this material allows for a wide range of energies, from about half the energy delivered to at least twice the delivered energy. Whether an internal energy source was triggered is still an open question undergoing much discussion [16, 17]. The material of the second phase had negligible kinetic energy compared to the hydrodynamically expelled material but contained most of the momentum of the ejecta.

Porosity

The porosity of an NEO is crucial both for estimating the mass, the dominant uncertainty in knowing how much momentum must be delivered, and for estimating the efficiency of momentum transfer, whether by kinetic impact or by nuclear explosion. The Deep Impact experiment measured sepa-

rately the porosity of the upper layers and the density of the bulk comet. The luminous efficiency (luminous energy output/kinetic energy input) of the impact was ~10^{-4}, indicating a very porous target at least to depths that were sampled by the impact trajectory, say 10–20 m. Ernst and Schultz [18] conducted a series of laboratory experiments with targets of varying density and varying composition to set a lower limit of 75 % on the porosity of this surface layer and a corresponding upper limit on the density of 0.55 g/cm^3. This very high porosity implies that the momentum transfer efficiency is likely to be not far above unity.

The porosity of the bulk nucleus is determined indirectly. The fallback of ejecta onto the surface of the nucleus yields a direct measure of the local gravitational acceleration. Although the impact site was beyond the observed limb during "lookback imaging", Richardson et al. [19] were able to measure the expansion of the base of the cone of ejecta long after the impact, this base being produced entirely by material falling back to the surface. They deduced a gravitational acceleration of only 0.34 mm/s^2. Combining this with the shape model for the nucleus they deduced a total mass and thus a bulk density of 0.4 g/cm^3. Given any of the typical values of the gas to dust ratio for comets, this yields a value for porosity in excess of 60 %, a value comparable to that found for the surface layers. This suggests a surprising homogeneity, in contradiction to the discussions of heterogeneity above. The low bulk density compensates for the low momentum transfer efficiency to make it easier to deflect a cometary nucleus of a given size.

Strength

The yield strength of the surface layer can also be measured by observing the base of the ejecta cone, but in this case, the fact that the base of the cone was over the limb allows one only to set an upper limit on the strength. The yield strength that is measured is closest to a tensile strength since it is the strength against the rarefaction behind the shock wave that propagates through the medium. The upper limit on this yield strength is very roughly 10 kPa (16, 19). This is substantially below the strength of solid ice (which in turn is much weaker than solid rock), and comparable to or less than that of highly fractured ice. The observations are consistent with zero strength.

Excavation & Momentum Efficiency

Estimating the mass of material ejected and the momentum it carries is very uncertain. A'Hearn [20] summarized the evidence. Observations of gas (OH and H_2O) show that roughly 5–10 kt of ice were excavated, although there is no model for how much of that gas might have sublimed from ice that fell back on the surface without being covered up by insulating, refractory material. Using dust/gas ratios measured by remote sensing for many comets, a reasonable estimate for the total mass of material ejected would be

20 kt, substantially greater than the total mass in the simulation by Richardson et al. [19] discussed above. Richardson's simulation yielded a momentum carried by the grains roughly comparable to the momentum delivered by the impactor. If the ejection were anti-parallel to the impactor's velocity vector (it was not), this would have provided a transfer efficiency of 2, toward the low end of the expected range and consistent with a highly porous target. Unless most of the gaseous water and OH came from ice that was excavated from the crater and then spread in an ejecta blanket without being insulated from sunlight, the ratio of mass ejected to mass delivered (1/3 t) was $>10^4$.

Ideally the momentum transfer efficiency should be directly measured by measuring the change in orbital velocity of the NEO. Because the Deep Impact experiment was a scientific search for sub-surface composition and physical properties rather than a mitigation test, the mass delivered was small compared to what can be delivered with current launch vehicles and the target was a relatively large cometary nucleus to ensure that it would not be disrupted and to simplify targeting. Experiments to directly measure the momentum transfer efficiency are likely to provide the biggest advance in our ability to deflect NEOs. This will require a much larger mass in the impactor than was the case for Deep Impact as well as a much smaller (sub-km) cometary nucleus.

Fragile Grains

Lisse *et al.* [21] used the Spitzer Space Telescope to study the composition of the ejecta. As a part of that effort, they determined the size distribution of the ejected grains and compared it with the size distribution of the grains observed in the ambient activity of the comet. In the ejecta, the size distribution of grains was much steeper than in the ambient activity, with a relative peak near 1 μm. This strongly suggests that the grains in the comet are porous, fragile, aggregates, which can easily be broken up by the shock wave of the impact but are not readily broken by the hydrodynamic drag that lifts grains from the surface.

The icy grains that were excavated, and which persisted in the coma for hours, also have sizes of order 1 μm, whereas what little ice was seen on the surface of the nucleus had grain sizes of order 50 μm [22, 13]. This strongly suggests that the refractory grains and the ice are independently fragile aggregates.

While the grain size is not directly relevant to mitigation, the fragility of the aggregate grains goes hand in hand with the idea that the nuclear material is very weak on larger scales, something that does matter for mitigation with impacts. The inability to detect large, coherent fragments in the ejecta suggest that no meter-sized or larger objects were strong enough to survive the

ejection process, whereas such rocks are found in ejecta from terrestrial impact craters.

Depth of Ice

There does appear to be some layering near the surface at the impact site. The very surface layer, down to something between 10 cm and 2 m below the surface [22, 23, 24], appears to be devoid of ice. There is probably additional layering in the ice *vs.* dust component at lower levels, but the evidence is not clear on this point. This might be important for impactor effectiveness, but the evidence that both ice and rock are in very fragile aggregates, with 1-micron basic units, suggests that layering of the ices is not going to be a significant issue for impactor effectiveness.

Deflection Calculation

In order to set the stage for a true mitigation experiment, it is useful to estimate how much deflection might have occurred in the Deep Impact experiment. I will assume a) that the momentum transfer efficiency is 2 (this could easily be wrong by a factor 2) and b) that the impactor velocity vector was directly opposed to the comet's orbital velocity at perihelion and directed more or less through the center of mass. The comet was nearly at perihelion at the time of impact, but the other parts of the latter assumption are definitely wrong: the impactor's entry track was only about 30° above the local horizontal, the impactor's velocity vector was significantly away from anti-parallel to the comet's orbital velocity, and the impact was not directed through the center of mass. These deviations from the assumptions reduce the effectiveness of the actual deflection by a factor of a few, but this is intended as an order of magnitude estimate for an experiment intended to deflect the comet nucleus rather than a scientific investigation of cometary composition.

Knowing the mass of the target [19], the mass of the impactor (372 kg), and the relative velocity of the impactor (10.3 km/s), we can easily calculate the change in velocity of the comet as $\Delta v = -0.17$ μm/s. Converting this to a change in kinetic energy of the comet (using the comet's velocity at perihelion) and thus to a change in semi-major axis of the orbit, $\Delta a = -17$ m. This corresponds to a change in orbital period $\Delta P = -0.01$ s. Using the comet's orbital velocity at perihelion, we can say that after successive orbital periods after the impact, the comet will be advanced in its orbit by $\Delta x = +0.28n$ km, where n is the integral number of orbital periods elapsed (the calculation is only valid near perihelion). This change in the orbital position after one period (280 m) is comparable to the sizes of the largest craters on the nucleus and far too small to be directly measured, even if there were no uncertainty in the non-gravitational acceleration from outgassing.

The significance of this calculation lies only in estimating what one can do with other comets. An impactor ten times larger than DI, say 3 t, is within the capability of existing, heavy-lift launch vehicles and an impact onto a comet with diameter 600 m (P/Tempel 1 had an effective diameter of 6.0 km) would yield 10^4 times the momentum change in the comet. This is already enough to displace a 600-meter cometary nucleus by more than the size of most keyholes after a single orbital period and it would allow one to displace the comet by an Earth-radius after 10–20 orbital periods. Multiple impactors could, of course, do this in a shorter interval. These numbers are, of course, consistent with numerous previous analytical studies of deflection by kinetic impactors. The details of carrying out an impacting mitigation are sensitive to the actual orbit of the comet, the possible trajectories to reach the comet, and the amount of warning time available. The limiting uncertainty in carrying out a deflection is likely to be the uncertainty in the non-gravitational acceleration from outgassing and in whether that non-gravitational acceleration changes after the impact. The second large uncertainty is likely to be lack of knowledge about how the physical properties vary from one comet to another, or even from place to place on a single cometary nucleus.

Summary and Conclusions

Deep Impact has demonstrated the capability to impact NEOs with a large mass and has thus demonstrated, at least in principle, the ability to deflect an NEO. The physical properties deduced from the Deep Impact experiment give us some confidence in narrowing the range of possible parameters relevant to impact mitigation, but considerable additional work needs to be done to ensure a robust capability for deflection.

This work was supported by NASA through the Deep Impact and EPOXI contracts. Participation in the meeting was also supported by the National Research Council.

References

1. *A'Hearn M. F. et al.* Deep Impact: Excavating Comet Tempel 1 // Sci. 2005. Vol. 310. P. 258–264.
2. Deep Impact at Comet Tempel 1 / Eds M. F. A'Hearn, M. C. Combi // Amsterdam: Elsevier, 2007 (also published as Icarus Vol. 191).
3. *De Meo F., Binzel R. P.* Comets in the Near-Earth Object Population // Icarus. Vol. 194. P. 436–449.
4. *Yeomans D., Baalke R.* http://neo.jpl.nasa.gov/cgi-bin/neo_elem.
5. *Belyaev N. A., Kresák L., Pittich E. M., Pushkarev A. N.* Catalogue of Short-Period Comets. Bratislava: Astronomical Institute of the Slovak Academy of Sciences, 1986.

6. *Carusi A., Kresák L., Perozzi E., Valsecchi G. B.* Long-term Evolution of Short-Period Comets. Bristol: Adam Hilger Ltd, 1985.
7. *Mastrodemos N., Kubitschek D. G., Synnott S. P.* Autonomous Navigation for the Deep Impact Mission Encounter with Comet Tempel 1 // Space Sci. Rev. 2005. Vol. 117. P. 95.
8. *Kubitschek D. G. et al.* The Challenges of Deep Impact Autonomous Navigation // J. Field Robotics. 2007. Vol. 24. P. 339.
9. *A'Hearn M. F. et al.* Deep Impact and Sample Return // Earth, Planets, Space. 2008. Vol. 60. P. 61.
10. *Thomas P. et al.* The Shape, Topography, and Geology of Tempel 1 from Deep Impact Observations // Icarus. 2007. Vol. 187. P. 4.
11. *Feaga L. M., A'Hearn M. F., Sunshine J. M., Groussin O. et al.* Asymmetries in the distribution of H_2O and CO_2 in the inner coma of comet 9P/Tempel 1 as observed by Deep Impact // Icarus. 2007. Vol. 190. P. 345.
12. *Belton M. J. S. et al.* The Internal Structure of Jupiter Family Cometary Nuclei from Deep Impact Observations: The Talps or "Layered Pile" Model // Icarus. 2007. Vol. 187. P. 332.
13. *Sunshine J. M. et al.* Exposed Water Ice Deposits on the Surface of Comet 9P/Tempel 1 // Sci. 2006. Vol. 311. P. 1453.
14. *Belton M. J. S., Feldman P. D., A'Hearn M. F., Carcich B.* Cometary cryo-volcanism: Source regions and a model for the UT 2005 June 14 and other mini-outbursts on Comet 9P/Tempel 1 // Icarus. 2008. Vol. 198. P. 189.
15. *Basilevsky A. T., Keller H. U.* Craters, Smooth Terrains, Flows, and Layering on the Comet Nuclei // Solar System Res. 2007. Vol. 41. P. 109.
16. *Holsapple K. A., Housen K. R.* A crater and its ejecta: an interpretation of Deep Impact // Icarus. 2007. Vol. 187. P. 345.
17. *Groussin O. et al.* Energy balance of the Deep Impact experiment // Icarus. 2009. (in press).
18. *Ernst C. M., Schultz P. H.* Evolution of the Deep Impact flash: Implications for the nucleus surface based on laboratory experiments // Icarus. 2007. Vol. 190. P. 334.
19. *Richardson J. E., Melosh H. J., Lisse C. M., Carcich B.* A ballistics analysis of the Deep Impact ejecta plume: Determining Comet Tempel 1's gravity, mass, and density // Icarus. 2007. Vol. 190. P. 357.
20. *A'Hearn M. F.* Deep Impact and the Origin and Evolution of Cometary Nuclei // Space Sci. Rev. 2008. Vol. 138. P. 237.
21. *Lisse C. M. et al.* Spitzer Spectral Observations of the Deep Impact Ejecta // Sci. 2006. Vol. 313. P. 635 (see the On-Line Only material).

22. *Sunshine J. M. et al.* The Distribution and Structure of Water Ice in the Interior of Comet Tempel 1 // Icarus. 2007. Vol. 190. P. 284.
23. *Groussin O. et al.* Surface Temperature of the Nucleus of Comet 9P/Tempel 1 // Icarus. 2007. Vol. 187. P. 16.
24. *Davidsson B. J. R., Gutiérrez P. J., Rickman H.* Physical properties of morphological units on Comet 9P/Tempel 1 derived from near-IR Deep Impact spectra // Icarus. 2009. Vol. 201. P. 335.

The Asteroid-Comet Hazard Conference Proceedings, 2009

INVESTIGATION OF NEOS IN SITU.
COUNTERACTION TO THE NEO HAZARD

The Engagement Space for Countermeasures Against Potentially Hazardous Objects (PHOs)

W. F. Huebner[1], D. C. Boice[1], P. Bradley[2], S. Chocron[1], R. Clement[2], A. Ghosh[1], P. T. Giguere[2], R. Goldstein[1], J. A. Guzik[2], L. N. Johnson[3], J. J. Keady[2], J. Mukherjee[1], W. Patrick[1], C. Plesko[2], M. Tapley[1], J. D. Walker[1], R. P. Weaver[2], K. Wohletz[2]

[1]Southwest Research Institute, San Antonio, TX, USA
[2]Los Alamos National Laboratory, Los Alamos, NM, USA
[3]Science Mission Directorate at NASA Headquarters, Washington, DC, USA

Abstract. We have proposed a comprehensive plan for counter-measures against PHOs: asteroids and comet nuclei on a collision course with Earth. Countermeasures include hyper-velocity impacts; surface and subsurface conventional explosions; and stand-off, surface, and subsurface nuclear explosions. We consider momentum transfer for complete deflection of a PHO as well as destruction of it with maximum dispersal of the fragments. Methods and procedures for applying counter-measures depend on many variables that are defined by a multi-dimensional engagement space. The dimensions and measures of the engagement space include the reaction time, the size of the PHO, its chemical composition, physical structure, shape, whether it is a binary, and its spin state. Reaction time is one of the most important variables, followed by the spin state and the size of the object. The type of countermeasures that would be effective depends heavily on the engagement space. Hyper-velocity kinetic impactors require intercept missions. The preferred methods of deploying chemical or nuclear explosives require rendezvous missions; however, if the available reaction time is too short, intercept missions must be chosen.

Introduction

Background

Last year, at the Tunguska Conference in Moscow, we proposed a comprehensive plan for countermeasures against potentially hazardous objects (PHOs: asteroids and comet nuclei) on a collision course with Earth [1]. The plan proposes ground-based launches and contains five options:

1. Kinetic impactors to deflect a PHO;
2. Strategically placed chemical explosives on the surface of a PHO to deflect it;
3. Chemical explosives on or below the surface of a PHO to destroy it and disperse the fragments;
4. Nuclear stand-off explosions to deflect a PHO;
5. Nuclear surface or subsurface explosions to destroy a PHO and disperse the fragments.

We consider momentum transfer for complete deflection of a PHO as well as destruction of a PHO with maximum dispersal of resulting fragments to minimize the remaining impact dangers. The methods and procedures for applying these countermeasures depend on many variables. These variables are defined by a multidimensional engagement space. Here we outline the dimensions and measures of the engagement space. These include the reaction time, the size of the threatening object, its chemical composition, physical structure, shape, whether it is a binary or multi-body object, and its spin state. If the available reaction time permits, a robotic precursor characterization spacecraft and a separate spacecraft to observe the effects of the countermeasures will significantly enhance the likelihood of success and provide confirmation of the success (or identify the need for follow up) of the countermeasure mission. The available reaction time is the warning time (time from realization that the object may impact the Earth to the time of the predicted impact) minus the time to prepare for the launch of the intended countermeasures, the launch campaign, the time to get to the PHO, and the time for application of the countermeasures. The warning time, which in turn defines the reaction time, is the most important variable, followed by the spin state and the size of the object. The type and magnitude of the countermeasures that are likely to be effective depend heavily on the engagement space. Hyper-velocity kinetic impactors will require an intercept (as opposed to a rendezvous) mission. Chemical explosives to be activated on or below the surface of a PHO require a rendezvous mission. The preferred method of deploying nuclear explosives would be a rendezvous mission, but if the reaction time is very short, an intercept mission may be more appropriate. Some countermeasure scenarios can be precalculated and collected in a playbook.

Observations of solid surface planets and their moons show that asteroids and comet nuclei have impacted them throughout the history of the planetary system. The evidence from the craters on the Moon and Mars is overwhelming. The Earth also has suffered many such collisions. A list of impact craters on Earth including their sizes, ages, names, locations, and images can be found at: *http://www.unb.ca/passc/ImpactDatabase/index.html* and at *http://tsun.sscc.ru/nh/impact.php*. The Planetary and Space Science Centre of the University of New Brunswick, Canada, maintains this database.

Collisions of PHOs with the Earth will occur in the future, even though we currently may not be able to predict when the inevitable collision may occur. The warning time (i. e., reaction time) to activate countermeasures for Earth collision avoidance may be very short (possibly only weeks) if the object is either small (e. g., Tunguska size: about 25–30 m diameter [2]) or a long-period comet (LPC) nucleus. We note that small PHOs are about 100 times more abundant than km-sized PHOs. Small PHOs will be difficult to detect unless they are very near the Earth, which may result in very short warning times. Long-period comet nuclei are typically larger than 10 km in diameter. Because they come from the outer solar system they approach with very high speeds, usually in orbits out of the ecliptic; about half of them in retrograde orbits. If a long-period comet approaches the Earth from behind the Sun, the warning time may be even shorter.

Early detection of PHOs is only effective if counter-measures are ready and available to be applied!

The necessary technologies that may be applied to countermeasures against PHOs have been developed over the last several decades. They are ready to be adapted and applied for the defense of Earth against cosmic impacts. It is ethically compelling for us to apply these technologies to defend and protect civilization. *We must not fail to exercise our responsibilities!* The first step in preparing countermeasures is to investigate in advance the optimum method of countering a PHO under various different circumstances. This Playbook with precalculated scenarios for potential countermeasures will be very useful as a guide when we face an impending collision with a cosmic object.

Goals of Countermeasures

Eferred option is to transfer momentum to deflect (e. g., retard or accelerate) the PHO in its orbit to avoid a collision with Earth. This requires a hypervelocity kinetic impactor, which itself can be a spacecraft on an intercept mission. Alternatively, since PHOs are typically not spherical in shape, conventional chemical explosives can be placed strategically on the surface to maximize the desired effects. Chemical explosives are appropriate for

PHOs that are too large for a kinetic impactor to deflect and too small to justify nuclear explosives. Placing conventional explosives on the surface would require a rendezvous mission and, therefore, more time. Nuclear explosives in stand-off mode may have to be used for larger PHOs either in an intercept mission if the warning time is too short or in a rendezvous mission if more time is available. An alternative approach is to disrupt the PHO and widely disperse its fragments to avoid or at least minimize effects of their collisions with the Earth. Nuclear surface or subsurface explosions would probably be used in extreme and hopefully rare circumstances on PHOs that are too difficult to deflect. In such a case, the utmost care must be taken to completely disperse all but the smallest fragments (preferably less than 10 m in diameter), and a rendezvous mission will be necessary.

The ultimate (long-term) goal is to be able to respond and apply countermeasures to a PHO with warning times as short as a few weeks. This will require launch vehicles continuously available for appropriation and the required countermeasure payloads to be on standby so that an intercept mission can be initiated within a day or two of warning.

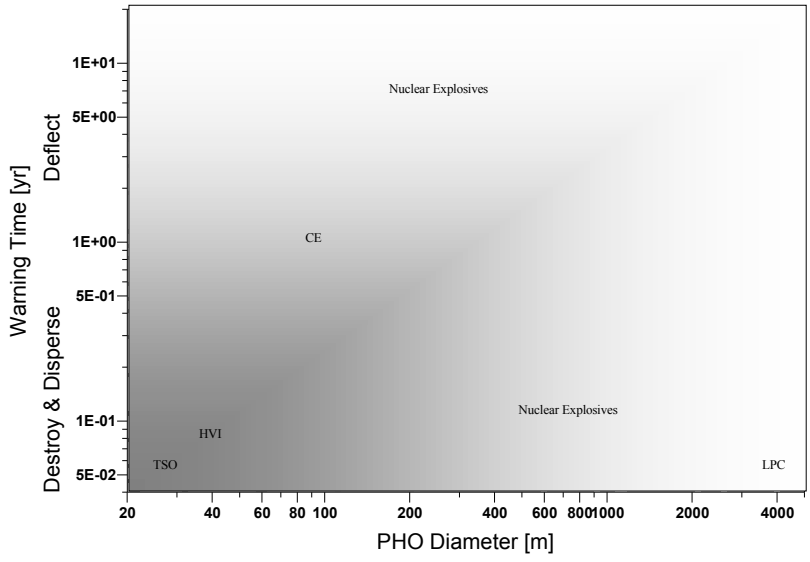

Fig. 1. Approximate relationship between warning time, size of PHO, probability of Earth impact, with a few examples of the type of objects and possible countermeasures. The intensity of the shading indicates the probability of an impact as a function of warning time and size of the object, the darker the more likely. TSO refers to a Tunguska sized object, and LPC to a long-period comet. Possible countermeasures are indicated by HVI for a hypervelocity impacts and CE for chemical explosions. Other possible counter measures are as indicated.

Engagement Space Variables

Input from observations of a PHO, such as the time available for reaction, the size of the object, its spin state, whether it is a binary, its shape, the elements of its trajectory, its chemical composition, and its physical structure will determine the type of the countermeasures. The types of countermeasures we consider include hypervelocity impacts, conventional explosions for surface and subsurface applications, and nuclear explosions for stand-off, surface, and subsurface applications. Fig. 1 relates in very general terms some of these variables to possible countermeasure responses and to the frequency of the objects. Countermeasures for warning times less than one year are intended as long-term goals as our technology advances.

The Playbook

Decisions to select the most effective type of countermeasures for any situation depend on engagement space variables. Pre-investigated scenarios will be useful as a guide, particularly if the warning time is short, as might be the case for some objects. The playbook we plan to develop will define specific countermeasure scenarios for a series of variables. It will also show the overlap of some scenarios. In Fig. 2, we outline the beginning of a Decision-Making Chart for the Playbook. As an example, the data from the threatening PHO are entered into the Decision-Making Chart. The most important variable is the warning time, which will be considered first. Once a warning time has been determined, a trajectory will be calculated how best

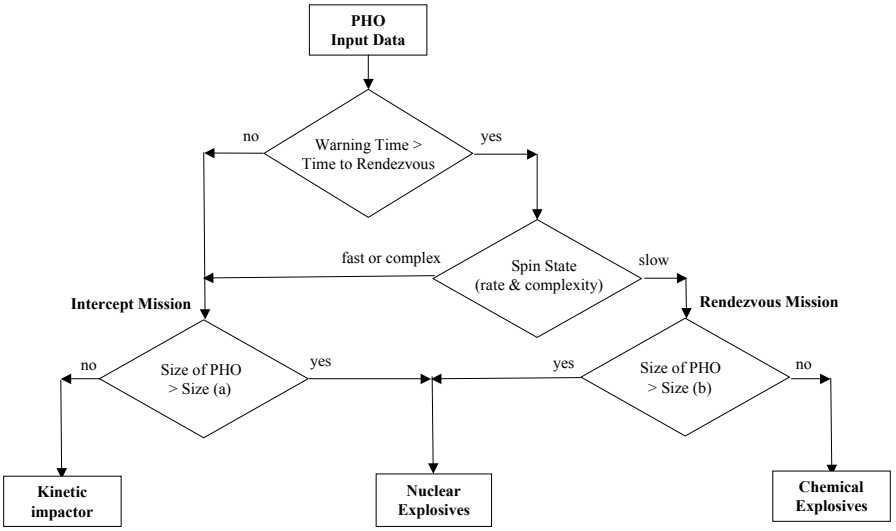

Fig. 2. Decision-Making Chart. More specific values for Size (*a*) and Size (*b*) will be determined from Engagement Space variables.

to reach the PHO. If the time needed to rendezvous with the object is longer than the warning time, then the mission will have to be an intercept (flyby type) mission. If time permits a rendezvous mission, then this option will be preferred. If the warning time is long enough to allow for a rendezvous mission, then the next test is to determine the spin state of the PHO. If the object is spinning fast or the spin state is complicated, for example the object spins about two axes, then placement of the countermeasures on or below the surface of the PHO may be difficult. In this case the decision should revert to an intercept mission. In either case of an intercept or a rendezvous mission, the size of the object must be considered. If the PHO is larger than a certain size, size (*a*) in case of an intercept mission or size (*b*) in case of a rendezvous mission, then nuclear explosives would be preferred. If the PHO is smaller than size (*a*) then a kinetic impactor may be appropriate for an intercept mission. If it is smaller than size (*b*), then chemical explosives appropriately placed on the surface or below the surface may be the preferable choice. Both size (*a*) and size (*b*) must be determined from more detailed analyses of the engagement space variables.

Not shown in Fig. 2 are decisions appropriate for a PHO that is a binary system. A number of known impact craters on Earth and other planets and moons have a companion crater nearby. It appears that they were formed by the nearly simultaneous impacts of similar-sized objects, suggesting impacts of a binary set of asteroids. One possible approach to counter binary asteroids is to disrupt and disperse one component of the binary system at the right moment in their mutual orbit. With one component eliminated, the other component will be deflected in its orbit. However, a detailed analysis of such a scenario is needed.

Data Required for the Analysis of the Engagement Space Variables

The most important data for physical properties come from observations and *in situ* investigations of asteroids and comet nuclei. However, such data are difficult to obtain particularly since they concern the interiors of these objects. Thus, to properly plan for and support appropriate decisions in real time, missing data must be substituted by simulated data (i. e., Earth-equivalent data) adjusted to conditions that we presume to be appropriate for asteroids and comet nuclei. Some data are impossible to obtain over the entire density-temperature region of interest. Such data must be supplemented from theoretical calculations. Opacities, equations of state (EOS), and nuclear cross sections fall in this category. Although many properties for asteroids and comet nuclei are similar, there also are significant differences. For this reason we present required properties separately for these objects.

Commission 15 of the International Astronomical Union is charged with the Physical Studies of Comets and Minor Planets (asteroids). This commis-

sion has set up several task groups to help with the interpretation of data from asteroids and comet nuclei. One task group in particular, the Task Group for Physical Properties of Near-Earth Objects (TGPPNEO) is collecting and analyzing data and making recommendations for the best available data. This task group has `met' once electronically via e-mails and it has planned additional meetings. Other task groups have been charged with improving methods to determine the size (via brightness) of asteroids and comet nuclei and the polarization — albedo relationship [3].

Required properties for asteroids include the size, shape, and mass of the object, the mass distribution in the object, the bulk density and spin state, the light curve, albedo, taxonomic classification, and polarimetric parameters, the chemical composition, and the reflectance spectra. Some of these properties describe the interior of an asteroid, while others describe its surface. It is hoped that analyses will relate some of the surface properties to interior properties such as structure and composition.

Global (whole body) properties, such as material strength and internal structure, can be determined best from the analyses of penetrating waves: artificially initiated seismology and multifrequency reflection and transmission radio tomography. The velocities of shear and compression waves relate to the modulus (deformability) of the material. Seismology provides the best geophysical data of near-Earth objects (NEOs) composed of consolidated materials while radio tomography provides the best geological data (e. g., the state of fracturing) of nonconducting media. Electromagnetic (radio) waves are rapidly attenuated in conducting media, while sound waves are rapidly dissipated in porous objects like comet nuclei or highly fractured asteroids. Thus, the two methods are complementary: seismology is best for stony and metallic asteroids, while radio tomography is best for comet nuclei and carbonaceous asteroids.

While some properties such as size, shape, mass of the object, mass distribution in the object, bulk density, spin state, light curve, and albedo, are of the same types as for asteroids, for comet nuclei we also need the gas production rate, the dust-to-gas mass ratio, and information about its dust trails and meteor streams. Bulk densities for asteroids and comet nuclei and sizes for some short-period comets are known and are publically available in our database located at *http://neodata.space.swri.edu*. It is surprising that the densities of asteroids and comet nuclei are quite low. Even the densities of S-type asteroids are lower than their stony structure would suggest. Besides the orbital parameters of a threatening object we will need the material properties of that object. Considering NEOs as a subgroup of asteroids and comet nuclei, it is hoped that the database will eventually contain representative data from asteroids and comet nuclei in general.

Material properties

We divide the material properties into three categories. In the first category, we list data obtained from remote sensing (e. g., observations) or *in situ* measurements at an asteroid or comet nucleus. However, not all the required data can be obtained from observations or measurements. Some useful data also can be obtained from comet — asteroid — meteorite — dust links. Additionally we can supplement the data with a second category: data measured in Earth environments but corrected for conditions in space (i. e., simulated for conditions expected to exist in or on asteroids and comet nuclei). A third category of data comprises pre-calculated information. On our website *http://neodata.space.swri.edu* the data in the first two categories are further divided into two subgroups: Static data for slow, nearly static countermeasures and dynamic data for impulsive countermeasures. However, since our proposed approach of countermeasures concentrates on impulsive methods, we concentrate primarily on that subgroup, although some of the static data also will be discussed because they also play an important role in impulsive countermeasures.

1. Observational (*in situ*) *data*

Dynamic data for countermeasures based on large but very short-duration impulse methods include: momentum coupling coefficients; strain rates, deformability (Young's modulus); Poisson ratios; yield, flow, and fracture stresses in compression and in tension; Hugoniots; Grüneisen parameters; and dissipation rates. These data are needed when a sudden (explosive) force is applied to an object, which may transmit a shock wave through the object causing spall on the opposite side. When spalled material flies off it reduces the amount of momentum imparted and thus reduces the effectiveness of the countermeasure.

Static data for long-duration long impulse countermeasures include densities, porosity, and pore radii in the ice — dust mixtures of comet nuclei, complex permittivities, thermal conductivities, heat capacities, enthalpies, and sound speeds.

2. Simulated (*Earth equivalent*) *data*

The dynamic elements of the simulated data encompass the same types as for the observational data listed above. The static part of the simulated data includes physical and mechanical properties of minerals, heat capacities of rock-forming minerals, vapor pressures and enthalpies in addition to the observational static data listed above.

3. Pre-calculated information (*theoretical calculations to fill in experimental data*)

Equations of State (EOS) and opacities will be needed for large regions of temperature and density. At high temperatures these data are usually available. However, for low temperatures special calculations may have to be carried out. For situations where chemical equilibrium can be assumed, the molecular EOS will be calculated taking phase changes (e. g., condensation) into account. The equilibrium abundances of the gas phase and any condensed species that may be present will be obtained by minimizing the total Gibbs free energy of the system with respect to the number of species present in each phase at a specified temperature and pressure (density). The procedure has been described, for example, by Sharp and Huebner [4]. EOS and opacity are important during the ablation phase, for example during a stand-off nuclear explosion. In addition appropriate nuclear cross sections are required.

Conclusions

It is our ethical responsibility to move forward. Governments (i. e., tax-paying members of the public, who also are those at risk to PHOs) have supported the basic research that will be used in this project for decades. It is time to apply the results of this research to a problem that benefits all mankind (e. g., to prevent a Tunguska phenomenon, or worse, on short notice). International participation will promote rapid success.

We propose that various teams investigate how to counter a Tunguska-sized asteroid on a collision course with the Earth. For example, we can:

1) Define the orbit of an assumed 50 m diameter stony asteroid,
2) Define its assumed geophysical and geological properties,
3) Define a short warning time that is too short for a rendezvous mission,
4) Develop models for effective countermeasures,
5) Present results at a future ACH-type meeting.

It will take a significant effort and, if not enough resources are provided, a long time to build a materials properties database. It is also important to acquire the basic geophysical and geological data we need to carry out successful countermeasures. Remote sensing for physical characterization should be increased, several dedicated asteroid and comet missions should be prepared for geophysical and geological investigations, and it is prudent to develop and prove the technology and learn how to make geophysical measurements on NEOs as soon as possible. We also must develop a long-term plan for sample returns.

Determination of whole-body properties is still funded poorly, but is nevertheless crucial for the development of countermeasure techniques. It

suffers from limited progress. We must develop and launch a number of coordinated multiple rendezvous missions, possibly based on relatively inexpensive microsatellite technology to visit different types of asteroids and comet nuclei to establish their detailed structure and physical properties. In particular seismology experiments are needed. It will not be possible to investigate all NEOs, but we must collect a statistically meaningful sample.

Long-period comets usually are ignored when discussing countermeasures, because they are extremely rare, impossible to predict (because their orbital periods range from 200 years to over one million years), very large and fast moving, and can have very short warning times. For example, a retrograde long-period comet can have a speed greater than 70 km/s relative to the Earth. Thus, since they are large (massive) and fast, they release enormous amounts of energy in an Earth collision, with the potential to destroy civilization. Although they ar rare, we must not ignore them. They must be included in countermeasures to protect the Earth. Hopefully we never will have to defend against one, but that is no reason to ignore them in countermeasure plans.

References

1. *Huebner W. F., Johnson L. N., Boice D. C., Bradley P. et al.* A Comprehensive Program for Countermeasures Against Potentially Hazardous Objects (PHOs) // Sol. Syst. Res. 2008. Vol. 43. P. 334–342.
2. *Harris A.* Estimating the NEO Population and Impact Risk: Past, Present and Future // Proc. of the Intern. conf. “Asteroid-Comet Hazard-2009”. St. Petersburg, September 21–25, 2009 (see this book).
3. *Cellino A.* The importance of polarimetry for NEA studies // Book of abstracts. Intern. conf. “Asteroid-Comet Hazard-2009”. St. Petersburg, September
   21–25, 2009. P. 44–46.
4. *Sharp C. M., Huebner W. F.* Molecular Equilibrium with Condensation. // Astrophys. J. Suppl. Ser. 1990. Vol. 72. P. 417–431.

The Asteroid-Comet Hazard Conference Proceedings, 2009

INVESTIGATION OF NEOS IN SITU. COUNTERACTION TO THE NEO HAZARD

Description of a NASA Study to Deflect Hazardous Asteroids

C. Maccone

International Academy of Astronautics, Paris, France

Abstract. In January 2007 this author served as Principal Investigator (P. I.) for the Kinetic Deflection of NEOs during a Study conducted by NASA at the Marshall Space Flight Center (MSFC) in Huntsville, Alabama, USA.

The well-known asteroid 99942 Apophis was used as asteroid test-case, and the Study foresaw three different ways of achieving its deflection by ***only*** resorting to the two brand-new NASA launchers, Ares I and Ares V. These three envisaged, alternative deflection techniques are, respectively:

Nuclear Deflection, achieved by virtue of a B83 nuclear warhead (Prof. John Remo of Harvard University served as P. I. for this nuclear deflection study);

Kinetic Deflection, i. e. deflection achieved by (at most) six impinging 1.5 t projectiles (this author served as P. I.);

Solar Collector, i. e. deflection achieved by a Sunlight beam focused by a two-mirror Solar Collector upon the asteroid (Prof. Gregory Matloff of NYC Technical College was P. I.).

The results of this NASA Study ([1]) were first presented publicly by Dr. Robert B. Adams, the Study Team Leader, at the Planetary Defense Conference held in Washington D. C., USA, March 5–8, 2007. In this author's view, however, the importance of these NASA plans for NEO deflection are such that he asked for and obtained from NASA full permission to present anew Dr. Rob Adam's 2007 Presentation at the "Solar System Bodies" Conference held in Kharkov, the Ukraine, May 26–29, 2008. Again, he presented this NASA Study anew at the St. Petersburg International Conference "Asteroid-Comet Hazard-2009" (ACH-2009), September 21–25, 2009. It is thus hoped that this new presentation will be of help to Russian and European Space Scientists interested in the Deflection of Hazardous NEOs.

Introduction

In 2004 NASA embarked on a new vision to explore space [2]. The architecture that resulted includes a human rated launch vehicle and a heavy lift cargo vehicle. Both vehicles are derived from shuttle technology.

The crewed launcher, the Ares I, is slated to be complete by 2014. However, here is an important note about the ARES I-X Test Launch, added by the author C. M. of this paper on February 28, 2010, and taken from the "ARES I" Wikipedia site: http://en.wikipedia.org/wiki/Ares_I :

"The Ares I prototype, Ares I-X, successfully completed a test launch on October 28, 2009. The launch pad 39B was damaged more than from a Space Shuttle launch. During descent, one of the three parachutes of the Ares I-X's first stage failed to open, and another opened only partially, causing the booster to splash down harder and suffer structural damage."

The heavy lift vehicle is called the Ares V and is currently scheduled to be completed by 2020. The vision defines the objectives of returning humans to the Moon in 2020 in preparation for future human exploration of Mars and other destinations.

In 2004 NASA published a review [3] of mitigation technologies for defending the planet from Near Earth Objects (NEO's). This review was completed at the George C. Marshall Space Flight Center and several of the authors of [1] were contributors. Although the results of the 2004 technical paper were preliminary, they suggested that mitigation methods would benefit greatly from the existence of a heavy lift launch vehicle (such as Ares V). Another result of the 2004 study was the need for advanced propulsion technologies. Many of these technologies are also applicable to human deep space exploration (such as Ares I).

Clearly, there is the potential for substantial synergy between the objective of human deep space exploration and planetary defense. Both missions will require delivery of considerable payloads with propulsion systems that produce substantial ΔV. Additionally both missions will experience similar environments in interplanetary space in the inner solar system where Earth and Mars both orbit. Finally, the Vision for Space Exploration requires preparation for human exploration of Mars and other destinations. Human visitation of an NEO would be an excellent candidate for an intermediate mission between returning to the Moon and the first landing on Mars; with a degree of difficulty in operations, ΔV and space environment between the two missions above.

What is also clear is that in the current political environment and the numerous issues faced by the United States, there is precious little extraneous funding for new missions like planetary defense. NASA has its hands full completing the near term task of returning to the Moon while maintaining agency priorities in Earth and space science, education, legacy infra-

structure, etc. The direction of the study described herein is to consider what can be done in the realm of planetary defense using the Vision for Space Exploration architecture and minimal new technology development. Perhaps in the future, planetary defense will rise high enough in the pantheon of the country's priorities.

Approach, groundrules, and assumptions

Many of the groundrules and assumptions for the study are derived from the dual requirements that the vehicles for the Vision for Space Exploration architecture are available and that minimal new funding is available to support development of a new planetary defense architecture. From this it is easily concluded that only near-term technologies should be considered. Times to bring vehicles from concept to operation can easily range from 5–10 years. Therefore, it is not unreasonable to assume that a planetary defense system, requiring minimal technology development, could be operational by the time the Ares V is brought on line, i. e. 2020.

Current knowledge of the NEO population is limited. Current knowledge of NEO's does not include a strong understanding of the densities or internal structure of most asteroids and comet nuclei. Whether the NEO in question has a dust cloud or satellites is not usually known. Current detection systems cannot determine orbital parameters, size or geometry with a high degree of accuracy. This study assumes that there is not a substantial increase in the capability of current detection systems or the understanding of the physical parameters of NEO's.

Concept of operations

Both the Ares I and Ares V vehicles are used in the operational concept for this study. At some point after 2020 current or future detection systems determine that a NEO has a substantial probability of striking the Earth in the near future. When the probability exceeds a threshold determined by the appropriate governing body (i. e. Congress or the President for a NASA developed system) the operational plan for NEO threat mitigation will be put into action.

The first step will be to launch an observer satellite on the Ares I to yield the required information on the NEO. This observer satellite will either rendezvous or fly-by the NEO. Observer operations will be designed to yield highly accurate information on the internal structure and possible composition of the NEO, as well as its geometry, rotation, orbital elements and the potential for orbiting dust, debris or small satellites.

With this information, the probability of impact as well as the consequences of impact can be estimated to a much higher level of accuracy. If the results suggest further action is needed to protect the population (again based

on guidelines ratified by the appropriate governing body) then one of the interceptor options will be launched.

Which interceptor is launched is determined by the results from the observer satellite. The most capable interceptor will be launched based on time before impact, size and composition of the NEO, etc. The interceptor will be launched on an Ares V launch vehicle. Based on the interceptor option, the interceptor will either collide with or rendezvous with the NEO. Each option has a different method of interacting with the NEO to mitigate the threat posed. It should be noted that if possible the observer satellite will rendezvous with the NEO. Not only will this offer additional time to characterize the NEO, it will give an additional asset to observe the NEO while it is being affected by the interceptor, should the interceptor be needed.

Ares launch vehicle description

The designs for the Ares I and Ares V are currently in the state of development. Other documents define the design and capabilities of these vehicles in detail. This section describes the Ares I and Ares V from the state of their design when this study was completed.

The stack of the Ares I vehicle is comprised of a first stage that is a Reusable Solid Rocket Motor (RSRM) modified from the current Shuttle Transportation System (STS) to add an additional fifth motor segment. The second stage is a new design utilizing liquid oxygen (Lox) and liquid hydrogen (LH2) propellants and a modified version of the J-2 engine used on the second and third stages of the Saturn V launch vehicle. The relevant parameters and performance of the Ares I are listed in Tab. 1. The Ares V vehicle design is based on the STS stack. The orbiter is removed from the stack. The external tank is extended and the payload is placed on top of it for the new Ares V design. The Ares V specifications and performance is also in Tab. 1.

Table 1. Performance and specifications for the Ares I and Ares V

Target Orbit/C3	Inclination	Ares I payload	Ares V payload
–30 · 100 nm	28.5º	52.592 lbm[1]	n/a
–30 · 100 nm	51.6º	49.260 lbm[1]	n/a
100 · 100 nm	28.5º	n/a	105.487 lbm[2]
–2.6 km^2/sec^2	n/a	n/a	134.483 lbm
–2.0 km^2/sec^2	n/a	5146 lbm	133.585 lbm
0 km^2/sec^2	n/a	n/a	129.600 lbm
10 km^2/sec^2	n/a	n/a	111.262 lbm

The Ares V performance to the various values of C3, are based on a direct ascent trajectory and the complete exhaustion of the EDS propellant. Ares V performance to LEO in the preceding table is based on burning 290,000 lbm of EDS propellant in a sub-orbital burn with 218,519 lbm of

propellant remaining. Propellant can be traded for payload in this configuration on a 1 : 1 basis, subtracting the added payload from the propellant remaining for an Earth departure burn.

Observer description and target classification

The observer satellite is loosely based on the Deep Impact spacecraft. The observer uses several of the same payload instruments, with some additional instruments specifically designed to yield the maximum amount of information on the NEO. Whenever possible the payload package was selected to give multiple instruments capable of measuring each aspect of the NEO. A list of instruments on the observer satellite, and the measurements and results expected from each instrument can be found in Tab. 2.

The primary mission of the scout probe is to supply the critical information necessary for a successful diversion. The principal data goals are verification of mass and local dynamics (i. e. three dimensional rotations relative to the trajectory) as well as geometry and composition (i. e. solid, fragmented or rubble pile). This data needs to be gathered in time to provide the mission planners with targeting and timing parameters for the diversion. The philosophy behind the design is redundancy of approach to gathering the data and multi-purpose sensors. To provide the maximum mission flexibility, the main power source is assumed to be RTG. This will allow greater flexibility in maneuvering the spacecraft relative to the target without Sun pointing or battery-life considerations.

Since the exact target and trajectory will not be known, a balance of capabilities and ΔV must be made. How fast the target can be reached versus

Table 2. Observer satellite instruments and expected measurements

Category	Instruments	Planned measurements
Optical	Laser ranger	Orbital elements
	Narrow field CCD	Surface mapping, geometry, dust environment
	Wide field CCD	Dust environment, geometry, potential satellites
	Spectrometer	Composition, density
Radar	MARSIS radar sounder	Density, internal structure
	Dual mode radar/data link	Internal structure
Other	Gravity sensor	Mass, gravitational field
	Chemical analysis package	Composition
	Seismic sensor	Internal structure
	Fly-by balls	Mass, gravitational field

how long a sensing period will be available will be addressed in follow on studies. A baseline design uses the lift capacity of the Ares I together with proven technologies.

The primary sensors of the probe will be a 30 cm optical system with an integral laser range finder and a MARSIS style subsurface radar sounder. In addition, the spacecraft will have on-board accelerometers/gravity sensors which, when combined with range data from either radar or laser, will provide mass estimates. The probe will also carry a lander and a box launcher for seismic impactors and gravity fly-by projectiles.

The optical system will have the laser transmitter(s) positioned in the shadow of the secondary and shared the 30 cm aperture (using a beam-splitter at the laser frequency) for the receiver portion of the range finder. The optical side will have both wide field and narrow field video systems with limited zoom capabilities. The basic optical package, with associated electronics would be a common design with the diversion spacecraft targeting system as both missions have similar targeting accuracy requirements.

The second mass determination method consists of launching a suitable mass (a shinny polished ball of aluminum) in a fly-by of the target. The laser ranger will supply velocity data and the optical system will track the sphere, the diversion of trajectory will be used to calculate the mass estimate. The box launcher, located on the central axis of the space craft will have a mix of seismic impactors and fly by spheres, thereby allowing multiple data acquisition attempts.

The lander will have a basic guidance system (similar to the diversion "bullets"), attitude control system and onboard command and control and data-link to the mother spacecraft.

The main sensors of the lander are three seismic sensors on the three (fairly long deployable) legs with spikes to establish a close contact with the hard surface of the target. Due to the low gravity, it is anticipated that a constant thrust motor will be required to hold the lander against the surface while the mother craft launches a series of impactors into the target. The seismic sensors will monitor the internal reflections, giving us a view of the structure. A solid rock will have one pattern, a collection of large masses will have a different pattern and a pile of rubble will have no internal signal. Together with the radar mapping of much of the interior and modeling of the external geometry from the video system, a detailed picture of the target can be developed.

The basic spacecraft will require a fairly robust attitude control and star tracking (or Sun–Earth tracking system) to locate itself in space. It is anticipated that the main up-link/down-link would be a gimbaled hi-gain (parabolic) antenna, to allow the craft's sensors to be aligned with the target while transmitting data to Earth. A second smaller hi-gain antenna would be on the

sensor side of the craft, to communicate with the lander and as a dual purpose radar system/ranger as backup to the optical system. This second (smaller) hi-gain could be the backup down link to Earth, but would require reorienting the spacecraft to transmit/receive.

The optical system could also have a "DEEP IMPACT" style spectrometer to look at the ejecta from the impactors and the lander could have LOCAD style chemical analyzers built into the spikes.

Since the target may be tumbling relative to the mother-craft during the lander portion of the mission, the lander will require data storage and burst transmission capabilities and probably an omni-directional antenna.

Most of the technologies required for this mission already have been demonstrated and flown. The oil exploration industry has the seismic mapping technologies. The Mars probes have the radar mapping technology. The image processing to calculate the rotation and geometry from the range and video stream (feature recognition and 2d-to-3d mapping from multiple images) already exists in various formats.

Observer design

Attached below the observer satellite will be two different main propulsion system stages, one with a reaction control system; each stage either has its own subsystems or shares resources with the other stages. The stages produce enough ΔV to escape Low Earth Orbit (LEO) as well as perform any needed interplanetary maneuvers. The stages were sized so that they, in combination with the observer satellite, use the full capability of the Ares I as listed in Tab. 1.

There were several constraints in laying out the observer satellite vehicle configuration. Several payloads required unobstructed fields of view. Also there are typical constraints for avionics, thermal and propulsion systems. The propulsion stages were configured to minimize height to allow for the stack to fit within the Ares I launch shroud while maintaining simplicity.

Performance

Behind the observer satellite are two of liquid bipropellant stages. The stages produce enough ΔV to escape Low Earth Orbit (LEO) and for some additional ΔV for interplanetary maneuvers. The stages were sized so that they, in combination with the observer satellite, use the full capability of the Ares I as listed in Tab. 1. The performance of the stages is shown in Tab. 3. In order to obtain a one-way outbound trajectory for the observer satellite, the high thrust tool called MAnE, or Mission Analysis Environment, which was developed by Jerry Horsewood of Space Flight Solutions, was used. After inputting such parameters as departure and arrival bodies (which were Earth and Apophis, respectively), specific impulse, approximate dates, and

Table 3. Performances of the trans-asteroid injection (TAI) stage and of the rendezvous kick stage for the observer satellite

Propulsion System	Thrust (lbf) / Number of Engines	Nominal Isp, seconds	ΔV capability, m/s	Propellant, kg
LOX/LH2	24750/1	465.5	4150	13860
Hydrazine/N2O4	1000/1	330	2000	2165
Hydrazine	5/16	234	60	107

time of flight, the code gives ΔV values, burn times, V-infinity values, and optimizes the departure and arrival dates.

Three different opportunities were run; the spacecraft left in the years 2019, 2020, or 2021. Two different ΔV's were computed, that to leave Earth and that to rendezvous with Apophis. As was shown above, the upper bound of the rendezvous ΔV was ground ruled at 2000 m/s. This assumption eliminated the 2019 case. The 2020 and 2021 cases both still were plausible missions, even when considering the Trans-Asteroid Injection burn, which had an upper bound of 4150 m/s. However, note that the intention of this study was to keep the trajectory analysis as general as possible so the observer could leave at any point in time after the Ares I was built.

Interceptor configuration

The interceptor proposed here is comprised of several elements. The individual technology options are integrated into a "bullet", sized so that six of them will fit into a single cradle. The cradle is standardized, so that one cradle will accommodate the entire interceptor technologies proposed herein. The cradle and bullets are propelled towards the NEO with a liquid bipropellant stage. As with the observer, the stage is sized so it and the cradle with the bullets will fully utilize the capabilities of the Ares V.

The term "cradle kickstage" refers to the stage that gets the vehicle out of LEO, which provides 4650 m/s in addition to the 3940 m/s that the launch vehicle's Earth departure generates. This cradle kick stage consists of a LOX/LH2 propulsion system and carries all six of the interceptors and their cradle. After it completes its burn, it is jettisoned and any remaining burns are either performed by the RCS on the cradle itself or by the one of the engines on the bullets. The cradle kickstage was sized using a propellant mass fraction of 0.85.

The next component to be sized was the cradle. It was assumed the cradle holds six bullets as well as some other hardware, such as a LIDAR and cameras for observation and a reaction control system for attitude control. The avionics and communication package is similar to the Observer.

Interceptor technology options

The study assumes three possible technologies for mitigation of the NEO threat. These technologies include nuclear deflection, kinetic interceptor, and solar collector. These technologies were selected as they are a representative subset of the wide array of options proposed in the literature for NEO mitigation. The nuclear option allows for high energy interaction with the NEO. The solar electric propelled kinetic interceptor delivers less energy, but with much more flexibility in achieving the optimum deflection angle. Finally the solar collector option delivers a very low power interaction with the NEO, but has the ability to sustain that interaction for months or years at a time.

Analysis of NEO deflection requirements

It was decided upon two computer applications for modeling the outbound and inbound trajectory legs for the deflection scenarios — Planetary Body Intercept (PBI) and Copernicus. PBI, which only considers impulsive maneuvers, was developed specifically for planetary body maneuvering analysis and was used in the previous study [3] to analyze the inbound planetary body trajectories. PBI reads from an input file the position and velocity vectors of the Earth and planetary body at the time of impact, integrates the equations of motion backward in time by a user-specified number of days, and then determines the impulsive ΔV required to make the planetary body miss Earth by a specified distance. For this study, the specified distance was 3 Earth radii (or 4 Earth radii from Earth's center). The impulsive ΔV directions can be varied, but given the study schedule and results from the previous study [3], the only directions analyzed for the impulsive deflection maneuvers were parallel to the planetary body's velocity vector, either in the same direction as the velocity vector or in the exact opposite direction. These maneuvers, specified with the keywords ACCEL or DECEL in the input file for PBI, generally result in the lowest ΔV requirement. The gravitating bodies included in the model are the Sun and the Earth. The effect of the Moon is not considered.

Copernicus is a generalized spacecraft trajectory design and optimization program developed by the Trajectory Optimization Group in the Department of Aerospace Engineering and Engineering Mechanics at The University of Texas at Austin. Copernicus can model both impulsive and finite thrust maneuvers, as well as perform constrained optimization. Trajectories are modeled as segments, with impulsive maneuvers possible at the beginning and end of each segment, and finite thrust possible throughout each segment. Successive segments can inherit the values of parameters from previous segments, or they can be independent. In fact, successively numbered segments are not even required to model the same orbit or spacecraft. These

features make Copernicus a very flexible trajectory modeling and optimization package. The only gravitating bodies included in this analysis were the Sun and the Earth, although Copernicus has the capability of including a large number of bodies in the model.

The planetary body named (99942) Apophis is anticipated to pass well within the Moon's orbit in April of 2029. Given this fact, the authors decided to make Apophis the subject of the deflection analysis. But before beginning, just as in the previous study [3], the analysts had to modify the orbital elements of Apophis to force it to collide with the Earth on or around April 2029. These calculations were done by Copernicus. The actual ephemeris data for Apophis came from the JPL Horizons ftp-server (*horizons.jpl.nasa.gov*) and was entered into Copernicus. Then several orbital elements were varied until the planetary body collided with Earth, dead center.

From these values the authors calculated the state vector for M-Apophis on the collision date (Tab. 4). The state vector for Earth and M-Apophis were then entered into PBI, which determined the impulsive ΔV values required to successfully deflect the asteroid. The number of days before impact, which represents the time at which the impulsive ΔV takes place, was allowed to vary in 50 day increments from 50 days before Earth impact to 3000 days before Earth impact. As a check, a few cases were also completed using Copernicus, and the results were nearly identical. PBI was used, however, because it can compute the ΔV's for all the impulsive cases in a single run.

Fig. 1 shows the impulsive ΔV values required to successfully deflect M-Apophis. Since the nuclear blast and the kinetic interceptor options are

Table 4. Orbital elements for Apophis and the modified orbital elements for the fictitious asteroid M-Apophis

Source	JPL Horizons ftp server
Epoch	2029 January 01, 0 hms (2462137.5)
Collision date	2029 April 22, 12:10:10.73
System	Heliocentric, ecliptic of J2000

	Original	Modified
SMA	137986931.808626	137978976.282590
Ecc	0.19114698829234	0.19091399221024
Inc	3.34145210222811	3.33334821309700
RAAN	203.87408043057400	212.35750466471000
AOP	126.69571964824600	127.46966492194000

modeled as impulsive events, Fig. 1 shows the ΔV values required from these two deflection mechanisms. As expected, the ΔV requirements are very large if the asteroid is only a few months away from collision. However, if intercepted far enough in advance, the required ΔV can be as low as approximately 5 cm/s.

While applying the impulsive maneuver 500 days or more before impact appears to lower the ΔV requirement, the cyclic component of the graph suggests that applying the ΔV at certain points in M-Apophis's orbit may be more advantageous. When one looks at the position of M-Apophis at the peaks and valleys on the plot, one will see that the valleys correspond to the times when the planetary body is near perihelion, and the peaks correspond to the times when the planetary body is near aphelion.

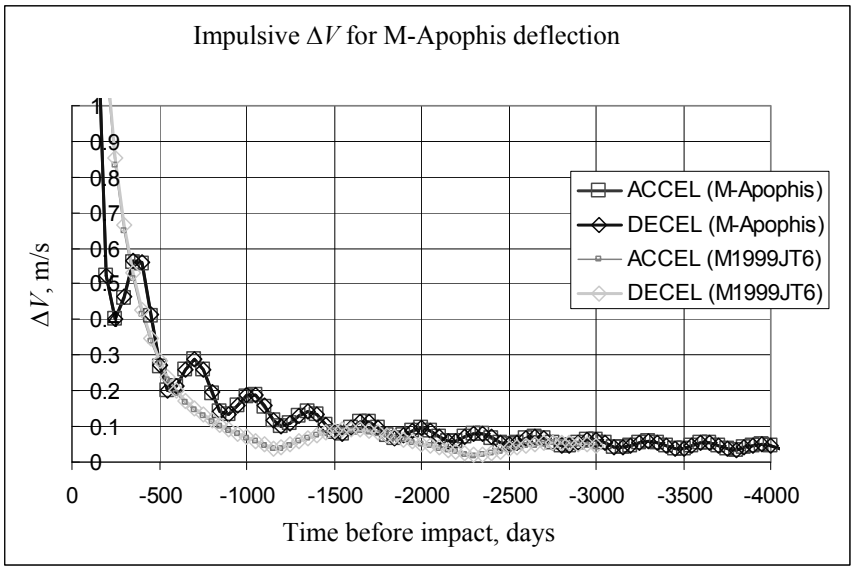

Fig. 1. Impulsive ΔV required to successfully deflect the fictitious asteroid M-Apophis and cause it to miss Earth's surface by 3 Earth radii. There is virtually no difference in the ΔV requirements for accelerating or decelerating the asteroid.

The finite thrust analysis, which corresponds to the solar collector deflection option, was analyzed using Copernicus. And while Copernicus can model the thrust in any direction, the authors decided to initially limit the thrusting to be parallel with the velocity vector of the asteroid, causing either acceleration or deceleration, and then allow Copernicus to optimize the thrusting direction for a few cases in order to compare the benefits of unconstrained thrust angles. The authors selected 1,000,000 kg as the mass of the asteroid; this data was entered into Copernicus, as well as the number of

days before Earth impact when the solar collector began working. With this information, Copernicus was allowed to determine the initial thrust required to successfully deflect the asteroid. The solar collector option was modeled as a solar electric propulsion system so that the effect of the distance from the Sun would be included. Given the mass of the asteroid and the force required, the authors could determine the acceleration required to deflect the asteroid.

The deflection requirements are shown in Fig. 2. Once again, there is little difference between accelerating and decelerating the asteroid, but clearly the length of time that the solar collector can act greatly influences the required acceleration. A rendezvous at 600 days before impact, and with continuous operation of the solar collector, requires an acceleration of $9.4 \cdot 10^{-9}$ m/s^2, which results in a thrust of 0.0094 N for our baseline one million kilogram asteroid. These values drop by an order of magnitude if the rendezvous occurs around 2000 days before Earth impact.

The kinetic deflection option resulted in the most complex trajectory models. The team assumed that the impulse applied by the kinetic interceptor would not be parallel to the velocity vector of M-Apophis, which means

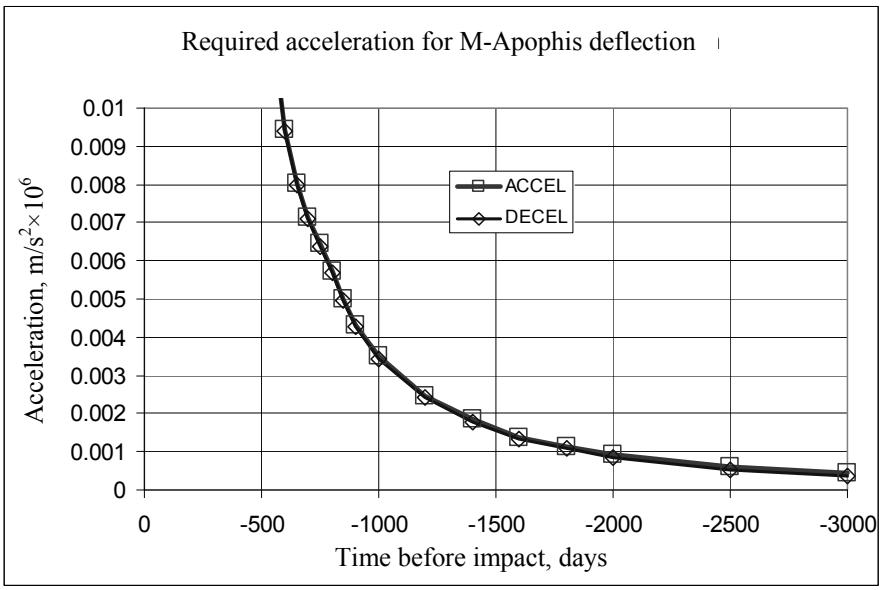

Fig. 2. Acceleration required to successfully deflect the fictitious asteroid M-Apophis versus the number of days before impact at which the deflection mechanism begins operating. As with the impulsive option, there is little difference between the accelerating and decelerating cases, although decelerating has a slight advantage if the operating time is greater than about 1500 days.

that the impulsive ΔV values from the ACCEL and DECEL maneuvers would not be applicable. The approach was to allow Copernicus, given the number of days before Earth impact at which the kinetic interceptor is to collide with M-Apophis, to determine the trajectory that resulted in the maximum encounter velocity relative to M-Apophis. In fact, the ΔV required to rendezvous with M-Apophis was actually determined, which maximized the relative encounter velocity. The TAI ΔV was constrained to a maximum of 8590 m/s, and the rendezvous ΔV to a maximum of 10000 m/s (due to limits of the targeting system). Given that the opposite direction of the rendezvous ΔV vector is the direction of the momentum exchange when the kinetic interceptor collides with the target, PBI was given that vector and used to determine the minimum ΔV in that direction that would successfully deflect the planetary body.

Table 5. Launch and encounter data for M-Apophis using the kinetic interceptor option. Knowing the required ΔV (final column), the encounter relative velocity (5th column), and the asteroid mass, one can determine the required kinetic impactor mass

TBI at Intercept (days) Intercept	TBI at TAI (days) Launch	Trip Time, days	TAI ΔV, km/s	Encounter, km/s	Req. ΔV, m/s
–50	–124.07	74.07	4.44	10.00	6.9312
–100	–176.07	76.07	6.82	10.00	1.8303
–150	–209.54	59.54	8.59	8.11	1.0094
–200	–297.38	97.38	3.55	10.00	5.4441
–250	–387.80	137.80	6.46	10.00	0.6762
–300	–422.09	122.09	8.59	8.34	0.4054
–350	–454.32	104.32	8.59	6.47	0.4199
–400	–475.70	75.70	8.59	7.38	0.7608
–450	–529.49	79.49	5.69	10.00	0.4262
–650	–858.36	208.36	8.59	6.85	0.1588
–700	–883.34	183.34	8.59	8.66	0.1841
–750	–958.47	208.47	5.91	10.00	1.2039
–2000	–2164.53	164.53	8.59	9.08	0.0826
–2100	–2299.94	199.94	4.96	5.68	0.0518
–2500	–2740.21	240.21	6.15	10.00	0.0422

Since the outbound and inbound analysis of the kinetic interceptor could not be decoupled (unlike the other deflection options), and the analysis was more complicated, only a portion of the trajectory trade space could be analyzed. However, the results shown in the table do provide insight into the kinetic deflection requirements. The kinetic interceptor does not generally

impart an impulse in a direction parallel to the planetary body's velocity vector, meaning that the results shown in Fig. 1 could not be used. Instead, the ΔV magnitude is the impulse required along the delta-velocity vector at collision, and does not necessarily agree with the values in Fig. 2. The first column in Tab. 5 is the time before Earth impact (TBI) at which the interceptor collides with the planetary body. The second column lists the number of days before Earth impact at which the interceptor departs from LEO. The far right three columns show the ΔV required to travel to M-Apophis, the relative velocity of the impact, and the required ΔV that the interceptor must deliver for a successful deflection, respectively. In most of the cases for which Copernicus could find a solution, either the TAI ΔV or the encounter relative velocity were at a maximum. The reason is that the encounter relative velocity was always maximized, but constrained, and the launch vehicle and departure stages provide plenty of ΔV for reaching Apophis. Given the required ΔV in the last column, the mass of the asteroid, and the relative encounter velocity, one can determine the required mass of the kinetic interceptor. Clearly, intercepting the asteroid 2000 to 2500 days before Earth impact requires a significantly smaller kinetic interceptor mass.

Conclusions

In conclusion it is evident that the nuclear interceptor option can deflect NEO's of smaller size (100–500 m) with 2 years or more time before impact, and larger NEO's with 5+ years warning. The kinetic interceptors may be effective for deflection of NEO's up to 300–400 m diameter but require 8–10 years warning time. Solar collectors show promise for deflection of NEO's if issues pertaining to long operation time can be overcome. And finally the Ares I and Ares V vehicles show sufficient performance to enable development of a near term categorization and mitigation architecture.

Open issues

The efforts described herein are the result of a short term intense study. There are many issues the authors would like to address in a more detailed long term design effort. The architecture has several issues outstanding, as does the design and modeling of each interceptor option.

For the architecture there are several issues to be addressed. First more detailed designs for all vehicles are indicated to drive out all issues not uncovered in our preliminary design. The interceptor stage was almost double the size of the observer TAI stage, which suggests possible reuse of Lox/LH2 stage in both observer and interceptor stacks. Finally the TAI stage was of similar mass to the existing Centaur stage which suggests possible use of an existing stage.

For the nuclear interceptor option there are details to be worked out in the design and modeling of the nuclear explosion and its interaction with the NEO. Future efforts should include neutron flux in asteroid deflection models. There is still significant uncertainty in asteroid composition, which should be addressed in the interaction model between the resultant neutron and x-ray spectrum and the asteroid composition. The authors would like to continue research into existing terminal guidance technologies under development for missile defense systems. And more investigation of the optimal stand-off distance and the ability to respond accurately enough to explode at the optimal stand off point should be addressed.

Finally, for the kinetic interceptor the authors were not able to include the design of the solar electric propulsion system effects in shaping the interceptor orbit to strike at the optimal velocity and impact direction. Modeling of the penetrator interaction with the asteroid is indicated. For the solar collector the authors wish to expand their investigation of the issues surrounding heating of secondary collector. Reaching a lower rejection temperature would enable higher TRL heat pipe technology. Estimates of beam divergence and focusing require refinement.

References

1. *Rob Adams et al.* Near-Earth-Object (NEO) Mitigation Options using Exploration Technologies // AIAA Planetary Defense Conf. held in Washington D. C., March 5–8, 2007 (the full text of this paper that can be freely downloaded from the web site: *http://www.aero.org/conferences/planetarydefense/2007papers/S3-8--Adams-Paper.doc*. Also, the relevant presentation used by author Rob Adams in March 2007 can be freely downloaded from the web site: *http://www.aero.org/conferences/planetarydefense/2007papers/S3-8--Adams-Brief.pdf*)
2. The Vision for Space Exploration", NP-2004-01-334-HQ, Washington, DC, February 2004.
3. *Adams R. B., Bonometti J. A. R., Chapman J., Fincher S. et al.* Survey of Technologies Relevant to Defense from Near-Earth Objects // NASA-TP-2004-213089, NASA-MSFC, July 2004.
4. *Maccone C.* Planetary Defense from Space: Part 1 — Keplerian Theory // Acta Astronautica. 2004. Vol. 55. P. 991–1006.
5. *Maccone C.* Planetary Defense from Space: Part 2 — (Simple) Asteroid Deflection Law // Acta Astronautica. 2006. Vol. 58. P. 662–670.

INVESTIGATION OF NEOS IN SITU. COUNTERACTION TO THE NEO HAZARD

The Level of Rapid Response Reaction of the Planetary Defense System

A. V. Zaitsev[1], A. Koroteev[2], B. Liaschuk[2], S. Popov[2]

[1]Non-profitable Partnership "Planetary Defense Center", Khimki, Russia
[2]Russian Academy of Cosmonautics by K. E. Tsiolkovsky, Moscow, Russia

Abstract. The necessity to include two basic levels — a level for rapid response reaction (RRR) and a level for deliberate and well-planned reaction — in the structure of the Planetary Defense System (PDS) has been substantiated in [1–3].

This article reviews results for the development of RRR principal components: a reconnaissance spacecraft and intercepting spacecraft. The reconnaissance spacecraft is intended for investigation of dangerous celestial bodies (DCBs), the intercepting spacecraft for their deflection or destruction. Feasibility to identify a DCB 2 to 3 days before its impact is shown.

The necessity of using nuclear methods and, in specific events, kinetic impactors in the RRR structure has been shown. The possibility of the deflection or destruction of a DCB up to hundreds meters of size is indicated.

Introduction

There is no doubt that development of defense measures against asteroid and comet nucleus impacts is required. One of possible ways to ensure the planetary safety can be the creation of Planetary Defense System (PDS) "Citadel' [1]. The basis for such a system has been presented by a first level of rapid response reaction (RRR) called "Citadel-1" [2, 3]. The creation of the RRR is dictated by the possibility of a sudden appearance of a dangerous celestial body (DCB, also known as potentially hazardous object or PHO) as short as a few days, weeks, or months before its collision with Earth.

The situation is attributable to the impossibility of early discovery and identification of all DCBs. As a rule, only rather large asteroids, larger than

hundred meters, can be discovered many years or decades before their collision with Earth. The discovery of asteroid Apophis is one such example.

Smaller asteroids of the size from tens (Tunguska type) to few hundreds of meters can be discovered during their close approaches to Earth. Yet undiscovered objects comprise 99.5 % of the total number of near-Earth asteroids.

The protection of our planet from such objects can be ensured only through the creation of the RRR a first level of the Planetary Defense System. It must be ready for immediate action against a space threat just a few days after a sudden discovery.

This paper deals with some results from research on determining the configuration of rocket-space defense of the PDS RRR Reconnaissance and Interception Service that was carried out by the Russian Academy of Cosmonautics named after Tsiolkovsky (RACTs) in association with the Planetary Defense Center. The work has been performed on instructions of TsNII Mash in the context of the research assignment "Prospects-RACTs", being carried out according to the Federal Space Program of Russia.

Plan of construction and operation of the RRR "Citadel-1"

The RRR has to incorporate the international ground- and space-based surveillance service, two regional segments of the reconnaissance and interception service — the European-Asian, "East", and the American, "West", and, accordingly, two regional Centers of Planetary Defense (CPD) [2,3].

The basis for the ground- and space-based surveillance service will be formed by the space surveillance segment (SSS). As one of possible variants of construction of the operative SSS, the SSS"Konus" [4] can be used.

The regional segments of the ground- and space-based reconnaissance and interception service are meant for a refinement of the DCB characteristics with the reconnaissance spacecraft and for deflecting the DCB from the impact trajectories or destruction of the DCB through the intercepting spacecraft.

The ground- and space-based reconnaissance and interception service must contain:

— rocket-space complexes with a reconnaissance spacecraft and an intercepting spacecraft;

— ground-based infrastructure incorporating the launch preparation hardware of the spacecraft, the launch itself, and its control.

The RRR will operate as follows:

After identification of a DCB all ground-and space-based systems available in the world will start to observe it. The Planetary Defense Centers using information acquired from the ground- and space-based systems will evaluate the degree of hazard and measures for its prevention will be devel-

oped. Upon coordination of a plan of the measures at the international level, instructions to launch the reconnaissance spacecraft and then to the intercepting spacecraft will be issued.

When approaching the DCB, the reconnaissance spacecraft using the patrolling equipment has to provide acquired data needed for constructing the engineering model of the dangerous asteroid or comet nucleus. For this purpose, the reconnaissance spacecraft's instrumentation must incorporate: high-resolution video cameras, an IR multispectral camera, a laser or radar finder, and some other instruments. On the basis of the data acquired the scheme for the interception and the countermeasures against the DCB will be refined.

Choice of methods for action on dangerous celestial bodies

To prevent asteroid-comet hazards, many variants of methods for action on a DCB are proposed. They can be broken down into two groups differing by duration of the action:

— the methods of short-term (impulse) action;

— the methods of gentle long-time action.

To the first group belong the methods of sudden impact (kinetic) and explosive types. For the kinetic impact methods, the spacecraft or some of its parts, kinetic impactors, or small celestial bodies ("space billiards") can be used. To the explosive methods belong the nuclear devices.

The second group can be divided into the methods of direct and distant action. The direct-action methods are rocket propulsion systems of various types (using chemical propellant; electric nuclear engines, using a substance from celestial bodies, and so on), methods for changing the DCB's albedo, etc. The distant-action means are laser facilities, solar concentrators, "gravitational tractor," and so on.

The first-group of methods are more flexible, they can be used both for deflection of a DCB and for its destruction.

The second-group of methods can be used only for the deflection of a DCB. Taking into account its low thrust-to-weight ratio because of the big masses of a DCB, these methods must be able to operate for many months and even years, in order to impart the necessary impulse to deflect the DCB. Therefore, their operative use is impossible for practical purposes. Thus, only the impulsive-action methods — kinetic impacts and explosives — can be applied in the RRR.

The estimates [5] reveal that stony asteroids with a diameter between 50 to 150 m can be destroyed by kinetic impactors with a mass of about 20 to 50 t. At small collision velocities they become inefficient, whereas nuclear devices (ND) can be applied over the whole range of possible DCB parameters. The efficiency of the ND application to the defense against a DCB was

presented in particular in [6] and some other works. The high efficiency of the ND, as well as such characteristics as compactness, reliability, and high availability to service, make the ND a main defense system in the RRR against a DCB.

This paper is concerned with a variant of the ND application to a subsurface explosion as the most efficient means of the action. The ND design of a single application of ~2 Mt of energy [7], was taken as a basis. It allows crushing a DCB of 200 to 250 m size, i. e., objects similar to asteroid Apophis. In the case of a group application of NDs [8], the efficiency of action on a DCB may be increased significantly.

The interception of a DCB by RRR nethods

Strict requirements for effectiveness of launch of the spacecraft, applied in the RRR, dictate using launch vehicles (LV) with a minimum time for launch preparation. For this purpose the LV Zenit, whose launch preparation period amounts to 1.5 hours total, is most promising.

The LV makes it possible to realize an acceleration of the reconnaissance and intercepting spacecraft up to asymptotic velocities of departure from Earth as high as 12 and 3.3 km/s, respectively. The masses of these spacecraft comprise approximately 120 and 4000 kg.

In the case of identification of a DCB two days before Earth impact at a DCB velocity of about 50 km/s, which is near the limiting possible velocity for asteroids, a rendezvous of the reconnaissance spacecraft with the DCB will occur at a range of 950,000 km, of the intercepting spacecraft — 180,000 to 270,000 km from the Earth.

During a flight to the DCB an orbit correction using spacecraft guidance systems will be carried out using data from the reconnaissance spacecraft to inject the intercepting spacecraft into the capture zone of the DCB. After that the final stage will start: the interception of the DCB, i. e., the delivery to it of the means for countermeasures.

Results of simulation of the DCB interception process revealed velocity requirements for the interception spacecraft to rendezvous and on the accuracy of the DCB ephemerides [9]. For instance, the magnitude of the interception ΔV will amount to 600 m/s with the relative velocity of the intercepting spacecraft and the DCB as high as 60 km/s.

Shown in Figure is the scenario of a DCB interception. During approach to the DCB the interception module separates from the spacecraft and heads for the DCB with the aid of low-thrust engines. The orbital module continues its motion on the flyover path and follows the interception process implementing the reconnaissance.

In the case of a miss or the need for additional action on the DCB another intercepting spacecraft is used.

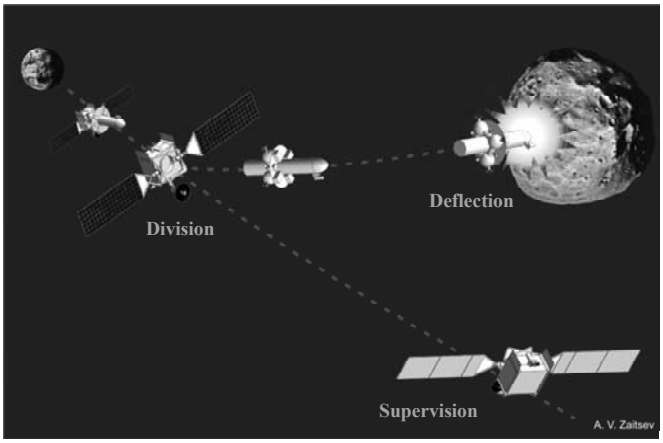

A scenario of a DCB interception.

In forming the operative interception scheme it is obviously necessary that it be governed by "the minimum damage criterion" such as the undesirability of explosions of the ND in the Earth magnetosphere and possible damage to objects on Earth and in near space by DCB fragments.

If necessary, the ND power in the intercepting spacecraft may be increased. For this purpose it is required to perform the docking of two units in near-earth orbit or to use, with an available time reserve, the high power LV Proton.

In both cases the ND mass can be nearly doubled and the ND power can attain 10 Mt [10]. In this case or with the method of groups of NDs it will be possible to destroy a 500 m stony asteroid or deflect an even larger DCB from an impact trajectory [8].

The concept of the proposed PDS suggests the use of the deflection as the main objective of defense against DCBs. In some events, however, in operating the RRR a situation may arise when the DCB would be unintentionally destroyed. This may happen when the energy necessary to deflect a DCB exceeds the energy for destroying it. In this case the DCB fragments can be hazardous. To prevent it, the rocket-space defense system may be applied to intercept the fragments before their entry into the Earth atmosphere [11].

Thus, having combined a few observational, reconnaissance, and intercepting spacecrafts into "operational patrol", we shall be able to ensure the defense against 99.5 % of Earth threatening asteroids.

Progress of observational methods suggests that the rest (0.5 %) of asteroids of size 0.5 to 1.0 km would be identified many years and even decades in advance. Characteristic velocities of asteroid deflection from an impact trajectory will be about 1 cm/s. For this purpose it will be sufficient to apply nuclear devices of the megaton class. Therefore, for the deflection of large-

asteroids the intercepting spacecraft at the level of rapid response reaction may be used. In so doing, the interception scheme will be similar to that of standard missions to Solar System objects.

Conclusion

From the research results we conclude:

The up-to-date level of rocket-space, nuclear, and other technologies allow the creation of a rapid response reaction of the Planetary Defense System against dangerous celestial bodies of the size from tens to hundreds of meters that can be identified in periods as short as a few days, weeks, or months before their collision with Earth.

Nuclear and kinetic impactor methods are most efficient for the action on a DCB at an operative interception. They make it possible, with the use of modern launching systems, to destroy asteroids of the size of about 500 m, and deflect larger celestial bodies.

If necessary, it will be possible on the basis of rapid response reactions to quickly form the level of long-time reaction to counteract larger and more dangerous celestial bodies. This allows us to completely solve the problem of the Earth defense against asteroids and, in part, comets (with nuclei of 0.5 to 1 km in size).

References

1. *Zaitsev A. V.* Planetary Defense System “Citadel”, the conceptual project. M., 2000. 70 p.
2. *Kovtunenko V. M., Zaitsev A. V.* Protecting Earth from Asteroid Hazards is a Real Task for the World Space States // Space Bull. 1995. Vol. 2, N 4. P. 25–27.
3. *Zaitsev A., Pitchkhadze K., Tchesnokov A.* Possible Approaches to Implementation of “Citadel-1” International Planetary Defense System Project // Rep. on Forty-fourth session of the Sci. and Technical Subcommittee of the Committee on the Peaceful Uses of Outer Space (12–23 February 2007).
4. *Dobrov A. V., Zaitsev A. V., Maglinov I. D. et al.* Possible Approaches to Forming of Space Observation Service for Asteroids and Comets // Intern. Conf. “Asteroid Hazard-96”. Program and abstracts. July 15–19, 1996. St. Petersburg. P. 49–50.
5. *Tedeschi W. J.* Mitigation of the NEO Impact Hazard Using Kinetic Energy // Proc. of the Planetary Defense Workshop Lawrence Livermore National Laboratory, Livermore, CA. May 22–26, 1995. P. 313–323.
6. *Shubin O. N., Nechai V. Z., Nogin V. N. et al.* Nuclear Explosion Near Surface of Asteroids and Comets. Common Description of the Phenomenon // Proceeding of the Planetary Defense Workshop Lawrence Li-

vermore National Laboratory, Livermore, CA. May 22–26, 1995. P. 383–396.
7. *Rodionov V. V., Vozovikov V. V., Zadvornov Yu. A. et al.* Nuclear means for affecting near-Earth-objects. Composition and scheme of operation // Chelyabinsk Sci. Center News, Special Issue "Space Protection of the Earth". 1997. P. 111–117.
8. *Simonenko V. A.* Space impacts mitigation: deflection and dispersion based on nuclear explosions // Materials of All-Russian conf. "Asteroid-Comet Hazard-2005". 3–7 October 2005. St. Petersburg, 2005. P. 295.
9. *Zaitsev A. V., Dobrov A. V., Kotin V. A., Simonov I. V.* Impact experiment for project Space Patrol // Intern. J. of Impact Engineering, Vol. 20. Proceedings of the 1996 Hypervelocity Impact Symp. P. 839–848.
10. *Koblov P. I., Simonenko V. A., Ivanov Yu. A. et al.* Main requirements to nuclear explosive device (NED) to be used in system of Earth protection against asteroids and comets // Chelyabinsk Sci. Center News. Special Issue "Space Protection of the Earth". 1997. P. 107–110.
11. *Arsenyev G. N., Semyonov B. I., Torgovkin S. N., Treckin V. V.* The possibility of two-fold use of missile-space defense systems for solving the problem of asteroid-comet hazard // Information-measuring and Control Systems. 2000. Vol. 4, N 5. P. 5–12.

INVESTIGATION OF NEOS IN SITU. COUNTERACTION TO THE NEO HAZARD

Design Parameters and Efficiency of a Space System for Warning about Small Celestial Bodies Approaching the Earth along Collision Trajectories

V. A. Emelyanov, Yu. K. Merkushev

Central Research Institute for Machine Building, Korolev, Moscow region, Russia

Abstract. The space-based system would operate in two modes:
— automatic near-Earth space surveillance,
— tracking of an earlier detected hazardous celestial body (HCB) for synchronous-basic position measurements.

The space telescopes (ST) would be placed at a long distance (such as $5 \cdot 10^7$ km) from the Earth to provide for detecting small (100 m) celestial bodies when they are moving to the Earth from the sunward direction. Also space telescopes would be deployed at a long distance (such as $5 \cdot 10^7$ km) from each other. This would result in a radical increase of synchronous-basic measurements on a small orbit arc. When the system operates in the first mode the narrow rotating telescopic fields of view form the barrier zone (BZ) of reliable detection of HCB before they impact Earth. The optimal version for development of this system was selected. The long-duration (up to 365 days) simulation modeling capture of a HCB by ST have been carried out. Apophis and three other groups of HCBs in orbits with their aphelion distances similar to the semi-major axes of Mars, Jupiter, and Pluto orbits were considered.

Introduction

Warning about collision of small hazardous bodies with the Earth is an actual problem. One can propose protective measures on Earth: evacuation of population from seashores, temporary stopping dangerous industrial enterprises all over the Earth, and evacuation of population from potentially hazardous areas. Reliable detection of small dangerous bodies with ground-based telescopes has to overcome some principal problems:

— continuous search and detection of objects approaching Earth from different directions,

— performing observations against the background of the Sun,

— determination of motion parameters for collision trajectories of objects moving along the optical axis of a telescope.

Principles of development and design parameters

Principles of development of space-based optoelectronic sensors to observe small celestial bodies are the following:

1. Forming a barrier zone (BZ) of reliable detection of bodies before their collision with the Earth.

2. Space-based telescopes should be located relative to the Earth so that the velocity vector of a body moving along a collision trajectory forms some significant angle with the optical axis of each telescope. Also, a body approaching the Earth from the Sun direction should be observed at a ignifycant angular distance from that direction.

3. Use of only two telescopes located in the Earth orbit with narrow (~ 6°) fields of view rotating with an optimal rate around the direction to the Earth (Figs. 1, 2) to form a closed barrier zone.

4. Use of a CCD-detector in the mode of time delay and charge accumulation to increase the valid signal from body to decrease the detector size and the needed processing speed of the on-board data processors.

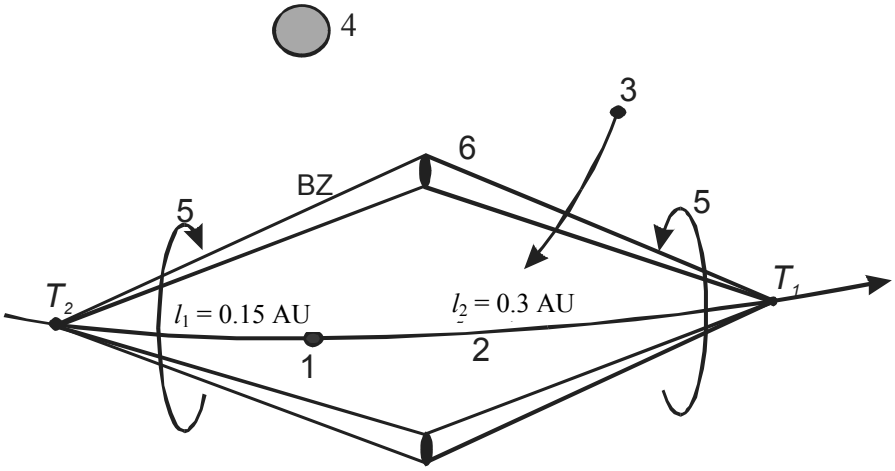

Fig. 1. The cut of the closed barrier zone by the ecliptic plane:
1 — the Earth; *2* — the Earth orbit; *3* — small body; *4* — the Sun; *5* — survey scans of near-Earth space with (*6*) rotating fields of view of the space telescopes T_1 and T_2 (barrier zone).

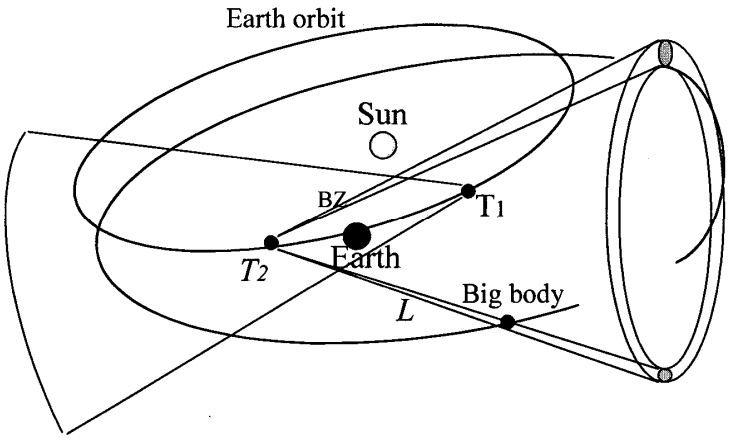

Fig. 2. A big asteroid is detected from a large distance L before its passage through the barrier zone.

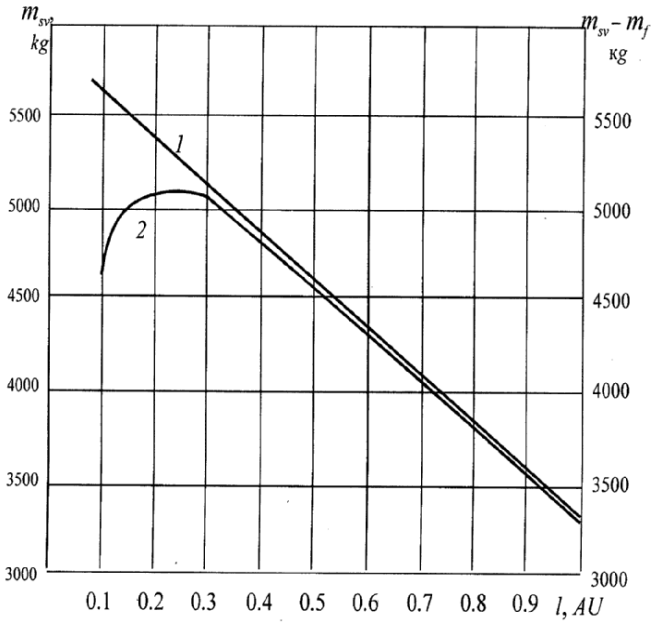

Fig. 3. The mass of a space vehicle placed in Earth orbit at different distances l from the Earth $m_{sv}(l)$ (straight line *1*); mass without the fuel needed to support spacecraft operation within 10 years $m_{sv}(l) - m_f(l)$ (curve *2*).

Algorithms for determining both the warning time, $T_в$, and the minimal size of detectable bodies, d, as a function of direction of body motion relatively to the Earth were developed.

The dependencies of these values on the distances l_1, and l_2 between each telescope and the Earth were determined. Dependencies of required characteristic velocities to launch space vehicles to operational orbits, for supporting them in orbits, and also the tolerable payload mass at these distances were taken into account (Fig. 3). The distances $l_1 = 0.3$ AU and $l_2 = 0.15$ AU are optimal. Both telescopes have identical design parameters: aperture ~1.5 m, 6 deg field of view, focal length ~ 3 m, $\sim 1.5 \times 10^4 \times 256$ CCD matrix.

Efficiency of a Space System

When space-based telescopes are operating in the mode of automatic search survey they have the following efficiency factors:

— the size of the detectable body averaged over all possible motion directions is 75 m,

— the time $T_в$ of warning about collision with the Earth averaged over all possible directions of motion is 40 days,

— warning time guarantied with the probability of 0.9 is 6 days.

The complex problem of determination of body motion parameters is solved by synchronous base line measurements with two telescopes placed at a large distance one from each other (~0.4 AU). In this case the telescopes are operating in the body-tracking mode.

We performed a long-time simulation (for a period ~ one year) of coverage of the body by the rotating fields of view of two telescopes operating in the mode of automatic observation. Three groups of bodies in orbits with aphelion distance Ra close to radius of orbits of Mars, Jupiter, and Pluto were considered.

For the five captures the asteroids size d should be more than 400, 700, 200, 230, 75 m. The warning times $T_в$ are 270, 150, 100, 50, 10 days. Tab. 1 and 2 show the size d and warning times $T_в$ when the small body passes through the closed barrier zone during the last capture before it approaches the Earth. The values d and $T_в$ of 80 m and 10 days do not depend much on inclination i or aphelion and perihelion distances Ra, Rp.

The errors in the course of determination of the body motion parameters decrease radically if synchronous base line observations with two telescopes are used. The measuring interval during tracking time was about 3 days. The errors of determination of angular elements were ~3 arc seconds. The errors (at 3σ level) of determination of other orbit parameters, position and velocity on this observation interval are presented in Tab. 3 for $Ra = 40$ AU, $Rp = 0.9$ AU.

Table 1. The size d and warning time $T_в$ for asteroids with Ra =1.6 AU

i,°	d, m	$T_в$, days
0.3	50	22
10	60	20
30	80	9
60	80	11

Ra = 1.6 AU, Rp = 0.9 AU

Table 2. The size d and warning time $T_в$ for asteroids with Ra = 6 AU and Ra = 40 AU

Rp, AU	d, m	$T_в$, days	Rp, AU	d, m	$T_в$, days
0.1	80	7	0.1	100	6
0.5	95	6	0.5	80	8
0.9	50	14	0.9	60	7
i =10°, Ra = 6 AU			i =10°, Ra = 40 AU		

Table 3. The errors of determination of orbit parameters

e, %	Δa, %	$\Delta\Omega$, arc sec	Δi, arc sec	ΔU, arc sec	ΔX, km	ΔV, m/s
0.01	0.2	3	4	3	500	1.4

We simulated a long time (up to 25 years) observation of Apophis. With operation of space telescopes in automatic search survey mode, the asteroid stays in the vision zone during the time equal to 4.25 years. This is longer than the time the asteroid stays in the vision zone of all ground-based telescopes, which is equal to 3.1 years.

Errors of determination of orbit elements, position and velocity vector at the moment of measuring, as well as flyby distance from the Earth center at the moment of subsequent Apophis passage through the ecliptic plane were assessed.

Simulation of synchronous base line tracking of Apophis for the period from February 21, 2011 to February 24, 2011 was performed. The positions of Apophis and telescope fields of view are shown in Fig. 4. At that time the observation distances L_1 and L_2 were equal 1.4 AU and 1.1 AU [1].

The calculated flyby distance error ΔL 147 days later when Apophis will be crossing the ecliptic plane is shown in Tab. 4. The ΔL value is 3000 km.

Observations were also simulated for the period from February 21, 2029 to February 23, 2029 when observation distances were ~0.2 and 0.3 AU, correspondingly. The error in determining of the flyby distance on April 13, 2029 (53 days after observation period) was assessed. It is equal to 550 km as is shown in Tab. 5.

Table 4. The errors in determining Apophis motion parameters for July 18, 2011

Δe, %	Δa, km	$\Delta\Omega$, arc sec	Δi, arc sec	$\Delta\omega_n$, arc sec	ΔU_a, arc sec	ΔX, km	ΔV, m/s	ΔL, km
0.01	9300	45	2	62	45	100	1.4	3000

Table 5. The errors of determining the Apophis motion parameters for April 13, 2029

Δe, %	Δa, km	$\Delta\Omega$, arc sec	Δi, arc sec	$\Delta\omega_n$, arc sec	ΔU_a, arc sec	ΔX, km	ΔV, m/s	ΔL, km
0.002	814	7.2	0.4	8.1	7.2	10	0.1	550

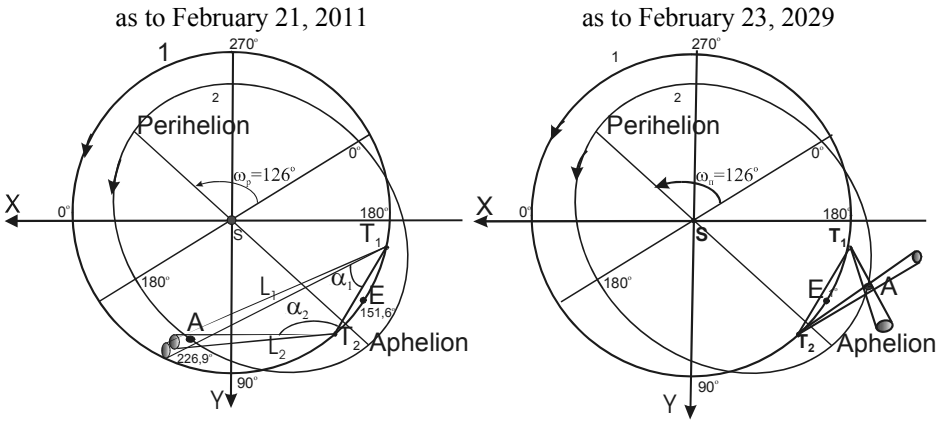

Fig. 4. Mutual positions of the Earth (E), Apophis (A), and the space telescopes (T_1, T_2) when Apophis is simultaneously captured by the two fields of view. *1* — Earth orbit, *2* — Apophis orbit.

The error in determining the body flyby distance from Earth depends on 3 factors. The first factor is the time interval from the moment measurements are made until the moment when the body passes through the ecliptic plane. The second factor are the real angles α_1, α_2 between the direction "telescope T_1 — telescope T_2" and the direction from each telescope to the body. The third factor are distances L_1, L_2 of the body from each telescope. The error of the determining the body flyby distance changed from 3000 to 550 km.

Conclusion

Small-sized 80-meter hazardous asteroids are detected in the barrier zone 10 days before they reach the Earth. Then, in the course of 3 days, their orbit parameters are measured by telescopes operating in the tracking mode. If aphelion *Ra* is 40 AU the error of determining the body position at the moment of measurement is about 500 km. Space telescopes will be highly efficient for warning about small celestial body collisions with Earth.

References

Emeljanov V. A., Lukjaschenko V. I., Merkushev J. K., Uspensky G. R. Tochnost opredelenia parametrov orbity asteroida Apophis, obespechi-

vaemaja kosmicheskimi teleskopami (Accuracy of determination of orbit parameters of asteroid Apophis provided by space telescopes) // Materialji mezdunarodnoji konferentsii "Okolozemnaya astronomiya – 2007" (Proc. of the Intern. conf. "Near-Earth Astronomy-2007"). Terskol, 3–7, September, 2007. P. 59–64 (in Russian).

INVESTIGATION OF NEOS IN SITU. COUNTERACTION TO THE NEO HAZARD

About Measures on Minimization of Damage from Collisions with Asteroids and Nuclei of Comets

N. A. Makhutov[1], V. A. Puchkov[2], D. Reznikov[1], A. Taranov[2], A. V. Zaitsev[3]

[1]A. A. Blagonravov Mechanical Engineering Research Institute of RAS, Moscow, Russia
[2]Ministry of the Russian Federation for Civil Defence, Emergencies and Elimination of Consequences of Natural Disaster, Moscow, Russia
[3]Non-profitable Partnership Planetary Defense Center, Khimki, Russia

Abstract. As the Planetary Defense System against dangerous celestial bodies is not created yet, it is necessary to consider how to minimize damage from possible collisions with them. Special attention should be paid to collisions with rather small bodies, of size from tens (Tunguska type) to hundreds of meters. The risk of collisions with such objects is especially high.

To mitigate possible consequences of impacts it is necessary to define in advance the place, time, and power from explosive damages. A Forecasting Service is necessary for this purpose. The complex methods for forecasting areas of impacts of asteroids and nuclei of comets on Earth should become a major element of the Service. These methods should model the consequences of impacts.

The expediency of creation of the Forecasting Service is substantiated in the article.

Introduction

The possibility of catastrophic collisions of asteroids and comet nuclei with the Earth makes it necessary to undertake measures on prevention or minimization of consequences of these collisions.

As the Planetary Defense System against dangerous celestial bodies (DCB) has not been created yet, special attention should be paid to relatively small bodies whose size is from tens (Tunguska type) to hundreds of meters.

They constitute about 99.5 per cent of the total number of 2 million of asteroids that come close to Earth. As only 6,000 of such bodies have been found so far, the probability of discovery of bodies on collision course with the Earth will increase as their dimensions decrease.

The explosion caused by a DCB impacting on an area of a large settlement, military or civilian nuclear facilities, stores of radioactive, chemicals, or other poisonous wastes can lead not only to large numbers of human casualties and material damages, but could also trigger ecological crisis or even nuclear war.

In order to prevent such consequences it is necessary to define the place, time, and power of explosion in advance and estimate its possible effects on the technological and natural objects in the area of a potential catastrophe.

The threat of asteroid and comet impacts belongs to those natural factors that can be forecast, which makes it possible for the Russian Ministry of Emergency Situations to undertake a number of measures to minimize the potential losses by, e. g., evacuation of people, materials, cultural assets, and hazardous materials and facilities. This can be done if the place and time of explosion are estimated with sufficient accuracy.

The realization of such measures is possible if a service for forecasting the regions to be hit by a DCB and the consequences of the impact are established. Creation of such service is a complicated scientific, technological, and organizational problem that requires an inter-disciplinary approach and broad international cooperation. The substantiation of the possibility to create such international service and to ensure its interaction with the National Center for the Management in Crisis Situations is presented in this paper.

Tasks and methods of forecasting the regions and consequences of a DCB impact

The resolution of the problem of accurate forecasting of the place, time, and power of explosion caused by a DCB impact, and the method for estimating its consequences can be divided into several phases that are considered below.

The DCB detection

At present asteroids and comets are detected by ground-based optical astronomic telescopes. However the ground-based optic devices have a number of drawbacks. They cannot find DCBs coming from the side of the Sun; they depend on weather and other factors. Therefore they do not ensure guarantied DCB detection.

Only a Space Observation Service (SOS) can be reliable at detecting a DCB. The Space Observation Service named KONUS [1, 2] could become a possible version of an efficient SOS. The estimates made show that scan-

ning of the cosmic zone under control of the system can be performed in intervals of several hours, which is sufficient to warn other services about the threat.

It is reasonable to begin creation of the forecasting service with the use of existing means of observations, and then build the SOS that will be one of the components of the future Planetary Defense System against the asteroid-comet threat [1, 2].

Forecasting of conditions for DCB entry into the Earth atmosphere.

To ensure the maximal accuracy of forecasting conditions of DCB entry into the Earth atmosphere it is desirable to engage not only astronomical observatories, but also radar telescopes. The main instruments for reliable determination of orbital and physical DCB characteristics are powerful planetary radars. Along with highly effective numerical methods for trajectory calculations this will allow one to ensure the high accuracy for obtaining the input data for the calculation of DCB motion in the Earth atmosphere.

To ensure continuous daytime observations it is necessary to use radar complexes of Russia (Ussurijsk), Ukraine (Yevpatoria), and USA (Goldstone). Such radar systems will allow one to conduct a continuous monitorring of the entire celestial sphere except southern latitudes

The calculation of DCB motion in the Earth atmosphere

For simulation of DCB motion in the Earth atmosphere it is reasonable to use the experience obtained in the space-rocket industry when developing space vehicles intended to descent in the atmosphere of the Earth and other planets of the Solar System. Methods for numeric simulation of aerodynamic characteristics of irregularly shaped bodies and heat and mass transfer processes when braking in the atmosphere can be applied.

The methods applied allow one to take into consideration not only possible variants of the entry conditions, but also physical characteristics of a DCB such as its size, shape, mass, chemical composition, etc. [3], which ensures an acceptable precision of forecasting the impact region.

Simulation of DCB explosion processes in different media

The final phase of DCB motion in the atmosphere can end in explosion above the Earth surface (like Tunguska explosion) or on the Earth surface, or in water. The power of the explosion and the scope of its consequences will depend on the DCB characteristics (mass, velocity, etc.) and on the medium in which the explosion may take place.

Organizations that took part in the development of nuclear weapons have an experience in theoretic simulation and in carrying out natural experiments on powerful explosions in different media. Their experience can be

used for DCB explosion simulation and for the simulation of the explosion effects such as shock and seismic waves, lightning pulse, tsunami, etc. [4, 5].

Assessment of possible consequences of DCB explosions

The high concentration of potentially hazardous facilities on our planet can provoke a dangerous development of events caused by the impact of a relatively small DCB, which can lead to a catastrophe on a regional or even global scale. The toolkit developed in fracture mechanics for assessing robustness and safety of complex technical systems could be used to forecast such events [6]. The developed theoretical methods are employed together with the methods of computational hydrodynamics and mechanics as well as with physical-mathematical and computer simulation methods. These methods allow one to carry out analysis of peculiarities in the development of dangerous processes caused by a DCB impact and simulation of these processes. Scenarios for development of natural and manmade catastrophes in complex interrelated systems can be worked out taking into account the interaction of initial and secondary catastrophic processes.

Thus, the existing and future means of observations as well as software and algorithm methods allow one to forecast the zone to be impacted by an asteroid or comet nucleus and to assess the consequences of the impact, which enables us to reduce the losses inflicted by these cosmic catastrophes.

The service of forecasting the regions of DCB impacts and their consequences

It is reasonable to have two regional segments of international service — Eurasian and American — with each having its Forecast Center. The service should include Cosmic Observation Segment, optical and radar ground instruments, and regional forecast centers and communication channels between all components of the service.

After a DCB is discovered, all optical instruments join the observations. Simultaneously, in response to the request of the Forecast Center the planetary radars of the Russian Space Agency, those of foreign space agencies, and military agencies will be drawn into the observations.

Once the complex processing of the orbital data has been made, the conditions of the DCB entry into the Earth atmosphere can be forecast, its motion in the atmosphere can be simulated, and the region of its impact can be determined. Then the simulation of explosion process and its potential consequences can be made. On the basis of the data, the decision on reducing the possible losses to be inflicted by the cosmic catastrophe can be estimated.

After the System of Planetary Defense is established, the decision is made in collaboration with the Planetary Defense Center. The possibilities to prevent the collision are examined. This aim can be achieved by deflecting

the body from hazardous trajectory or by fragmentizing it into small particles.

In order to work out the methods and means of interaction between the components of the Forecast Service, it is necessary to carry out international physical and computational experiments. This will allow one to form a reliable basis for forecasting the conditions of the DCB entry into earth atmosphere (time, velocity, and coordinates) and DCB characteristics (size, shape, mass, composition, etc.)

Conclusion

1. The existing means of space monitoring and algorithm methods allow one to perform simulation of processes of collision between the Earth and a DCB, and to take effective measures to reduce potential losses.
2. In order to make an effective prediction of the time, place, and power of explosion caused by a DCB impact it is necessary to develop national and international research program and to set up the International Forecast Service.
3. To develop methods, means, and interactions between the components of the Service it is necessary to carry out an international demonstrative experiment, using a real DCB flying by the Earth as an experimental object.

References

1. International Conference “Asteroid Hazard-96”. Program and abstracts. July 15–19, 1996. St. Petersburg. 152 p.
2. *Zaitsev A. V.* The Planetary Defense System “Citadel”. The conceptual project // Lavochkin Association. 2000. 70 pp.
3. *Derugin V., Zaitsev A., Kozlov I.* Evaluation of possible dispersion of places of falls of celestial bodies on the Earth surface // Abstracts. Intern. conf. “Space Protection of the Earth-96”. 23–27 September 1996. Snezhinsk (Chelyabinsk-70). P. 99–100.
4. Katastroficheskie vozdejstviya nebesnykh tel (Catastrophic Impacts of Celestial Bodies) / Eds V. V. Adushkin, I. V. Nemchinov. Akademkniga, 2005. 310 p (in Russian).
5. *Simonenko V. A.* Mathematical modeling of megatsunamis / EDs V. A. Simonenko, N. A. Scorkin, V. P. Elsukov, A. S. Uglov // Herald of South-Ural State University, Mathemathics, Physics, Chemistry series. Chelabinsk, 2006. Is. 11, N. 22. P. 62–69.
6. *Frolov K. V., Makhutov N. A., Vorobiev V. L., Putchkov V. A. et al.* Safety of Russia. Legal, Social and Economic, Research and Development Aspects. Vol. 1–33. M.: Znanie publ., 1998–2008 (in Russian).

The Asteroid-Comet Hazard Conference Proceedings, 2009

INVESTIGATION OF NEOS IN SITU. COUNTERACTION TO THE NEO HAZARD

Rotational Mass Driver — an Efficient NEO Deflection Concept

Z. M. Ilitz

Subotica, Serbia

Abstract. There is an Olympic athletic discipline — throwing of a ball on a chain. This paper explores the possibility of using the same method for asteroid deflection. Instead of a chain, however, a tether (or a rope) must be used.

As it turns out, the method has many merits. It offers high precision and controllability, is safe, efficient, and has a wide applicability range.

The performance envelope for the rotational mass driver specifically covers binaries, rubble piles, and large objects on a direct collision course that need a ΔV of cm/s. The method is comparably efficient to nuclear methods, but is much safer.*

Introduction

In order to deflect an asteroid, any applicable method must change its velocity by a small amount called ΔV. Assuming a warning time of several years, this value should be on the order of cm/s for a deflection comparable with the Earth radius, or on the order of μm/s for a deflection comparable with dimension of a keyhole to prevent a future collision. Although these values seem to be small, they have to be applied to a sizeable object of a few hundred meters in diameter, and this should be done autonomously and with the amount of equipment that weights only a few hundred kilogramm.

So far, there is neither a cheap, nor an easy solution for this problem.

---

*Editorial note: The concept presented in this paper merits interest, but as pointed out in several footnotes, it may be difficult to put into practice with some efficiency.

Preparations

Space is a rather harsh environment, imposing strict limitations for tether material. However, there exists a material that fulfills all the needed criteria and is perfect for this job: "M5" fiber from DuPont, manufacturer of kevlar. The most important property of this material is that it is the only one that actually *strengthens* when exposed to UV radiation, while most of the others deteriorate if unprotected, sometimes very rapidly. Moreover it is resistant to temperatures encountered in Venus-like solar orbit, and it has tensile strength comparable to zylon (which needs coating protection against UV rays). A "comparably strong" *zylon* Z180 weights 2.44 kg/km, has a diameter of 1.02 · 3.43 mm, tensile strength of 5783 N, and a modulus of elasticity of 124 GPa [3]. Several other, less suitable choices exist, like PBI (material for spacesuits) or *kevlar*.

An attachment to the unknown, and probably unstable surface of the asteroid is needed. Considering how light-weight these tethers are, the idea is to loop them, like many "tentacles", all the way around the asteroid. The spacecraft (S/C) will then mount the asteroid as a rider mounts a horse. To do this, tentacles are deployed in space during descend to the asteroid surface, and on touchdown their momentum will carry them, like whips, all around the surface (Fig. 1). Hereby, *entanglement is a desired outcome*, not a danger. The whole operation should last about 20 minutes, and the tentacles should only be kept from entangling each other during their deployment, not after that. Once they start whipping the asteroid, it is desirable for them to entangle on the opposite side to provide better attachment. For this purpose, they should be a little longer than necessary. Small hooks and bags of clay at their ends would ensure that they don't bounce back, but stay attached, securing the S/C. Usage of Hoytethers ™, and redundancy in their numbers provides safety against accidental cutting.*

The best place to mount a NEO is on its lighted rotational pole (see Fig. 1). While this is not a requirement for this concept to work, the landing on a pole does makes things easier, as it also enables a "*Tug boat"* concept to be used as an alternative backup method of asteroid deflection.

---

* Editorial note: Anchoring on the surface of an asteroid is very problematic as was recognized by the proponents of the tugboat concept for moving an asteroid. Using several tethers for reasons of redundancy brought about another problem, because tethers could entangle themselves, rendering them useless. These were the main reasons why the proponents switched to the gravity tractor concept, which uses no tethers.

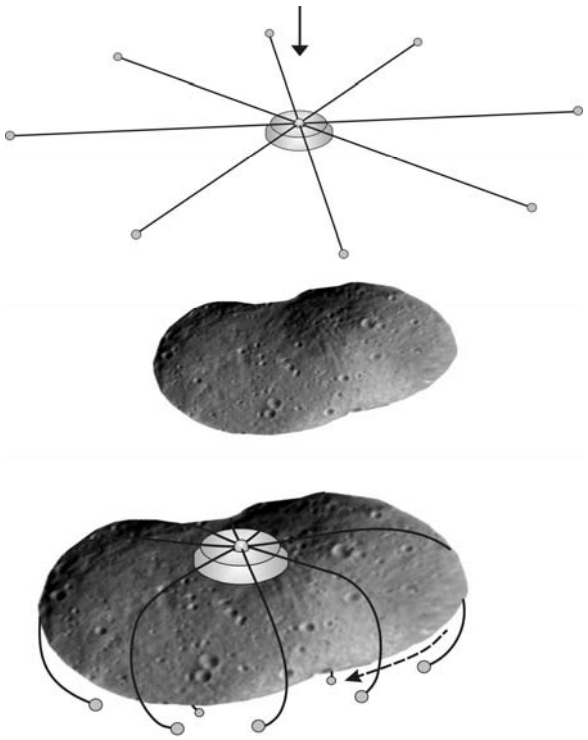

Fig. 1. Mounting: initial deployment and "whipping" of asteroid with tentacles.

The tentacles can be reeled in and out, which provides extra stability for the S/C, protecting it even in case of a total surface collapse under it. Additionally, reeling of tentacles gives to S/C a modest possibility to reposition itself (octopus-like movement).

One also needs some heavy weight that can be rotated away to provide momentum upon release. Since most of the asteroids are believed to be rubble piles, there is an excess number of loose boulders lying around, as it was found on Itokawa. To deflect Apophis from the keyhole it would be enough to throw away 1 or 2 of 30–50 t boulders with a speed of 10–20 m/s. But, we need to be able to collect them and to tie them.

Note also that these "massive" boulders weigh only several N on the asteroid, like a small fish on Earth. Thus, instead of a crane, we can use a light fishing rod to manipulate them gently. When one casts a fishing string on Earth, gravity curves the string down and air drag, which is a function of speed, causes it to spiral. In space, there is no drag and gravity is almost negligible. So, the only force acting on a string is the tension force.

Lack of drag allows exceptional lengths of tethers, on the order of many kilometers. Increase of tether length allows alterations of payload mass, an-

gular speed, and V parameters in a favorable way. However, if the material of a tether is conductive, motion will generate currents and additional electromagnetic forces. Dynamics of such scenario are not explored here.

On top of S/C, should be a turret with a `fishing rod' with 2 degrees of freedom of movement (up/down and around). Instead of bait, at the end of each string is a small, or medium sized spiderbot (a robot that looks like a spider and behaves like a spider) [1]. The purpose of these spiderbots is for them to be thrown by a "fishing rod" to the chosen place on the surface of the asteroid and perform various tasks, like exploration, requisition of boulders, sample retrieval, and similar tasks. For safety, they also carry a reeling mechanism, so that their string can be reeled from 2 directions. The energy for their operation can be provided by either solar power, batteries, evanescent coupling, or directly through a cable cord.

To secure a boulder, a spiderbot only needs to do what spiders do: to encircle it in an entanglement of strings, and then attach it to the tether connected to the "fishing rod" on a S/C, perhaps using glue, a hook, or some other small mechanism. After that it should crawl back over the tether string, and the accelerating operation may begin. Alternatively, a simple *lasso* would probably do the job as well. Since we intend to later swing away these boulders, the S/C should land on a place where it has a 360° clearance to perform the required operation.*

Energy requirements are very modest, only a few kWh/boulder, and are identical for any boulder size (6), but the more massive boulders provide more momentum in return. Dramatic energy effectiveness results from propelling of a LARGE mass with a SMALL relative speed; instead of the other way around. The whole operation is doable in several hours. Usage of formidable force of an electromotor makes it swift.

Deflection

Angular momentum is slowly applied over the tether by the fishing rod's electromotor, or by transferring it directly from the asteroid (the latter case is only applicable on a fast spinning asteroid.)

When the force in the tether exceeds a predefined limit, the tether is allowed to extend, thus keeping the force strength acceptable and allowing a *continual buildup of angular momentum* and consequently a speed increase. *The final length of a tether should be on the order of several km*.

---

* Editorial note: It may be difficult to accelerate a boulder without it hitting another boulder or obstacle in its way. Manipulating a boulder with the "fishing rod" and with tethers during the acceleration and release processes may present additional difficulties related to material properties of the equipment.

While the thinner strings of the same material have larger modulus of elasticity, and hence larger relative strength per mass unit, overly thin and long ones are vulnerable to micrometeoroids. The solution is to use Hoytethers [4].

The momentum to the asteroid is delivered instantly with boulder release (Fig. 2). The end state becomes known in real time.*

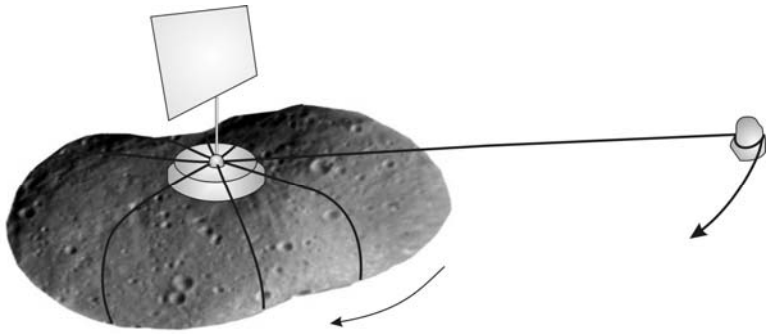

Fig. 2: Deflection by throwing boulders. Momentum changes upon release. Wrapped by tentacles, the asteroid is mounted on its pole; solar panels deployed.

As a bonus to being swift, this concept provides *fine calibrating of every aspect of operation*: the angular speed of the rotated mass is very low, enabling a timely accurate release; the mass amount is measurable; its velocity vector is easily controllable; thus we can set what goes where and when, even how much of it. By providing slow, controllable buildup of angular momentum, and its accurate, instant transmission to an asteroid's linear momentum change upon release, *all potential political hustles about how to deflect along the line of variations are being bypassed*. However, the issue on *who* controls it, and potential for a deliberate misuse still remains.

---

* Editorial note: The maximum momentum transfer to an asteroid is achieved if a boulder is released in the direction (or the opposite direction) of the orbital velocity vector of the asteroid. This is always possible if the S/C is on a pole and the spin axis is normal to the orbital plane of the asteroid. However, considering the more common case that the S/C may land on some other places on the asteroid and the orientation of the spin axis and the orbital velocity vector of the asteroid are such that the boulder cannot be released in a direction aligned with the velocity vector of the asteroid's orbit, then the release of the boulder will still lead to transfer of momentum to the asteroid but with reduced effectiveness. The components of impulse *not* aligned with the orbital velocity must be taken into consideration in the plans for changing the asteroid's orbit.

Moreover, this is an excellent way to deflect binaries. Surprisingly, it is possible to separate them by transferring angular momentum from one to the other over 2 connecting tethers (the main one is typically a fast rotator). Once separated, their mass center may "hit" the Earth, but they would not, as one of them would come too early, and the other too late.

Important note: This is still 1–2 orders of magnitude less than what is required for deflection of asteroid towards the Earth. (For this, a bypassing PHA would need to be diverted for several lunar distances at least, while remaining undetected; which means it would need ΔV of several m/s to be able to do it within reasonable amount of time.) This means that the fishing rods are very effective for defense, but almost useless for offensive purpose.

Example

Let us take deflection of Apophis as an example (initial phases skipped).

Deflection part: (tons are assumed to be metric ones):

- Throw a lasso over any of suitable nearby boulders (10–10,000 t). Most asteroids are rubble piles, so we can safely assume that there is a lot of suitable boulders littered around to choose one from. If the asteroid is monolithic, a bit of explosive can change it.
- Pull the tether with max available force until the boulder achieves the orbital speed of several cm/s. Surface gravity acceleration is on the order of 10^{-4} m/s², thus 10 t of mass has ~1 N of weight. 10,000 t has a weight of ~1,000 N. Not much indeed.

Moreover, to pull it, we must overcome not the weight, but the drag force. In worst case scenario this should not exceed 0.6 of weight. On the other hand we must also overcome the Van der Waals forces and bonding with ground (the boulder could be partially buried). The tether can presumably withstand a force of 5,000 N max, which is enough to overcome the resistance even of the largest rocks. However, for safety reasons, we should keep the force as low as possible. If we stay under 1 kN at all times, it would still be enough to pull a 100 t boulder (~5 m in diameter) into orbital speed in 10–20 s time, over a "runway" length of ~2 m.

$$\vec{F} = \vec{F}_{\max} - \sum \vec{F}_{resistance}, \tag{1}$$

$$t_{assel} = \frac{\left(m_{\text{boulder}} \times V_{\text{orbital}}\right)}{F} \text{ (acceleration time)}, \tag{2}$$

$$S = \frac{\left(m_{\text{boulder}} \times V^2_{\text{orbital}}\right)}{F} \text{ (minimal "runway" length).} \tag{3}$$

While keeping the tension force in tether under a threshold, swing the boulder away until the tether is sufficiently extended (~10 km). The

operation is automatic: linear electromotor rotates the boulder around while the reeling mechanism allows the tether to extend whenever the force in tether is above the threshold. For a 100 t boulder, 10 km tether length, 1 kN max tension, we can achieve the $V_{\max}$ of 10 m/s, with an angular speed of $\omega = 0.001$ rad/s. That corresponds to 1 : 44 : 43 revolution period:

$$V_{\max} = \sqrt{\frac{F_{\max} \times r_{\max}}{m_{\text{boulder}}}} \text{ (final speed of the boulder),} \tag{4}$$

$$\omega = \frac{V_{\max}}{r_{\max}} \text{ (final angular velocity of the boulder).} \tag{5}$$

To avoid the complexity of transmission, the electromotor is envisioned as a linear electromotor. This one practically has no moving parts and can deliver almost all of the supplied energy to the tether without the need to use gears for transmission. If we assume that the electromotor can steadily supply the boulder with 500 W of additional kinetic energy, it would require >10,000 s to achieve $V_{\max}$. That is 2 : 46 : 40 (at least). Few additional seconds of operation cover all the kinetic energy that would be delivered to a tether (with a mass of ~20–30 kg) and to the (Apophis) asteroid on the other side.

Note that after the tether length exceeds r_{synch} radius, further acceleration can be achieved by directly stealing the angular momentum from the asteroid (over the tether). This would probably require further robotic assistance. It would be possible to do this, but not as an easy, straight forward task.

M_{EM}, P_{EM} — angular momentum and power of the electromotor; ξ_i — coefficients of power losses in transmission.

$$E_{k\text{boulder}} = \frac{m_{\text{boulder}} \cdot V_{\max}^2}{2} = \frac{F_{\max} \cdot r_{\max}}{2} = \text{const}, \tag{6}$$

$$E_{k\text{tether}} = \frac{m_{\text{tether}} \cdot V_{\max}^2}{6} = \text{(few hJ)}, \tag{7}$$

$$\Delta\omega_{ast} = \frac{M_{\text{EM}} \cdot t_{\text{operation}}}{I_{zast}}, \tag{8}$$

$$\Delta E_{\text{rotast}} = \frac{I_{\text{zast}} \cdot \Delta\omega_{\text{ast}}^2}{2} = \text{(few J)}, \tag{9}$$

$$t_{\text{operation}} = \frac{\sum E_{ki}}{\prod \xi_i \cdot P_{EM}} \text{ (~10,000 s).} \tag{10}$$

When the time is right, release the boulder. Note that there is only one instance in every revolution suitable for boulder releasing (when velocity vector of a boulder most completely aligns with the heliocentric velocity vector of the asteroid in a desired direction).*

Operation is to be repeated with other boulders until a desired ΔV_{ast} is reached (ΔK is given *per boulder*). If there are few scores of loose boulders on the surface of Apophis, it can be deflected even in 2034 (during several weeks). (11) yields ΔV_{ast}:

$$\Delta K = \Delta\left(m_{\text{ast}} \cdot V_{\text{ast}}\right) = m_{\text{boulder}} \cdot V_{\max} \simeq 10^7 \ \text{kg}\frac{\text{m}}{\text{s}}, \tag{11}$$

$$\Delta V_{\text{err}} - \Delta V_{\text{ast}} \cdot \left(1 - \cos\left(\omega_{\text{ast}} \cdot t_{errrelease}\right)\right). \tag{12}$$

Other potential applications

The fishing rod mechanism can also be used to launch back a small *sample return capsule* with a respectable velocity. (Reduction of the amount of thrown mass allows the increase of its velocity.)

Term definition: "*Potentially* capturable NEO (PC NEO)" — approaches the Earth with a V_∞ < ~5 km/s with a ΔV required for shifting into a capturing trajectory by the Earth–Moon system small enough to be timely deflected with available means.

Since we can control the velocity of ejected mass, we can use this method to throw *ore shipments* into a capturing trajectory by the Earth-Moon system, which opens for the first time the real possibility for economically profitable asteroid mining. However, these should be *bare* rocks, with no regolith upon them to avoid creating a debris problem.

Last, but not least, operation "*Einstein"*, as it may be called, would retrieve two suitably sized boulders, named "*Albert"* and "*Mileva"*, in order for one or both of them to be used *as foundation rocks for a new generation space station*, one with artificial gravity. PC NEA 1999 AO10 is the best target candidate (known so far) for the operation "*Einstein"*. Comes back every 26 years, and is about 60 m in size (H = 23.855). If visited in 2018 or 2019, we may have a payload returned from it in 2026 and inserted into Earth orbit. If something goes wrong, and the mission fails, we can learn from our mistakes and try again 26 years later.

While an automatic launching and orbit boost station would require only ~600 t [4], a manned station would need to have a diameter of at least 40 m

---

* See Editorial note in section "Deflection".

to allow creation of a (variable) artificial gravity [2] However, the boulder should be small enough not to cause any damage on the surface of the Earth if ever perturbed into a collision course.

Then, by placing a framework around it, it can be used as a solid ground to hold a S/C launching station using a rotational mass driver. Velocities of 3 km/s, relative to station, are swiftly, and safely achievable this way. This is enough to reach either Mars, Moon, or LEO. With no fuel required for this. The costs of sending S/Cs to Mars and Moon would thus drop by 80–90 %.

The station can also be used to promptly send kinetic impactors to a suddenly appearing small hazardous object (with low warning times). Material mined on spot should be used as ballast weight (Don Quijotes), attached to a small S/C for guidance, and impact monitoring (Sancho). Few of these, docked on standby, would serve as a planetary defense. The following issues need further examination:

Abrasive properties of asteroid surfaces. If edges are too sharp, they may shred the tentacles. This is critical during mounting phase and could be mitigated later (not an issue if Hoytethers are used).

Influence of the elasticity of a tether, when the tether is very long. This could be an issue, but there are some options to workaround.

Lorentz forces acting on a long tether in the interplanetary plasma environment. Probably not an issue on an asteroid, but possibly on a launch station because it would reside within the Earth's magnetosphere.

References

1. *Mark Tilden* interview (inventor of the BEAM robotics): *http://www.exhibitresearch.com/tilden/*
2. *Hall T.* Artificial Gravity and the Architecture of Orbital Habitats, 1997: *http://www.spacefuture.com/archive/artificial_gravity_and_the_architecture_of_orbital_habitats.shtml*
3. *Tibert G. Gardsback M.* Space Webs Final Report, *http://www.esa.int/gsp/ACT/ACT-APT-06-4109a-ARIADNA-SpaceWebs-KTH.pdf*
4. *Sorensen K. F.* Conceptual Design and Analysis of an MXER Tether Boost Station, American Institute of Aeronautics and Astronautics: *http://www.tethers.com/papers/AIAA_2001-3915_MXER.pdf*, *http://www.tethers.com/Hoytether.htm*

The Asteroid-Comet Hazard Conference Proceedings, 2009

INVESTIGATION OF NEOS IN SITU. COUNTERACTION TO THE NEO HAZARD

Evolution of Apophis Orbit for 1000 Years and New Space Targets

J. J. Smulsky[1], Ya. J. Smulsky[2]

[1]Institute of Earth's Cryosphere of RAS, Tyumen, Russia
[2]Institute of Thermophysics of RAS, Novosibirsk, Russia

Abstract. Analysis of publications establishes that the uncertainty of trajectories of Apophis are caused by imperfections in the methods of its determination. The differential equations of motion of Apophis, planets, the Moon, and the Sun are integrated by new numerical methods and the evolution of the asteroid orbit is investigated. Apophis will pass by the Earth at a distance of 6.1 Earth radii on April 13th, 2029. It will be its closest approach to Earth during the next 1000 years. The possibility of transforming Apophis' orbit to an Earth satellite orbit that could be used for various tasks, is considered.

It is known from the publications (see for example [1]) that asteroid Apophis will pass Earth on April 13, 2029 at a distance from 5.62 to 6.3 Earth radii. Because this will change the orbit of Apophis, further predictions of its motion become uncertain. However, there is some probability of its encounter with Earth in 2036.

We have analyzed papers [1–4] and have established that uncertainties of the Apophis trajectory are caused by imperfections in the methods of orbit computations. We have developed [5] a new method for integration of the differential equations of interaction of the asteroid with the Sun, planets, and the Moon under Newton's law of gravitation

$$\frac{d^2\vec{r}_i}{dt^2} = -G\sum_{k\neq i}^{n}\frac{m_k\vec{r}_{ik}}{r_{ik}^3}, \quad i = 1, 2, \ldots, n, \tag{1}$$

where $\vec{r}_i$ is the position vector of a body with mass m_i relative to the Solar System barycenter; G is the gravitational constant; $\vec{r}_{ik} = \vec{r}_i - \vec{r}_k$ and r_{ik} is its module; $n = 12$.

As a result of numerical experiments and their analysis we came to the conclusion, that finite-difference methods of integration do not provide the necessary accuracy. For the integration of equations (1) we have developed an algorithm and a program "Galactica". The value of a function at time $t = t_0 + \Delta t$ is determined with the help of a Tailor series expansion. For coordinate x it looks like:

$$x = x_0 + \sum_{k=1}^{K} \frac{1}{k!} x_0^{(k)} (\Delta t)^k , \qquad (2)$$

where $x_0^{(k)}$ is the derivative of order k at the initial moment t_0.

The value of velocity x_0' is defined by a similar formula, and the acceleration x_0'' by formula (1). Higher derivatives $x_0^{(k)}$ are determined analytically as a result of differentiation of equations (1). The calculation uses the algorithm of the sixth order, i. e. with $K = 6$. The mass of bodies, and also their initial coordinates and velocities are given for the epoch of November 30.0, 2008 at: *http://www.ikz.ru/~smulski/Data/OrbtData/* in a folder AsApophs, and their description is in a file ReadMeOREn.pdf.

By this numerical method we have integrated the differential equations (1) of motion for Apophis, the major planets, the Moon, and the Sun and investigated the evolution of the asteroid orbit.* On April 13, 2029 Apophis will pass at a distance $R_{\min}$ = 38,907 km from the Earth's center and during the next 1000 years there will be no close approaches of the asteroid with planets.

The minimum distances $R_{\min}$ of the asteroid from planets and the Moon were determined for a number of successive intervals of time of duration ΔT each. The examinations have been executed over three time spans: 0 ÷ +100 yr (Fig. 1, *a*), 0 ÷ –100 yr (Fig. 1, *b*) and 0 ÷ +1000 yr (Fig. 1, *c*).

In Fig. 1 the points connected by a broken line give the minimal distances, $R_{\min}$, of the asteroid from bodies, which are marked by points connected by a horizontal line. That is, the ordinate of a point in the broken line is equal to the minimum distance attained by the asteroid during time inter-

* Editorial note: When integrating equations (1), the author uses initial values of coordinates and velocities of Apophis and the major planets that were found under more general suppositions than is done in this paper.

val ΔT = 1 yr from a body that is noted by a point in a horizontal line at the same moment.

As Fig. 1, *a* shows, for 100 yr, starting November 30.0, 2008, there will be only one very close approach to the Earth (point A) at T_A = 0.203693547133403 centuries (on April 13, 2029, $21^h45^m47^s$ of Greenwich time) at a distance R_{minA} = 38906.9 km. The following close approach (point B) will be also with the Earth at T_B = 0.583679164042455 centuries (on April 13, 2067) at a distance R_{minB} = 622231 km, which is 16 times greater than the distance of the first approach. As to the other bodies, the closest approach will be only with the Moon (point D) (see Fig. 1, *b*) at T_D = –0.106280550824626 centuries at a distance R_{minD} = 3545163 km.

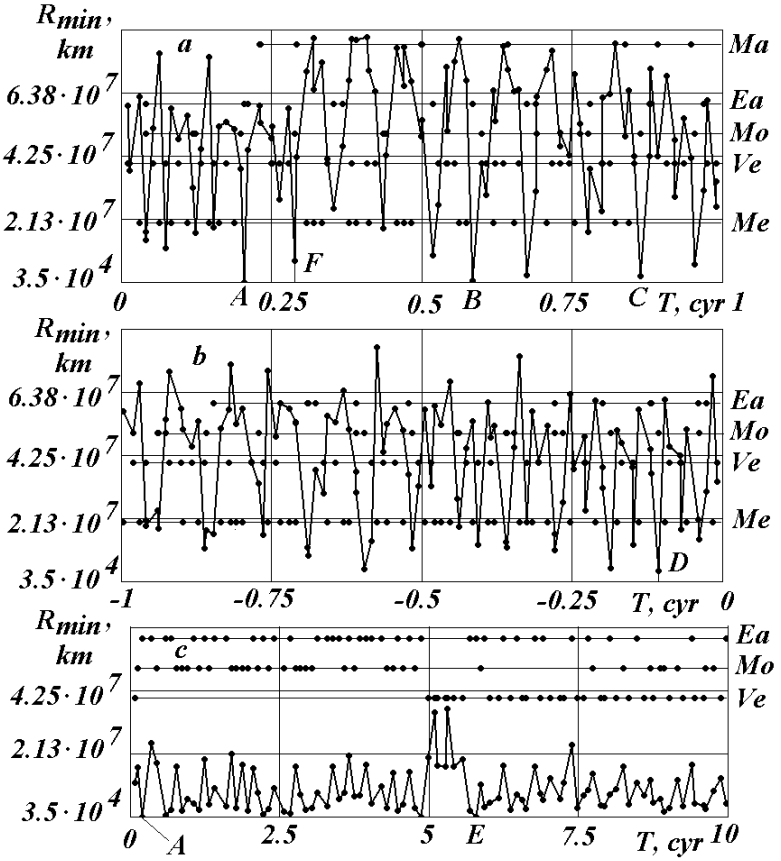

Fig. 1. Apophis' minimum distance R_{min} (in kilometers) for successive intervals of time, ΔT, with celestial bodies: Mars (Ma), the Earth (Ea), the Moon (Mo), Venus (Ve) and Mercury (Me); a and b: ΔT = 1 yr; c: ΔT = 10 yr. T, cyr — time in Julian centuries from epoch JD0 = 2454800.5 = November 30.0, 2008.

When the equations of motion (1) were integrated for the 1000 yr period (see Fig. 1, *c*), the minimum approach distances of the asteroid with bodies were counted every 10 yr. In doing so, we do not show the approaches with Mercury and Mars since approaches to the other bodies are closer. There is an approach with the Earth at T_A that can be seen as well on Fig. 1, *a*. The second close approach also occurs with the Earth (point E) at T_E = 5.778503 centuries (on October 10, 2586) at a distance R_{minE} = 74002.9 km, i. e. at the distance from the Earth, which is almost twice as large as at T_A.

Thus, on April 13, 2029 Apophis will pass by the Earth 38907 km from its centre and such close approaches to the Earth will not occur again for 1000 yr.* Therefore, thanks to an unusual opportunity, the possibility to capture Apophis into a satellite orbit about the Earth and then into a manned station is of considerable interest. Other applications of such satellite are also possible. It can serve as a base for space launches. It can be used as a "shuttle" for delivery of loads to the Moon. In this case the satellite should have an elongated orbit with perigee distance close to radius of a geostationary orbit and apogee distance that approaches the distance of the perigee of the Moon orbit. Then loads from a geostationary orbit could be shifted to an Apophis-satellite at perigee and then, at apogee, these loads could be delivered to the Moon. The last two applications are possible, if the satellite motion coincides in direction with Earth's rotation and the Moon's motion.

In Fig. 2, *a* the trajectory of Apophis relatively to the Earth is shown for two years. Apophis moves on the trajectory *1* from point Ap_0 to point Ap_1. At point Ap_e it approaches the Earth, and the Ap_f is final point of its trajectory. The loops of Apophis trajectory represent its returnable motions relatively to the Earth. The fraction of Apophis' trajectory near point Ap_e is shown on a large scale in Fig. 2, *b*. The origin of coordinates (point 2) coincides with the Earth. The Sun is located in the upper right quadrant. Velocity of the asteroid relative to the Earth in point Ap_e is equal v_{AE} = 7.39 km/s. Velocity of the Earth's satellite in a circular orbit with radius R_{min} is equal v_{cE} = 3.2 km/s. To transform the asteroid into a satellite requires slowing its velocity v_{AE} to v_{cE}. When reducing Apophis' velocity at point Ap_e it would transform it into the Earth's satellite, however, into a satellite with retrograde motion.

If Apophis (see Fig. 2, *b)* passes the Earth on the other side (see point *3*), then after reducing its velocity it would be transformed into a satellite with prograde motion. For the purpose of a numerical experiment, equations (1)

---

* Editorial note: This inference is based on the results of integration of equations (1) with the initial conditions referenced above. Under different set of initial conditions taken within limits of their possible errors the results could be quite different.

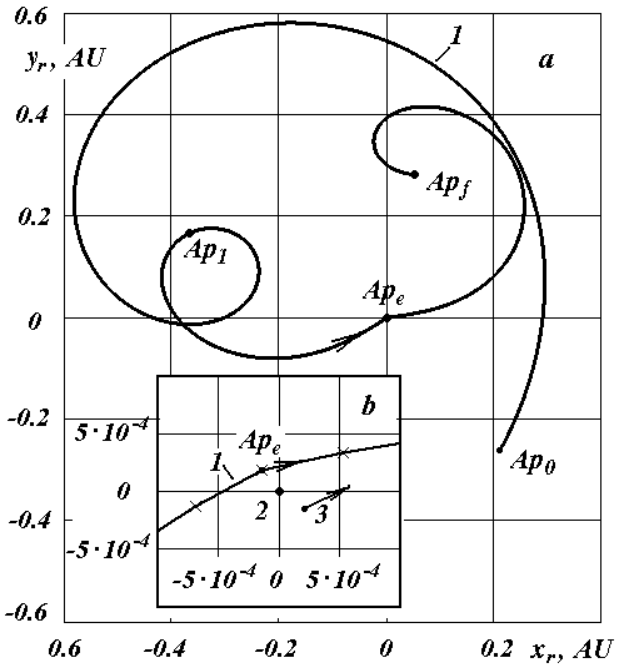

Fig. 2. Trajectory of Apophis (*1*) in a geocentric equatorial frame $x_r y_r$; Ap_0 and Ap_f — initial and final points of the Apophis trajectory; Ap_e — the point of Apophis minimum distance to the Earth: *a* — in usual scale, *b* — in the enlarged scale at the moment of Apophis approach with the Earth (*2*); *3* — position of Apophis at the moment of its approach with the Earth after correction of its trajectory with coefficient of reduction of velocity $k = 0.9992$; coordinates x_r and y_r are given in AU.

has been integrated with a changed asteroid velocity at point Ap_1. In the experiment the velocity components were proportionally changed by the same factor, i. e. they were multiplied by coefficient *k.* As a result it has been shown that at reduced velocity the asteroid starts to approach more closely to the Earth and at $k = 0.9999564$ Apophis encounters the Earth. With further reduction of velocity the asteroid approaches the Earth from the other side of the globe and at $k = 0.9992$ the asteroid passes the Earth at almost the same distance $R_{\min}$.

In this case the asteroid velocity relative to the Earth also is equal $v_{AE} = 7.39$ km/s. With it's a velocity reduction by 1.9 Apophis is transformed into an Earth satellite with a steady orbit and with revolution period of 2.436 days.

Thus, to transform Apophis into a satellite with direct orbital revolution it is necessary to reduce its velocity by 2.54 m/s 0.443 yr prior to its approach

to Earth, and during approach with the Earth it is necessary to reduce it further by 3.5 km/s.

The reduction of velocity by 3.5 km/s of a body of mass 30 million tones represents now a serious scientific and technical problem. But we have 20 yr and the experience of creating the first artificial Earth satellite will challenge society to successfully accomplish it.

References

1. *Georgini J. D., Benner L. A. M., Ostro S. I., Nolan H. C. et al.* Predicting the Earth encounters of (99942) Apophis // Icarus. 2008 Vol. 193. P. 1–19.
2. *Sokolov L. L., Bashakov A. A. , Pit'ev N. P.* O vozmozhnykh sblizhenijakh ACZ 99942 Apofis s Zemlej // Okolozemnaja astronomija. 2007. Materialy mezhdunar. konf. 3–7 sentjabrja 2007 g., Terskol. Mezhdunarodnyj centr Astronomicheskikh i mediko-ekologicheskikh issledovanij Nacional'noj akademii nauk Ukrainy i Institut astronomii RAN. Nal'chik, 2008. P. 33–38. (On the possible approaches of NEA 99942 Apophis with the Earths) (in Russian).
3. *Smirnov E. A.* Sovremennye chislennye metody integrirovanija uravnenij dvizhenija asteroidov, sblizhajushchihsja s Zemlej // Ibidem. P. 54–59. (Modern numerical methods of integration of equations of motion of the asteroids approaching with the Earth). (in Russian).
4. *Bykova L. E., Galushina T. Ju.* Evoljucija verojatnoj oblasti dvizhenija asteroida 99942 Apofis // Ibidem. P. 48–54. (Evolution of probable areas of a motion of the asteroid of 99942 Apophis) (in Russian).
5. *Smulsky J. J.* Optimisation of a passive orbit with the help of a gravity-assist maneuver // Kosmicheskie Issledovaniya. 2008. Vol. 46, N 5. P. 484–492 (in Russian) *http://www.ikz.ru/~smulski/Papers/KOS0484.pdf.*
6. *Smulsky J. J.* Optimization of Passive Orbit with the Use of Gravity Maneuver // Cosmic Res. 2008. Vol. 46, N 55. P. 456–464 (in English). *http://www.ikz.ru/~smulski/Papers/COSR456.PDF*.

INVESTIGATION OF NEOS IN SITU. COUNTERACTION TO THE NEO HAZARD

On the Approach to Form International-Legal Foundations to Ensure Planetary Defense

A. V. Zaitsev, A. A. Klapovsky

Not-profitable Partnership "Planetary Defense Center", Khimki, Russia

Abstract. The building of the planetary defense system (PDS) against asteroid and comet nucleus impact hazards will require adequate international legal instruments that may take the form of an international treaty "On the principles of ensuring the Earth's defense against asteroid and comet nucleus impact hazards".

This report reviews the basic elements of the approach to forming this treaty. More specifically, the treaty should contain principles governing the establishment and use of a security fund of humanity with the aim to financially supporting the development, exploitation and modernization of the system.

It is noted that the United Nations could coordinate the PDS formation and exploitation. For this purpose we need to establish under the aegis of the United Nations an international planetary defense center and its regional offices.

The report provides an explanation for the necessity of reservations to be introduced into some international space law provisions with respect to the issue of the PDS formation, management, and application. In particular, it regards the issue of mitigating hazardous celestial bodies by means of nuclear devices.

Introduction

Identifying the existence of asteroid and comet nucleus impact hazards helped many countries to conduct studies with a view to create a PDS against such hazards. Those studies led to the understand that PDS formation, management, and application will require significant international legal foundations [1–3].

The reasons are as follows:

1. Given the technical and organizational complexity of the defensive measures, their scope, and the cost of implementation, it is unlikely that one or several countries will have enough resources to carry them out. However, entrusting this issue to an international institution or association will require adequate international legal instruments.

2. Technical components that may be used for building the PDS (rocket and space capabilities, etc.) are currently under the jurisdiction of individual countries. Technical and legal integration into a global international infrastructure will be needed.

3. Nuclear capabilities are deemed to be the most effective for mitigating hazardous celestial bodies. For this reason countermeasures should be exempted from international laws banning nuclear explosions in outer space.

4. While developing (or under the guise of developing) the PDS, capabilities potentially posing a threat to national security of other countries might develop. Measures to eliminate such possibilities should be envisaged.

The arguments cited above show that the issue of asteroid and comet nucleus impact hazards can be undertaken only at the international level and with the adequate international legal instruments, which may take the form of an international treaty "On the principles of ensuring the Earth's defense against asteroid and comet nucleus impact hazards" (hereafter referred to as the Treaty).

International organizational and legal steps that should be reflected in this Treaty, as indicated below, may be linked, for illustration purposes, to the tasks of specific activities.

Concept stage

Evidently, as the first step in building the PDS, we should prepare and sign an international treaty that will serve as a foundation for creating the PDS and financial support for it.

We outline general principles that will be needed.

When drafting the Treaty it is desirable to have a concept for the PDS, drafted by the international community. "Citadel" [4] is one of the options to be considered.

We need to attribute international status to the legal instruments governing the PDS formation, use, and application.

The legal instruments should be of a lawfully binding nature for the countries involved in the establishment of the PDS.

The legal instruments may be structured according to the basic areas to be encountered (scientific, technical, organizational, financial etc.), and the stages of building of the PDS etc. [2].

Furthermore, the treaty should contain a provision that prohibits countries united in a single military and political association to be the sole or independent creators and developers of the PDS. This is necessary in order to avoid a so-called "no-use dilemma" [1], which allows for the possibility for the association to refuse to defend other countries or exert influence on them with a view to change a geopolitical situation or even to destroy them.

It is necessary to include into the treaty general principles for allocating and using a special international fund, that one may call a security fund for humanity [5], in order to guarantee financial support for PDS development, use, management, and modernization.

Stage of developing the PDS project

The PDS development will require resourceful decisions in terms of organization. For this reason it is relevant to put into the draft treaty the following principles:

High priority should be given to international activities aimed at building the PDS, and they should be managed by an international organization specially created for this purpose.

The PDS formation may be conducted on the basis of specially established international components and national capabilities.

Measures should be incorporated to eliminate the possibility to use the PDS activities for the purposes of developing prohibited types of space weapons.

A status "Patrimony of Mankind" should be attributed to the technologies used in the PDS for the sake of their guaranteed preservation until these technologies are replaced by new ones, without detriment to the PDS "permanent readiness status."

To address the threat of a global catastrophe we need to develop "a mobilization plan for Earth's defense" in order to engage all the necessary resources of mankind [6].

Stage of building and testing of the PDS components

The Organization of the United Nations, in particular a specific ad hoc organism created under its aegis, could coordinate the PDS building.

One of the most important problems at that stage will be the issue of live testing of nuclear devices, as one of the most probable ways of mitigating hazardous celestial bodies. The same will apply to the stage of PDS applications.

We will need to adopt for these purposes reservations with respect to some international space law provisions. It regards the Treaty Banning Nuclear Tests in the Atmosphere, in Outer Space and under Water (1963), the Outer Space Treaty (1967) and the Convention on Registration of Objects Launched into Outer Space (1977). It is evident that nuclear devices, in case

of their use in the PDS, should not be understood as components of "a nuclear weapon".

With regard to the Russian-Chinese draft PPWT we will need to agree upon the fact that space assets with destructive capabilities tailored for mitigating hazardous celestial bodies are not related to the notion of a nuclear weapon "of any kind".

We need to point out that under the guise of establishing the PDS components, outer space may be used as a testing ground for developing new kinds of weapon. For example, new models of hyper-velocity impacts (needed to assess the efficiency of a new kinetic type of weapon) may be tested. Whereas in the future it is possible to create "an asteroid weapon" — i. e., the use of small asteroids for bombarding objects on the Earth.

For this reason the treaty must contain provisions that exclude the possibility to produce means of mitigating hazardous celestial bodies for the purposes of developing prohibited and new kinds of space weapon.

Stage of "a standby alert"

Among the most important problems that could emerge at this stage, if the appropriate measures are not taken, are [1]:

The dilemma of reporting. It consists in the possibility to delay or conceal data on a hazardous object. Such an incident took place on January 13, 2004, when American astronomers concealed data on asteroid 2004AS1, which, by preliminary estimates, fortunately false one, was to impact Earth. Evidently such situations should be eliminated or minimized.

Another dilemma is whether to notify the population about an upcoming threat. To solve this dilemma we will need to develop provisions governing the order of notifying the population about the upcoming threat from outer space and eliminating the possibility of a massive panic.

The important role in solving these problems might be to establish an international Center of Planetary Defense under the aegis of the United Nations, as well as two regional offices — "East" — in the eastern hemisphere, and "West" — in the western hemisphere.

The Treaty should contain provisions governing the work of these Centers.

Stage of application of the PDS components

The timely decision on the use of the PDS components is the important condition of the Earth's secure protection against hazardous celestial bodies. It should be taken in coordination with all governments, and — in case of emergency — by the United Nations Secretary General. At the same time we need to eliminate, as indicated above, the "no-use dilemma".

We need to envision the possibility to use technical instruments of the military agencies, for example, missile space defense capabilities [7].

Stage of PDS application consequences

Since destruction of hazardous celestial bodies near Earth may generate debris, we need to consider measures in order to compensate possible damage to the appropriate countries and regions.

We need to envisage activities with a view to preserve a minimum of immaterial and material values, which will allow regeneration of losses in case of any regional — or global — scale catastrophes.

While the PDS is being developed, we will need to solve many other problems of great importance. All these proposals could be put in practice through legal norms, developed and adopted at the international level in the framework of this treaty.

In addition to existing international treaties and agreements, we need to adopt concerted understandings with provisions covering the issue of defense against asteroid and comet nucleus impact hazards.

Conclusion

We conclude that:

1. Undertaking the issues of defense against asteroid and comet nucleus impact hazards requires development of international legal instruments that could take the form of an international treaty "On the principles ensuring the Earth's defense against asteroid and comet nucleus impact hazards".

2. The formation of the international legal instruments providing for the Earth's defense against asteroid and comet nucleus impact hazards should correlate with the PDS concept, provisionally agreed to by the international community.

3. In order to establish a comprehensive set of juridical norms regulating PDS formation and work we need to develop governing principles and coordinate them at the international level. They will serve as a point of departure for further work.

4. While developing the legal instruments for the PDS formation and application we need to take into account the current international space law provisions and change some of its juridical framework such as technical assets tailored for mitigating hazardous celestial bodies.

5. The Organization of the United Nations, more specifically, the international Center of Planetary Defense, specially created for these purposes under its aegis, and its regional offices could coordinate the PDS formation and applications.

References

1. *Zaitsev A. V.* Some of Problems and Sequences of Development of the Planetary Defense System. // Chelyabinsk Sci. Center News. Special Issue "Space Protection of the Earth". 1997. P. 243–246.

2. *Zaitsev A. V., Klapovsky A. A., Koulik S. V.* Organizational and legal aspects of Planetary Defense System creation and application // Materials of All-Russian conference "Asteroid-Comet Hazard-2005" (ACH-2005), October 3–7, 2005, St. Petersburg. P. 148–150.
3. *Zaitsev A. V., Klapovsky A. A.* Scientific and Technical, Organizational-Legal and Moral Aspects of Ensuring of Defense of the Earth from Asteroid-Comet Dangers // Abstracts Intern. Conf. "100 years since Tunguska phenomenon: Past, present and future". June 26–28, 2008. M. P. 187.
4 *Bashilov A. S., Konyukhov S. N., Pichkhadze K. M., Pobedonostsev K. A. et al.* The Planetary Defense System "Citadel", Proposals. Planetary Defense Center, 2001. 23 p.
5. *Zaitsev A. V.* The Planetary Defense System "Citadel". The conceptual project // Lavochkin Association. M. 2000. 70 p.
6. *Kovtunenko V. M., Zaitsev A. V.* "Protecting Earth from Asteroid Hazards is a Real Task for the World Space States" // Space Bull. 1995. Vol. 2, N 4. P. 25–27.
7. *Arsenyev G. N., Semyonov B. I., Torgovkin S. N., Treckin V. V.* The possibility of two-fold use of missile-space defense systems for solving the problem of asteroid-comet hazard // Information-measuring and Control Systems. 2000. Vol. 4, N 5. P. 5–12.

INVESTIGATION OF NEOS IN SITU. COUNTERACTION TO THE NEO HAZARD

About the Interaction of the "Citadel" Planetary Defense System with the Missile-Space Defense Systems

B. I. Semyonov[1], S. N. Torgovkin[1], V. V. Treckin[1], A. V. Zaitsev[2]

[1]4-th Central Scientific-and-Research Institute of Russian Ministry of Defence, Yubilejnyj, Russia
[2]Non-profitable Partnership "Planetary Defense Center", Khimki, Russia

Introduction

Dangerous celestial bodies (DCBs) also known as potentially hazardous objects (PHOs), i. e., asteroids and comet nuclei with dimensions of tens to hundreds of meters in diameter, can be detected several days to weeks before impacting Earth [1]. One of possible ways of ensuring planetary safety is the creation of the International Planetary Defense System (PDS) "Citadel" [2]. One level of this system, "Citadel-1" [3], must be on a permanent alert and interacting with the Missile-Space Defense systems [4].

The possibility of the technical realization of "Citadel-1"

Because of the potentially extremely short time for responding to a threat from space, a mode of permanent readiness of the system demands automating the process of controlling and integrating the regional Center of the Short-term Response. In connection with this, the latest achievements of information technology realized during designing and building the Missile-Space Defense systems — Ballistic Missile Early Warning systems, Space Control systems, and Missile Defense systems — should be used in conjunction with existing nuclear-missile technologies during development of "Citadel-1".

The technical feasibility and effectiveness of the Rapid Response Level of "Citadel-1" based on converting the missile-space complex and also adopting the existing and to be developed Missile-Space Defense systems are illustrated in this paper by the example of the Earth defense from suddenly appearing DCBs of hectometer (Apophis size) and decameter (Tunguska

size) scales. By suddenly appearing we mean detection several days before Earth impact.

In spite of the very low probability of this scenario, the cost of possible losses would be enormous. The success of intercepting such a DCB depends first of all on its timely detection. For the scenario under investigation we show in this paper the possibility of neutralizing this threat by means of the suggested Rapid Response Level "Citadel-1" when interacting with the Missile-Space Defense systems to minimize the losses [5]. We must also remember that a successful intercept of a DCB of hectometer and decameter size using nuclear-missile technologies can impose certain restrictions on developing "Citadel-1" information technologies that are assumed as a basis of its construction [6].

The problems of interaction of "Citadel-1" with the Missile-Space Defense systems

While researching the feasibility of the above-mentioned variants of intercepting and neutralizing a DCB it was found that the following information technologies used for building the Missile-Space Defense [7] are needed: (1) centralized control of all systems and complexes from a common single post on the basis of which the control outline of the Missile-Space Defense systems is centered; (2) interaction of all systems in automatic mode in real time; (3) open architecture, enabling increases in the single Missile-Space Defense System information base with methods belonging to various departments (planetary radars of deep space communication, observatories of organizations belonging to the Russian Academy of Science, and others).

It appears natural that these technologies should be used in designing and building "Citadel-1" and in organizing the interaction of this Level, in particular, with the Missile-Space Defense systems. The interaction of the Missile-Space Defense System Command Post with the regional Center of Planetary Defense (CPD) can be carried out with the aid of the Data Exchange Center, assuming in particular also international exchange. The organization of such interactions enables one to solve a number of problems in the interest of planetary defense against DCBs:

1. Timely target designations to Missile-Space Defense systems for an individual DCB of decameter size detected by various observation devices of the Rapid Response Level of the PDS or for decameter fragments of larger asteroids or comet nuclei destroyed by an Operative Level of the PDS at distances of several hundred thousand km from Earth.

2. Tracking the detected DCB of decameter size by means of the Space Control System net and provision of the target designation to the National Missile Defense System. The algorithm developed on the basis of theory of multipoint boundary value problems is suggested for use to determine the

DCB's orbit on the sites of the Control System [8]. This algorithm enables reconstruction of the trajectory not only of the incoming DCB, but also for attacking DCBs on the basis of position measurements of angular coordinates with proper accuracy.

3. Tracking — through target designation of the Rapid Response Level — the cloud of fragments of an asteroid or a comet nucleus destroyed in the operative Level of the PDS by the high-potential phased-array radars of the Ballistic Missile Early Warning System in the mode of packet signals that must provide the target designation to the Missile Defense radar for decameter fragments attacking the central regions of a country.

4. Realizing with the aid of the Ballistic Missile Early Warning System radars autonomous regular searches of DCBs that were not detected by other means till approaching Earth. Detecting them is possible up to a distance of 70,000 km.

5. Acquiring international exchange of information on flyby and possible impact of a DCB of meter and decameter size = on Earth — a measure that allows for the possibility of alerting the population in advance. The exchange of similar information decreases the risk of triggering a nuclear-missile conflict.

6. The International monitoring of technological litter of near-Earth space and a periodic update of corresponding catalogues will help to select the anthropogenic background while carrying out the programs of observing DCBs.

In addition a number of supporting functions (such as continuous monitoring of the space in close proximity to the Earth, keeping and updating of corresponding catalogues) may be entrusted to the Space Control System.

Conclusion

Attaining an acceptable cost of building the Rapid Response Level "Citadel-1" is possible through converting and adapting missile-space technology and the shared use of systems being adopted and used for permanent alert and readiness.

The performed analysis and derived estimates do not only confirm the feasibility of solving the problems of neutralizing investigated dangerous celestial bodies but also give the opportunity for developing new methods taking into account their possible shared use in the interests of solving the problem of defense against DCBs. Thus, additional requirements for shared use in the technical specifications referring to methods and complexes being developed, in particular, for Missile-Space Defense [9] should be provided.

References

1. Catastrophic influence of space bodies / Eds V. V. Adushkin, I. V. Nemchinov. Moscow: Akademkniga, 2005 (in Russian).
2. *Zaitsev A. V.* Planetary Defense System "Citadel", the conceptual project. Moscow, Lavochkin Association 2000. 70 pp.
3. *Zaitsev A. V., Petrov D. V., Shubin O. N.* The international project "Citadel-1" is a real basis for guarantee of planetary safety // Int. Conf. "100 years since Tunguska phenomenon: past, present and future", M. June 26–28, 2008. P. 188–189.
4. *Semyonov B. I., Treckin V. V., Zaitsev A. V.* The possible use of missile-space defense system as part of the "Citadel" Planetary Defense System for neutralizing hazardous space bodies of decameter scale // Int. Conf. "100 years since Tunguska phenomenon: past, present and future", M. June 26–28, 2008. P. 209–210.
5. *Arsenyev G. N., Semyonov B. I., Torgovkin S. N., Treckin V. V.* The possibility of two-fold use of missile-space defense systems for solving the problem of asteroid-comet hazard // Information-measuring and Control Systems. 2000. Vol. 4, N 5. P. 5–12.
6. *Batyr G. S., Semyonov B. I., Treckin V. V.* Some Restrictions of Nuclear Missile Technology of Neutralizing Threatening Space Objects // Int. Conf. "Asteroid Hazard–96", St. Petersburg, July 15–19, 1996. P. 33–37.
7. *Repin V. G.* Osnovnye etapy sozdanija RKO. (The main stages of building Missile-Space Defense system) // The corporation "Vympel" Missile-Space Defense system. The publishing house "Weapon and Techology". Moscow, 2004. P. 50–72 (in Russian).
8. *Bogdanova Yu. P., Semyonov B. I.* The application of multipoint boundary problem theory for the space object determination // Cosmic Res. 1989. Vol. 27, N 2. P. 299–302.
9. *Fateev V. F., Suchanov S. A.* Kontseptsiya razvitiya RKO Rossii (The conception of developing Missile-Space Defense of Russia) // Aerospace defense. 2007. N 2(33) P. 20–27 (in Russian).

The Resolution of the ACH-2009 Conference

St. Petersburg, September 25, 2009

An International Conference ACH-2009 organized by the Institute of Applied Astronomy of RAS with support from the Russian Academy of Sciences and the Russian Foundation for Basic Research was held on 21–25 September, 2009 in St. Petersburg.

The main topics of the Conference were:

1. Study of small bodies of the Solar System (physics, dynamics, and origin and evolution of asteroids, comets, meteoroids).
2. Origin and dynamic evolution of objects approaching the Earth, observations, physical properties, cataloging, databases, estimating collision probabilities with the Earth and other Solar System bodies.
3. Collisions of cosmic bodies with the Earth (study of the traces of past catastrophic collisions, modeling of collisions, and consequences of such collisions).
4. Counteraction (discovering hazardous cosmic objects, methods and means of acting upon near-Earth objects, organization of passive and active countermeasures against impacts by asteroids and comet nuclei, technologies to address the study of asteroids and comets in near-Earth space, missions to hazardous bodies).
5. International legal aspects of counteracting the impact hazard. Collaboration of different countries in solving the problem.

About 150 scientists of more than 110 institutions and other organizations took part in the Conference. 120 papers were presented and discussed at the Conference. As a result of discussions and presentations this Resolution of the ACH-2009 Conference was approved.

1. During the last several years significant progress has been achieved in studying the problem of asteroid-comet hazards. This is particularly true for the discovery of thousands of asteroids and comets that approach or cross Earth's orbit. Collisions with such bodies are dangerous for human life and fraught with significant material losses. As a result of the international observing program Spaceguard the number of identified asteroids larger than 1 km approaching Earth's orbit within a distance of less than 0.3 AU has increased more than four times and is now about 800. Among them about 20 % are potentially hazardous objects (PHOs). A collision with such an object would cause a global catastrophe. Due to their dis-

covery and identification the risk of unpredictable collisions with them decreased approximately by a factor of ten.

2. In the USA and in Italy monitoring, tracking, and cataloging all cosmic objects approaching Earth within 0.3 AU, regardless of their size, has been established. Predictions of possible collisions with Earth are carried out and disseminated on a routine basis. Because of these services we now know that a number of objects have small, but not negligible probability of collision with Earth in the 21st century.
3. Significant progress has been made in studying the origin, evolution, mineralogy, size, and surface properties of minor planets and comet nuclei. In spite of these achievements their internal structure, composition, and material strengths remain largely unexplored. The A–C hazard continues to be one of the global problems that deserve broad and detailed attention of the scientific community and the public.
4. Discovery, characterization, and cataloging 90 % of all potentially hazardous objects larger than 140 m in size has been proposed as a task for the next 15 years. This task is by approximately two orders of magnitude more complicated than the first phase of the Spaceguard program. New and more powerful instruments are planned and are under construction to carry out this second phase of the Spaceguard program. New approaches for discovery and follow-up observations are under development. During execution of "Spaceguard-2" the amount of data to be analyzed and the probability of discovering PHOs on a collision course with Earth will increase enormously.
5. It must be kept in mind that discovering, tracking, and identifying PHOs is a very important and essential first step in defending Earth against collisions from objects in space. However, this first step is only useful if we also develop countermeasures to deflect or destroy such objects regardless of their size or projected impact frequency.
6. In this connection concluding internationally and politically binding agreements, possibly within the framework of the UN is an essential and urgent next step. Defense against PHOs is an international problem for the benefit of all peoples of the world and requires international participation and combined efforts of all nations.
7. The Conference participants highly appreciate the initiative of the USA Congress to commission NASA with fulfilling the second phase of the Spaceguard program in collaboration with other countries. The Conference urges astronomical institutions of all coun-

tries, including Russia, to actively participate in the realization of this program.

8. The Conference calls on scientists of all countries, including Russia, to broaden their international participation in studying the asteroid-comet hazard and to participate in developing effective countermeasures against potentially hazardous objects.
9. The Conference supports efforts directed to concluding an international agreement within the framework of the UN on developing common countermeasures against objects threatening Earth.

List of Participants

Surname	Name	Country	E-mail
A'Hearn	Michael	USA	ma@astro.umd.edu
Abramov	Vladimir	Russia	vva85@mail.ru
Adushkin	Vitaly	Russia	adushkin@idg.chph.ras.ru
Alehin	Vladimir	Russia	alehin@ipa.nw.ru
Alekseev	Vladimir	Russia	lilialeks@yandex.ru
Aleshkina	Ekaterina	Russia	aek3@list.ru
Artemieva	Natalia	Russia	nata_artemeva@rambler.ru
Bancelin	David	France	bancelin@imcce.fr
Batrakov	Yurii	Russia	batrakov@ipa.nw.ru
Berezhnoi	Andrei	Russia	berezhnoyaa@gmail.com
Bondarenko	Yurii	Russia	jura.bondarenko@gmail.com
Bubnov	Mikhail	Russia	aviacapellan@mail.ru
Cellino	Alberto	Italy	cellino@oato.inaf.it
Chernetenko	Yuliya	Russia	cya@ipa.nw.ru
Chubei	Markiyan	Russia	mchubey@gao.spb.ru
Danilin	Anatolii	Russia	anatol-48@mail.ru
Denisov	Sergei	Russia	denisovsergey777@rambler.ru
Desmars	Josselin	France	desmars@imcce.fr
Di Martino	Mario	Italy	dimartino@oato.inaf.it
Drobyshevskii	Eduard	Russia	emdrob@mail.ioffe.ru
Egorova	Lidiya	Russia	egorova@imec.msu.ru
Elenin	Leonid	Russia	l.elenin@qmail.com
Emel'yanenko	Vyacheslav	Russia	vvemel@inasan.ru
Emel'yanov	Vladimir	Russia	vaem45@mail.ru
Finkelstein	Andrey	Russia	amf@ipa.nw.ru
Fominov	Alexander	Russia	fominov@ipa.nw.ru
Gaftonyuk	Ninel'	Ukraine	oplnel@yahoo.com
Galushina	Tat'yana	Russia	volna@sibmail.com
Gayazov	Iskandar	Russia	gayazov@ipa.nw.ru
Gladysheva	Ol'ga	Russia	olga.gladysheva@mail.ioffe.ru
Glebova	Nina	Russia	glebova@ipa.nw.ru
Gritsevich	Mariya	Russia	gritsevich@list.ru
Gusyakov	Vyacheslav	Russia	gvk@sscc.ru
Harris	Alan	USA	awharris@spacescience.org
Hestroffer	Daniel	France	hestro@imcce.fr

Honkova	Michaela	Czech Rep.	mhonkova@klet.cz
Huebner	Walter	USA	WHuebner@swri.edu
Ikhsanov	Nazar	Russia	nazar_ikhsanov@yahoo.com
Ilitz	Zoran	Serbia	springsoft@tippnet.rs
Ivanova	Tamara	Russia	itv@ipa.nw.ru
Kalinin	Dmitrii	Russia	sunny-sko@mail.ru
Kankiewicz	Pawel	Poland	pawel.kankiewicz@pu.kielce.pl
Karachkina	Ludmila	Ukraine	morozova4848@mail.ru
Kastel’	Galina	Russia	kastel@ipa.nw.ru
Khazins	Valerii	Russia	khazins@idg.chph.ras.ru
Kiselev	Aleksei	Russia	alexxki@gmail.com
Kocer	Michal	Czech Rep.	kocer@klet.cz
Kochetova	Ol'ga	Russia	kochet_54@mail.ru
Korsmeyer	David	USA	david.j.korsmeyer@nasa.gov
Kosmodamianskij	Georgij	Russia	gak_83@mail.ru
Kristensen	Leif	Denmark	LKK@Phys.au.dk
Krugly	Yurij	Ukraine	krugly@astron.kharkov.ua
Kulichkov	Sergey	Russia	snk@ifaran.ru
Kuz’micheva	Marina	Russia	mkuzm@mail.ru
Landis	Rob	USA	rob.r.landis@nasa.gov
Lopez Garcia	Alvaro	Spain	alvaro.lopez@uv.es
Loseva	Tat’yna	Russia	losseva@idg.chph.ras.ru
Lupishko	Dmitrij	Ukraine	lupishko@astron.kharkov.ua
Lukashova	Marina	Russia	lmv@ipa.nw.ru
Maccone	Claudio	Italy	clmaccon@libero.it
Marchuk	Andrei	Russia	mag@omzg.sscc.ru
Margot	Jean-Luc	USA	jlm@ess.ucla.edu
Masaitis	Viktor	Russia	victor_masaitis@vsegei.ru
Medvedev	Yurii	Russia	medvedev@ipa.nw.ru
Michel	Patrick	France	michel@oca.eu
Naroyenkov	Sergey	Russia	snaroenkov@inasan.ru
Netsvetaeva	Galina	Russia	gan@ipa.nw.ru
Netsvetaev	Ilia	Russia	equal90@gmail.com
Nikishin	Vladimir	Russia	
Nikol'skii	Genrik	Russia	gnik777@mail.ru
Novikov	Fedor	Russia	fedornovikov@rambler.ru
Ogneva	Ol'ga	Russia	olga.f.ogneva@gmail.com
Pechernikova	Galina	Russia	pechernikova@idg.chph.ras.ru
Perov	Nikolai	Russia	perov@yspu.yar.ru

Petrov	Nikita	Russia	petrov@astro.spbu.ru
Pitjeva	Elena	Russia	evp@ipa.nw.ru
Polyakhova	Elena	Russia	pol@astro.spbu.ru
Popova	Ol'ga	Russia	olga_idg@rambler.ru
Pozhalova	Zhanna	Ukraine	pza1900@mail.ru
Pravec	Petr	Czech Rep.	ppravec@asu.cas.cz
Prialnik	Dina	Israel	dina@planet.tau.ac.il
Saifullin	Nazym	Russia	ppark2@ya.ru
Semenov	Boris	Russia	news197@mail.ru
Sharkov	Vladimir	Russia	vlash@ipa.nw.ru
Shefer	Vladimir	Russia	shefer@niipmm.tsu.ru
Shevchenko	Ivan	Russia	iis@gao.spb.ru
Shor	Viktor	Russia	shor@ipa.nw.ru
Shustov	Boris	Russia	bshustov@inasan.ru
Shuygina	Nadia	Russia	nvf@ipa.nw.ru
Sidorenko	Vladislav	Russia	sidorenk@spp.keldysh.ru
Skorov	Yuri	Germany	skorov@mpi.mpg.de
Smolentsev	Sergey	Russia	smolen@ipa.nw.ru
Smul'skii	Iosif	Russia	Jsmulsky@mail.ru
Sokolov	Leonid	Russia	lsok@astro.spbu.ru
Sokolov	Viktor	Russia	vix@gao.spb.ru
Stikhno	Kirill	Russia	fn2cyril@gmail.com
Sveshnikov	Mikhail	Russia	sml@ipa.nw.ru
Tihonova	Ulyana	Russia	ulyana.tihonova@qmail.com
Timofeev	Kirill	Russia	hillcitu@yandex.ru
Tishchenko	Valentina	Russia	kulikova@iate.obninsk.ru
Tochenov	Vladimir	Russia	
Usanin	Vladimir	Russia	VUsanin@yandex.ru
Valyaev	Valery	Russia	viv@ipa.nw.ru
Vega	Tatyana	Russia	tatyanavega@yandex.ru
Vinogradova	Tamara	Russia	vta@ipa.nw.ru
Virtanen	Jenni	Finland	jenni.virtanen@fgi.fi
Vityazev	Andrei	Russia	AVityazev@gmail.com
Wlodarczyk	Ireneusz	Poland	astrobit@ka.onet.pl
Yagudina	Eleonora	Russia	eiya@ipa.nw.ru
Yatskiv	Yaroslav	Ukraine	director@mao.kiev.ua
Yeomans	Donald	USA	donald.k.yeomans@jpl.nasa.gov
Zabotin	Aleksandr	Russia	shooreek@gmail.com
Zaitsev	Anatolii	Russia	pdc@berc.rssi.ru
Zamarashkina	Marina	Russia	m_zam@mail.ru
Zausaev	Anatolii	Russia	zausaev_af@mail.ru
Zheleznov	Nikolai	Russia	znb@ipa.nw.ru

Издание осуществлено с оригинал-макета,
подготовленного к печати
в Институте прикладной астрономии РАН

Подписано к печати 30.06.2010.
Формат 60×84 1/16. Печать офсетная.
Усл. печ. л. 26,7. Заказ № 310.
Тираж 250 экз.

ЗАО «Полиграфическое предприятие» № 3
191104, Санкт-Петербург, Литейный пр., д. 55.

ISBN 978-5-02-025514-2